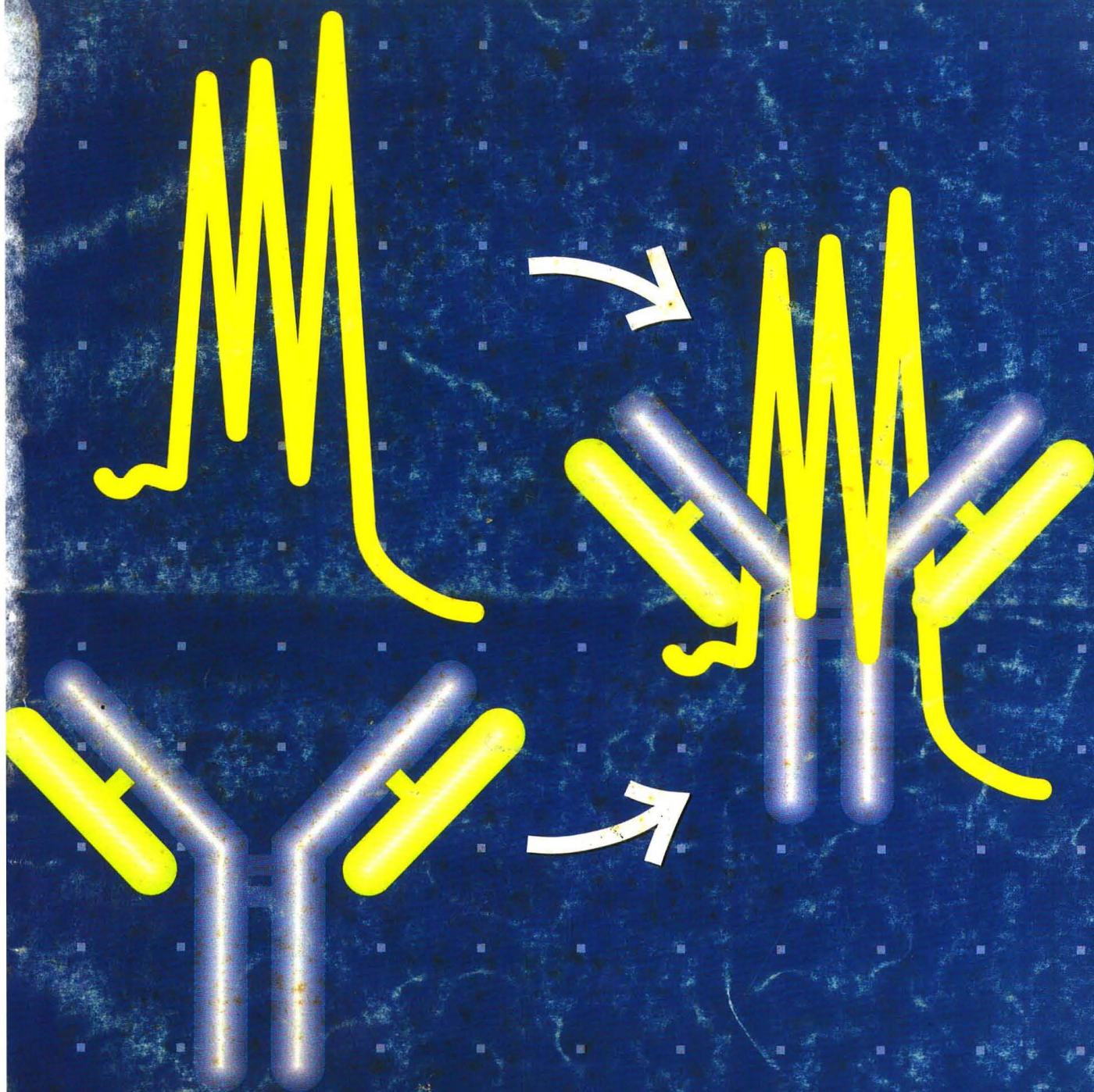


JANUARY 1, 1993

Analytical CHEMISTRY



**Tandem Chromatographic-
Immunological Analyses**

17 A

The Dawn of a New Era in Ion Analysis

Introducing revolutionary *AutoSuppression*.
Precise, reliable ion chromatography that's easier than ever.

Enter a new era in ion analysis, with *AutoSuppression* for ion chromatography.

AutoSuppression increases analyte signal and significantly reduces background noise, giving you detection limits up to *100 times* better than other ion analysis techniques. You get superb detection limits, broad dynamic ranges and ultimate matrix flexibility.

For inorganic anions to organic acids. And for Group I & Group II cations, ammonium and amines.

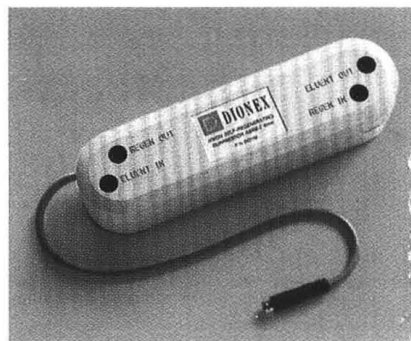
In short, the most powerful, versatile ion analysis technology available.

And *AutoSuppression* is effortless. Just plug it in and you're ready.

- No regenerants.
- No maintenance.
- No complicated eluents.

Just a *Self-Regenerating Suppressor* that you can completely forget.

Find out more about the advantages of *AutoSuppression* and the future of ion chromatography. In the U.S., call **800-227-1817 ext. 440**. Outside the U.S., call the Dionex office nearest you or **408-737-0700 ext. 4223**.

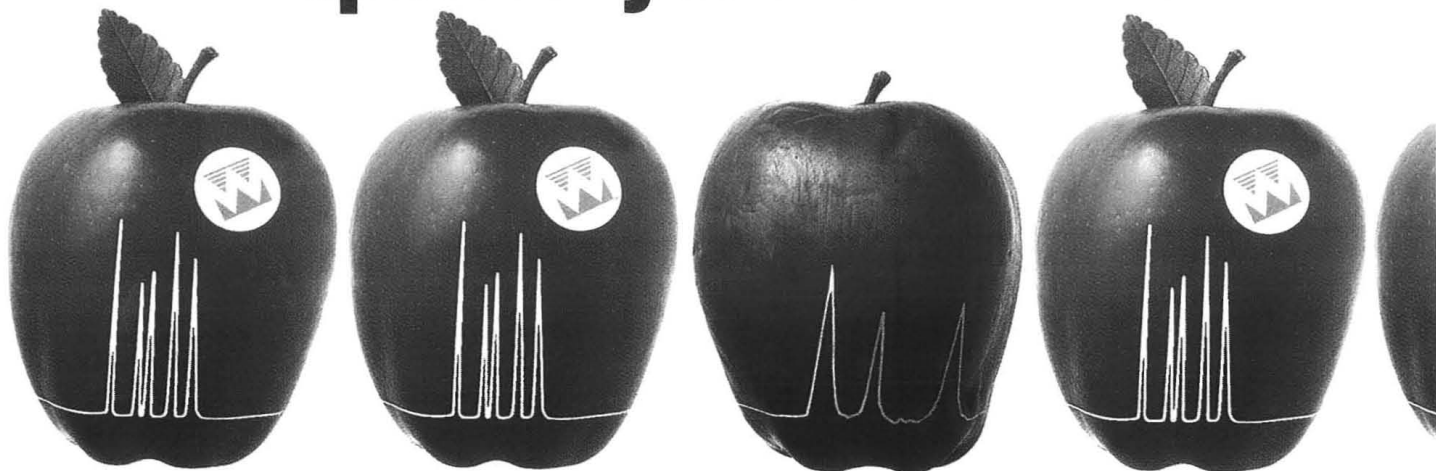


AutoSuppression is provided by our unique *Self Regenerating Suppressor (SRS™)*, available for the entire line of Dionex Systems. Ask about upgrading your existing system with SRS.

Dionex Corp. Sunnyvale, CA (408)737-0700 FAX (408)730-9403 **Canada** Dionex Canada Ltd. (416)855-2551 **France** Dionex S.A. (1)46 21 66 66 **Germany** Dionex GmbH (06126)9955-0 **Italy** Dionex S.r.l. (06)3715454 **Japan** Nippon Dionex K.K. (06)885-1213 **Netherlands** Dionex B.V. 076-714800 **United Kingdom** Dionex (UK) Ltd. (0276)691722 SRS and *AutoSuppression* are trademarks of Dionex Corporation. ©1992 Dionex Corp.

 **DIONEX**
A BETTER SOLUTION

Why let one bad apple spoil all your work?



Get reproducible results with Whatman.

Call 1-800-242-7530
for a free sample and more information.

Reproducibility problems are more than just frustrating: They cast doubt on the validity of your analysis. Why not get the reproducible results you need from Whatman?

Whatman has the most complete line of sample prep products in the industry—over 500 in all—and every one is unconditionally guaranteed to work within your exacting tolerances. In fact, reproducible results are the #1 reason so many professionals have made the switch to Whatman.

Our technical staff is ready to help you improve your method's reproducibility—whether your problems are procedural or involve the shortcomings of another manufacturer's product.

So the next time you're less than satisfied with the results you're getting, call Whatman. We'll spoil *you*, not your work.

CIRCLE 118 ON READER SERVICE CARD



Whatman Laboratory Division

Whatman Inc., 9 Bridewell Place, Clifton, New Jersey 07014

Telephone: 201-773-5800 Telex: 133426 Fax: 201-472-6949

Whatman (word and device) and Whatman (word only) are trademarks of Whatman Paper Ltd. 746-11-203

The reproducible results you need. Guaranteed.

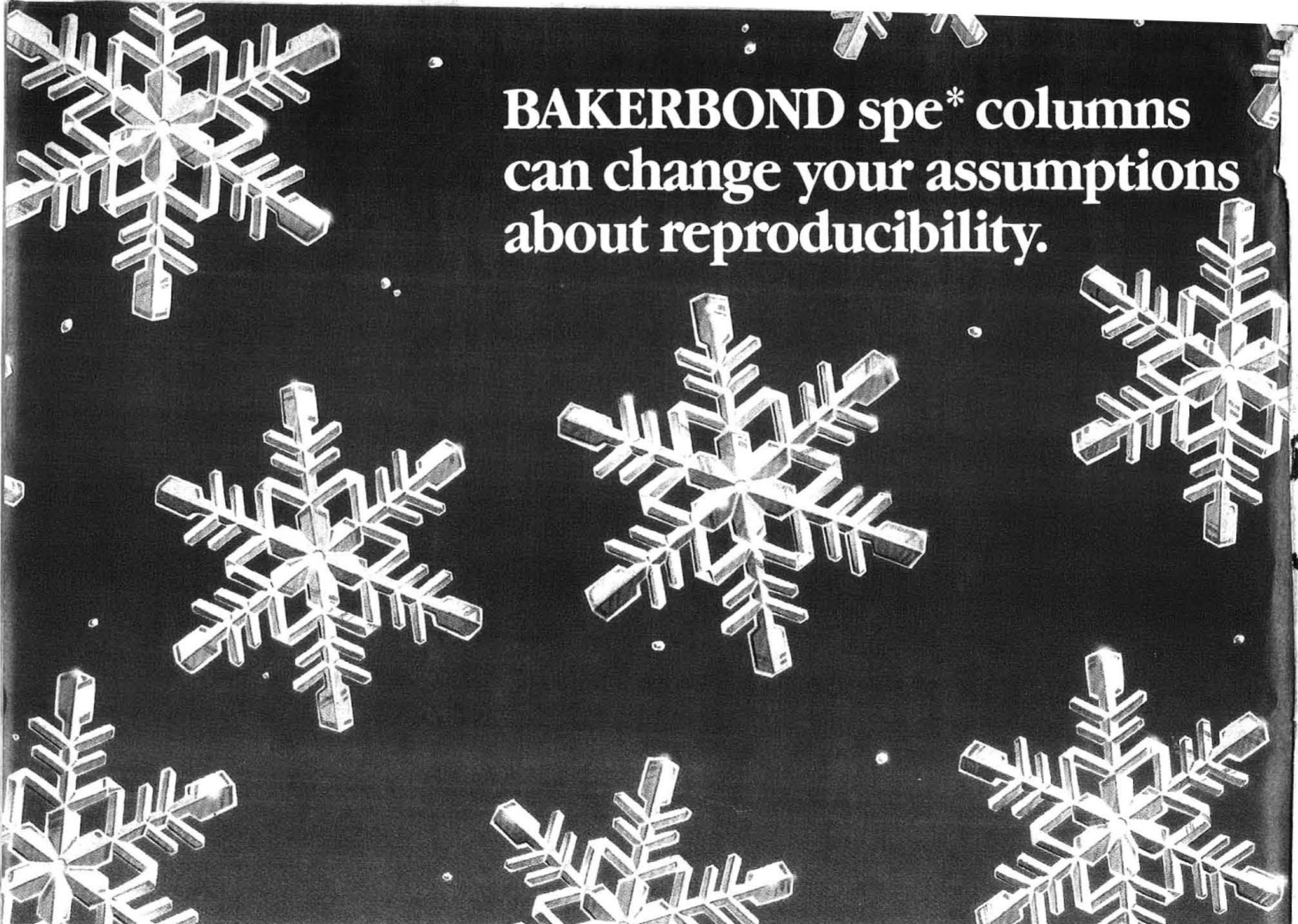


WHATMAN
ODS-1



WHATMAN
SPE ODS-1





BAKERBOND spe* columns can change your assumptions about reproducibility.

J.T.Baker's proprietary technology makes accurate, reproducible results easy to achieve.

Everyone knows a better solid phase extraction column gives you better results.

So if you want outstanding reproducibility, choose BAKERBOND spe* columns. Because J.T.Baker has the expertise and the technology that help you improve your results:

- Our proprietary technology gives us exceptional control over trifunctional bonding chemistry... and exceptional reproducibility in your sample preparation.
- Highly stable BAKERBOND* bonded phases produce clean extracts, giving you virtually interference-free sample preparation and highly reproducible results.
- To ensure high quality, our C₁₈ columns undergo more than 25 quality control tests throughout manufacturing. And our Reports of Analysis allow you to see our test data yourself.
- Our Application Notes provide pre-developed methods for over 100 applications, helping you save lab time and obtain high recoveries.

For solid proof of BAKERBOND spe column excellence, call J.T.Baker for our free brochure. Then compare your current solid phase extraction column performance to ours. The results will speak for themselves... and change your perception of reproducibility.

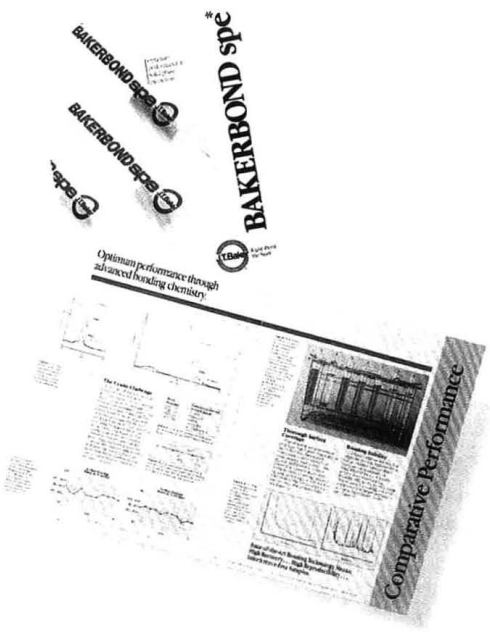
Contact J.T.Baker Inc., 222 Red School Lane, Phillipsburg, NJ 08865.
1-800-JTBAKER or 908-859-2151.
FAX: 908-859-9318.

1-800-JTBAKER

*BAKERBOND and BAKERBOND spe are trademarks of J.T.Baker Inc. ©1992 J.T.Baker Inc.



J.T.Baker *Right from the Start.*



J.T.Baker's free brochure provides definitive evidence of outstanding BAKERBOND performance.

Visit JT Baker at PITCON 93
Exhibit Hall E, Rows 4700-4701

Registered in U.S. Patent and Trademark Office;
©Copyright 1992 by the American Chemical Society

EDITOR: ROYCE W. MURRAY, University of North
Carolina

ASSOCIATE EDITORS: Catherine C. Fenselau,
University of Maryland Baltimore County, William
S. Hancock, Genentech, James W. Jorgenson,
University of North Carolina, Robert A. Os-
teryoung, North Carolina State University, Edward
S. Yeung, Iowa State University/Ames Laboratory

Editorial Headquarters, research section
Department of Chemistry
Venable and Kenan Laboratories
University of North Carolina
Chapel Hill, NC 27599-3290
Phone: 919-962-2541
Fax: 919-962-2542
E-mail: Murray @ uncvx1.oit.unc.edu

Editorial Headquarters, A-page section
1155 Sixteenth St., N.W.
Washington, DC 20036
Phone: 202-872-4570
Fax: 202-872-4574
E-mail: rmh96 @ acs.org

Managing Editor: Mary Warner

Senior Editor: Louise Voress

Associate Editor: Grace K. Lee

Assistant Editor: Felicia Wach

Editorial Assistant: Deborah Noble

Contributing Editor: Marcia Vogel

Head, Graphics and Production: Leroy L.
Corcoran

Art Director: Alan Kahan

Designers: Peggy Corrigan, Robert Sargent

Production Editor: Elizabeth Wood

Electronic Composition: Wanda R. Gordon

Circulation: David Schulbaum

LabGuide

Managing Editor of Directories and Databases:
Kathleen Strum

Associate Editor: Joanne Mullican

Assistant Editor: Susan Barclay

Journals Dept., Columbus, Ohio

Editorial Office Manager: Mary E. Scanlan

Journals Editing Managers: Kathleen E. Duffy,
Anne C. O'Melia, Joseph E. Yurvati

Assistant Editors: Stephanie R. Harrell,
Diane E. Needham

Advisory Board: Michelle V. Buchanan, Bruce
Chase, M. Bonner Denton, Joseph G. Gordon,
David M. Haaland, Joel M. Harris, Timothy D.
Harris, Franz Hillenkamp, Kiyokatsu Jinno, Den-
nis C. Johnson, Richard A. Keller, Philip D.
LaFleur, Gary E. Maciel, Geraldine Richmond,
Ralph Riggin, Michael Thompson
Ex Officio: Joseph L. Glajch

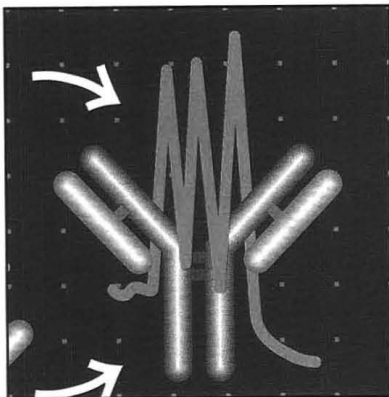
Instrumentation Advisory Panel: Anna Braj-
ter-Toth, Raymond E. Clement, Therese M. Cot-
ton, Norman J. Dovichi, Jack D. Henion, Mary
Ellen P. McNally, John W. Olesik, Dallas L. Ra-
benstein, J. Michael Ramsey

Publications Division

Director: Robert H. Marks

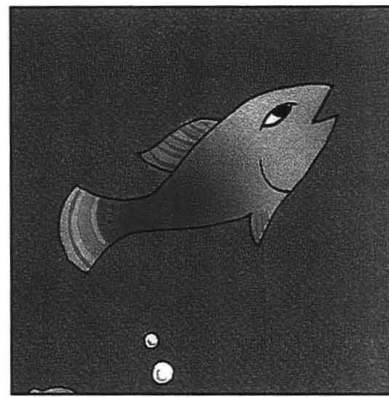
Head, Special Publications: Anthony Durniak

Head, Journals: Charles R. Bertsch



REPORT 17 A

**On the cover. Chromatograph-
ic-immunological analyses.** For more than half a century, liq-
uid chromatography and immuno-
logical assays have developed
along independent routes. Mer-
cedes de Frutos and Fred E. Reg-
nier of Purdue University describe
how the complementary features
of these two techniques can be
combined to produce analytical
systems with superior selectivity,
speed, and sensitivity



ANALYTICAL APPROACH 32 A

**Egyptian civilization and the
environment before the Pha-
raohs.** The importance of the Nile
River to the development of Egyp-
tian civilization has long been re-
cognized. Ralph O. Allen of the
University of Virginia and coau-
thors describe how studies of pre-
dynastic archaeological sites have
provided new evidence of major
climatic changes in Africa during
this period, leading to the postula-
tion that adaptation to the envi-
ronment may have triggered the
creation of the first nation state

UPCOMING RESEARCH 11 A

EDITORIAL 13 A

A macromolecular proposal. The large role of polymers in our everyday
lives warrants an increased emphasis on the study of polymers in our un-
dergraduate and graduate curricula

NEWS 15 A

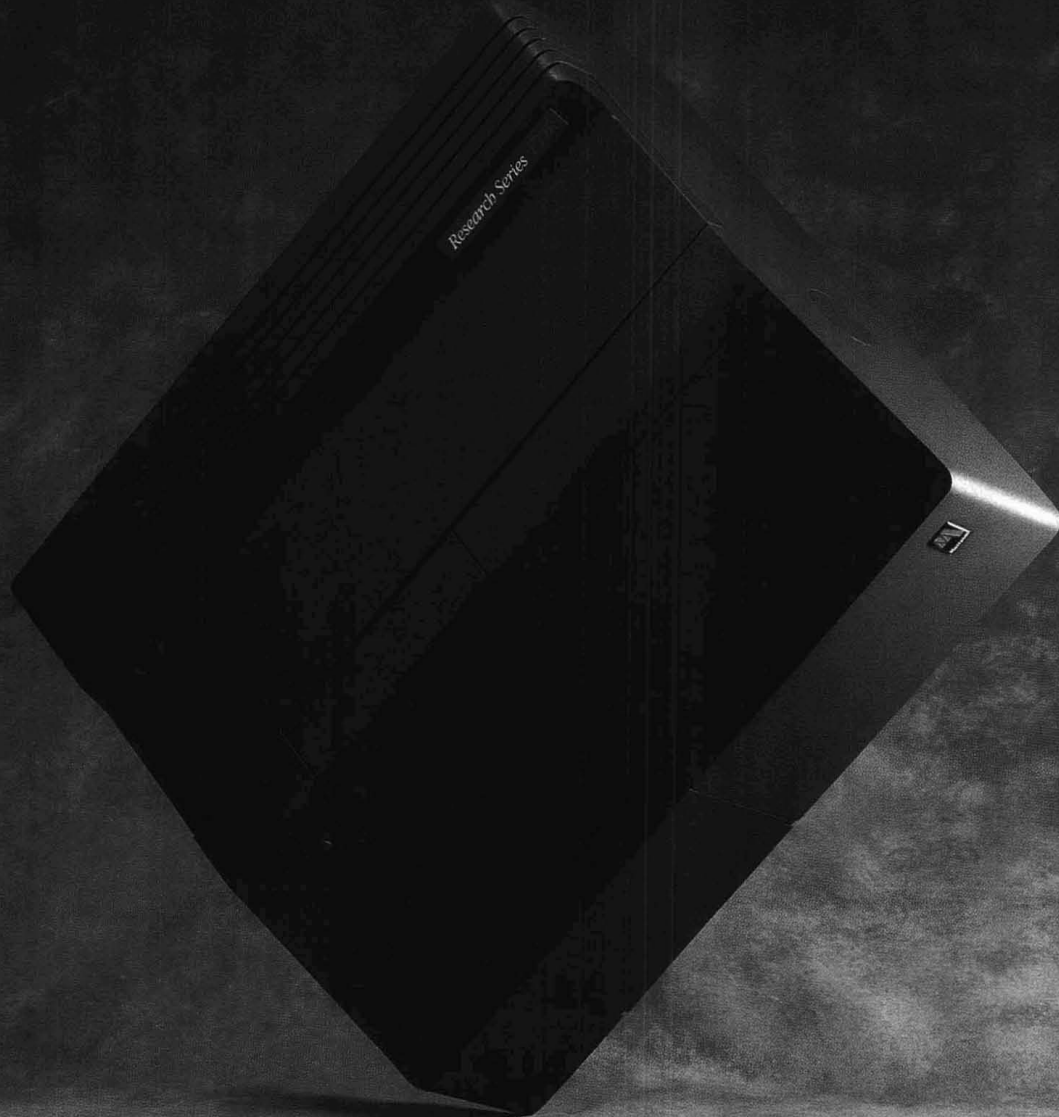
**Bruce Chase, Joseph L. Glajch, Joseph G. Gordon, David M. Haa-
land, Kiyokatsu Jinno, and Gary E. Maciel** join ANALYTICAL CHEM-
ISTRY's Advisory Board. • Deborah Noble joins the AC staff

MEETINGS 26 A

1993 comprehensive listing

NEW PRODUCTS AND MANUFACTURERS' LITERATURE 30 A

We put a new spin on our Research Series™ FTIR spectrometer.



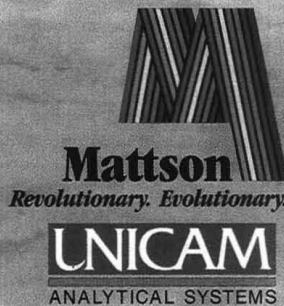
New added features make it better than ever.

Now it's even more precise. We've pushed perfection to the limit and improved the Research Series signal-to-noise ratios to better than 80,000:1 measured peak-to-peak.

Even more flexible. Choose from our conductively-cooled ICE™ source or ultra-hot fluid-cooled glowbar. Change beamsplitters and detectors for extended spectral range. Use the two external beams and separate emission port. Add FT-Raman, high-capacity TGA and sensitive GC interfaces, our Quantum Infrared Microscope™ — and more.

And more comprehensive, more powerful than ever. As the leaders in easy-to-use FTIR software, we created WinFIRST™ software specifically for Microsoft® Windows™ 3.1. (We didn't just adapt it.) Exclusives such as our WinFIRST Infrared Tool Bar™ help you work faster, while in-depth control lets you take your work to the limits. And nothing beats our EZ-annotation™ report generator for creating fast, professional reports.

Call us today at (608) 831-5515. Or fax us at (608) 831-2093. Our new, improved Research Series will take you into the future. And beyond.



1001 Fourier Drive Madison, WI 53717

**Cahn, Orion, Mattson and Unicam are
operating divisions of Analytical Technology, Inc.**

© 1993, Mattson Instruments, Inc.

CIRCLE 70 ON READER SERVICE CARD

ANALYTICAL CHEMISTRY (ISSN 0003-2700) is published semimonthly by the American Chemical Society, 1155 Sixteenth St., N.W., Washington, DC 20036. Second-class postage paid at Washington, DC, and additional mailing offices. Postmaster: Send address changes to ANALYTICAL CHEMISTRY, Member & Subscriber Services, P.O. Box 3337, Columbus, OH 43210. Canadian GST Reg. No. R127571347.

Copyright Permission: An individual may make a single reprographic copy of an article in this publication for personal use. Reprographic copying beyond that permitted by Section 107 or 108 of the U.S. Copyright Law is allowed, provided that the appropriate per-copy fee is paid through the Copyright Clearance Center, Inc., 27 Congress St., Salem, MA 01970. For reprint permission, write Copyright Administrator, Publications Division, ACS, 1155 Sixteenth St., N.W., Washington, DC 20036.

Registered names and trademarks, etc., used in this publication, even without specific indication thereof, are not to be considered unprotected by law.

Subscription and Business Information

1993 subscription rates include air delivery outside the U.S., Canada, and Mexico. Canadian subscriptions are subject to 7% GST.

	Members	Nonmembers (personal)	Nonmembers (institutional)
U.S.	\$ 36	\$ 78	\$ 415
Canada and Mexico	72	114	451
Europe	117	230	496
Other countries	141	254	520

Nonmember rates in Japan: Rates above do not apply to nonmember subscribers in Japan, who must enter subscription orders with Maruzen Company Ltd., 3-10, Nihonbashi 2-chrome, Chuo-ku, Tokyo 103, Japan. Tel: (03) 272-7211.

For multi-year and other rates, call toll free 800-227-5558 in the U.S. and Canada; in the Washington, DC, metropolitan area and outside the U.S., call 202-872-4363; fax 202-872-4615.

Single issues, current year, \$16.00 except review issue, \$50.00, and LabGuide, \$50.00; **back issues and volumes and microform editions** available by single volume or back issue collection. For information or to order, call the number listed for subscription orders by phone; or write the Microform & Back Issues Office at the Washington address.

Subscription orders by phone may be charged to VISA, MasterCard, or American Express. Call toll free 800-333-9511 in the continental U.S.; in the Washington, DC, metropolitan area and outside the continental U.S., call 202-872-8065. Mail orders for new and renewal subscriptions should be sent with payment to American Chemical Society, Department L-0011, Columbus, OH 43268-0011.

Changes of address must include both old and new addresses with ZIP code and a recent mailing label. Send all address changes to the ACS Columbus address. Please allow 6 weeks for change to become effective. **Claims for missing numbers** will not be allowed if loss was due to failure of notice of change of address to be received in the time specified; if claim is dated (a) North America—more than 90 days beyond issue date, (b) all other foreign—more than 180 days beyond issue date. Hard copy claims are handled at the ACS Columbus address.

ACS membership information: Lorraine Bowlin (202-872-4567)

Articles

- Heat-Induced Conformational Changes in Proteins Studied by Electro spray Ionization Mass Spectrometry **1**
*Urooj A. Mirza, Steven L. Cohen, and Brian T. Chait**
- Structure-Specific Collision-Induced Fragmentations of Ceramides Cationized with Alkali-Metal Ions **7**
*Qinghong Ann and Jeanette Adams**
- Matrix-Assisted Laser Desorption of Biological Molecules in the Quadrupole Ion Trap Mass Spectrometer **14**
David M. Chambers, Douglas E. Goeringer, Scott A. McLuckey, and Gary L. Glish*
- Determination of Atrazine in Water at Low- and Sub-Parts-per-Trillion Levels by Using Solid-Phase Extraction and Gas Chromatography/High-Resolution Mass Spectrometry **21**
Zongwei Cai, V. M. Sadagopa Ramanujam, Daryl E. Giblin, Michael L. Gross, and Roy F. Spalding*
- Effects of Buffer pH on Electroosmotic Flow Control by an Applied Radial Voltage for Capillary Zone Electrophoresis **27**
*Mark A. Hayes, Indu Kheterpal, and Andrew G. Ewing**
- NMR Study of the State of Water in Ion-Selective Electrode Membranes **32**
*Andy D. C. Chan and D. Jed Harrison**
- Self-Assembled Monolayers in Electroanalytical Chemistry: Application of ω -Mercapto Carboxylic Acid Monolayers for the Electrochemical Detection of Dopamine in the Presence of a High Concentration of Ascorbic Acid **37**
*Franck Malem and Daniel Mandler**
- pH-Metric log *P*. 3. Glass Electrode Calibration in Methanol-Water, Applied to pK_a Determination of Water-Insoluble Substances **42**
Alex Avdeef, John E. A. Comer, and Simon J. Thomson*
- Optimization of Waveforms for Pulsed Amperometric Detection of Carbohydrates Based on Pulsed Voltammetry **50**
*William R. LaCourse and Dennis C. Johnson**
- Examination of Conditions under Which the Reduction of the Cobaltocenium Cation Can Be Used as a Standard Voltammetric Reference Process in Organic and Aqueous Solvents **56**
*R. S. Stojanovic and A. M. Bond**
- Long-Term, On-Line Monitoring of Microbial Biofilms Using a Quartz Crystal Microbalance **65**
David E. Nivens, James Q. Chambers, Tina R. Anderson, and David C. White*
- Vector Representation, Feature Selection, and Fingerprinting: An Application of Pattern Recognition to Pyrolysis-Gas Chromatography/Mass Spectrometry of Nucleosides **70**
*Rachhpal S. Sahota and Stephen L. Morgan**


*Corresponding author

continued on p. 9 A

FT-IR down-time?



No Problem!

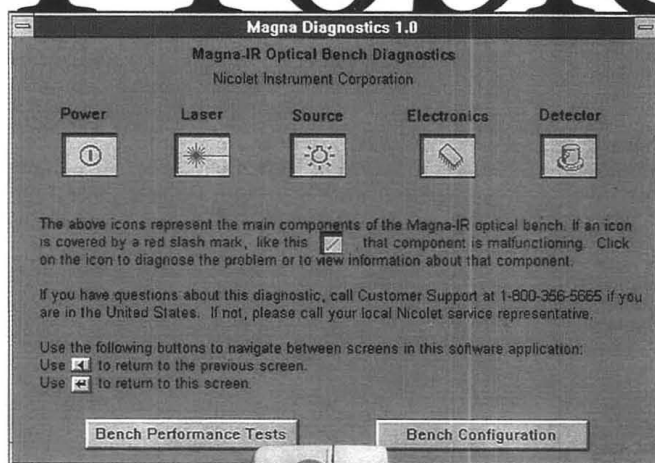
 Nicolet's new Magna-IR™ and Impact™ spectrometers with OMNIC™ software will change the way you think about FT-IR technology.

You can easily replace the source, laser, detectors, and power supply—without getting in over your head.

The only tool kit you'll ever need is a screwdriver.

Nicolet offers the first FT-IR systems with user-changeable components.

Each is pinned-in-place, eliminating complicated alignment adjustments and a service call. This saves you time and money.



Plus, you are ensured of reliable FT-IR performance through Nicolet's advanced diagnostics program. With a click of the mouse, you are instantly updated on the system's operating status.



Magna-IR 750

*No guessing.
No waiting.
No problem!*

Contact Nicolet at 800-356-8088 for an eye opening demonstration or circle the reader service number to receive more information.

Nicolet
INSTRUMENTS OF DISCOVERY
The intelligent FT-IR choice!

5225 Verona Road / Madison, WI 53711-4495 / TEL: 608/271-3333 / FAX: 273-5046

CIRCLE 80 ON READER SERVICE CARD

Editorial Information

Instructions for authors of AC RESEARCH are published in the January 1 issue, p. 91. Guidelines for the INSTRUMENTATION, REPORT, ANALYTICAL APPROACH, and A/C INTERFACE features are published in the January 1 issue, p. 90. Please consult these instructions and guidelines prior to submitting a manuscript for consideration for publication.

Manuscripts for publication in AC RESEARCH (4 copies of text and illustrative material) should be submitted to the Editor at the University of North Carolina address. Please include a signed copyright status form; a copy of this document appears on p. 95 of the January 1 issue. Manuscripts for publication in the A-page section should be submitted to the Washington editorial staff.

For individual reprints of AC RESEARCH or A-page articles, please contact the authors directly. Bulk reprints of individual articles are available from ACS. For information, write or call the Distribution office at the ACS Washington address (202-872-4539; fax 202-872-4615).

ACS Division of Analytical Chemistry

Chair, Joseph L. Glajch (508-671-8413)
Secretary, Sarah Rutan (804-367-1298)

ACS Information

Library Services	202-872-4515
Education Division	202-872-4388
Meetings Dept.	202-872-4397
Member Services	202-872-4414
Employment Services	202-872-6120
Public Outreach	202-872-4091

Supplementary material is noted in the table of contents with a ■. It is available as photocopy (\$10.00 for up to 3 pages and \$1.50 per page for additional pages, plus \$2.00 for foreign postage) or as 24X microfiche (\$10.00, plus \$1.00 for foreign postage). Canadian residents should add 7% GST. See supplementary material notice at end of journal article for number of pages. Orders *must* state whether for photocopy or for microfiche and give complete title of article, names of authors, journal, issue date, and page numbers. Prepayment is required and prices are subject to change. Order from Microforms & Back Issues Office at the ACS Washington address.

The paper used in this publication meets the minimum requirements of American National Standard for Information Sciences—Permanence of Paper for Printed Library Materials, ANSI Z39.48-1984.

Journals Department

American Chemical Society
2540 Orlentangy River Road
P.O. Box 3330
Columbus, OH 43210
614-447-3600, Ext. 3171
TELEX 6842086; Fax 614-447-3745

Member & Subscriber Services

American Chemical Society
P.O. Box 3337
Columbus, OH 43210
614-447-3776
800-333-9511

Advertising Office: Centcom, Ltd., 1599 Post Road East, P.O. Box 231, Westport, CT 06881

The American Chemical Society and its editors assume no responsibility for the statements and opinions advanced by contributors. Views expressed in the editorials are those of the editors and do not necessarily represent the official position of the American Chemical Society.

Quantitative Analysis by On-Line Supercritical Fluid Extraction/
Fourier Transform Infrared Spectrometry **78**
*Cynthia Hume Kirschner and Larry T. Taylor**

Technical Notes

Real-Time Measurement of Dimethyl Sulfoxide in Ambient Air **84**
H. Berresheim, D. J. Tanner, and F. L. Eisele*

Method for Batch Processing Small Wood Samples to Holocellulose
for Stable-Carbon Isotope Analysis **87**
Steven W. Leavitt and Shelly R. Danzer*

A-Page Feature Article Guidelines **90**

AC Research Manuscript Requirements **91**

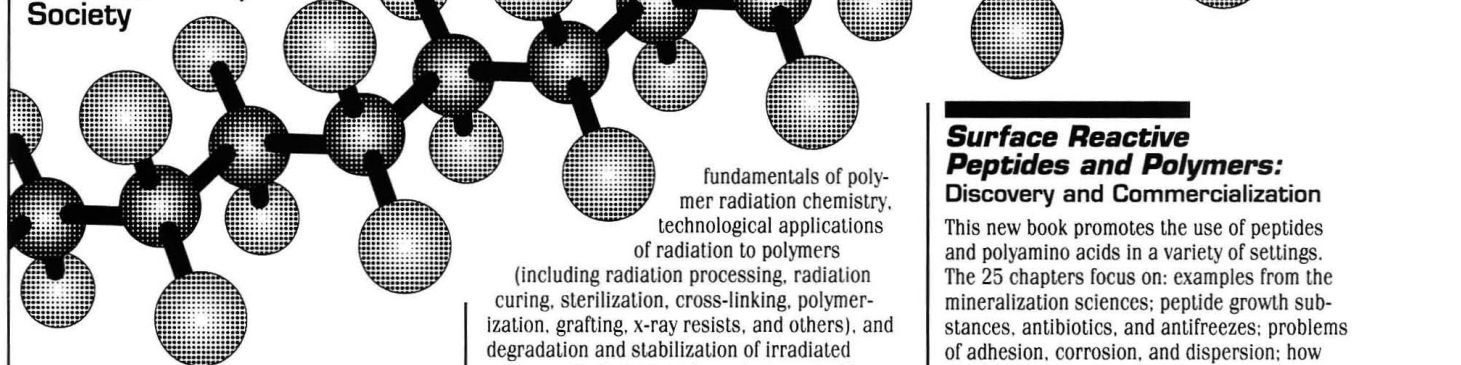
Ethical Guidelines to Publication of Chemical Research **93**

Copyright Status Form **95**

Author Index **96**

New Books on POLYMERS & PLASTICS

from the
American
Chemical
Society



Spectroscopy of Polymers

The definitive reference book for those who have a basic knowledge of polymer chemistry and the common spectroscopic methods, but who lack the specific knowledge required to apply the modern techniques of FTIR, Raman, and NMR spectroscopy to the polymer system at hand. Eleven chapters cover the fundamental aspects and experimental applications of the primary spectroscopic methods and examine the advantages and disadvantages of the various techniques for particular polymer systems.

Jack L. Koenig

ACS Professional Reference Book
450 pages (1991)
Clothbound: ISBN 0-8412-1904-4
■\$89.95
Paperbound: ISBN 0-8412-1924-9
■\$49.95

Particle Size Distribution II Assessment and Characterization

Features the latest technology now in use for particle size distribution assessment. Among the new techniques discussed are capillary hydrodynamic fractionation, field flow fractionation, disc centrifuge photosedimentometry, on-line measurements, fractals, electrophoretic characterization, image analysis, and electric sensing zone. A review chapter examines turbidimetry, an old technique that has been revitalized with new mathematical approaches.

Theodore Provder, Editor

ACS Symposium Series No. 472
400 pages (1991)
Clothbound: ISBN 0-8412-2117-0
■\$89.95

Radiation Effects on Polymers

Reviews the chemistry and physics of polymer-radiation interaction and examines recent progress in major areas of the field. Covers

fundamentals of polymer radiation chemistry, technological applications of radiation to polymers

(including radiation processing, radiation curing, sterilization, cross-linking, polymerization, grafting, x-ray resists, and others), and degradation and stabilization of irradiated polymers (including nuclear plants, scintillation detectors for particle physics, and others).

Roger L. Clough and Shalaby W. Shalaby, Editors

ACS Symposium Series No. 475
640 pages (1991)
Clothbound: ISBN 0-8412-2165-0
■\$109.95

Polymeric Drugs and Drug Delivery Systems

Covering a broad spectrum of methods of drug delivery and focusing on the use of polymers and materials, this volume presents new materials and methods for controlled drug release. Emphasizes selection of materials for drug delivery rather than just reviewing current methods. Included is an examination of recent advances in biodegradable and bioerodible polymer matrices for drug delivery.

Richard L. Dunn and Raphael M. Ottenbrite, Editors

ACS Symposium Series No. 469
314 pages (1991)
Clothbound: ISBN 0-8412-2105-7
■\$74.95

Water-Soluble Polymers Synthesis, Solution Properties, and Applications

This new volume provides readers with necessary information on the organic and physical chemistry of synthetic and natural polymers, as well as recent developments in polymer synthesis and modification. Its 33 chapters are divided into five sections covering polymers and intermediates, polymer synthesis and modification, physicochemical aspects of aqueous solutions, biomedical and industrial applications, and advances in less conventional systems.

Shalaby W. Shalaby, Charles L. McCormick, and George B. Butler, Editors

ACS Symposium Series No. 467
526 pages (1991)
Clothbound: ISBN 0-8412-2101-4
■\$99.95

Surface Reactive Peptides and Polymers: Discovery and Commercialization

This new book promotes the use of peptides and polyamino acids in a variety of settings. The 25 chapters focus on: examples from the mineralization sciences; peptide growth substances, antibiotics, and antifreezes; problems of adhesion, corrosion, and dispersion; how organisms regulate silica deposition; how silica deposits are dealt with in industrial settings.

C. Steven Sikes and A. P. Wheeler, Editors

ACS Symposium Series No. 444
432 pages (1991)
Clothbound: ISBN 0-8412-1886-2
■\$69.95

Polyelectrolyte Gels Properties, Preparation, and Applications

Presents an overview of current research and a review of historic contributions on polyelectrolyte gels, with particular emphasis on their unique characteristics. Leading researchers in the field offer contributions covering such topics as polyelectrolyte gel properties; gel phase behavior; novel synthesis methods; mass transport, gel thermodynamics, molecular interaction, and principle applications. The book's fundamental approach aids readers in solving developmental objectives and provides an in-depth understanding of the physical and theoretical bases of polyelectrolyte gels.

Ronald S. Harland and Robert K. Prud'homme, Editors

ACS Symposium Series No. 480
314 pages (1992)
Clothbound: ISBN 0-8412-2176-6
■\$79.95

ORDER FROM:
American Chemical Society
Distribution Office
Department 27
1155 Sixteenth Street, N.W.
Washington D.C. 20036

**or CALL TOLL FREE
800-227-5558
or in Washington D.C.
202-872-4363
and use your credit card!**

UPCOMING RESEARCH

Optimization of pH for the Separation of Organic Acids in Capillary Zone Electrophoresis

Mobility in CZE is successfully predicted as a function of pH by using a mathematical model. The optimum pH for the separation is obtained on the basis of only four initial experiments.

Scott C. Smith and Morteza G. Khaledi*, Department of Chemistry, North Carolina State University, Box 8204, Raleigh, NC 27695-8204

Bicyclic Ketone as a Solid-State ^{13}C NMR Intensity Reference

A carbonyl ^{13}C -labeled bicyclic ketone is synthesized and characterized as a cross-polarization intensity standard for solid-state NMR. The 217-ppm chemical shift avoids most spectral overlaps.

Randal A. Hall, Antoni Jurkiewicz, and Gary E. Maciel*, Department of Chemistry, Colorado State University, Fort Collins, CO 80524-0002

Selective Detection of Free Thiols by Capillary Electrophoresis—Electrochemistry Using a Gold/Mercury Amalgam Microelectrode

A thiol-specific amperometric detector for CE is described. The detection method is highly selective and is based on the catalytic oxidation of thiols at a gold/mercury amalgam electrode. Detection limits for glutathione are 0.53 fmol or $2.1 \times 10^{-8}\text{M}$.

Thomas J. O'Shea and Susan M. Lunte*, Center for Bioanalytical Research, University of Kansas, 2095 Constant Avenue, Lawrence, KS 66047

Window Evolving Factor Analysis for Assessment of Peak Homogeneity in Liquid Chromatography

The performance of fixed-size window evolving factor analysis is assessed for peak purity control using an LC system that also allows for testing of peak homogeneity algorithms.

Hans R. Keller and Désiré L. Massart*, Pharmaceutical Institute, Vrije Universiteit Brussel, Laarbeeklaan 103, B-1090 Brussels, Belgium and **Jacques O. De Beer**, Institute for Hygiene and Epidemiology, J. Wytmanstraat 14, B-1050 Brussels, Belgium

Expert System for Data Acquisition To Achieve a Constant Signal-to-Noise Ratio: Application to Imaging of DNA Sequencing Gels

The idea of data acquisition and processing to achieve a constant signal-to-noise ratio rather than constant time is evaluated for use in analyzing DNA sequencing gels.

Lance B. Koutny and Edward S. Yeung*, Department of Chemistry and Ames Laboratory—USDOE, Iowa State University, Ames, IA 50011

Photochemical Sensor for Catalase Activity Based on the In Situ Generation and Detection of Substrate

Reagentless sensors for the automation of enzyme immunoassay require in situ substrate generation. A device that photochemically generates and electrochemically detects peroxide, a substrate of the enzyme catalase, is described.

Claudia B. Cohen and Stephen G. Weber*, Department of Chemistry, University of Pittsburgh, Pittsburgh, PA 15260

Origin of Indirect Detection in the Liquid Chromatography of a Neutral Sample with an Ionic Probe Using an ODS Bonded Phase and Aqueous Mobile Phase

Simultaneous sorption of butanol sample and naphthalene-2-sulfonate probe on Partisil 10 ODS-3 involves a direct competition for space.

Laura L. M. Glavina and Frederick F. Cantwell*, Department of Chemistry, University of Alberta, Edmonton, Alberta, Canada T6G 2G2

The Use of Tetraalkylammonium Ion-Sensitive Electrodes for the Liposome Marker Release Assay

Tetraalkylammonium ions with alkyl chain lengths shorter than that of a propyl group are trapped stably in the inner aqueous phase of liposomes and are used for the assay of liposomal membrane permeability.

Takashi Katsu, Faculty of Pharmaceutical Sciences, Okayama University, Tsushima, Okayama 700, Japan

Native Fluorescence Detection of Nucleic Acids and DNA Restriction Fragments in Capillary Electrophoresis

Detection of nucleotides and DNA fragments separated by capillary electrophoresis can be accomplished by laser excitation at 275 nm and by monitoring of native fluorescence at levels well below absorption detection.

Robert E. Milofsky and Edward S. Yeung*, Department of Chemistry and Ames Laboratory—USDOE, Iowa State University, Ames, IA 50011

These articles are scheduled to appear in AC RESEARCH in the near future.

*Corresponding author

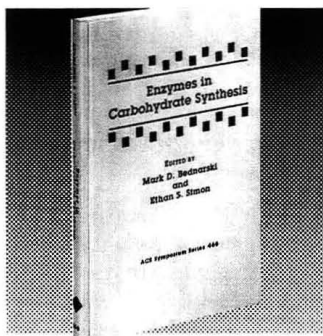
HOT Topics, HOT Books!

New Titles in Medicinal and Pharmaceutical Chemistry From the American Chemical Society

Polymeric Drugs and Drug Delivery Systems

Covering a broad spectrum of methods of drug delivery and focusing on the use of polymers and materials, this volume presents new materials and methods for controlled drug release. Emphasizing selection of materials for drug delivery rather than just reviewing current methods, the editors challenge researchers to venture into new areas and consider new methods. Included is an examination of recent advances in biodegradable and bioerodible polymer matrices for drug delivery.

Richard L. Dunn and Raphael M. Ottenbrite, Editors
ACS Symposium Series No. 469
314 pages (1991) Clothbound
ISBN 0-8412-2105-7
\$74.95



Protein Refolding

Bridging the gap between fundamental and applied studies in protein refolding, this volume addresses such topics as in vivo protein refolding, protein aggregation and inclusion body formation, elucidation of the folding pathway, characterization of folding intermediates, and practical considerations in protein renaturation. An overview chapter provides historical highlights of the key aspects of protein folding, aggregation, and refolding, both in the laboratory and in industry.

George Georgiou and Eliana De Bernardez-Clark, Editors
ACS Symposium Series No. 470
216 pages (1991) Clothbound
ISBN 0-8412-2107-3
\$49.95

Selective Fluorination in Organic and Bioorganic Chemistry

Recent applications of organofluorine chemistry to problems in biological chemistry are explored in this new volume. Its 14 chapters address theoretical and synthetic problems, as well as applications of selective fluorination to biological systems. The overview chapter, an excellent tutorial, begins with the fundamental and unique aspects of fluorine chemistry and reviews methods of introducing fluorine into molecules and work done on biomolecules.

John T. Welch, Editor
ACS Symposium Series No. 456
215 pages (1991) Clothbound
ISBN 0-8412-1948-6
\$57.95

Cell Separation Science and Technology

Providing theoretical and practical information on the state of the science of cell separation, this new volume covers the four principal modern methods: flow sorting and optical methods; sedimentation and flow fractionation; affinity adsorption and extraction methods; and electrophoresis and magnetic methods. Readers will be able to choose, evaluate, and in some cases, build cell separation procedures and equipment for their own purposes based on the contents of the book, which also covers many applications of each method.

Dhinakar S. Kompala and Paul Todd, Editors
ACS Symposium Series No. 464
302 pages (1991) Clothbound
ISBN 0-8412-2090-5
\$69.95

Chiral Separations by Liquid Chromatography

Here is the definitive reference for researchers working on problems involving chirality. Presenting state-of-the-art information, this volume covers all the major modes of separation and offers contributions from the leading researchers who developed these techniques. Four chapters provide a detailed review of the commonly used

columns: brush type, cyclodextrin, polysaccharide carbonate, and protein. Many of the papers focus on HPLC, a technique which is also ideally suited for large scale preparation of optical isomers. In addition, the volume provides significant discussion on the use of chiral discriminators or selectors.

Satinder Ahuja, Editor
ACS Symposium Series No. 471
240 pages (1991) Clothbound
ISBN 0-8412-2116-2
\$59.95

Cholinesterases: Structure, Function, Mechanism, Genetics, and Cell Biology

Presenting the proceedings of the Third International Meeting on Cholinesterases, this volume provides a wealth of new information on current cholinesterase research, including important advances resulting from new concepts and methodologies such as monoclonal antibodies and molecular genetics. Among the topics covered in its 49 full papers and 140 posters papers are polymorphism and structure, cellular biology, gene structure and expression, catalytic mechanism, pharmacological utilization of anticholinesterase agents, and noncholinergic roles of cholinesterases.

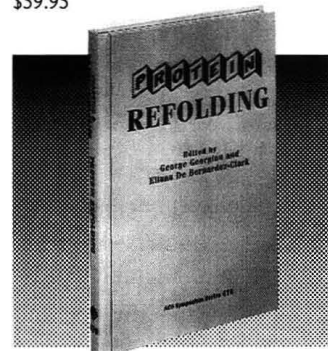
Jean Massoulie, Francis Bacou, Eric Barnard, Arnaud Chatonnet, Bhupendra P. Doctor, and Daniel M. Quinn, Editors
Conference Proceedings Series
400 pages (1991) Clothbound
ISBN 0-8412-2008-5
\$89.95

Inositol Phosphates and Derivatives: Synthesis, Biochemistry, and Therapeutic Potential

This new volume examines the synthesis, biochemistry, and pharmacological evaluation aspects of inositol phosphate research. Two overview chapters provide comprehensive background information on stereochemistry and nomenclature of inositol phosphates, basic biochemistry, synthetic challenges, and related pharmacology. Subsequent chapters describe novel methods of

preparation, including the use of unusual starting materials and mediation by microorganisms, therapeutic potential and bioactivity, structure-activity relations, and separation.

Allen B. Reitz, Editor
ACS Symposium Series No. 463
224 pages (1991) Clothbound
ISBN 0-8412-2086-7
\$59.95



Enzymes in Carbohydrate Synthesis

Not only assessing the past, present, and future uses of enzymes to synthesize carbohydrates, this volume also illustrates the significance of carbohydrate chemistry and describes how the combination of use of modern enzyme chemistry can advance exploration in the field. It details research at the interface of chemistry and biology for carbohydrate chemistry by demonstrating how to integrate chemical reactions and biological techniques that can be used to synthesize complex bioactive monosaccharides, oligosaccharides, and glycoconjugates.

Mark D. Bednarski and Ethan S. Simon, Editors
ACS Symposium Series No. 466
132 pages (1991) Clothbound
ISBN 0-8412-2097-2
\$34.95

Order from:

American Chemical Society
Distribution Office, Dept. 162
1155 Sixteenth St., N.W.
Washington, DC 20036
or CALL TOLL FREE
800-227-5558
or in Washington DC
(202) 872-4363
and use your credit card!

A Macromolecular Proposal

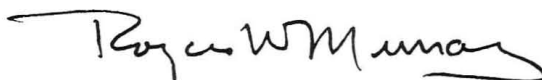
Ask yourself which chemical material contributes the most to our society's everyday convenience and well-being. It shouldn't require a long moment to think of polymers, organic plastics, and inorganic ceramics. We wear them, drive them, pack our travel clothes in them, write with them, dial numbers with them, and buy our food wrapped in them. Sports fishermen cast plastic baits on plastic lines from plastic reels on plastic rods. Great authors compose their thoughts on a plastic keyboard, store them on plastic disks, and print them with plastic inks. Polymers are indispensably everywhere.

By now you are asking: Why this extolling? I recently attended an interesting conference of the Society of Polymer Science of Japan and, besides learning about some very nice research, I was reminded of how little I hear about polymers. The central challenge for analytical chemists in today's world is inventing and developing new concepts, applications, and products. A second, also important, challenge is to teach how new knowledge in chemistry has affected our lives.

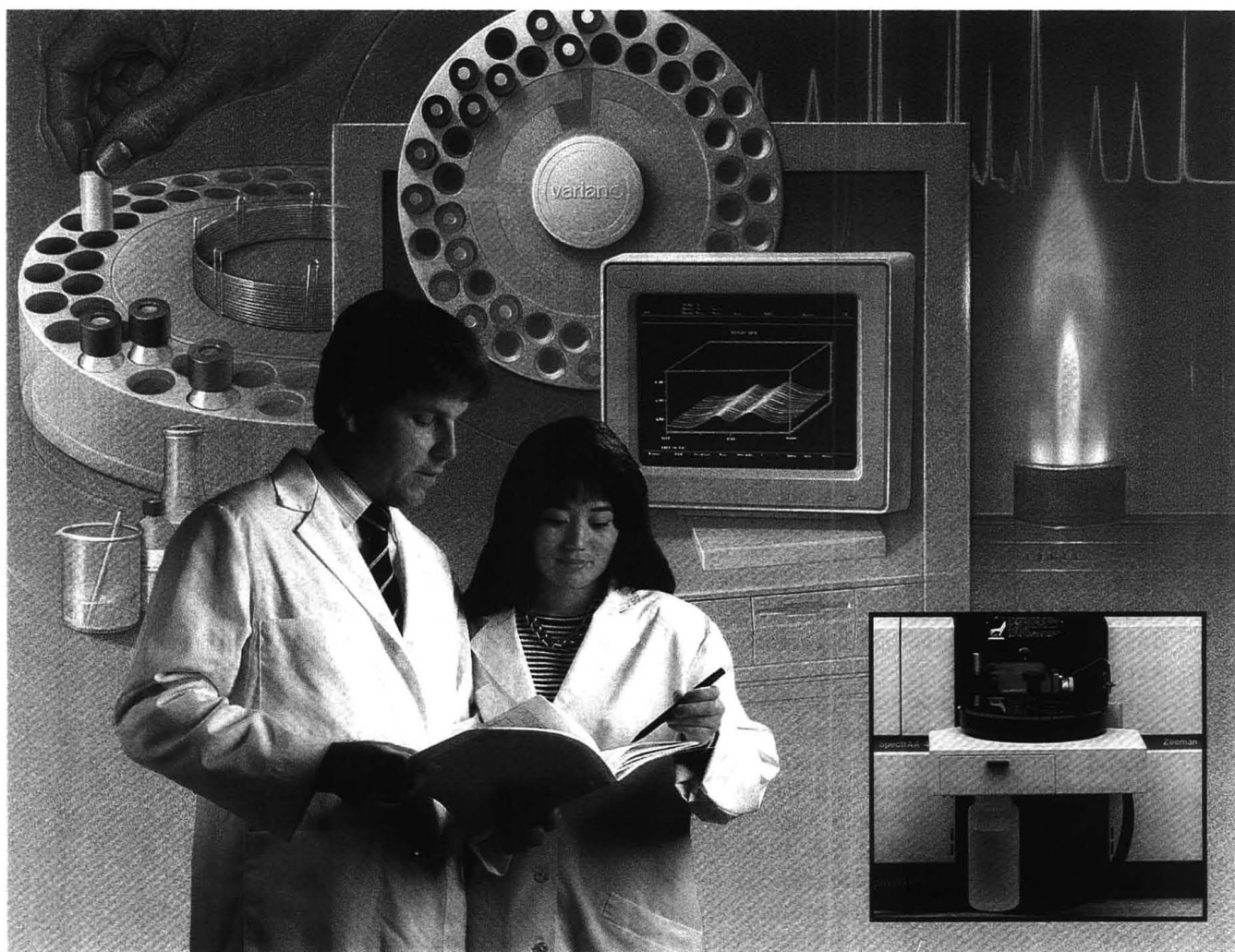
Polymers provide such easily recognizable examples that it is difficult to defend their virtual absence from curricula. If one of our educational goals is to give students an appreciation of

how analytical chemistry affects their lives, and how a career in it can enhance the lives of others, a case can be made that instruction in polymers should command a higher priority.

General chemistry is practically devoid of discussion about these important materials, which certainly will attract students' attention more than will ideal gases! Ion-exchange and gel polymers are introduced in analytical courses as separation phases and membranes in ion-selective electrodes, but basic ideas underlying permeation and transport, optical and thermal measurement of crystallinity, molecular weight measurement and distribution, and electrolyte acid-base equilibria are not found. The steady introduction of modern aspects of analytical measurements into undergraduate courses over recent years is laudable, particularly in spectroscopy and separations science. I think it is time that measurement concepts for polymeric materials also begin to find some space in our crowded undergraduate (and graduate) programs. The large role of polymers in our lives, by itself, warrants this proposal.



Everyone Agrees. Zeeman AA is Outstanding.



Even our competitors agree that Zeeman background correction gives outstanding graphite furnace performance. That's why they promote it like it's their own invention.

In fact, Varian invented Zeeman background correction. While our competition is selling technology that we first patented in 1972, we've perfected Zeeman to meet your demands today.

With Varian SpectrAA Zeeman you get the most accurate results with the

fastest correction available and polynomial interpolation of background signals. Fast Furnace Analysis cuts cycle times in half. Sensitivities and detection limits are unbeatable and optimum platform design minimizes interferences.

Varian's patented Zeeman atomic absorption technology is remarkable. Even our competitors agree. Call Varian at 1-800-944-1826. In Canada call 1-800-387-2216

1993 Board Members Appointed

Six new members have been selected to serve three-year terms on ANALYTICAL CHEMISTRY's Advisory Board. Each January, membership is rotated as new appointees replace members whose terms have expired. Biographical sketches of the new members follow.



Bruce Chase, a member of the research staff of Du Pont since 1975, received his B.A. degree from Williams College in 1970 and his Ph.D. from Princeton University in 1975.

Chase has conducted research in vibrational spectroscopy applied to industrial analytical problems. His current research interests include

detection methods for near-IR Raman spectroscopy and instrument development for Raman measurements. Chase served on ANALYTICAL CHEMISTRY's Instrumentation Advisory Panel from 1988 to 1990.



Joseph L. Glajch, associate director of the New Product Chemistry Group at Du Pont Merck Pharmaceutical Co., received his A.B. degree from Cornell University in 1975 and his Ph.D. from the University of Georgia in 1978.

Glajch is responsible for formulation and methods development of radiopharmaceuticals at Du Pont

Merck. The author of more than 30 publications, he also has four patents in analytical chemistry and diagnostic imaging. He is the current chairman of the ACS Division of Analytical Chemistry and is the ex officio member of the Board representing the Division.



Joseph G. Gordon, a research staff member and manager of Materials Science and Analysis at IBM Research Division's Almaden Research Center, received his A.B. degree from Harvard College in 1966 and his Ph.D. from MIT in 1970.

His research focuses on the composition and structure of solid-

liquid interfaces using a variety of in situ characterization techniques.



David M. Haaland, a member of the technical staff at Sandia National Laboratories, received his B.S. degree from the University of New Mexico in 1968 and his Ph.D. from the University of Rochester in 1972.

Haaland's interests include quantitative IR spectroscopy and chemometrics applied to gas analysis, en-

vironmental monitoring, microelectronics quality control, and noninvasive monitoring of blood glucose.



Kiyokatsu Jinno, professor of materials science at Toyohashi University of Technology (Japan), received his B.S. degree (1968) and his Ph.D. (1973) from Nagoya University.

His research focuses on the characterization of organic and biological compounds, computer techniques for chromatography/spectroscopy analyses, and design and synthesis of stationary phases based on molecular recognition.



Gary E. Maciel, professor of chemistry at Colorado State University, received his B.S. degree from the University of California (Berkeley) in 1956 and his Ph.D. from MIT in 1960.

Maciel's primary research interest is NMR spectroscopy of solids and surfaces with applications in catalysts, silica surfaces,

organic polymers, ceramics, and coal.

Established in the 1940s to advise the JOURNAL's Editors, the board meets formally once a year at ACS headquarters. The board members are a vital link between the editors and the analytical community, providing guidance and advice on editorial content and policy.

Leaving the Board are Alan G. Marshall, Ohio State University; John F. Rabolt, IBM; Debra R. Rolison, Naval Research Laboratory; Shigeru Terabe, Himeji Institute of Technology; and ex officio member Charles L. Wilkins, University of California, Riverside.

Continuing to serve are Michelle V. Buchanan, Oak Ridge National Laboratory; M. Bonner Denton, University of Arizona; Joel M. Harris, University of Utah; Timothy Harris, Bell Laboratories; Franz Hillenkamp, University of Münster; Dennis C. Johnson, Iowa State University; Richard A. Keller, Los Alamos National Laboratory; Philip D. LaFleur, Eastman Kodak Co.; Geraldine L. Richmond, University of Oregon; Ralph Riggan, Lilly Research Laboratories; and Michael Thompson, University of Toronto.

New ANALYTICAL CHEMISTRY Staffer



Deborah Noble has joined the staff of ANALYTICAL CHEMISTRY as an Editorial Assistant. Her responsibilities include handling BOOKS and NEW PRODUCTS, and writing FOCUS articles for the A-pages.

She comes to the JOURNAL from *Clinical Chemistry News*, where she worked as a staff writer. She received her B.A. degree in chemistry

from the University of Virginia and worked there for several years in a biochemistry research laboratory.

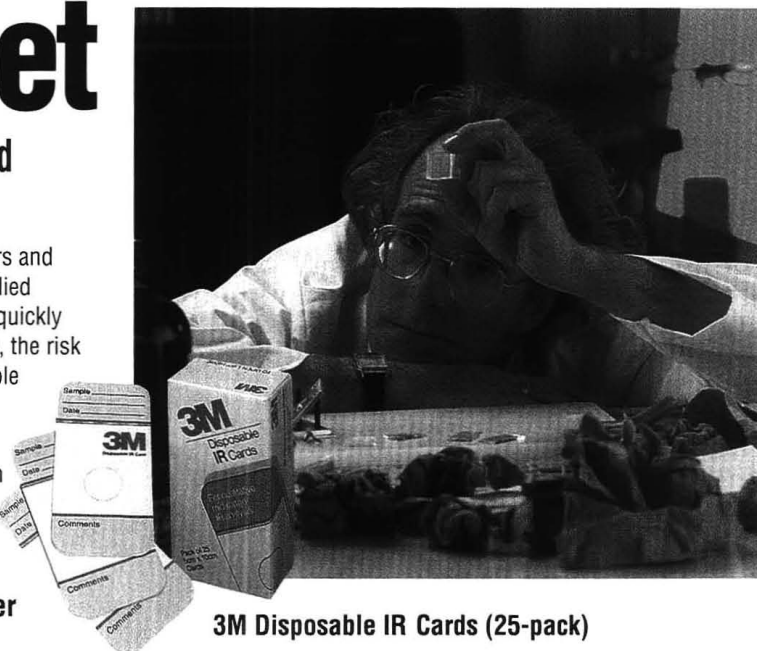
Put your samples on a salt-free diet

Tired of cleaning salt plates? Try quick and easy 3M Disposable IR Cards.

These disposable sample cards fit major FTIR spectrometers and reduce time-consuming sample preparation. Samples are applied directly onto the microporous, polyethylene substrate, which quickly absorbs and holds the analyte. Since the cards are disposable, the risk of cross-contamination is eliminated. Likewise, no more sample clean-up translates into savings in both time and supplies.

3M Disposable IR Cards are non-hygroscopic and require no special storage or handling. They work most favorably with organic liquids, samples soluble in organic solvents, and semisolids or pastes. The cards are especially effective with water-containing samples.

To order 3M Disposable IR Cards, contact either Fisher Scientific or VWR Scientific.



3M Disposable IR Cards (25-pack)

3M Disposable Products Division

3M Center
St. Paul, MN 55144-1000

CIRCLE 72 ON READER SERVICE CARD



INDUSTRIAL & ENGINEERING CHEMISTRY RESEARCH



Editor: Donald R. Paul
University of Texas, Austin
Published by the American Chemical Society

Quality information that gives you the leading edge

Covering the broad, interdisciplinary field of chemical engineering and industrial chemistry, *Industrial & Engineering Chemistry Research* delivers peer-reviewed, monthly reports with a focus on the fundamental and theoretical aspects of chemical engineering, process design and development, and product R&D.

A typical issue contains original studies in the areas of kinetics and catalysis, materials and interfaces, process engineering and design, separations, and other topics, with an emphasis on new areas of science and technology.

Don't miss a single issue, Subscribe Today!

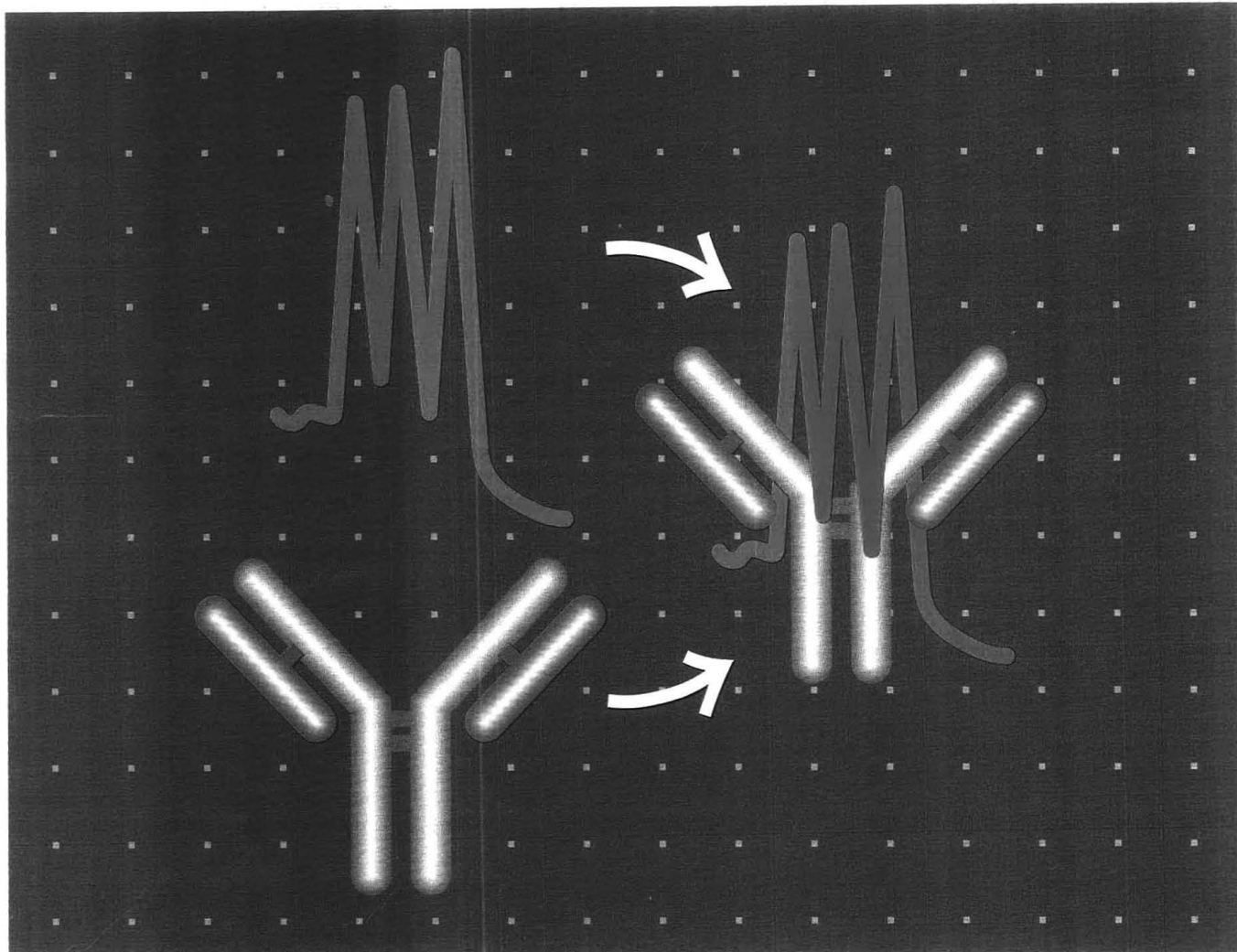
Call Toll Free (U.S. only): 1-800-333-9511
Outside the U.S.: 614-447-3776
FAX: 614-447-3671

Or Write:
American Chemical Society
Member and Subscriber Services
P.O. Box 3337
Columbus, OH 43210

Volume 32 (1993) Printed	U.S.	Canada & Mexico	Europe*	All Other Countries*
ACS Members				
One Year	\$ 64	\$ 84	\$108	\$120
Two Years	\$115	\$155	\$203	\$227
Nonmembers	\$567	\$587	\$611	\$623

* Air Service Included.

Member subscription rates are for personal use only. Subscriptions are based on a calendar year. Foreign payment must be made in U.S. currency by international money order, UNESCO coupons, or U.S. bank draft, or order through your subscription agency. For nonmember rates in Japan, contact Maruzen Co., Ltd. This publication is available on microfilm, microfiche, and the full text is available online on STN International.



Tandem Chromatographic- Immunological Analyses

Mercedes de Frutos and Fred E. Regnier

Department of Chemistry
Purdue University
West Lafayette, IN 47907

Liquid chromatography (LC) and immunological assays (IAs) are cornerstones of modern analytical biochemistry. For more than half a century, these two techniques have developed along independent routes. The use of antibodies as analytical agents for the determination of microorganisms, viruses, proteins, drugs, hormones, and toxins evolved in the laboratories of microbiologists and clinical chemists. Today analytical immunology is widely used in clinical laboratories for the determination of *known* substances. LC, by contrast, evolved in research laboratories where it was used for purifying and characterizing *unknown* substances. In this REPORT we will examine how

the complementary features of these two techniques allow them to be combined to produce analytical systems with superior selectivity, speed, and sensitivity.

Molecular discrimination in immunology and chromatography

Antibodies generally possess enormous selectivity, targeting unique structural elements (epitopes) that

REPORT

consist of 3–12 amino acids in polypeptides or a few carbohydrate residues in oligosaccharides (1). In contrast to their behavior with polypeptides and polysaccharides, the immune systems of higher animals generally do not respond to small molecules. Only by conjugating non-immunogenic species (haptens) to immunogenic macromolecules can

antibodies to low molecular weight drugs (2), hormones (3), toxins (4), and pesticides (5) be produced.

Immunological recognition is based on the spatial complementarity of groups in the epitope of the antigen with those in the paratope of the antibody (1). In the case of macromolecules, each antibody recognizes a specific epitope that generally constitutes a fraction of the total structure. This microscopic identification of complex macromolecular species can be both an asset and a liability, as will be shown below. In favorable cases, antibodies can be used to recognize a single substance in the presence of several thousand similar species. This is the basis for the broad use of immunological assays in clinical chemistry.

The problem with substance-specific immunological assays is that antibodies target epitopes, not the whole antigen. Multiple substances may have the same or similar

epitopes. When this is true, antibodies fail to discriminate by "cross-reacting" with structurally similar species (1). "False positives" are a negative feature of immunological assays when the goal is to determine a single molecular species. In contrast, cross-reactivity is a positive attribute when the goal is to isolate families of molecules of similar structure. We will show that tandem LC-IA systems deal easily with both cases.

In an effort to overcome the false-positive problem, a second level of immunological discrimination is often used. An enzyme-linked immunosorbent assay (ELISA), sometimes referred to as a "sandwich" assay, with monoclonal antibodies is a good example of a double-discrimination assay. Subsequent to capture by an immobilized monoclonal antibody, antigen is targeted at a different epitope by a second, enzyme-tagged, monoclonal antibody (1). By assaying the bound enzyme, the amount of product formed can be related to the

quantity of antigen. Although this double-discrimination assay is of much higher specificity, cross-reactivity is still possible.

Whereas antigen:antibody (Ag:Ab) recognition depends on spatial complementarity among functional groups on two heterogeneous surfaces, molecular discrimination in chromatographic systems is based on the differential interaction of functional groups at the relatively homogeneous surface of a sorbent with those on the heterogeneous surface of an analyte (6). It is commonly thought that Ag:Ab interactions provide a much higher level of discrimination. Although it is true that the heterogeneous paratope of the antibody is vastly superior to the homogeneous surface of the chromatography column in recognizing and capturing families of molecules with common structural elements, chromatography systems are generally superior in discriminating among the members of an antigen family (7). Because chromatographic sorbents

probe a larger portion of the molecule's surface, LC provides a more holistic view of a molecule. Chromatographic discrimination among variants of small molecules such as drugs, hormones, or steroids (8) and a series of proteins such as subtilisin (9), lysozyme (10), calcitonin (11), insulin (12), and human growth hormone (13) provides examples of the power of homogeneous surfaces to recognize small differences between molecules. Figure 1 shows an ion-exchange separation of two subtilisin variants of 35 kDa that vary by a single methylene group (9).

Enhancement of discrimination with LC-IA. A variety of LC-IA methods have been used to deal with the immunospecificity problem. These methods may be divided into two groups: those in which immunodiscrimination precedes chromatography and those in which immunological determinations are made after the separation. The analytical protocol is frequently determined by antigen concentration and

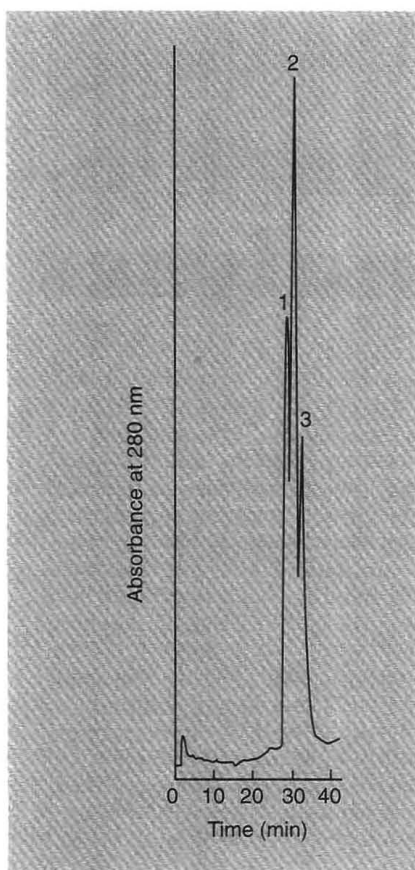


Figure 1. Separation of (1) D 166 variant (Asp in 166), (2) E 166 variant (Glu in 166) and (3) wild-type subtilisin (Gly in 166).

LC was performed at pH 5.0, using a 90-min linear gradient from 0 to 0.15 M NaCl at a 0.5 mL/min flow rate. (Adapted from Reference 9.)

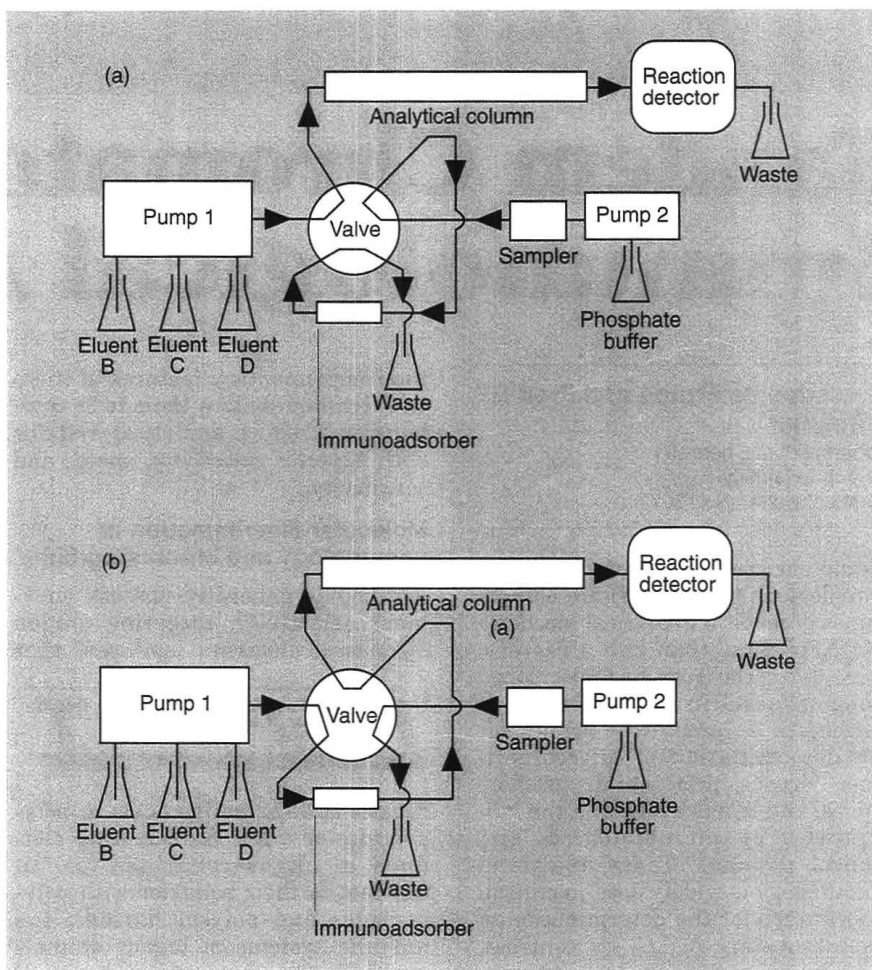


Figure 2. Arrangement of the valve-switching module with immunoaffinity and reversed-phase columns.

Valve setting for (a) solute adsorption and (b) elution. (Adapted with permission from Reference 17.)

the laboratory environment. At high antigen concentrations (> 10–100 ng/mL), detection can often be achieved directly by an absorbance detector.

One technique for identifying antigenic species at high concentrations is immunosorbent subtraction chromatography (14). In this technique, a precolumn immunosorbent cartridge is used to subtract antigens from the chromatographic stream. The immunosorbent is prepared in situ by biospecific adsorption of the antibody onto a protein A or G cartridge. Antibody is easily adsorbed and desorbed from immobilized protein A or G by

manipulation of pH. Comparison of chromatograms obtained before and after antibody immobilization on the protein A or G cartridge reveals that antigens are subtracted when the sample passes through the immunosorbent. Detection of human growth hormone monomer and dimer was achieved by immunosorbent subtraction coupled with size exclusion chromatography. Although multimer formation is common in therapeutic protein formulations, it is difficult to detect with conventional immunological assays. Immunosorbent subtraction should be possible in all chromatographic modes.

A second approach is to analyze the captured haptens and antigens (2–4, 8, 10, 15–24). Subsequent to capture, antigen is released from the immunosorbent and reconcentrated on a chromatographic column. Generally, a reversed-phase column is used and the immunosorbent is taken out of the flow path before gradient eluting the chromatographic column. The advantage of this method (Figure 2) is that the immunosorbent can concentrate antigens from a large volume of sample while greatly reducing the amount of nonantigenic species. Occasionally, elution from the immunosorbent will irreversibly alter the structure of antigen species. This means that chromatograms of the native antigen will be different from those obtained by antigen release from the immunosorbent.

Immunospecific capture and enrichment of haptens followed by reversed-phase chromatography was first used in drug analysis (15). Cortisol was captured from human serum by an immunosorbent cartridge coupled to an LC system through an injection valve. Through this valve the immunosorbent could be coupled in tandem with a reversed-phase column. After nonbinding impurities had been washed from the cartridge, cortisol was desorbed with a methanol–water mobile phase and transferred to the reversed-phase column. A 5-min isocratic elution resolved cortisol from interfering substances, allowing detection by UV absorbance. This technique subsequently was used with more sophisticated valving and elution to determine a number of haptens such as phenytoin (2), nortestosterones (3, 16), digoxin (17), clenbuterol (18), estrogens (8), aflatoxin (4), and cytokinins (19). The utility of immunospecific prefractionation of a cytokinin sample before LC analysis is shown in Figure 3.

Interference can be reduced in the case of steroid hormone analyses by biospecifically displacing the analyte from the immunosorbent with an analogue of longer chromatographic retention (3, 8, 16). Complications in displacement elution are poor desorption kinetics and the need to find a displacer that has both high displacing power and the proper chromatographic behavior. Still another refinement is the incorporation of a dialysis membrane into the system to protect the immunosorbent from proteolytic enzymes in samples (4).

The use of an immunosorbent to capture and enrich antigens has several additional advantages beyond

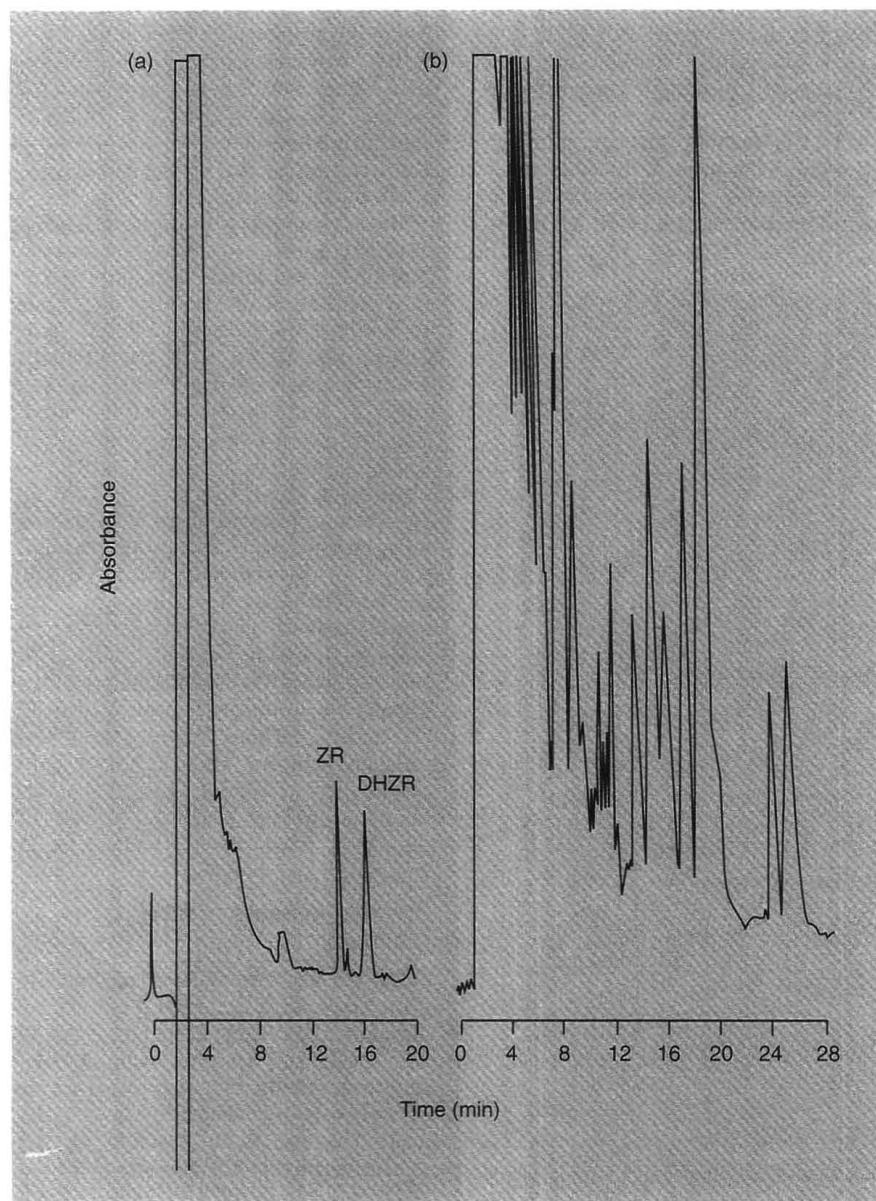


Figure 3. Separation of zeatin riboside (ZR) and dihydrozeatin riboside (DHZR) from a methanolic extract of 10 mm soybean embryo (40 mg fresh weight) by HPLC.

Chromatogram obtained (a) after anti-ZR CNBr-activated sepharose 4B immunoaffinity purification and (b) with no prior purification. Samples were separated on Ultrasphere ODS and detected by absorbance at 268 nm. (Adapted with permission from Reference 19.)

increasing selectivity. One is that the immunosorbent can capture analytes from large volumes of sample. Detection down to 200 ng/mL has been achieved with UV absorbance by concentrating the analyte from 10 to 20 immunosorbent cartridge volumes of sample, as in the case of estrogens in urine (8). A second advantage is that even sequestered antigens are captured. It is often the case in the analysis of drugs and hormones that binding proteins sequester analytes and interfere with the determination. Because the binding constants of antibodies are generally 3–4 orders of magnitude greater than those of serum binding proteins, analytes are generally stripped from serum by the immunosorbent (2). Capture and enrichment techniques have been equally efficacious in the analysis of proteins such as interferon α -2 (20), lysozyme (10, 21), immunoglobulin G (22), transferrin (23), and viral coat proteins (24). Figure 4 shows the efficiency of this technique for the

analysis of interferon α -2. The method is also useful in the analysis of antibodies. Figure 5 indicates how a given setup can be used to quantitate either antigens or antibodies (23).

Still another strategy is to separate variants and interfering substances before immunodiscrimination. Immunological determinations by this approach are generally achieved off line by a standard assay procedure such as ELISA or enzyme-multiplied immunoassay technique (EMIT). It is important to remember that in postseparation immunodiscrimination the separation process may alter the structure of antigens, particularly in the case of reversed-phase separations of macromolecules with organic solvents. When this occurs, it is possible that a monoclonal antibody will no longer recognize the antigen.

Off-line, postchromatographic immunological assays have been used in several cases. A recent review (25) examines the combination of HPLC

with radioimmunological assays in the determination of metabolites of arachidonic acid, collectively known as eicosanoids. Here again, the broad cross-reactivity of antibodies is exploited in the search for compounds with common structural elements. These studies establish that LC-IA may be used to isolate unknown species.

The ability to exploit the cross-reactivity of antibodies is extremely valuable in metabolism studies, such as in the case of rolipram (26). A cross-reacting metabolite of rolipram is found in human plasma but not in the plasma of animals (Figure 6). The limit of detection by this method is as low as 20 pg/mL (27). Off-line enzyme immunoassays are equally sensitive. Nortestosterones were determined at concentrations of < 10 pg/mL (28, 29), which is an order of magnitude greater than the sensitivity achieved by direct absorbance detection (8).

Several cases of automated post-separation immunodiscrimination have been reported. A highly sensitive method was recently described in which fluorescently labeled antibodies are mixed with the effluent from a microcolumn and passed through a microreactor before introduction into a microcolumn of immobilized antigen (30). When antigens elute from the column, they form an Ag:Ab complex and elute through the antigen column to a fluorescence detector. In the absence of antigen, the fluorescently labeled antibodies are quantitatively captured by the immobilized antigen column. This system reportedly is capable of detecting picograms of antigen and operating for a day without regenerating the antigen column. The real-time process-monitoring system described below is another example. The lower detection limit of this system is in the range of 1 μ g/mL.

Positive aspects of cross-reactivity

Occasionally one wishes to identify all species with a common structural element that vary at other sites in the molecule. In this case, cross-reacting antibodies may be used to capture and concentrate these variants. The success of tandem LC-IA in this application depends on broad cross-reactivity of the immunosorbent and the ability of the chromatography column to resolve the variants.

One example of this approach is provided by the study of penicillin conjugation to serum albumin. Be-

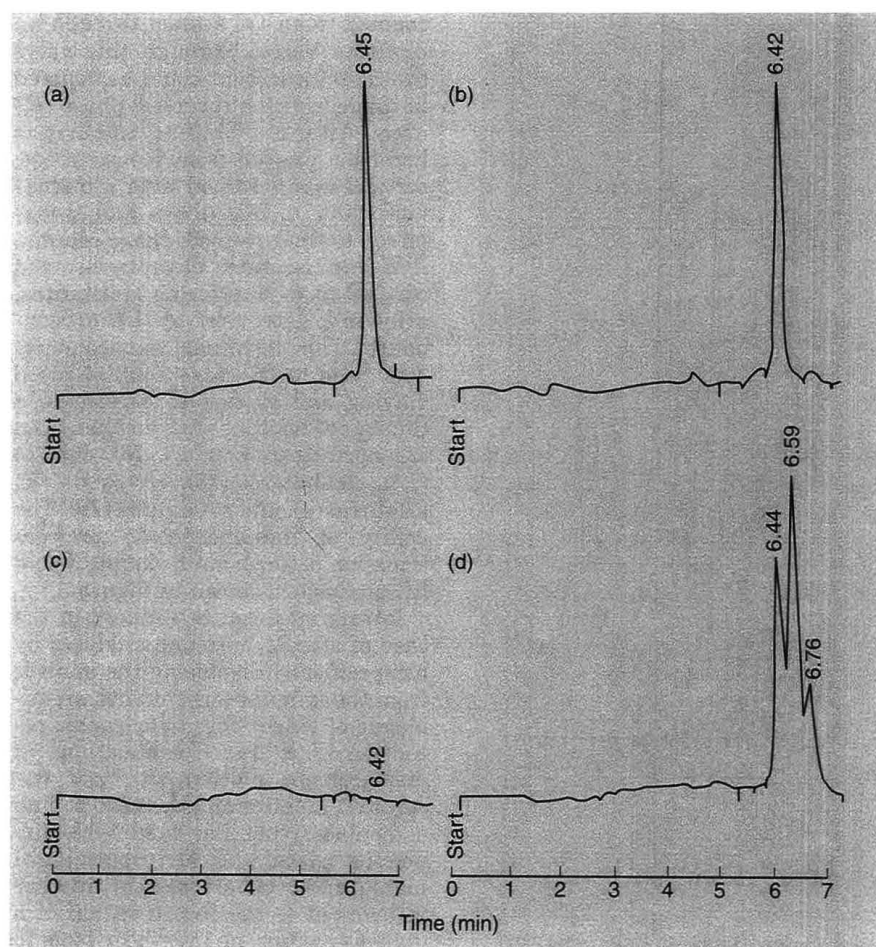


Figure 4. Determination of interferon α -2.

Reversed-phase chromatograms of (a) loading buffer supplemented with interferon α -2 monomer, (b) yeast lysate (interferon α -2 gene deleted) supplemented with interferon α -2 monomer, (c) yeast lysate (interferon α -2 gene deleted), and (d) yeast lysate (interferon α -2 gene inserted). Samples were purified on a monoclonal antibody LIT-1 column. (Adapted with permission from Reference 20.)

Valuable References for Analytical Chemists



from the American Chemical Society



Measurement Challenges in Atmospheric Chemistry

Presents discussions on state-of-the-art techniques and instrumentation used for atmospheric measurements. Summarizes progress in a variety of areas of atmospheric research and identifies areas that should now be addressed by the research community. Provides in-depth coverage of the measurement of both aerosols and gases. Reviews techniques for measuring species in the troposphere and mesosphere. Serves as an excellent reference for atmospheric scientists as well as an introduction to the field for analytical and gas-phase researchers interested in atmospheric measurement.

Leonard Newman, Editor

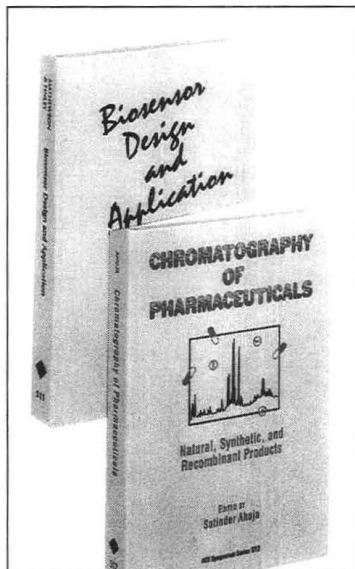
Advances in Chemistry
Series No. 232
338 pages (1993)
Clothbound
ISBN 0-8412-2470-6
\$94.95

Chromatography of Pharmaceuticals: Natural, Synthetic, and Recombinant Products

Describes the role of chromatography in the development of new drugs. Features chapters on the analysis of natural and recombinant pharmaceutical products. Covers new techniques such as capillary electrophoresis and a number of hyphenated techniques that combine liquid chromatography or gas chromatography with mass spectrometry. Describes such applications as impurity analysis, chiral separations, metabolic studies, robotics, and support of biotechnology products. Also describes trace and ultratrace analyses in a variety of matrices.

Satinder Ahuja, Editor

ACS Symposium Series No. 512
214 pages (1992) Clothbound
ISBN 0-8412-2498-6
\$59.95



Biosensor Design and Application

Presents a contemporary discussion of currently available and potential applications of biosensors. Examines diverse approaches to the basic problems of microsizing analytical instrumentation, including the use of intact crustacea antenna, various forms of redox reactions, use of antibody-mediated reactions, and optical- and spectrophotometric-based methods. Describes requirements for using biosensors in experiments conducted in space as well as an interesting approach to the development of more efficient procedures for commercialization of biosensor technologies.

Paul R. Mathewson and John W. Finley, Editors

ACS Symposium Series
No. 511
204 pages (1992)
Clothbound
ISBN 0-8412-2494-3
\$54.95

Element-Specific Chromatographic Detection by Atomic Emission Spectroscopy

Offers fundamental research studies and reviews by the most active groups in the field, including those involved in instrument development. Includes discussions on a wide variety of techniques, including LC/GC, SFC, atomic emission spectroscopy, plasma spectroscopy, microwave induced plasmas, inductively coupled plasmas, direct current plasmas, and inductively coupled plasma/mass spectroscopy. A valuable source of information for analytical and environmental chemists, toxicologists, medicinal and pharmaceutical chemists, and instrument developers.

Peter C. Uden, Editor

ACS Symposium Series No. 479
345 pages (1992) Clothbound
ISBN 0-8412-2174-X
\$74.95

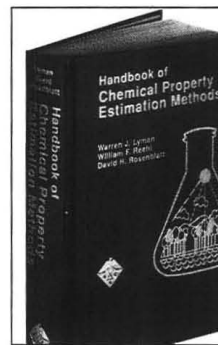
Instrumentation in Analytical Chemistry, 1988-1991

An anthology of 48 articles that first appeared in *Analytical Chemistry*, this volume provides an excellent overview of the entire field of analytical instrumentation and features state-of-the-art developments. This fourth volume in the series focuses on robotics, computers, and laboratory data management; atomic and molecular spectroscopy, electroanalytical chemistry and chemical sensors; separations; mass spectroscopy; and surface analysis. Also included is an introduction by Royce Murray, editor of *Analytical Chemistry*.

Louise Voress, Editor

350 pages (1992)
Clothbound: ISBN 0-8412-2191-X
\$44.95
Paperbound: ISBN 0-8412-2202-9
\$28.95

Handbook of Chemical Property Estimation Methods: Environmental Behavior of Organic Compounds



Presents simple estimation methods for 26 important properties of organic chemicals that are of environmental concern. Facilitates the study of problematic chemicals in such applications as chemical fate modeling, environmental

assessments, priority ranking of large lists of chemicals, chemical spill modeling, chemical process design, and experimental design. Provides step-by-step instructions to quickly and easily obtain the needed estimations.

Warren J. Lyman, William F. Reehl, and David H. Rosenblatt

First published by McGraw-Hill Book Company (1982)
960 pages (1990) Clothbound
ISBN 0-8412-1761-0
\$49.95

Order From: American Chemical Society, Distribution Office Dept. 55, 1155 Sixteenth St., NW, Washington, DC 20036.
Or CALL TOLL FREE 800-227-5558 (in Washington, DC, 872-4363) and use your credit card. FAX: 202-872-6067.

GOOD NEWS FOR ATOMIC ABSORPTION SPECTROSCOPY



Hamamatsu Hollow Cathode Lamps are now available from major lab suppliers.

Hamamatsu single and multi-element Hollow Cathode Lamps offer superior stability, spectral purity and output intensity, even for such elements as arsenic and selenium. They are compatible with most commercial spectrophotometers, including Beckman, Zeiss and Perkin-Elmer. And best of all, they're available from your local lab supplier.

For Application Information, Call
1-800-524-0504
1-908-231-0960 in New Jersey

HAMAMATSU

HAMAMATSU CORPORATION
 360 FOOTHILL ROAD
 P. O. BOX 6910
 BRIDGEWATER, NJ 08807
 PHONE: 908/231-0960
 International Offices in
 Major Countries of
 Europe and Asia.

© Hamamatsu Corporation, 1990

CIRCLE 46 ON READER SERVICE CARD

REPORT

cause penicillin reacts with proteins, a benzylpenicilloyl-serum albumin conjugate (BPO-HSA) is formed in the serum of individuals who are on penicillin therapy or who consume food from treated animals. This conjugate triggers an immune response in sensitive individuals. In an effort to locate the site of BPO binding in HSA, the conjugate was digested with trypsin and the peptide fragments captured on an anti-BPO immunosorbent (31). Three peptides containing the common structural element, BPO, were identified.

Structural variants of proteins are of concern in biotechnology because they may be immunogenic when chronically administered during drug therapy. Variants in genetically engineered proteins arise from expression errors, improper folding, incomplete or incorrect post-translational

modification, and chemical degradation. It is probable that LC-IA will play a role in identifying such variants in the future. Lysozyme variants that differ by one or more amino acids have been resolved by this technique (21).

The isolation of viral coat proteins and bacterial membrane proteins is another case in which the use of cross-reacting antibodies can be helpful. Animals immunized with viruses or bacteria will produce antibodies that target external structural components. These antibodies may then be used to capture and identify external proteins in extracts of the organism. *Sendai* virus F₂ coat protein was identified in this way by tandem LC-IA in amounts down to 1 ng through the use of microbore columns (24).

Both antibodies and LC probe the

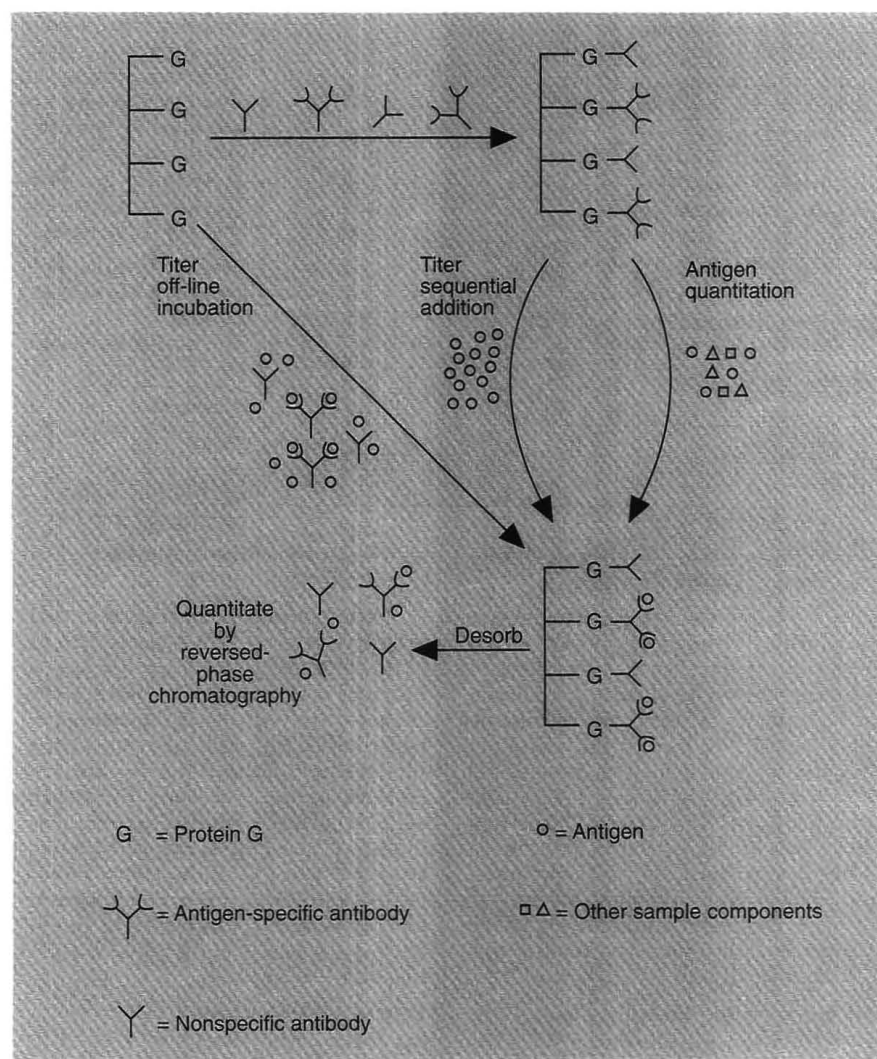


Figure 5. Schematic diagram of antibody titer determination and antigen quantitation by dual-column immunoassays using protein G affinity chromatography.

(Adapted from Reference 23.)

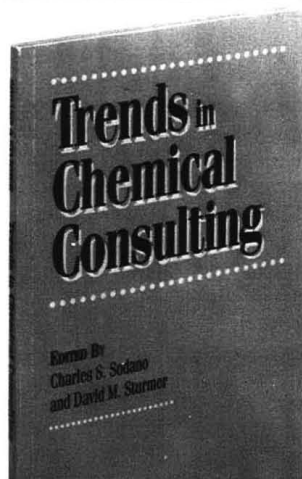
surface of molecules. Variants can be recognized only when one or more preconditions are met: Structural variations occur at the surface of the molecule, structural variations alter the external structure of the variant, or internal points of variation are revealed by conformational changes during the chromatographic step.

Detection in LC-IA

A number of cases have been described above in which antigen is detected directly, generally at concentrations > 1 ng/mL. At lower levels of antigen it is necessary to use some type of indirect detection method. Off-line methods based on enzyme amplification and competitive binding radioimmunological assays have already been described. Assays in which the ligand is tagged with an acridinium ester are another alternative (32). Detection in these systems is based on chemiluminescence. Several methods based on enzyme amplification, fluorescence, and chemiluminescence have been described in which immunodiscrimination, chromatography, and detection were combined.

In the case of enzyme-amplified immunological assays, chromatographic systems have been used to enhance detection of the enzyme product by removing interfering substances. Two-dimensional chromatographic resolution of NADH with flow-amperometric detection in a homogeneous EMIT assay is one example (33). Linear calibration plots were obtained over the range of 0.55–7.5 ng/mL. A problem with this assay is that the ability of the antibody to inhibit enzyme activity of the enzyme-labeled digoxin is poor, producing a substantial blank. ELISA may also be treated this way. Conversion of phenyl phosphate to phenol by alkaline phosphatase conjugated to the second antibody in a conventional ELISA was monitored by LC with electrochemical detection (34, 35). The lower detection limit was ~ 1 ng/mL. Sensitivity was increased by 3 orders of magnitude by carrying out the assay in a 70- μ L capillary and transferring the entire contents of the capillary to the chromatography column after product formation (36). The assay requires 25 min, has a linear range of 5 orders of magnitude, and has a detection limit of 4.6×10^{-21} mol or 2800 ± 150 molecules.

Assays equivalent to the classical ELISA have also been achieved by carrying out the individual steps in a flow-through immunosorbent cartridge. The sandwich for a mouse



Trends in Chemical Consulting

Restructuring in the chemical industry has created a wealth of opportunities for consultants. Companies are now more willing to seek outside help than in the past as they recognize the value of experienced specialists.

But what constitutes the efficient use of a consultant? And is consulting for you? *Trends in Chemical Consulting* explores these issues through contributions from chemical consultants, those who have used the services of a consultant, and participants in cooperative arrangements. Presentations focus on those considerations specific to consulting relationships between scientific professionals.

Chemists, chemical engineers, and other scientific professionals in support areas to the chemical industry will find this an indispensable resource of information on chemical consulting.

Contents

- Consulting to the Chemical Industry
- Industrial Expectations for Consultants and Consulting Services
- Understanding, Selecting, Managing, and Compensating Consultants
- An Academic Perspective on Consulting
- University-Industrial Relationships
- Accessing Federal Laboratories Know-How
- What Consulting Practices Look Like
- Defining and Marketing Your Consulting Specialty
- Opportunities for Retired Chemists
- Using Consultants to Interpret Regulatory Initiatives
- Major Chemical Company Retirees as Consultants and Market Developers
- Robotic Servicing on the Space Station Freedom
- Consultation in Sensory Evaluation
- Chemical Information Consultants

Charles S. Sodano and David M. Sturmer,
Editors

174 pages (1991) Paperbound
ISBN 0-8412-2106-5
\$29.95

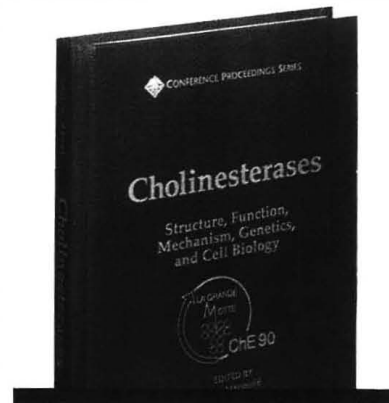
O · R · D · E · R · F · R · O · M

American Chemical Society
Distribution Office, Dept. 11
1155 Sixteenth St., N.W.
Washington, DC 20036

or CALL TOLL FREE

800-227-5558

(in Washington, D.C. 872-4363) and use your credit card!



Cholinesterases Structure, Function, Mechanism, Genetics, and Cell Biology

Presenting the proceedings of the Third International Meeting on Cholinesterases, this inaugural volume in the Conference Proceedings Series offers a wealth of new information on current and future cholinesterase research, including important advances resulting from new concepts and methodologies such as monoclonal antibodies and molecular genetics.

The volume's 49 full papers and 140 poster papers are divided into six sections covering:

- Polymorphism and Structure of Cholinesterases
- Cellular Biology of Cholinesterases
- Gene Structure and Expression of Cholinesterases
- Catalytic Mechanism of Cholinesterases: Structure-Function Relationships of Anticholinesterase Agents, Nerve Agents, and Pesticides
- Pharmacological Utilization of Anticholinesterase Agents. Neuropathology of Cholinergic Systems
- Noncholinergic Roles of Cholinesterases

This volume will be of great interest to a broad spectrum of readers, including those interested in the evolution of cholinesterase catalysis, researchers developing agricultural chemicals, scientists seeking up-to-date information on the treatment of glaucoma and such neurological diseases as Alzheimer's disease and myasthenia gravis, those interested in the design of drugs to bind the enzyme itself or to cholinergic receptors, as well as those who follow the progress toward complete structure elucidation of cholinesterases.

Jean Massoulie, Centre National de la Recherche Scientifique, *Editor*
Francis Bacou, Institut National de la Recherche Agronomique, *Editor*
Eric Barnard, Medical Research Council, *Editor*

Arnaud Chatonnet, Institut National de la Recherche Agronomique, *Editor*
Bhupendra P. Doctor, Walter Reed Army Institute of Research, *Editor*

Daniel M. Quinn, University of Iowa, *Editor*
Conference Proceedings Series
414 pages (1991) Clothbound
ISBN 0-8412-2008-5
\$89.95

O · R · D · E · R · F · R · O · M

American Chemical Society
Distribution Office, Dept. 13
1155 Sixteenth St., N.W.
Washington, DC 20036

or CALL TOLL FREE

800-227-5558

(in Washington, D.C. 872-4363) and use your credit card!

anti-bovine immunoglobulin G (IgG) assay was constructed by introducing the sample of mouse anti-bovine IgG and a goat anti-mouse IgG–glucose oxidase conjugate sequentially into an immunosorbent cartridge with immobilized bovine IgG (37). Hydrogen peroxide formed by the enzymatic oxidation of glucose was monitored electrochemically. Three injections of glucose were made to determine the amount of immobilized conjugate; the correlation coefficient and accuracy increased when the area of the second or third injection was used. This phenomenon was attributed to the desorption of nonspecifically bound enzyme conjugate with the first injection of glucose. Interassay precision was $\pm 3\%$ with a lower detection limit of a few femtomoles.

A competitive binding version of this assay for IgG was shown to be sensitive into the picomole range (38), and a recent report of a flow-based ELISA indicates that the assay will detect 10–100 pg/mL of antigen (39). The current limits of ELISA-based detection schemes are determined by nonspecific adsorption of the enzyme conjugate. As nonspecific adsorption is diminished, the background is decreased, and the detection limit is lowered.

Sandwich assays have also been used with chemiluminescent detection (32). Plasma and acridinium ester-labeled anti-parathyroid hormone (PTH) antibodies [anti-(1–34 PTH)] directed against amino acids 1–34 were preincubated for 1 h to allow immunological complex formation. The sample containing the complex was then injected into an immunosorbent cartridge containing immobilized anti-(44–68 PTH) antibodies. Nonbound species were eluted from the cartridge, and the sandwich was desorbed into a post-

column reactor where the column effluent was mixed with alkaline peroxide. The resulting light production was monitored with a chemiluminescence detector. The response was linear over 2–3 orders of magnitude, and the lower limit of detection for a 66- μ L plasma sample was 16 amol, or 2.4×10^{-13} M.

Parallel vs. serial assays

Conventional immunological assays are generally carried out in a disposable kit format in which reagent addition, separation steps, and detection are achieved by either manual or robotic operations. The large number of mechanical steps used in this format tends to make assays slow and requires that they be conducted in parallel to achieve high sample throughput. Increasing the speed of immunological assays could be very important because it would allow serial processing of samples, elimination of robotic operations, repeated use of the immunosorbent, detection in a single sample cuvette, and the use of assay data in feedback control. In short, the system would approach an immunosensor.

High-sensitivity immunological assays achieved in a few minutes are probably just around the corner. At antigen concentrations $> 1 \mu\text{g/mL}$, immunological assays have been conducted in 10–20 s (39). By using an LC system fitted with an immunosorbent column, identical pre- and postcolumn sample loops, and a UV absorbance detector, absorbance was determined before and after antigen was subtracted by the immunosorbent. Sample from the postcolumn inlet gave the total absorbance, whereas that from the precolumn inlet gave absorbance after antigen was subtracted by passage through the immunosorbent. Antigen concentration and purity were calculated

from the difference between these two absorbance values. By using an immunosorbent capable of binding 200–1000 μg of antigen, it was possible to carry out several hundred assays before the immunosorbent had to be recycled. More than 200 assays per hour have been made with this system. When this high-speed immunological assay system was coupled to a process-scale chromatography system, it was possible to monitor the elution of both antigens and impurities and also to control fraction collection in real time. It is likely that systems such as this will allow automation of therapeutic protein production in biotechnology.

Summary

The function of conventional immunological assays is to determine the presence and amount of known substances. Cross-reactivity of antibodies with unknown species of similar structure is a problem that can be circumvented by using chromatography in a second level of discrimination.

Tandem LC–IA systems increase the selectivity and the sensitivity of assays by removing interfering species. For cases in which the goal is to prove that similar species are absent from a sample or to identify antigen variants, conventional assays fail. LC–IA systems are adept at dealing with these tasks. The necessary steps of metering reagents, separating Ag:Ab complex from other species, and enhancing detection in an immunological assay are easily accommodated by the LC system. In fact, the LC system provides a wide variety of new, high-sensitivity, high-speed methods for carrying out immunological assays. On the basis of the enormous versatility, selectivity, and sensitivity that LC–IA brings to analytical chemistry, we believe this technique will become increasingly important for monitoring analytes in complex biological matrices.

M. de Frutos wishes to acknowledge Fulbright/MEC (Spain) for a scholarship.

References

- (1) Weir, D. M.; Herzenberg, L. A.; Blackwell, C.; Herzenberg, L. A. *Handbook of Experimental Immunology*, 4th ed.; Blackwell Scientific Publications: Boston, 1986; Vol. 1.
- (2) Johansson, B. *J. Chromatogr.* **1986**, *381*, 107–13.
- (3) Haasnoot, W.; Schilt, R.; Hamers, A.R.M.; Huf, F. A.; Farjam, A.; Frei, R. W.; Brinkman, U.A.T. *J. Chromatogr.* **1989**, *489*, 157–71.
- (4) Farjam, A.; van de Merbel, N. C.; Nieman, A. A.; Lingeman, H.; Brinkman, U.A.T. *J. Chromatogr.* **1992**, *589*, 141–49.

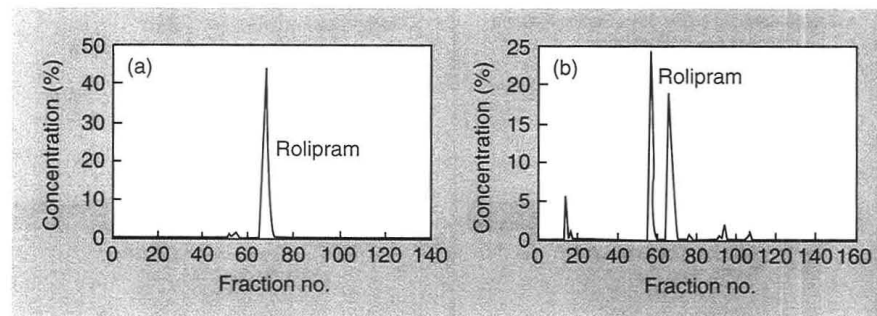


Figure 6. Use of LC–IA in metabolism studies.

High-performance liquid chromatograms of (a) rabbit plasma obtained 1 h after oral administration of 10 mg/kg [^3H] rolipram and (b) human plasma obtained 4 h after oral administration of ~ 0.01 mg/kg [^3H] rolipram. Radioimmunoassay activity was measured in fractions from plasma extracted with diethyl ether. (Adapted with permission from Reference 26.)

- (5) Van Emon, J. M.; Lopez-Avila, V. *Anal. Chem.* **1992**, *64*, 79-88.
- (6) Regnier, F. E. *Science* **1983**, *222*, 245-52.
- (7) Fausnaugh-Pollitt, J.; Thevenon, G.; Janis, L.; Regnier, F. E. *J. Chromatogr.* **1988**, *443*, 221-28.
- (8) Farjam, A.; Brugman, A. E.; Soldaat, A.; Timmerman, P.; Lingeman, H.; de Jong, G. J.; Frei, R. W.; Brinkman, U.A.T. *Chromatographia* **1991**, *31*, 469-77.
- (9) Chiciz, R. M.; Regnier, F. E. *Anal. Chem.* **1989**, *61*, 2059-66.
- (10) Janis, L. J.; Regnier, F. E. *J. Chromatogr.* **1988**, *444*, 1-11.
- (11) Heintz, M. L.; Flanigan, E.; Orłowski, R. C.; Regnier, F. E. *J. Chromatogr.* **1988**, *443*, 229-45.
- (12) Farid, N.; Atkins, L. M.; Becker, G. W.; Dinner, A.; Heiney, R. E.; Miner, D. J.; Riggan, R. M. *J. Pharm. Biomed. Anal.* **1989**, *1*, 185-88.
- (13) Riggan, R. M.; Shaar, C. J.; Dorulla, G. K.; Lefeber, D. S.; Miner, D. J. *J. Chromatogr.* **1988**, *435*, 307-18.
- (14) Riggan, A.; Sportsman, J. R.; Regnier, F. E. *J. Chromatogr.* in press.
- (15) Nilsson, B. *J. Chromatogr.* **1988**, *276*, 413-17.
- (16) Farjam, A.; de Jong, G. J.; Frei, R. W.; Brinkman, U.A.T.; Haasnoot, W.; Hamers, A.R.M.; Schilt, R.; Huf, F. A. *J. Chromatogr.* **1988**, *452*, 419-33.
- (17) Reh, E. *J. Chromatogr.* **1988**, *433*, 119-30.
- (18) Haasnoot, W.; Ploum, M. E.; Paulussen, R.J.A.; Schilt, R.; Huf, F. A. *J. Chromatogr.* **1990**, *519*, 323-35.
- (19) Davis, G. C.; Hein, M. B.; Chapman, D. A. *J. Chromatogr.* **1986**, *366*, 171-89.
- (20) Rybacek, L.; D'Andrea, M.; Tarnowski, S. J. *J. Chromatogr.* **1987**, *397*, 355-64.
- (21) Janis, L. J.; Grott, A.; Regnier, F. E.; Smith-Gill, S. J. *J. Chromatogr.* **1989**, *476*, 235-44.
- (22) Riggan, A.; Regnier, F. E.; Sportsman, J. R. *Anal. Chim. Acta* **1991**, *249*, 185-93.
- (23) Janis, L. J.; Regnier, F. E. *Anal. Chem.* **1989**, *61*, 1901-06.
- (24) Van Der Zee, R.; Welling, G. W. *J. Chromatogr.* **1985**, *327*, 377-80.
- (25) Gelpi, E.; Ramis, I.; Hotter, G.; Biogue, G.; Bulbena, O.; Rosello, J. *J. Chromatogr.* **1989**, *492*, 223-50.
- (26) Krause, W.; Kuhne, G. *J. Chromatogr.* **1992**, *573*, 303-08.
- (27) Pellegatti, M.; Braggio, S.; Sartori, S.; Franceschetti, F.; Bolelli, G. F. *J. Chromatogr.* **1992**, *573*, 105-11.
- (28) Meyer, H.H.D.; Hartmann, F.-X.; Rapp, M. *J. Chromatogr.* **1989**, *489*, 173-80.
- (29) Rapp, M.; Meyer, H.H.D. *J. Chromatogr.* **1989**, *489*, 181-89.
- (30) Irth, H.; Oosterkamp, A. J.; van der Welle, W.; Tjaden, U. R.; van der Greef, J. Presented at the 19th International Symposium on Chromatography, Aix-en-Provence, France, Sept. 13-18, 1992.
- (31) Yvon, M.; Wal, J. M. *J. Chromatogr.* **1991**, *539*, 363-71.
- (32) Hage, D. S.; Kao, P. C. *Anal. Chem.* **1991**, *63*, 586-95.
- (33) Wright, D. S.; Halsall, H. B.; Heineman, W. R. *Anal. Chem.* **1986**, *58*, 2995-98.
- (34) Doyle, M. J.; Halsall, H. B.; Heineman, W. R. *Anal. Chem.* **1984**, *56*, 2355-60.
- (35) Jenkins, S. H.; Heineman, W. R.; Halsall, H. B. *Anal. Biochem.* **1988**, *168*, 292-99.
- (36) Halsall, H. B.; Heineman, W. R.;

Jenkins, S. H. *Clin. Chem.* **1988**, *34*, 1702.

(37) de Alwis, W. U.; Wilson, G. S. *Anal. Chem.* **1985**, *57*, 2754-56.

(38) de Alwis, W. U.; Wilson, G. S. *Anal. Chem.* **1987**, *59*, 2786-89.

(39) Afeyan, N. B.; Gordon, N. F.; Regnier, F. E. *Nature* **1992**, *358*, 603-04.

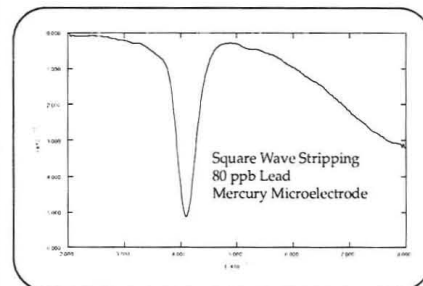


Mercedes de Frutos received her B.S. degree (1980) and her M.S. degree (1983) in chemistry from Autonoma University (Madrid, Spain). Her Ph.D. thesis (1989) focused on high-performance chromatographic techniques for the analysis of dairy products and was performed at the Consejo Superior de Investigaciones Cientificas (Madrid, Spain). For the past two years she has been a Fulbright scholar in the chemistry department at Purdue University under the direction of Fred E. Regnier. Her current work focuses on the development of immunochromatographic techniques and their applications.



Fred E. Regnier has been professor of chemistry at Purdue University since 1990. After completing a Ph.D. at Oklahoma State University (1965) and post-doctoral work at the University of Chicago (1967) and Harvard University (1969), he became assistant professor of biochemistry at Purdue (1969). During 20 years in the Biochemistry Department at that institution, he served as associate professor (1971-76), professor (1976-90), and associate director of the Agricultural Experiment Station (1976-78). He is the author of 150 publications and 15 patents on various aspects of chemistry, biochemistry, and separation techniques and their application to proteins. A recipient of the Dal Nogare Award for Achievements in Chromatography in 1987 and the ACS Award in Chromatography in 1989, he continues to pursue his interest in the rapid separation of proteins in both the analytical and preparative modes.

Say Goodbye to Either/Or Electrochemistry



Most electrochemical software is designed to do *either* sophisticated research *or* routine measurements. In the past, if your lab did both, you were stuck.

Either you had to buy two separate packages, which meant satisfying the compatibility requirements for both and learning two very different environments. Or you had to buy one package and make do.

Well say goodbye to *either/or* electrochemistry. The Model 270 Electrochemical Analysis software from EG&G Princeton Applied Research is unmatched on all counts—power, versatility, and ease of use.

Consider just this small selection of Model 270 advantages:

- Both time-tested hardware (Model 273 Potentiostat) and state-of-the-art computer environment (IBM platform, pull-down menus)
- Automatic control of both the PARC Model 303A SMDE and a selection of microelectrodes
- Traditional voltammetry/polarography and fast Square Wave
- Easy-to-learn Standard Mode for routine use and feature-rich Expert Mode for finer experimental control

So if you typically do ground-breaking research one day and routine measurements the next, say hello to *total* electrochemistry. Call for information today at 1-609-530-1000.

EG&G PARC

P.O. BOX 2565 • PRINCETON, NJ 08543-2565
(609) 530-1000 • FAX: (609) 883-7259

Circle 30 for Literature.
Circle 31 for Sales Representative.

Conferences

- **1993 European Winter Conference on Plasma Spectrochemistry.** Jan. 10–15. Granada, Spain. Contact: *Alfredo Sanz-Medel, Dept. of Physical and Analytical Chemistry, Faculty of Chemistry, University of Oviedo, C/Julián Clavería, s/n-33006 Oviedo, Spain (34 85 10 34 71 or 34 85 10 34 74; fax 34 85 23 78 50)*
- **Sanibel Conference on Mass Spectrometry of Carbohydrates.** Jan. 23–26. Sanibel Island, FL. Contact: *Judith A. Sjöberg, American Society for Mass Spectrometry, 815 Don Gaspar, Santa Fe, NM 87501 (505-989-4517; fax 505-989-1073)*
- **5th International Symposium on High-Performance Capillary Electrophoresis (HPCE '93).** Jan. 25–28. Orlando, FL. Contact: *Shirley E. Schlessinger, Symposium Manager, HPCE '93, Suite 1015, 400 E. Randolph Dr., Chicago, IL 60601 (312-527-2011)*
- **7th International Forum on Process Analytical Chemistry (IFPAC).** Jan. 26–27. Houston, TX. Contact: *InfoScience Services, Inc., Conference Div., 3000 Dundee Rd., Suite 313, P.O. Box 153, Northbrook, IL 60065 (708-291-9161; fax 708-291-0097)*
- **Envirolab Conference.** Jan. 26–27. Houston, TX. Contact: *InfoScience Services, Inc., Conference Div., 3000 Dundee Rd., Suite 313, P.O. Box 153, Northbrook, IL 60065 (708-291-9161; fax 708-291-0097)*
- **On-Site Analysis Conference and Exhibition.** Jan. 26–27. Houston, TX. Contact: *InfoScience Services, Inc., Conference Div., 3000 Dundee Rd., Suite 313, Northbrook, IL 60065 (708-291-9161; fax 708-291-0097)*
- **IS&T/SPIE Symposium on Electronic Imaging: Science and Technology.** Jan. 31–Feb. 5. San Jose, CA. Contact: *Conference Manager, The Society for Imaging Science and Technology, 7003 Kilworth Lane, Springfield, VA 22151 (703-642-9090; fax 703-642-9094)*
- **International Conference on Energy, Environment, and Electrochemistry.** Feb. 10–12. Karaikudi, Tamilnadu, India. Contact: *K. C. Narasimham, Conference Convener, Central Electrochemical Research Institute, Karaikudi-623 006, Tamilnadu, India (91 04565 3161 2368 or 2064; fax 91 04565 2088)*
- **2nd International Symposium on Automation, Robotics, and Artificial Intelligence Applied to Analytical Chemistry and 2nd International Conference on Robotics in Laboratory Medicine.** Feb. 23–26. Montreux, Switzerland. Contact: *Scitec SA, Av. de Provence 20, CH-1000 Lausanne 20, Switzerland (41 21 24 15 33; fax 41 21 24 15 49)*
- **3rd International Specialty Conference on Field Screening Methods for Hazardous Wastes and Toxic Chemicals.** Feb. 23–26. Las Vegas, NV. Contact: *Marci Mazzei, Air & Waste Management Association, P.O. Box 2861, Pittsburgh, PA 15230 (412-232-3444; fax 412-232-3450)*
- **Pittcon '93. The 44th Pittsburgh Conference & Exposition on Analytical Chemistry and Applied Spectroscopy.** March 8–12. Atlanta, GA. Contact: *Pittcon '93, 300 Penn Center Blvd., Suite 332, Pittsburgh, PA 15235-5503 (412-825-3220)*
- **34th Experimental Nuclear Magnetic Resonance Conference.** March 14–18. St. Louis, MO. Contact: *Judith A. Sjöberg, ENC, 815 Don Gaspar, Santa Fe, NM 87501 (505-989-4573; fax 505-989-1073)*
- **Symposium on Possibilities and Limitations of Chiral Separation Techniques.** March 19. Antwerp, Belgium. Contact: *Royal Flemish Chemical Society (KVCV), Working Party on Chromatography, c/o R. Smits, BASF Antwerpen N. V., Central Laboratory, Scheldelaan, B-2040 Antwerp, Belgium (32 3 568 28 31; fax 32 3 568 32 50)*
- **Interpex USA.** March 29–April 1. New York, NY. Contact: *Conference Department, 1350 East Trouhy Ave., P.O. Box 5060, Des Plaines, IL 60017-5060 (708-390-2479)*
- **1993 Spring Meeting of the Materials Research Society.** April 12–16. San Francisco, CA. Contact: *Materials Research Society, 9800 McKnight Rd., Pittsburgh, PA 15237 (412-367-3003; fax 412-367-4373)*
- **Scanning '93.** April 21–23. Orlando, FL. Contact: *Scanning '93, P.O. Box 832, Mahwah, NJ 07430 (201-818-1010; fax 201-818-0086)*
- **46th Annual Conference of the Society for Imaging Science and Technology.** May 9–14. Cambridge, MA. Contact: *Conference Manager, The Society for Imaging Science and Technology, 7003 Kilworth Lane, Springfield, VA 22151 (703-642-9090; fax 703-642-9094)*
- **17th International Symposium on Column Liquid Chromatography.** May 9–14. Hamburg, Germany. Contact: *Gesellschaft Deutscher Chemiker, Abteilung Tagungen, Postfach 90 04 40, Varrentrappstr. 40-42, D-6000 Frankfurt am Main 90, Germany (49 069 79 17 360; fax 49 069 79 17 475)*
- **Analysis of Peptides.** May 24–26. Stockholm, Sweden. Contact: *Swedish Academy of Pharmaceutical Sciences, P.O. Box 1136, S-111 81 Stockholm, Sweden (46 8 24 50 85; fax 46 8 20 55 11)*
- **5th International Symposium on Quantitative Luminescence Spectrometry in Biomedical Sciences.** May 25–27. Ghent, Belgium. Contact: *Willy R. G. Baeyens, University of Ghent, Pharmaceutical Institute, Harelbekestraat 72, B-9000 Ghent, Belgium (32 091 21 89 51 ext. 254 or 248; fax 32 091 21 79 02)*
- **41st ASMS Conference on Mass Spectrometry and Allied Topics.** May 30–June 4. San Francisco, CA. Contact: *Judith A. Sjöberg, American Society for Mass Spectrometry, 815 Don Gaspar, Santa Fe, NM 87501 (505-989-4517; fax 505-989-1073)*
- **38th International Symposium on Analysis of Peptides.** June 2–4. Stockholm, Sweden. Contact: *The Swedish Academy of Pharmaceutical Sciences, P.O. Box 1136, S-111 81 Stockholm, Sweden (46 8 24 50 85; fax 46 8 20 55 11)*
- **86th Annual Meeting and Exhibition of the Air & Waste Management Association.** June 13–18. Denver, CO. Contact: *Lisa Bradley, Air & Waste Management Association, P.O. Box 2861, Pittsburgh, PA 15230 (412-232-3444; fax 412-232-3450)*
- **28th Colloquium Spectroscopicum Internationale.** June 29–July 4. York, UK. Contact: *Colloquium Spectroscopicum Internationale Secretariat, Department of Chemistry, Loughborough University of Technology, Loughborough, Leicestershire LE11 3TU, U.K. (44 0 509 222575; fax 44 0 509 233163)*

These events are newly listed in the JOURNAL. See back issues for other events of interest.

An efficient, economical way to train employees and keep them up-to-date with a minimum of disruption to operations!

Analytical Chemistry by Open Learning

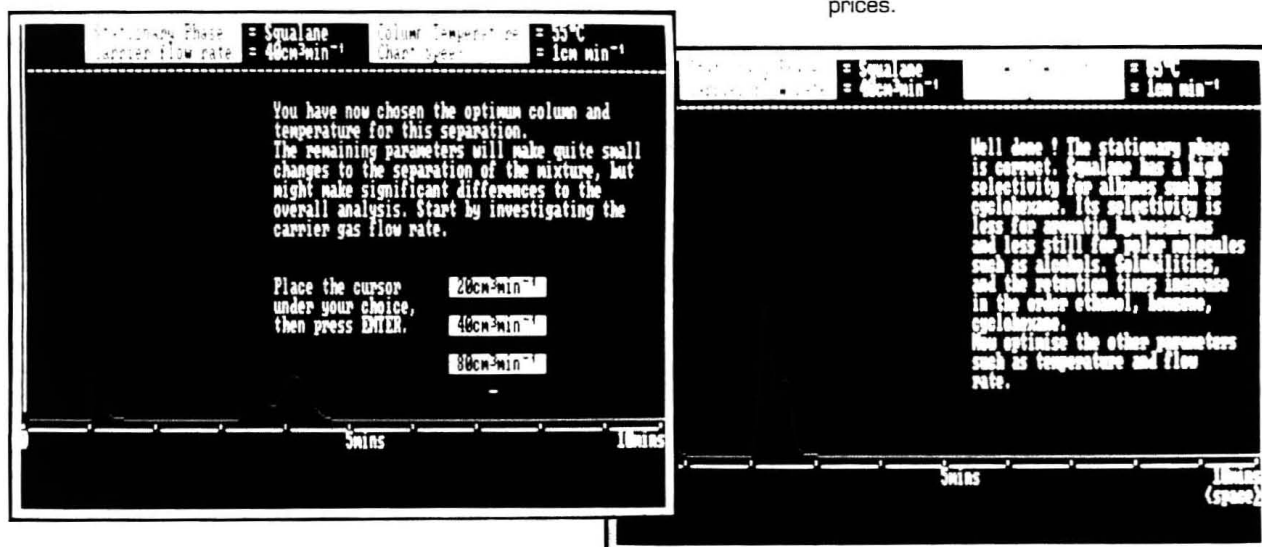
ACOL, an interactive teaching/training series, utilizes software and text to teach seven of the most widely used techniques in analytical science. It is designed to permit users to "work with" instrumentation online, without tying up company equipment, and to work at their own pace, on premises, at times when it is most convenient for both company and personnel.

ACOL offers the user a choice of instrument configurations and other variables such as calibration standards, pH, flow rate, stationary phase, wavelength, and attenuation. The outcome of each choice, together with relevant reinforcement or guidance, if necessary, is seen immediately on the screen, simulating instrument output. Plus, companies can stress those applications specific to their needs from the basic principles and practices covered in the program.

HOW DOES IT WORK?

Self-contained and interactive, ACOL provides all the benefits of classroom teaching without the drawbacks. The texts are planned to keep users alert and interested via frequent activities and self-assessment checks scattered throughout the text. Not only that, books and software both include commentaries on the answers selected and suggest additional options to clarify, correct, and reinforce the user's understanding.

EXAMPLE



Each section concludes with a summary of essential points and a checklist of objectives that the user should have learned.

WHO SHOULD USE IT?

- Chemists, scientists, and technicians in other disciplines who are expected to carry out analytical procedures with skill and proficiency, but who may have never received formal training.
- Staff who are about to use a new technique, or
- Those who need a refresher course.

ACOL has become a standard part of routine training for many companies. Once they've tried one program, they are so impressed with the results they usually come back for more!

MODULES AVAILABLE

- Atomic Absorption Spectroscopy
- Gas Chromatography
- High Performance Liquid Chromatography
- Polarography
- Radiochemistry
- Fluorescence Spectrometry
- Quantitative IR and UV

List price \$395
Member price \$355
Academic price \$295

Additional books may be purchased separately. Also available in Opening-Learning books are *Nuclear Magnetic Resonance Spectroscopy* and *Mass Spectroscopy*. Please inquire for prices.

To order call 1-800-227-5558
In Washington, DC 202-872-4363
by FAX 202-872-6067

American Chemical Society
Distribution Office, Dept. 41
1155 16th Street, NW
Washington, DC 20036

NEW PRODUCTS



Benchtop GC/MS system combines an HP 5972A mass-selective detector with the 5890 Series II GC, optional electronic pressure control, and mass spectrometry software for trace component analysis in the fg/g range for SIM mode or in the pg/g range for full-scan mode. The MSD allows reproduction of spectra, including ion ratios, and electronic pressure control automatically calculates carrier gas flow rate to compensate for the MSD's vacuum environment. Hewlett Packard 402

Instrumentation

Dissolved oxygen monitoring. DO-166FT micro flow-through oxygen probe can be used in line in bioreactors, oxygen consumption studies, FIA, HPLC, and water analysis. The probe, with an internal volume of 120 μL , has a P_{O_2} electrode, a micro flow cell, and an electronic signal conditioner, and can be hooked up directly to a standard pH/mV meter or strip chart recorder. LAZAR Research Laboratories 401

Extraction. Zero-headspace extractor is designed for use with EPA's toxicity characteristic leaching procedure for measuring the mobility of volatile organic and inorganic contaminants in solid and liquid wastes. The stainless steel extractor separates liquids from solids, can be inserted into standard rotary agitators, and features both a side-view pressure gauge and an underdrain disc

that forces hazardous samples to flow to the center of the disc for minimal risk of operator exposure. Gelman Sciences 403

Near-IR. Three process measurement packages are based on the Quantum 2000 NIR process analyzer: a batch-monitoring system; a beer analyzer for blending processes; and an octane number measurement system for MOGAS blending, reformat units, and FCC units. Each package contains a dispersive near-IR spectrometer, a probe, fiber-optic cables, and application-specific software. LT Industries 404

FT-IR. Industrial process on-line IR analyzer system monitors up to 10 analytes simultaneously with temperature-controlled, closed-loop sampling in either batch or continuous process modes. Concentrations are displayed as percentages and plotted against time, and alarms in-

dicating stray from product target formulations. On-Line Scientific 405

XRF. Two on-line analyzers measure sulfur in petroleum products. The 682-LP analyzes low concentrations (≥ 50 ppm) of sulfur in refined petroleum products by XRF, and the 682-HP measures high concentrations (0.1–10%) in crude oil using X-ray transmission. Both can be operated in remote locations. ASOMA Instruments 406

FT-IR. MICRO FT/IR-200 spectrometer has a resolution capability of 1 cm^{-1} and allows confirmation of both sample and reference positions on the screen. The aperture opens and closes in two directions and can be rotated to any angle. The system is menu-driven and includes a computer data station with a printer/plotter. Jasco 407

Octane analysis. Process FT-IR/FT-near-IR analyzer, designed to replace knock engine methods for industrial measurement of octane number, can measure research or motor octane number with a precision of $< 0.2\%$. The unit includes dedicated software for instrument control, diagnostics, data acquisition, octane number prediction, and data output. It can communicate with other plant analyzers and distributed control systems. Applied Automation 408

Gas monitoring. GasPro SGM-1000 battery-powered portable single-gas monitors use electrochemical gas sensors to detect specific toxic gases or oxygen depletion in the field. They operate with a simple on/off switch and their audible and visual alarms alert the user to toxic levels of H_2S (0–550 ppm; alarm 10 ppm), CO (0–999 ppm; 35 ppm), SO_2 (0–20 ppm; 2 ppm), or Cl_2 (0–10 ppm; 1 ppm), or to depleted O_2 (0–50%; 19% V/V). Lumidor Safety Products 409

For more information, please circle the appropriate numbers on one of our Readers' Service Cards.



Wavelength-dispersive XRF analyzer rapidly measures sulfur, phosphorus, chlorine, calcium, barium, and zinc in lubricant oil additives for quality control with little sample preparation or operator intervention. Oil samples are analyzed in as-received condition in the QX system, which includes a 72-position autosampler for long unattended or overnight runs. Oxford Instruments **413**

Spectroscopy. RSM computerized spectrophotometry system, optimized for studies of spectrally distant reaction intermediates, combines diode array and double-beam technology for scanning speeds of 1000 scans/s with 220-nm span, routine range of 180–1000 nm, and S/N better than ± 0.0001 ABS units. The system has both fluorescence and absorbance modes, an $f/4.5$ optical system with 250-mm focal length, bandwidths selectable from 0.5 nm, and user-accessible gratings. On-Line Instrument Systems **410**

CCD detector. Spectrum One detection system uses a 1024×256 pixel format CCD detector array for enhanced spectral coverage. The 1-in. chip offers high-speed spectral acquisition and low S/N. SPEX **411**

Software

LIS demonstration. Demonstration software package based on the full-function version of LabVIEW for Windows graphic programming software provides an overview of the system, basic concepts, and hands-on examples. The user can explore or build a virtual instrument program for instrument driving, data acquisition, and data processing. National Instruments **412**

Size exclusion chromatography. Turbochrom 3 SEC software package features automatic generation of

user-selected SEC reports and plots and has five curve-fitting options for molecular weight calibration, including point-to-point; first-, second-, and third-order; and cubic spline. The software uses either narrow or broad molecular weight standards to generate the calibrations and provides a universal calibration option, automatic updating of calibration curves, and retention time correction based on internal reference peaks. Perkin Elmer **414**

Polymer modeling. ChemPolymer integrates polymer building and property calculation by using interactive analysis and display functions, including spectral displays of polymer properties. Building functions include branching, kinetic control for mixed copolymers, stereochemical control, and crystalline packing. Physical and bulk property calculations are displayed as 2D spectra that can be viewed alongside the polymer model and stored in databases. Chemical Design **415**

Manufacturers' Literature

Newsletter. *Supelco Reporter* contains articles on HPLC and SPE techniques for monitoring pesticides and PCBs in indoor air, measuring cyclosporin A in blood, and measuring vanillin in food and other products. Other topics include applications for Rezorian A-161 analytical cartridges, and CLOT and Petrocol

capillary columns. The newsletter consolidates material from Supelco's other periodicals: *Biotext*, *Liquid Currents*, *Food Analysis Digest*, and *The Environmental EDGE*. 28 pp. Supelco **416**

HPLC. Brochure describes ID ImmunoDetection cartridges for HPLC and applications such as assays analogous to standard, competitive, and sandwich immunoassays performed on microtiter plates. Experimental examples are provided, and chemistries for the cartridges are illustrated. 8 pp. PerSeptive Biosystems **417**

Particle counting. Product literature describes a line of in situ monitors, spectrometers, and data acquisition systems for determining filter efficiency and particulate levels. The instruments offer sizing sensitivities at $0.05 \mu\text{m}$ for DI water and at $0.065 \mu\text{m}$ for process chemicals. 4 pp. Particle Measuring Systems **418**

Gas monitoring. *8th Edition Detector Tube Handbook* is a field reference for users of Dräger gas detector tubes. The book, in compliance with IUPAC standards, lists more than 220 Dräger tubes and provides information on ranges, reaction principles, cross-sensitivity, and operating conditions. Graphics and tables of physical, chemical, toxicological, and international exposure limit information are included, as well as references to U.S. occupational exposure regulations and safety organizations. 318 pp. National Draeger **419**

Catalogs

Training seminars. Brochure lists training seminars and analytical assistance for ICP-AES for environmental, geological, rare earth, and precious metals studies. Locations, topics, and duration are given. 4 pp. J-Y Emission **420**

Software. Catalog describes test and measurement, data acquisition, image analysis, chromatography, and line scan hardware and software products for common microcomputers. The catalog is available alone or as part of a three-book set that includes a 144-page source handbook with compatible products and services from more than 175 companies as well as a 164-page applications handbook with articles on applications and technology. 288 pp. Data Translation **421**

Impact of the Environment on Egyptian

Ralph O. Allen

Department of Chemistry
University of Virginia
Charlottesville, VA 22901

Hany Hamroush

Faculty of Science
Cairo University
Giza, Egypt

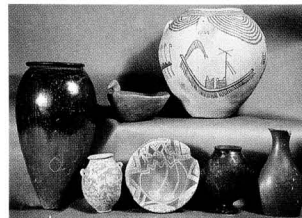
Daniel J. Stanley

U.S. Museum of Natural History
Smithsonian Institution
Washington, DC 20560

Most people can appreciate the intricate methods used by historians who study letters, manuscripts, and art objects to deduce relationships and organize events. Efforts to understand the history of one of mankind's first great civilizations, Tawy (Two Lands), are aided by an immense amount of written material, some carved in the stone of magnificent ancient Egyptian monuments. It has

Hence understanding anything about the factors leading to this unification is important in developing a better sense of mankind's evolution.

Legends suggest that when Menes founded the first dynasty, he and the protodynastic kings who preceded him (Narmer and Scorpion) were followers of the hawk-headed god Horus who came from the city Nekhen, or, as the ancient Greeks later named it, Hierakonpolis (city of the hawk). Some scholars believed that Nekhen was more symbolic than historical, but discoveries of the largest predynastic settlement area in upper Egypt (by James E. Quibell, an Englishman trained in chemistry and the classics) in 1897 have suggested otherwise. Among these discoveries were symbolic maceheads and commemorative stone palettes purported to document the efforts of the protodynastic kings Narmer and Scorpion. Figure 1 is a drawing of Scorpion, taken from the stone macehead, wearing the crown of upper Egypt.



Predynastic pottery used in burials of important leaders who were the forefathers of the Pharaohs.

further evidence of the historical importance of Nekhen. These studies have enabled researchers to see this ancient society in a more complete context and have drawn on the concepts of the pioneer environmental archaeologist Karl Butzer. These studies have also pointed out the importance of developing an ecological perspective to better understand the complex interrelationships between the natural setting (e.g., biology, climate, landforms) and the culture of the people.

Factors influencing the environment

The paleoenvironment of Egypt during these prehistoric times was governed mainly by three factors: the Nile floods, local climatic conditions, and the paleogeography of the Nile Valley. The annual floods carried fresh sediments that were deposited when the water overflowed the banks and that were instrumental to the agricultural system. Seeds spread on the water, became trapped by the banks as the flood receded, and settled to the bottom along with the fresh Nile sediment. Because the floods provided a unique planting opportunity for the growth of food, it was important to predict their onset. Anticipating the floods likely became one of the key elements in the development of religious customs and practices. The location of settlement areas at Nekhen suggests that, in addition to the existence of agriculture near the Nile, the sediments could have been used beyond the flood plain. Archaeologists have inter-

ANALYTICAL APPROACH

been possible to reconstruct the well-ordered list of 32 historic Pharaonic dynasties, which stretches from the unification of the nation state under one of the first Pharaohs, Menes, in about 3200 B.C. (5200 B.P. [before present]) to the ill-fated alliances of Cleopatra in 31 B.C. In contrast, the time before the Pharaohs is a mystery to researchers using a normal historical approach. The type of material that has survived from this earlier "predynastic" period lends itself more to examination through the methods of the geologist, the botanist, and the analytical chemist.

Throughout Egyptian history the writings emphasize the Two Lands of upper (southern) and lower (northern) Egypt and the Nile River, which ties them together. The unification of these lands into the first nation state is looked upon as the prerequisite for the development of civilization.

Depicted in the figure is the ritual digging or perhaps the opening of an irrigation canal.

Modern interdisciplinary studies of this area, notably under the leadership of the late American archaeologist Michael Hoffman, have provided



Ponds created by water from the Nile. In the past, these ponds were filled by overflowing banks; water is now pumped for irrigation purposes.

ILLUSTRATION: LOEL BARR

Civilization before the Pharaohs

preted the Scorpion macehead as evidence of the importance of irrigation to this protodynastic king, and—as our more recent studies have suggested—to the genesis of the Egyptian civilization. Thus understanding the landforms and environmental conditions at Nekhen is important for understanding the evolution of the nation state concept.

Trying to decipher the factors influencing the paleoenvironment has been difficult, because archaeological studies tend to focus on localized sites. Concentrating on the local scale can result in a failure to see larger scale and regional differences that may offer clues to the environment. However, along the Nile the greatest problem has been inaccessibility.

Most early archaeological sites such as Nekhen are located on the flood plain of the Nile bordering or under the modern cultivation zone. Geographical and geomorphical investigations suggest that during predynastic times the general character of the flood plain along the banks of the Nile was very similar to that of 60 years ago, before completion of the Aswan Dam. The flood plain was convex and accumulated sediments through bank overflow of suspended sediments. By contrast, flat flood plains are built up through repeated channel shifts and lateral accretion of bed-load sediments (such as those in the delta of northern Egypt). This formation implies that most evidence of Egypt's prehistoric heritage is situated under the sediments over which 50 million people now live. Rather than being exposed in outcrops and easily visible by geological examination, the geological records of the Nile's past 7000 years are covered by successive deposits of Nile sediments. These sediments are, however, themselves a record of the past if they can be deciphered.

The analytical approach

Obtaining information from Nile sediments is a complex problem, but the analytical approach can be better understood by considering the origin of the material deposited by the floods. These sediments are fragments of

minerals from the rocks covering the terrains of the Nile headwaters in eastern and central Africa. The fine-grained materials in the sediments are mostly clay minerals that have resulted from the chemical alteration (weathering) of certain minerals in the source rocks. The coarse-grained material (described as the sand-sized fraction) comes mainly from the physical fragmentation of certain hard minerals that retain their chemical and physical characteristics. Much of the sand is quartz (SiO_2), which has a mineral structure that contains little contamination from trace element impurities.

When the sediment sample is analyzed, it is found to be a mixture of clay minerals, rock fragments, and organic material. Chemical differences are often difficult to understand, even when corrected for the organic content. Even when Nile sediments have been analyzed for trace elements with techniques such as neutron activation analysis (NAA), which pro-



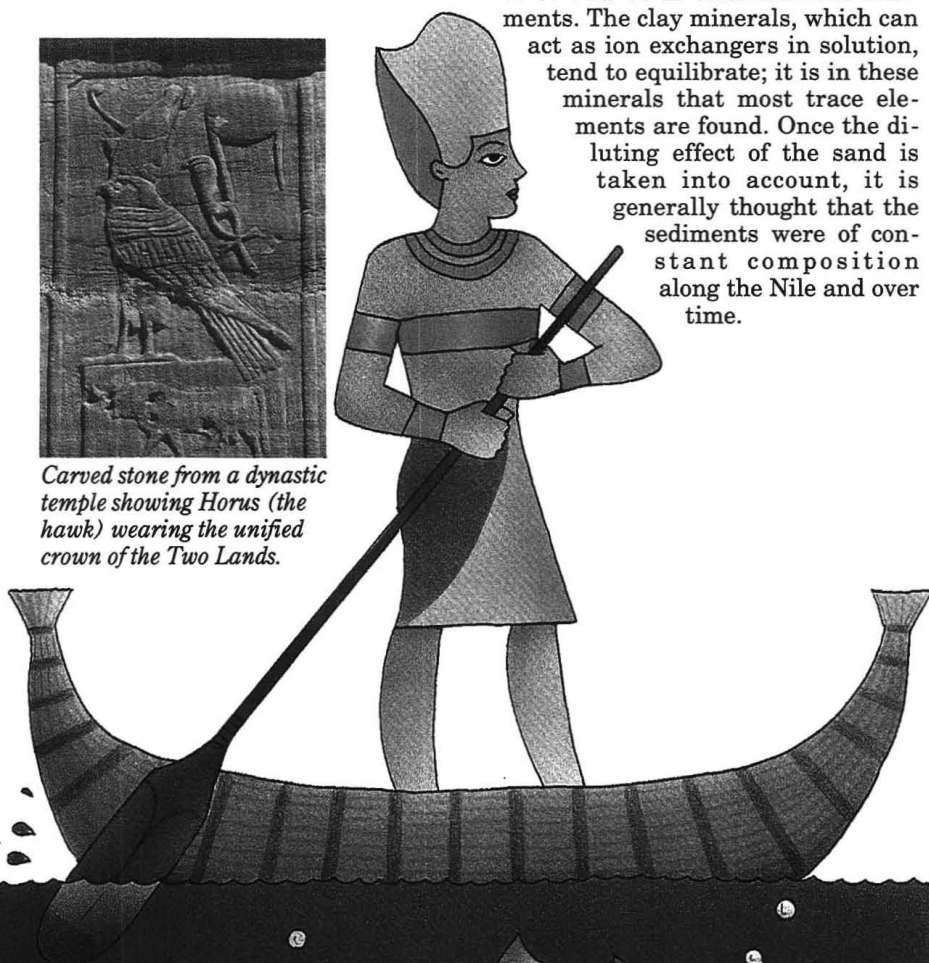
Temple with a column made in the shape of a palm.

vides good accuracy and precision, there is variability. The quartz sand acts as a dilutant; thus, trace element concentrations vary as a function of the relative amount of sand.

When the sediments are deposited by the Nile, the relative portions of coarse-grained sand and fine silt vary with local hydrological conditions. The dilution effect of the quartz can be seen in a binary plot (Figure 2), which shows the variation of Sc and Co in different Nile sediments. The clay minerals, which can act as ion exchangers in solution, tend to equilibrate; it is in these minerals that most trace elements are found. Once the diluting effect of the sand is taken into account, it is generally thought that the sediments were of constant composition along the Nile and over time.



Carved stone from a dynastic temple showing Horus (the hawk) wearing the unified crown of the Two Lands.



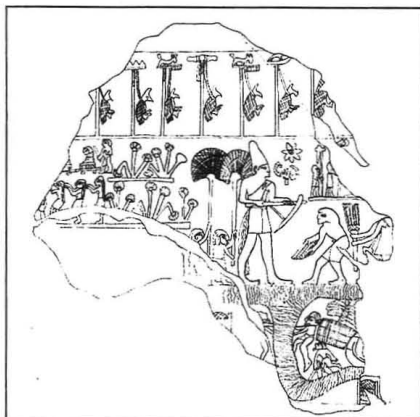
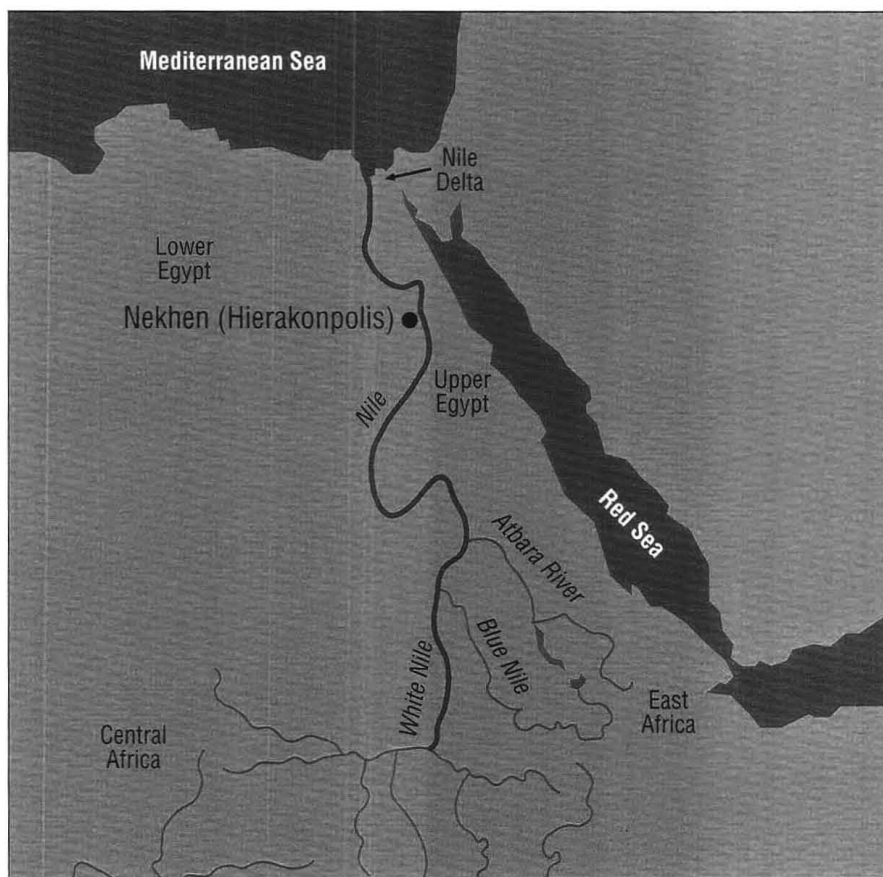


Figure 1. Drawing taken from the carved stone ceremonial macehead found at Nekhen.

This macehead shows a predynastic king of upper Egypt (note the tall crown of upper Egypt) called Scorpion; the image of the scorpion is in front of his face. Scorpion holds an agricultural implement that is thought to have been used to control or open the irrigation canals represented at his feet.

The Nile River sediment composite shown in Figure 2 is the average of more than 30 individual analyses of modern Nile sediments. The ceramic samples shown here were made from these same Nile sediments. In special cases, the interpretation of trace element concentrations in Nile sediments has been complicated by the fact that local material was mixed with river sediments coming from the headwaters area. When the sand-sized fractions (mineral fragments) were separated and analyzed, it was possible to detect differences among Nile sediments deposited during different time periods and locally derived (non-Nile) sediments and mixtures. This important observation suggested an analytical approach for classifying particular Nile sediments by their trace element "fingerprints."

When the sand fraction for Nile sediment samples was analyzed, con-



siderable variability existed because of the differing amounts of quartz. To discover meaningful relationships, several pattern recognition programs (statistical packages such as Systat and Arthur) were used. Although statistical methods do not prove that materials are different, they can help provide insight by showing possible differences. When sand fraction sediments were analyzed with NAA, 18 elemental concentrations were detected with analytical uncertainties (based on counting statistics) better than $\pm 10\%$. When large numbers of samples were analyzed, it was difficult to observe trends without the use of computer-based statistical

programs. Examination of the data with pattern recognition programs suggested that several groups of elements in the sand-sized fraction could be used to "classify" sediments from different layers. The variability attributable to dilution by quartz could be normalized by using appropriate elemental ratios.

The normalization method shown in Figure 3 takes the sum of three elemental concentrations (Cr, Hf, and Th) and displays the fraction of each in the sum. This approach, commonly used by mineralogists to describe the composition of certain minerals, eliminates the effect of dilution by the quartz grains. By try-

**What is the chemical structure of a polymer system?
Get the answer in this definitive new resource...**

Spectroscopy of Polymers

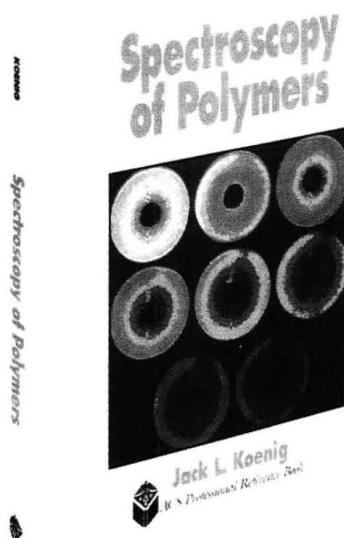
by **JACK L. KOENIG**

*Department of Macromolecular Science
Case Western Reserve University*

At last—the definitive resource for scientists, engineers, and graduate students in polymer science on the primary spectroscopic methods of polymer characterization that continues where introductory-level texts end.

Spectroscopy of Polymers was written for those whose knowledge of polymer chemistry includes some familiarity with the basic vibrational and resonance spectroscopic methods, but who have limited experience in applying the modern techniques of FTIR, Raman, and/or NMR spectroscopy. The book provides a solid background in the fundamental aspects and experimental applications of the primary spectroscopic methods and their advantages and disadvantages for particular polymer systems. It brings both professional and student up-to-date on the current techniques and facilitates communication with others in the field.

Throughout the eleven chapters of this book, Koenig provides clear, concise examples to demonstrate the strengths and weaknesses of the various vibrational and NMR techniques and offers the reader practical knowledge of how to select the most appropriate solutions to polymer structure problems. Numerous illustrations accompany both text and examples.



ACS Professional Reference Book

450 pages (1992)

Clothbound: ISBN 0-8412-1904-4 \$89.95

Paperback: ISBN 0-8412-1924-9 \$49.95

TO ORDER CONTACT:

American Chemical Society
Distribution Office, Dept. 31
1155 Sixteenth Street, N.W.
Washington, DC 20036

To charge your order by phone,

call **TOLL-FREE** 1-800-227-5558.

In Washington, DC, call 202-872-4363.

Or FAX your order to 202-872-6067.

ABOUT THE AUTHOR

Jack Koenig is the J. Donnell Institute Professor of the Departments of Macromolecular Science and Chemistry at Case Western Reserve University, Cleveland, Ohio, and has over 25 years teaching and research experience to his credit. He has published over 430 papers, edited or authored 5 monographs, and has won numerous awards, among them the prestigious Pittsburgh Spectroscopy Award, the New York Society of Spectroscopy Gold Medal, the Society of Plastics Engineers Research Award, the ACS Doolittle Award.

CONTENTS

Theory of Polymer Characterization
Vibrational Spectroscopy of Polymers
Experimental IR Spectroscopy of Polymers
Applications of IR Spectroscopy to Polymers
Raman Spectroscopy of Polymers
High-Resolution NMR Spectroscopy of Polymers
in Solution
Special Editing Techniques for High-Resolution NMR
Spectroscopy of Polymers
High-Resolution NMR Spectroscopy of Solid Polymers
Applications of High-Resolution Solid-State NMR
Spectroscopy of Polymers
NMR Relaxation Spectroscopy of Polymers
NMR Imaging of Polymeric Materials

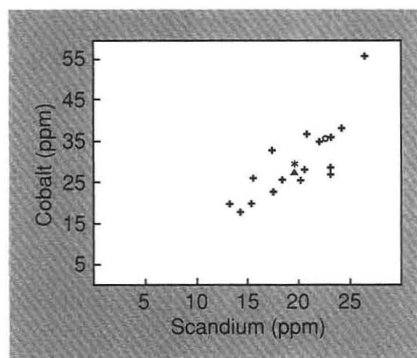


Figure 2. Concentrations of Co and Sc in Nile sediments found in the area around Nekhen in upper Egypt (+).

The triangle (\blacktriangle) is the average of 30 individual analyses of Nile muds and sediments from the length of the Nile, the circle (\circ) is the average of nearly 200 ceramic samples made from Nile sediments, and the star ($*$) is the average of 30 ceramic samples from Nekhen.

ing different combinations, we have found that the best separations occurred when the elements used had different geochemical properties. The fact that the sand fraction contains a variety of minerals from the weathering of rocks suggests variability in the type of mineral present.

Earlier petrological studies of heavy minerals in the sand-sized fraction of Nile sediments had indeed shown such differences over time. These were interpreted as a reflection of changing contributions to the sediment load from the two main sources of the Nile: the Ethiopian and the Central African plateaus. These same differences seem to be reflected in trace element data. Cr

occurs in markedly higher concentrations in basaltic rocks, such as those in the Ethiopian plateau (which is drained by the Blue Nile and the Atbara rivers) than in granite and quartzite rocks, such as those in the Central African plateau (which is drained by the White Nile). Hf and Th are more concentrated in Central African rocks than in those of the Ethiopian plateau. Because the Nile sediments are derived from these two different geological terrains, the variation in the trace element data suggests changes over time in the relative contributions from these two sources.

Thus the identification of appropriate trace elements in the sand-sized fraction of the Nile sediments, as seen in elemental ratios or plots such as Figure 3, provides a means of measuring the relative contributions to the sediments from the two geological areas drained by the White Nile and the Blue Nile. Data suggest that changes in the relative contributions have occurred over time. Studies of the sediments from Nekhen provided an example of how the ability to distinguish among sediments deposited at different times or from different sources can provide insight into environmental changes.

To obtain samples it was necessary to bore down through the sediments and get a core of samples representing earlier periods. Ceramic shards included in the cores provided a convenient means of establishing the age of the sediment layers in which they were found (a process reinforced by ^{14}C dating). Sediment samples

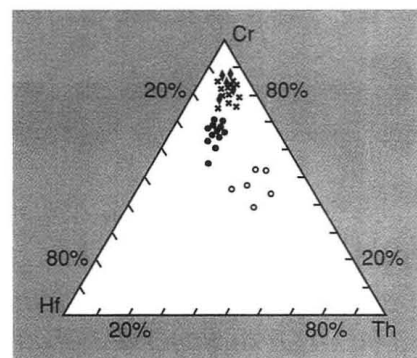
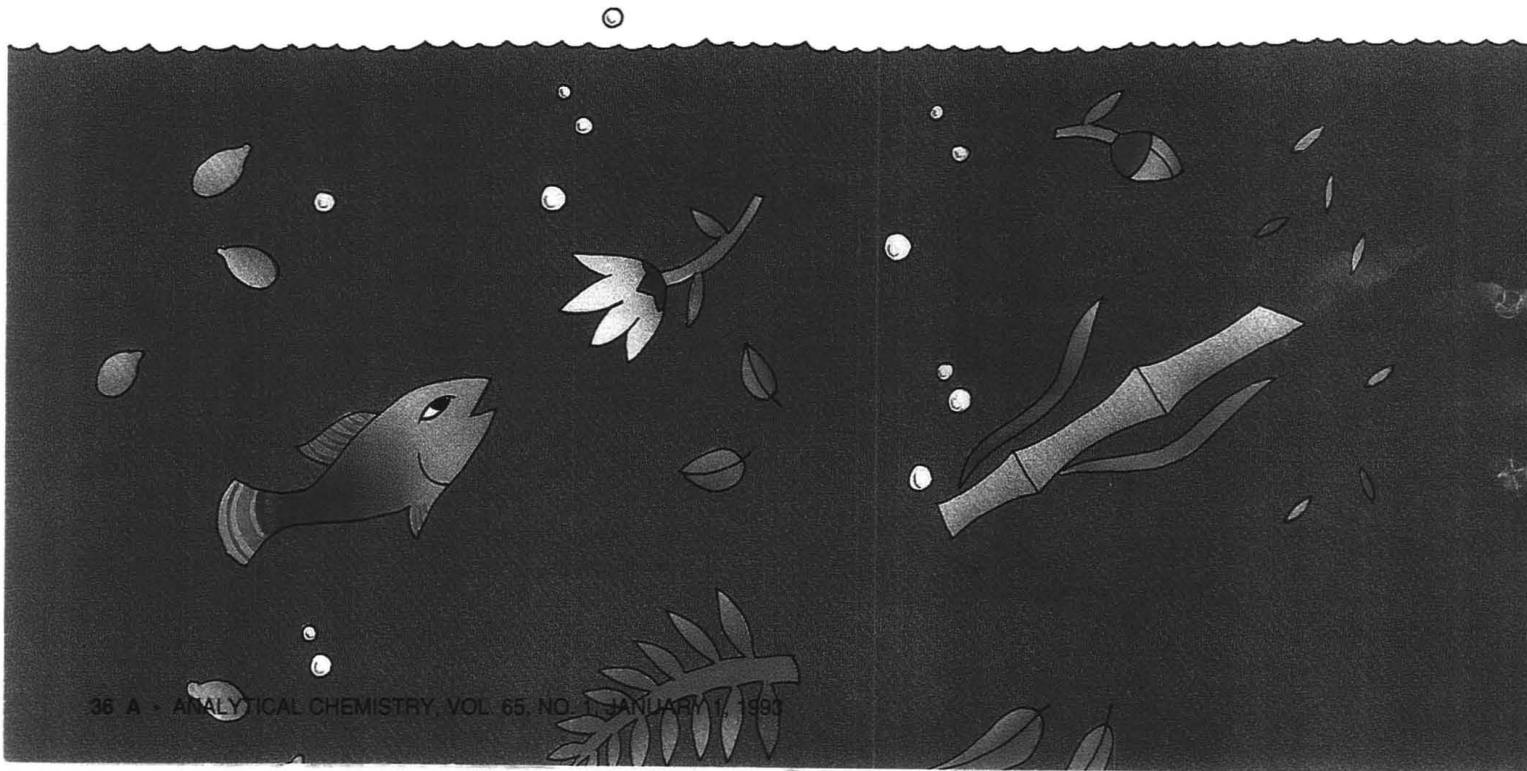


Figure 3. Interelement correlation diagram for relative concentrations of Cr, Hf, and Th in sand-sized fractions of Nile sediments at Nekhen.

Samples from the Nekheh geological formation (deposited from ~ 7000 B.P. to ~ 5200 B.P.) were taken from Nekhen (X) and across the Nile at El Kab (\blacklozenge). Nile samples deposited between 4500 B.P. and 2300 B.P. are indicated as solid circles (\bullet). The open circles (\circ) are described as wadi deposits made up of a mixture of much older Nile sediments (before 10,000 B.P.) deposited in the wadi and much older sedimentary material from the Esna shale deposits along the wadi. These were deposited between the Nekheh formation and later Nile sediments between 5200 B.P. and 4500 B.P. The concentrations of Cr, Th, and Hf are summed, and the ratio of each element to the sum is plotted on the diagram.

were sieved to recover the sand-sized fractions ($> 63 \mu\text{m}$), which were analyzed and compared (Figure 3). Using the sediment layer thickness, the sample depth, and the area covered, it was possible to interpret the evolution of the land around Nekhen.

There is clear evidence that Nile sediment deposits from at least 6000 B.P. to 5200 B.P. were substantial, and then the pattern changed. Floods



Here are 26 of the World's Most Prestigious Periodicals in Chemical Science Today!

ACCOUNTS OF CHEMICAL RESEARCH*

ISSN 0001-4842

Fred W. McLafferty, Editor; Cornell University

Monthly offering short, critical reviews written by scientists active in the research described.

	U.S.	Canada & Mexico	Europe	All Other Countries
Members				
One Year	\$ 28	\$ 35	\$ 38	\$ 41
Two Years	\$ 50	\$ 64	\$ 70	\$ 76
Nonmembers	\$ 177	\$ 184	\$ 187	\$ 190

ANALYTICAL CHEMISTRY

ISSN 0003-2700

Royce W. Murray, Editor; University of North Carolina, Chapel Hill

The world's foremost publication in the vital field of measurement science. Semi-monthly.

	U.S.	Canada & Mexico	Europe	All Other Countries
Members				
One Year	\$ 36	\$ 72	\$ 117	\$ 141
Two Years	\$ 61	\$ 133	\$ 223	\$ 271
Nonmembers (One Year)				
Personal	\$ 78	\$ 114	\$ 230	\$ 254
Institutional	\$ 415	\$ 451	\$ 496	\$ 520

BIOCHEMISTRY*

ISSN 0006-2960

Gordon G. Hammes, Editor; Duke University

Results of original research in all recognized or developing areas of biochemistry. Weekly.

	U.S.	Canada & Mexico	Europe	All Other Countries
Members				
One Year	\$ 107	\$ 204	\$ 346	\$ 421
Two Years	\$ 192	\$ 386	\$ 670	\$ 820
Nonmembers	\$ 1186	\$ 1283	\$ 1425	\$ 1500

BIOCONJUGATE CHEMISTRY*

ISSN 1043-1802

Claude F. Meares, Editor; University of California, Davis

Six times a year, chemists, biochemists, and molecular biologists find the most important research in conjugation chemistry in this one publication.

	U.S.	Canada & Mexico	Europe	All Other Countries
Members				
One Year	\$ 29	\$ 36	\$ 41	\$ 44
Two Years	\$ 52	\$ 66	\$ 76	\$ 82
Nonmembers	\$ 273	\$ 280	\$ 285	\$ 288

BIOTECHNOLOGY PROGRESS* Co-published with AICHE

ISSN 8756-7938

Jerome S. Schultz, Editor; University of Pittsburgh

This bimonthly publication focuses on the application of fundamental chemical and engineering principles to biological phenomena and to process or product design.

	U.S.	Canada & Mexico	Europe	All Other Countries
ACS/AICHE Members	\$ 30	\$ 38	\$ 47	\$ 53
Nonmembers	\$ 325	\$ 333	\$ 342	\$ 348

CHEMICAL & ENGINEERING NEWS

ISSN 0009-2347

Michael Heylin, Editor

The official publication of the ACS that reports weekly on news and information of interest to chemical professionals. Members receive as part of their dues.

	U.S.	Canada & Mexico	Europe	All Other Countries
Nonmembers				
One Year	\$ 110	\$ 148	\$ 164	\$ 179
Two Years	\$ 198	\$ 274	\$ 306	\$ 336

CHEMICAL RESEARCH IN TOXICOLOGY*

ISSN 0893-228X

Lawrence J. Marnett, Editor; Vanderbilt University

Bimonthly international journal reporting chemical approaches to the solution of toxicological problems.

	U.S.	Canada & Mexico	Europe	All Other Countries
Members				
One Year	\$ 46	\$ 54	\$ 61	\$ 65
Two Years	\$ 82	\$ 98	\$ 112	\$ 120
Nonmembers	\$ 311	\$ 319	\$ 326	\$ 330

CHEMICAL REVIEWS*

ISSN 0009-2665

Josef Michl, Editor; University of Colorado, Boulder

Reviews of research in various areas of chemistry that eliminate the need to scan scores of articles concerning particular fields. 8 issues per year.

	U.S.	Canada & Mexico	Europe	All Other Countries
Members				
One Year	\$ 33	\$ 47	\$ 68	\$ 77
Two Years	\$ 59	\$ 87	\$ 129	\$ 147
Nonmembers	\$ 346	\$ 360	\$ 381	\$ 390

CHEMISTRY & INDUSTRY

ISSN 0009-3068

Andrew Miller, Editor; Society of Chemical Industry, Great Britain

Features news, reviews, and comments on current research, business, and public policy, with a special emphasis on Europe. Semi-monthly.

	U.S., Canada & Mexico	Europe & All Other Countries
Members		
One Year	\$ 59	**
Nonmembers	\$ 330	**

**Contact: Society of Chemical Industry, The Distribution Centre, Blackhorse Road, Letchworth, Herts SG6 1HN, England

CHEMISTRY OF MATERIALS*

ISSN 0897-4756

Leonard V. Interrante, Editor; Rensselaer Polytechnic Institute

This monthly journal gives direction in the fundamentals of materials preparation, characterization, and processing science and technology.

	U.S.	Canada & Mexico	Europe	All Other Countries
Members				
One Year	\$ 49	\$ 64	\$ 80	\$ 89
Two Years	\$ 88	\$ 118	\$ 150	\$ 168
Nonmembers	\$ 375	\$ 390	\$ 406	\$ 415

CHEMTECH

ISSN 0009-2703

Abraham P. Gelbein, Editor

Stimulating, personal monthly helping chemists and engineers arrive at innovative solutions to real problems.

	U.S.	Canada & Mexico	Europe	All Other Countries
Members				
One Year	\$ 39	\$ 48	\$ 55	\$ 60
Two Years	\$ 66	\$ 84	\$ 98	\$ 108
Nonmembers (One Year)				
Personal	\$ 79	\$ 88	\$ 95	\$ 100
Institutional	\$ 370	\$ 379	\$ 386	\$ 391

ENERGY & FUELS*

ISSN 0887-0624

John W. Larsen, Editor; Lehigh University

Bimonthly journal covering all aspects of the transformation, utilization, formation, and production of fuels and non-nuclear energy in addition to studies of fuel structure and properties.

	U.S.	Canada & Mexico	Europe	All Other Countries
Members				
One Year	\$ 48	\$ 56	\$ 64	\$ 68
Two Years	\$ 86	\$ 102	\$ 118	\$ 126
Nonmembers	\$ 345	\$ 353	\$ 361	\$ 365

ENVIRONMENTAL SCIENCE & TECHNOLOGY*

ISSN 0013-936X

William H. Glaze, Editor; University of North Carolina, Chapel Hill

Published monthly for those engaged in environmental study and maintenance through the application of chemical principles.

	U.S.	Canada & Mexico	Europe	All Other Countries
Members				
One Year	\$ 43	\$ 63	\$ 86	\$ 100
Two Years	\$ 73	\$ 113	\$ 159	\$ 187
Nonmembers (One Year)				
Personal	\$ 89	\$ 109	\$ 132	\$ 146
Institutional	\$ 444	\$ 464	\$ 487	\$ 501

MAIL THIS ORDER FORM TODAY!

1993

Please enter my subscription(s) for the following:

Title _____ 1 yr. _____ 2 yrs. _____

Title _____ 1 yr. _____ 2 yrs. _____

(If you wish to enter more than two subscriptions, please use a separate piece of paper and mail with this coupon in an envelope.)

Name _____

Employer _____

Title _____

Address Business Home _____

City _____ State _____ ZIP _____

Payment enclosed. (Payable to American Chemical Society)

Bill Me Bill Company Charge my VISA/MasterCard

Card No. _____

Expires _____ Signature _____

I am an ACS Member I am not an ACS Member

Please send me information on how to become an ACS Member

All journal subscriptions are based on a calendar year. Subscriptions to ANALYTICAL CHEMISTRY, CHEMICAL & ENGINEERING NEWS (nonmembers only), CHEMTECH, and ENVIRONMENTAL SCIENCE & TECHNOLOGY will start the month the order is placed and expire one year later unless subscriber specifies otherwise. Allow 45 days to receive your first issue.

Foreign payment must be made in U.S. dollars by international money order, UNESCO coupons, or U.S. bank draft. Orders accepted through your subscription agency. For nonmember rates in Japan contact Maruzen Co., Ltd.

Air Service Delivery included in all rates listed for countries outside the U.S., Canada, and Mexico.

In a hurry? Call TOLL FREE (800)333-9511 (U.S. only). Outside the U.S. call (614)447-3776.

FAX: (614) 447-3671.

American Chemical Society publications offer:

Reliable and Accurate Research • Techniques • Trends • Discoveries
• Reviews • Developments • And much more!

Take advantage of the most current chemical research and general scientific reporting available — from many respected researchers worldwide.

Use the postage-paid order card below to order your 1993 subscriptions.

INDUSTRIAL & ENGINEERING CHEMISTRY RESEARCH* ISSN 0888-5885

Donald R. Paul, Editor; University of Texas, Austin

This monthly provides timely reports on original work in the broad field of chemical engineering and industrial chemical research.

	U.S.	Canada & Mexico	Europe	All Other Countries
Members				
One Year	\$ 64	\$ 84	\$ 108	\$ 120
Two Years	\$ 115	\$ 155	\$ 203	\$ 227
Nonmembers	\$ 567	\$ 587	\$ 611	\$ 623

INORGANIC CHEMISTRY* ISSN 0020-1669

M. Frederick Hawthorne, Editor; University of California, Los Angeles

Biweekly journal publishes fundamental studies, experimental and theoretical, in all phases of inorganic chemistry.

	U.S.	Canada & Mexico	Europe	All Other Countries
Members				
One Year	\$ 90	\$ 129	\$ 179	\$ 207
Two Years	\$ 162	\$ 240	\$ 340	\$ 396
Nonmembers	\$ 949	\$ 988	\$ 1038	\$ 1066

JOURNAL OF AGRICULTURAL AND FOOD CHEMISTRY* ISSN 0021-8561

Irvin E. Liener, Editor; University of Minnesota

Monthly reporting on original research into the chemical aspects of agriculture and food.

	U.S.	Canada & Mexico	Europe	All Other Countries
Members				
One Year	\$ 32	\$ 50	\$ 72	\$ 85
Two Years	\$ 57	\$ 93	\$ 137	\$ 163
Nonmembers	\$ 335	\$ 353	\$ 375	\$ 388

JOURNAL OF THE AMERICAN CHEMICAL SOCIETY* ISSN 0002-7863

Allen J. Bard, Editor; University of Texas, Austin

Most quoted journal of the widest possible interest to research workers and students in all areas of chemistry. Biweekly.

	U.S.	Canada & Mexico	Europe	All Other Countries
Members				
One Year	\$ 96	\$ 152	\$ 243	\$ 292
Two Years	\$ 172	\$ 284	\$ 466	\$ 564
Nonmembers	\$ 1055	\$ 1111	\$ 1202	\$ 1251

JOURNAL OF CHEMICAL AND ENGINEERING DATA* ISSN 0021-9568

Kenneth N. Marsh, Editor; Texas A&M University

This quarterly journal publishes high-quality experimental data of lasting value.

	U.S.	Canada & Mexico	Europe	All Other Countries
Members				
One Year	\$ 36	\$ 41	\$ 46	\$ 48
Two Years	\$ 64	\$ 74	\$ 84	\$ 88
Nonmembers	\$ 309	\$ 314	\$ 319	\$ 321

JOURNAL OF CHEMICAL INFORMATION AND COMPUTER SCIENCES* ISSN 0095-2338

George W.A. Milne, Editor; National Institutes of Health

Bi-monthly reporting on new R&D. concepts, systems, and programs in all areas of information and computers relative to chemistry.

	U.S.	Canada & Mexico	Europe	All Other Countries
Members				
One Year	\$ 20	\$ 26	\$ 33	\$ 37
Two Years	\$ 36	\$ 48	\$ 62	\$ 70
Nonmembers	\$ 180	\$ 186	\$ 193	\$ 197

JOURNAL OF MEDICINAL CHEMISTRY* ISSN 0022-2623

Philip S. Portoghesi, Editor; University of Minnesota

Biweekly articles on the relationship of chemistry to biological activity. Includes rapid communication of major advances in drug design and development.

	U.S.	Canada & Mexico	Europe	All Other Countries
Members				
One Year	\$ 54	\$ 79	\$ 118	\$ 136
Two Years	\$ 97	\$ 147	\$ 225	\$ 261
Nonmembers	\$ 586	\$ 611	\$ 650	\$ 668

THE JOURNAL OF ORGANIC CHEMISTRY* ISSN 0022-3263

Clayton H. Heathcock, Editor; University of California, Berkeley

Biweekly offering critical accounts of original work and interpretive reviews of existing data that present new viewpoints in organic chemistry.

	U.S.	Canada & Mexico	Europe	All Other Countries
Members				
One Year	\$ 75	\$ 124	\$ 196	\$ 235
Two Years	\$ 135	\$ 233	\$ 377	\$ 455
Nonmembers	\$ 785	\$ 868	\$ 940	\$ 979

JOURNAL OF PHYSICAL AND CHEMICAL REFERENCE DATA* ISSN 0047-2689

Jean W. Gallagher, Editor; National Institute of Standards & Technology

Published bimonthly with the American Institute of Physics and NIST. Presents critically evaluated data on physical and chemical properties.

	U.S.	Canada & Mexico	Europe	All Other Countries
Members (ACS, AIP and affiliated societies)	\$ 85	\$ 95	\$ 105	\$ 105
Nonmembers	\$ 420	\$ 430	\$ 440	\$ 440

THE JOURNAL OF PHYSICAL CHEMISTRY* ISSN 0022-3654

Mostafa A. El-Sayed, Editor; University of California, Los Angeles

Experimental and theoretical research on fundamental aspects of physical chemistry and chemical physics. Weekly.

	U.S.	Canada & Mexico	Europe	All Other Countries
Members				
One Year	\$ 97	\$ 174	\$ 257	\$ 308
Two Years	\$ 174	\$ 328	\$ 494	\$ 596
Nonmembers	\$ 1140	\$ 1217	\$ 1300	\$ 1351

LANGMUIR* ISSN 0743-7463

William A. Steele, Editor; The Pennsylvania State University

Broad coverage of all areas of fundamental surface and colloid science, wet surface chemistry, UHV surface chemistry, disperse systems, electrochemistry. Monthly.

	U.S.	Canada & Mexico	Europe	All Other Countries
Members				
One Year	\$ 68	\$ 89	\$ 116	\$ 129
Two Years	\$ 122	\$ 164	\$ 218	\$ 244
Nonmembers	\$ 715	\$ 736	\$ 763	\$ 776

MACROMOLECULES* ISSN 0024-9297

Field H. Winslow, Editor; AT&T Bell Laboratories

Biweekly publication of original material on all fundamental aspects of polymer chemistry. Critical surveys review history of progress in specific fields.

	U.S.	Canada & Mexico	Europe	All Other Countries
Members				
One Year	\$ 83	\$ 129	\$ 194	\$ 232
Two Years	\$ 149	\$ 241	\$ 371	\$ 447
Nonmembers	\$ 920	\$ 966	\$ 1031	\$ 1069

ORGANOMETALLICS* ISSN 0276-7333

Dietmar Seyferth, Editor; Massachusetts Institute of Technology

Interdisciplinary approach to organometallic chemistry; synthesis; structure and bonding; reactivity and mechanism; application in organic, inorganic, polymer, solid state chemistry, and materials science. Monthly.

	U.S.	Canada & Mexico	Europe	All Other Countries
Members				
One Year	\$ 79	\$ 104	\$ 141	\$ 160
Two Years	\$ 142	\$ 192	\$ 266	\$ 304
Nonmembers	\$ 850	\$ 875	\$ 912	\$ 931

*Indicates periodicals printed on acid-free paper.

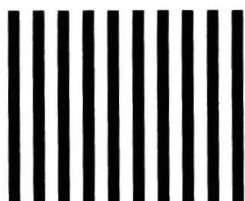
AMERICAN CHEMICAL SOCIETY
Attn: Marketing Communications Department
1155 Sixteenth Street, N.W.
Washington, D.C. 20037-5768

POSTAGE WILL BE PAID BY THE ADDRESSEE

BUSINESS REPLY MAIL
FIRST CLASS PERMIT NO. 10094 WASHINGTON D.C.



NO POSTAGE
NECESSARY
IF MAILED
IN THE
UNITED STATES



stopped carrying sediments up onto areas that are presently at the edge of the cultivation zone. Local conditions resulted in the deposition of sediments derived from the wadi or valley running perpendicular to the Nile at Nekhen. The trace element characteristics indicated that this local wadi material differed from the normal Nile sediments. The limited area covered by this sediment layer (deposited between 5200 B.P. and 4500 B.P.) suggested that it was deposited by water flowing through the wadi toward the Nile. This result could indicate that the Nile floods were not as great, thus limiting the normal agricultural pattern along the Nile; but the area along the wadi could have still supported a form of agricultural activity requiring irrigation. In this light the Scorpion macehead may be a reflection of the growing importance of irrigation as a focal point of community organization and perhaps political power.

About 4500 B.P., well after unification of the Two Lands, the Nile sediments were again deposited in the area far beyond its banks, but the total amount of sediment was less. We have observed that there was a difference in the trace element ratios between the pre-5200 B.P. Nile sediments and those deposited after 4500 B.P. This was interpreted as a change in the relative contribution from the two Nile sources.

The observations made at Nekhen are important for understanding the predynastic period and could be explained by a model involving major changes in the climate of central and east Africa and reflecting the local conditions in southern Egypt. This model could be tested by looking for similar changes elsewhere in the Nile sediments. Samples to test the model of climatic changes that affect the sediment composition were available as cores taken from the accumulated sediments in the Nile Delta.

The Nile Delta and its continuous

submarine extension are the repository for the sediments transported by the Nile from areas in central and east Africa, some of which are more than 6000 km away. Evidence of oscillations in the climatic conditions of the Nile drainage basins have been supported by observations of relic lake levels, locations of playa (flat-floored bottom of a desert basin) and wadi deposits, changes in the sediment yield, and the grain size distribution in the Nile sediments. Several investigators have observed that although the amounts of certain heavy (more dense) mineral fragments in the sand-sized fraction were small, the differences over time could be related to the relative contributions of materials from the different geological terrains.

The Nile Delta

As part of a project directed toward a better understanding of the Mediterranean and the Nile, the Smithsonian Institution obtained more than 100 core samples from the Nile Delta. Observations of the heavy minerals in these core samples indicated oscillations in the total sediment load and the relative contributions from the different terrains in Africa.

The major problem with using the heavy minerals as an index of change in Nile sediments is a statistical one. The small abundance of the minerals used, and irregularities in local transport and deposition of the suspended sediments, creates considerable variability (noise). Detailed studies of sediments at Nekhen suggested that the analysis of the light mineral fraction (by far the most abundant) of the sand-sized grains could provide a statistically reliable index of the same changes. Thus NAA was used to analyze more than 90 samples (light minerals from sand-sized fractions) from three separate cores of Nile sediments from the northeastern part of the delta.

The elements studied were based in part on observations made in the Nekhen studies and new data on trace element concentrations in sediments from the Blue Nile and the White Nile. Cr was studied, and Sc (which could be measured with greater precision than Th or Hf) was used as an indication of material from central Africa. Analysis of samples of material from the Blue Nile and the White Nile indicated that although rare-earth elements (lanthanides) were present in both, relative distributions (e.g., the ratio of La to Lu) differed.

When the central African source contributes more to the sediment load, the La/Lu ratio should be higher and should decrease because a greater percentage of the sedimentary material was found to originate from the east African (Ethiopian) region. When the sand fraction from the Nile Delta core samples was analyzed, the La/Lu ratio varied significantly. The oscillation observed with depth for one of the core samples is shown in Figure 4. Variations in the elemental ratios for the sand fraction in the different cores could not be compared on the basis of depth. The delta is a flat flood plain through which channels of water have moved over time, resulting in variations in depositional patterns. There was no pottery to provide approximate dates as at Nekhen, but ^{14}C dating for some samples in the core provided a means of estimating the deposition (Figure 4). For lack of a more exact method, it was assumed that the sediments had accumulated at a constant rate (cm/yr) between times where there was a ^{14}C date. Using this information, it was possible to relate the samples taken at various levels in each core to an estimated time in the past.

Although this averaging method is inexact, it does allow for the comparison of samples from different cores that were deposited at approximately

©

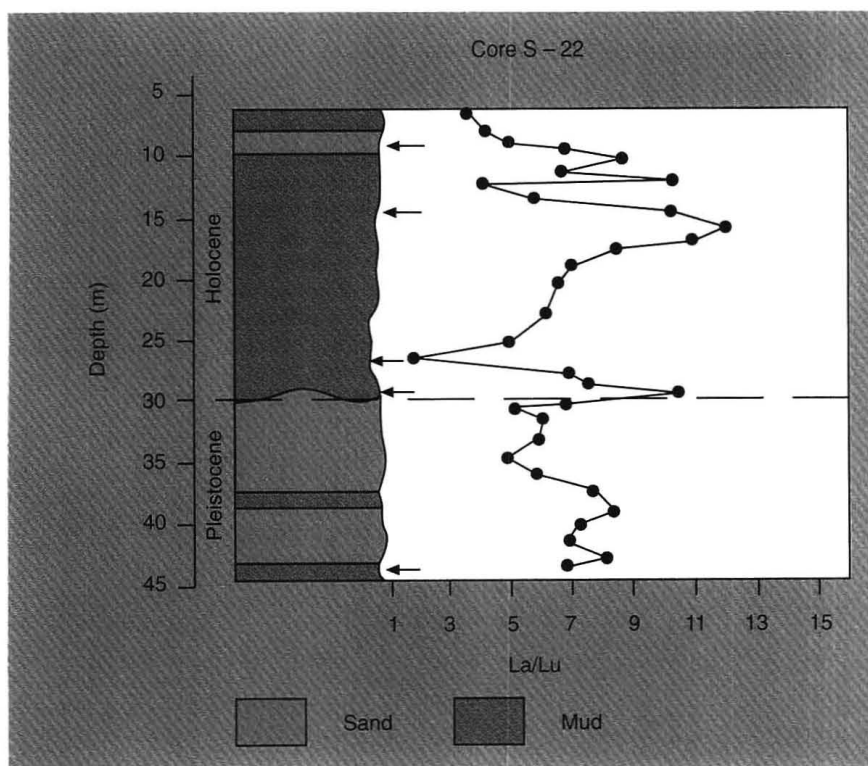


Figure 4. Ratio of normalized concentrations of La and Lu in samples from one core (designated S-22) taken about 25 km south of Port Said in the northeastern Nile Delta.

The 32 samples of sand-sized material from this core were analyzed by NAA, and the lanthanide concentrations were normalized to the concentrations in chondritic meteorites ($La = 0.33$ ppm, $Lu = 0.034$ ppm) before calculation of the La/Lu ratio shown. The material, ranging from sandy coarser sediments (designated sand) to finer silt (designated mud), represents changing depositional conditions over time. The exact rate of accumulation is not known, but five different segments of the core yielded ^{14}C dates noted by the arrows. Starting from near the surface at ~ 10 m depth, the dates were 3770 ± 90 B.P.; 4670 ± 80 B.P.; 6630 ± 150 B.P.; 7540 ± 70 B.P.; and, at about 45 m, $24,320 \pm 230$ B.P.

the same time. The samples deposited contemporaneously did match quite well in terms of the elemental ratios. Figure 5 represents the average of the concentration ratios for the three cores examined within an estimated time period (± 200 years) as a function of time. Variations in the Cr/Sc ratio in the sand fraction as a function of time are interpreted as being directly related to the climatic conditions at the Nile headwaters.

For example, during a wet phase on the Ethiopian plateau, the sediment load from the Blue Nile and the Atbara rivers would increase and thus the Cr/Sc ratio in the sand fraction should increase. The detailed interpretation of variations in the chemistry of mineral grains in the sand fraction may be more complex

than simply determining which area had more rain. For example, it has been suggested that after a wet phase began, a denser vegetation coverage and therefore a lesser amount of eroded soil would result. Although the flood water levels would remain high, the sediment load (and deposition) could decrease. Details of the changes in climate may not be clearly understood, but the variations in these elemental ratios do seem to indicate long-term changes in the climatic conditions throughout the large region of central and east Africa.

The periodic changes suggested in Figure 5 require further investigation; however, some changes are worth noting because they coincide with major anthropological events in Egypt. The model explaining why

these trace element ratios change suggests that around 6400 B.P. there was a maximum of flooding and sediment load from the Ethiopian plateau. This theory is consistent with independent geological observations in Ethiopia. Interestingly, this is the time frame for the beginning of what archaeologists have described as the predynastic period in Egypt.

The other notable change is between 5600 B.P. and 5200 B.P., when floods and sediments from Ethiopia were at a minimum. This low sediment load (low accumulation rate) from one source appears to have been exacerbated around 5200 B.P., when floods from central Africa (the major source of the sediment load) also decreased dramatically. The lower levels of flood waters were apparent at Nekhen between 5200 B.P. and 4500 B.P., as suggested by the accumulation rates indicated by the Delta cores. Whereas the overall amount of sediment (floods) decreased, relative contributions from the two general sources changed. The Cr/Sc ratio increased somewhat, and the La/Lu ratio changed dramatically.

These changes coincide with the era that marks the beginning of the dynastic period with the unification and creation of the first nation state. All of this information may indicate that the climatic changes that dramatically affected the Nile floods throughout the valley and over extended periods of time may have been important to the evolution of the society along the banks of the river.

Another factor may have influenced the development of the state of early Egypt. The so-called predynastic culture with its characteristic pottery was associated with upper Egypt and not the delta. Archaeological sites from the same early period have been found in lower Egypt, but this area may not have been as predictable and as easy for communities to develop. It may be important to understand more about the development of the delta itself. The level of the present Mediterranean Sea differed considerably in the past; beach-level studies indicate that the water level of the Mediterranean was much lower 7000 years ago. Data suggest a steady increase in sea level from 7000 B.P. From a sedimentological

PAPERED OVER?



Let CA SELECTS® Uncover You!

Subscribe to CA SELECTS. We will free you from mounds of extraneous papers... and uncover the information you need.

CA SELECTS is a series of nearly 250 different current-awareness publications. These printed bulletins provide the same bibliographic information, abstracts, and structure diagrams (when available) that you find in CHEMICAL ABSTRACTS® but focused on specialized topics.

With CA SELECTS, you can relax while a computer profile searches for current literature relevant to your interests. This information is sent to you automatically every two weeks.

All this is yours for just pennies per abstract. Annual subscription: \$210 in the U.S.; \$229 in Canada, Mexico, and Central America; \$242 elsewhere. Ask for our FREE catalog.

Let CA SELECTS strip away your mounting mass of papers! Act Now!

For faster response, complete the coupon, and FAX this ad to 614/447-3713!

YES! Please send me the catalog describing nearly 250 topics.

Name _____

Job Title _____

Organization _____

Address _____

City _____ State/Zip _____

Country _____

Business Phone _____



Marketing Dept. 30693
2540 Olentangy River Road
PO. Box 3012
Columbus, Ohio 43210-0012 U.S.A.



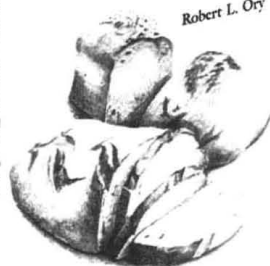
ORY

GRANDMA CALLED IT
Roughage

Fiber Facts and Fallacies

GRANDMA CALLED IT *Roughage*

Robert L. Ory



Grandma Called It Roughage

Fiber Facts and Fallacies

This semi-technical volume, written specifically for non-scientists, is must-reading for anyone concerned about health and nutrition. With scientific facts to support the statements made about the known health benefits of fiber, Dr. Ory offers an interesting, sometimes humorous, approach that will appeal to the general reader.

Although not intended to be the final word on dietary fiber (research goes on continually), the book is intended to quell rumors about dietary fiber and to inform those who don't understand enough about fiber's benefits and limitations.

The author also offers some of his own recipes for simple and tasty high-fiber foods, including Bread Pudding, New Orleans Style Red Beans, and Eggplant Lasagna.

Contents

- Fibermania and How It Began
- What Is Fiber and Where Do We Find It?
- Fiber and Metabolism vs. Fat and Cholesterol
- Can Fiber Fight Fat?
- Fiber and the Big "C"—Constipation!
- Can Fiber Cure Cancer, Diabetes, or Other Diseases?
- Fiber and Mineral Nutrition
- Is Fiber an Essential Nutrient?
- Breakfast Cereals: The Battle of the Brans
- Fiber in Fruits and Vegetables
- Can Fiber Be Good for You and Still Taste Good?

Robert L. Ory, Ph.D.

160 pages (1991)

Clothbound: ISBN 0-8412-1749-1

\$22.95

Paperbound: ISBN 0-8412-1764-5

\$12.95

O · R · D · E · R · F · R · O · M

American Chemical Society
Distribution Office, Dept. 21
1155 Sixteenth St., N.W.
Washington, DC 20036

or CALL TOLL FREE

800-227-5558

(in Washington, D.C. 872-4363) and use your credit card!

ANALYTICAL APPROACH

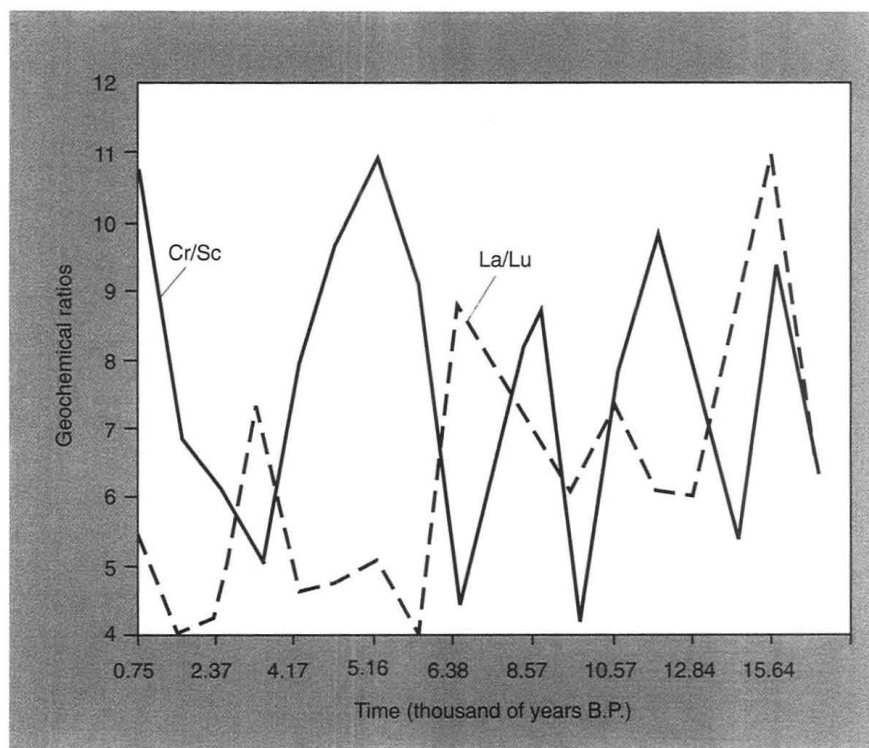


Figure 5. Change in the normalized La/Lu and Cr/Sc ratios in light sand-sized fractions of cores from the Nile Delta.

The values represent the averages for three cores, each of which accumulated at different and varying rates over time. ^{14}C dates for each core were used to estimate accumulation rates among dated samples and to convert the sample depth to an approximate date when it was deposited. Although the dates of deposition are probably no better than ± 200 years, samples from different cores or different depths can be compared and averages determined for samples that were deposited within a similar time frame (400 years). Changes in each ratio reflect differences in the relative contributions of sediments over time from the major sources of the Nile.

point of view, an increase in the sea level and in high floods with large sediment loads (as suggested by the trace element ratios and the heavy minerals) would result in the development of a broad delta. Thus a new landform was rapidly being built up from 7000 B.P. to about 5200 B.P. At this point (on the basis of the results at Nekhen), the level of Nile floods decreased markedly.

It is interesting to speculate that when agricultural practices in upper Egypt (which depended on large annual floods) became more difficult to maintain, a large area of more usable agricultural land had formed in the north. The delta region had grown, and with less flooding it probably became more useful for crops—especially with the implementation of irrigation techniques. Could climatic changes have caused a disruption of the agricultural practices and hence society in the south? A need to create extensive irrigation and possibly share resources may have evolved. It is perhaps a simplification to propose a model to explain how environmental stress could lead to increased de-

pendency on irrigation and thus to managerial bureaucracy and eventually despotic control.

Although the unification of upper and lower Egypt may be, as has been suggested by some Egyptologists, attributable to a new race of conquerors, the climatic changes suggested by the sediments may provide a more satisfying explanation. The people in the south may have united in an effort to adapt to environmental changes. Whether they united voluntarily or whether the people of the south conquered the people of the north (as suggested by legends) because they had a large, relatively new and fertile land mass that could be used to help feed the populace, is still not known. These are only speculations, but it is becoming clearer that major climatic changes disrupted this society. However unification occurred, the people along the Nile did overcome the adversity and survived.

Summary

Data on elemental concentrations of trace constituents in complex natural

samples have been made possible by advances in analytical instrumentation. However, as more data of known quality (accuracy) are produced, methods for data analysis and interpretation become more vital to analytical chemists. Pattern recognition is aided by statistical programs, but ultimately we must be able to understand something about the materials being analyzed. Choice of samples or portions of samples to be analyzed should be based on an understanding of the materials and the questions to be addressed. Often, reasonable interpretations and the development of new ideas result from interaction between the analyst and investigators from other disciplines. This article demonstrates the value of this approach.

Without insight developed from geological, geochemical, meteorological, and archaeological input, the analytical data would not have led to the important hypothesis that climatic changes in Africa, and the response to those changes, resulted in the cultural and societal changes that were so important in the evolution of civilization.

Suggested reading

- Archaeological Chemistry IV*; Allen, R. O., Ed.; American Chemical Society: Washington, DC, 1989.
- Allen, R. O.; Hamroush, H. A.; Hoffman, M. A. *Anal. Chem.* **1986**, *58*, 572 A-575 A.
- Butzer, K. W. *Environment and Archaeology*; Aldine Publishing Co.: New York, 1966.
- Followers of Horus*; Friedman, R.; Adams, B.; Eds.; Oxbo Monograph 20; Petrie Museum of Egyptian Archaeology: Oxford, England, 1992.
- Hamroush, H. A.; Stanley, D. J. *Episodes* **1990**, *13*, 264-69.
- Hoffman, M. A. *Egypt before the Pharaohs: The Prehistoric Foundation of Egyptian History*; Knopf: New York, 1979.
- Problems of Prehistory: North Africa and the Levant*; Wendorf, F.; Marks, A., Eds.; SMU Press: Dallas, TX, 1975.

Ralph O. Allen is a professor of chemistry and a professor of environmental sciences at the University of Virginia. He received a B.A. degree from Cornell College (IA) in 1965 and a Ph.D. in analytical chemistry from the University of Wisconsin-Madison in 1970. His research interests include studies of trace elements in a variety of different geological materials such as lunar, meteoritic, and archaeologically significant materials. He directs the university's environmental health and safety program.

Hany Hamroush teaches at Cairo University (Giza, Egypt) and at the American University in Cairo. He is also scientific attaché at the American Embassy in Cairo. His bachelor's and master's degrees in geology are from Cairo University, and he received a Ph.D. in chemistry at the University of Virginia in 1985. His research interests lie in the geochemical behavior of trace elements in Nile sediments and the impact of environmental changes on the monuments and the heritage of Egypt.

Daniel J. Stanley is senior oceanographer and director of the Mediterranean Basin Program at the U.S. Museum of Natural History, Smithsonian Institution, in Washington, DC. He received a B.S. degree from Cornell University in 1956, a M.Sc. degree from Brown University in 1958, and a D.Sc. from the University of Grenoble (France) in 1961. He has been involved in geological investigations emphasizing the origin of the Atlantic margin off North America and the Mediterranean. He has directed the Nile Delta project, an international and multidisciplinary effort to study the origins of the Nile Delta and its relationship to the Nile River Valley.

For Those Involved in the Vital Field of Surface and Colloid Chemistry

Langmuir

The ACS Journal of Surfaces and Colloids

Each month, *Langmuir* subscribers receive broad coverage that brings together research from all aspects of the field: ultra-high vacuum surface chemistry and spectroscopy, heterogeneous catalysis, and all aspects of interface chemistry involving fluids, and disperse systems.

Langmuir publishes peer-reviewed research in:

- * "Wet" Surface Chemistry * "UHV" Surface Chemistry
- * Disperse Systems * Electrochemistry
- * Surface Structure; tunneling electron microscopy

EDITOR

William A. Steele, The Pennsylvania State University

ASSOCIATE EDITORS

- A. Bradshaw, Max Planck Institute, Germany
- R.L. Rowell, University of Massachusetts
- J.T. Yates, Jr., University of Pittsburgh

1993 Rates	ACS Members*		Nonmembers
	1 year	2 years	1 year
U.S.	\$ 68	\$122	\$715
Canada & Mexico	\$ 89	\$164	\$736
Europe**	\$116	\$218	\$763
All Other Countries**	\$129	\$244	\$776

* Member rate is for personal use only.
** Air service included.

ISSN 0743-7463

For more information or to subscribe, write:
American Chemical Society
Member and Subscriber Services
P.O. Box 3337
Columbus, OH 43210

In a hurry?

Call Toll Free (800) 333-9511 (within the U.S.), or (614) 447-3776 (outside the U.S.), or Fax your order to (614) 447-3671.

LABORATORY SERVICE CENTER

NMR ANALYSIS

Multinuclear Multifield
Liquid or Solid State
GLP Compliance

Spectral Data Services, Inc.
818 Pioneer, Champaign, IL 61820
(217) 352-7084 Fax (217) 352-9748

FREE DATA, FAST

To quickly amass data on all of the products you need, consult the Lab Data Service section on our *Analytical Chemistry* reader reply card insert.

LABORATORY SERVICE CENTER

(Equipment, Materials, Services, Instruments for Leasing), Maximum space — 4 inches per advertisement. Column width, 2-3/16"; two column width, 4-9/16". Artwork accepted. No combination of directory rates with ROP advertising. Rates based on number of inches used within 12 months from first date of first insertion.

Per inch: 1" — \$185; 12" — \$180; 24" — \$175; 36" — \$170; 48" — \$165.

CALL OR WRITE JANE GATENBY

ANALYTICAL CHEMISTRY

1599 Post Road East
P.O. Box 231
Westport, CT 06881
203-256-8211
FAX: 203-256-8175

HELP WANTED ADS

ROP display at ROP rates. Rate based on number of insertions within contract year. Cannot be combined for frequency.

Unit	1-TI	6-TI
1" (25 mm)	\$210	\$190
	12-TI	24-TI
	\$180	\$170

CALL OR WRITE JANE GATENBY

ANALYTICAL CHEMISTRY

1599 Post Road East
P.O. Box 231
Westport, CT 06881
203-256-8211
FAX: 203-256-8175

**Supplementary
Material
is available
for this journal!**

**Need more information
than is provided in an article?
Need tables? Diagrams?**

Supplementary Material is the answer!

Articles with Supplementary Material available have a black box by the page number in the table of contents. And, a notice of its availability will appear at the conclusion of the paper.

To order your Supplementary Material. . .

Send your order with payment for either photocopies or 24X microfiche to:

American Chemical Society
Microforms and Back Issues Office
1155 Sixteenth St., N.W.
Washington, D.C. 20036

The rates are: \$10 for microfiche (add \$1 for postage outside the U.S. and Canada)

\$10 for photocopies up to 3 pages, plus \$1.50 per page for each additional page (Add \$2 for postage outside the U.S. and Canada)

Please give complete title of article, authors' names, journal, issue date, and page numbers.

Or call 202-872-4554 and charge your order to your MasterCard, VISA, or American Express.

An annual subscription to Supplementary Material is available. . .

If you want all the Supplementary Material as it is published, why not enter an annual subscription to Supplementary Material? Annual subscription rates (available in microfiche only) are listed on the masthead page. Or, subscribe to the package plan, where you will receive all Supplementary Material (those with subscriptions and those without subscriptions) for \$400 (U.S.) or \$550 (for all other countries).

INDEX TO ADVERTISERS IN THIS ISSUE

Advertising Management for the American Chemical Society Publications

CIRCLE INQUIRY NO.	ADVERTISERS	PAGE NO.
12	*J.T. Baker, Inc. Stiegler, Wells & Brunswick, Inc.	4A
24	*Dionex Corporation Brooks Communications, Inc.	IFC
30, 31	*EG&G Princeton Applied Research Kilgore Associates	25A
46	*Hamamatsu Corporation SSD&W	22A
72	3M Disposable Products Division Campbell-Mithun-Esty	16A
70	*Mattson Instruments, Inc. Fourier Court Advertising	6A
80	*Nicolet Analytical Instruments	8A
90	PITTCON '93 The Pittsburgh Conference	OBC
112	*Varian Lanig Associates	14A
118	Whatman	3A

CENTCOM, LTD.

President

James A. Byrne

Executive Vice President

Benjamin W. Jones

Joseph P. Stenza, *Production Director*

1599 Post Road East
P.O. Box 231
Westport, Connecticut 06881-0231
(Area Code 203) 256-8211
Fax No. 203-256-8175

DIRECTOR, ADVERTISING SALES, LABORATORY PRODUCTS

Bruce E. Poorman

ADVERTISING PRODUCTION MANAGER

Jane F. Gatenby

SALES REPRESENTATIVES

Philadelphia, PA. . . . Matthew J. McCloskey, CENTCOM, LTD. GSB Building, Suite 405, 1 Belmont Ave., Bala Cynwyd, PA. 19004. Telephone: 215-667-9666, FAX: 215-667-9353

New York/New Jersey . . . Dean A. Baldwin, John F. Rafferty, CENTCOM, LTD., Schoolhouse Plaza, 720 King Georges Post Road, Fords, NJ 08863, Telephone: 908-738-8200, FAX: 908-738-6128

Westport, CT./Boston, MA. . . . Dean A. Baldwin, Michael J. Pak, CENTCOM, LTD., 1599 Post Road East, P.O. Box 231, Westport, CT 06881-0231. Telephone: 203-256-8211, FAX: 203-256-8175

Cleveland, OH. . . . Bruce E. Poorman, Dean A. Baldwin, CENTCOM, LTD., 325 Front St., Suite 2, Berea, OH 44017. Telephone: 216-234-1333, FAX: 216-234-3425

Chicago, IL. . . . Michael J. Pak, CENTCOM, LTD., 540 Frontage Rd., Northfield, IL. 60093. Telephone: 708-441-6383, FAX: 708-441-6382

Houston, TX./Atlanta, GA. . . . Edward M. Black, CENTCOM, LTD., 1599 Post Road East, P.O. Box 231, Westport, CT 06881-0231. Telephone: 203-256-8211, FAX: 203-256-8175

San Francisco, CA. . . . Paul M. Butts, Jay S. Francis, CENTCOM, LTD., Suite 808, 2672 Bayshore Parkway, Mountain View, CA 94043. Telephone: 415-969-4604, FAX: 415-969-2104

United Kingdom, Scandinavia and Europe (Except: Germany, Switzerland, Austria) . . . Malcolm Thiele, Technomedia Ltd., Wood Cottage, Shurlock Row, Reading RG10 0QE, Berkshire, England. Telephone: 0734-343302, FAX: 0734-343848

Germany, Switzerland, Austria . . . InterMedia Partners, GmbH, Deutscher Ring 40, 5600 Wuppertal 11, Germany. Telephone: (0202) 711091, FAX: (0202) 712431

Tokyo, Japan . . . Sumio Oka, International Media Representatives Ltd., 1-11-5-502, Tamazutsumi, Setagaya-ku, Tokyo 158 Japan. Telephone: 502-0656, Telex #22633, FAX: 5706-7349

Asia (Except Japan) . . . Bruce E. Poorman, CENTCOM, LTD., 325 Front St., Suite 2, Berea, OH 44017. Telephone: 216-234-1333, FAX: 216-234-3425

South America . . . Bruce E. Poorman, CENTCOM, LTD., 325 Front St., Suite 2, Berea, OH 44017. Telephone: 216-234-1333, FAX: 216-234-3425

Directory section, see page 44A.

* See ad in ACS LabGuide.



**NEW RELEASES FROM THE
ACS SYMPOSIUM SERIES**

ACS BOOKS

Phenolic Compounds in Food and Their Effects on Health I: Analysis, Occurrence, and Chemistry

Covers the study of the occurrence and analytical methodology of polyphenol complexation in food. Examines the effects of phenolic compounds on the flavor, taste, color, texture, and nutritional quality of food. Explores the use of phenolic antioxidants in foods.

Chi-Tang Ho, Chang Y. Lee, and Mou-Tuan Huang, Editors

ACS Symposium Series No. 506
338 pages (1992)
Clothbound
ISBN 0-8412-2475-7
\$74.95

Phenolic Compounds in Food and Their Effects on Health II: Antioxidants and Cancer Prevention

Examines the sources of phenolic antioxidants. Covers the chemical and biological activities of phenolic compounds in food and their health effects, especially the biological properties of phenolic compounds on the modulation of tumor development in experimental animal models and possibly in humans. Explores flavonoids, green tea, and other phenolic compounds in relation to cancer prevention. Together with *Phenolic Compounds in Food and Their Effects on Health I*, this volume represents the most up-to-date studies of the antioxidative and anticarcinogenic activities of phenolic compounds in food.

Mou-Tuan Huang, Chi-Tang Ho, and Chang Y. Lee, Editors

ACS Symposium Series No. 507
402 pages (1992) Clothbound
ISBN 0-8412-2476-5
\$84.95

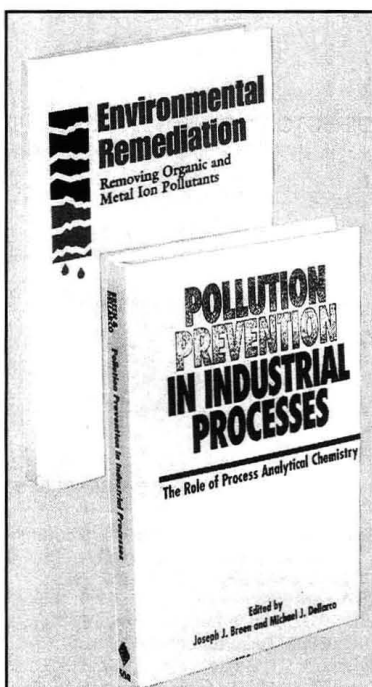
Two-volume set
ISBN 0-8412-2501-X
\$149.95

Pollution Prevention in Industrial Processes: The Role of Process Analytical Chemistry

Features chapters from industry on the successful application of modern process analytical chemistry to problems of waste minimization, source reduction, and pollution prevention. Examines recent academic and U.S. Department of Energy efforts in the development and potential use of on-line analysis to monitor industrial processes. Showcases the National Science Foundation's highly successful university-industry-government cooperative research program at University of Washington's Center for Process Analytical Chemistry.

Joseph J. Breen and Michael J. Dellarco, Editors

ACS Symposium Series No. 508
316 pages (1992)
Clothbound
ISBN 0-8412-2478-1
\$79.95



Biosensor Design and Application

Presents a contemporary discussion of currently available and potential applications of biosensors. Examines diverse approaches to the basic problems of microsizing analytical instrumentation, including the use of intact crustacea antenna, various forms of redox reactions, use of antibody-mediated reactions, and optical- and spectrophotometric-based methods.

Paul R. Mathewson and John W. Finley, Editors

ACS Symposium Series No. 511
204 pages (1992) Clothbound
ISBN 0-8412-2494-3
\$54.95

Environmental Remediation: Removing Organic and Metal Ion Pollutants

Examines waste treatment and the applications of separation science to waste minimization and preconcentration. Presents fundamental research for developing new technologies in the remediation of contaminated aquifers and surface and subsurface media. Includes an overview chapter examining the extent of environmental abuse, the high cost of cleanup, and the federal regulations that govern cleanup and disposal of present waste.

G. F. Vandegrift, D. T. Reed, and I. R. Tasker, Editors

ACS Symposium Series No. 509
270 pages (1992) Clothbound
ISBN 0-8412-2479-X
\$66.95

Pesticide Waste Management: Technology and Regulation

Discusses the disposal of pesticides and pesticide containers. Analyzes the current status of pesticide disposal and identifies problems yet to be resolved. Examines progress in the development of pesticide disposal technology and highlights successful implementation of disposal programs. Includes case studies of Minnesota state pesticide waste management programs. Reviews the current regulations pertinent to the area.

John B. Bourke, Allan S. Felsot, Tomas J. Gilding, Janice King Jensen, and James N. Seiber, Editors

ACS Symposium Series No. 510
278 pages (1992) Clothbound
ISBN 0-8412-2480-3
\$64.95

Chromatography of Pharmaceuticals: Natural, Synthetic, and Recombinant Products

Features chapters on the analysis of natural and recombinant pharmaceutical products. Covers new techniques such as capillary electrophoresis and a number of hyphenated techniques that combine liquid chromatography or gas chromatography with mass spectrometry. Describes such applications as impurity analysis, chiral separations, metabolic studies, robotics, and support of biotechnology products. Also describes trace and ultratrace analyses in a variety of matrices.

Satinder Ahuja, Editor

ACS Symposium Series No. 512
214 pages (1992) Clothbound
ISBN 0-8412-2498-6
\$59.95

ORDER FROM:
American Chemical Society, Distribution Office, Dept. 53, 1155 16th St., N.W., Washington, DC 20036. Or CALL TOLL FREE 800-227-5558, or in Washington, DC, 202-872-4363 and use your credit card!

AC RESEARCH

Heat-Induced Conformational Changes in Proteins Studied by Electrospray Ionization Mass Spectrometry

Urooj A. Mirza, Steven L. Cohen, and Brian T. Chait*

The Rockefeller University, New York, New York 10021

A simple and effective device for investigating heat-induced denaturation of proteins by electrospray ionization mass spectrometry is described. Results are presented for the denaturation as a function of temperature and solution pH of bovine ubiquitin and bovine cytochrome *c*. These results are in concert with and extend the earlier results of LeBlanc et al. (*Org. Mass Spectrom.* 1991, 26, 831). The cooperative effects of pH and temperature on the denaturation of ubiquitin and cytochrome *c* were investigated. Electrospray ionization mass spectrometry is also shown to be a useful probe of the reversibility of heat-induced denaturation of proteins. Finally, it is demonstrated that heat-induced denaturation can be used to improve the mass spectrometric response of proteins that do not normally yield useful spectra when the solubilized protein is electrosprayed at ambient temperatures.

INTRODUCTION

In their native state, globular proteins are tightly folded, compact structures that can be denatured and caused to unfold by subjecting them to extremes of pH, denaturants such as guanidinium hydrochloride, organic solvents, detergents, and high temperatures.¹ A variety of techniques have been applied to the measurement of conformational changes of proteins in solution, including acid-base titrations, calorimetry, spectrophotometry, viscometry, circular dichroism, fluorescence, and nuclear magnetic resonance.^{2,3} Recently, we and others have demonstrated that conformational changes of proteins can also be detected by electrospray ionization mass spectrometry.⁴⁻⁸

Electrospray is a gentle method of ionization that produces intact, multiply protonated gas-phase ions directly from

(1) Creighton, T. E. *Proteins: Structures and Molecular Principles*; W. H. Freeman: New York, 1984. Dill, K. A.; Shortle, D. *Ann. Rev. Biochem.* 1991, 60, 795-825.

(2) Ghelis, C.; Yon, J. *Protein Folding*; Academic Press: New York, 1982. Lapanje, S. *Physical and Chemical Aspects of Protein Denaturation*; Wiley Interscience: New York, 1978.

(3) Wuthrich, K. *NMR Of Proteins and Nucleic Acids*; Wiley Interscience: New York, 1986.

(4) Chowdhury, S. K.; Katta, V.; Chait, B. T. *J. Am. Chem. Soc.* 1990, 112, 9012.

(5) Katta, V.; Chait, B. T. *Rapid Commun. Mass Spectrom.* 1991, 5, 214.

(6) Katta, V.; Chait, B. T. *J. Am. Chem. Soc.* 1991, 113, 8534.

(7) Loo, J. A.; Loo, R. R. O.; Udseth, H. R.; Edmonds, C. G.; Smith, R. D. *Rapid Commun. Mass Spectrom.* 1991, 5, 101.

(8) Le Blanc, J. C. Y.; Beuchemin, D.; Siu, K. W.; Guevremont, R.; Berman, S. S. *Org. Mass Spectrom.* 1991, 26, 831.

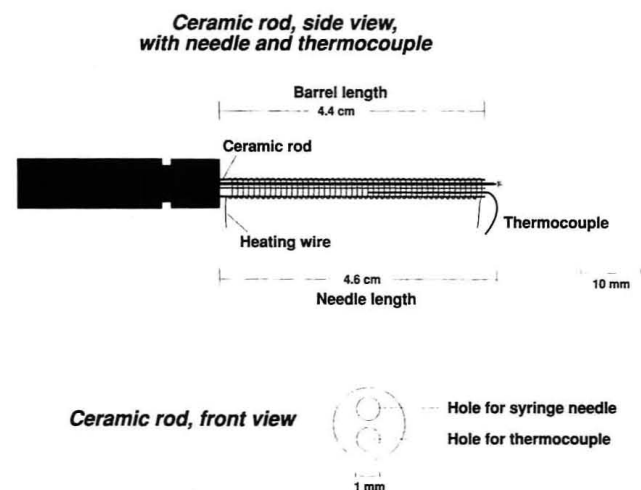


Figure 1. Apparatus for heating and controlling the temperatures of protein solutions just prior to electrospray.

protein molecules in solution.⁹⁻¹² The multiply charged ions observed in the positive-ion spectra are produced by proton attachment to basic and deprotonated acidic sites in the protein and reflect, to some extent, the degree of protonation in solution.¹³ Because the accessibility and the effective pK values of the acidic and basic side chains are determined by the precise conformation that the protein assumes under the conditions of study, the conformation can be probed by the extent to which the protein is observed to be protonated in electrospray ionization.⁴⁻⁸

Chowdhury, Katta, and Chait⁴ demonstrated this new probe in an investigation of conformational changes in bovine cytochrome *c*, bovine ubiquitin, and yeast ubiquitin induced by changes in pH and by the addition of organic solvent denaturants. Dramatic differences were observed in the charge state distributions obtained from the native versus denatured proteins. The conformations of these proteins were

(9) Fenn, J. B.; Mann, M.; Meng, C. K.; Wong, S. F.; Whitehouse, C. M. *Science* 1989, 246, 64.

(10) Covey, T.; Bonner, R. F.; Shushan, B. I.; Henion, J. *Rapid Commun. Mass Spectrom.* 1988, 2, 249.

(11) Smith, R. D.; Loo, J. A.; Edmonds, C. C.; Barinaga, C. J.; Udseth, H. R. *Anal. Chem.* 1990, 62, 882.

(12) Chowdhury, S. K.; Katta, V.; Chait, B. T. *In Methods and Mechanisms for Producing Ions from Larger Molecules*; Standing, K. G., Eds.; Plenum Press: New York, 1991; p 201.

(13) Guevremont, R.; Siu, K. W. M.; Le Blanc, J. C. Y.; Berman, S. S. *J. Am. Soc. Mass Spectrom.* 1992, 3, 216.

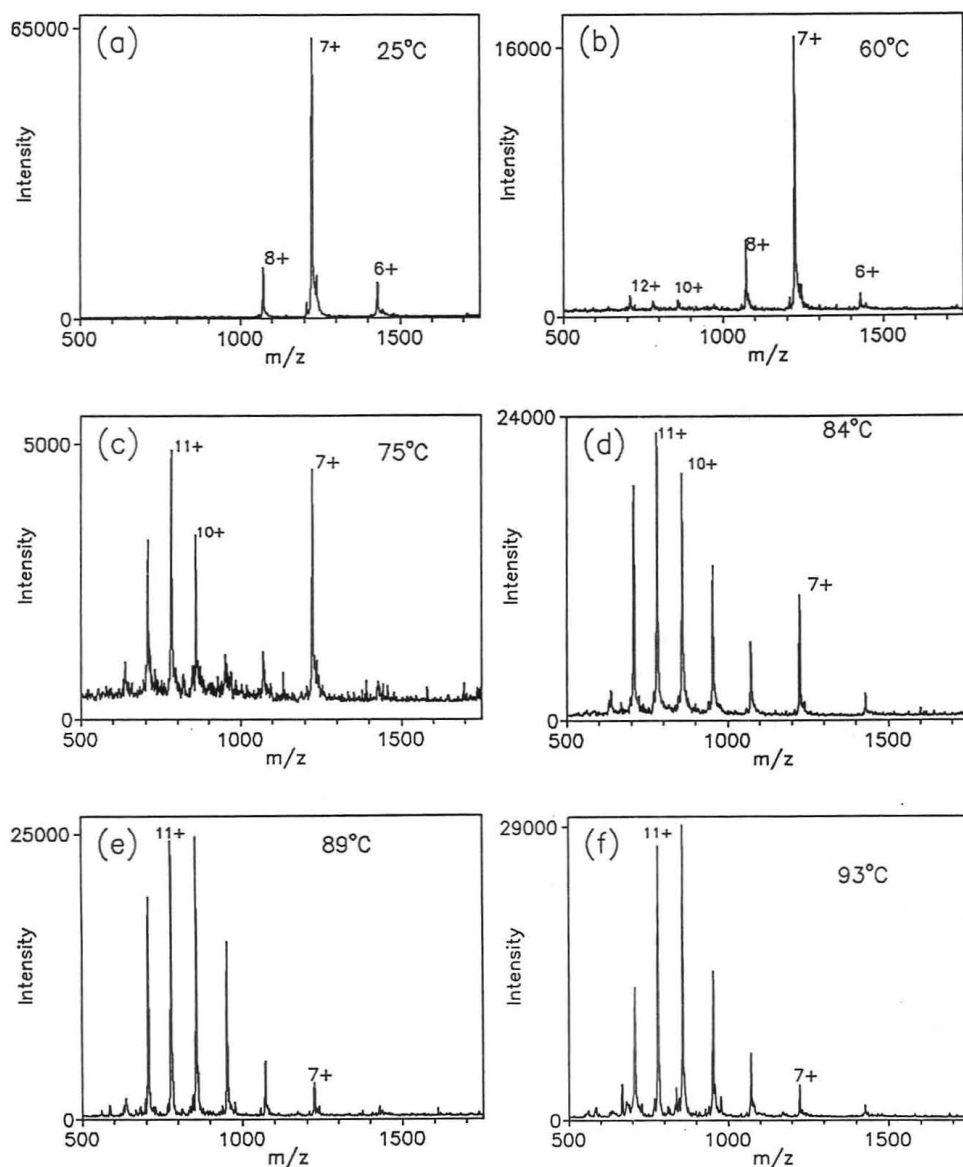


Figure 2. Electro spray ionization mass spectra of bovine ubiquitin in water and acetic acid (pH 2.8) obtained at a series of different temperatures. Protein concentration: 2×10^{-5} M.

also probed by electro spray ionization mass spectrometric determination of the rate of hydrogen/deuterium exchange in solution.⁵ The rate of hydrogen/deuterium exchange was observed to be much enhanced in the unfolded forms of the proteins versus the folded forms, and the rates of exchange correlated closely with the observed differences in charge-state distributions of the different forms as well as changes in conformation determined by circular dichroism measurements. Loo et al.⁷ have used charge-state distribution determinations by electro spray ionization mass spectrometry to monitor changes in the higher order structures of hen egg lysozyme, bovine ubiquitin, and yeast ubiquitin induced by changes in pH and organic solvent composition and have noted significant changes in the charge-state distributions of the oxidized and reduced forms of several proteins. Le Blanc et al.⁸ studied the effects of heat on the electro spray spectra of a number of globular proteins, observing a dramatic increase with increasing temperature of the charge states of ions produced from equine cytochrome *c* and chicken egg lysozyme as well as a strong increase of the ion intensity from cytochrome *c*. These workers attributed the changes in the observed charge states to heat-induced denaturation of the proteins, leading to an effective increase in the pK_a values of

the carboxylic acid groups. Allen and Vestal¹⁴ have described an electro spray interface in which the spray chamber is heated. These authors have proposed that the special facility of their source for producing intense spectra from certain proteins that do not normally give intense electro spray ion peaks (e.g. subtilisin Carlsberg) may be related to the heating of the sample.

In the present study, we describe a simple and effective device for investigating heat-induced denaturation of proteins by electro spray ionization mass spectrometry. Results are presented for the denaturation as a function of temperature and solution pH of bovine ubiquitin and bovine cytochrome *c*. These results are in concert with and extend the earlier results of LeBlanc et al.⁸ Electro spray ionization mass spectrometry is also shown to be a useful probe of the reversibility of heat-induced denaturation of proteins. Finally, it is demonstrated that heat-induced denaturation can be used to improve the mass spectrometric response of proteins (such as wheat germ agglutinin) that do not normally yield useful spectra when the solubilized protein is electro sprayed at ambient temperatures.

(14) Allen, M. H.; Vestal, M. L. *J. Am. Soc. Mass Spectrom.* 1992, 3, 18.

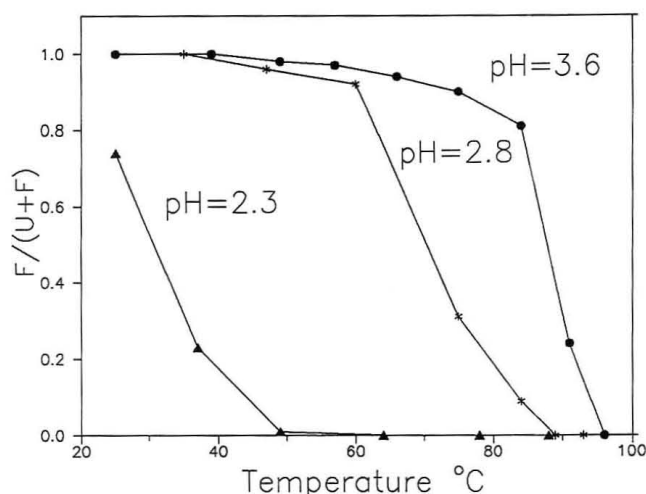


Figure 3. Denaturation transition curves for bovine ubiquitin plotted as a function of temperature for three different values of solution pH. *F* designates a tightly folded form of ubiquitin and *U* designates less tightly folded forms of the protein. See ref 20 for a discussion of the method by which the ratio $F/(U + F)$ was determined.

EXPERIMENTAL SECTION

Figure 1 shows the apparatus that we constructed for the purpose of controlling and measuring the temperature of the solution just prior to electro spraying. It consists of a cylindrical ceramic rod (length 4.4 cm, diameter 3 mm) containing two holes (diameter 1 mm) running parallel to the long axis of the rod. A stainless steel electro spray syringe needle (length 4.6 cm, o.d. 0.7 mm, i.d. 0.15 mm, electropolished to produce a sharpened tip¹⁵) is inserted through one of the holes in the ceramic rod such that the syringe needle is covered along its length by the rod and protrudes from the ceramic rod for a length of 2 mm. An iron/constantan thermocouple (connected to an Omega Engineering Model DP-701 thermocouple gauge) is inserted into the second hole in the ceramic rod to provide a measure of the temperature of solutions that are pumped through the electro spray syringe needle. A chromel wire was wound tightly around the outside of the ceramic rod and cemented in place with a layer of high-temperature castable ceramic (Aremco Products Inc., NY). The temperature of the ceramic rod and the protein solution flowing through the electro spray syringe needle is controlled by passing an appropriate current through the chromel heating wire using a low-voltage power supply (Kepco Model JQE, 0–6 V, 0–10 A). Heating wire currents in the range 0–3.5 A produced electro spray syringe needle temperatures in the range 25–96 °C. Because the dead volume in the heated syringe needle is 1 μ L and the flow rate of the protein solution is typically 0.5 μ L/min, the solution is normally heated for at least 2 min at the controlled temperature prior to electro spray ionization. Temperature measurements were made prior to and after each electro spray ionization mass spectrometric measurement by inserting the thermocouple wire into the second hole in the ceramic rod. The temperatures prior to and after electro spray generally coincided to within ± 1 °C. Temperature measurements were not normally made during the electro spray measurement to avoid the perturbing effect of the thermocouple wires on the field applied to the syringe needle. The walls of the ceramic rod provided adequate electrical insulation between the potentials applied to the spray capillary (<5 kV) and the heating wire (<5 V). The arrangement described above allowed protein solutions to be electro sprayed with temperatures ranging between 25 and 98 °C.

The electro spray ionization mass spectrometer and the sample preparation procedures have been described previously.¹⁶ Briefly, the sample solution was pumped through the stainless steel syringe needle using a syringe pump (Harvard Model 2400-001) and electro sprayed in ambient laboratory air. The resulting highly charged droplets and solvated ions were transported into

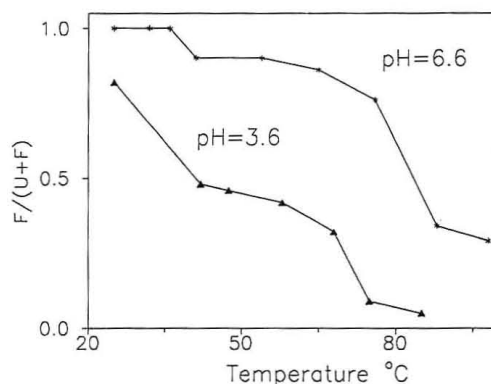


Figure 4. Denaturation transition curves for bovine cytochrome *c* plotted as a function of temperature for two different values of solution pH. *F* designates a tightly folded form of cytochrome *c* and *U* designates less tightly folded forms of the protein. See ref 20 for a discussion of the method by which the ratio $F/(U + F)$ was determined.

the vacuum of a quadrupole mass spectrometer (Vestec Model 201) through a 20-cm-long, 0.5-mm-i.d. heated capillary tube. The flow rate of the analyte through the spray needle (0.2–0.7 μ L/min) was adjusted to produce stable electro spray and depended on the solvent composition and temperature of the spray solution. Electro spray was performed by applying a dc voltage of 3–5 kV to the syringe needle. The distance between the tip of the syringe needle and the capillary leading into the mass spectrometer vacuum ranged between 4 and 5 mm. The capillary leading into the mass spectrometer vacuum was sharpened by electropolishing to focus the field lines from the spray needle and improve the transport of charged droplets and ions into the capillary. The spectra were acquired using a commercially available data system (Tecknivent Vector II) on an IBM compatible computer. Data collection times ranged between 2 and 4 min.

The protein samples were obtained from Sigma Chemical Co. (St. Louis, MO) and were used without further purification. The samples, catalog numbers, and molecular masses (MM) are bovine ubiquitin (U-6253, MM 8565 u), bovine cytochrome *c* (C-3256, MM 12 229 u), chicken egg lysozyme (L-6876, MM 14 306 u), thermolysin from *Bacillus proteolysis* (P-1512, MM 34 420 u), subtilisin Carlsberg from *Bacillus subtilis* (P-5380, MM 27 300 u), and wheat germ agglutinin (L-9640, MM 17 000 u). The protein concentrations of the electro spray solutions were in the range 10–20 μ M.

RESULTS AND DISCUSSION

Denaturation of Bovine Ubiquitin. Our first studies of heat-induced conformational changes by electro spray ionization mass spectrometry were carried out on bovine ubiquitin. This protein was chosen because we have previously carried out extensive mass spectrometric investigations of conformational changes in ubiquitin brought about by changes in pH and organic solvent content of the spray solution⁵ and because heat-induced conformational changes in ubiquitin have previously been investigated by nuclear magnetic resonance measurements.^{17,18} Bovine ubiquitin is a tightly folded protein (molecular mass 8565 u, no disulfide bonds, 13 basic sites, 4 acidic sites) that is very resistant to denaturation.¹⁸ The extreme stability of the protein has been attributed to the pronounced hydrophobic core and the fact that some 90% of the residues in the polypeptide chain appear to be involved in intramolecular hydrogen bonding.¹⁹

Figure 2(a–f) compares the electro spray ionization mass spectra of bovine ubiquitin obtained at a number of different temperatures of the spray solution. In each case, the protein

(17) Linkinski, R. E.; Chen, D. M.; Clickson, J. D.; Goldstein, G. *Biochem. Biophys. Acta* 1977, 126, 494.

(18) Cary, P. C.; King, D. S.; Robinson, C. C.; Bradburry, E. M.; Rabbani, A.; Goodwin, G. H. *Eur. J. Biochem.* 1980, 112, 577.

(19) Kumar, S. V.; Bugg, C. E.; Cook, W. J. *Mol. Biol.* 1987, 194, 531.

(15) Chowdhury, S. K.; Chait, B. T. *Anal. Chem.* 1991, 63, 1660.

(16) Chowdhury, S. K.; Katta, V.; Chait, B. T. *Rapid Commun. Mass Spectrom.* 1990, 4, 81.

was sprayed from a 1% acetic acid solution in water (pH 2.8) at a flow rate of 0.5 $\mu\text{L}/\text{min}$. Figure 2a shows the mass spectrum of ubiquitin obtained at the ambient laboratory temperature (25 °C). The spectrum is dominated by an ion corresponding to the intact protein containing seven additional protons and conferring on it a charge state of +7. Small contributions from the adjacent +6 and +8 charge states are also observed. From previous NMR measurements¹⁸ and from our earlier circular dichroism electrospray ionization studies,⁵ we conclude that Figure 2a represents the spectrum obtained from the native state of the protein. Raising the temperature of the spray solution to 60 °C produces little change in the distribution of charge states (Figure 2b). As the temperature is further raised to 75 °C (Figure 2c), the mass spectrum undergoes a substantial change and a second distribution of charge states (centered about +11) becomes apparent. We⁴ and others⁷ have attributed such bimodal charge-state distributions to the presence in solution of two populations of conformers, one population that is relatively tightly folded and one that is less tightly folded. Further heating of the protein solution leads to a shift of the bimodal distribution (Figures 2d-f) toward the higher charge-state component. Above 89 °C there remains little evidence for the presence of the lower charge-state component.

The data given in Figure 2 are presented in a different form in the central curve shown in Figure 3, where the proportion of ionized molecules in the tightly folded conformation (F) relative to the total in both tightly (F) and loosely (U) folded conformations is plotted against temperature (see ref 20 for a discussion of the calculation of the values of F and U). We interpret this data as evidence for a two-state transition, where the transition temperature for half-denaturation of bovine ubiquitin in aqueous acetic acid at pH 2.8 is 71 ± 5 °C (see ref 21 for a discussion of the uncertainty in this measure). Transition curves obtained from analogous experiments performed at pH 2.3 and pH 3.6 are also given in Figure 3, yielding half-denaturation temperatures of respectively 31 ± 5 and 88 ± 5 °C. The half-denaturation temperatures are observed to fall off rapidly with decreasing pH in accord with the expectation that heat and low pH act as additive denaturants.² Our findings are in agreement with the results of Cary et al.¹⁸ who investigated the effects of heat on the NMR spectra of ubiquitin. At pH 3.9, with no added salt, these workers observed denaturation to occur as a two-state process over the range 70–95 °C with a half-denaturation temperature of 85 °C.

Denaturation of Bovine Cytochrome *c*. We have previously investigated the effect of pH, at a constant solution temperature (25 °C), on the electrospray ionization spectra of bovine cytochrome *c*,⁴ finding dramatic variations in the charge-state distributions as a function of pH. For example, at pH 2.6, a single distribution was observed centered about the +16 charge state, which we identified with a denatured form of the protein. At pH 3.0, on the other hand, a bimodal

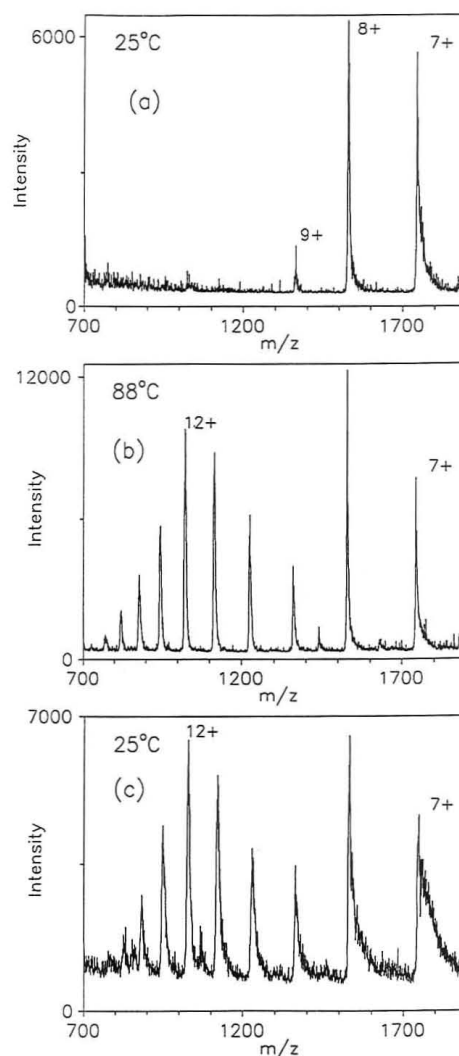


Figure 5. Illustration of a three step experiment designed to probe the reversibility of conformational changes in bovine cytochrome *c* by electrospray ionization mass spectrometry. The spectra were obtained by electrospraying bovine cytochrome *c* in water (pH 6.6, 5 mM ammonium acetate buffer) at a spray needle solution temperature of (a) 25 °C and (b) 88 °C. (c) Spectrum obtained after heating the protein solution at 90 °C for 4 min in a test tube and subsequently cooling the solution to 25 °C prior to electrospray.

distribution was observed where, in addition to the distribution centered around +16, a second distribution was observed centered about +8. The latter distribution was identified with a more tightly folded form of the protein. In the present set of experiments, electrospray ionization mass spectra of bovine cytochrome *c* were obtained at pH 3.6 for temperatures ranging between 25 and 85 °C and at pH 6.6 between 25 and 98 °C. Again, bimodal distributions of charge states were observed, leading to the temperature transition curves given in Figure 4. The shapes of these temperature transition curves appear more complex than those obtained for ubiquitin (Figure 3), with an indication of two temperature transitions. At pH 3.6 (bottom curve of Figure 4), the first transition occurs between 25 and 40 °C and the second between 67 and 75 °C. At pH 6.6, corresponding transitions take place at temperatures some 10 deg above those observed in the pH 3.6 solution, in accord with the greater predicted stability of cytochrome *c* at pH values closer to neutrality. We note that transitions between more than two conformational states of cytochrome *c*, at acidic pHs, have previously been inferred from spectroscopic,²² circular dichroism,²³ and mass spectrometric measurements.⁴

Probing the Reversibility of Conformational Changes by Mass Spectrometry. Certain proteins, after being

(20) The values of F (or U) were calculated by summing the heights of the spectral peaks corresponding to ions originating from proteins in tightly folded (or loosely folded) conformations. For example, the values of $F/(U+F)$ yielding the central curve in Figure 3 (pH = 2.8) were extracted from Figure 2 using the following assumptions: (i) The distribution of charge states obtained at room temperature (Figure 2a) originated completely from proteins in a tightly folded conformation. (ii) The distribution of charge states at 93 °C (Figure 2f) originated completely from proteins in a loosely folded conformation. At intermediate temperatures, the values of U and F were obtained by unfolding the distribution of charge states corresponding to proteins in tightly folded conformations from that corresponding to proteins in loosely folded conformations.

(21) The largest source of uncertainty in determining the half-denaturation temperatures arises from uncertainties in the efficiency of the mass analyzer as a function of m/z . For the present measurements we assume that the efficiency for the analysis and detection of ions between m/z 800 and m/z 1200 varies by less than a factor of 2.

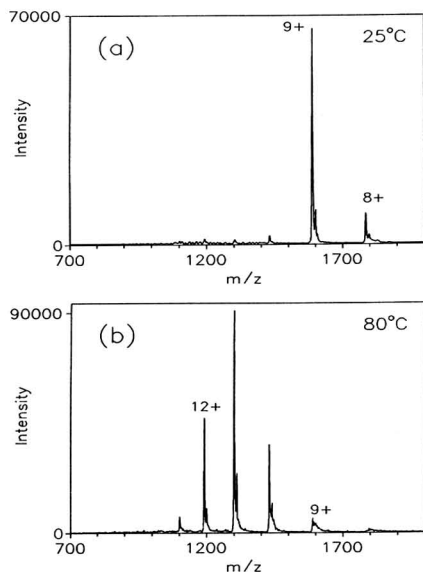


Figure 6. Electro spray ionization mass spectra of chicken egg lysozyme in water and acetic acid (pH 3.1), obtained at two different temperatures: (a) 25 °C; (b) 80 °C. Protein concentration: 1×10^{-5} M.

subjected to heat-induced denaturation, are able to refold into their native forms when the solution temperature is lowered; others are irreversibly denatured.² To investigate the potential of electro spray ionization as a probe of the reversibility of conformational changes in proteins, the three-step experiment described below and illustrated in Figure 5 was carried out on a solution of bovine cytochrome *c* maintained at pH 6.6.

Step 1. A mass spectrum was obtained from a solution sprayed at 25 °C (Figure 5a). At this temperature, the protein is largely in a tightly folded conformation (see the top curve of Figure 4).

Step 2. A mass spectrum was obtained from a solution sprayed at 88 °C (Figure 5b). At this temperature, both folded and denatured forms of the protein are present in solution (see top curve of Figure 4).

Step 3. A solution of the protein was heated to 90 °C, in a test tube, maintained at this elevated temperature for 4 min, recooled to 25 °C, and then electro sprayed to give the spectrum shown in Figure 5c.

The spectrum obtained after recoiling the solution to 25 °C (Figure 5c) has the same distribution of charge states as that obtained by electro spraying the solution at 88 °C, indicating that the protein has not renatured in the time required for cooling (25 min). A similar indication of irreversible denaturation was observed for a solution of cytochrome *c* maintained at pH 3.6 where the temperature was raised to 75 °C (data not shown). By contrast, an analogous experiment performed on bovine ubiquitin (pH 3.0) demonstrated complete reversibility of the denaturation observed upon heating the solution to 92 °C (data not shown). These results demonstrate that electro spray ionization provides a useful probe of the reversibility of heat-induced conformational changes in proteins.

Improving the Mass Spectra of Proteins by Heating the Electro spray Solutions. We have previously experienced considerable difficulty in obtaining useful electro spray

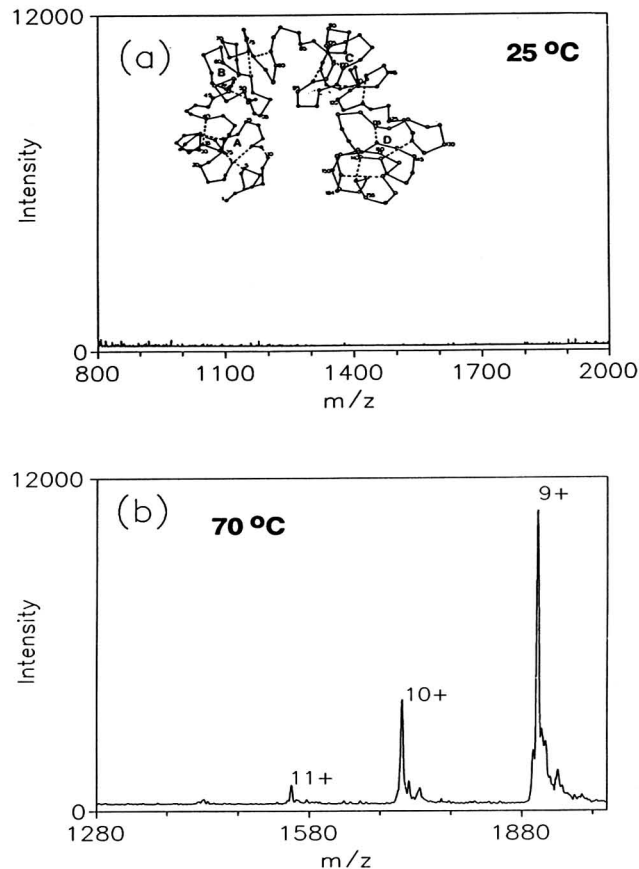


Figure 7. Electro spray ionization mass spectrum of wheat germ agglutinin in 45% water, 50% methanol, and 5% acetic acid obtained at two different temperatures: (a) 25 °C; (b) 70 °C. Protein concentration: 1×10^{-5} M. The structure of wheat germ agglutinin is indicated in the top panel.

ionization mass spectra of some members from certain classes of protein,¹² including those that contain a large number of disulfide bonds or are otherwise highly stabilized against unfolding. Because our analyzer has an upper *m/z* limit of 2000, we hypothesized that one possible reason for this lack of success was the low number of charges that attach to these proteins.

Chicken egg lysozyme is a highly basic protein ($pI = 11.1$) containing 4 disulfide bonds. Even though this protein contains a large number (19) of basic groups, the dominant ion in the mass spectrum obtained at 25 °C from an acidic solution (pH 3.1) of lysozyme contains only 9 positive charges and has a *m/z* of approximately 1600 (Figure 6a). It is readily seen that a mass analyzer having a *m/z* upper limit of less than 1600 would fail to yield a useful mass spectrum under these circumstances. Such a limitation could be eliminated by shifting the charge-state distribution to higher values, and as we have seen heat provides an effective means for bringing about such shifts. Figure 6b shows the spectrum of chicken egg lysozyme obtained by heating the spray solution to 80 °C, where the dominant ion species are now shifted into the *m/z* range 1200–1400 (+12 to +10). The present result for lysozyme is in concert with that previously obtained by Le Blanc et al. using heat-induced denaturation⁸ and Loo et al. using acid- and methanol-induced denaturation.⁷

A somewhat similar but more challenging example is provided by wheat germ agglutinin, a 171 amino acid residue

(22) Artyukhov, V. G.; Kryuchkova, V. T.; Loboda, T. *Biophysics* 1980, 24, 614.

(23) Mayer, Y. P. *Biochemistry* 1968, 7, 768.

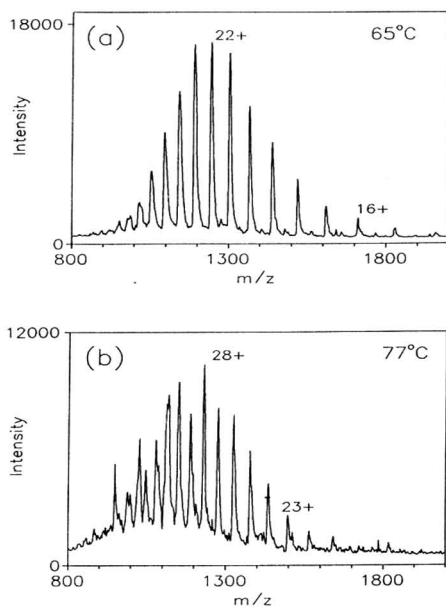


Figure 8. Electro spray ionization mass spectra of (a) subtilisin Carlsberg in 45% water, 50% methanol, and 5% acetic acid (pH 2.3) obtained at 65 °C and (b) thermolysin in 45% water, 50% methanol, and 5% acetic acid (pH 2.3) obtained at 77 °C. Protein concentration: 1×10^{-5} M.

lectin containing only 12 basic groups. The protein contains an unusually high density of disulfide bridges (16), which confers upon it a high degree of stabilization against denaturation (Figure 7a). Thus, at 25 °C even when 50% methanol is added to a highly acidified (pH 2.4) spray solution, no discernable protonated molecule ions are observed with m/z value less than 2000 (Figure 7a). However, when this spray solution is heated to 70 °C, intense ions are observed that correspond to the +9, +10, and +11 charge states of the intact lectin (Figure 7b). The elevation in temperature apparently induces denaturation, leading to an elevation in the number of charges that attach to the protein and allowing for the

collection of an analytically useful mass spectrum.

Subtilisin Carlsberg and thermolysin are additional examples of proteins having high conformational stability that yield very weak electrospray ionization spectra at room temperature even from acidified spray solutions containing 50% methanol. Figure 8 shows that intense mass spectra can be obtained from these two intractable enzymes when the temperature of the spray solution is raised substantially, confirming the earlier result of Allen and Vestal¹⁴ with these compounds.

CONCLUSIONS

The effects of heat on the electrospray ionization mass spectra of several proteins were investigated using a simple and effective new apparatus. The described measurements demonstrate that heat provides an effective means for inducing denaturation of proteins prior to electrospray ionization in concert with previous results obtained by LeBlanc et al.⁸ and that denaturation transition curves can be deduced from the resulting mass spectrometric data. Different transition temperatures obtained for the heat-induced denaturation of bovine ubiquitin and cytochrome *c* at different values of the solution pH indicate the cooperative effect of pH and temperatures on the unfolding of these proteins. The reversibility of heat-induced denaturation and refolding of proteins can also be probed by the present technique. Finally, the heat-induced denaturation technique is found to be useful for obtaining mass spectra of proteins (e.g., wheat germ agglutinin, subtilisin Carlsberg, thermolysin) that do not yield analytically useful electrospray ionization mass spectra under more conventional electrospray conditions.

ACKNOWLEDGMENT

This work was supported by Grants RR00862 and GM38274. We thank Gladys McMilleon for typing this manuscript.

RECEIVED for review June 3, 1992. Accepted October 5, 1992.

Structure-Specific Collision-Induced Fragmentations of Ceramides Cationized with Alkali-Metal Ions

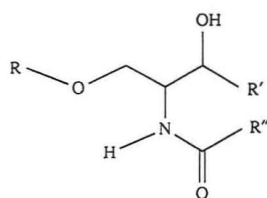
Qinghong Ann and Jeanette Adams*

Department of Chemistry, Emory University, Atlanta, Georgia 30322

Collision-induced and metastable ion fragmentations of gas-phase $[M + \text{Cat}]^+$ complexes between five alkali-metal ions, Li^+ , Na^+ , K^+ , Rb^+ , and Cs^+ , and seven structurally diverse ceramides and two mixtures of ceramides are reported. The collision-induced decomposition (CID) spectra of the $[M + \text{L}]^+$ ions provide immediate information about the lengths of the sphingoid base and fatty acyl chains and locations of substituents such as double bonds and hydroxyl groups on the fatty acyl chain. Structures of individual components of complex mixtures can be determined, and the detection limit for structural determination of *N*-palmitoyl-DL-sphinganine by CID is 8 pmol. Relative product ion abundances, which change with increasing size of alkali-metal ion, cannot be explained by classic kinetic arguments. They can be at least partially explained, however, from decompositions of different populations of structurally distinct precursor ions.

INTRODUCTION

Ceramides are a class of molecules that form the backbone of the biologically important sphingolipids. Ceramides (structure 1, $R = \text{H}$) comprise a long-chain sphingoid base, such as (4*E*)-sphinganine ($R' = \text{CH}_2=\text{CH}(\text{CH}_2)_{12}\text{CH}_3$) or



structure 1

sphinganine ($R' = (\text{CH}_2)_{14}\text{CH}_3$), and a fatty acyl chain (R'') substituted at the sphingoid amino group. Sphingolipids ($R = \text{sugar}$ or other group in structure 1) are ubiquitous components of plasma membranes and are present at the outer leaflet of the membrane bilayer.¹ Sphingolipids can act as cell-surface interactants and transducers, cellular antigens, cell-surface markers, and as receptors for cellular recognition.²⁻⁴ Ceramides act both as precursors in the biosynthesis⁵ and as intermediates in the degradation⁶ of sphingolipids. They also can be enzymatically hydrolyzed *in vivo* into their sphingoid base and fatty acid components.⁶ Because structures of ceramides can vary substantially along with their biological activity, their characterization has been of interest and a challenge in analytical chemistry.

There have been several approaches for elucidating the structure of ceramides. One of the earliest methods employed chemical hydrolysis followed by derivatization and gas chromatography (GC) of the liberated sphingoid bases⁷ and fatty acids.^{8,9} This approach for structure determination of the sphingoid bases was later improved by the addition of electron ionization (EI) GC-mass spectrometry (GC-MS).¹⁰ Samuelsson and Samuelsson,^{11,12} however, were the first to determine ceramides as intact molecules by derivatization to trimethylsilyl ethers followed by GC-MS. They and others used GC-MS of the trimethylsilyl ethers to identify ceramides that contained α -hydroxy fatty acyl groups¹³⁻¹⁶ and ones that contained phytosphingosine (4-D-hydroxysphinganine).^{16,17} Similar approaches involved chemical ionization of acetylated ceramides¹⁸ or EI of permethylated species.^{19,20}

Fast atom bombardment (FAB) MS of both $[M + \text{H}]^+$ and $[M - \text{H}]^-$ ions has provided a new avenue for determining the molecular weights of ceramides released from sphingolipids.²¹⁻²⁴ Unfortunately, interfering matrix ions and poor sensitivity associated with detection of fragment ions precludes unequivocal structural characterization by FAB alone. High-energy (kiloelectronvolt) tandem mass spectrometry (MS-MS) can alleviate some of these problems, but the exact location of substituents such as double bonds in the *N*-acyl chain cannot be determined.²⁵⁻²⁸ Costello and co-workers, however, have demonstrated that either permethylation or hydroboration and oxidation of intact ceramides coupled with MS-MS of the $[M + \text{H}]^+$ ions could be used to determine their structures.^{27,28}

(7) Karlsson, K.; Holm, G. A. L. *Acta Chem. Scand.* **1965**, *19*, 2423-2425.

(8) Sweeley, C. C. *J. Lipid Res.* **1963**, *4*, 402-406.

(9) Morrison, W. R. *Biochim. Biophys. Acta* **1969**, *176*, 537-546.

(10) Polito, A. J.; Akita, T.; Sweeley, C. C. *Biochemistry* **1968**, *7*, 2609-2614.

(11) Samuelsson, B.; Samuelsson, K. *Biochim. Biophys. Acta* **1968**, *164*, 421-423.

(12) Samuelsson, B.; Samuelsson, K. *J. Lipid Res.* **1969**, *10*, 41-46.

(13) Samuelsson, K.; Samuelsson, B. *Chem. Phys. Lipids* **1970**, *5*, 44-79 and references therein.

(14) Hammarström, S.; Samuelsson, B.; Samuelsson, K. *J. Lipid Res.* **1970**, *11*, 150-157.

(15) Hammarström, S. *Eur. J. Biochem.* **1970**, *15*, 581-591.

(16) Hayashi, A.; Matsuura, F. *Chem. Phys. Lipids* **1973**, *10*, 51-65.

(17) Hammarström, S. *J. Lipid Res.* **1970**, *11*, 175-182.

(18) Markey, S. P.; Wenger, D. A. *Chem. Phys. Lipids* **1974**, *12*, 182-200.

(19) Egge, H. *Chem. Phys. Lipids* **1978**, *21*, 349-360.

(20) Hansson, G.; Li, Y. T.; Karlsson, H. *Biochemistry* **1989**, *28*, 6672-6678.

(21) Hemling, M. E.; Robert, K.; Yu, R.; Sedgwick, D.; Rinehart, K. L. *Biochemistry* **1984**, *23*, 5706-5713.

(22) Pahlsson, P.; Nilsson, B. *Anal. Biochem.* **1988**, *168*, 115-120.

(23) Suzuki, M.; Seine, M.; Yamakawa, T.; Suzuki, A. *J. Biochem.* **1989**, *105*, 829-833.

(24) Suzuki, M.; Yamakawa, T.; Suzuki, A. *J. Biochem.* **1990**, *108*, 92-98.

(25) Singh, B. N.; Costello, C. E.; Levery, S. B.; Walenga, R. W.; Beach, D. H.; Mueller, J. F.; Holz, G. G. *Mol. Biochem. Parasitol.* **1987**, *26*, 99-112.

(26) Domon, B.; Costello, C. E. *Biochemistry* **1988**, *27*, 1534-1543.

(27) Domon, B.; Vath, J. E.; Costello, C. E. *Anal. Biochem.* **1990**, *184*, 151-164.

(28) Costello, C. E.; Vath, J. E. In *Methods in Enzymology*; McCloskey, J. A., Ed.; Academic Press: San Diego, CA, 1990; Vol. 193 pp 738-768.

(1) Kanfer, J. N.; Hakomori, S. *Sphingolipid Biochemistry, Handbook of Lipid Research*; Plenum Press: New York, 1983; Vol. 3.

(2) Yogeewaran, G.; Hakomori, S. *Biochemistry* **1975**, *14*, 2151-2156.

(3) Ando, S.; Yamakawa, T. *J. Biochem.* **1973**, *73*, 387-396.

(4) Helting, T. B.; Zwisler, O.; Wiegandt, H. *J. Biol. Chem.* **1977**, *252*, 194-198.

(5) Basu, S.; Kaufman, B.; Roseman, S. *J. Biol. Chem.* **1968**, *243*, 5802-5807.

(6) Leibovitz, Z.; Gatt, S. *Biochim. Biophys. Acta* **1968**, *152*, 136-143.

As an alternative to chemical derivatization, we have been exploring the use of metal ions as adducts to direct mass spectral fragmentation pathways to improve structural determination. Earliest work involved collision-induced decomposition (CID) of FAB-desorbed $[M + \text{Cat}]^+$ or $[M + 2\text{Cat} - \text{H}]^+$ ions, in which Cat = alkali-metal ion, to determine structures of fatty alcohols and acids.²⁹⁻³² This approach has since been applied to structure determination of prostaglandins,³³ fatty acid esters,³⁴ and peptides.³⁵⁻³⁷ Others have likewise used this approach to elucidate structures of sugars and oligosaccharides³⁸⁻⁴² and other compounds.^{43,44} Preliminary data were recently presented for structure determination of ceramides and neutral glycosphingolipids by CID of $[M + \text{Li}]^+$ ions.⁴⁵ Here we report in more detail the use of this technique for determining structures of intact ceramides.

EXPERIMENTAL SECTION

Reagents. Seven ceramides and two mixtures of ceramides (Sigma, St. Louis, MO) were used in this investigation. The ceramides are *N*-lignoceroyl-DL-sphinganine (*N*-tetracosanoyl-DL-sphinganine), *N*-palmitoyl-DL-sphinganine (*N*-hexadecanoyl-DL-sphinganine), *N*-stearoyl-DL-sphinganine (*N*-octadecanoyl-DL-sphinganine), *N*-palmitoyl-(4*E*)-sphinganine (*N*-hexadecanoyl-(4*E*)-sphinganine), *N*-oleoyl-(4*E*)-sphinganine (*N*-cis-9-octadecanoyl-(4*E*)-sphinganine), *N*-nervonoyl-(4*E*)-sphinganine (*N*-cis-15-tetracosanoyl-(4*E*)-sphinganine), and *N*-stearoyl-(4*E*)-sphinganine (*N*-octadecanoyl-(4*E*)-sphinganine). One of the mixtures, ceramide type IV, which contains α -hydroxy-*N*-lignoceroyl-(4*E*)-sphinganine as a dominant component,⁴⁶ was used to study ceramides that contain an α -hydroxy fatty acyl chain. Another mixture, ceramide type III, was used for mixture analysis.

Procedure. The samples were dissolved in $\text{CHCl}_3/\text{MeOH}$ (2:1 v/v), and $\sim 1 \mu\text{L}$ of this solution was added to the FAB matrix on the stainless-steel FAB probe tip. The $[M + \text{H}]^+$ and $[M - \text{H}]^-$ ions were desorbed from a matrix of 3-nitrobenzyl alcohol (3-NBA). The $[M + \text{Cat}]^+$ complexes of most ceramides were prepared by using 3-NBA saturated with different alkali-metal iodides. Complexes of the α -hydroxy fatty acyl ceramides were instead prepared by using 3-NBA saturated with alkali-metal hydroxides. Deuterium-labeled α -hydroxy-*N*-lignoceroyl-(4*E*)-sphinganine-*d*₄ was desorbed as $[M + \text{Li}]^+$ ions by dissolving the ceramide in $\text{CDCl}_3/\text{MeOD}$ (2:1, v/v) and then adding $\sim 1 \mu\text{L}$ of this solution to deuterium-exchanged 3-NBA, saturated with LiOD and D₂O. The deuterium-exchanged 3-NBA was prepared by dissolving it in D₂O and then evaporating the D₂O under vacuum four times.

Mass spectrometric experiments were conducted by using a VG 70-S forward-geometry (EB, where E is electrostatic analyzer, or ESA, and B is magnetic analyzer) mass spectrometer equipped

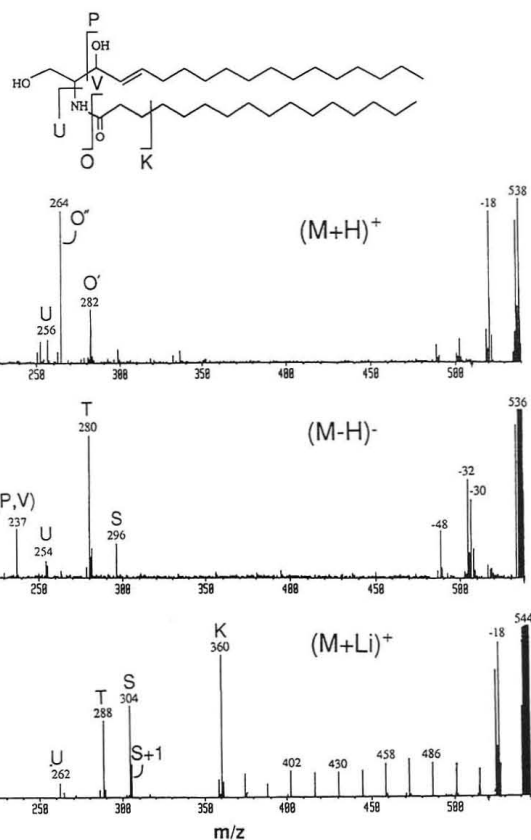


Figure 1. CID spectra of (a) $[M + \text{H}]^+$, (b) $[M - \text{H}]^-$, and (c) $[M + \text{Li}]^+$ ions of *N*-palmitoyl-(4*E*)-sphinganine. See Figure 2 for nomenclature for the cleavages. In all spectra, the masses of the precursor and product ions are shown without their positive mass defects (e.g., m/z 538 is actually m/z 538.5).

with an Ion Tech saddle-field FAB gun and a commercial FAB ion source. Precursor ions were produced by bombarding the sample with 7-keV Ar or Xe atoms at a gun current of 2 mA. Sample ions desorbed from the FAB matrix were accelerated to 8-keV translational energy, and product ions formed either metastably or by CID in the first field-free region between the ion source and ESA were observed by using scans at a constant ratio of B/E. Helium was used as collision gas, and the beam transmission was reduced to $\sim 50\%$. An aqueous solution of LiI (1.5 F), NaI (4.5 F), KI (0.01 F), RbI (0.01 F), and CsI (1.0 F) was prepared and mixed 5:1 (v/v) with acetonitrile for calibration.⁴⁷ Experiments were performed at a product ion resolution of ~ 1000 (10% valley), and 10–15 scans were signal-averaged, smoothed, centroided, and mass-measured by using commercial software. Background subtraction of matrix and other spectra was acquired for all experiments, and this was especially important in determining the detection limit and performing the mixture analysis.³⁴

RESULTS AND DISCUSSION

Structural Determination. In an earlier communication,⁴⁵ we reported that CID of $[M + \text{Li}]^+$ ions of ceramides provides more structural information than CID of either $[M + \text{H}]^+$ or $[M - \text{H}]^-$ ions. Examples of the type of structural information that can be obtained from CID of the three different precursor ions are shown in Figure 1 for *N*-palmitoyl-(4*E*)-sphinganine. The nomenclature used to label the peaks in the spectra is defined in Figure 2. Loss of water is one major fragmentation route for $[M + \text{H}]^+$ ions of ceramides that contain both (4*E*)-sphinganine (Figure 1a) and sphinganine. There are also O' and O'' ions that presumably arise

(47) Sato, K.; Asada, T.; Ishihara, M.; Kunihiro, F.; Kammei, Y.; Kubota, E.; Costello, C. E.; Martin, S. A.; Scoble, H. A.; Biemann, K. *Anal. Chem.* 1987, 59, 1652–1659.

- (29) Adams, J.; Gross, M. L. *J. Am. Chem. Soc.* 1986, 108, 6915–6921.
 (30) Adams, J.; Gross, M. L. *Anal. Chem.* 1987, 59, 1576–1582.
 (31) Adams, J.; Gross, M. L. *Org. Mass Spectrom.* 1988, 23, 307–316.
 (32) Adams, J.; Deterding, L. J.; Gross, M. L. *Spectroscopy (Ottawa)* 1987, 5, 199–228.
 (33) Contado, M. J.; Adams, J.; Gross, M. L. *Adv. Mass Spectrom.* 1989, 11B, 1034–1035.
 (34) Contado, M. J.; Adams, J. *Anal. Chim. Acta* 1991, 246, 187–197.
 (35) Teesch, L. M.; Adams, J. *J. Am. Chem. Soc.* 1990, 112, 4110–4120.
 (36) Teesch, L. M.; Adams, J. *J. Am. Chem. Soc.* 1991, 113, 812–820.
 (37) Teesch, L. M.; Orlando, R. C.; Adams, J. *J. Am. Chem. Soc.* 1991, 113, 3668–3675.
 (38) Wright, L. G.; Cooks, R. G.; Wood, K. V. *Biomed. Mass Spectrom.* 1985, 12, 159–162.
 (39) Orlando, R.; Bush, C. A.; Fenselau, C. *Biomed. Environ. Mass Spectrom.* 1990, 19, 747–754.
 (40) Zhou, Z.; Ogden, S.; Leary, J. A. *J. Org. Chem.* 1990, 55, 5444–5446.
 (41) Hofmeister, G. E.; Zhao, Z.; Leary, J. A. *J. Am. Chem. Soc.* 1991, 113, 5964–5970.
 (42) Puzo, G.; Prome, J. C. *Adv. Mass Spectrom.* 1979, 8, 1003–1011.
 (43) Teesch, L. M.; Adams, J. *Org. Mass Spectrom.*, in press.
 (44) Teesch, L. M.; Adams, J. In *Experimental Mass Spectrometry*; Russell, D. H., Ed.; Plenum Press (in press).
 (45) Ann, Q.; Adams, J. *J. Am. Soc. Mass Spectrom.* 1992, 3, 260–263.
 (46) Carter, H. E.; Rothfus, J. A.; Gigg, R. *J. Lipid Res.* 1961, 2, 228–234.

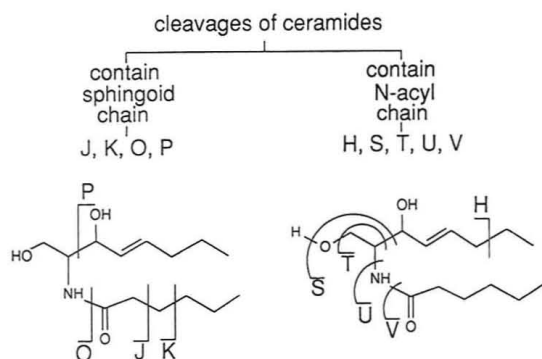
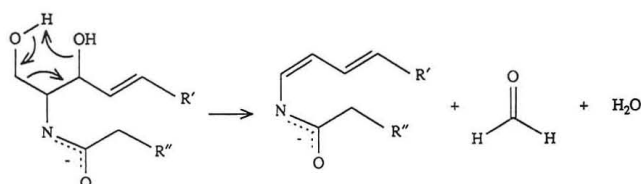


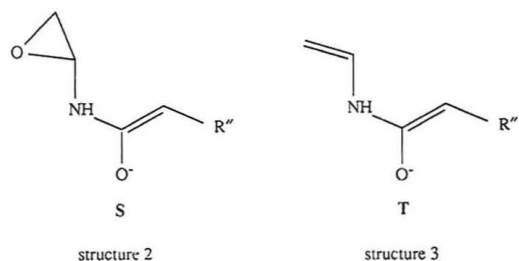
Figure 2. Nomenclature for cleavages of precursor ions of ceramides.

Scheme I



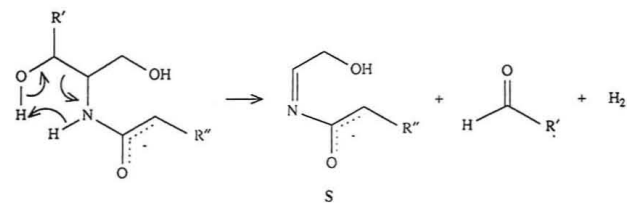
via loss of one or two molecules of water from undected O ions, which are formed by cleavage of the amide bond with charge retention on nitrogen. For ceramides that contain sphinganine instead of (4*E*)-sphinganine, the O ion can be detected, and the relative abundance of the O' ion is greater than that of the O'' ion. The O, O', and O'' series of product ions provides information about the molecular weights of the sphingoid and fatty acyl residues. Costello and co-workers^{27,28} showed that after borane reduction of the ceramide amide to an amine and hydroboration of the double bonds in olefin ceramides, more structurally informative product ions, such as charge-remote ions,^{29-34,48-51} arise from decompositions of the $[M + H]^+$ ions. The charge-remote product ions can provide information about the presence and location of double bonds on both chains.

CID of $[M - H]^-$ ions of ceramides provides complementary information. For example, $[M - H]^-$ ions of ceramides that contain both (4*E*)-sphinganine (Figure 1b) and sphinganine lose 32 u, presumably as CH_3OH . We have no mechanistic evidence, but loss of 48 u (Figure 1b) may arise from a charge-remote cleavage reaction to give formaldehyde and water, perhaps as suggested in Scheme I. The peaks labeled, P, S, T, U, and V all give information about the molecular weights of the fatty acyl and sphingoid chains. The structures of the S and T ions were previously proposed to be structures 2 and 3.^{26,28} We suggest, however, that the S ions are more stable

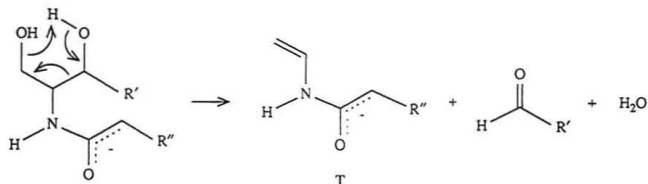


than those shown in structure 2, and perhaps arise via the reaction in Scheme IIa. The conjugated structure for the

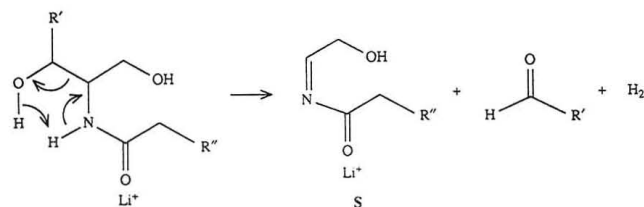
Scheme IIa



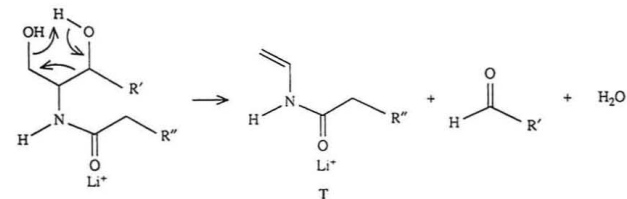
Scheme IIb



Scheme IIIa



Scheme IIIb



S ions shown in Scheme IIa would be more stable than the epoxide proposed previously. The T ions might likewise arise via a concerted reaction, as suggested in Scheme IIb, to give the homoconjugated structure 3 previously proposed. Both reactions would involve a resonance-stabilized form of the precursor anion and would be nominally charge-remote fragmentations. The close proximity of the anionic charge site, however, would polarize the bonds involved in the reactions,⁵² thus lowering the transition-state energies. The major effect of changing (4*E*)-sphinganine to sphinganine is a significantly reduced loss of 30 u, which is presumably loss of $\text{H}_2\text{C}=\text{O}$ in analogy to fragmentations of $[M - H]^-$ ions of fatty alcohols.²⁹

CID spectra of $[M + \text{Li}]^+$ ions of ceramides (Figure 1c) also reveal S, T, and U ions that we believe are analogous to those in the spectra of $[M - H]^-$ ions. Indeed, similar mechanisms can explain the formation of the S and T ions from the cationized precursors (Scheme IIIa,b, respectively). The Li^+ ion should be preferentially bonded to the amide carbonyl oxygen, as this site has the greater Li^+ affinity than the other functional groups.⁵³ Spectra of $[M + \text{Li}]^+$ ions also show some new product ions that primarily involve cleavages of the N-acyl chain. These C-C bond cleavages are classic examples of charge-remote losses of $\text{C}_n\text{H}_{2n+2}$ that are useful for elucidating structures of alkyl chains.^{29-34,48-51} There is a particularly abundant peak labeled K, which is more abundant than either the S or T ion, and it also gives information about the molecular weights of the fatty acyl and sphingoid residues. The formation of the K ion can be

(48) Adams, J. *Mass Spectrom. Rev.* 1990, 9, 141-186 and references therein.

(49) Jensen, N. J.; Tomer, K. B.; Gross, M. L. *J. Am. Chem. Soc.* 1985, 107, 1863-1868.

(50) Adams, J.; Gross, M. L. *J. Am. Chem. Soc.* 1989, 111, 435-440.

(51) Contado, M. J.; Adams, J.; Jensen, N. J.; Gross, M. L. *J. Am. Soc. Mass Spectrom.* 1991, 2, 180-183.

(52) Bates, D. R. *Int. J. Mass Spectrom. Ion Processes* 1987, 80, 1-16.

(53) Taft, R. W.; Anvia, F.; Gal, J.-f.; Walsh, S.; Capon, M.; Holmes, M. C.; Hosn, K.; Oloumi, G.; Vasanwala, R.; Yazdani, S. *Pure Appl. Chem.* 1990, 62, 17-23.

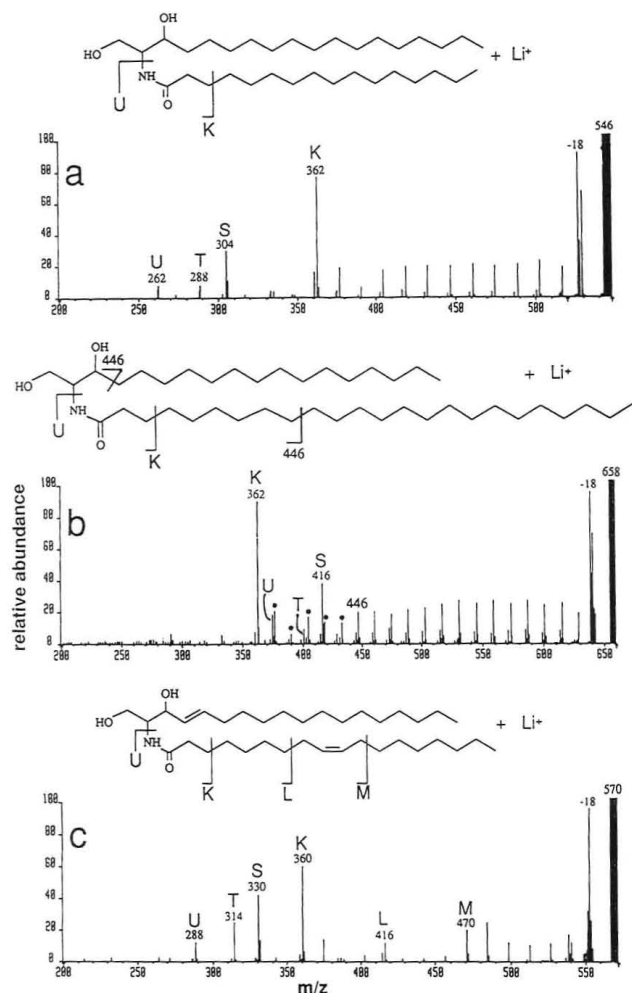
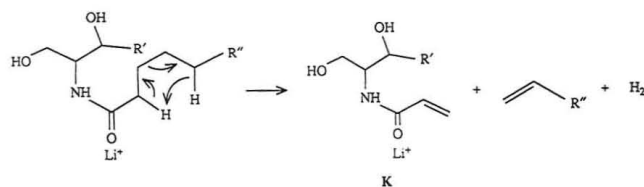


Figure 3. CID spectra of $[M + Li]^+$ ions of (a) *N*-palmitoyl-DL-sphinganine, (b) *N*-lignoceroyl-DL-sphinganine, and (c) *N*-oleoyl-(4*E*)-sphinganine.

Scheme IV



described by a charge-remote 1,4-elimination, such as originally proposed for fatty acids (Scheme IV).^{30,49} Here, however, the transition-state energy would be lowered and the rate of the reaction increased, as a result of the close proximity of the charge site,⁵² more favorable transfer of an α -hydrogen,⁵⁴ and the formation of a stable conjugated product ion. Hence, K ions have greater abundances than the higher mass ions also formed by losses of C_nH_{2n+2} . These higher mass charge-remote cleavages, however, give immediate information about the length of and possible substituents in the fatty acyl chain, information that is lacking in the spectra of $[M + H]^+$ and $[M - H]^-$ ions (Figure 1a,b). The more favorable charge-remote cleavages of the *N*-acyl vs the sphingoid chain are demonstrated in Figure 3. For example, abundances of charge-remote product ions, relative to each other, in CID spectra of $[M + Li]^+$ ions of *N*-palmitoyl-DL-sphinganine (Figure 3a) and *N*-lignoceroyl-DL-sphinganine

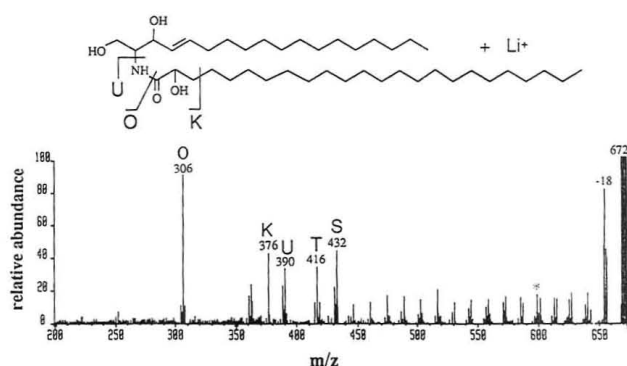
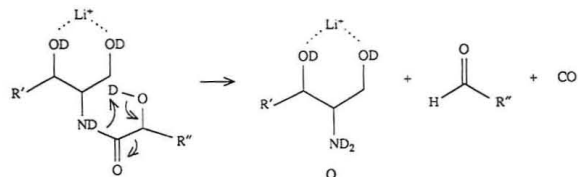


Figure 4. CID spectrum of $[M + Li]^+$ ions of predominantly α -hydroxy-*N*-lignoceroyl-(4*E*)-sphinganine. This spectrum also shows product ions (one is labeled with an *) from $[M + Li]^+$ precursor ions of α -hydroxy-*N*-nervonyl-(4*E*)-sphinganine of m/z 670. See text for discussion.

Scheme V



(Figure 3b) are virtually identical, although the fatty acyl chain in *N*-lignoceroyl-DL-sphinganine is eight methylene groups longer than the acyl chain in *N*-palmitoyl-DL-sphinganine. If charge-remote fragmentations of the sphingoid chain were competing effectively against fragmentations of the *N*-acyl chain, abundances of the lowest mass charge-remote ions in Figure 3b (of $m/z \leq 432$, labeled with dots) would be expected to be $\sim 50\%$ of the abundances of the ions of $m/z \geq 446$ because the lower mass ions can only arise from the *N*-acyl chain. The ions of $m/z \leq 432$ are instead only decreased by $\sim 30\%$. Furthermore, the spectrum in Figure 3c of $[M + Li]^+$ ions of *N*-oleoyl-(4*E*)-sphinganine shows a clear 54-u gap between peaks labeled L and M that is a result of unfavorable cleavages vinylic to and through the double bond in the *N*-acyl chain. From this gap, the exact location of the double bond can be determined. If fragmentations of the sphingoid chain were more competitive, however, the three weakly abundant peaks present in the gap instead would be formed at approximately twice their observed abundances. Preferential cleavage of the *N*-acyl chain is quite analytically useful because it is this chain, as opposed to the sphingoid chain, that is most structurally varied in biological samples.⁸

Fragmentations of $[M + Li]^+$ ions also can be used to determine α -hydroxy fatty acyl ceramides such as α -hydroxy-*N*-lignoceroyl-(4*E*)-sphinganine, which is a dominant component⁴⁶ of the ceramide type IV mixture (Figure 4). There are still charge-remote fragmentations that reveal details of the *N*-acyl chain, and the typical K, U, S, and T ions. In addition, however, there is a new highly abundant diagnostic peak labeled O. The O ion, as with $[M + H]^+$ precursors of ceramides (Figure 1a), arises from cleavage of the amide *N*-CO bond. To investigate the details of the reaction, α -hydroxy-*N*-lignoceroyl-(4*E*)-sphinganine-*d*₄ was prepared by deuterium exchange and collisionally activated. The deuterated precursor decomposes to give an O ion of m/z 310 that contains four deuterons. A mechanism that accounts for this can be suggested (Scheme V). Thus it appears that the high abundance of the O ion is a result of favorable transfer of the α -hydroxy hydrogen, which is significantly more facile than analogous transfer of a β -methylene hydrogen. In contrast to the spectra shown in Figures 1–3, the K ion in the

(54) Lowry, T. H.; Richardson, K. S. In *Mechanism and Theory in Organic Chemistry*; Berger, L. S., MacErlce, E., Eds; Harper & Row: New York, 1987; pp 296–326.

(55) Yan, J. F.; Momany, F. A.; Hoffmann, R.; Scheraga, H. A. *J. Phys. Chem.* 1970, 74, 420–433.

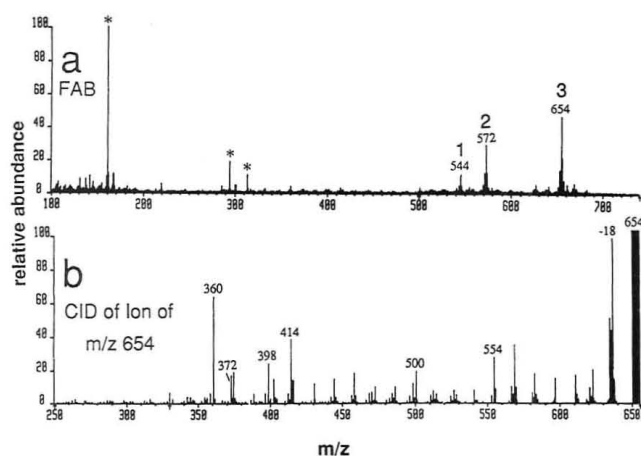


Figure 5. Mass spectra of ceramides type III mixture: (a) FAB spectrum of mixture in 3-NBA/LII, in which asterisks (*) indicate matrix ions; (b) CID spectrum of the ion of m/z 654 from the FAB spectrum shown in (a). The CID spectrum of $[M + Li]^+$ ions of pure *N*-nervonyl-(4*E*)-sphinganine gave the same spectrum as in (b).

spectrum of α -hydroxy ceramides (Figure 4) is much less abundant.

The spectrum in Figure 4 also demonstrates problems inherent with poor precursor ion resolution in first field-free region B/E scans: Product ions from $(M + Li)^+$ precursors of m/z 670 of α -hydroxy-*N*-nervonyl-(4*E*)-sphinganine also are present (an example is the peak labeled with an *). The identity of α -hydroxy-*N*-nervonyl-(4*E*)-sphinganine was determined nonetheless from its own CID spectrum because product ions from the adjacent precursor (of m/z 672) were of reduced abundance. Another abundant component of the ceramide type IV mixture, of m/z 588, was determined from its CID spectrum to be the $(M + Li)^+$ ions of α -hydroxy-*N*-stearoyl-(4*E*)-sphinganine. We have not yet studied ceramides that contain hydroxyl groups in other positions in the *N*-acyl chain, but the presence and location of the hydroxyl group should be easily determined by the patterns of charge-remote fragmentations.^{31,32,34} Other types of substituents on the fatty acyl chain also should be easily identified in the same way.

Another commercially available mixture of ceramides, ceramides type III, which are obtained from bovine brain by the action of phospholipase C on bovine brain sphingomyelin, was analyzed. Three main components were found in the FAB spectrum of the mixture (Figure 5a), which give $[M + Li]^+$ ions of m/z 544, 572, and 654. The CID spectrum of the FAB-desorbed ion of m/z 654 is shown in Figure 5b, which is same as the spectrum of pure *N*-nervonyl-(4*E*)-sphinganine. Because there are no abundant FAB-desorbed ions in the vicinity of the ion of m/z 654 that is present in the mixture (Figure 5a), background subtraction³⁴ is not needed. The other two components of the mixture were also identified from their CID spectra: Compound 1 is *N*-palmitoyl-(4*E*)-sphinganine, and compound 2 is *N*-stearoyl-(4*E*)-sphinganine.

Another test of the analytical utility of this method is the detection limit for structural determination by CID. A 1-ng (2-pmol) amount of the $[M + Li]^+$ ions of *N*-palmitoyl-DL-sphinganine can be detected in the FAB spectrum at a signal-to-noise ratio of approximately 10 with Xe as fast atoms (Figure 6a). This spectrum of 2 pmol is comparable to that of 20 pmol for FAB-desorbed chemically derivatized ceramide $[M + H]^+$ ions reported previously.²⁸ A CID spectrum of 8 pmol of *N*-palmitoyl-DL-sphinganine, after subtraction of the matrix background, is shown in Figure 6b. The CID detection limits here are hampered because of poor precursor ion resolution of the first field-free region B/E linked scans. We previously⁴⁵ reported a slightly higher, 10-pmol, detection

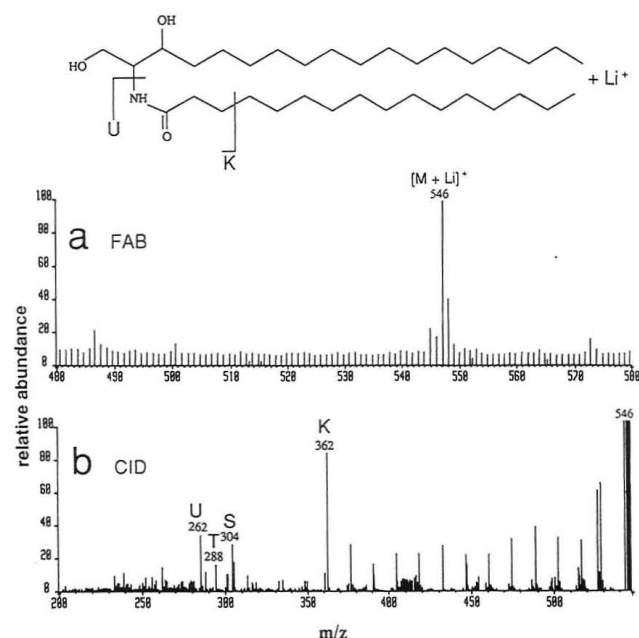


Figure 6. Mass spectra of *N*-palmitoyl-DL-sphinganine: (a) FAB spectrum of 2 pmol; (b) CID spectrum of 8 pmol after subtraction of matrix background. Xe is used as the FAB gas.

limit, but this was improved here by narrowing the α restrictors that are immediately before the ESA in the VG 70-S. The collision cell in the first field-free region is after the source slit and thus is not at an ion optical focal point. Narrowing the α restrictors, which are after the collision cell, improves beam directional focusing, and this results in improved precursor ion resolution. Although some artifacts from chemical noise are still present, the spectrum can be interpreted (compare Figure 6b to Figure 3a). The detection limits should be significantly lowered by using true tandem mass spectrometric techniques and multichannel array detectors.²⁸

Effects of Other Alkali-Metal Ions. Effects of the larger alkali-metal ions on the CID detection limit and fragmentation patterns were also studied. For example, CID spectra of $[M + Cat]^+$ ions, where Cat = alkali-metal ion, of *N*-palmitoyl-(4*E*)-sphinganine are shown in Figure 7. Several changes occur in the spectra with increasing size of alkali-metal ion. One is that increasingly competitive release of Cat^+ significantly reduces the abundances of the structurally informative product ions. Although losses of Li^+ , Na^+ , and K^+ are indeterminable from the B/E scans used here, we do observe losses of Rb^+ and Cs^+ . This results in an increased CID detection limit of 20 pmol for the $[M + Na]^+$ ions and a significantly poorer CID detection limit for the higher mass $[M + Cat]^+$ ions. The increased release of Cat^+ with increasing ionic radius has also been observed in CID spectra of cationized peptides^{36,56,57} and monosaccharides.⁵⁸ This is not surprising because ion-molecule interaction energies⁵⁹ and ligand-Cat⁺ bond energies⁶⁰ decrease with increasing ionic radius of the alkali-metal ion. There are more interesting changes in the spectra, however, that involve the relative abundances of open-shell (radical) product ions (labeled H + 1^{•+}, J + 1^{•+}, and S + 1^{•+}). The H + 1^{•+} ions, which are missing in spectra of ceramides that contain sphinganine instead of (4*E*)-sphinganine, arise from homolytic, allylic cleavages to give nominally an allylic radical site. The J + 1^{•+} ions nominally contain

(56) Grese, R. P.; Gross, M. L. *J. Am. Chem. Soc.* **1990**, *112*, 5098-5104.

(57) Mallis, L. M.; Russell, D. H. *Anal. Chem.* **1986**, *58*, 1076-1080.

(58) Röllgen, F. W.; Giessmann, U.; Borchers, F.; Levsen, K. *Org. Mass Spectrom.* **1978**, *13*, 459-461.

(59) Smith, S. F.; Chandrasekhar, J.; Jorgensen, W. L. *J. Phys. Chem.* **1982**, *86*, 3308-3318.

(60) Eliezer, I.; Krindel, P. *J. Chem. Phys.* **1972**, *57*, 1884-1891.

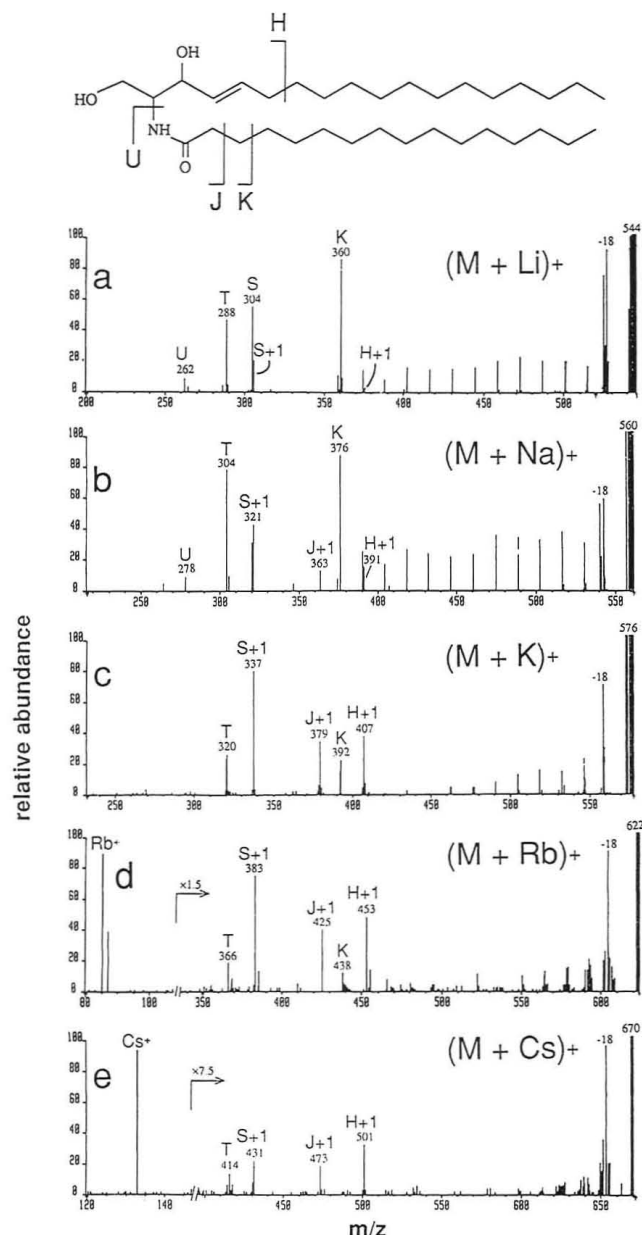


Figure 7. CID spectra of $[M + \text{Cat}]^+$ complexes of *N*-palmitoyl-(4*E*)-sphingine.

an acyl radical site, and the $S + 1^{++}$ ions nominally contain a homoallylic radical site (refer to Scheme IIIa). Similar spectra are obtained from seven ceramides studied. If these homolytic C–C bond cleavages arose remote from the charge site, the radical cations could conceivably be stable distonic ions^{61,62} in which the radical site would be on a carbon, and the charge site, an alkali-metal ion, would preferentially be on the carbonyl oxygen. Interestingly, formation of each radical cation becomes increasingly competitive with increasing size of the alkali-metal ion.

To understand this chemistry further, metastable ion decompositions were studied. The most obvious difference between metastable ion and CID spectra of $[M + \text{Li}]^+$ ions is that the higher mass closed-shell product ions formed by charge-remote losses of C_nH_{2n+2} are not detected as metastable ion fragmentations. The lower mass closed-shell S and K product ions and the $S + 1^{++}$ radical cations, are formed

Table I. Relative Abundances of $S + 1$ and S Product Ions in Metastable Ion and CID Spectra of *N*-Palmitoyl-(4*E*)-sphingine^a

alkali-metal ion	product ion	meta-stable ^b (%)	CID ^c (%)	% increase ^d	(S + 1)/S metastable	(S + 1)/S CID
Li ⁺	S + 1	0.10	0.03	30		
	S	0.13	0.24	185	0.77	0.35
Na ⁺	S + 1	0.06	0.13	217		
	S	0.03	0.11	366	2.0	1.2
K ⁺	S + 1	0.04	0.20	500		
	S	<0.001	<0.05	4900	<40	<4.1
	S + 1					

^a The abundances are expressed as percent relative to the main beam, not including the loss of the alkali-metal cations, which are not observable in the B/E linked scans. Losses of the metal ions metastably should be undetected.^{29,63} Losses by CID should be comparable to those reported for $[M + \text{Cat}]^+$ ions of fatty alcohols and acids.^{29,30} ^b True metastable ion decomposition spectra cannot be obtained because of residual FAB gas in the first field-free region. Thus, these values represent a maximum percent abundance. ^c This is the percent abundance in the CID spectra after subtracting contributions from metastable ion fragmentations. ^d This is the percent increase in abundance as a result of decompositions in the CID time frame.

metastably, however. One of the most interesting changes that occurs both metastably and by CID is the changes in relative abundances of the $S + 1^{++}$ and S ions with increasing size of the metal ion. The data for the $[M + \text{Cat}]^+$ ions of *N*-palmitoyl-(4*E*)-sphingine, in which Cat = Li⁺, Na⁺, and K⁺, are presented in Table I.

One way to try to interpret the data in Table I is from a classic kinetics point of view. This would require formation of $S + 1^{++}$ and S product ions from a population of structurally identical precursor ions that simply decompose via two (or more) competitive fragmentation routes. Because the ratios of the abundances of the $S + 1^{++}$ to the S ions are always greater in the metastable ion than in the CID time frame (compare columns 6 and 7 in Table I), the data would suggest that formation of $S + 1^{++}$ radical cations always involves a slower, lower energy reaction than the reaction that gives S closed-shell ions. This interpretation is unreasonable, however, from known reaction kinetics: To cleave the same C–C bond, a homolytic, direct bond cleavage (to give an $S + 1^{++}$ ion) should be a faster, higher energy reaction than a rearrangement (to give an S ion) (see Scheme IIIa).⁶⁴ Thus, the transition state for the $S + 1^{++}$ radical ions should be looser than, and its threshold energy greater than, the transition state for the S closed-shell ions. This means that the log $k(E)$ vs E curves for the $S + 1^{++}$ ions should be more steeply sloped than, and displaced to the right of, those for the S ions. Furthermore, the effect of the proximity of the charge site on the homolytic cleavage that gives the $S + 1^{++}$ radical cation should not be significantly different from its effect on the rearrangement that gives the S closed-shell ion. Indeed, formation of both $S + 1^{++}$ and S product ions from $[M + \text{Li}]^+$ precursors competes in the metastable ion time frame, and this indicates that they both have lower energy requirements than the more distal charge-remote losses of C_nH_{2n+2} that are not observed metastably. Thus, both $S + 1^{++}$ and S ions are better described as arising from lower energy, charge-induced reactions.

The inconsistencies between the experimental observations and a classic kinetic interpretation suggests that the different

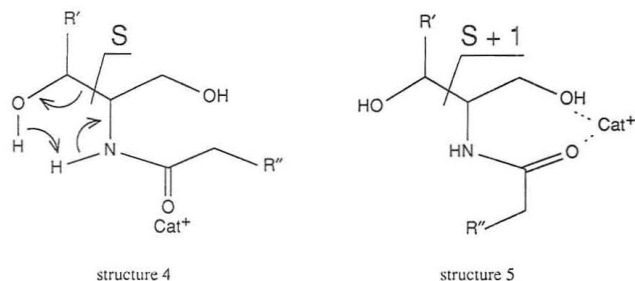
(61) Hammerum, S. *Mass Spectrom. Rev.* 1988, 7, 123–202 and references therein.

(62) Sack, T. M.; Cerny, R. L.; Gross, M. L. *J. Am. Chem. Soc.* 1985, 107, 4562–4564.

(63) Adams, J. Unpublished results.

(64) Benson, S. W.; O'Neal, H. E. *Kinetic Data on Gas Phase Unimolecular Reactions* (NSRDS-NBS 21); National Bureau of Standards, U.S. Government Printing Office: Washington, DC, 1970.

fragmentations arise from different sets of structurally distinct precursor ions. Furthermore, it would appear that the relative populations of the isomeric precursors change with increasing size of metal ion. Two such possible isomers are shown by structures 4 and 5. Structure 4 is proposed to be the primary



source of S product ions, and structure 5, to be the primary source of S + 1⁺ ions. The bases for these proposals are the chemistry of alkali-metal ion interactions with multifunctional compounds⁶⁵ and the data in Table I. For example, structure 4 would be expected to contribute more to the population of [M + Li]⁺ precursors because, for the small Li⁺, more energy would be intrinsically required to contract the open-chain structure shown by structure 4 into the cyclic chelate represented by structure 5.⁶⁵ With increasing size of metal ion, however, the cyclic structure 5 would be characterized by larger torsional angles and smaller repulsive interactions that would increase its thermodynamic stability and thus its relative population. These ideas are schematically depicted in Figure 8. Increasing formation of the more stable structure 5 (Figure 8c) results in a reduced population of structure 4, which in turn results in decreased formation of the S ions in both the metastable ion and CID time frames (columns 3 and 4 in Table I). Formation of the S + 1⁺ radical cations is virtually unchanged in the metastable ion time frame (column 3) but becomes increasingly competitive with larger metal ions in the CID time frame (column 4). As depicted in Figure 8, with increasing size of metal ion, the rate of the reaction

(65) Rode, B. M.; Hannongbua, S. V. *Inorg. Chim. Acta* 1985, 96, 91-97.

(66) Zhao, H.; Reiter, A.; Teesch, L. M.; Adams, J. *J. Am. Chem. Soc.*, in press.

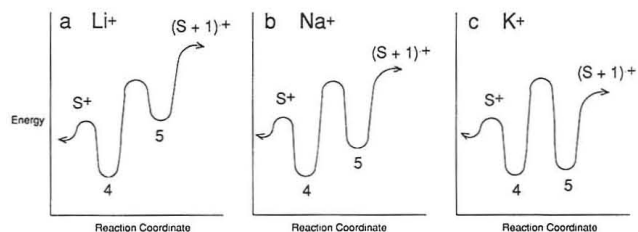


Figure 8. Schematic that describes increasingly competitive formation of structure 5 and S + 1⁺ radical cations with increasing size of metal ion. It should be noted that the threshold energies for both reactions remain the same, but formation of S⁺ involves a tight transition state whereas formation of S + 1⁺ involves an orbiting (loose) transition state. The barrier between the two structures is the isomerization barrier.

that involves the loose transition state that leads to the S + 1⁺ radical ions, as opposed to the tight transition state that gives the S ions, will become significant especially at higher energies, as in CID. Competitive fragmentations of different populations of precursor isomers here are similar to fragmentations of peptides complexes with alkaline-earth-metal ions^{35,66} in which the precursor ion beam is likewise composed of different structural isomers. The chemistry here, however, differs from that of peptides complexed with alkali-metal ions³⁷ in which relative product ion abundances can be adequately addressed by classic kinetics.

ACKNOWLEDGMENT

We acknowledge funding from the Petroleum Research Fund (Grant 25280-AC), which is administered by the American Chemical Society, the NSF (Grant CHE-9113272), and the Emory University Research Fund. Preliminary reports of this work were presented at the 1991 Sanibel Conference on Mass Spectrometry, Sanibel Island, FL, January, 1991; at the 201st National Meeting and Exposition of the American Chemical Society, Atlanta, GA, April, 1991; and at the 39th ASMS Conference on Mass Spectrometry and Allied Topics, Nashville, TN, May, 1991. We also acknowledge M. J. Contado for early technical work.

RECEIVED for review February 13, 1992. Accepted October 5, 1992.

Matrix-Assisted Laser Desorption of Biological Molecules in the Quadrupole Ion Trap Mass Spectrometer

David M. Chambers,[†] Douglas E. Goeringer,* Scott A. McLuckey, and Gary L. Glish[‡]

Analytical Chemistry Division, Oak Ridge National Laboratory, Oak Ridge, Tennessee 37831-6365

Matrix-assisted laser desorption (MALD), which has been proven to be an effective ionization technique for biological molecules, has been implemented on a quadrupole ion trap mass spectrometer (ITMS). In the instrumental configuration used for this work both the sample probe and the laser beam are brought through holes in the ring electrode, thereby enabling MALD-generated ions to expand directly into the ion trap cavity. This approach for directly introducing MALD-generated ions complements the capabilities of the ITMS to obtain low detection limits and to perform tandem mass spectrometric analysis. For example, detection limits in the single-unit femtomole regime have been achieved for small polypeptides such as leucine enkephalin, bradykinin, and neuromedin U-8. Furthermore, structural information has been acquired via multiple stages of mass spectrometry. One limitation that currently exists is an unanticipated drop in sensitivity and resolution as the mass/charge ratio for ions exceeds 3000.

INTRODUCTION

Since its introduction in 1988^{1,2} matrix-assisted laser desorption (MALD) coupled with mass spectrometry has experienced rapid application development³⁻⁹ as well as recent gains in understanding of the ionization mechanism itself.¹⁰⁻¹⁴ This activity has resulted in part because of the ease in which MALD can be implemented and because of current demands in analytical biotechnology for techniques that provide molecular weight and structural information on biological molecules.¹⁴ In MALD, an analyte such as a polypeptide is combined with a 100-50 000 molar excess of matrix and placed on a probe tip. The sample/matrix combination is irradiated with a laser pulse short enough to heat only the matrix. Provided that the matrix has a high absorption coefficient at the wavelength of the laser radiation, does not efficiently transfer energy to the analyte, and has a low heat of

sublimation, its transition from solid to gas phase results in transport of the analyte into the gas phase. As the matrix and analyte are desorbed from the substrate surface, a free-jet expansion is believed to form, collisionally cooling the analyte molecules.¹³ This process produces stable, intact analyte species that at some point become protonated.¹⁵

Mass analysis of MALD-derived ions has been carried out most often with time-of-flight (TOF) mass spectrometers³⁻⁹ due primarily to their inherent compatibility with pulsed ionization techniques and high-mass range. Although the compact ion packet produced by MALD is well-suited for TOF mass analysis, the kinetic energy spread of such ions is detrimental to high-resolution measurements. Decay of ions along the flight tube is thought to contribute to degradation in resolution as well.¹⁶ Currently, mass resolution ($m/\Delta m$, full-width at half-maximum, fwhm) up to 1170 at m/z 5734 has been reported for MALD/TOF using a two-stage reflectron.¹⁶ Another drawback of the TOF instrument is the limited ability to perform tandem mass spectrometric analysis (MS^n), which is useful for obtaining ionic structural information. Furthermore, because MS^n with TOF instruments is tandem-in-space, each step of analysis requires an additional TOF stage.

The use of other types of mass analyzers has been explored as a means for circumventing disadvantages associated with TOF. For example, a high-performance hybrid mass spectrometer (EB/TOF) has been utilized for CID of MALD-derived ions.¹⁷ In that particular study subfemtomole detection limits were demonstrated for the angiotensin II parent ion, but resolution for parent and product ions was low due to a relatively broad arrival time distribution of $[M + H]^+$ ions. Other promising results have been reported employing the MS-2 of a tandem mass spectrometer of EBEB configuration.¹⁸ To offset the disadvantages associated with pulsed ionization on conventional scanning mass spectrometers, an integrating focal-plane detector was used. In these studies a few picomoles of sample was typically used to produce spectra from substances with molecular weights up to the instrumental mass limit of m/z 14 000 (10-kV accelerating voltage). Mass resolution up to 2600 at m/z 1348 was reported.

Another class of mass analyzer based on ion trapping, the Fourier transform ion cyclotron resonance (FT/ICR) mass spectrometer, has been under investigation for use with MALD.¹⁹⁻²² The advantages of combining MALD with FT/ICR were evident from earlier studies,²⁰ namely high-

[†] Present address: Lawrence Livermore National Laboratory, Chemistry and Materials Science Department, Livermore, CA 94550.

[‡] Present address: University of North Carolina, Department of Chemistry, Chapel Hill, NC 27599.

- (1) Karas, M.; Hillenkamp, F. *Anal. Chem.* 1989, 60, 2299.
- (2) Tanaka, K.; Waki, H.; Ido, Y.; Akita, S.; Yoshida, Y.; Yoshida, T. *Rapid Commun. Mass Spectrom.* 1988, 2, 151.
- (3) Beavis, R. C.; Chait, B. T. *Rapid Commun. Mass Spectrom.* 1989, 3, 436.
- (4) Beavis, R. C.; Chait, B. T. *Anal. Chem.* 1990, 62, 1836.
- (5) Overberg, A.; Karas, M.; Bahr, U.; Kaufmann, R.; Hillenkamp, F. *Rapid Commun. Mass Spectrom.* 1990, 4, 293.
- (6) Overberg, A.; Karas, M.; Hillenkamp, F. *Rapid Commun. Mass Spectrom.* 1991, 5, 128.
- (7) Brown, R. S.; Gilfrich, N. L. *Anal. Chim. Acta* 1991, 248, 541.
- (8) Chan, T. W. D.; Colburn, A. W.; Derrick, P. J. *Org. Mass Spectrom.* 1991, 26, 342.
- (9) Doktycz, S. J.; Sowickas, P. J.; Krueger, D. A. *Rapid Commun. Mass Spectrom.* 1991, 5, 145.
- (10) Vertes, A.; Gijbels, R.; Levine, R. D. *Rapid Commun. Mass Spectrom.* 1990, 4, 228.
- (11) Spengler, B.; Cotter, R. J. *Anal. Chem.* 1990, 62, 793.
- (12) Beavis, R. C.; Chait, B. T. *Chem. Phys. Lett.* 1991, 181, 479.
- (13) Vertes, A. *Microbeam Anal.* 1991, 26, 25.
- (14) Carr, S. A.; Hemling, M. E.; Bean, M. F.; Roberts, G. B. *Anal. Chem.* 1991, 63, 2803.

(15) Kammer, H. F. *Proc. Phys. Small Syst.* 1990, 3, 61.

(16) Spengler, B.; Kirsch, D.; Kaufmann, R. *Rapid Commun. Mass Spectrom.* 1991, 5, 198.

(17) Strobel, F. H.; Solouki, T.; White, M. A.; Russell, D. H. *J. Am. Soc. Mass Spectrom.* 1991, 8, 91.

(18) Hill, J. A.; Annan, R. S.; Biemann, K. *Rapid Commun. Mass Spectrom.* 1991, 5, 395.

(19) Nuwaysir, L. M.; Wilkins, C. L. *Proc. SPIE—Int. Soc. Opt. Eng.* 1991, 1437, 112.

(20) Hettich, R. L.; Buchanan, M. V. *J. Am. Soc. Mass Spectrom.* 1991, 2, 22.

(21) Hettich, R. L.; Buchanan, M. V. *J. Am. Soc. Mass Spectrom.* 1991, 2, 402.

resolution and tandem-in-time mass spectrometry capabilities. Recent successes include the ability to analyze ions with m/z 34 000 and achieve resolution of 3300 at m/z 2847.²²

In this work a different type of ion-storage device, the quadrupole ion trap mass spectrometer (ITMS), is investigated for the analysis of MALD-generated ions. Many of those strengths that make FT/ICR attractive for MALD are also shared by ITMS, namely high sensitivity,²³ the capability of multistep, tandem-in-time mass spectrometry,²⁴ mass range extending beyond m/z 45 000,²⁵ and a demonstrated mass resolution of up to 10^6 .²⁶⁻²⁸ The capability for multistep, tandem-in-time mass spectrometry of laser-desorbed ions has also been demonstrated.²⁹ Moreover, in contrast to the FT/ICR, the ITMS is normally operated with a helium buffer gas in the millitorr pressure regime. Collisional damping of ion motion in the ion trap is known to moderate ion kinetic energies, a phenomenon that might prove advantageous for trapping MALD-derived ions.

The capabilities and limitations of the standard commercial ITMS when used as a mass analyzer for MALD are evaluated in this paper. This study includes examination of detection limits, mass range, resolution, and tandem mass spectrometric analysis capabilities for selected polypeptides. In addition, several fundamental studies that reveal paths for future development are reported.

EXPERIMENTAL SECTION

Apparatus and Procedures. Experiments were performed using a Nd:YAG laser (Quanta-Ray, DCR-2A) and a Finnigan ITMS. The Q-switched, frequency-quadrupled output (266 nm) from the laser was first directed through a 3-mm aperture and suitably attenuated (Newport, 935-5 variable attenuator) before it was finally focused with a 45-mm focal length lens into the ITMS. Modifications to the ion trap ring electrode, as described elsewhere,²⁹ included drilling two horizontally aligned holes that permitted the laser beam to pass radially through the trap cavity. MALD was performed *in situ* by inserting the sample probe through the hole opposite the impinging laser beam. Laser power was adjusted to maximize $[M + H]^+$ signals while minimizing fragmentation from thermal decomposition. Typical laser power densities at the probe surface were estimated to be 1×10^6 W/cm². To aid high-mass measurement, the standard ITMS detector was replaced with a high-voltage conversion dynode unit from a Finnigan TSQ-700 tandem quadrupole mass spectrometer. The dynode of the replacement detector was operated at -10 kV. The uncorrected, static bath gas (helium) pressure in the vacuum housing was typically 1.0×10^{-4} Torr, as determined with a Bayard-Alpert ionization gauge. Dynamic pressure increases were produced when desired by periodically introducing additional bath gas through a pulsed valve (Newport, BV 100).

Laser desorption was synchronized with the ion trap scan function via the software-adjustable ITMS electron-gate pulse that triggered the laser. When several spectral scans were averaged, each individual scan was summed in computer memory before the average spectrum was displayed. Because the interval required for real-time display of the averaged data was somewhat longer than a single-scan period, a variation in the laser-pulse

repetition rate occurred. This variation resulted in pulse-to-pulse laser-power fluctuations due to thermal lensing in the YAG rods. The power variations could be reduced by firing just the laser flashlamps a few times prior to the UV-desorption/data-acquisition sequence. Although the standard Nd:YAG controls can be adjusted to trigger only the flashlamps via an external signal, the Q-switch must be manually triggered each time an optical pulse is required. Thus, the Q-switch circuit was modified to permit electronic control by connecting a transistor in parallel with the manual enable switch.

A single-scan sequence began by issuing three laser trigger signals at 100-ms intervals to initially trigger only the flashlamps; a software-actuated trigger signal was then given prior to the next laser-trigger signal to enable the Q-switched optical output. Thus, an optical (266-nm) pulse occurred on every fourth flashlamp pulse. The pulsed valve was also actuated by the trigger signal when a brief pressure increase was required. The trigger signal was taken directly from the scan-acquisition processor board and was amplified and extended with a pulse generator (Berkeley Nucleonics Corp., Model 8010). Following the optical-pulse sequence, one of the various ion manipulation procedures described below was then performed and a data-acquisition mass scan was subsequently made. One scan was composed of such a sequence of events; five scans were typically averaged to generate spectra for the data presented here.

After the laser desorption event, trapped ions were stored for a period of 5–10 ms to allow for collisional cooling. The stored ions were then manipulated in an experimentally dependent manner. MALD mass spectra were obtained using resonance ejection³⁰ to extend the mass range above the nominal limit of m/z 650 associated with the mass-selective instability mode. Tandem mass spectrometry experiments were initiated by resonance ejection of ions with m/z values less than the parent species.³¹ Once isolated, parent ions were collisionally activated via resonance excitation. A modified version of the scan editor obtained from Finnigan Corp. permitted the excitation frequency to be directly specified, thereby enabling ions above m/z 650 to be kinetically excited to effect collision-induced dissociation (CID). When multiple stages of mass spectrometry were performed, each additional stage used ejection of low- m/z CID products before collisional activation. Data acquisition followed the final stage of isolation and CID.

Samples. The matrix used was a 50 mM solution of commercially obtained nicotinic acid dissolved in methanol and high-performance liquid chromatography grade water (30/70 v/v) and trifluoroacetic acid (0.1%). Stock analyte solutions of 10–100 μ M were separately prepared by dissolving the requisite amount of sample in the same solvent mixture used to prepare the matrix solutions. These stock solutions were diluted as needed. Before sample analysis 1 μ L each of the analyte and matrix solutions was applied to the probe tip (borosilicate glass), and the sample was then rapidly admitted to the probe pump-out region and allowed to dry. The probe tip diameter was 2 mm.

For detection limit determinations, the concentration values resulting from serial dilutions were such that 1 μ L corresponded to a sample loading close to the detection limit (within the same order-of-magnitude). Five single-laser-shot spectra were averaged for detection limit determinations. To obtain the highest sensitivity the laser power was increased and the time between consecutive laser pulses was minimized. Analyte-signal peak heights such spectra were extrapolated linearly to determine detection limits corresponding to a net signal-to-background noise ratio of 3. The noise was estimated as one-fifth the peak-to-peak variation of the background.³²

RESULTS AND DISCUSSION

Detection Limits and Upper Mass Capabilities. Detection limits and mass/charge range are important figures of merit to evaluate so instrumental limitations can be defined

(22) Castro, J. A.; Köster, C.; Wilkins, C. *Rapid Commun. Mass Spectrom.* 1992, 6, 239.

(23) Goeringer, D. E.; Whitten, W. B.; Ramsey, J. M. *Int. J. Mass Spectrom. Ion Processes* 1991, 106, 175.

(24) Louris, J. N.; Cooks, R. G.; Syka, J. E. P.; Kelley, P. E.; Stafford, G. C.; Todd, J. F. *J. Anal. Chem.* 1987, 59, 1677.

(25) Kaiser, R. E., Jr.; Cooks, R. G.; Stafford, G. C.; Syka, J. E. P.; Hemberger, P. H. *Int. J. Mass Spectrom. Ion Processes* 1991, 106, 79.

(26) Schwarz, J. C.; Syka, J. E. P.; Jardine, I. *J. Am. Soc. Mass Spectrom.* 1991, 2, 198.

(27) Goeringer, D. E.; McLuckey, S. A.; Glish, G. L. *Proceedings of the 39th ASMS Conference on Mass Spectrometry and Allied Topics*, Nashville, 1991; p 532.

(28) Williams, J. D.; Cox, K.; Morand, K. L.; Cooks, R. G.; Julian, R. K., Jr.; Kaiser, R. E., Jr. *Proceedings of the 39th ASMS Conference on Mass Spectrometry and Allied Topics*, Nashville, 1991; p 1481.

(29) Glish, G. L.; Goeringer, D. E.; Asano, K. G.; McLuckey, S. A. *Int. J. Mass Spectrom. Ion Processes* 1989, 94, 15.

(30) Kaiser, R. E., Jr.; Louris, J. N.; Amy, J. W.; Cooks, R. G. *Rapid Commun. Mass Spectrom.* 1989, 3, 225.

(31) McLuckey, S. A.; Goeringer, D. E.; Glish, G. L. *J. Am. Soc. Mass Spectrom.* 1991, 2, 11.

(32) Hieftje, G. M. *Anal. Chem.* 1972, 44, 81A.

Table I. Detection Limits for Several Polypeptides

polypeptide	mol wt	detn limit
leucine enkephalin	555.6	4 fmol
bradykinin	1060.2	1 fmol
neuromedin U-8	1111.3	6 fmol
neurotensin ^a	1672.9	15 fmol
melittin ^c	2846.5	90 fmol
bovine insulin ^b	5733.5	9 pmol
horse cytochrome c ^c	12360	22 pmol

^a Dynamic He pressure, 5×10^{-4} Torr uncalibrated. ^b Static Ar pressure, 10×10^{-4} Torr uncalibrated. ^c Static Ar pressure, 20×10^{-4} Torr uncalibrated.

and eventually understood. Consequently, the detection limits and characteristics of high mass/charge operation for MALD/ITMS are examined empirically in this section. As previously noted, ion trap mass spectra for $\text{Cs}(\text{CsI})_n^+$ cluster ions with m/z values exceeding 45 000 have been obtained using resonance ejection at reduced β_z values.³⁰ In that study the ion trap electronics were also modified for operation at a reduced rf drive frequency and ramp rate, and cluster ions were produced external to the ion trap by Cs^+ bombardment and subsequently injected into the ion trap. In contrast, our experimental configuration involved internal generation of MALD ions, and the ion trap electronics were not modified.

Table I lists molecular weight and detection limit data for the polypeptides examined. Below m/z 2000, detection limits were in the low-femtomole range; however these limits rose as m/z 6000 was approached. Shown in Figure 1 are typical spectra for neurotensin (100 fmol), melittin (500 fmol), bovine insulin (163 pmol), and horse cytochrome *c* (160 pmol). These data reflect not only the increase in detection limit with mass but also a decrease in resolution that is discussed further in a later section. An explanation for this inverse correlation between mass and detection limit can be postulated from the results obtained by Beavis and Chait for the kinetic energy of MALD-generated ions.¹² Their experiments indicate that gas dynamic acceleration of the laser-induced, free-jet expansion imparts a mass-independent, most-probable velocity of approximately 750 m/s to analyte ions. Thus, they predicted that analytes of increasingly higher mass should require correspondingly greater trapping fields because kinetic energy of MALD-derived ions scales directly with mass. The ramifications of their prediction on MALD/ITMS mass limits can be seen using the harmonic oscillator model of ion motion in the quadrupole ion trap. In that model, the radial pseudopotential well depth for the ion, D_r , is given by

$$D_r = -eV_\Omega^2/4mr_0^2\Omega^2 = q_r^2mr_0^2\Omega^2/16e$$

where m is ion mass, e is charge, r_0 is the radius of the ring electrode, V_Ω and Ω are the fundamental rf voltage (0-pk) and radial frequency, respectively, and q_r represents the working point in the radial plane. Note that D_r decreases with increasing mass/charge for fixed values of operating parameters but increases with mass for a fixed q_r . If the upper kinetic energy limit for trapping MALD-derived ions is assumed to be equal to D_r , then calculations ($r_0 = 1$ cm, $V_\Omega = 7500$ V, $\Omega = 1.1$ MHz, ion velocity = 750 m/s) yield a high-mass limit of m/z 9830 for MALD/ITMS. However, given that there is a distribution of translational energies it would be expected that higher masses could be trapped, although with less efficiency, if the potential well depth is important to the trapping process.

To gain further insight into the MALD/ITMS combination, we distinguished the action of capturing ions (referred to as "trapping") from the action of storing ions once their trajectories have been stabilized via collisionally cooling (referred to as "storage") by temporal separation of the processes. In the first group of experiments the effect of rf

trapping level during laser desorption was studied for several polypeptides. Figure 2 depicts the scan functions used. For each of the experiments the rf level during and 5 ms after desorption was held at a specific value (Figure 2, region a). Then the rf amplitude was reduced to a storage level of 2308 V (low-mass cutoff = m/z 200) over a 15-ms period (Figure 2, region b), and the mass spectrum was then obtained. Results were taken with the mass range extended by a factor of 5 by resonance ejection. The data, which were acquired for the $[\text{M} + \text{H}]^+$ ions of neuromedin U-8, neurotensin, and melittin, are plotted in Figure 3. On the basis of the kinetic energy/well depth reasoning presented above, the ion signal would be expected to increase at some m/z -dependent rf trapping level. A threshold for increase in ion signal, which is m/z dependent, is seen in the data in Figure 3. The slope of the rising portion of such a signal vs rf level curve would also be predicted to decrease with increasing m/z (i.e., as the kinetic energy distribution of desorbed ions becomes broader). The curves in Figure 3 show such behavior. Beavis and Chait found rather broad ion kinetic energy distributions (e.g., 10–100 eV for m/z 15 590) that might be caused by interactions among charged species in regions of the expansion where ion movement is no longer dominated by neutral flow (analogous phenomena are documented in gas dynamic studies³³). Consequently, the availability of MALD-derived ions with the proper kinetic energy for trapping, presumably those in the low-energy tail of the distribution, suggests it may be possible to obtain MALD/ITMS spectra for larger molecules at relatively low rf levels. However, for each of the curves the ion signal falls off at higher rf trapping levels. This behavior is inconsistent with an argument for increased well depth with rf trapping level; such reasoning would predict a plateau for desorbed ion signal above some rf level. A possible explanation is that although the well depth increases with rf trapping level, the effective trapping volume decreases. We have attributed experimental results from the electron ionization and photoionization of vapor-phase species, which showed a reduction in the number of ions formed as the rf level increased, to such an effect.³⁴ Similar behavior has also been observed in ion injection experiments.³⁵

The dependency of ion signal (neurotensin $[\text{M} + \text{H}]^+$) on rf storage level was studied in the second group of experiments. The scan function shown in Figure 4 was used. For these experiments the rf level during and 15 ms after desorption was held at 2308 V (low-mass cutoff = m/z 200). The rf amplitude was then reduced to a specified storage level over a period no shorter than 5 ms (Figure 4, region b). As shown in Figure 5 (data points represented by squares) the ion signal for neurotensin fell sharply when the rf storage level was brought below 856 V (low-mass cutoff = m/z 75). Further experiments involved inserting a 50-ms delay following desorption (Figure 4, region a) to ensure sufficient time for kinetic cooling before the rf level was lowered. The same low-mass cutoff at m/z 75 was seen (Figure 5, data points represented by circles). The lower ion signals in the plateau region for this latter experiment resulted from a decrease in laser repetition rate and concomitant power reduction; this fact was confirmed when the 50-ms delay was moved to the end of the scan function with no discernible effect on Figure 5 results (data points represented by circles). The data in Figure 5 indicate that neurotensin ion-storage inefficiencies occur below an rf level of 856 V.

Similar analyses to those shown in Figure 5 were made for ions with a range of m/z values to investigate the m/z

(33) Spokes, G. N.; Evans, B. E. *Tenth Symposium (International) on Combustion*; Combustion Institute: Pittsburgh, PA, 1965; p 644.

(34) Hart, K. J.; McLuckey, S. A.; Glish, G. L. *Proceedings of the 39th ASMS Conference on Mass Spectrometry and Allied Topics*, Nashville, 1991; p 1495.

(35) McLuckey, S. A.; Glish, G. L.; Asano, K. G. *Anal. Chim. Acta* 1989, 225, 25.

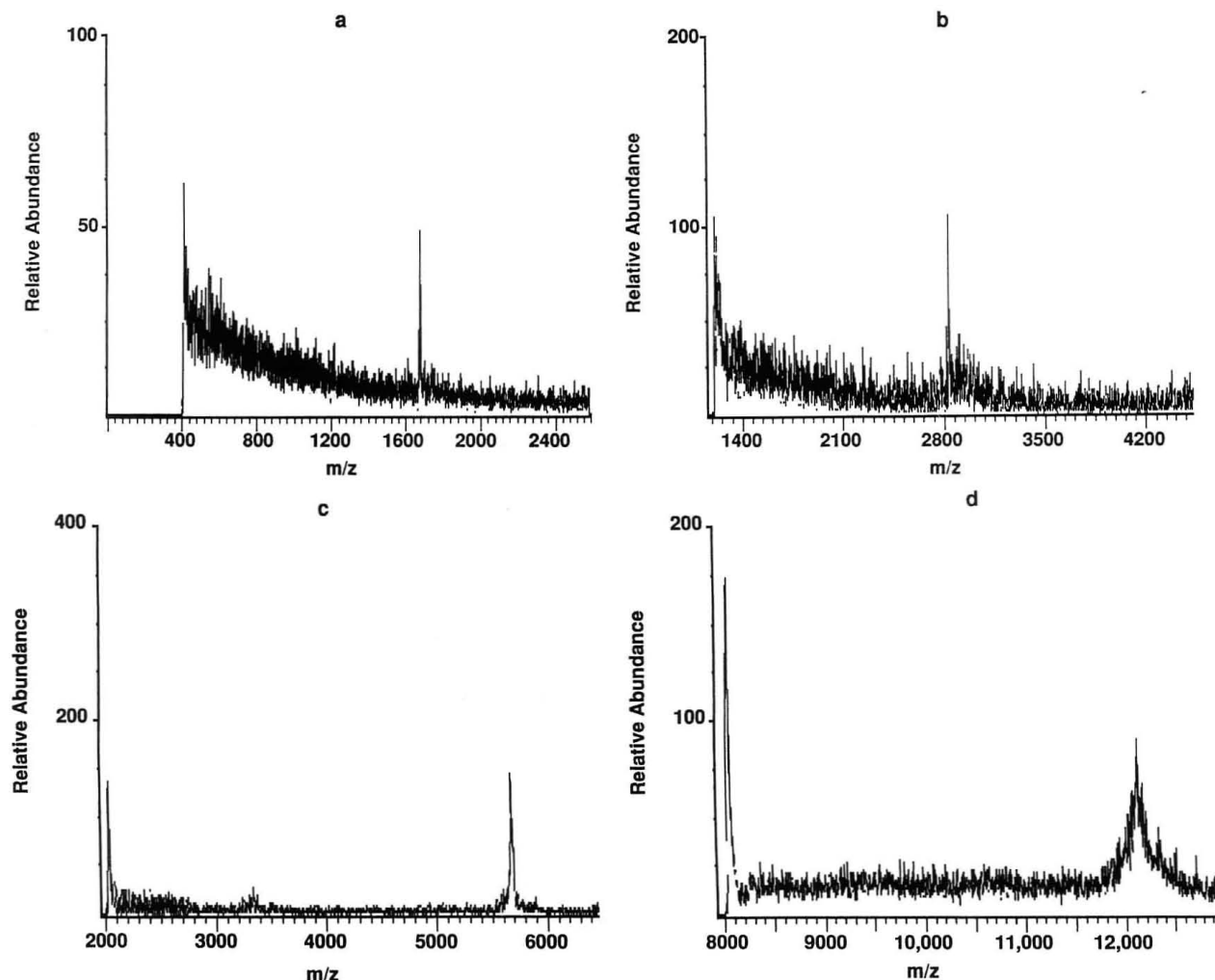


Figure 1. Matrix-assisted laser desorption of (a) 100 fmol of neurotensin, (b) 500 fmol of melittin, (c) 163 pmol of bovine insulin, (d) and 160 pmol of horse cytochrome *c*. The mass/charge axes were not determined via internal standard calibration but were assigned from resonance ejection frequencies (mass range extension factors) based on instrument software.

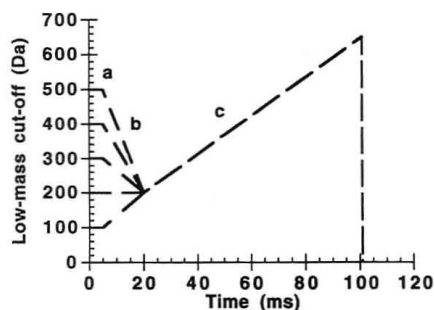


Figure 2. Scan functions used to deduce the effect of the rf level on trapping efficiency: (a) desorption/delay; (b) rf ramp; (c) data acquisition rf ramp.

dependence of ion storage. For these experiments a scan function similar to that shown in Figure 4 was used, with the exception that the initial rf level was adjusted to be sufficiently above the ion-storage drop-off level for each particular m/z . In Figure 6 the desorbed ion signal drop-off point is plotted as a function of the ion-storage rf level. A theoretical upper mass limit of m/z 17 600, corresponding to a sustained low-mass cutoff of m/z 650 ($V_{\Omega} = 7500$ V, $\Omega = 1.1$ MHz, $r_0 = 1$ cm), can be linearly extrapolated from the plot. These data are significant because they indicate that a variable upper m/z limit for ion storage of MALD-generated ions exists and is a function of the fundamental rf amplitude. However, detection limits and resolution degraded significantly before the projected upper limit for ion storage was approached experimentally.

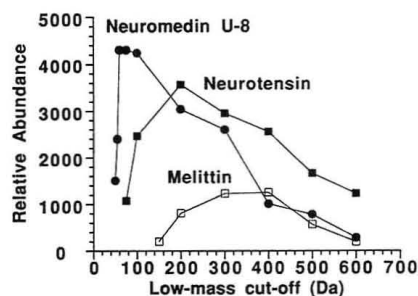


Figure 3. Effect of rf trapping level on neuromedin U-8, neurotensin, and melittin $[M + H]^+$ ion signals. Data were collected with the scan function shown in Figure 2.

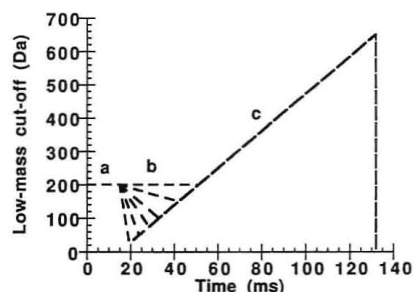


Figure 4. Scan functions used to discern the effect of the rf level on storage efficiency: (a) laser desorption/delay; (b) rf ramp; (c) data acquisition rf ramp.

Pulsed Pressures during Laser Desorption. As described in the previous section, two competing processes might be responsible for the drop in sensitivity as m/z increases.

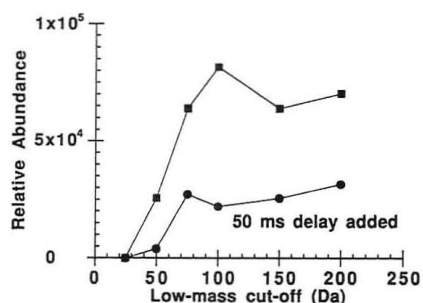


Figure 5. Dependence of neurotensin $[M + H]^+$ ion signal on rf storage level. Results plotted with circles (●) represent data taken with the scan function plotted in Figure 2 where a 15-ms delay occurs after the laser desorption pulse. Results plotted with squares (■) were taken with an additional 50 ms added after the initial 15-ms laser desorption delay (Figure 2, region a).

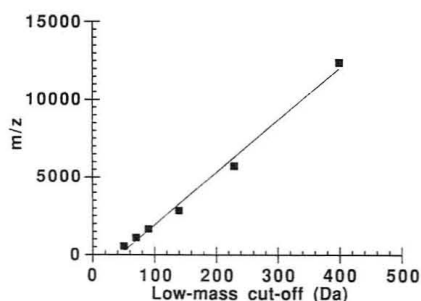


Figure 6. Onset of ion-storage plateau (see Figure 3) as a function of ion mass.

First, strong fields are likely needed to trap large ions that possess high kinetic energies. Second, as the rf level is raised, the trapping volume is believed to decrease, requiring some mechanism to collapse ions closer to the trap center. The effect of dynamic and static pressure increases on ions with high- m/z values was pursued to study collisional damping of ions desorbed from the probe surface as well as of ions toward the center of the trap. Dynamic pressure surges were initially implemented to provide a temporarily elevated pressure that could moderate initial ion kinetic energies that desorbed species obtain from gas dynamic acceleration. However, because this momentary pressure surge exceeded the time to execute a typical scan function, higher pressures also persisted during ion storage and ejection. In later studies the pressure was statically controlled, which produced results similar to those using the dynamic approach. The effects of increased collisional damping by the argon on heavy species should be similar to that demonstrated on lighter ions when a helium buffer gas is used (i.e., enhanced resolution and sensitivity).³⁶ Even though heavier buffer gases promote ion loss through collisional scattering of low-mass ions, the kinematics of a 2500-Da ion colliding with Ar is analogous to a 250-Da ion colliding with He. As a result it is difficult to isolate the effect of pulsed or elevated pressure on gas dynamic acceleration and collisional damping; thus, either of these mechanisms should be considered as possible explanations for the aforementioned enhancement.

The results provided below demonstrate the enhancement obtained from pulsing argon before laser desorption. Although the pulsed argon was not found to improve signals of ions with m/z values below 2000, a significant gain was seen for both melittin and bovine insulin. An example of this enhancement is depicted in Figure 7 where the signal for the melittin $[M + H]^+$ ion was increased over 1 order of magnitude as peak Ar pressure (achieved after four consecutive scans) approached 2×10^{-3} Torr. In a similar manner, bovine insulin,

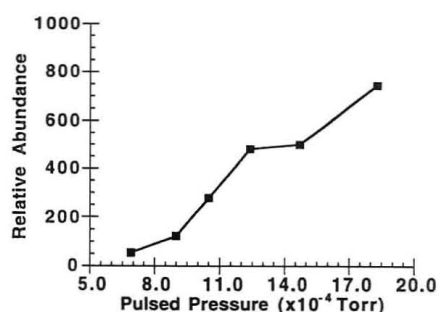


Figure 7. Intensity of melittin $[M + H]^+$ ion signal (m/z 2848) as a function of pulsed argon pressure.

which was initially undetectable, could be detected as the static Ar pressure reached 10×10^{-3} Torr (refer to Figure 1c). At a static Ar pressure of 20×10^{-3} Torr horse cytochrome *c* was detectable but exhibited poor resolution (Figure 1d). Gains in resolution with higher pulsed argon pressures were realized for melittin and bovine insulin, yet lower mass ions such as bradykinin and neuromedin exhibited modest declines. At a static Ar pressure of 20×10^{-3} Torr bradykinin and neuromedin were not readily detectable.

Mass Resolution and Mass Accuracy. Extended mass range operation via resonance ejection at reduced β_z values is not without consequence on mass resolution. Specifically, if the fundamental rf ramp rate remains unchanged, this technique causes an effective increase in the mass/charge scan rate that scales directly with the mass range extension factor. Such an increase in scan rate has been shown experimentally²⁶ and theoretically³⁷ to result in resolution degradation. Furthermore, because the number of points digitized per unit time also remains constant under such conditions, the number of sample points defining a mass peak shape decreases directly with the extension factor as well.

The effects of extended m/z scans are evident in Figure 8, which show spectra of bradykinin taken at mass range extension factors of 2 and 9. Under these conditions, the corresponding resolutions were 570 (Figure 8a) and 142 (Figure 8b). These values are a factor of roughly 2 and 9 times lower, respectively, than generally obtained using the standard rf ramp rate near the high- m/z limit of the normal m/z 650 range. The effects of extending the m/z range on resolution can be compensated for by reducing the rf ramp rate.²⁵ However, the electronic modifications necessary to perform this type of experiment have not been made on our instrument.

The spectrum for horse cytochrome *c* in Figure 1d (mass range extension factor 20) shows resolution lower than that expected simply from higher effective scan rates. The poorly resolved peak for the molecular ion (12 360 units) is similar in shape to those seen under conditions of excessive ion space charge, which is known to degrade resolution in the ion trap.³⁶ Because ions are normally ejected from low to high m/z during a mass scan, such effects on resolution are often more evident at lower m/z values. The presence of adduct clusters, commonly seen in MALD spectra (especially for higher molecular weight compounds), may also account for the poorly resolved $[M + H]^+$ ion.

Mass accuracy is defined in this discussion as mass assignment error divided by the ion mass and is taken as a percentage. One convenient method for mass calibration involved generating a calibration plot using two peptides of known mass/charge. For example, a mass accuracy of 0.05% could readily be obtained for the neurotensin $[M + H]^+$ ion (1673.9 units) from a calibration plot made using MALD-generated melittin ($[M + H]^+$, 2846.5 units) and bradykinin ($[M + H]^+$, 1061.2 units) ions. It is important to note that mass accuracy does not vary significantly from one MS stage

(36) March, R. E.; Hughes, R. J. In *Quadrupole Storage Mass Spectrometry*; Winefordner, J. D., Kolthoff, I. M., Eds.; Chemical Analysis Series 102; Wiley: New York, 1989.

(37) Goeringer, D. E.; Whitten, W. B.; Ramsey, J. M.; McLuckey, S. A.; Glish, G. L. *Anal. Chem.* 1992, 64, 1434.

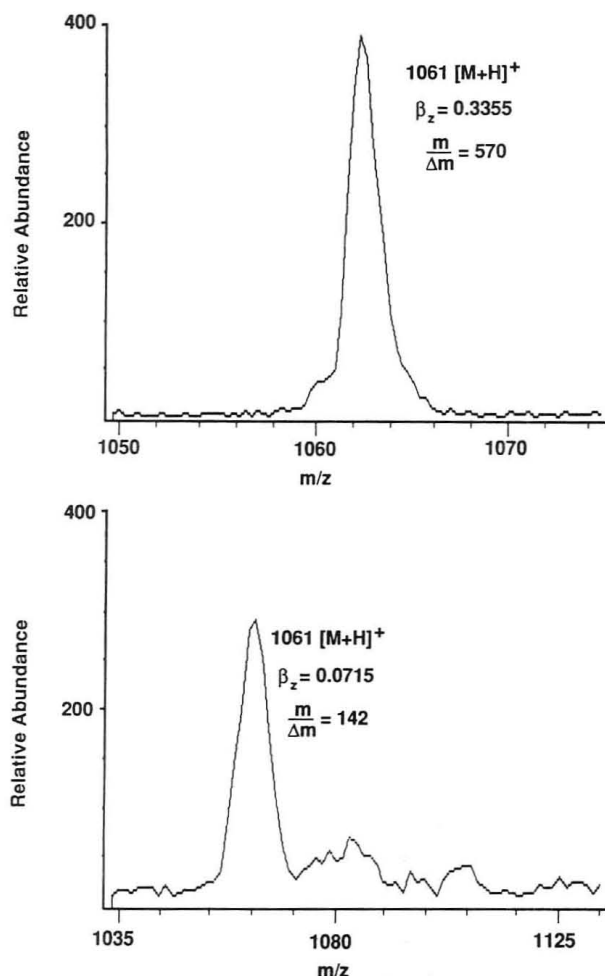


Figure 8. Comparison of mass resolution as the mass range for bradykinin mass scans was extended by factors of (a, top) 2 ($\beta_z = 0.336$) and (b, bottom) 9 ($\beta_z = 0.0715$).

to the next in the ITMS, so similar accuracy can be expected in MS^n experiments. Normally, a calibration plot could be used reliably throughout the day. Problems with mass calibration were encountered in those instances where excessive ion density was incurred, resulting in a peak shift to higher m/z values. This effect is caused by space-charge-induced changes in ion secular frequency and can be visualized as a distortion in the stability diagram.³⁶

Multiple Stages of Mass Spectrometry. One of the most appealing features of the ion trap is the tandem-in-time MS^n -experiment,²⁴ which can be performed repeatedly as long as sufficient ion populations are available from the previous stage of the experiment.³⁸ This procedure has already been demonstrated for peptides using Cs^+ desorption ionization followed by ion injection into an ion trap.³⁹ In that study sequence information was obtained from CID experiments with up to four stages of mass spectrometry. Similar mass spectrometric capabilities are presented below to demonstrate CID on MALD-generated polypeptide ions. Acquisition of such tandem mass spectra requires tuning the resonance excitation frequency, amplitude, and duration for kinetic excitation of targeted ions at each stage of MS; such an empirical process typically requires a few minutes to tens of minutes depending on the operator's experience. Once the optimum conditions have been established, each stage of MS then requires ~ 100 ms.

Plotted in Figures 9 and 10 are MS^4 and MS^3 experiments on 100 pmol of bradykinin and 1 pmol of neurotensin,

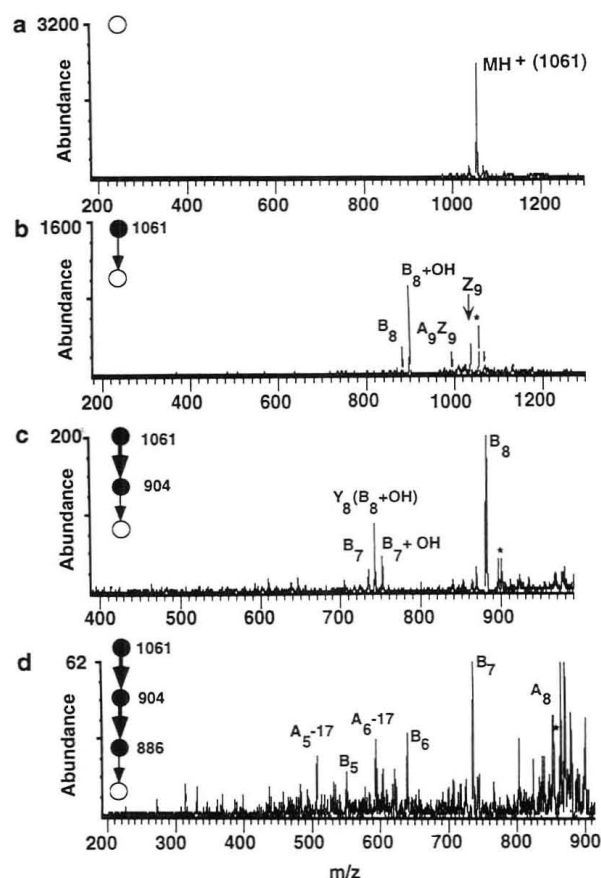


Figure 9. Four stages of mass spectrometry on 100 pmol of bradykinin [RPPGFSPFR]: (a) full mass scan; (b) first-generation product ions of $[M + H]^+$ (m/z 1061); (c) second-generation product ions of $[B_8 + OH]^+$ (m/z 904); (d) third-generation products of $[B_8]^+$ (m/z 886).

respectively. The product ions are identified using guidelines derived from Roepstorff nomenclature.⁴⁰ Several stages of mass spectrometry were performed on bradykinin, and as a result higher sample quantities were needed. Although the ability to perform tandem mass spectrometric analysis on lower molecular weight ions is encouraging, it was difficult to control the fragmentation of the higher molecular weight species, like neurotensin. This phenomenon is also seen on other types of tandem mass spectrometry instruments on which CID is performed.⁴¹ As a result, fewer stages of mass spectrometry could be performed on neurotensin and lower analyte concentrations were used.

First-generation CID products of bradykinin $[M + H]^+$ are shown in Figure 9b. An ion of m/z 904 was the most abundant product seen from this initial phase of CID. The MS/MS efficiency, defined as the percentage of the parent ion signal appearing as first-generation product ion signals, was estimated at 70%. Accurate measurement of MS/MS efficiency could not be made due to relatively large laser shot-to-shot fluctuations in the parent ion signal. Subsequent CID of the m/z 904 ion yielded second-generation products distinguished mainly by loss of 18 units (Figure 9c). Presumably, this loss was due primarily to cleavage at the C terminus. Finally, dissociation of ions with m/z 886 ($[B_8]^+$) resulted in numerous third-generation products, mostly from losses at the C-terminus side.

Low-energy CID of bradykinin (FAB ionization) on a BEqQ instrument has been previously reported.⁴² In these studies the m/z 904 ion is attributed to the loss of the C-terminal

(40) Roepstorff, P.; Fohlman, J. *J. Biomed. Mass Spectrom.* 1984, 11, 601.

(41) Bordas-Nagy, J.; Jennings, K. R. *Int. J. Mass Spectrom. Ion Processes* 1990, 100, 105.

(42) Thorne, G. C.; Ballard, K. E.; Gaskell, S. J. *J. Am. Soc. Mass Spectrom.* 1990, 1, 249.

(38) McLuckey, S. A.; Glish, G. L.; Van Berkel, G. J. *Int. J. Mass Spectrom. Ion Processes* 1991, 106, 213.

(39) Kaiser, R. E., Jr.; Cooks, R. G.; Syka, J. E. P.; Stafford, G. C. *Rapid Commun. Mass Spectrom.* 1990, 4, 31.

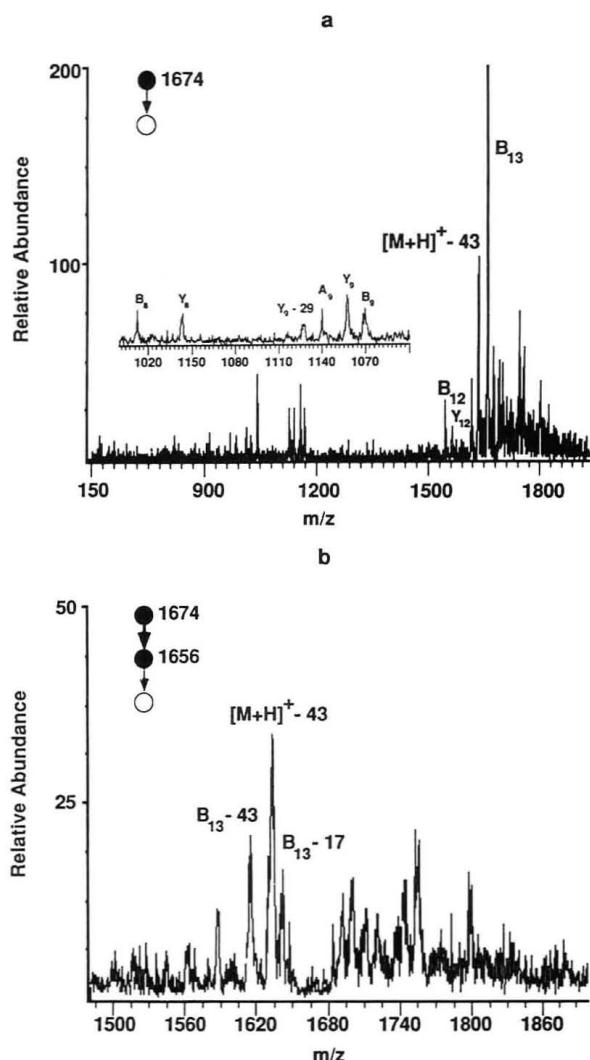


Figure 10. CID of $[M + H]^+$ from 1 pmol of neurotensin [pELYEN-KPRRPYIL] yielding mainly (a) first-generation products $[B_{13}]^+$ and $[M + H] - 43]^+$ ions. Main second-generation products (b) were $[B_{13} - 17]^+$ and $[B_{13} - 43]^+$. The $[M + H] - 43]^+$ product persisted from the previous stage of mass spectrometry.

arginine residue with retention of the arginine OH through rearrangement. The second- and third-generation products we obtained from CID of the $[B_8 + OH]^+$ and B_8^+ ions were also similar to those they reported for the decomposition of the $[B_8 + OH]^+$ ion. The main difference noted for CID performed in the ITMS was that the internal energy deposition appeared to be somewhat lower than in the BEqQ. Specifically, bradykinin product ions tended toward higher m/z products and required additional stages of mass spectrometry for comparable dissociation.

One of the difficulties that arose in MS^n structural analysis was low product ion resolution caused by increased effective scan rates during mass range extension. Poor resolution also complicated mass assignment in the case where two peaks with similar intensities merged as one. Shown in Figure 11 are first-generation products from bradykinin (see also Figure 9b) where resolution has been improved by lowering the mass range extension factor from 2 to approximately 1.4, thereby decreasing the effective scan rate. Baseline resolution reveals peaks at m/z 886 and 887 and at m/z 904 and 905 that were previously unresolved. As a result, mass assignments in these studies were determined from peak maxima because of the obvious presence of multiple peaks.

Shown in Figure 10a are results from CID of the neurotensin parent $[M + H]^+$. Difficulty was encountered in assigning masses to neurotensin product ions as well, where a mass

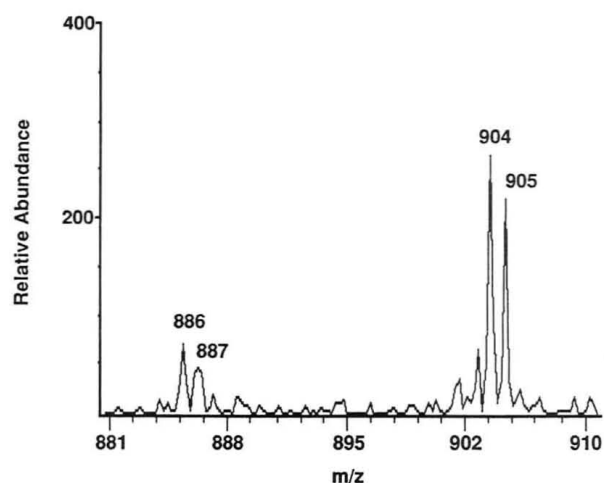


Figure 11. First-generation CID products of bradykinin $[M + H]^+$ ions acquired at an effective scan rate of 7900 Da/s (normal scan rate is approximately 5556 Da/s).

range extension factor of 3 was used. Efficient loss of C-terminal OH and loss of approximately 43 Da accounted for the major products. Weaker peaks have been given possible assignments in the figure.

Second-generation product ions from CID of the $[B_{13}]^+$ ion are shown in Figure 10b. Ions resulting from a loss of approximately 43 and 17 Da, which were the only ones that appeared to be produced, were analogous to those losses seen for the parent $[M + H]^+$ ion. A first-generation product ion with m/z 1631, labeled in Figure 10b as $[M + H]^+ - 43$, persisted from the previous stage of mass spectrometry. This anomaly was deduced upon careful comparison with the first-generation product ion spectra. This peculiarity is likely the result of subsequent fragmentation of high-mass ions following resonance ejection of the lower mass species during ion isolation. Lower intensities apparent in Figure 10b were from attenuating the laser power to achieve a constant ion signal so a meaningful comparison could be made.

CONCLUSION

The goal of this study was to evaluate the capabilities of the standard commercial ITMS for MALD of biological molecules. For relatively low molecular weight compounds, those species with m/z values below 3000, low-femtomole detection limits were readily obtainable. For species with higher m/z values, a degradation in detection limits and a drop in resolution beyond that attributable to high effective scan rates were observed. Experimental findings indicate that the current limitations at high mass are dependent, at least in part, on standard ITMS parameters. In light of these experimental results the primary challenge in MALD/ITMS now appears to be overcoming the limitations at high mass. Possible methods for circumventing these drawbacks include electrostatically moderating ion energies as they are desorbed from the sample probe and altering the ITMS electronics so fields are better suited to trap ions with high kinetic energies.

ACKNOWLEDGMENT

Research sponsored by the U.S. Department of Energy, Office of Basic Energy Sciences, under Contract DE AC05 84OR21400 with Martin Marietta Energy Systems, Inc. D.M.C. acknowledges an appointment to the U.S. Department of Energy, Laboratory Cooperative Postgraduate Research Training Program, administered by Oak Ridge Associated Universities.

RECEIVED for review May 11, 1992. Accepted October 5, 1992.

Determination of Atrazine in Water at Low- and Sub-Parts-per-Trillion Levels by Using Solid-Phase Extraction and Gas Chromatography/High-Resolution Mass Spectrometry

Zongwei Cai, V. M. Sadagopa Ramanujam, Daryl E. Giblin, and Michael L. Gross*

Midwest Center for Mass Spectrometry, Department of Chemistry, University of Nebraska, Lincoln, Nebraska 68588-0304

Roy F. Spalding

Water Center, University of Nebraska, Lincoln, Nebraska 68588-0844

A capillary column gas chromatography/high-resolution mass spectrometry (GC/HRMS) method was developed to determine atrazine in water at low- and sub-parts-per-trillion (ppt) levels. The method fills a need when the detection limits of routine GC, GC/MS, and high-performance liquid chromatography (HPLC) are inadequate for studies to evaluate transport and fate of herbicides in deep ground water systems. Atrazine and the added internal standard [¹³C₃]atrazine were extracted from water samples by solid-phase extraction using a C₁₈ bonded silica cartridge. A column chromatography procedure with Florisil was developed to reduce when necessary further interferences in the sample extract. The analysis was performed by GC/HRMS with the mass spectrometer operated in the selected ion monitoring (SIM) mode; mass profiles were acquired. The precision and accuracy of the method are 15% (relative standard deviation, n = 8) and >85%, respectively, for standard water samples containing atrazine at 1 ppt. The method, which gives detection limits of 200–500 parts-per-quadrillion (ppq), has been successfully used to analyze water samples containing atrazine at concentration levels of 1–500 ppt.

Atrazine (2-chloro-4-(ethylamino)-6-(isopropylamino)-1,3,5-triazine) is one of the most widely used herbicides for a broad spectrum of crops. It was first marketed in 1957 and soon became a very popular herbicide for broadleaf weed control in corn and milo. Residues of atrazine are frequently found in environmental samples of soil and water owing to its persistence and relatively high solubility in water. Currently used methods for the analysis of atrazine in water involve sample enrichment by liquid-liquid¹⁻³ or solid-phase extraction⁴⁻¹² followed by reconcentration and determination

by gas chromatography (GC),^{1,2,4-7,13,14} gas chromatography/mass spectrometry (GC/MS),^{3,10-12,15-28} and high-performance liquid chromatography (HPLC).²⁹⁻³⁶

Improved methods with lower detection limits allow for the determination of ultratrace levels of this agrochemical in more pristine surface or near surface ground water. Such low levels also occur in semiconfined and/or deep formation waters. The presence of atrazine in even parts-per-quadrillion (ppq) levels in ground water indicates that the water is a product of relatively recent recharge (post-1960) from the surface. Low detection limits are also required to support research focused on environmental kinetics of the degradation of herbicides in both soil and water. Additional applications for methods with ultratrace detection limits include evaluations of the efficacy of activated carbon in purifying atrazine-contaminated waters and as an early warning indicator of herbicide breakthrough from activated carbon filters.

(13) Grob, K.; Li, Z. *J. Chromatogr.* 1989, 473, 423-430.

(14) Edgell, K. W.; Jenkins, E. L.; Lopez-Avila, V.; Longbottom, J. E. *J. Assoc. Off. Anal. Chem.* 1991, 74, 295-309.

(15) Durand, G.; Barcelo, D. *J. Chromatogr.* 1990, 502, 275-286.

(16) Rostad, C. E.; Pereira, W. E.; Leiker, T. F. *Biomed. Environ. Mass Spectrom.* 1989, 18, 820-827.

(17) Huang, L. Q.; Mattina, M. J. I. *Biomed. Environ. Mass Spectrom.* 1989, 18, 828-835.

(18) Barcelo, D. *Chromatographia* 1988, 25, 295-299.

(19) Eichelberger, J. W.; Behymer, T. D.; Budde, W. L. *Method 525. Determination of Organic Compounds in Drinking Water by Liquid-Solid Extraction and Capillary Column Gas Chromatography/Mass Spectrometry*, Revision 1.0, 2.0, 2.1; 1988; pp 325-356.

(20) Thurman, E. M.; Meyer, M.; Perry, C.; Schwab, P. *Anal. Chem.* 1990, 62, 2043-2048.

(21) Kadokami, K.; Morimoto, M.; Haraguchi, K.; Koga, M.; Shinohara, R. *Anal. Sci.* 1991, 7, 247-252.

(22) Benfenati, E.; Tremada, P.; Chiappetta, L.; Frassanito, R.; Bassi, G.; DiToro, N.; Fanelli, R.; Stella, G. *Chemosphere* 1990, 21, 1411-1421.

(23) Huang, L. Q. *J. Assoc. Off. Anal. Chem.* 1989, 72, 349-354.

(24) Schuette, S. A.; Smith, R. G.; Holden, L. R.; Graham, J. A. *Anal. Chim. Acta* 1990, 236, 141-144.

(25) Pereira, W. E.; Rostad, C. E.; Leiker, T. *J. Anal. Chim. Acta* 1990, 228, 69-75.

(26) Davolin, E.; Benfenati, E.; Bagnati, R.; Fanelli, R. *Chemosphere* 1987, 16, 1425-1430.

(27) Kraut-Vass, A.; Thoma, J. *J. Chromatogr.* 1991, 538, 233-240.

(28) Durand, G.; Barcelo, D. *Anal. Chim. Acta* 1991, 243, 259-271.

(29) Owens, D. S.; Sturrock, P. E. *Anal. Chim. Acta* 1986, 188, 269-274.

(30) Froehlich, D.; Meier, W. *J. High Resolut. Chromatogr.* 1989, 12, 340-342.

(31) Brown, D. F.; McDonough, L. M.; McCool, D. K.; Papendick R. I. *J. Agric. Food Chem.* 1984, 32, 195-200.

(32) Reupert, R.; Ploeger, E. *Fresenius' Z. Anal. Chem.* 1988, 331, 503-509.

(33) Stahl, M.; Luehrmann, M.; Kicinski, H. G.; Kettrup, A. *Z. Wasser Abwasser Forsch.* 1989, 22, 124-127.

(34) Kicinski, H. G. *Lebensm.-Biotechnol.* 1990, 7, 159-164.

(35) Di Corcia, A.; Marchetti, M. *Anal. Chem.* 1991, 63, 580-585.

(36) Battista, M.; Di Corcia, A.; Marchetti, M. *Anal. Chem.* 1989, 61, 935-939.

(1) Graves, R. L. *Method 507. Determination of Nitrogen- and Phosphorus-Containing Pesticides in Water by Gas Chromatography with Nitrogen-Phosphorus Detector*, revision 2.0; 1989; pp 143-170.

(2) Lee, H. B.; Stokker, Y. D. *J. Assoc. Off. Anal. Chem.* 1986, 69, 568-572.

(3) Lopez-Avila, V.; Hirata, P.; Kraska, S.; Flanagan, M.; Taylor, J. H.; Hern, S. C. *Anal. Chem.* 1985, 57, 2797-2801.

(4) Popl, M.; Voznakova, Z.; Tatar, V.; Strnadova, J. *J. Chromatogr. Sci.* 1983, 21, 39-42.

(5) Woodrow, J. E.; Majewski, M. S.; Seiber, J. N. *J. Environ. Sci. Health* 1986, B21, 143-164.

(6) Richard, J. J.; Junk, G. A. *Mikrochim. Acta* 1986, 1, 387-394.

(7) Junk G. A.; Richard, J. *J. Anal. Chem.* 1988, 60, 451-454.

(8) Sherma, J. *J. Liq. Chromatogr.* 1986, 9, 3433-3438.

(9) Nash, R. G. *J. Assoc. Anal. Chem.* 1990, 73, 438-442.

(10) Mangani, F.; Bruner, F. *Chromatographia* 1983, 17, 377-380.

(11) Bagnati, R.; Benfenati, E.; Davoli, E.; Fanelli, R. *Chemosphere* 1988, 17, 59-65.

(12) Di Corcia, A.; Marchetti, M.; Samperi, R. *J. Chromatogr.* 1987, 405, 357-363.

Although ultratrace levels of atrazine are useful as environmental tracers for dating and in remediation, they likely have no obvious health relevance. The maximum contaminant level for atrazine in potable water is 3 µg/L, and the first observable adverse effects are in the milligram per liter range—more than 1 million times greater than detection levels reported in this paper.

Increased analytical sensitivity and specificity can be gained by using a high-resolution mass spectrometry (HRMS) technique involving a double-focusing magnet sector instrument. Combined with capillary GC, HRMS has been successfully used for trace analysis of dioxins.³⁷ GC/HRMS, however, is yet to be applied to the ultratrace analysis of atrazine and related herbicides.

A serious impediment to establish detection limits at low- or sub-parts-per-trillion (ppt) levels is the increased background and interferences at low levels. The interferences tend to grow exponentially as the detection limit is lowered. HRMS provides both high sensitivity and high resolving capacity for separating interfering compounds from the analytes. Moreover, the application of the mass profile mode operated in selected ion monitoring (SIM) gives a high certainty of identification because it has high diagnostic capability.³⁸ The quantification of atrazine is based on the internal standard method in which [¹³C₃]atrazine is used as an internal standard and added to the water prior to extraction. Thus, the method accuracy and precision should not be adversely affected by problems with sample preparation and recovery of atrazine. These advantages of the internal standard method are most important at low-concentration levels and for complex matrices.

The most often commonly reported isotopically labeled atrazine is atrazine-*d*₅ in which hydrogen atoms of the ethylamino group are replaced with deuterium.^{3,22-26} Atrazine-*d*₅ is effective as an internal standard in the extraction process. The ability to recognize the parent compound and to gain insight into its degradation products, however, is essential. The most frequently found decomposition compounds of atrazine in the environment are deethylatrazine and deethylatrazine-type compounds in which the ethyl group of atrazine is metabolized or replaced by other groups.^{15,25,28,39,40} Therefore, the choice of atrazine-*d*₅ as an internal standard is not satisfactory to simulate the native atrazine in the study of atrazine transport in the environment because the degradation products of both native atrazine and atrazine-*d*₅ are not differentiated. For environmental fate and transport studies, an isotopically stable compound is recommended. Atrazine with isotopically labeled carbons on the ring structure (¹³C₃) was synthesized as the internal standard in this research. Because it has similar chemical and physical properties as the native atrazine and because it possesses chemical stability in the GC separation and MS analysis processes, it is an ideal internal standard. In addition, [¹³C₃]atrazine is stable in environmental conditions.

EXPERIMENTAL SECTION

Reagents and Samples. Native atrazine standard was purchased from AccuStandard Inc., New Haven, CT. The internal standard [¹³C₃]atrazine (isotope purity of more than 99%) was specially synthesized for the Water Center, University of Nebraska-Lincoln (UNL) by Merck Frosst (Canada). Organic

solvents were pesticide quality or HPLC grade and were purchased from Fisher Scientific. Stock standards were prepared by dissolving 1.0 mg of native and labeled atrazine in 10 mL of methanol, respectively. The solutions were further diluted to obtain the fortifying standard solutions of 100 pg/µL in methanol. The standard solutions for GC/HRMS calibration were prepared with nine solutions at concentrations of 10–1000 pg/µL for native atrazine and 200 pg/µL for [¹³C₃]atrazine in methylene chloride.

Environmental Sep-Pak C₁₈ cartridge (1 g) was purchased from Waters Chromatography, Millipore. Anhydrous sodium sulfate of analytical grade was purchased from Fisher Scientific and was purified by Soxhlet extraction with methanol for 48 h and by heating overnight at 450 °C. Florisil (Fisher Certified ACS, 60–100 mesh) was activated overnight at 200 °C before using for the column chromatography procedure.

For standard water samples, distilled water was further purified by passing it through a four-module NANOpure cartridge system (Fisher/Barnstead) installed in the Water Center, UNL. The standard water samples were prepared by adding native atrazine standard solution into the water. The environmental water samples were collected by the Water Center, UNL, and two tap water samples were obtained from the Department of Chemistry, UNL, on November 11, 1991, and January 30, 1992. After the internal standard [¹³C₃]atrazine was added at the 5 ppt level, the samples were directly submitted to the solid-phase extraction.

Procedure. A C₁₈ bonded silica cartridge was sequentially prewashed with 5 mL each of methanol, methylene chloride, ethyl acetate, methanol, and clean water at a flow rate of 1–2 mL/min. The [¹³C₃]atrazine standard solution (20 µL) was added to 500 mL of water. The sample was allowed to flow through the cartridge at approximately 10 mL/min under water aspirator vacuum. After the sample had been applied, the solid-phase cartridge was allowed to flow for another 5 min to remove residues of water. The atrazine and the internal standard were then eluted by passing 2 mL of ethyl acetate through the cartridge at a flow rate of 1 mL/min. The extract was then dried with approximately 0.5 g of anhydrous sodium sulfate and concentrated to 20–50 µL under a slow stream of nitrogen.

The elimination of nonpesticide interferences from the tap water extracts was effected with a clean glass pipet filled with 0.8 g of activated Florisil. After packing, the column was rinsed with 6 mL of hexane. The water extract in ethyl acetate (0.5 mL) was quantitatively transferred onto the column and rinsed with 3 mL of 6% ethyl ether in hexane. The atrazine was eluted from the column by using 5 mL of 50% ethyl ether in hexane, and the fraction was evaporated to approximately 20 µL for GC/HRMS analysis.

GC/HRMS Analysis. The GC/HRMS analyses were performed on a Carlo-Erba GC/Kratos MS-50 double-focusing mass spectrometer system. An aliquot (2 µL) of a sample extract was injected into a DB-1 fused-silica capillary GC column (30 m × 0.32 mm, J&W Scientific) with on-column injection at 50 °C, hold for 1 min, followed by a programmed increase in temperature to 250 °C at a rate of 15 °C/min. The entire column effluent was passed directly into the source via an interface operated at 250 °C. The GC carrier gas was helium at a head pressure of 1.5 kg/cm². The retention time of atrazine by the GC conditions was 10.50 min. It is important that the atrazine retention time be kept small to avoid decomposition on the GC column.

The mass spectrometer was operated in the electron ionization (EI) mode at 70 eV, source temperature 250 °C and resolution 8000–10 000 (10% valley definition). Data acquisition and processing for the mass spectrometer were controlled by a Kratos MACH-3 computer system. A selected ion monitoring group in the mass profile mode was used for the qualitative and quantitative analyses. Three ions were selected for the analysis of atrazine: *m/z* 200.0703 and *m/z* 203.0805 as the quantification ions for native atrazine and [¹³C₃]atrazine, respectively, and *m/z* 202.0674 as the confirmation ion for the identification of atrazine. The mass profiles of the selected ions were obtained during GC elution. The identification was based on examination of mass profile peak shape, central mass shift, isotopic ratio of *m/z* 202.0674 to *m/z* 200.0703, and retention time of GC separation. The area of the mass profile peaks of the quantification ions was used for the quantitative analysis of atrazine; specifically, a relative response factor (RRF) of native atrazine signal to that

(37) Gross, M. L.; Sun, T.; Lyon, P. A.; Wojinski, S. F.; Hilker, D. R.; Dupuy, A. E.; Heath, R. G. *Anal. Chem.* 1981, 53, 1902–1906.

(38) Tong, H. Y.; Giblin, D. L.; Lapp, R. L.; Monson, S. J.; Gross, M. L. *Anal. Chem.* 1991, 63, 1772–1780.

(39) Durand, G.; Forteza, R.; Barcelo, D. *Chromatographia* 1989, 28, 597–604.

(40) Vermeulen, N. M.; Apostolides, Z.; Potgieter, D. J. J. *J. Chromatogr.* 1982, 240, 247–253.

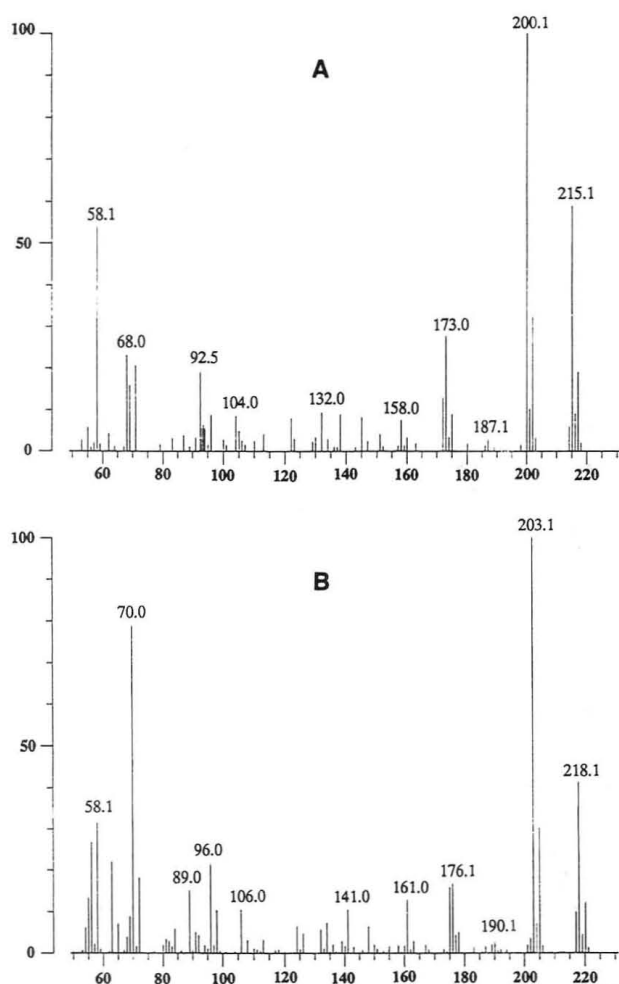


Figure 1. High-resolution EI mass spectra of (A) native atrazine and (B) [$^{13}\text{C}_3$]atrazine.

of its corresponding internal standard [$^{13}\text{C}_3$]atrazine was used for the quantitative analysis to improve the accuracy of the method:

$$\text{RRF} = (A_x C_{is}) / (A_{is} C_x) \quad (1)$$

where A_x and A_{is} are the mass profile peak areas of atrazine at m/z 200.0703 and [$^{13}\text{C}_3$]atrazine at m/z 203.0805 and C_x and C_{is} are the concentrations of native atrazine and [$^{13}\text{C}_3$]atrazine in the calibration standards, respectively.

The concentration of atrazine in an unknown water sample was calculated by the formula

$$C_x = [(C_{is})(A_x/A_{is})] / \text{RRF} \quad (2)$$

where C_x is the concentration of analyzed atrazine in sample, C_{is} is the concentration of the added [$^{13}\text{C}_3$]atrazine, and A_x and A_{is} are the mass profile peak areas for signals at m/z 200.0703 and m/z 203.0805, respectively.

RESULTS AND DISCUSSION

Qualitative and Quantitative Analysis. High-resolution EI (70 eV) mass spectra for atrazine and [$^{13}\text{C}_3$]atrazine were obtained at 10 000 resolution (10% valley definition) (Figure 1) to provide the necessary information for the analysis of atrazine by using SIM. In the SIM technique, ions for quantification were chosen on the basis of maximum abundance, maximum selectivity, and low susceptibility to interference from other compounds that may be present. Thus, consideration was given primarily to the most abundant ions in the mass spectra to achieve the maximum instrument response. As indicated by the spectra, it is possible to select the ions of m/z 200.0703 and m/z 203.0805 as quantification ions for native atrazine and [$^{13}\text{C}_3$]atrazine, respectively. The

ion of m/z 202.0674, which is the ^{37}Cl -containing fragment ion, was selected to provide confirmation for the presence of atrazine.

The mass spectrum of [$^{13}\text{C}_3$]atrazine illustrates that the labeled atrazine gives no significant ions at m/z 200 and m/z 202. Thus, the internal standard does not interfere with the analysis of native atrazine when both compounds are present.

The criteria we use for determining the presence of atrazine at low levels are as follows.

1. The retention time of the native atrazine, as determined from the mass chromatogram of the m/z 200.0703 ion, must be equal to within 2 s to that of the internal standard m/z 203.0805 ions.

2. The masses of the m/z 200.0703 and m/z 202.0674 ions must be within ± 5 ppm of the true values.

3. The isotope abundance ratio of the m/z 202.0674 and the m/z 200.0703 ions must be 0.35 ± 0.10 .

The mass profile mode is better-suited for meeting these criteria than the peak top monitoring mode.³⁸ The ability to establish accurate mass measurements and isotope abundance ratios as well as to detect the presence of interferences is particularly useful for determining with certainty that atrazine is present in the sample.

The spectrum of native atrazine shows a signal at m/z 203.0696 with an abundance of 3.2%, which results from ^{13}C and ^{37}Cl contribution to the $[M - 15]^+$ fragment ion at m/z 200.0703. Thus, this ion contributes to the quantification ion abundance. To separate the interference ion (m/z 203.0696) from the quantification ion of [$^{13}\text{C}_3$]atrazine (m/z 203.0805), a resolving power of more than 19 000 would be required. Although this higher resolution can be reached by using many magnet sector mass spectrometers, the sensitivity will be decreased by at least a factor of 2 compared to that at resolving power 10 000. Because the percentage of the isotopic contribution from the native atrazine base peak is determinant, the analytical error caused by the interference ion can be minimized by an area correction according to the following equation:

$$A([\text{C}_3]\text{atrazine}) = A(203.0805) - A(200.0703) \times 0.032 \quad (3)$$

where $A([\text{C}_3]\text{atrazine})$ is the actual area of [$^{13}\text{C}_3$]atrazine peak after the correction and $A(203.0805)$ and $A(200.0703)$ are areas of the m/z 203.0805 and m/z 200.0703 peaks, respectively.

By using this equation, the area of the m/z 203.0805 ion for the internal standard was corrected for the 3.2% contribution from the ion m/z 200.0703 of native atrazine. When the concentration of native atrazine is similar to or less than the concentration of the added [$^{13}\text{C}_3$]atrazine, the correction is not necessary because the presence of native atrazine does not significantly interfere with the determination of the labeled atrazine. Better accuracy, however, was achieved after using the correction, especially when the concentration of atrazine is more than 5 times higher than the concentration of the added [$^{13}\text{C}_3$]atrazine.

The calibration curve, presented in Figure 2, shows a linear dynamic range over 3 orders of magnitude. For the calibration data points, the concentration of [$^{13}\text{C}_3$]atrazine was kept at 200 pg/ μL whereas the concentration of atrazine was varied from 10 to 1000 pg/ μL . The area of [$^{13}\text{C}_3$]atrazine was adjusted only for the atrazine concentration of 1000 pg/ μL because no significant changes were obtained by the correction for the other calibration points.

For the internal standard method, a concentration ratio of less than 10 of analyte-to-internal standard was recommended

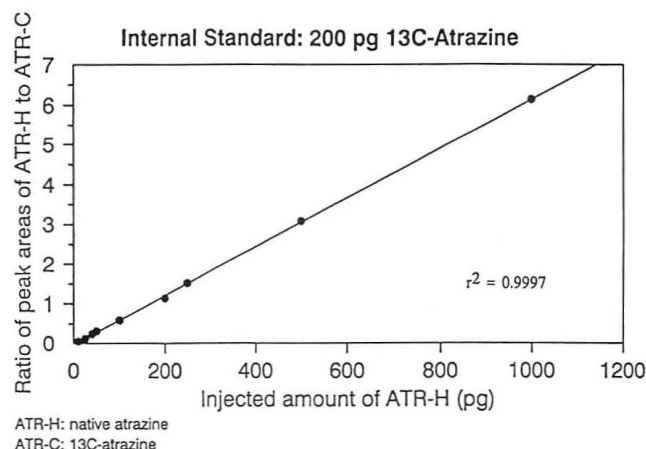


Figure 2. Linear dynamic range for the GC/HRMS analysis of atrazine when the injected amount of [$^{13}\text{C}_3$]atrazine was 200 pg.

Table I. Relative Response Factors of Native Atrazine Relative to [$^{13}\text{C}_3$]Atrazine

injected amt (pg)		RRF ^a
native atrazine	[$^{13}\text{C}_3$]atrazine	
10	206	0.99
20	206	0.97
40	206	1.19
50	206	1.23
100	206	1.17
200	206	1.12
250	206	1.20
500	206	1.22
1000	206	1.21
av \pm SD ^b		1.14 \pm 0.10
RSD, % (n = 9) ^d		8.7

^a Relative response factor. ^b Average RRF \pm standard deviation. ^c Relative standard deviation. ^d Number of determinations.

to obtain the best accuracy.⁴¹ For unknown environmental samples, the actual concentration ratio may exceed this factor. If the analysis of a water sample indicated that the concentration of native atrazine was a factor of more than 10 times that of the added [$^{13}\text{C}_3$]atrazine, a second analysis was carried out for this sample by using a more suitable concentration of the internal standard, which had been estimated from the first analysis.

To improve further the method accuracy, a relative response factor (RRF) was used for the analysis. The RRF of native atrazine to [$^{13}\text{C}_3$]atrazine was obtained from the GC/HRMS results for standard solutions of native atrazine and [$^{13}\text{C}_3$]atrazine (Table I). Under ideal conditions, the RRF should be equal to 1. The deviation from unity may be due to the different purities of standards and to errors introduced in the preparation of the standard solutions and in the GC/HRMS analysis. Thus, the RRF was determined with standards containing at least three different concentration ratios of the native atrazine to [$^{13}\text{C}_3$]atrazine each day samples were analyzed. If a standard solution was changed, the RRF was determined again with at least six points in the dynamic range shown in Figure 2.

Recovery and Detection Limit. Because the internal standard, which is the stable isotopically labeled form of the analyte, was added into the water samples prior to the sample preparation, the quantification of the native compound is based on the instrument response and has minimal dependence on recovery. The detection limit, however, can be improved when good recovery is achieved. Nevertheless, the

Table II. Recoveries of Atrazine by Solid-Phase Extraction of 500 mL of Water at Three Concentration Levels

analysis	recovery (%)		
	1 ppt	5 ppt	10 ppt
1	67	79	80
2	77	79	77
3	78	78	91
4	84	78	80
5	81	81	78
6	75	68	81
av \pm SD, ^a %	77.0 \pm 5.8	77.2 \pm 4.6	81.2 \pm 5.0
RSD, ^b % (n = 6) ^c	7.6	6.0	6.2

^a Average recovery \pm standard deviation. ^b Relative standard deviation. ^c Number of determinations.

Table III. Accuracy and Precision Data for Atrazine Analysis by Solid-Phase Extraction and GC/HRMS

added (ppt)	found ^a (ppt)	DL ^b (ppt)
1.04	1.05	0.20
1.04	0.81	0.22
1.04	0.78	0.38
1.04	1.05	0.20
1.04	1.00	0.24
1.04	0.95	0.14
1.04	1.05	0.15
1.04	0.73	0.29
av \pm SD ^c	0.93 \pm 0.13	0.23 \pm 0.08
relative error, %	-10.6	
RSD, ^d % (n = 8) ^e	14.3	34

^a Order of data presentation was the order of analysis. ^b Detection limit. ^c Average concentration of atrazine \pm standard deviation. ^d Relative standard deviation. ^e Number of determinations.

data in Table II demonstrate excellent recoveries of atrazine in water at the concentration levels of 1, 5, and 10 ppt by employing the solid-phase extraction procedure with the C_{18} cartridge. The average recoveries and the relative standard deviations (RSD) were determined from six GC/HRMS detections of three sample extractions.

The sample volumes for the recovery tests were 500 mL. The C_{18} cartridge (1 g) was tested for the extraction of atrazine at ppt to ppb levels in larger water volume. No significant breakthrough at up to 1000 mL water, however, was found. The capacity of the same kind of C_{18} (360 mg) for some triazine herbicides in water was determined, and the breakthrough for atrazine was 3200 mL of water.²⁰

The typical instrument detection limit for atrazine at a signal-to-noise (S/N) ratio of 3 is 10 pg/injection, which corresponds to a procedure detection limit of 200 ppq if the sample volume is 500 mL and 2 of 20 μL from the final extract is injected into the GC column. The procedure detection limit, however, depends upon the nature of the samples and the quality of extraction. The detection limits for the standard water samples are defined as the concentration of atrazine required to produce a signal with an amplitude of at least 3 times the baseline noise; they are listed in Table III for the analyses conducted in this research. Detection limits can be lowered further if a large volume of sample is used, if the sample extract is further concentrated, or if the mass resolving power is reduced. It is noted that contemporary magnet sector instruments have higher sensitivities than the 16-year-old instrument used here. To measure lower ppq levels of atrazine and other related herbicides, a preconcentration step (e.g., evaporation of the water) could be used before the solid-phase extraction. The background noise from a larger volume of water samples, however, will also increase and possibly cause interferences. In such cases, column chromatography with Florisil can be used to eliminate or reduce the interferences in the sample extracts.

(41) Colby, B. N.; Rosecrance, A. E.; Colby, M. E. *Anal. Chem.* 1981, 53, 1907-1911.

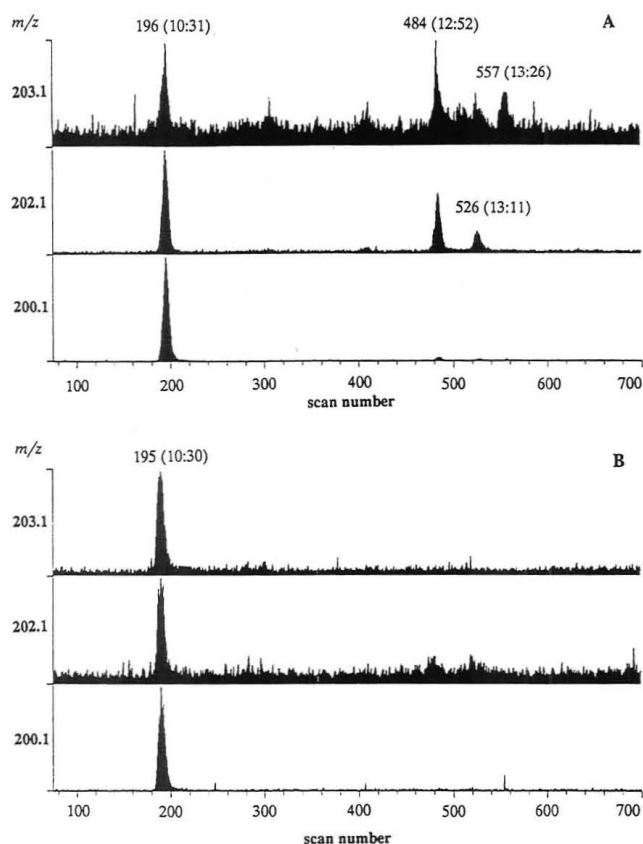


Figure 3. TIC chromatograms of the C_{18} cartridge eluants for a tap water sample (A) before and (B) after the Florisil column chromatography procedure.

Interferences. The interferences include method interferences caused by contaminants in solvents, glassware, C_{18} cartridge, and other sample processing apparatus and matrix interferences caused by contaminants that are coextracted from the water samples. Alkanes, alkenes, plasticizers, and antioxidants were identified as possible interferences by extracting components of the C_{18} bonded silica cartridge that interfered with the analysis of herbicides by GC with high-sensitivity electron capture detection⁴² and by GC/quadrupole MS.⁴³ The interferences from the C_{18} cartridge, however, do not affect the determination of atrazine by GC/HRMS because this method has higher selectivity than GC/low-resolution MS.

The need for an additional chromatography step for application of the solid-phase extraction and GC/HRMS analysis depends on the cleanliness of the matrix. The extent of matrix interferences will vary considerably with the source of the water sample. The cartridge eluants of the standard water samples and the relatively clean groundwater samples in this study did not have significant interferences so that the Florisil chromatography step was not used for those eluants. The chromatography procedure, however, was required for the eluant of a tap water sample. Figure 3 shows the TIC chromatograms (containing the three selected ions) of the sample extract of tap water before and after the chromatography step. The final volume as well as the injection volume of both samples were kept similar so that the background noise and interferences peaks could be reliably compared with each other. Because the GC/HRMS technique has high selectivity, the background noise and interference peaks are small relative to the intense peak of atrazine, as

Table IV. Results of the Analyses of Water Samples from the Aquifer in the Southeast of Grand Island, Nebraska (MLE), and Tap Water Samples from the Department of Chemistry, UNL (TAP)

samples	C_{is} (ppt) ^a	C_z (ppt) ^b
MLE 75	52	132
MLE 80	52	107
MLE 85	52	21.5
MLE 90	52	12.5
MLE 95	52	22.4
MLE 100	52	15.7
MLE 105	52	2.5
MLE 110	52	11.5
blank 1	52	ND (0.59) ^c
MLE 105	5.2	3.4
blank 2	5.2	ND (0.48)
TAP 1	52	463
TAP 2	104	428

^a Concentration of added internal standard. ^b Detected concentration of native atrazine. ^c Not detected (detection limit).

shown in Figure 3. The S/N ratio for the sample analysis after the chromatography step is better than that of the sample analysis before the chromatography step, and interference peaks (scan numbers 484, 526, and 557 in Figure 3A) are not seen.

The recoveries of atrazine in the Florisil column chromatography procedure were 83% and 80% for 1 and 10 ng of atrazine, respectively. This indicates that the procedure detection limit will be affected minimally (decreased by less than 20%) by introducing the chromatography procedure. This additional chromatography step was found to be necessary when a dirty sample was analyzed because intense interferences shorten the lifetime of the GC column and contaminate the ion source of a system operated at high sensitivity, reducing GC resolution, S/N ratio, and ultimately the sensitivity.

Method Accuracy and Precision. Eight standard samples containing 1 ppt atrazine in 500 mL of water were analyzed by GC/HRMS after solid-phase extraction. The accuracy and precision data are presented in Table III. The average error for the determination of atrazine is less than $\pm 15\%$. The method precision given as relative standard deviation (RSD) is better than 15% ($n = 8$) for the standard water samples.

Ground water samples from a Pleistocene age sand and gravel aquifer in southeast Grand Island, NE⁴⁴ and two tap water samples containing ground water from the city of Lincoln municipal supply line were analyzed (see Table IV for results). The Grand Island samples were obtained from a specially installed multilevel sampling system capable of extracting ground water from discrete 5-ft. levels throughout the 100-ft. saturated zone.⁴⁵ The concentrations of atrazine in the samples from Grand Island range from low ppt in the deep samples to more than 100 ppt in the shallower samples. The data indicate a decrease in atrazine concentration with depth, and this is in accord with the hypothesis that the deeper water is older. Recharge to these deep ground water zones may have contained less atrazine, and the residual atrazine may have undergone more retardation and degradation.

The concentration of the added internal standard was 52 ppt for all unknown samples and one of the blank samples. A second round of analysis with a fortifying concentration of 5.2 ppt was performed for the sample MLE 105 as well as the

(42) Junk, G. A.; Avery, M. J.; Richard, J. J. *Anal. Chem.* 1988, 60, 1347-1350.

(43) Johnson, W. E.; Fendinger, N. J.; Plimmer, J. R. *Anal. Chem.* 1991, 63, 1510-1513.

(44) Spalding, R. F.; Exner, M. E.; Martin, G. E.; Snow, D. D. *J. Hydrol.*, in press.

(45) Spalding, R. F.; Exner, M. E.; Burbach, M. E. *Groundwater Residue Sampling Design*; ACS Symposium Series; American Chemical Society: Washington, DC, 1991; Chapter 15, 255-261.

other blank sample. These samples were also analyzed by a GC/quadrupole MS at the Water Center, UNL.⁴⁶ For samples MLE 75, MLE 80, MLE 85, and MLE 95, in which atrazine concentrations were above the detection limit of the method using low-resolution GC/MS, the results from the two methods are in close agreement.⁴⁶ Results for the blank samples show high reliability of the solid-phase extraction and GC/HRMS for the analysis of atrazine.

Conclusion. The method using solid-phase extraction and GC/HRMS is satisfactory for the analysis of atrazine in water at ultratrace levels and gives good accuracy and precision at these levels. The use of the high-resolution mass spectrometry technique supported by an optional Florisil column chromatography procedure can eliminate most of the interferences

that are introduced from samples and the method itself. The method, which already has been successfully used to analyze ground water samples, can be incorporated in other studies such as the metabolism of atrazine and related herbicides in the environment. Moreover, it is expected that this GC/HRMS method will be applicable to investigation of movement and degradation of selected herbicides in the environment.

ACKNOWLEDGMENT

This study was supported by the University of Nebraska Water Center by the Nebraska Research Initiative and the National Science Foundation (Grant No. DIR 9017262).

(46) Cassada, D. A.; Z. Cai; Spalding, R. F.; Gross, M. L. Manuscript in preparation.

RECEIVED for review July 20, 1992. Accepted October 5, 1992.

Effects of Buffer pH on Electroosmotic Flow Control by an Applied Radial Voltage for Capillary Zone Electrophoresis

Mark A. Hayes, Indu Kheterpal, and Andrew G. Ewing*

Department of Chemistry, Penn State University, 152 Davey Laboratory, University Park, Pennsylvania 16802

Electroosmotic flow has been shown to be controlled via an applied radial voltage. Many factors determine the effectiveness of this control, and one major factor is buffer pH. In this study the effectiveness of the applied radial voltage for controlling electroosmotic flow while varying buffer pH is examined. Previously developed theory is applied and compared to experimental results for a pH range from 1.4 to 6.32. Analysis time is dramatically reduced by applying a radial voltage for separation of a peptide mixture at pH 1.4. Theory predicts laminar flow profiles under some conditions when applying this technique. However, experimental evidence at pH 6.32 and 1.4 shows no evidence of band broadening from a laminar flow profile. Theoretical and experimental results indicate the largest range of effective electroosmotic flow control via an applied radial voltage occurs at low pH. Furthermore, a sigmoidal relationship between electroosmotic flow and applied radial voltage is clearly apparent under these conditions. In contrast, at high buffer pH (>6) the relationship appears to be linear and is only over a limited range of flow velocities.

INTRODUCTION

Capillary electrophoresis (CE) is a high-efficiency, low-volume separation technique. This and related techniques (micellar electrokinetic capillary chromatography (MECC), capillary gel electrophoresis, etc.) separate charged and neutral species in aqueous solution with a wide range of applicability.^{1,2} Applications include cations, anions, and neutrals from single atomic ions³ to proteins and nucleic acids with molecular weight in excess of 130 000 Da⁴. One important factor in the applicability of CE to such a large range of analytes is electroosmotic flow (EOF). This flow, generated at the wall of the capillary, typically causes the elution of cations, anions, and neutrals at one end of the capillary, allowing the use of a single detector.⁵ In addition, a term for electroosmotic flow appears in the equations for both resolution and efficiency in MECC⁶ and CE.⁵ Hence, the control of EOF may have a large effect in improving resolution and efficiency and is one of the most important aspects of controlling reproducibility in CE.

Electroosmotic flow may be altered in many ways. These include derivatizing the inner surface of the capillary,⁷⁻⁹

altering the buffer pH¹⁰⁻¹² or concentration,^{10,13-15} the addition of surface active species (surfactants, glycerol, etc.)^{7,8,16} or organic modifiers¹⁷ to the buffer, and the application of applied radial voltage to the capillary wall.¹⁸⁻²²

One of these methods, the variation of pH, has a strong effect on electroosmotic flow.^{10,11,23} The variation of buffer pH may essentially stop electroosmotic flow at low values (pH <2.5) and induce a maximum flow at high values (pH >7) in fused silica capillaries. Thus, buffer pH defines the full range of electroosmotic flow with the value of the electroosmotic flow coefficient ranging from approximately zero to 1×10^{-3} cm/V s.¹¹ Since a term appears for electroosmotic flow in the resolution equation for CE and MECC, buffer pH may be optimized for resolution. However, many separations, especially biological, are limited in pH by the instability of biomolecules or by adsorption of the solutes to the capillary wall.¹² Furthermore, pH alters the charge on proteins and peptides and therefore may alter their electrophoretic mobilities.²⁴⁻²⁶ By altering their mobilities the separation of protein and peptide mixtures may be realized by optimized pH. Thus, pH may be adjusted to optimize analysis time, resolution, and efficiency or be held at a given value. In situations where the pH range that can be employed is limited, it would be advantageous to vary the electroosmotic flow independently.

Independent control of EOF with an applied radial voltage has been investigated in several recent publications.¹⁸⁻²² This work has identified some important factors which influence the ability of the radial voltage to control EOF and to define the limits of this effect. Theoretical aspects of this effect come from established double-layer theory from electrochemistry and colloid science.^{20,27,28} Experimentally, we have developed a novel means to create this effect with a Nafion-

(10) Lukacs, K. D.; Jorgeonson, J. W. *J. High Res. Chromatogr. Chromatogr. Commun.* 1985, 8, 407.

(11) Lambert, W. J.; Middleton, D. L. *Anal. Chem.* 1990, 62, 1585.

(12) McCormick, R. M. *Anal. Chem.* 1988, 60, 2322.

(13) Issaq, H. J.; Atamna, I. Z.; Muschik, G. M.; Janini, G. M. *Chromatographia* 1991, 32, 155.

(14) Atamna, I. Z.; Metral, C. J.; Muschik, G. M.; Issaq, H. J. *J. Liq. Chromatogr.* 1990, 13, 2517.

(15) Atamna, I. Z.; Metral, C. J.; Muschik, G. M.; Issaq, H. J. *J. Liq. Chromatogr.* 1990, 13, 3201.

(16) Bruin, G. J. M.; Chang, J. P.; Kuhlman, R. H.; Zegers, K.; Kraak, J. C.; Poppe, H. *J. Chromatogr.* 1989, 471, 429.

(17) Van Orman, B. B.; Liversidge, G. G.; McIntire, G. C.; Olefirowicz, T. M.; Ewing, A. G. *J. Microcol. Sep.* 1990, 2, 176.

(18) Lee, C. S.; Blanchard, W. C.; Wu, C.-T. *Anal. Chem.* 1990, 62, 1550.

(19) Lee, C. S.; McManigill, D.; Wu, C.-T.; Patel, B. *Anal. Chem.* 1991, 63, 1519.

(20) Hayes, M. A.; Ewing, A. G. *Anal. Chem.* 1992, 64, 512.

(21) Wu, T.-T.; Lopes, T.; Patel, B.; Lee, C. S. *Anal. Chem.* 1992, 64, 886.

(22) Lee, C. S.; Wu, C.-T.; Lopes, T.; Patel, B. *J. Chromatogr.* 1991, 559, 133.

(23) Towns, J. K.; Regnier, F. E. *Anal. Chem.* 1991, 63, 1126.

(24) Foret, F.; Fanali, S.; Bocek, P. *J. Chromatogr.* 1990, 516, 219.

(25) Sustacek, V.; Foret, F.; Bocek, P. *J. Chromatogr.* 1989, 480, 271.

(26) Bocek, P.; Deml, M.; Pospichal, J.; Sudor, J. *J. Chromatogr.* 1989, 470, 309.

(27) Bard, A. J.; Faulkner, L. R. *Electrochemical Methods: Fundamentals and Applications*; John Wiley & Sons: New York, 1980.

* To whom all correspondence should be addressed.

(1) Kuhr, W. G. *Anal. Chem.* 1990, 62, 403R.

(2) Lauer, H. H.; Ooms, J. B. *Anal. Chim. Acta* 1991, 250, 45.

(3) Gross, L.; Yeung, E. S. *J. Chromatogr.* 1989, 480, 169.

(4) Drossman, H.; Luckey, J. A.; Kostichka, A. J.; D'Cunha, J.; Smith, L. M. *Anal. Chem.* 1990, 62, 900.

(5) Jorgenson, J. W.; Lukacs, K. D. *Anal. Chem.* 1981, 53, 1298.

(6) Terabe, S.; Otsuka, K.; Ando, T. *Anal. Chem.* 1985, 57, 834.

(7) Jorgenson, J. W.; Lukacs, K. D. *Science* 1983, 222, 266.

(8) Hjerten, S. *J. Chromatogr.* 1985, 347, 191.

(9) Moseley, M. A.; Deterding, L. J.; Tomer, K. B.; Jorgenson, J. W. *Anal. Chem.* 1991, 63, 109.

coated CE capillary,²⁰ and this apparatus has many practical advantages to previous systems which control EOF by applied radial voltage. The new design system leaves the polyimide coating intact on the capillary and simply covers it with a flexible ionomer. Hence, the capillaries retain their flexibility and strength in these experiments.

Although the control of EOF appears to have several advantages as outlined above, under specific conditions this technique might lead to laminar flow and associated band broadening.²² In all published experimental apparatuses there are sections of the capillary which are not covered by the radial voltage control sheath. Since the effect is assumed to be directly radial inward, then the flow at the inner wall of the capillary can be expected to differ from the unsheathed sections versus the sheathed sections. This may lead to laminar flow and band broadening. A series of experiments are presented to determine the magnitude of this effect.

In this paper, the effect of buffer pH on the control of electroosmotic flow by applied radial voltage is examined, both theoretically and experimentally. For a buffer pH ranging from 1.4 to 6.32 excellent agreement is found between theory and experimental data for the rate of EOF. In addition, an application of this method to the separation of peptides at low pH is examined. Finally, the effect of EOF control on band broadening is examined.

THEORY

Theoretical considerations for the control of EOF with an applied radial voltage have been developed.^{19,20} Briefly, these considerations are that the ionized surface silanol groups of the fused silica capillary indirectly define the ζ potential and, hence, EOF. These ionized groups generate surface charge density, σ_{Si} , which is related to solution pH by the following relationship:

$$\sigma_{Si} = \gamma / (1 + ([H^+]/K)) \quad (1)$$

where γ is the total of both the ionized and protonated surface silanol group concentrations, $[H^+]$ is the bulk buffer hydrogen ion concentration, and K is the dissociation constant. This surface charge density is related to the ζ potential by the following relationship:

$$\zeta = \exp(-\kappa x) (2kT/e) \sinh^{-1} (\sigma_{Si} [500\pi/\epsilon_b RCT]^{1/2}) \quad (2)$$

and

$$\kappa = 2\eta_0 Z^2 e^2 / \epsilon_b kT \quad (3)$$

where ϵ_b is the permittivity of the buffer, η_0 is the viscosity of the buffer, Z is the electronic charge, e is the elementary charge, T is the temperature, κ is the inverse Debye length, x is the thickness of the counterion, k is the Boltzmann constant, C is the electrolyte concentration, and R is the molar gas constant. The ζ potential is related to electroosmotic flow velocity, v_{eo} , by

$$v_{eo} = \zeta (\epsilon_b / \eta_0) E_{app} \quad (4)$$

where E_{app} is the separation potential field strength. By applying eqs 1, 2, and 4, it can be seen that buffer pH directly effects EOF through the ionization of surface silanol groups. This effects the EOF through variation of the ζ potential according to eq 2 which predicts the characteristic sigmoidal shape of the relationship between buffer pH and EOF shown by previous studies.^{10,11,23}

Surface charge may also be induced via a radially applied voltage. The relationship between applied radial voltage, V_r ,

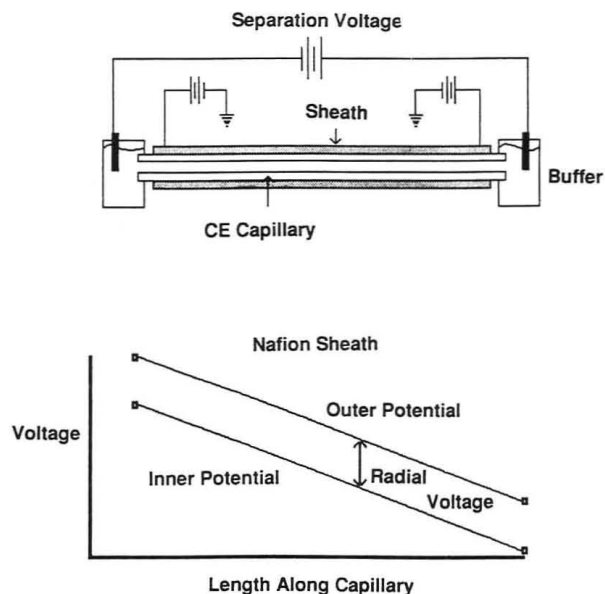


Figure 1. Schematic of the experimental apparatus used to control EOF by applied radial voltage. The high-voltage lead in the buffer on the left is isolated in an interlock Plexiglas box. The sheath (Nafion coating) and both high-voltage leads are isolated in a separate interlock box. The bottom section shows the expected potential drop inside the capillary assuming a homogeneous buffer versus length along the capillary. Also plotted is the potential field of the Nafion outer coating which is manipulated by the independent adjustment of each power supply, defining the end point potential. In this apparatus, the applied radial voltage (inner potential–outer potential) may be manipulated to be constant across the length of the capillary.

and surface charge density, σ_v (due only to effects of V_r), has been described^{19,20} as

$$\sigma_v = (\epsilon_Q V_r / R_1) (1 / \ln (R_0 / R_1)) \quad (5)$$

where ϵ_Q is the permittivity of the fused silica capillary, R_0 is the outer radius of the capillary, and R_1 is the inner radius of the capillary.

This surface charge density due to the applied radial voltage enhances or depletes the surface charge density due to the ionization of the surface silanol groups (σ_{Si}) and therefore directly effects v_{eo} . The nature of the interaction between σ_{Si} and σ_v is assumed to be additive. By inserting both sources of surface charge into eq 2 and combining with eq 3, a relationship between applied voltage, buffer pH, and EOF may be developed as follows:

$$v_{eo} = (\epsilon_b / \eta_0) E_{app} \exp(-\kappa x) (2kT/e) \times \sinh^{-1} ((\sigma_v + \sigma_{Si}) [500\pi/\epsilon_b RCT]^{1/2}) \quad (6)$$

EXPERIMENTAL SECTION

Apparatus. The Nafion-sheathed capillary for application of an applied radial voltage was described in a previous study.²⁰ Briefly, the system used two Plexiglas interlock boxes designed for operator safety. The high-voltage lead for the separation potential and the injection end of the polyimide-coated fused silica capillary were enclosed in the first box. The second box contained the Nafion-coated section of the capillary and high-voltage electrodes on either end of the sheath to adjust the radial potential field (Figure 1). The radial voltage field was manipulated by calculating the linear voltage drop in the buffer-filled interior and adjusting the outer sheath voltage to match the gradient, offset at the experimental value (Figure 1, bottom). The capillaries used for the variation of buffer pH studies were 50 cm in length, 10- μ m i.d.; 141- μ m o.d. and 25- μ m i.d.; 250- μ m o.d. (Polymicro, Pheonix, AZ). Capillaries were used as received without further modification. Electroosmotic flow was monitored with phenol as the neutral marker. Detection was carried out on-column through a window where the polyimide was removed

**Effects of Buffer pH on Electroosmotic Flow
Control by an Applied Radial Voltage for Capillary
Zone Electrophoresis**

Mark A. Hayes, Indu Kheterpal, and Andrew G.
Ewing* (*Anal. Chem.* 1993, 65, 27-31).

Equation 3 is incorrect. It should read

$$\kappa = (2N_0 Z^2 e^2 / \epsilon_b kT)^{1/2}$$

where N_0 is the number concentration of counterions at the surface, not the viscosity.

The terms for the elementary charge (e) and the permittivity of the buffer (ϵ_b) have been defined according to more conventional symbols.

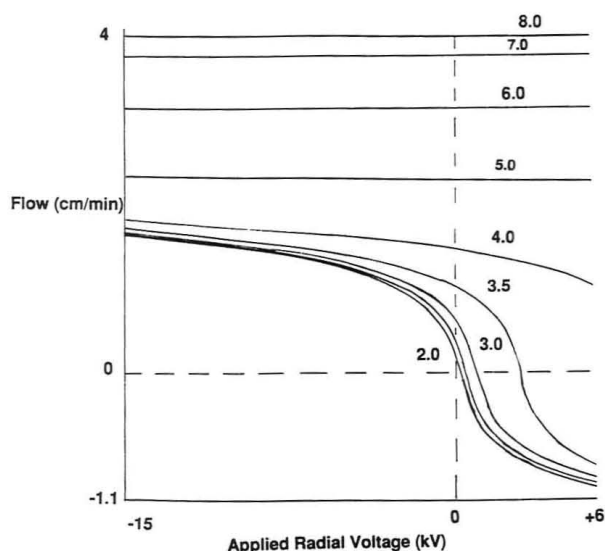


Figure 2. This graph shows a plot of eq 6 for a series of buffer pH values. The specific values for all variable input parameters are separation potential, 140 V/cm; capillary, 50 cm \times 10- μ m i.d. \times 150- μ m o.d.; temperature, 298 K; concentration, 1 mM; dissociation constant, 1×10^{-7} ; width of counterion, 1.5×10^{-10} m; dielectric coefficient, 78, viscosity, 0.000 89 kg/m s; and surface silanol group concentration, 5×10^{14} groups/cm².

by heat. Detection was by absorbance (Linear 200, Reno, NE) at 214 nm.

This apparatus was used to separate a series of peptides. A 25 mM phosphate buffer at pH 1.4 was used with a 20- μ m-i.d., 144- μ m-o.d., and 52-cm-long capillary. In one set of experiments, the capillary was coated with a thin layer of highly conductive silver paint (Ernest F. Fullham, Latham, NY; P/N 14810) and attached to a 0–30 kV power supply (Spellman, Plainview, NY).

Chemicals. Solutions were made from NaH₂PO₄ (Sigma, St. Louis, MO) and adjusted to the desired pH with H₃PO₄ (Baker Chemical, Phillipsburg, NJ) or NaOH. Phenol solutions were made from "phenol liquefied" (Fisher, Fairlawn, NJ). Peptide standards were prepared in operating buffer. Nafion (a perfluorosulfonic acid polymer) was obtained as a 5% solution in methanol/water from Solution Technology, Inc. (Mendenhall, PA). All chemicals were used as received with no further purification. Twice distilled (Megapure-Corning, Corning, NY) water was used for all buffers and solutions.

RESULTS AND DISCUSSION

Effect of pH on EOF Control. In previous publications, applied radial voltage has been shown to alter EOF to a large degree.^{18,22} This dynamic method of EOF control shows great promise, and the investigation of the fundamental properties of this process is important. The controlling effect is based on a capacitive charge across the wall of the capillary resulting from the application of the radial voltage. This capacitive charge is assumed to affect the ζ potential in an additive manner with those charges that are due to ionization of surface silanol groups. Since the surface charge is a function of the buffer pH, the effectiveness of control by radial voltage should also be effected by pH. The effect of varying the pH has been theoretically examined and the resulting plot is shown in Figure 2. This figure is a plot showing the theoretical flow versus applied radial voltage (eq 6), where pH values are set from 2 to 8. The specific input values are listed in the figure legend. As the hydrogen ion concentration increases, the operand decreases and lowers EOF due to the reduced number of surface charges from the silanol ionization. This, in turn, allows a greater relative control with the applied radial voltage. The less charge on the surface due to ionized functional groups on the inner surface allows greater absolute control of the flow by the applied radial voltage. Also, as control of EOF

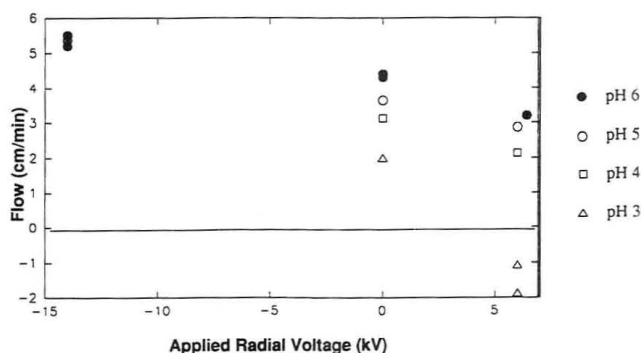


Figure 3. Graph of experimental results for control of EOF by an applied radial voltage at a series of buffer pH values using phenol as a neutral marker. Data for pH 6 shows two data points for each radial voltage setting. Data for pH 4 and 5 have only one data point per radial voltage setting. The data for pH 3 indicate a reversal of flow for the +6-kV radial voltage setting. Experimental conditions: separation potential, 140 V/cm; capillary, 50 cm \times 25- μ m i.d. \times 250- μ m o.d.; concentration, 1 mM phosphate buffer; detection, absorbance at 214 nm.

increases at lower pH the sigmoidal shape of the hyperbolic inverse sine function becomes apparent.

Electroosmotic flow control by applied radial voltage has also been examined experimentally over the range of pH from 3.00 to 6.00. The results obtained at applied radial voltages of -14 kV, no applied radial voltage, and at +6 kV are shown in Figure 3. Experimental trends in the data are clearly in agreement with the theoretical plots of eq 6 shown in Figure 2. A relatively linear relationship exists between EOF and applied radial voltage for the pH values of 4, 5, and 6 (correlation coefficients of 0.9997, 0.9992, and 0.947, respectively). Experimental data at these pH values (Figure 3), indicates that the EOF is altered over the entire range of applied voltages by 59, 48, and 22%, respectively. The linear relationship between EOF and radial voltage under these experimental conditions has led to the suggestion that a linear relationship exists at all accessible applied radial voltages.^{19,22} However, at lower pH values it appears that EOF velocity approaches an asymptotic limit when controlled by increasing applied radial voltages. It also appears that altering the surface charge by extreme pH values also causes flow to approach this limit, and it is likely to be due to some saturation of the surface/buffer interface. In addition to these interesting effects, the data set obtained at pH 3 shows a large effect on the flow, shows a flow reversal, and is clearly not a linear relationship.

At pH 3.00, EOF can be varied from ca. 3.5 cm/min to ca. -1.87 cm/min at applied radial voltages from -14 to +6 kV, respectively. Figure 4 shows several experimental data points plotted along with a line representing eq 6 (multiplied by 3.9 to match the absolute magnitude of the flow) for these same experimental conditions. At this pH, it is clear that the control of EOF by an applied radial voltage is much more effective in the presence of fewer ionized silanol surface charges than are present at higher pH. It is also clear that eq 6 predicts the sigmoidal shape of this data set. Equation 6 also predicts more effective control of EOF with the 10- μ m-i.d., 140- μ m-o.d. capillary versus the 25- μ m-i.d., 250- μ m-o.d. capillary, although comparing Figures 3 and 4 shows better control for the 25- μ m-i.d. capillary. These relatively small differences have been attributed to capillary to capillary variation; hence, group data sets are considered here. However, the relationship between EOF control and capillary radius is the subject of current study in our laboratory. Electroosmotic flow control does not follow a linear relationship under these conditions, and it would seem that accuracy near the steepest portion of the curve would be difficult. However, since this section of

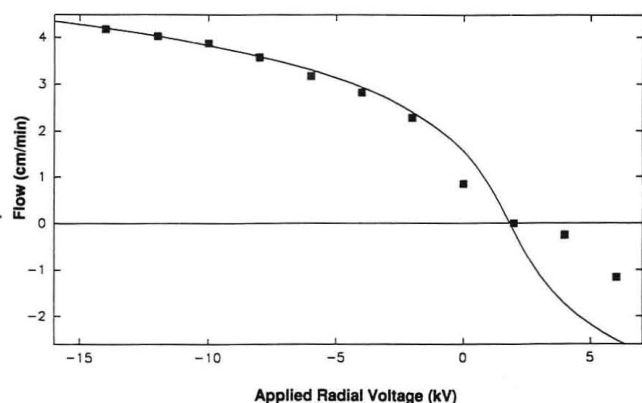


Figure 4. Comparison of experimental data and theory from eq 6 at pH 3.00. Each box represents the average of several neutral marker experiments, with $n = 1$ for data at -14 and 0 kV and $n = 3$ or more for all others. The solid line is theoretical data from eq 6 employing the same variables as in the experiments (multiplied by 3.9 to match the magnitude—see text). Experimental conditions: separation potential, 140 V/cm; capillary, 50 cm \times 10 - μ m i.d. \times 144 - μ m o.d.; concentration, 1 mM phosphate buffer; detection, 214 nm. Additional variables for eq 6: dielectric coefficient, 78 ; viscosity, 0.00089 kg/m s; counterion diameter, 1.5×10^{-10} m; dissociation constant, 5×10^{-7} ; surface silanol group concentration, 5×10^{14} groups/cm 2 .

the curve occurs near zero flow rate, it becomes experimentally unimportant for many applications.

Values of EOF generated by eq 6 had to be increased by a factor of 3.9 to match the magnitude of the experimental data points in Figure 4. While the trends predicted by the theory are clearly supported by the experimental evidence, the exact magnitude is not. This points out the limitations of the fundamental theory, some of which have been discussed previously.²⁰ The theory developed assumes that a monovalent buffer system and a perfectly cylindrical inner capillary wall are utilized. Also, the dissociation constant for surface silanol groups has been reported at values ranging over 8 orders of magnitude.²⁹ The inherent limitation of the double-layer theory which is based on Debye-Huckel approximations assumes constant viscosity and dielectric properties across the double layer, of which there is much evidence to the contrary.²⁸ Finally, it is not clear what error the unshathed portions at the ends of the capillary are contributing to the flow. Understanding these assumptions and limitations, the theory, as developed, predicts all of the experimentally observed trends in this study. The usefulness of eq 6 in assessing the effect of pH on EOF control is clearly apparent in Figure 4. In addition, in the absence of any applied radial voltage, eq 6 is consistent with experimental results for varying pH,^{10,11,23} temperature,³⁰ and concentration¹³ in normal unshathed CE systems.

Enhanced Time of Analysis for Low pH Separations of Peptides. A separation was carried out to demonstrate the utility of EOF control. McCormick¹² has used a low pH buffer system to separate a series of di- and tripeptides while preventing adsorption of these solutes to the capillary wall. At a pH of 1.5, EOF is nearly eliminated and the interaction of the analytes with the wall of the capillary is minimized. In the previous work, the absence of EOF has been described as an advantage due to irreproducibility of this flow from run to run. In the experimental scheme presented in this paper, EOF control reduces the analysis time and the flow is considerably more reproducible owing to independent control. Two electropherograms are shown in Figure 5 for the separation of several peptides. Figure 5a shows the separation in the absence of an applied radial voltage and Figure 5b with

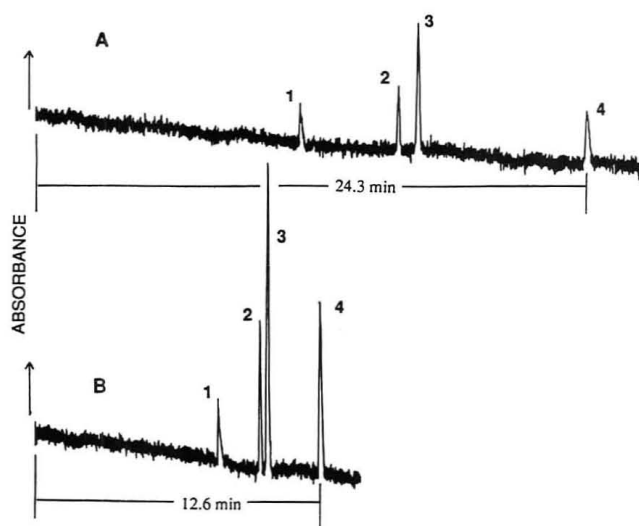


Figure 5. Separation of di- and tripeptides at pH 1.4 with and without EOF control: (A) no applied radial voltage and (B) the same separation with the applied radial voltage of -14 kV. Analytes: (1) L-lysyl-L-lysine, (2) L-glycyl-L-alanyl-L-alanine, (3) L-histidyl-L-phenylalanine, and (4) L-lysyl-L-phenylalanine. Experimental conditions: separation potential, 140 V/cm; capillary, 52 cm \times 20 μ m-i.d. \times 144 - μ m o.d., 44 cm to detector; concentration, 25 mM phosphate buffer; detection, absorbance at 200 nm.

an applied radial voltage of -14 kV. The total analysis time has been nearly divided in half under conditions of EOF control. In addition, the peak height (signal to noise) has improved and all components are completely resolved in the electropherogram with the -14 -kV applied radial voltage.

Use of a Conductive Sheath for EOF Control. Since we realize a possible disadvantage of the EOF control technique is band broadening due to possible laminar flow, this has been investigated further. Theory to date assumes that capacitive charging of the double layer inside the capillary only occurs in the portions of the capillary covered by the sheath. According to the theory previously developed, there should be a large differential in the ζ potential (and therefore flow at the wall) in the unshathed sections at the ends of the capillary. This effect may lead to a systematic error in experiments where the flow is reversed. In addition, the differential flows might be expected to lead to significant band broadening due to laminar flow profiles near and in these regions. The magnitude of this effect is not great enough to observe it in the separation of the peptides shown in Figure 5. So, to test this predicted band broadening under more extreme conditions, a conductive sheath²⁰ has been applied over the length of the capillary and held at 0 V. Since the radial voltage drop across the fused silica wall over the length of the capillary would be varying in direct relation to the linear potential drop inside the capillary, this should induce differential flow at the wall over the length of the capillary. This is in contrast to the Nafion-coated apparatus where the applied radial voltage is constant everywhere except over the uncoated portions of the capillary. The experiments have involved two probes and two different pH values. Efficiency has been evaluated with phenol (pH 6.32) and L-histidyl-L-phenylalanine (pH 1.4). Theoretical plates (N) have been calculated in the usual manner where $N = 5.54 (t_r/w_h)^2$, where t_r is the elution time and w_h is the peak width at half height. The experimental results are shown in Table I. No evidence of band broadening is present at either pH. In fact, the applied radial voltage appears to slightly increase efficiency. This phenomenon is the subject of further investigation in our laboratory. These initial experiments appear to indicate that the application of this technique does not detract from the advantages of the plug-type flow in electroosmosis.

(29) Nawrocki, J. *Chromatographia* 1991, 31, 177.

(30) Tsuda, T. *J. Liq. Chromatogr.* 1989, 12, 2501.

Table I. Change in Theoretical Plates upon Application of Grounded Conducting Sheath

experimental condition	theoretical plates ^a	<i>n</i>
pH 1.4 (L-Histidyl-L-phenalanine)		
no sheath	44 327 ± 217	5
conductive sheath (60% of capillary)	59 291 ± 2	5
pH 6.32 (Phenol)		
no sheath	87 700 ± 9200	6
conductive sheath (60% of capillary)	101 000 ± 6300	6

^a Errors are standard deviations.

CONCLUSION

The effects of varying pH on the control of EOF, both theoretically and experimentally, have been examined. A theory has been presented that successfully predicts the range and relationship between applied radial voltage and EOF. The effect of applied radial voltage on EOF is significantly

amplified at low pH relative to high pH. The usefulness of EOF control has also been demonstrated by providing an improvement in the separation of peptides at low pH. Finally, preliminary data to examine the effect of different EOF values along the capillary appears to indicate that, at least for the conditions of EOF control by an applied radial voltage, solute band broadening is not affected.

ACKNOWLEDGMENT

This work was supported, in part, by the National Institutes of Health and the National Science Foundation. A.G.E. is a National Science Foundation Presidential Young Investigator (NSF CHE-8657193) and a Camille and Henry Dreyfus Teacher-Scholar.

RECEIVED for review June 1, 1992. Accepted September 30, 1992.

NMR Study of the State of Water in Ion-Selective Electrode Membranes

Andy D. C. Chan and D. Jed Harrison*

Department of Chemistry, University of Alberta, Edmonton, Alberta, Canada T6G 2G2

Variable-temperature ^1H and ^2D NMR studies of H_2O and D_2O uptake in poly(vinyl chloride) (PVC) based ion-selective membranes were employed to evaluate the state of water. The data show that water (heavy or light) in the membranes is present as "freezable" water, indicating it is present as droplets or clusters. The water freezes between 0 and -15°C , and calculations suggest the minimum droplet diameter is about $0.016\ \mu\text{m}$, but a large size range exists. The light scattering centers observed during water uptake must be due to these droplets, at least in part. The NMR chemical shift of water is a function of the concentration of $\text{KB}(\text{C}_6\text{H}_5)_4$ added to the membrane, and the range of chemical shifts demonstrates there are a range of environments for water.

INTRODUCTION

Ion-selective electrode (ISE) membranes based on a poly(vinyl chloride) (PVC) and plasticizer matrix are extensively used in analytical measurements. Considerable effort has been directed toward understanding the selective extraction and transport of ions in these membranes with regards to the mechanism of development of membrane potential.¹⁻³ Water has been identified as playing an important role;^{2,3} however, there is little data on the behavior, distribution, or chemical state of H_2O in PVC-based membranes.

Recently, we have used a spectroscopic probe to image the internal concentration profile of water and of light-scattering centers generated by the uptake of water within ISE membranes.⁴⁻⁶ This work established that water penetrates the membrane in a two-stage process. The first stage involves a fast uptake of water and very little perturbation of the membrane and is attributed to water miscible in the membrane phase. The second stage involves a phase transformation in the polymer over a much longer time period and is evidenced by the formation of a large number of light-scattering centers. We have postulated⁴⁻⁶ that these light-scattering centers are water droplets in the membrane phase, as have others.^{2,3,7} However, there is little direct evidence for this assumption. Other effects, such as phase separation of the plasticizer and PVC and changes in the fraction of polymer crystallinity are known to occur as the PVC to plasticizer

ratio varies, or the mixture is aged environmentally.⁸ It is possible that water uptake induces light scattering by such a process. Since the chemical state of water in the membrane will govern its effect on transport and the equilibria of other species, it is important to determine whether water droplets are indeed formed. Likewise, interpretation of our optical studies of light scattering in the membrane will be facilitated by identification of the nature of the light-scattering centers.

^1H NMR has proven useful in identifying the various forms of water present in polymer matrices⁹⁻¹⁵ and has revealed the sensitivity of water's structural organization to polymer mobility.^{12,13} Variable-temperature NMR can also be used, as in the probing of bound water in protein and polypeptide systems.^{9,14,15} In a study of water in polymers there is always a difficulty in distinguishing between the different chemical states present. From the perspective of this report the terms "freezable" and "nonfreezable" are perhaps most useful. Water which is miscible in another medium (e.g. alcohol) is molecularly dispersed and can be categorized as dissolved water. If it is dispersed, but specifically associated with another molecule or ion, then it is frequently described as "bound" water.^{9,14,15} Neither of these states will freeze, since this is a cooperative function of water aggregates, and so these environments give rise to "nonfreezable" states of water. When small amounts of water are absorbed in a restrictive environment such as a polymer, it can be expected that H bonding and aggregation will be affected.^{16,17} Nonetheless, the water in polymers is generally perceived to form mobile clusters.^{18,19} If the water molecules aggregate in large enough clusters, they will freeze. Very large aggregates will exhibit the properties of bulk water, while smaller aggregates may not.²⁰ Freezable water than can be distinguished from bulk water by a change in a bulk parameter such as the freezing point is often referred to as a cluster or droplet.

In this study ^1H and ^2D NMR have been used at various temperatures to probe the state of H_2O and D_2O absorbed in PVC/DOA membranes. The effect of the lipophilic salt potassium tetraphenylborate (KBPh_4), which is commonly

(8) Mark, H. F.; Bikales, N. M.; Overberger, C. G.; Menges, G., Kroschwitz, J. I., Eds. *Plasticizers*. In *Encyclopedia of Polymer Science and Engineering, Supplement Vol.*; John Wiley & Sons: New York, 1989; pp 568-648.

(9) Kuntz, I. D.; Kauzmann, W. *Adv. Protein Chem.* 1974, 28, 239.

(10) Boyle, N. G.; McBrierty, V. J.; Douglass, D. C. *Macromolecules* 1983, 16, 75.

(11) McCall, D. W.; Douglass, D. C.; Blyler, L. L., Jr.; Johnson, G. E.; Jelinski, L. W.; Blair, H. E. *Macromolecules* 1984, 17, 1644.

(12) Quinn, F. X.; Kampff, E.; Smyth, G.; McBrierty, V. J. *Macromolecules* 1988, 21, 3191.

(13) Smyth, G.; Quinn, F. X.; McBrierty, V. J. *Macromolecules* 1988, 21, 3198.

(14) Kuntz, I. D.; Brassfield, T. S.; Law, G. D.; Purcell, G. V. *Science* 1969, 163, 1329.

(15) Kuntz, I. D. *J. Am. Chem. Soc.* 1971, 93, 514.

(16) Resing, H. A.; Thompson, J. K.; Krebs, J. J. *J. Phys. Chem.* 1964, 68, 1621.

(17) Dransfeld, K.; Frisch, H. L.; Wood, E. A. *J. Chem. Phys.* 1962, 36, 1574.

(18) Hoeve, C. A. *J. ACS Symp. Ser. (Water Polym.)* 1980, 127, 135.

(19) Brown, G. L. *ACS Symp. Ser. (Water Polym.)* 1980, 127, 441.

(20) Stillinger, F. H. *ACS Symp. Ser. (Water Polym.)* 1980, 127, 11.

* Author to whom correspondence should be addressed.

(1) Morf, W. E. *The Principles of Ion-Selective Electrodes and of Membrane Transport*; Elsevier: New York, 1981.

(2) Morf, W. E.; Simon, W. *Helv. Chim. Acta* 1986, 69, 1120.

(3) Armstrong, R. D.; Horvai, G. *Electrochim. Acta* 1990, 35, 1.

(4) Li, X.; Petrović, S.; Harrison, D. J. *Sensors Actuators* 1990, B1, 275.

(5) Li, X.; Harrison, D. J. *Anal. Chem.* 1992, 63, 2168.

(6) Harrison, D. J.; Li, X.; Petrović, S. In *Biosensors and Chemical Sensors*; Edelman, P. G., Wang, J. Eds.; ACS Symposium Series 487; American Chemical Society: Washington, D.C., 1992; Chapter 23, pp 292-300.

(7) Marian, S.; Jagur-Grodzinski, J.; Kedem, O.; Vofsi, D. *Biophys. J.* 1970, 10, 901.

added to ion-selective membranes to improve permselectivity,^{1-3,21,22} has also been examined. The results show that freezable water is present in the membrane. This substantiates the hypothesis that the light-scattering centers observed upon water uptake are due to water droplet formation.

EXPERIMENTAL SECTION

Sample Preparation. Samples for NMR analysis were prepared from solutions of 150 mg of bis(2-ethylhexyl) adipate (DOA) (Fluka, Selectophore grade) and 75 mg of poly(vinyl chloride) (PVC) (Polysciences, chromatographic grade) in 3 mL of freshly distilled tetrahydrofuran (THF) (BDH, distilled from potassium). Appropriate aliquots of potassium tetrphenylborate (KBPh₄) in THF were added. KBPh₄ was prepared by precipitation from NaBPh₄ (Terochem).²³ Small aliquots of the membrane cocktail were added to a 5-mm NMR tube. Between each addition, the sample tube was dried in a 60 °C oven for 24 h in order to ensure uniform casting and complete solvent evaporation. Final samples were about 2 cm in height in the tube. Membranes were allowed to equilibrate for several days with either nanopure H₂O (Barnstead) or 99.8% D₂O (General Intermediates) before NMR experiments. During NMR analysis either the head of water was removed when present (and the tube was capped to prevent evaporation) or it remained and the NMR tube position was adjusted so that the head of water was above the coils. Both methods produced the same results.

Membrane samples for IR analysis were prepared by dissolving 200 mg of DOA and 100 mg of PVC in 3 mL of THF. These solutions were cast in Teflon rings (inner diameter, 4 cm) clamped onto a Teflon sheet to form master membranes according to the method of Craggs et al.²⁴ A flexible membrane of ca. 120- μ m thickness (determined with a micrometer) remained after complete evaporation of the THF solvent. Samples for FTIR analyses 1.5 cm in diameter were cut from the master membrane.

Potassium ion-selective electrodes were prepared from membranes cast onto glass slides.²⁴ The following membrane composition was used: 66% DOA, 33% PVC, 1% valinomycin (Sigma), and 0.01% KBPh₄.²¹ For calibration, 10⁻²–10⁻⁶ M KCl solutions were prepared by serial dilutions of a 10⁻¹ M KCl stock solution.

Apparatus. ¹H and ²D NMR measurements were made on a Bruker WH-200 spectrometer operating in the pulsed Fourier transform mode at Larmor frequencies of 200 and 30 MHz, respectively. For the ¹H measurements a ²D-lock was established using a DOA/CDCl₃ sample with TMS added as the chemical shift reference. Membrane samples were then measured with the spectrometer unlocked. For ²D measurements a sample of pure D₂O provided both the initial lock and chemical shift reference. All chemical shifts are reported in ppm relative to TMS. The probe temperature was regulated with a Bruker B-VT-1000 temperature controller using liquid nitrogen and measured with an Analogic AN2572 thermocouple (± 1 °C). The spectrometer was relocked and reshimmied at each temperature using the DOA/CDCl₃/TMS or D₂O samples. Membrane samples were accordingly stored at ambient temperature, in the refrigerator, or in the freezer in order to minimize extreme temperature modulations during this procedure.

Fourier transform infrared (FTIR) spectroscopic measurements were made on a Nicolet 7199 Fourier transform spectrometer with a resolution capability of 0.06 cm⁻¹. Potential measurements were made with a Fisher 825 MP meter. A saturated NaCl calomel electrode was used as the reference electrode (SSCE). The temperature of the calibration solutions

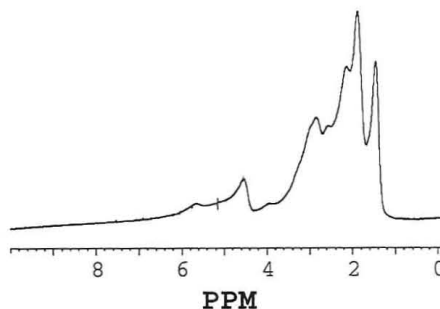


Figure 1. ¹H NMR spectrum of a dry 66% DOA/PVC membrane sample.

was adjusted by immersion in a Lauda K-4/RD circulator bath using a 50% methanol/water mixture as the thermostatic medium.

RESULTS AND DISCUSSION

To evaluate the sensitivity of ¹H NMR to H₂O in PVC/DOA membranes, NMR and infrared spectra of neat DOA were first obtained. NMR spectra of neat DOA sampled directly from the reagent bottle showed no evidence of H₂O present. Shaking the plasticizer with an equal volume of H₂O for 1 h produced a suspension of water droplets, evidenced by the translucence of the sample. Even after allowing 1 h for settling, integration of the proton signal indicated 0.7 wt % H₂O remained. However, centrifugation of the sample produced a clear liquid that gave no discernable NMR signal for H₂O in the DOA (<0.2 wt %).

Infrared spectroscopy is much more sensitive to water, and FTIR spectra of neat DOA showed the presence of H₂O as a low intensity, broad band at 3450 cm⁻¹ due to the OH stretch. Saturation of DOA with water, followed by centrifugation, resulted in a significant increase in the OH stretch, although it remained a relatively low intensity peak. These results show that H₂O has some limited solubility in DOA and that NMR has insufficient sensitivity for its detection. NMR does have the sensitivity required for the determination of water droplets suspended in DOA.

A membrane matrix composed of 33 wt % PVC and 66 wt % DOA was examined by transmission FTIR before exposure to water. The radiation was completely attenuated for the major vibrational modes of the membrane components, including the CH stretch (2900 cm⁻¹), CO stretch (1750 cm⁻¹), and C–C stretch and CH bending (1100–1500 cm⁻¹) modes of the plasticizer.^{25,26} However, a well-defined OH stretch was clearly seen at 3450 cm⁻¹, indicating the presence of water. This band increased in intensity if the membrane was first soaked in H₂O for several hours, allowed to dry for up to 15 min, and then reexamined. After this limited drying the ~120- μ m-thick membranes were transparent and showed no evidence of light scattering. However, the ratio of the peak intensity at 3450 cm⁻¹ to a membrane band at 490 cm⁻¹ indicated about an 18% increase in water content following the procedure described above, but this value should depend on the drying time. Quantitative data was not obtained due to constraints on use of the FTIR spectrometer.

The ¹H NMR spectrum shown in Figure 1 is relatively broad and the features are poorly resolved; however, the resolution is sufficient for studying water absorption within these membranes. Alternatively, ²D NMR measurements of D₂O-soaked membranes were employed in order to eliminate spectral interferences from the other membrane components.

(25) Kellner, R.; Fischböck, G.; Götzinger, G.; Pungor, E.; Tóth, K.; Polos, L.; Lindner, E. *Fresenius' Z. Anal. Chem.* 1985, 322, 151.

(26) Kellner, R.; Zippel, E.; Pungor, E.; Tóth, K.; Lindner, E. *Fresenius' Z. Anal. Chem.* 1987, 328, 464.

(21) Band, D. M.; Kratochvil, J.; Treasure, T. J. *Physiol. (London)* 1976, 265, 2P.

(22) Verpoorte, E. M. J.; Harrison, D. J. *J. Electroanal. Chem. Interfacial Electrochem.* 1992, 325, 153.

(23) Bassett, J.; Denney, R. C.; Jeffery, G. H.; Mendham, J. *Vogel's Textbook of Quantitative Inorganic Analysis*, 4th ed.; Longman: London, 1978.

(24) Craggs, A.; Moody, G. J.; Thomas, J. D. R. *J. Chem. Ed.* 1974, 51, 541.

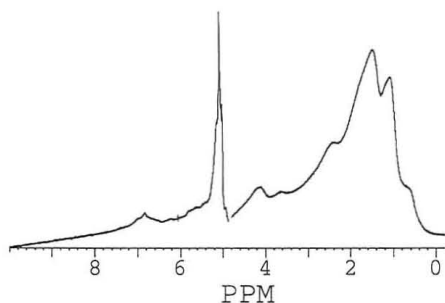


Figure 2. ^1H NMR spectrum of a H_2O -soaked 66% DOA/PVC membrane containing 0.1% KBPh_4 salt.

0.01% KBPh_4 Membranes. A ^1H NMR spectrum of a 66% DOA/PVC membrane containing 0.01% KBPh_4 salt soaked in H_2O is shown in Figure 2. A period of about 2 days was usually required for the NMR signal to develop and then stabilize. Analogous ^2D NMR measurements on D_2O -soaked membranes confirm that these are water resonances and not due to chemical shift changes of the membrane components. The water droplets in the neat plasticizer led to a single sharp resonance, yet in the membrane phase there is a spread between 4.9 and 5.4 ppm. This observation is not too surprising given the complex nature of the PVC/DOA phase, which likely contains a number of possible environments for water.

We have observed that the exact chemical shifts and the fine structure of the water signal are not completely reproducible between different H_2O -soaked membrane samples. This seems to suggest that the absorbed water molecules do not exist in well-defined, static environments. It is likely that water clusters of various sizes exist and that these are randomly distributed throughout the membrane phase and differ between samples due to inhomogeneities in the samples. These clusters will present an assortment of different chemical environments and could account for the observed spread in the water signal and the differences between samples. We had some concerns regarding the possibility of magnetic inhomogeneities in the samples which might affect the observed chemical shifts and lead to broadening. To evaluate this several PVC/DOA samples were soaked in 10 wt % tetramethylammonium chloride (Me_4NCl) aqueous solutions. The Me_4NCl resonance in the membranes did not vary by more than ± 0.1 ppm from its value of 2.9 ppm in pure D_2O solvent. Additionally, a soaking period of about 24 h was required before the Me_4NCl resonance was detectable. This important observation demonstrates that it is the aqueous phase within the membrane which is probed and not merely the "head" of solution above the sample.

Variable-temperature (VT) NMR can provide considerable insight into the character of water absorbed in the PVC/DOA matrix. Water which is dissolved in the membrane matrix will be measurable at all temperatures, at least above the glass transition of the matrix, whereas water present in clusters or small droplets will become frozen at low enough temperatures. The line width of ice is on the order of 10^5 Hz, so that once frozen the water resonance is not observed with a solution-phase instrument.

^2D VT-NMR spectra of a D_2O -soaked membrane are shown in Figure 3. Analogous ^1H VT-NMR spectra of H_2O -soaked membranes were also obtained. These show the same behavior as the ^2D spectra but appear more complex due to the broad membrane resonances. The spectra in Figure 3 show that the D_2O eventually freezes out in the PVC/DOA matrix. From Figure 3 we can also see that the process of crystallization and subsequent thawing does not appear to significantly affect the distribution of water in the membrane. The similarity of the D_2O resonances at $+25^\circ\text{C}$ both before

and after freezing suggests that similar states of water are present. Spectral intensity decreases were apparent as the temperatures was decreased below 0°C , and this is reflected in the observed signal-to-noise ratios in Figure 3. However, the results are only semiquantitative, as the spectral intensities depend on the placement of the sample relative to the rf receiver coil. Measurements at each temperature involved repositioning the sample in the spectrometer when adjusting the magnetic field, so that the changes in intensity are subject to some error.

The resonance for absorbed D_2O began to decrease between 0 and -5°C , well below the freezing point of bulk heavy water ($+3.78^\circ\text{C}$), and was completely eliminated between -10 and -15°C . This temperature is well above the membrane glass transition temperature.⁸ Note that the sensitivity of NMR is insufficient for observation of any unfrozen water still dissolved in the membrane at these temperatures, consistent with the results for water in DOA plasticizer. The data in Figure 3 provides clear evidence that much of the water in the PVC/DOA matrix is present as water clusters or droplets, so that it has characteristics similar to bulk water. The freezing point depression observed, and the distribution of chemical shifts, indicate that there are some differences though.

A freezing point depression of 15 – 20°C cannot be due to simple colligative effects of the added KBPh_4 salt, since the molal freezing point depression constant for water is only $1.86\text{ K}\cdot\text{kg}/\text{mol}$. This supercooling effect is not unique to these membranes but has been observed in other polymer–water systems as well. Freezing point depressions of up to 35°C are not uncommon¹⁴ and can result if the polymer is able to trap water in sufficiently small channels or pores.^{16,17} Space restrictions within these cavities may then preclude the formation of ice crystals from the absorbed water. In addition there may also be kinetic difficulties in nucleating crystallization of ice clusters of limited size.²⁰ Furthermore, between -10 and 0°C , the surface of ice is believed to be covered by a mobile liquid-like layer containing bifurcated H bonds and odd-sided polygons.²⁷ The increased number of water molecules in the surface region due to these small clusters will also contribute to a proportionately greater amount of "liquid" fraction below the normal freezing point.

Analogous ^1H NMR VT experiments on H_2O -soaked membranes show that absorbed H_2O does not completely freeze until about -15°C . We can use this result to calculate the radius of the water cluster required to cause a freezing point depression of this magnitude. Higuti and Iwagami²⁸ have derived a correlation between the freezing point depression (ΔT) and the radius of pore (r) in which a liquid is condensed on the basis of thermodynamic considerations. This is given by

$$\frac{\Delta T}{T_0} = \frac{2\gamma M}{\rho r \Delta H_{\text{fus}}} \quad (1)$$

where T_0 , M , and ΔH_{fus} are the normal freezing point (273 K), the molecular weight ($18.01\text{ g}/\text{mol}$), and the heat of fusion ($6.01 \times 10^{10}\text{ erg}/\text{mol}$) for the bulk liquid, respectively, and γ and ρ are the surface tension ($75.6\text{ dynes}/\text{cm}$ at 0°C) and the density ($0.9998\text{ g}/\text{cm}^3$ at 0°C) of the supercooled liquid. Numeric values for the various physical constants can be approximated by values at 0°C for a small range of ΔT . From this calculation, the radius (r) of the water clusters may be estimated as $0.008\ \mu\text{m}$ for a ΔT of 15°C . The diameter of these water clusters in the membrane phase is, therefore, approximately $0.016\ \mu\text{m}$. It is interesting to note that

(27) Fletcher, N. H. *The Chemical Physics of Ice*; Cambridge U.P.: Cambridge, 1970.

(28) Higuti, I.; Iwagami, Y. *J. Phys. Chem.* 1952, 56, 921.

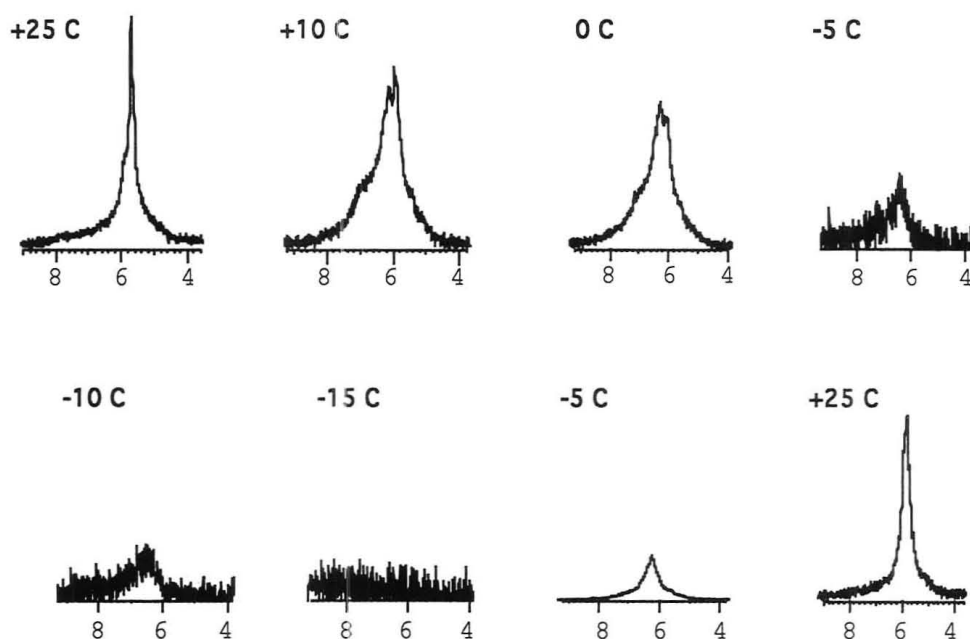


Figure 3. Variable temperature ^2D NMR spectra of a D_2O -soaked 66% DOA/PVC membrane containing 0.01% KBPh_4 salt.

Stillinger²⁰ has estimated that the content of spherical water clusters with a $0.01\text{-}\mu\text{m}$ diameter is 1.75×10^4 water molecules, of which 4.7×10^3 , or 27%, are within 5 \AA of the surface. Stillinger estimated that this surface water to bulk water ratio would be sufficient to lower the well-known density maximum of water at $3.98 \text{ }^\circ\text{C}$ by about $17 \text{ }^\circ\text{C}$. Clearly, such a significant fraction of water molecules in a surface rather than bulk environment could account for the observed deviations from the behavior of bulk H_2O seen in the NMR spectra.

From Figure 3 it can be seen that the amount of water observed decreases as the temperature is decreased. This means the maximum freezing point depression corresponds to the smallest droplet size and not the average size. In fact much larger light-scattering centers can also be observed by optical microscopy, and this corresponds to the observations that water begins to freeze just below the normal freezing point.

0.1% KBPh_4 Membranes. When the level of KBPh_4 in the membranes is increased 10-fold to 0.1 wt % there is a significant increase in the extent of light scattering observed. Initially transparent 0.01% KBPh_4 -doped membranes become translucent as water is taken up, while 0.1% doped membranes become white and opaque upon soaking in water. Previous work^{9,29} has shown that the presence of salt in a polymer increases the water uptake, and the increased degree of light scattering observed in PVC/DOA⁶ is consistent with this.

Figure 4 shows that the increased salt content leads to a significant change in the water environment. The chemical shifts for H_2O in the 0.1% KBPh_4 membranes indicate an increase in the number of distinct environments. Multiple water peaks have previously been reported for different states of water within polymer and protein phases.^{9,30} These arise from the high sensitivity of the ^1H chemical shifts to solvent and H-bonding effects.

Typically three H_2O peaks were observed for 0.1% KBPh_4 membranes, but the relative peak heights and exact chemical shifts differed between samples. As seen in Figure 4 the chemical shifts observed in the membrane are 1–2 ppm downfield from bulk water (ca. 4.8 ppm), although a peak at

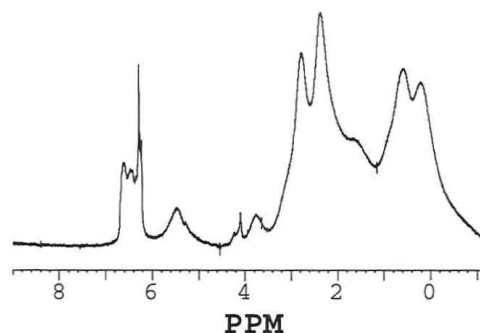


Figure 4. ^1H NMR spectrum of a H_2O -soaked 66% DOA/PVC membrane containing 0.1% KBPh_4 salt.

5.4 ppm may arise from water, the membrane, or both. These are relatively small shifts since, for example, the shift from water liquid to water vapor is +6 ppm at room temperature. Hence, this implies that the water environments do not have radically different H-bonding patterns from each other and from bulk water.⁹ It is likely that the higher concentration of water in the 0.1% KBPh_4 membrane results in the formation of a larger range of water droplet sizes than in 0.01% doped membranes, and this is supported by the increased light scattering and opaqueness. The higher concentration of salt in the membrane may assist in this process by providing nucleation sites. Such a range of droplet sizes would lead to a multitude of chemical shifts for water. Furthermore, since these environments are resolved on the NMR time scale, this indicates that any exchange process between the different environments must not be too rapid and that the water droplets are relatively isolated entities.

^2D NMR VT spectra for a 0.1% KBPh_4 membrane soaked in D_2O are shown in Figure 5. Three peaks were typically observed, but the range of chemical shifts was somewhat broader for the ^2D spectra, as seen by comparing Figures 4 and 5. We again observed a supercooling effect for the freezing of D_2O . The lowest field components, while still present below the freezing point of D_2O , were substantially attenuated by $-5 \text{ }^\circ\text{C}$. In addition, after freezing and rewarming to $+25 \text{ }^\circ\text{C}$ it appears that there is one preferred environment at about 4.9 ppm. This is at higher field than the peak at 5.4–5.8 ppm for D_2O in 0.01% KBPh_4 membranes and is similar to that of bulk water. This suggests that the ice crystallization process led to aggregation of the water droplets so that it became

(29) Southern, E.; Thomas, A. G. *ACS Symp. Ser. (Water Polym.)* 1980, 127, 375.

(30) Pesek, J. U. J.; Pesok, R. L. *Anal. Chem.* 1972, 44, 620.

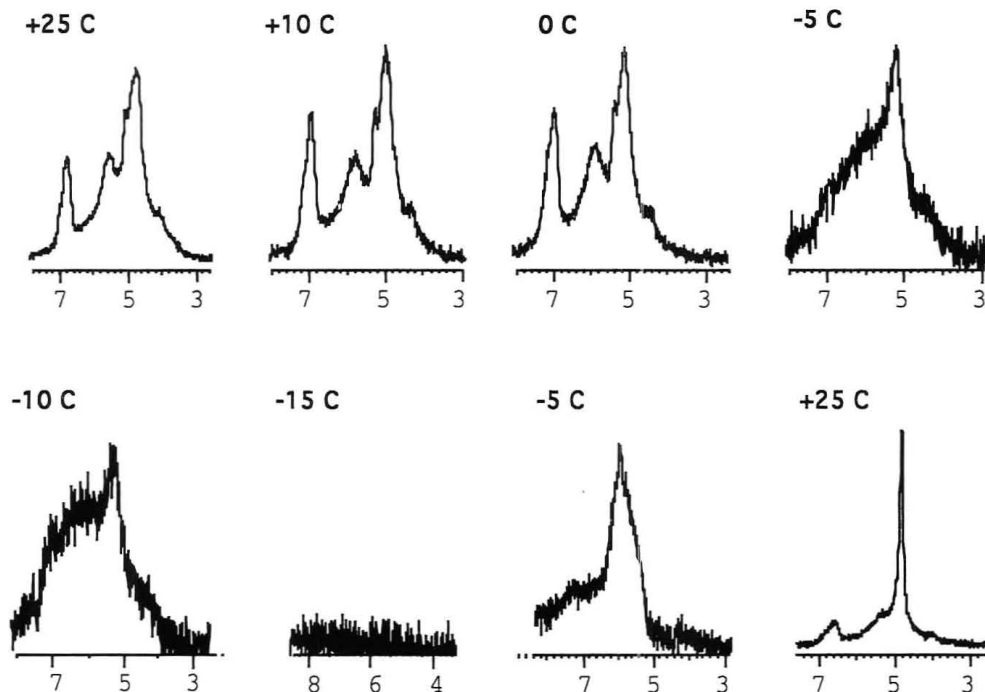


Figure 5. Variable temperature ^2D NMR spectra of a D_2O -soaked 66% DOA/PVC membrane containing 0.1% KBPh_4 salt.

more bulk-like and is consistent with the fact that ice crystals act as nucleation centers for further crystallization.

Further interpretation of the distribution of water environments is difficult. The different peaks may represent different droplet sizes, although if this is so then it seems likely the smallest droplets would have the greatest chemical shift from bulk water. The smallest droplets should also freeze out at the lowest temperatures, but in fact the peaks at about 6 and 7 ppm decrease at higher temperature than that at 5 ppm. Alternatively, the different peaks may reflect the chemical content of the droplets, or be related to the water solvation shells of the anions and cations, as observed in other ion-containing polymers.^{9,30} Further work will be required to determine the meaning of the shifts; however, it is clear this will be complicated by the variability between samples.

Effect of Temperature on EMF Measurements. There is a significant reorganization in the distribution of water within an ISE membrane at temperatures above the freezing point. This is particularly pronounced for those membranes containing 0.01% KBPh_4 , as evidenced by the considerable change in the NMR spectra of D_2O at temperatures between +25 and +10 $^\circ\text{C}$ shown in Figure 3. It is relevant to learn what effect, if any, this water reorganization has on the electrochemical performance of these membranes as ISE devices.

In order to evaluate the effect of temperature on ISE performance, potentiometric data were acquired over a range of temperatures. There is no anomalous behavior for the electrode slope of response to $\log [\text{K}^+]$ between +25 and 0 $^\circ\text{C}$. However, the slope of the electrode standard cell potential versus temperature does appear to show a discontinuous change just above 10 $^\circ\text{C}$, as seen in Figure 6. The effect of the change is small, but it is interesting to speculate that it is related to the changes in the water environment within the membrane evidenced by the NMR studies.

CONCLUSIONS

The infrared studies confirm that water can be present in PVC-based ion-selective membranes at a concentration below which light scattering centers are detectable. In conjunction with previous optical imaging studies it is reasonable to conclude that this represents water miscible within the

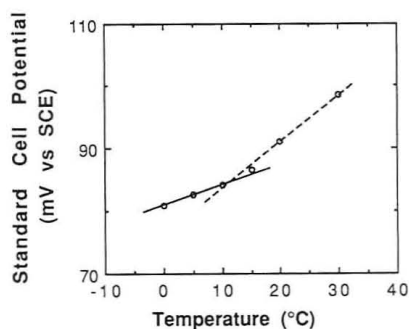


Figure 6. Standard cell potentials vs SSCE for 0.01% KBPh_4 doped K^+ -sensitive ISE membrane as a function of temperature. The size of the data points represents the experimental uncertainty.

membrane matrix. At higher water content, when light scattering centers are present, NMR studies show that "freezable" water droplets are also present within the membranes. The minimum droplet size is around $0.016 \mu\text{m}$ in diameter, and larger droplets are also present, based on the range of freezing point depression observed. These observations confirm that at least some fraction of the light-scattering centers observed during water uptake are due to water droplet formation. Taken together, the NMR and IR data confirm that there is more than one chemical state or environment for water within the membrane matrix, and the NMR data shows the range of these environments is significant. Consequently, models for the role and behavior of water in ion-selective membranes should consider the heterogeneity of these systems.

ACKNOWLEDGMENT

We thank the Natural Sciences and Engineering Research Council of Canada for support, and A.D.C.C. thanks the University of Alberta for a Graduate Research Assistantship.

RECEIVED for review July 29, 1992. Accepted October 8, 1992.

Self-Assembled Monolayers in Electroanalytical Chemistry: Application of ω -Mercapto Carboxylic Acid Monolayers for the Electrochemical Detection of Dopamine in the Presence of a High Concentration of Ascorbic Acid

Franck Malem and Daniel Mandler*

Department of Inorganic and Analytical Chemistry, The Hebrew University of Jerusalem, Jerusalem 91904, Israel

Self-assembled monolayers of ω -mercapto carboxylic acids, $\text{HS}(\text{CH}_2)_n\text{CO}_2\text{H}$ ($n = 2, 5, 10$), C_n , on gold electrodes were used as a means to induce electrochemical differentiation between a neurotransmitter, dopamine (DO), and ascorbic acid (AA). Optimum differentiation is found for $n = 5$, and it is attributed to a compromise between a well-organized system that requires long ω -mercapto carboxylic acids and a reasonable rate of electron transfer which is observed with short ω -mercapto carboxylic acids.

INTRODUCTION

Electrochemical techniques have proved to be significantly advantageous to the biosciences.¹ The application of ultramicroelectrodes in neuroscience, which has been pioneered by Adams,² to monitor the concentration of neurotransmitters in the central nerve system (CNS) has had a special impact. Several of the neurotransmitters, e.g. dopamine, are electroactive and therefore can be detected electrochemically. As a result, ultramicroelectrodes, of the order of microns, have been developed as microprobes for the measurement of neurotransmitters in the extracellular fluid of the CNS.^{3,4}

Nevertheless, the wide application of such voltammetric analysis suffered from lack of specificity. The voltammetric response of the neurotransmitters is hindered by electroactive species, mostly ascorbic acid, which is present at substantially higher concentration than the neurotransmitters. An elegant approach to resolve this problem, i.e. to introduce specificity, was demonstrated by Adams.^{5,6} The approach was based on precoating carbon electrodes with a negatively-charged polymer, Nafion, which repelled the ascorbic acid and other negatively charged species, while attracting positively-charged neurotransmitters, such as dopamine and 5-hydroxytryptamine. Although this approach has been very successful in creating the desired specificity, some issues have been questionable. The reported diffusion coefficients of the neurotransmitters inside the film were relatively low ($D_{\text{dopamine}} = 2.3 \times 10^{-9} \text{ cm}^2\text{s}^{-1}$), implying that very thin films must be used for fast measurements.⁷ On the other hand, the presence of other cations especially at high concentrations, have

affected the electrochemical measurements as a result of saturating the negative sites in the polymer.⁸

We report on a different approach, although also based on electrostatic interactions, to achieve electrochemical differentiation between dopamine and ascorbic acid. We have applied negatively-charged monolayers, i.e. ω -mercapto carboxylic acids $\text{HS}(\text{CH}_2)_n\text{CO}_2\text{H}$, on gold electrode. We found that dopamine could be determined electrochemically in the presence of high concentrations of ascorbic acid through the use of electrodes modified with these monolayers. The application of this approach to ultramicroelectrodes has also been successfully examined.

EXPERIMENTAL SECTION

All chemicals were purchased from Aldrich or Sigma (Milwaukee, WI) and were used as received. Solutions of dopamine (DO) and ascorbic acid (AA) were prepared daily using triple distilled water and were kept under nitrogen. Phosphate buffer (0.1 M, pH 7.4) was used for all measurements, unless otherwise written. 6-Mercaptohexanoic acid, C_6 , was prepared from ϵ -caprolactone according to the procedure by Khim and Field.⁹ 11-Mercaptoundecanoic acid, C_{11} , was synthesized from 11-bromoundecanoic acid in a modified procedure.¹⁰ 11-Bromoundecanoic acid was used as a starting material. The product was extracted with ether and washed with water before it was recrystallized from hexane. All the syntheses gave satisfactory microanalysis results. Gold wire for microelectrodes (10- μm diameter) was ordered from Goodfellow (Cambridge, UK), and the assembly of microelectrodes followed conventional methods.¹¹

Electrochemical experiments were conducted on an Electrochemical Analyzer (BAS 100B). Gold disk electrodes (0.25- or 0.5-mm diameter) sealed in a soldering glass were constructed by us.¹² The electrodes were polished first with emery paper followed by alumina (1.0, 0.3, and 0.05 μm). After rinsing with water, the electrodes were electrocycled in 1 M H_2SO_4 (1.4 V - (-0.7) V vs $\text{Hg}/\text{Hg}_2\text{SO}_4$) until a reproducible voltammogram was obtained. Modification of gold electrodes was carried out in ethanolic solutions that consisted of 50 mM of the thiol. The electrodes were left in the stirred solution for 24 h and then washed with ethanol and water before cyclic voltammetry was recorded. The excess of surface coverage was determined by comparing the charge associated with the reduction of surface gold oxide¹³ in 1 M H_2SO_4 before and after modification. In addition, the method reported by Rubinstein et al.¹⁴ which involves the underpotential deposition and stripping of copper as a means for determining

(1) Junter, G.-A. *Electrochemical Detection Techniques in the Applied Biosciences*; Halsted Press: New York, 1988.

(2) Adams, R. N. *Anal. Chem.* 1976, 48, 1126A-1138A.

(3) Adams, R. N.; Marsden, C. A. In *Handbook of Psychopharmacology*; Iversen, L. L., Iversen, S. D., Snyder, S. H., Eds.; Plenum: New York, 1982; Vol. 15, pp 1-74.

(4) Gerhardt, G. A.; Oke, A. F.; Nagy, G.; Moghaddam, B.; Adams, R. N. *Brain Res.* 1984, 290, 390-395.

(5) Wightman, R. M.; May, L. J.; Michael, A. C. *Anal. Chem.* 1988, 60, 769A-779A.

(6) Rice, M. E.; Oke, A. F.; Bradberry, C. W.; Adams, R. N. *Brain Res.* 1985, 340, 151-155.

(7) Kristensen, E. W.; Kuhr, W. G.; Wightman, R. M. *Anal. Chem.* 1987, 59, 1752-1757.

(8) Nagy, G.; Gerhardt, G. A.; Oke, A. F.; Rice, M. E.; Adams, R. N.; Moore, R. B.; Szentirmay, M. N.; Martin, C. R. *J. Electroanal. Chem. Interfacial Electrochem.* 1985, 188, 85-94.

(9) Khim, Y. H.; Field, L. *J. Org. Chem.* 1972, 37, 2714-2720.

(10) Noll, K. M.; Donnelly, M. I.; Wolfe, R. S. *J. Biol. Chem.* 1987, 262, 513-515.

(11) Fleischmann, M.; Pons, S.; Rolison, D.; Schmidt, P. P. *Ultra-microelectrodes*; Datatech Systems: Morgantown, NC, 1987.

(12) Malem, F.; Mandler, D. *J. Electrochem. Soc.* 1992, 139, L65.

(13) Woods, R. *Electroanalytical Chemistry*; Bard, A. J., Ed.; Marcel Dekker, Inc.: New York, 1976; Vol. 9, pp 1-162.

(14) Rubinstein, I.; Steinberg, S.; Tor, Y.; Shanzer, A.; Sagiv, Y. *Nature* 1988, 332, 426-429.

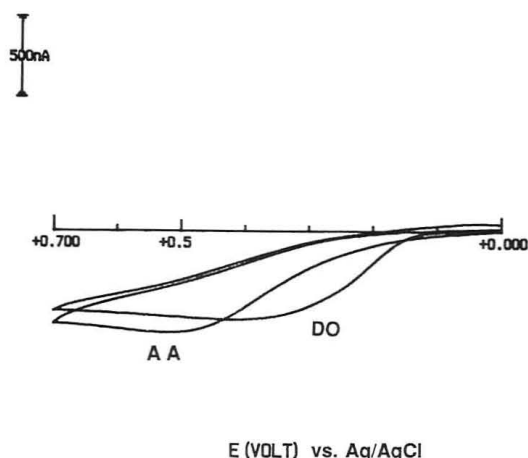
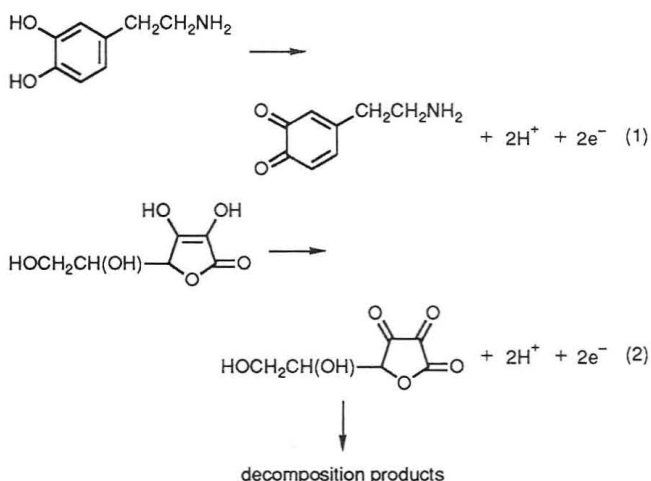


Figure 1. Cyclic voltammety of 5 mM dopamine (DO) and 5 mM ascorbic acid (AA) solutions (pH 7.4) taken with a bare gold electrode and a scan rate of 50 $\text{mV}\cdot\text{s}^{-1}$.

the excess of surface coverage has been employed as well. All quoted potentials are versus Ag/AgCl reference electrode unless otherwise written.

RESULTS AND DISCUSSION

The cyclic voltammety of dopamine (DO) and ascorbic acid (AA), recorded with a bare gold electrode, is shown in Figure 1. Both species exhibit sluggish electrochemical kinetics on gold surfaces. The electrochemical oxidation of these species has been studied mostly on carbon electrodes¹⁵⁻¹⁷ and corresponds to a two-electron, two-proton process (eqs 1 and 2). Both of these electrochemical reactions are irreversible; however, their electrochemical oxidation has been widely used to determine their concentrations. Although the oxidation wave of DO is slightly less positive ($E_{\text{pk}} = 0.38 \text{ V}$) on gold electrodes than that of AA ($E_{\text{pk}} = 0.5 \text{ V}$), this difference is obviously insufficient for electroanalytical purposes. Moreover, this task becomes more difficult due to the fact that the concentration of AA is several orders of magnitude higher than DO in biological environments.



Recently, gold electrodes have been intensively explored as a superior surface for self-organized assemblies.¹⁸⁻²¹ Long-chain thiols have been adsorbed onto gold surfaces, thus

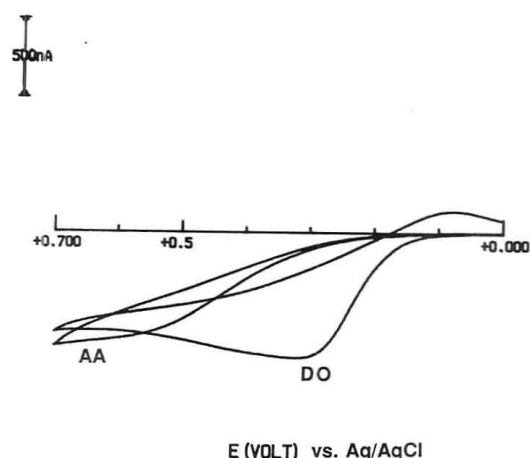


Figure 2. Cyclic voltammety of 5 mM dopamine (DO) and 5 mM ascorbic acid (AA) solutions (pH 7.4) taken with a gold electrode modified with $\text{HS}(\text{CH}_2)_2\text{CO}_2\text{H}$ and a scan rate of 50 $\text{mV}\cdot\text{s}^{-1}$.

forming self-assembled monolayers. These modified surfaces exhibit new electrochemical and physical properties that stem from the organic monolayer. The functionalization of self-assembled monolayers has also been reported as a means to selectively extract metal ions¹⁴ as well as to recognize biological molecules.²²

Thus, we anticipated that such monolayer, if appropriately designed, i.e. functionalized, will enable us to differentiate between AA and DO electrochemically. The amine group of DO is positively charged, whereas the hydroxyl next to the carbonyl group of AA is negatively charged at neutral pH ($\text{p}K_{\text{B}} = 8.87$ and $\text{p}K_{\text{A}} = 4.10$, respectively). Therefore, we have applied ω -thio carboxylic acids, $\text{HS}(\text{CH}_2)_n\text{CO}_2\text{H}$ ($n = 2, 5, 10$), C_n , as a means of attracting the DO while repelling the AA. Figure 2 shows the cyclic voltammety of DO and AA at pH 7.4 with a gold electrode modified with 3-mercaptopropanoic acid, C_3 . It can be clearly seen that while the oxidation wave of DO shifted to less positive potentials ($E_{\text{pk}} = 0.3 \text{ V}$), AA is oxidized at more positive potentials as compared to a bare gold electrode. The shift in the peak potentials is due to a kinetic effect. A substantial increase in the rate of electron transfer from DO is observed. This shift can be attributed to more favorable interactions between DO and the positively charged monolayer. At the same time, the rate of electron transfer from AA is decreased as a result of the introduction of the negatively-charged monolayer. Since short alkyl thiols do not form highly organized self-assembled monolayers, *vide infra*, and the fact that DO is shifted cathodically indicate that the shifts in the oxidation wave must have been ascribed to the existence of the negatively-charged monolayer, rather than to a blocking effect. The cyclic voltammety of DO and AA under the same conditions, however, with a gold electrode modified with 2-mercaptoethanol was examined. Interestingly, no changes in the oxidation waves of DO and AA were detected, suggesting that the negative charge in the C_3 -modified electrode plays an essential role in the electrochemical differentiation between DO and AA.

These results encourage us to synthesize longer ω -mercapto carboxylic acids where more highly organized self-assembled monolayers were expected. Figures 3 and 4 show the cyclic voltammety of DO and AA obtained with gold electrodes modified with 6-mercapto hexanoic acid, C_6 , and 11-mercapto

(15) Dryhurst, G.; Kadish, K. M.; Scheller, F.; Rennenberg, R. *Biological Electrochemistry*; Academic Press: New York, 1982, Vol. 1.

(16) Deakin, M. R.; Kovach, P. M.; Stutts, K. J.; Wightman, R. M. *Anal. Chem.* 1986, 58, 1474-1480.

(17) Hu, I.-F.; Kuwana, T. *Anal. Chem.* 1986, 58, 3235-3239.

(18) Bain, C. D.; Troughton, E. B.; Tao, Y.-T.; Evall, J.; Whitesides, G. M.; Nuzzo, R. G. *J. Am. Chem. Soc.* 1989, 111, 321-335.

(19) Bain, C. D.; Whitesides, G. M. *Adv. Mater.* 1989, 4, 522-528.

(20) Nuzzo, R. G.; Zegarski, B. R.; Dubois, L. H. *J. Am. Chem. Soc.* 1987, 109, 733-740.

(21) Sabatani, E.; Rubinstein, I.; Maoz, R.; Sagiv, J. *J. Electroanal. Chem. Interfacial Electrochem.* 1987, 219, 365-371.

(22) Haussling, L.; Ringsdorf, H.; Schmitt, F.-J.; Knoll, W. *Langmuir* 1991, 7, 1837-1840.

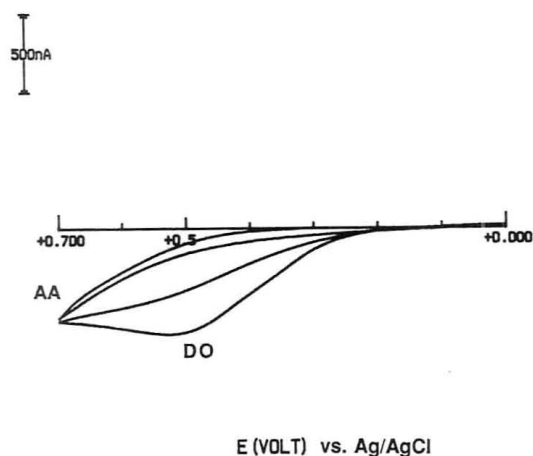


Figure 3. Cyclic voltammety of 5 mM dopamine (DO) and 5 mM ascorbic acid (AA) solutions (pH 7.4) taken with a gold electrode modified with $\text{HS}(\text{CH}_2)_5\text{CO}_2\text{H}$ and a scan rate of $50 \text{ mV}\cdot\text{s}^{-1}$.

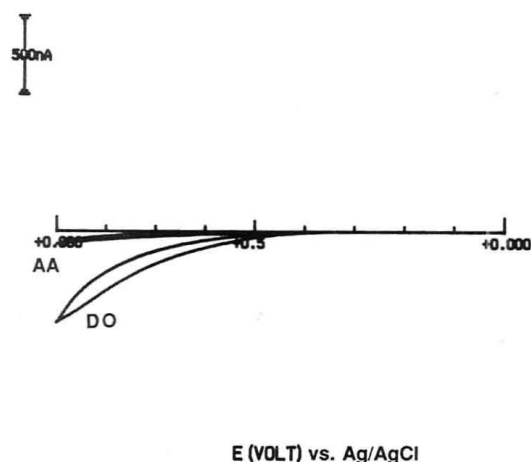


Figure 4. Cyclic voltammety of 5 mM dopamine (DO) and 5 mM ascorbic acid (AA) solutions (pH 7.4) taken with a gold electrode modified with $\text{HS}(\text{CH}_2)_{10}\text{CO}_2\text{H}$ and a scan rate of $50 \text{ mV}\cdot\text{s}^{-1}$.

undecanoic acid, C_{11} , respectively. As expected, the oxidation wave of ascorbic acid is shifted anodically. The peak potential of the anodic wave using a C_6 -coated electrode is shifted to potentials more positive than 0.7 V. The oxidation wave of dopamine is also shifted ($E_{\text{pk}} = 0.52 \text{ V}$) with a C_6 -coated gold electrode. On the other hand, a substantial decrease in the rate of the electron transfer is observed with a C_{11} gold electrode for both AA as well as DO (Figure 4).

These results suggest that two factors are likely to govern the kinetics of electron transfer, i.e. the negative charge of the monolayer plus the length of the chain. However, whereas the effect of the charge affected the rate of electron transfer of ascorbic acid solely, the length of the thiol chain influenced the kinetics of both dopamine and ascorbic acid. To confirm this hypothesis, we conducted two sets of experiments. First, we examined the oxidation wave of dopamine and ascorbic acid at acidic pH with modified electrodes. Although both waves were shifted anodically because of the pH, we found that almost no difference is observed at pH 3 in the rate of electron transfer between the two substances using a C_6 -modified gold electrode. In other words, the same rate of electron transfer for the electrooxidation of DO and AA is observed when the carboxylic acid monolayer is no longer charged. It should be noted that according to a recent report by Ward and his co-workers, there is a substantial difference between the pK_a of a ω -mercapto carboxylic acid in monolayer as compared to a homogeneous solution.²³ The measured pK_a of a self-assembled monolayer was reported to be essentially more basic.

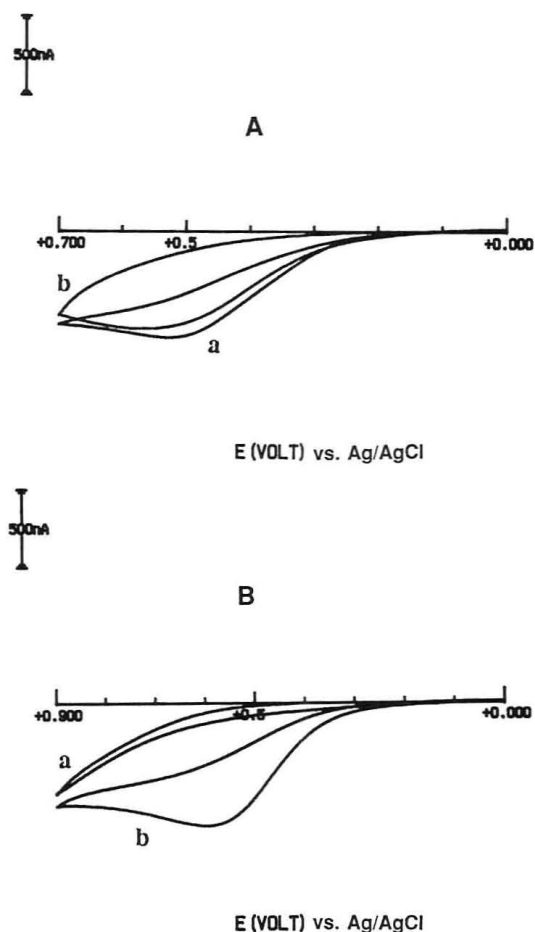


Figure 5. Cyclic voltammety of (A) 5 mM dopamine (DO) and (B) 5 mM ascorbic acid (AA) taken with gold electrodes modified with (a) $\text{HS}(\text{CH}_2)_5\text{CO}_2\text{H}$ and (b) $\text{HS}(\text{CH}_2)_5\text{CH}_3$ and a scan rate of $50 \text{ mV}\cdot\text{s}^{-1}$.

Therefore, we can conclude that the negative charge of the monolayer is responsible for the anodic shift of AA at pHs higher than the pK_a of the monolayer.

In the second set of experiments, the oxidation waves of AA and DO were examined and compared using a gold electrode coated with 6-mercaptohexanoic acid and 6-hexyl mercaptan (Figure 5). We found that while the oxidation wave of DO was not influenced by the presence of the negative monolayer (Figure 5A) as compared to a neutral monolayer, there is a remarkable effect on the anodic wave of AA (Figure 5B). Namely, 6-mercaptohexanoic acid monolayer shifted anodically the oxidation wave of AA to a substantial extent than a 6-hexyl mercaptan monolayer. Obviously, the effect of a monolayer of 6-hexyl mercaptan on the kinetics of AA is not electrostatically driven. The packing of a 6-hexyl mercaptan monolayer is expected to be more dense, i.e. more highly organized, than that of 6-mercaptohexanoic acid. Indeed, examination of the excess of surface coverage of gold electrodes modified with the two monolayers confirmed this assumption. Nonetheless, the negatively-charged monolayer affected, i.e. decreased, more the rate of electron transfer from AA. Therefore, these results can be interpreted only if we attribute the shifts of the anodic wave to both the charge of the monolayer as well as the length of the monolayer chain.

The effect of the length of a monolayer on its electrochemical and physical characteristics has been the subject of recent research.²⁴ Although several explanations have been

(23) Wang, J.; Frostman, L. M.; Ward, M. D. *J. Phys. Chem.* 1992, 96, 5224-5228.

(24) Bain, C. D.; Whitesides, G. M. *J. Am. Chem. Soc.* 1989, 111, 7164-7175.

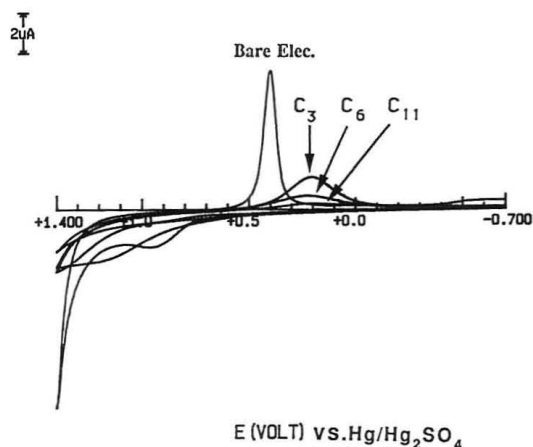


Figure 6. Cyclic voltammetry of 1 M H_2SO_4 solution taken with a bare gold electrode and with gold electrodes modified with C_3 , C_6 , and C_{11} .

suggested, it is usually believed that a better coverage of the surface is obtained by increasing the length of the hydrophobic part of the thiol chain. Submonolayer coverage by short alkyl thiols has been interpreted as pinholes. The existence and determination of such pinholes has been carried out electrochemically.²⁵

Figure 6 shows the cyclic voltammogram of gold electrodes modified with the three different ω -mercapto carboxylic acids, $\text{HS}(\text{CH}_2)_n\text{CO}_2\text{H}$ ($n = 2, 5, 10$), in 1 M H_2SO_4 . The sharp cathodic peak is assigned to the reduction of surface bound gold oxide.¹³ Thus, the excess of surface coverage can be determined through the decrease of the area associated with this electrochemical surface process.^{26,27} It can be seen that the charge, i.e. the area, that is related to the reduction of gold oxide is inversely proportional to the length of the thiol. The extent of surface coverage, θ , is 0.32, 0.61, and 0.76, for $n = 2, 5$, and 10, respectively.

As expected, longer alkyl groups possess stronger hydrophobic interactions resulting in electrodes which are more highly organized. Similar results, although less clear, were obtained by applying the procedure reported by Rubinstein¹⁴ who determined the excess of surface coverage through the underpotential deposition and stripping of copper. It should be pointed out that the latter technique is less sensitive. Hence, we can conclude that two main parameters control the electrochemical differentiation between DO and AA. These two parameters are controlled by the length of the monolayer chain. On one hand, the negative charge of the ω -mercapto carboxylic acid monolayer repels AA from the electrode. This effect is more pronounced by increasing the chain length. Longer thiols form better organized self-assembled monolayers which are pinhole-free, thus better blocking the access of AA to the electrode. The net negative charge is also increased as a function of the surface coverage. On the other hand, the rate of electron transfer is markedly affected by the monolayer which serves as a spacer between the electrode and the electroactive species. Increasing the length of the chain affects the kinetics transfer of both DO and AA and thus shifting anodically their oxidation waves.

To summarize, longer ω -mercapto carboxylic acid monolayers are required to form better and more highly charged monolayers, whereas shorter monolayers are preferred in order to increase the rate of electron transfer. As a result, an optimum is the electrochemical differentiation between DO and AA is found using the ω -mercaptohexanoic acid monolayer.

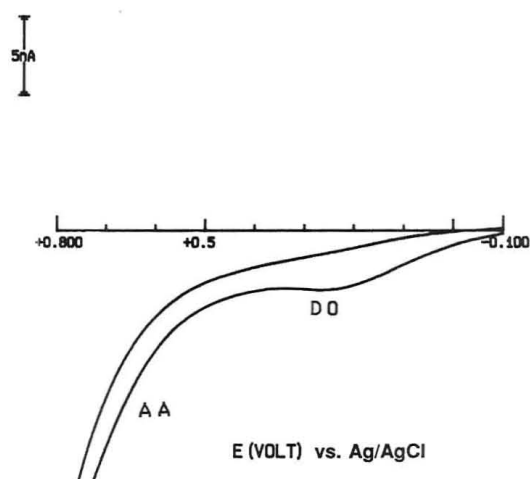


Figure 7. Cyclic voltammetry of a solution containing 2 mM dopamine and 200 mM ascorbic acid taken with a gold electrode modified with C_3 and a scan rate of $50 \text{ mV}\cdot\text{s}^{-1}$.

The success of this approach must be determined through its applicability to microelectrodes. Although these results are interesting from their scientific point of view, the implication of these results for the neurosciences depends totally on the possibility of applying this method to ultramicroelectrodes. Figure 7 shows the cyclic voltammogram of a $10\text{-}\mu\text{m}$ gold electrode, which was modified with 3-mercaptopropionic acid, prior to immersing it in a solution containing 2 mM dopamine and 200 mM ascorbic acid. The cyclic voltammetry of ultramicroelectrodes differs from that of a regular-size electrode.²⁸ A sigmoidal voltammogram is obtained in which the steady-state current, i , depends linearly on the number of electrons transferred per molecule, n , the Faraday constant, F , the diffusion coefficient of the electroactive species, D , its concentration, C , and the electrode radius, r (eq 3).

$$i = 4nFDc_r \quad (3)$$

It can be seen that, in spite of the fact that the concentration of AA is 100 times higher than that of DO, a small anodic wave that is associated with the oxidation of DO is observed at 0.3 V.

An important issue that needs to be taken into consideration is the electrocatalytic oxidation of dopamine by ascorbic acid.²⁹⁻³¹ Namely, oxidized dopamine, i.e. dopamine-*o*-quinone, is chemically reduced by ascorbic acid. Thus, one would anticipate that the oxidation wave of DO will be affected by the concentration of ascorbic acid. We carefully examined the steady-state current of DO at an ultramicroelectrode in the presence of increasing concentrations of AA. No difference is detected while changing the concentration of AA from 0 to 100 mM, applying a 6-mercaptohexanoic acid modified ultramicroelectrode. This can be explained by the small thickness of the diffusion layer.³² Notice also that the current obtained in the presence of AA (Figure 7), is comparable to that obtained without AA (Figure 8).

A calibration curve for DO carried out with a $10\text{-}\mu\text{m}$ -modified ultramicroelectrode is shown in Figure 8. It is clear that DO can be determined electrochemically by an ultra-

(28) Wightman, R. M.; Wipf, D. O. *Electroanalytical Chemistry*; Bard, A. J., Ed.; Marcel Dekker: New York, 1988, Vol. 15, pp 267-353.

(29) Dayton, M. A.; Ewing, A. G.; Wightman, R. M. *Anal. Chem.* 1980, 52, 2392-2396.

(30) Freed, C. R.; Echizen, H. *Abs. Soc. Neurosci.* 1983, 9, 999.

(31) Justice, J. B., Jr.; Jaramillo, A. *J. Electrochem. Soc.* 1984, 131, 106C.

(32) Justice, J. B., Jr. In *Voltammetry In The Neurosciences, Principles, Methods, and Application*; Justice, J. B., Jr., Ed.; Humana Press: Clifton, NJ, 1987; pp 2-101.

(25) Porter, M. D.; Bright, T. B.; Allara, D. L.; Chidsey, C. E. D. *J. Am. Chem. Soc.* 1987, 109, 3559-3568.

(26) Finklea, H. O.; Avery, S.; Lynch, M. *Langmuir* 1987, 3, 409-413.

(27) Sabatani, E.; Rubinstein, I. *J. Phys. Chem.* 1987, 91, 6663-6669.

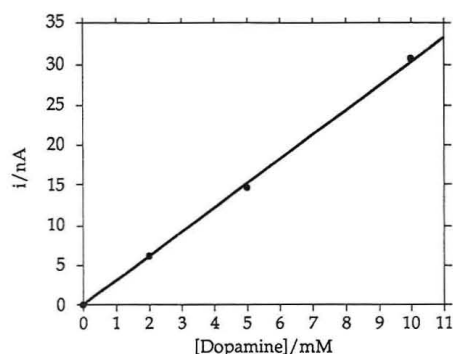


Figure 8. Calibration curve for dopamine taken with a 10- μm gold electrode modified with C_3 and a scan rate of 50 $\text{mV}\cdot\text{s}^{-1}$.

microelectrode at the sub-millimolar level. Although the reported concentrations of DO at the CNS are in the nanomolar level,³³ higher sensitivity can be achieved if other electrochemical methods, such as differential pulse voltammetry or square wave voltammetry, are used. We wish to signify that this preliminary work emphasizes the potential of self-assembled monolayers as a versatile tool to modify electrochemical probing for analytical purposes. The ability to fine-tune the properties of microprobes will evidently have further implication in the biosciences.

CONCLUSIONS

A novel approach for the utilization of self-assembled monolayers in electroanalytical chemistry is described. The advantage in electrodes, modified by monolayers, originates from our ability to fine-tune the properties of the monolayer. ω -Mercapto carboxylic acid monolayers, which are negatively charged at neutral pH, control the rate of electron transfer of two substances, dopamine and ascorbic acid, that differ in their net charge. Positively-charged dopamine is attracted electrostatically to the monolayer and is being oxidized at relatively low potentials. On the other hand, ascorbic acid, being negatively charged, is repelled from the electrode due

to the negatively-charged monolayer, shifting its electrooxidation to more positive potentials. The length of the monolayer chain tremendously affects the electrochemical differentiation between the two species. Long-chain monolayers exhibit highly charged and organized surfaces that efficiently repel ascorbic acid, therefore affecting the rate of electron transfer of dopamine as well due to their length. On the other hand, short-chain monolayers neither influence the kinetics of dopamine nor do they tend to form highly organized systems. As a consequence, an optimum in the electrochemical differentiation between dopamine and ascorbic acid is achieved using medium-length ω -mercapto carboxylic acids, i.e. $\text{HS}(\text{CH}_2)_5\text{CO}_2\text{H}$.

This approach offers several advantages over the method which applies a polyelectrolyte such as Nafion. Most of these advantages stem from the thickness of a monolayer as compared to a polymer film. Fast measurements should be possible since the diffusion of the electroactive species is not slowed down by the monolayer. No accumulation of species is expected on the electrode and the influence of high concentrations of other ions like sodium ions should be minimal. Although the time of modification in this study was long, i.e. overnight, recent data indicate that this time can be substantially shortened without affecting the organization of short- and medium-length monolayers.

Finally, the success in determining dopamine in the presence of high concentrations of ascorbic acid using microelectrodes implies that this approach can be applied to *in vivo* studies.

ACKNOWLEDGMENT

I. Rubinstein is warmly acknowledged for helpful discussions. This research was supported by the Basic Research Foundation administered by the Israel Academy of Sciences and Humanities.

(33) Parson, L. H.; Justice, J. B., Jr. *J. Neurochem.* 1992, 53, 212-218.

RECEIVED for review May 6, 1992. Accepted September 28, 1992.

pH-Metric log *P*. 3. Glass Electrode Calibration in Methanol-Water, Applied to pK_a Determination of Water-Insoluble Substances[†]

Alex Avdeef,* John E. A. Comer, and Simon J. Thomson

Sirius Analytical Instruments Ltd., Manor House, Lewes Road, Forest Row, East Sussex, RH18 5AF United Kingdom

A series of semiaqueous HCl solutions of known concentration, containing 0.1 M KNO₃ (as ionic strength adjuster) and 0-70 wt % methanol, was titrated at 21, 25, and 37 °C with standardized KOH, pH 2-12. The pH measuring circuit (Ross-type electrode) was calibrated with an aqueous pH buffer (Nernst slope assumed). The operational pH readings were related to p_cH ($= -\log [H^+]$) by the four-parameter equation: $pH = \alpha + Sp_cH + f_H[H^+] + f_{OH}[OH^-]$. The parameters were determined by a weighted nonlinear least squares procedure, which allows for CO₂ corrections. This calibration procedure was applied at 25 °C in titrations to determine the pK_a values of acetic acid, benzoic acid, 4-*n*-butoxyphenol, 4-ethoxyphenol, 1-benzylimidazole, (\pm)-propranolol, and *N*-methyl-D-glucamine and of two water-insoluble highly lipophilic benzoic acid derivatives of pharmaceutical interest, with the aim of determining their octanol-water partition coefficients. Yasuda-Shedlovsky plots were used to extrapolate semiaqueous apparent pK_a 's to zero methanol.

INTRODUCTION

Knowledge of the aqueous ionization constant, pK_a , of a substance is very important in the pharmaceutical industry (drug design and pretest regulatory compliance), in the new-chemical manufacturing industry (environmental impact compliance), and in the environmental field (environmental fate of toxic substances). Since many new substances of interest are very poorly soluble in water, the determination of the pK_a in aqueous solution can be difficult and problematic. Potentiometry can be a quick technique for such determination,¹ provided the solubility of the substance is at least 10⁻⁴ M. Solutions as dilute as 10⁻⁵ M can still be analyzed, but special attention must be given to electrode calibration, and ambient carbon dioxide must be excluded (or corrections for its presence must be incorporated). If the substance is only soluble to the extent of 10⁻⁶ M and possesses an analytically useful chromophore, then spectroscopic methods can be applied.¹ If the compound is virtually insoluble, then a mixed-solvent approach can be tried. Where possible, methanol is the solvent of choice for this purpose, because its general effect on pK_a 's has been studied so extensively. It is thought to be the least "error-prone" of the common solvents.¹ Mixed-solvent solutions of various methanol-water proportions are prepared, and the p_sK_a (the apparent pK_a) is determined in each mixture. The aqueous pK_a is deduced by extrapolation of the p_sK_a values to zero methanol.

The above technique was first used by Mizutani in 1925.²⁻⁴ Numerous examples may be cited of pK_a 's determined by

extrapolation in mixtures of methanol,⁵⁻⁹ ethanol,¹⁰⁻¹⁴ propanol,¹⁵ dimethyl sulfoxide,^{16,17} dimethylformamide,¹⁸ acetone,¹⁹ and dioxane.²⁰ Plots of p_sK_a versus weight percent organic solvent, $R = 0-60$ wt %, show either a "hockey-stick" shape or a "bow" shape, but rarely a straight line. For $R > 60$ wt %, S-shaped curves are sometimes observed. (Generally, p_sK_a values from titrations with $R > 60$ wt % are not suitable for extrapolation to zero methanol because ion-pairing starts to play a significant role.)

For values of $R < 60$ wt %, the hockey-stick/bow nonlinearity can be ascribed partly to electrostatic long-range ion-ion interactions. Extensions of the Born electrostatic model, drawing on Bjerrum's theory of ion association, were introduced by Yasuda²¹ and Shedlovsky.²² It was recognized that equilibrium quotients in mixed solvents of varying proportions ought to explicitly incorporate the concentration of water. It was thus proposed that the plot of $p_sK_a + \log [H_2O]$ versus $1/\epsilon$ should produce a straight line for solutions with dielectric constant, ϵ , greater than 50, which for methanol at 25 °C means $R < 60$ wt %. The slope in such a plot is expected to be inversely proportional to the average ionic diameter of the solvated molecule.²²

Recently, we have been involved in developing the potentiometric technique for determining the octanol-water partition coefficient, P (or K_{ow}), of substances.²³⁻²⁵ In the cited industries, $\log P$ of a substance is a very useful parameter in quantitative structure-activity relationships (QSAR).²⁶ It is as important a physicochemical parameter as pK_a . The pH-

(5) Bacarella, A. L.; Grunwald, E.; Marshall, H. P.; Purlee, E. L. *J. Org. Chem.* 1955, 20, 747-762.

(6) Shedlovsky, T.; Kay, R. L. *J. Am. Chem. Soc.* 1956, 60, 151-155.

(7) de Ligny, C. L. *Recl. Trav. Chim. Pays-Bas* 1960, 79, 731-736.

(8) de Ligny, C. L.; Loriaux, H.; Ruitter, A. *Recl. Trav. Chim. Pays-Bas* 1961, 80, 725-739.

(9) Chatten, L. G.; Harris, L. E. *Anal. Chem.* 1962, 34, 1495-1501.

(10) Hall, N. F.; Sprinkle, M. R. *J. Am. Chem. Soc.* 1932, 54, 3469-3485.

(11) Grunwald, E.; Berkowitz, B. J. *J. Am. Chem. Soc.* 1951, 73, 4939-4944.

(12) Gutbezahl, B.; Grunwald, E. *J. Am. Chem. Soc.* 1953, 75, 565-574.

(13) Marshall, P. B. *Br. J. Pharmacol.* 1955, 10, 270-278.

(14) Edmonson, T. D.; Goyan, J. E. *J. Am. Pharm. Assoc., Sci. Ed.* 1958, 47, 810-812.

(15) Papadopoulos, N.; Avranas, A. *J. Solution Chem.* 1991, 20, 293-300.

(16) Halle, J.-C.; Garboriaud, R.; Schaal, R. *Bull. Soc. Chim. Fr.* 1970, 2047-2053.

(17) Siow, K.-S.; Ang, K.-P. *J. Solution Chem.* 1989, 18, 937-947.

(18) Garrett, E. R. *J. Pharm. Sci.* 1963, 52, 797-799.

(19) Cavill, G. W. K.; Gibson, N. A.; Nyholm, R. S. *J. Chem. Soc.* 1949, 2466-2470.

(20) Van Uitert, L. G.; Haas, C. G. *J. Am. Chem. Soc.* 1953, 75, 451-455.

(21) Yasuda, M. *Bull. Chem. Soc. Jpn.* 1959, 32, 429-432.

(22) Shedlovsky, T. In *Electrolytes*; Pesce, B., Ed.; Pergamon Press: New York, 1962; pp 146-151.

(23) Avdeef, A. In *QSAR: Rational Approaches to the Design of Bioactive Compounds*; Silipo, C., Vittoria, A., Eds.; Elsevier: Amsterdam, 1991; pp 119-122.

(24) Part 1 of the series: Avdeef, A. *Quant. Struct.-Act. Relat.*, in press.

(25) Part 2 of the series: Avdeef, A. *J. Pharm. Sci.*, in press.

* To whom correspondence is to be addressed.

[†] Part 2 of the series is ref 25.

(1) Albert, A.; Serjeant, E. P. *The Determination of Ionization Constants*, 3rd ed.; Chapman and Hall: London, 1984.

(2) Mizutani, M. *Z. Phys. Chem.* 1925, 116, 350-358.

(3) Mizutani, M. *Z. Phys. Chem.* 1925, 118, 318-326.

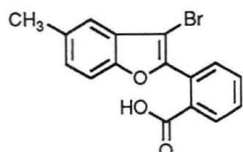
(4) Mizutani, M. *Z. Phys. Chem.* 1925, 118, 327-341.

metric log P method^{23-25,27-31} requires the knowledge of aqueous pK_a . Also, determination of log P by the more commonly used shake-flask, HPLC, and filter-probe techniques require the value of pK_a if the substance partially ionizes near the pH of interest.³² Hence if a molecule is not soluble in water, the determination of log P can be uncertain.

In the present paper we introduce a new procedure for calibrating the glass pH electrode in methanol-water mixtures. The procedure is based on a four-parameter equation originally applied to aqueous solutions³³ and is an extension of an earlier work of Van Uitert and Haas.²⁰ Several water-soluble and -insoluble acids and bases were selected (a) to test the mixed-solvents' electrode standardization procedure, (b) to characterize the shapes of p_sK_a vs R curves, and (c) to assess the effectiveness of the Yasuda-Shedlovsky extrapolation procedure.

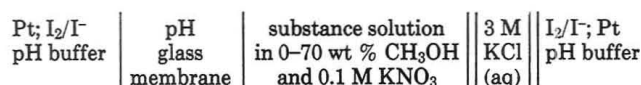
EXPERIMENTAL SECTION

Reagents. The preparation and standardization of HCl (Fisons), KOH (Volucon, Rhône Poulenc) are described elsewhere.³⁴ Sodium acetate trihydrate (Aldrich, 99+%), benzoic acid (Fisons, analytical reagent), 4-ethoxyphenol (Aldrich, 99%), 4-*n*-butoxyphenol (Aldrich, 99+%), 1-benzylimidazole (Aldrich, 99%), (\pm)-propranolol hydrochloride (Aldrich, 99%), and *N*-methyl-D-glucamine (Fluka, >99%) were used without further purification. Water-saturated partition-coefficient grade octanol-1-ol (Fisons) was used. Methanol (Fisons, analytical reagent, <0.05% water) was used without further purification. 4-(*n*-Decyloxy)benzoic acid (DOBA) was a gift from Rhône-Poulenc Rorer. Substance GR127810X was kindly supplied by Glaxo Group Research Ltd.



GR127810X

Apparatus. The computerized titration instrument we used to perform the pK_a and log P assays has been described elsewhere.²³⁻²⁵ It was equipped with a pH-sensing circuit ($10^{15}\text{-}\Omega$ impedance) of our own design and a semimicro Ross-type double-junction combination pH electrode (Orion 8103SC). The potentiometric cell may be denoted as



Readings of pH in a titration are not recorded until a certain stability criterion is satisfied. The stirrer is turned on as titrant is added. Vigorous stirring continues for 3 s after the addition. Then the stirrer is turned off. A sequence of 15 pH readings is made, one reading every 0.3 s. At the end of the sequence, pH versus time are fitted to a straight line. If the slope of the fit is greater than 0.01 pH min^{-1} in magnitude, the sequence is repeated. The best-fit value of pH at the end of the sequence is recorded and the next titrant addition is made. In buffered solutions, pH readings stabilize typically in 5-15 s. In unbuffered solutions,

for example, at pH 7 in a strong-acid, strong-base titration, readings often do not satisfy the stability criterion. In such cases, the instrument records the pH anyway if 180 s is exceeded. Such data are not of good quality; the weighting scheme (described below) appropriately takes this into account.

Electrode Standardization. A series of semiaqueous HCl solutions of known concentration, containing 0.1 M KNO_3 and 0-70 wt % methanol, was titrated with standardized KOH, in the pH interval 2-12. To establish the operational pH scale,³⁵ the measuring circuit was first calibrated with a single aqueous pH 7 phosphate buffer and the Nernst slope was assumed. Since all equilibrium constants reported in this study are on the concentration scale with reference to a particular value of fixed ionic strength (about 0.1 M here), it is necessary to convert the operational pH to p_cH , that is, the pH scale based on concentration. Since p_cH ($= -\log [H^+]$) is known at each point in the HCl- KNO_3 vs KOH standardization titrations, the operational pH reading can be related to the p_cH values by a multiparametric equation. This relationship is then employed in the semiaqueous titrations of uncharacterized substances.

In aqueous solutions the four-parameter equation

$$\text{pH} = \alpha + S p_cH + j_H [H^+] + j_{OH} K_w / [H^+] \quad (1)$$

has been used for this purpose.^{33,36} The parameters are determined by a weighted nonlinear least squares procedure. Typical aqueous values of the adjustable parameters at 25 °C and 0.1 M ionic strength are $\alpha = 0.09 \pm 0.01$, $S = 1.001 \pm 0.001$, $j_H = 1 \pm 0.2$, and $j_{OH} = -1 \pm 0.4$.^{33,36} The intercept parameter α in aqueous solution mainly corresponds to the negative logarithm of the activity coefficient of H^+ at the working temperature and ionic strength. The j_H term corrects pH readings for the nonlinear pH response due to liquid junction and asymmetry potentials in moderately acidic solutions (pH 1.5-2.5), while the j_{OH} term corrects for high-pH (pH >11) nonlinear effects.

In the present study the aqueous procedure was applied to semiaqueous solutions. The ionization constants of water in methanol-water mixtures, ${}_sK_w = [H^+][OH^-]$, were taken from Wooley et al.³⁷ The aqueous constants, K_w , as a function of ionic strength and temperature, were taken from Sweeton et al.³⁸

Carbonate Corrections. Every time the "CO₂-free" KOH titrant is standardized with potassium hydrogen phthalate, the carbonate concentration is also determined by least squares analysis, using literature carbonic acid pK_a values. In the procedure, the concentration of carbonate in KOH is initially estimated to be 0.05% of the KOH concentration. The least squares procedure iteratively refines the KOH concentration factor.²⁵ The measure of the quality of the fit is expressed by the "goodness-of-fit" index (GOF, see below).²⁵ A higher value of CO₂ in KOH is then picked and the calculation is repeated. Typically, the GOF changes; the direction of change indicates the subsequent guess for the CO₂ value. The process converges to a minimum GOF in three to five such passes. Typically, values of 0.1% (or higher) carbonate are found in commercial sources of KOH concentrates. (The titrant is not used if the carbonate concentration exceeds about 0.3%.) In processing titration data, including the standardization titration above, contribution from the carbonate is incorporated into the calculations. In this study we determined the two ionization constants of carbonic acid in methanol-water mixtures, in order to effect such corrections properly.

p_sK_a Determination. Butoxyphenol and propranolol were only sparingly soluble in water, and it was necessary to work with $<5 \times 10^{-4}$ M solutions for $R < 30$ wt % methanol. Solutions with the water-soluble compounds were otherwise 0.005-0.01 M. The two water-insoluble benzoic acid derivatives, GR127810X and DOBA, could only be dissolved in solutions with $R > 34$ and $R > 46$ wt % methanol, respectively; sample concentrations were $<5 \times 10^{-4}$ M.

(26) Hansch, C.; Leo, A. *Substituted Constants for Correlation Analysis in Chemistry and Biology*; Wiley-Interscience: New York, 1979.

(27) Brandstrom, A. *Acta Chem. Scand.* 1963, 17, 1218-1224.

(28) Seiler, P. *Eur. J. Med. Chem.* 1974, 9, 663-665.

(29) Kaufman, J. J.; Semo, N. M.; Koski, W. S. *J. Med. Chem.* 1975, 18, 647-655.

(30) Clarke, F. H. *J. Pharm. Sci.* 1984, 73, 226-230.

(31) Clarke, F. H.; Cahoon, N. M. *J. Pharm. Sci.* 1987, 76, 611-619.

(32) Dearden, J. C.; Bresnen, G. *Anal. Quant. Struct.-Act. Relat.* 1988, 7, 133-144.

(33) Avdeef, A.; Bucher, J. J. *Anal. Chem.* 1978, 50, 2137-2142.

(34) Avdeef, A.; Sofen, S. R.; Bregante, T. L.; Raymond, K. N. *J. Am. Chem. Soc.* 1978, 100, 5362-5370.

(35) Bates, R. G. *CRC Crit. Rev. Anal. Chem.* 1981, 10, 247-278.

(36) Avdeef, A. *Anal. Chim. Acta* 1983, 148, 237-244.

(37) Wooley, E. M.; Tomkins, J.; Hepler, L. G. *J. Solution Chem.* 1972, 1, 341-351.

(38) Sweeton, F. H.; Mesmer, R. E.; Baes, C. F., Jr. *J. Solution Chem.* 1974, 3, 191-214.

In a typical titration 0–20 mL of a methanol solution (80% v methanol, 0.1 M KNO₃) is added to a weighed sample and any additional 0.1 M KNO₃ (aq) is added if required to make a total solution volume of 20 mL. Standardized HCl is added to lower the pH to 2.5, and the solution is titrated with KOH to about pH 11.5. (In the case of the two water-insoluble compounds, the solutions were first made basic and were titrated with acid to about pH 3.) After each titrant addition, pH is measured. The initial estimates of the p_cK_a's in the semiaqueous solution are obtained from the "difference" (Bjerrum) plots.^{24,39} These approximate values are then refined by a weighted nonlinear least squares procedure.^{25,40}

The dielectric constants, ϵ , of methanol–water mixtures, needed for the Yasuda–Shedlovsky plots and for calculating activity coefficients, were taken from Albright and Gosting.⁴¹

log P Determination. The octanol–water partition parameter, log P, where $P = [H_jA]_{\text{octanol}}/[H_jA]_{\text{water}}$, for a species H_jA may be determined from the difference between the aqueous pK_a of the species and the *apparent* pK_a, p_cK_a, determined from a titration of the substance in the presence of octanol (or any other useful organic partition solvent that is immiscible with water).^{23–32} For compounds which are insoluble in water, it is desirable to perform two titrations, each with a different amount of octanol; p_cK_a(1) and p_cK_a(2) are determined from the resultant difference plots. Two octanol-containing titrations are usually needed because strongly lipophilic molecules can partition into octanol both as neutral species and usually to a lesser extent as ion-paired ionized species. The difference between p_cK_a(1) and p_cK_a(2) can indicate the presence of ion-pair partitioning.^{24,31} The aqueous pK_a, derived from Yasuda–Shedlovsky extrapolation, is necessarily provided as a fixed contribution during the log P least squares refinement stage using the octanol-containing data.

For monoprotic weak acids one can employ the approach in ref 24 and derive log P(neutral) and log P(anion) explicitly from pK_a, p_cK_a(1), p_cK_a(2), r₁, and r₂ (volume ratio, $r = V_{\text{octanol}}/V_{\text{water}}$) as

$$P_{\text{neutral}} = \frac{r_2 10^{p_{c}K_a(2) - pK_a} - r_1 10^{p_{c}K_a(1) - pK_a} - (r_2 - r_1) 10^{p_{c}K_a(1) + p_{c}K_a(2) - 2pK_a}}{r_1 r_2 (10^{p_{c}K_a(1) - pK_a} - 10^{p_{c}K_a(2) - pK_a})} \quad (2a)$$

$$P_{\text{anion}} = \frac{r_1 10^{p_{c}K_a(2) - pK_a} - r_2 10^{p_{c}K_a(1) - pK_a} + r_2 - r_1}{r_1 r_2 (10^{p_{c}K_a(1) - pK_a} - 10^{p_{c}K_a(2) - pK_a})} \quad (2b)$$

The equations are valid only if ion-pair partitioning takes place, that is, when pK_a ≠ p_cK_a(1) ≠ p_cK_a(2) and both P > 0.

Function Minimized in Least Squares Refinement. The approximate equilibrium constants, estimated from the difference plots^{24,39} and eq 2, form the "seed" values for the iterative least squares procedure for both pK_a and log P refinement. The "best" (refined) values are those which produce an absolute minimum in the sum of the weighted squares of residuals:

$$S = \sum_i \frac{(pH_i^{\text{obs}} - pH_i^{\text{calc}})^2}{\sigma_i^2(\text{pH})} \quad (3)$$

N_o is the number of pH measurements; σ_i^2 is the estimated variance in the measured pH_i^{obs}. The model equation, pH_i^{calc}, is a function of the pK_a and log P parameters, as well as the independent variables.^{25,40}

Weighting Scheme and Goodness-of-Fit. Both the dependent variable, pH, and the independent variable, volume of titrant, are assumed to be subject to error.^{34,36} The weighting

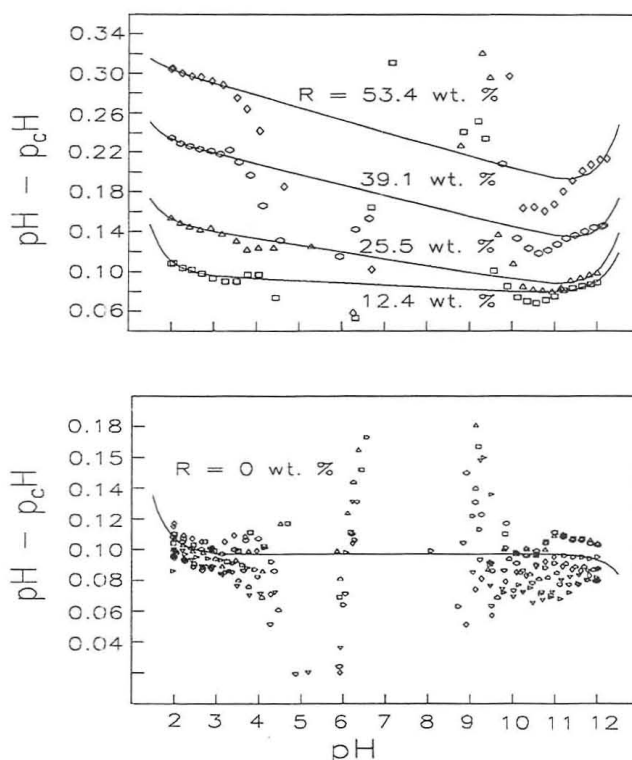


Figure 1. Differences between the operational and concentration pH values as a function of weight percent methanol. The solid lines represent eq 1 best-fit curves.

scheme used in eq 3 is constructed from the variances

$$\sigma^2(\text{pH}) = \sigma_c^2 + (\sigma_v dpH/dV)^2 \quad (4)$$

The values of σ_c and σ_v are experimental uncertainties, where $\sigma_c = 0.005$ (units of pH), the fixed contribution to the variance in the measured pH, and $\sigma_v = 0.001$ mL, the estimated standard deviation in the volume of titrant. The weighting scheme properly recognizes that measurements of pH near the end point of a titration (where dpH/dV is large) are not as reliable as those from the buffered portion.

After each iterative cycle a test of the progress of refinement is indicated by the goodness-of-fit, GOF, which is defined by

$$\text{GOF} = \sqrt{\frac{S}{N_o - N_r}} \quad (5)$$

where N_r is the number of refined parameters (that is, the number of pK_a's and log P's). A GOF value of 1 is ideal. It would mean that on the average the calculated titration curve and the observed curve are about one standard deviation apart in pH (about 0.005 pH units in the buffer regions). GOFs 0.5–1.5 are often obtained for well-behaved compounds. GOF > 2 indicates that the substance may not be pure, the KOH titrant may have absorbed some ambient CO₂, pH measurements are of poor quality, or the assumed equilibrium model is incorrect.

RESULTS AND DISCUSSION

Differences between pH and p_cH. Figure 1 shows plots of pH – p_cH versus pH at 25 °C and R = 0–53 wt % methanol. The solid curves in the figure are based on eq 1 best-fit parameters. As can be seen, the deviation of data points from the solid curves in the interval pH 4–9 is large. Reliable measurements of pH and calculations of p_cH are untenable in the unbuffered neutral pH region of the strong-acid, strong-base titration. The key to successful application of eq 1 to such data is a proper weighting scheme: provided the experimental errors in pH measurements are properly assessed, large deviations do not skew the four-parameter fit. (For the strong-acid, strong-base titration, the weighting scheme, eq 4, assigns errors as 0.006, 0.01, 0.08, 0.6, 1.1, 2.2,

(39) Irving, H. M.; Rossotti, H. S. *J. Chem. Soc.* 1954, 2904–2910.

(40) Avdeef, A. In *Computational Methods for the Determination of Formation Constants*; Leggett, D., Ed.; Plenum Press: New York, 1985; pp 355–473.

(41) Albright, P. S.; Gosting, L. J. *J. Am. Chem. Soc.* 1946, 68, 1061–1063.

(42) Yasuda, M.; Yamsaki, K.; Ohtaki, H. *Bull. Chem. Soc. Jpn.* 1960, 23, 1067.

Table I. Methanol-Water Electrode Standardization Parameters^a

<i>t</i> (°C)	<i>R</i> (wt %)	α	<i>S</i>	<i>j_H</i>	<i>j_{OH}</i>
21	0	0.092	1.0027	0.8	-0.6
	10	0.089	1.0008	0.9	-0.1
	20	0.120	0.9971	0.9	0.4
	30	0.178	0.9927	0.8	0.8
	40	0.249	0.9889	0.6	1.5
	50	0.316	0.9868	0.3	2.4
	60	0.355	0.9876	-0.2	3.7
25	0	0.096	1.0001	0.9	-0.3
	10	0.098	0.9994	1.0	0.3
	20	0.129	0.9970	1.0	0.7
	30	0.184	0.9940	0.8	1.1
	40	0.251	0.9916	0.5	1.4
	50	0.314	0.9907	0.2	1.8
	60	0.344	0.9922	-0.2	2.5
37	0	0.068	1.0039	1.3	-0.3
	10	0.085	1.0019	1.2	-0.2
	20	0.119	1.0003	1.2	-0.2
	30	0.165	0.9995	1.2	-0.1
	40	0.215	1.0002	1.2	0.0
	50	0.252	1.0028	1.2	0.1
	60	0.257	1.0078	1.3	0.1
25	0 ^b	0.099	0.9993	0.1	-0.6
	0 ^c	0.118	1.0007	-0.1	-0.9

^a 0.11 M ionic strength (0.1 M KNO₃). Values interpolated to whole-number weight percent; the group at 25 °C represents the mean whole-number interpolation of three standardization series. ^b HCl-KCl vs KOH, 0.11 M ionic strength.³³ ^c Universal buffer mixture of HCl, acetic, phosphoric, and boric acids titrated with KOH; 0.11 M ionic strength.³³

2.0, 1.3, 0.09, 0.01, and 0.005, for pH 2, 3, ..., 11, and 12, respectively.)

In aqueous calibrations, a universal buffer mixture consisting of HCl, acetic, phosphoric, and boric acids was used to extend the reliability of the pH - p_cH data into the neutral-pH region.³³ It is noteworthy that the four calibration parameters were found to be in good agreement with those obtained from strong-acid, strong-base titration (Table I).

Figure 1 for *R* = 0 wt % includes nine standardization titrations, performed at regular intervals over a 20-day period. The magnitude of dispersion of points about the solid curve is a good indication of the expected errors in pH readings if electrode standardizations are not done frequently. For pH 2-3.5 the errors appear to be ±0.01 and for pH 10-12, ±0.02. Similar reproducibility was observed in neutral-pH solutions.³³ These values are in agreement with expectations cited by Bates.³⁵

Figure 1 for *R* = 12-53 wt % clearly shows that pH - p_cH decreases with increasing pH, the effect being greatest at the highest values of *R*. This trend was not observed by Van Uitert and Haas²⁰ who worked with low ionic strength dioxane-water mixtures. Dependence of pH - p_cH on pH had been reported in aqueous standardizations at moderate ionic strength (0.2 M KCl).³³

Standardization Parameters. Table I lists the α , *S*, *j_H*, and *j_{OH}* parameters at 21, 25, and 37 °C, at regular intervals of *R* = 0-70 wt %, for ionic strength 0.11 M (KNO₃). The parameters are depicted as a function of *R* in Figure 2, drawing on the results of 53 titrations. At 25 °C and *R* = 0 wt % the parameters agree well with our previous values,³³ suggesting that the calibration procedure may be independent of the specific glass electrode used (assuming high-quality electrodes are used).

The α values increase with increasing amount of methanol and reach a maximum point in the *R* 55-65 wt % region, after

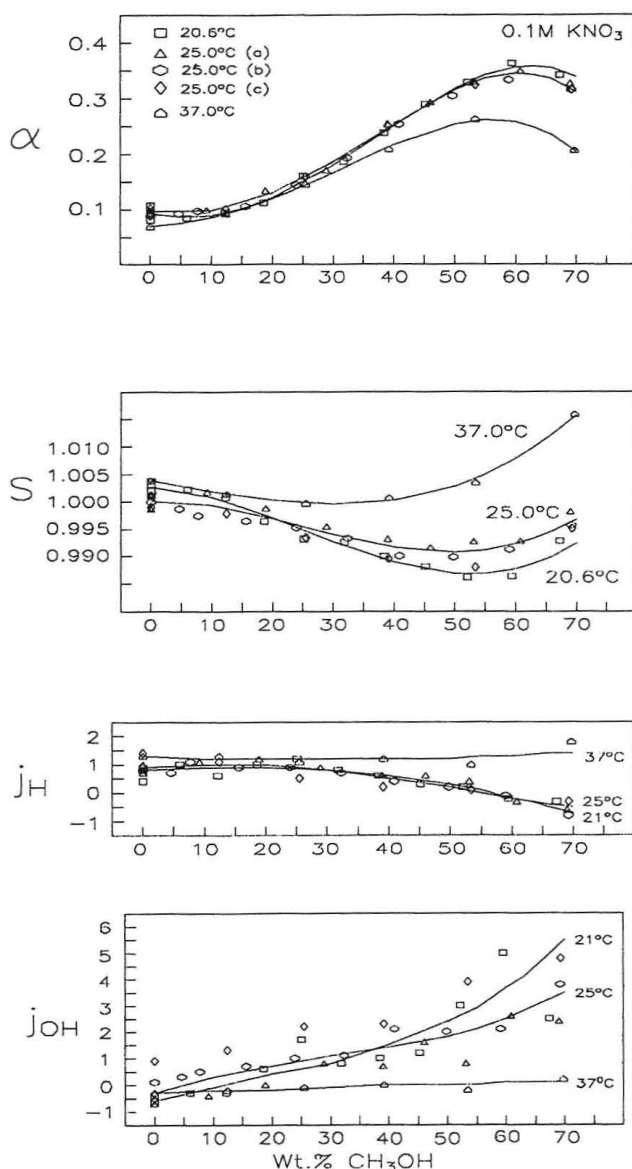


Figure 2. Calibration parameters as a function of weight percent methanol. The solid lines are smoothing fits for each temperature, using a fourth-order power series.

which the values decline. The α curves in Figure 2 appear to have the same shapes as what Bates called the "δ" curve.³⁵ Values of δ are the differences between the operational pH (calibrated with aqueous buffer) and p_aH*, the activity of hydrogen ions in the mixed solvent with the mixed solvent taken as the standard state. At zero methanol, δ = 0. Interlaboratory agreement between measured δ values is good,^{12,43,44} and it has been suggested by Bates that the use of δ would be a possible route to p_aH* values without the need for reference solutions in each different mixture of semi-aqueous solvent, albeit with some sacrifice of precision.³⁵

For methanol-water mixtures, Bates et al.⁴³ observed a maximum δ = 0.13 at *R* = 52 wt %, while Gelsema et al.⁴⁵ reported the maximum δ = 0.22 at *R* = 64 wt %. From Table I, $\alpha(R=60) - \alpha(R=0) = 0.25$, which is in reasonable agreement with δ, within the expected level of interlaboratory reproducibility. This suggests that in mixed solvents $\alpha \approx \delta - \log f_{\text{H}}$, where $\delta = -\log f_{\text{H}} + \bar{E}_{\text{H}}$,⁴³ *f_H* is the activity coefficient of H⁺ in water (*R* = 0), *f_H* is the transfer activity coefficient of

(43) Bates, R. G.; Paabo, M.; Robinson, R. A. *J. Phys. Chem.* **1963**, *67*, 1833-1838.

(44) Gelsema, W. J.; de Ligny, C. L.; Remijnse, A. G.; Blijleven, H. A. *Recl. Trav. Chim. Pays-Bas* **1966**, *85*, 647-660.

(45) Davies, C. W. *Ion Association*; Butterworths: London, 1962; p 41.

Table II. Equilibrium Constants in Methanol-Water^a

benzoic acid		acetic acid		4-ethoxyphenol		4- <i>n</i> -butoxyphenol	
<i>R</i> (wt %)	<i>p</i> _s <i>K</i> _a	<i>R</i> (wt %)	<i>p</i> _s <i>K</i> _a	<i>R</i> (wt %)	<i>p</i> _s <i>K</i> _a	<i>R</i> (wt %)	<i>p</i> _s <i>K</i> _a
1.6	4.018 (2) ^b	0.0	4.548 (1)	6.4	10.110 (4)	6.4	10.330 (32)
6.3	4.107 (2)	9.4	4.681 (1)	16.4	10.310 (5)	13.1	10.442 (39)
16.1	4.306 (1)	19.3	4.836 (2)	26.9	10.523 (6)	20.0	10.570 (131)
26.5	4.539 (2)	29.8	5.015 (2)	38.0	10.758 (7)	34.5	10.768 (13)
41.0	4.912 (3)	40.7	5.213 (4)	49.6	10.933 (8)	42.0	10.878 (8)
48.5	5.106 (1)	51.7	5.425 (2)	61.8	11.065 (9)	49.9	10.991 (20)
56.1	5.252 (1)	63.5	5.668 (2)	62.0	11.087 (7)	58.0	11.105 (19)
64.6	5.450 (1)						
1-benzylimidazole		(±)-propranolol		<i>N</i> -methyl- <i>D</i> -glucamine			
<i>R</i> (wt %)	<i>p</i> _s <i>K</i> _a	<i>R</i> (wt %)	<i>p</i> _s <i>K</i> _a	<i>R</i> (wt %)	<i>p</i> _s <i>K</i> _a		
0.0	6.681 (2)	0.0	9.461 (34)	0.0	9.575 (2)		
6.3	6.626 (2)	0.0	9.500 (16)	6.3	9.546 (3)		
16.1	6.532 (2)	9.7	9.388 (9)	15.3	9.490 (3)		
26.4	6.373 (3)	20.0	9.315 (6)	26.4	9.411 (4)		
37.0	6.182 (3)	34.5	9.113 (15)	37.1	9.308 (7)		
48.4	5.983 (4)	42.2	9.026 (14)	49.1	9.192 (7)		
60.2	5.795 (5)	50.1	8.918 (9)	61.3	9.060 (7)		
60.2	5.790 (5)	58.3	8.808 (5)				
GR127810X		DOBA		carbonic acid			
<i>R</i> (wt %)	<i>p</i> _s <i>K</i> _a	<i>R</i> (wt %)	<i>p</i> _s <i>K</i> _a	<i>R</i> (wt %)	<i>p</i> _s <i>K</i> _a		
33.8	4.393 (36)	46.1	5.675 (95)	0.0	6.14 (5)		
39.0	4.552 (32)	50.1	5.913 (41)	20.0 ^c	6.19 (6)		
42.8	4.627 (26)	54.1	5.807 (56)	40.0 ^c	6.34 (8)		
48.7	4.800 (17)	58.2	5.990 (50)	60.0 ^c	6.60 (20)		
52.5	4.914 (13)	62.5	6.011 (101)		9.93 (5)		
					9.93 (9)		
					9.95 (20)		
					9.97 (40)		

^a 25 °C, 0.11 M ionic strength (0.1 M KNO₃). ^b Estimated standard deviation in the least significant digit. ^c Interpolated values from the fitted curve (Figure 7).

H⁺ in the mixed-solvent medium (*R* > 0), related to the free energy of transfer, and \bar{E}_j is a slight residual junction potential (log scale).

Figure 2 shows that the slope factor, *S*, depends on *R* in a way that mirrors the *R* dependence of α . (The extreme are at lower values of *R*.) This is consistent with the observation that pH - *p*_sH depends on pH and *R*, as is evident in Figure 1. The *R* dependence of the slope factor is not an expected result, in view of the cited work in low ionic strength media.³⁵ It is not entirely clear what the origin of this pH dependence may be. Errors in the ionic products of water, ${}_sK_w$ ³⁷ and *K*_w³⁸ may cause such an anomaly. Alternatively, the *R* dependence of *S* may indicate that the residual liquid junction potential changes slightly with pH. It is usually accepted that the residual junction potential does not depend on pH in the interval 2.5–10 for ionic strengths less than 0.1 M.^{35,43}

The *j*_H and *j*_{OH} parameters account for the departure from straight lines in the solid curves in Figure 1. The low-pH region parameter, *j*_H, tends to be around 1 in aqueous solution^{33,36} and appears to decrease with increasing methanol content. The high-pH parameter, *j*_{OH}, tends to be a negative number in aqueous solution^{33,36} and appears to increase more rapidly with increasing amounts of methanol, compared to *j*_H. The upward turns in the solid curves for pH < 2 in Figure 1 appear to be of comparable magnitude to the deviations seen in Figure 1 in ref 43. The *j*_H term most likely compensates pH measurements for the expected increase in the liquid junction potential due to increased hydrogen ion concentration for pH < 2.5.

Dissociation Constants. Table II lists the *p*_s*K*_a values obtained from 62 separate titrations, *R* = 0–65 wt %, for the 10 studied compounds. Figure 3 shows the plots of *p*_s*K*_a vs *R* for the weak acids, and Figure 4 shows similar plots for the bases. It is characteristic of acids to have positive slopes and bases to have negative slopes, both of which slightly lessen in magnitude near zero methanol. The sparingly soluble 4-*n*-butoxyphenol seems to show the reverse trend: the slope is

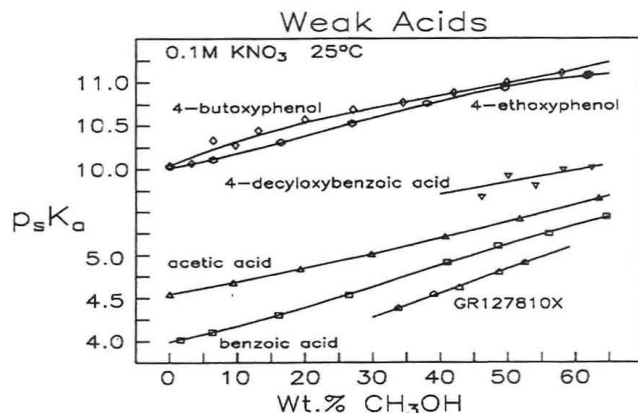


Figure 3. Methanol-water apparent *p*_s*K*_a's, *p*_s*K*_a's, of weak acids as a function of weight percent methanol.

greater in the water-rich region than in the methanol-rich region. 4-Ethoxyphenol seems to show a pronounced S-shaped curve. Benzoic acid and 1-benzylimidazole also show such a shape, although with much less distortion.

The largest errors in the refined *p*_s*K*_a's (Table II) were generally associated with the least water-soluble compounds (particularly DOBA), presumably because the titrated solutions were very dilute. Carbonate corrections were more critical in these solutions. The GOF of the refinements were in the range 0.2–1.2, consistently being lower for the more water-soluble compounds.

Acetic and benzoic acids were chosen for study because very reliable methanol-water data already existed in the literature, determined from high precision conductance data⁶ (requiring no pH electrode) and pH data employing junctionless reference electrodes.⁵ Figure 5 compares our acetic acid results to the literature values. Our acetic and benzoic acid constants, determined at 0.11 M ionic strength, *I*, were corrected to zero ionic strength using the relation $pK_a(0) =$

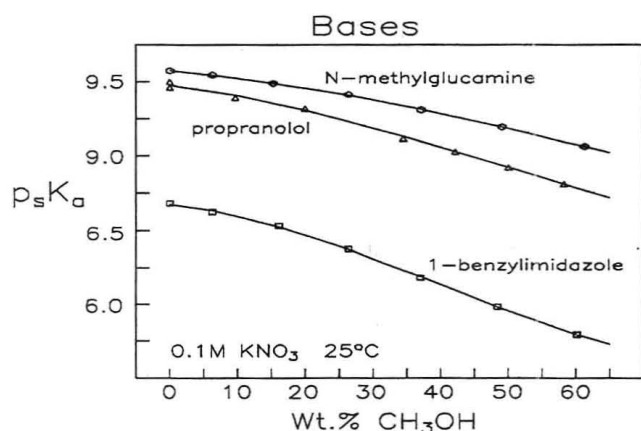


Figure 4. Methanol-water apparent pK_a 's, $p_s K_a$'s, of bases as a function of weight percent methanol.

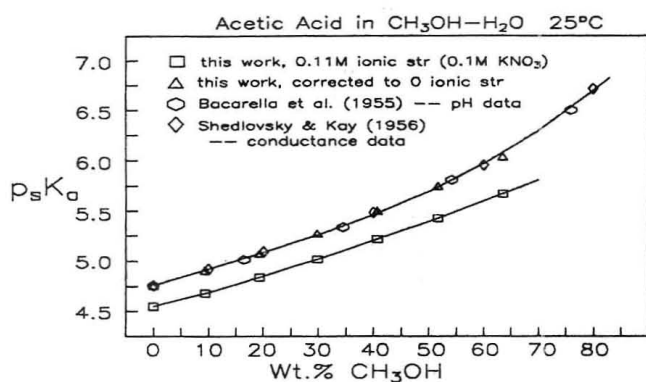


Figure 5. Comparison of literature values of acetic acid $p_s K_a$'s as a function of weight percent methanol.

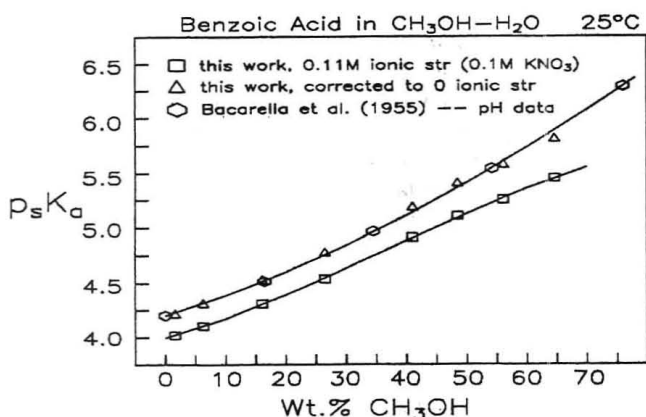


Figure 6. Comparison of literature values of benzoic acid $p_s K_a$'s as a function of weight percent methanol.

$pK_a(I) - 2 \log f$,²⁵ where f is the activity coefficient of the ions, calculated from the extended Debye-Huckel equation

$$\log f = - \frac{Az^2\sqrt{I}}{1 + Ba\sqrt{I}} \quad (6)$$

where $z = \pm 1$; A and B are functions of the dielectric constant and temperature. In Figure 5, $a = 5.9$. The agreement between the three results is superb. Figure 6 is a comparison of our benzoic acid results (corrected to $I = 0$ using eq 6 with $a = 6.3$) to those reported by Bacarella et al.⁵ The agreement is very good. We used eq 6 rather than the Davies expression⁴⁵ because we found the latter not to work well in methanol-rich solutions. (The original Davies empirical expression, based on aqueous data, has a factor $1/2$ which approximates A of eq 6. When we used the (ϵ, T) -dependent form of A in the Davies expression, our zero-corrected values were increasingly un-

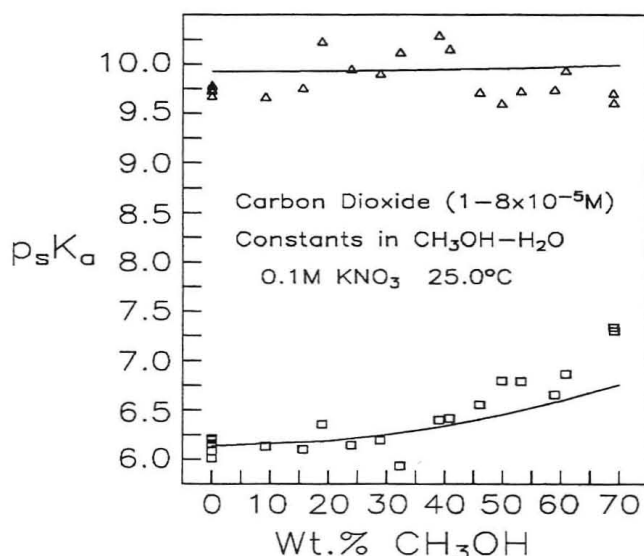


Figure 7. Ionization constants of carbonic acid in methanol-water mixtures. The solid lines represent weighted power-series smoothing curves.

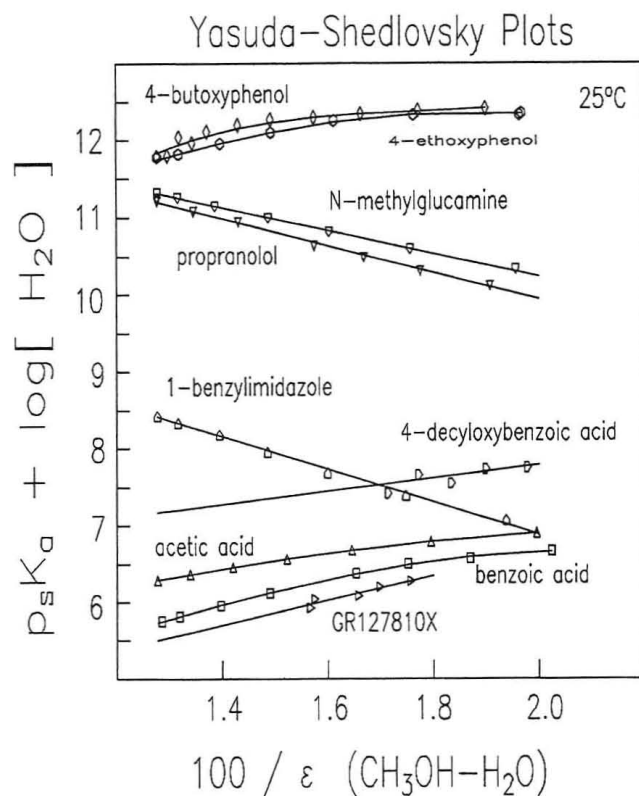


Figure 8. Yasuda-Shedlovsky plots for the nine compounds studied here.

derestimating the literature values for increasing R , by nearly 0.1 at 60 wt %.)

Figure 7 shows the $p_s K_a$ vs R plot for the two constants of carbon dioxide. The errors in the constants are high, largely due to the very low concentrations of carbonate employed in the determination ($(1-8) \times 10^{-5}$ M). The weighted averaging from many determinations produces constants of a quality suitable for use in correcting methanol-water data for absorbed ambient CO_2 .

Yasuda-Shedlovsky Plots. Figure 8 contains plots of $p_s K_a + \log [H_2O]$ vs $1/\epsilon$ for the studied compounds. Table III summarizes the values extrapolated to zero methanol, and draws comparisons with literature values.

The three bases studied here produce straight lines in the Yasuda-Shedlovsky plots. However, the soluble weak acids do

Table III. Aqueous pK_a from Yasuda–Shedlovsky Plots^a

	0–65 %/ w	30–65 %/ w	bias corr	lit.
benzoic acid	3.99	4.38	4.04 (12)	4.01, ^b 3.99 (2), ^c 4.04 ^d
acetic acid	4.55	4.72	4.38 (12)	4.53 ^b
4-ethoxyphenol	10.00	10.45	10.11 (12)	10.03 (1) ^e
4- <i>n</i> -butoxyphenol	10.09	10.45	10.11 (12)	10.04 (8) ^e
1-benzylimidazole	6.67	6.49	6.61 (8)	6.70 (3) ^c
(±)-propranolol	9.46	9.35	9.47 (8)	9.53 (6), ^c 9.72 ^d
<i>N</i> -methyl-D- glucamine	9.57	9.54	9.66 (8)	
GR127810X		3.76	3.42 (12)	
DOBA		5.43	5.09 (12)	

^a 25 °C, 0.11 M ionic strength (KNO₃); quantities in parentheses are the estimated standard deviations in the least significant digit.

^b 25 °C, 0.1 M ionic strength.⁴² ^c 0.11 M ionic strength (KNO₃); 20 °C (benzoic), 25 °C (benzylimidazole and propranolol).²⁵ ^d 25 °C, 0.15 M NaCl.³¹ ^e 0.1 M (KNO₃), 20 °C (butoxy), 24 °C (ethoxy).²³

not reveal such a simple relationship. Even acetic acid indicates a slight bow shape. (This distortion is also evident for $1/\epsilon < 0.02$ in Shedlovsky's paper.²²) Benzoic acid and the two alkoxyphenols appear to exhibit two straight-line segments, with the transition occurring at about $1/\epsilon = 0.016$. In the Shedlovsky²² derivation of the relationship, it was assumed that the ionic diameter of the solvated molecule remains constant over a range of alcohol–water mixtures. The appearance of two straight line segments may indicate a transition in the solvation structure enveloping the molecule, with a concomitant change in the ionic diameter. The calculated slopes suggest that ionic diameters of molecules decrease with increasing water content.

The two water-insoluble benzoic acid derivatives, GR-127810X and DOBA, were assumed to possess a linear relationship for the purpose of extrapolation to zero methanol. How reliable are such "long-distance" extrapolations? The water-soluble compounds may suggest the answer.

Bias Correction in Long-Distance Extrapolation. The present extrapolation technique was applied to water-soluble compounds not with the sole aim of getting aqueous pK_a 's, but rather to assess the magnitudes of errors to be expected if the extrapolations were based on data taken only from the methanol-rich region ($R > 30$ wt %). Table III contains the extrapolated pK_a 's, for data taken only from such a methanol-rich region. It appears that the pK_a 's extrapolated over long distance for weak acids are systematically *overestimated* (positive bias) by 0.34 on the average, while those of bases are *underestimated* (negative bias) by about 0.12.

These observations may be applied to water-insoluble compounds in the following practical way. (a) If a long distance extrapolated pK_a value is that of a *weak acid*, subtract from it the bias value 0.34 and assume the estimated standard deviation is 0.12 (based on the scatter of individual biases about the mean value of 0.34). (b) If the pK_a value is that of a *base*, then *add* the bias value 0.12 to it and assume the estimated standard deviation is 0.08 (based on scatter of individual biases). Table III lists the bias-corrected aqueous pK_a 's.

Although the water-soluble compounds we picked are a small sampling, it is expedient to assume they are representative and put the information to practical use. The assigned correction factors (biases) and errors (scatter in the biases) seem reasonable on the basis of other reported alcohol–water studies.^{2–6,10,15} However, we cannot confidently extend such estimates to solvents other than low molecular weight alcohols. For example, the DMSO–water determinations of the $p_s K_a$ of 2,4-dinitrophenol show a very sharp and substantial transition at about $1/\epsilon = 0.013$. The system was studied as

Table IV. Octanol–Water Partition Coefficients

	pK_a (aq)	log $P_{neutral}$		log P_{anion} this work
		this work	HPLC ^a	
GR127810X	3.42	5.19 (13) ^b		0.88 (8)
DOBA ^c	5.09 ^d	5.48 (16)	6.51	2.00 (17)
	4.49 ^e	6.06 (15)	7.12	1.97 (17)

^a B. Slater, Rhône-Poulenc, unpublished results. ^b Numbers in parentheses are the estimated standard deviations in the least significant digit. ^c Weighted mean values, $N = 16$. ^d Yasuda–Shedlovsky extrapolated value, bias-corrected. ^e Homologous series extrapolated value, corrected to $I = 0.1$ M.

a function of temperature, 20–40 °C, and the Gibbs free energy was found to have a large changing entropy component in the water-rich region. This suggested that the solute–solvent interactions of the nonelectrostatic nature were playing an important role in controlling the enthalpy and entropy of ionization.

pK_a 's for Water-Insoluble Compounds. For the homologous series of water-soluble compounds, 4-ROC₆H₄-COOH, R = CH₃ to C₅H₁₁, the aqueous pK_a 's at 20 °C range from 4.43 to 4.55 ($I = 0$), respectively.¹⁹ Linear extrapolation to compound DOBA might suggest a pK_a value of 4.70, or 4.49 when corrected to 0.1 M ionic strength. This value is lower than the Yasuda–Shedlovsky bias-corrected value of 5.09 ± 0.12 (Table III). It is difficult to say which is the correct value. Both values are considered in determining the partition coefficient (Table IV).

log P Determination of the Water-Insoluble Compounds. Table IV summarizes the log P values for the two substituted benzoic acid derivatives. One dual-octanol titration was performed to establish the log P 's of GR127810X. In the case of DOBA six dual-octanol titrations were performed, where the concentrations of the acid were systematically varied from 8.1×10^{-5} to 8.7×10^{-4} M. We wanted to test for the possibility of micelle formations. No clear indication of such self-association reactions was found. The scatter of results was large, but seemed nonsystematic. It was very important to correct data for carbon dioxide absorption at elevated pH, because the sample solutions were quite dilute.

As can be seen in Table IV, both compounds are extremely lipophilic and partition as neutral and as ion-paired species. The table lists two sets of log P for DOBA: one assuming that the Yasuda–Shedlovsky-based aqueous pK_a is correct and the other assuming that the homologous-series-based pK_a is correct. The difference in the log P (neutral) values is exactly equal to the difference in the two possible pK_a 's. The ion-pair log P is unaffected by the choice of aqueous pK_a . The HPLC-determined log P (which, like the pH-metric technique, requires the aqueous pK_a) is about one log unit greater than the potentiometric result. Such differences hint of complications probably not fully addressed by either technique and suggest that further work is required to shed a consistent light on the matter.

CONCLUSION

This work shows that by using a pH electrode which has been subjected to a four-parameter titrimetric calibration procedure in methanol–water mixtures, reliable values for apparent pK_a ($p_s K_a$) may be obtained from titrations done in solutions up to a methanol–water ratio (R) of 60 %/w. Albert and Serjeant¹ appear not to recommend pK_a determination

by extrapolation of p_sK_a vs R unless a molecule is soluble in the R 10–20 wt % region and suggest that the Yasuda–Shedlovsky extrapolation is expected to be more reliable. Our results using p_sK_a values obtained after the four-parameter calibration suggest that Yasuda–Shedlovsky extrapolations for values of R between 30 and 60 wt % give errors in pK_a no greater than ± 0.2 for weak acids and ± 0.1 for weak bases, provided bias corrections are made. We conclude that pK_a determination for water-insoluble, methanol-soluble compounds may be reliably performed according to the procedures described in this paper.

ACKNOWLEDGMENT

Discussions of the $\log P$ results with Dr. Bryan Slater and Ann McCormack of Rhône-Poulenc Rorer are appreciated. We are grateful for their determination of $\log P$ of DOBA by HPLC. Part of this work was supported by the U.K. Department of Trade and Industry, through stages I and II SMART grants.

RECEIVED for review May 11, 1992. Accepted October 1, 1992.

Optimization of Waveforms for Pulsed Amperometric Detection of Carbohydrates Based on Pulsed Voltammetry

William R. LaCourse[†] and Dennis C. Johnson*

Department of Chemistry, Iowa State University, Ames, Iowa 50011

Liquid chromatography (LC) with pulsed amperometric detection (PAD) at Au electrodes has gained prominence for analysis of complex mixtures of polyalcohols and carbohydrates. The most commonly used PAD waveform consists of three potentials and four time parameters, all of which can be varied independently but the effects of which are not necessarily mutually exclusive. Choice of potential values in PAD waveforms has traditionally been based on cyclic voltammetry (CV). However, CV data are useless for educing optimal values for time parameters, and these values are usually approximated using the trial-and-error method during multiple injections in LC-PAD systems. An automated procedure is described for optimization of all potential and time parameters in PAD waveforms on the basis of pulsed voltammetry (PV) at a rotated disk electrode (RDE). General and optimized waveforms are presented for detection of carbohydrates, and effects on LC-PAD response are illustrated.

INTRODUCTION

Pulsed amperometric detection (PAD) at Au electrodes has become popular for the sensitive and direct detection of many polar aliphatic organic compounds separated by liquid chromatography (LC).¹⁻³ These compounds typically exhibit little or no chromophoric and/or fluorophoric activity, and furthermore, many do not give persistent amperometric response for a constant (dc) applied potential at noble-metal electrodes.

PAD at Au electrodes in alkaline media exploits surface-catalyzed oxidations of various functional groups under management by multistep potential waveforms ($E-t$) to alternate the processes of amperometric detection with anodic and cathodic polarizations to clean and reactivate the Au surface. Presently, the most prominent application of PAD is for anodic detection of polyalcohols and carbohydrates in flow-through electrochemical cells following their separations by high-performance ion-exchange chromatography (HPIC) using an alkaline mobile phase.¹⁻⁶ Sensitivity for monosaccharides is comparable for aldoses and ketoses with detection limits at the picomolar level.

A typical PAD waveform is described in Table I for carbohydrate detection at Au electrodes in 0.1 M NaOH. The detection potential (E_{det}) is applied for the time period t_{det} , and the electrode current is sampled by electronic integration over the time period t_{int} following a delay of t_{del} to allow charging current to diminish toward zero (i.e., $t_{\text{del}} = t_{\text{del}} +$

t_{int}). The output voltage signal can be proportional to the integrated charge (q , coulombs) or the average current ($i_{\text{avg}} = q/t_{\text{int}}$, coulombs per second). The oxidative desorption of adsorbed detection products and/or solution impurities occurs simultaneously with anodic formation of surface oxide at $E_{\text{oxd}} \gg E_{\text{det}}$ applied during the period t_{oxd} . Subsequently, the inert oxide produced at E_{oxd} is cathodically dissolved at $E_{\text{red}} \ll E_{\text{det}}$ applied for the period t_{red} .

Whereas PAD has matured as a detection technology, the approach to waveform optimization continues to be rather primitive. Traditionally, choice of potential values in PAD waveforms has been based on the $i-E$ response from cyclic voltammetry (CV) recorded for triangular waveforms ($E-t$).^{2,7} However, CV is virtually useless for educing optimal time parameters for PAD waveforms and their choice has been based largely on the results of repetitive injections in LC-PAD systems while the effect on peak heights of changes in the time parameters produced manually is observed. This approach is tedious, and therefore, it is common to rely on published waveforms and anecdotal information, especially for new compounds available only in small quantities.

Choice of optimal E_{det} values for PAD waveforms is most logically based on the voltammetric response obtained when a PAD waveform is applied at a hydrodynamic electrode with a small incremental change in E_{det} for each cycle of the multistep waveform. Hence, the resulting $i-E_{\text{det}}$ plot is a true representation of PAD response over a range of E_{det} values. Such applications of a three-step waveform at noble-metal electrodes have been called "pulsed voltammetry"⁸⁻¹¹ and "pulse voltammetry".¹³ Here, we use "PV" to represent this voltammetric strategy. Previous applications of PV from our laboratory have focused primarily on the optimization of E_{det} for use in LC-PAD.⁸⁻¹² Here we extend the concept to study the effect of all waveform parameters on PAD response. The premise of this technique is the repeated application of a PAD waveform with small incremental changes of the individual parameters (i.e., E_{det} , t_{det} , t_{del} , t_{int} , E_{oxd} , t_{oxd} , E_{red} , or t_{red}).

EXPERIMENTAL SECTION

Reagents. All solutions were prepared from reagent grade chemicals. Triply-distilled water was purified further in a Millipore Milli-Q system (Millipore Corp., Bedford, MA). All solutions of NaOH were diluted from a 50% (w.w) stock solution (Fisher Scientific, Springfield, NJ). Acetonitrile (MeCN) was HPLC grade (Fisher Scientific). All mobile phases were filtered

[†] Present address: Department of Chemistry and Biochemistry, University of Maryland Baltimore County, Baltimore, MD 21228.

(1) Johnson, D. C.; LaCourse, W. R. *Anal. Chem.* 1990, 62, 589A-97A.
(2) LaCourse, W. R.; Johnson, D. C. *Carbohydr. Res.* 1991, 215, 159-78.

(3) Johnson, D. C.; LaCourse, W. R. *Electroanalysis* 1992, 4, 367-80.
(4) Rocklin, R. D.; Pohl, C. A. *J. Liq. Chromatogr.* 1983, 6, 1577-90.

(5) Olechno, J. D.; Carter, S. R.; Edwards, W. T.; Gillen, D. G. *Am. Biotechnol. Lab.* 1987, 5, 38-50.

(6) Paskach, T. J.; Lieker, H. P.; Reilly, P. J.; Thielecke, K. *Carbohydr. Res.* 1991, 215, 1-14.

(7) Andrews, R. W.; King, R. M. *Anal. Chem.* 1990, 62, 2130-4.

(8) Neuburger, G. G.; Johnson, D. C. *Anal. Chem.* 1987, 59, 150-4.

(9) Neuburger, G. G.; Johnson, D. C. *Anal. Chem.* 1987, 59, 203-4.

(10) Neuburger, G. G.; Johnson, D. C. *Anal. Chim. Acta* 1987, 192, 205-13.

(11) Vandenberg, P. J.; Kawagoe, J. L.; Johnson, D. C. *Anal. Chim. Acta* 1992, 260, 1-11.

(12) Larew, L. A.; Johnson, D. C. *J. Electroanal. Chem. Interfacial Electrochem.* 1989, 262, 167-82.

(13) Chem, T. K.; Lau, Y. Y.; Wong, D. K. Y.; Ewing, A. G. *Anal. Chem.* 1992, 64, 1264-8.

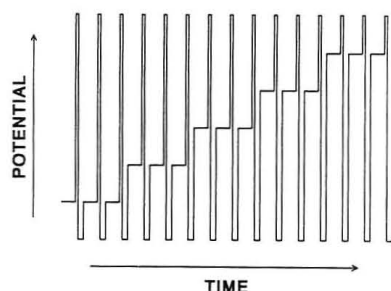


Figure 1. Typical pulsed voltammetric waveform.

with 0.45- μm filters and a solvent filtration apparatus (Rainin Corp., Woburn, MA). Solutions were deaerated with dispersed N_2 .

Apparatus. Voltammetric data were obtained at a Au rotated disk electrode (RDE, ca. 0.18 cm) using a Model RDE4 potentiostat (Pine Instrument Co., Grove City, PA). Cyclic voltammetric data were recorded on a Model 3025 X-Y recorder (Yokogawa Corp. of America, Peachtree City, GA).

PV data were obtained at the Au RDE with a computer-controlled potentiostat using a DAS-16F high-speed A/D-D/A expansion board (MetraByte Corp., Taunton, MA) in an IBM-AT compatible computer (Everex Systems, Inc., Fremont, CA). PV waveforms were generated with ASYST scientific software (Asyst Software Technologies, Inc., Rochester, NY).

LC separations were performed using a CarboPac-PA1 separator column in an isocratic/gradient chromatography system (Dionex Corp., Sunnyvale, CA). Pulsed amperometric detection was performed at a Au working electrode (ca. 0.15 cm^2) with a Ag/AgCl reference in a Model PED detector (Dionex).

Procedures. The PAD waveform used to obtain the PV response is depicted in Figure 1. The PV response was monitored for independent variations of all potential and time parameters. Because the duration of PV experiments at the RDE is not limited, as would be the case for LC-PAD, the waveform for each set of parametric values can be repeated to improve the precision of the current measurement. Hence, for the PV experiments described, each data point shown represents an average response for nine cycles of the PAD waveform ($n = 9$).

The signal-to-noise ratio (S/N) was calculated as follows:

$$S/N = i_d/\sigma_d = (i_a - i_r)/(\sigma_a^2 + \sigma_r^2)^{1/2} \quad (1)$$

In eq 1, i_a , i_r , and i_d are the average values of the analytical, residual, and difference currents, respectively; and σ_a , σ_r , and σ_d are the corresponding standard deviations.

All PV data correspond to O_2 -free solutions, unless otherwise noted. All potentials were controlled with respect to a Ag/AgCl reference and are reported with respect to this reference. Table I describes the useful ranges as well as the optimal values for all parameters in the most popular triple-step waveform applied in PAD for carbohydrates at Au electrodes in 0.1 M NaOH.

RESULTS AND DISCUSSION

The compounds studied are representative of the majority of carbohydrates. They are sorbitol, a nonreducing sugar alcohol; fructose, a nonreducing ketose; glucose, a reducing aldose; sucrose, a nonreducing disaccharide composed of glucose and fructose units bonded via an acetal-ketal linkage; and maltose, a reducing disaccharide composed of two glucose units bonded via an acetal-acetal linkage. For potential scan rates typical of CV ($50\text{--}200 \text{ mV s}^{-1}$), the response of sorbitol and glucose is under transport control, that of sucrose and maltose is under surface (kinetic) control, and that of fructose is under mixed control. The nature and ramifications of these differences has been considered.²

Voltammetry. The residual CV response (i - E) is shown in Figure 2 for the Au RDE in 0.1 M NaOH with (---) and without (—) dissolved O_2 . The anodic signals for the positive scan correspond to formation of surface oxide (wave A, ca. +200 to +700 mV) and anodic discharge of H_2O to produce

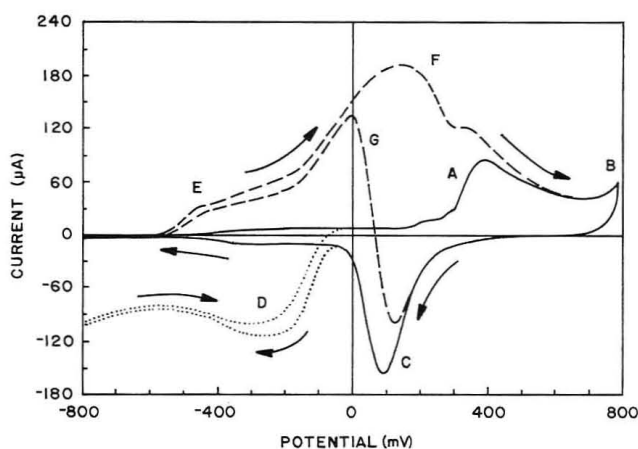


Figure 2. Cyclic voltammogram response for glucose at the Au RDE in 0.1 M NaOH. Conditions: 900 rpm rotation speed; 200 mV s^{-1} scan rate. Solutions: (---) aerated 0.1 M NaOH; (—) deaerated 0.1 M NaOH; (- - -) 0.4 mM D-glucose in deaerated 0.1 M NaOH.

Table I. General and Optimal Waveform Parameters for Pulsed Amperometric Detection (PAD) at a Au Working Electrode in 0.1 M NaOH

variable	potential (mV vs Ag/AgCl)		time (ms)		
	general	optimized	variable	general	optimized
E_{det}	-200 to +400	+200	t_{det}	>40	440
			t_{del}	>20	240
			t_{int}	>20	200
E_{oxd}	+300 to +800	+800	t_{oxd}	>60	180
E_{red}	-800 to +100	-300	t_{red}	>60	360

O_2 (wave B, greater than ca. +700 mV). The cathodic peak signal for the subsequent negative scan corresponds to reduction of the surface oxide (wave C, ca. +300 to -100 mV). A cathodic wave is observed for dissolved O_2 during the positive and negative scan (wave D, less than ca. -100 mV). Wave D for O_2 is well resolved from waves A and C. This is in sharp contrast to the residual CV response for Pt electrodes wherein there is significant overlap of the wave for O_2 reduction with those for oxide formation and dissolution. This difference is a significant factor in the selection of Au over Pt for detection of carbohydrates in LC-PAD. As will be apparent, the background signal in PAD can be minimized if a value of E_{det} is chosen which gives maximum response for carbohydrates with little or no O_2 reduction or oxide formation.

The CV response for glucose (---) in deaerated 0.1 M NaOH is also shown in Figure 2. Glucose produces a very definitive two-step anodic response during the positive scan beginning at ca. -600 mV. The first step corresponds to oxidation of the aldehyde group to produce the carboxylate anion in this alkaline media (wave E, ca. -600 to -200 mV).¹² The second step has the form of a peak (wave F, ca. -200 to +400 mV) and corresponds to the combined oxidations of the aldehyde and alcohol groups of glucose.¹² The anodic signal during the positive scan is attenuated abruptly (greater than ca. +200 mV), corresponding to the onset of oxide formation (wave A). The absence of signal on the subsequent negative scan in the

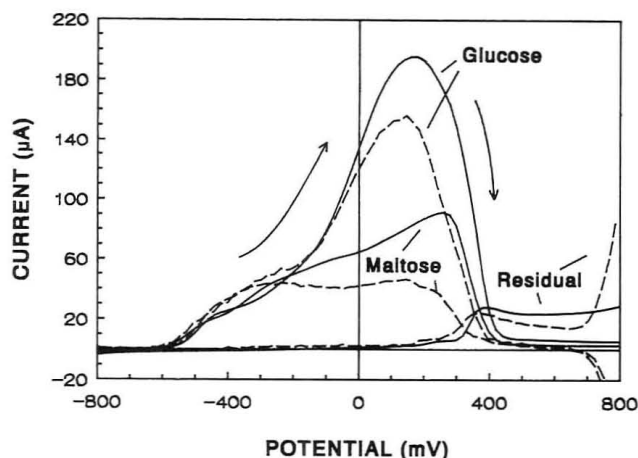


Figure 3. Comparison of PV response ($i-E_{\text{det}}$) (—) and CV response ($i-E$) (---) for 0.4 mM glucose and 0.4 mM maltose at the Au RDE in 0.1 M NaOH. Conditions: 900 rpm rotation speed; 50 mV s^{-1} CV scan rate; PV, optimized PAD waveform (Table I).

region ca. +800 to +200 mV indicates the absence of activity for the oxide-covered Au surface. Following cathodic dissolution of the oxide (wave C), the reactivity of the Au surface returns for glucose oxidation and an anodic peak is observed (wave G, ca. +50 to -600 mV).

Figure 3 compares the $i-E$ responses during the positive scans for glucose and maltose obtained by CV (---) and PV (—). Only the data for the positive scans are shown because this response is relevant to the PAD waveforms in which the anodic response is measured following a positive step from E_{red} to $E_{\text{det}} \gg E_{\text{red}}$. The $i-E$ curves for glucose and maltose correspond to the background-corrected response obtained by subtraction of the response obtained the presence and absence of analyte. Hence, the anodic signal in the region of oxide formation (greater than ca. +400 mV) is virtually zero for the presence of glucose and maltose. Those signals shown correspond to the anodic processes discussed above for glucose (see Figure 2).

A comparison of the maltose response in Figure 3 obtained by CV (---) and PV (—) reveals that the optimal value of E_{det} to be applied in PAD cannot be based accurately on the CV data. This difference between PV and CV response is attributable to the coupling of time and potential in the CV waveform. Hence, the anodic response during the positive scan in CV is attenuated as a result of surface fouling. In contrast to maltose, the response peaks for glucose obtained by CV and PV are virtually equivalent. We conclude these data indicate that the Au electrode surface is fouled more rapidly by the detection products of maltose as compared to glucose.

Optimization of E_{det} , t_{del} , and t_{int} in the PAD Waveform.

The optimum value of E_{det} for LC-PAD can be easily and accurately chosen on the basis of PV data obtained during application of the PAD waveform at a hydrodynamic electrode. Figure 4 shows the $i-E_{\text{det}}$ response for a positive scan of E_{det} at the Au RDE for equimolar concentrations of representative carbohydrates in 0.1 M NaOH. They are sorbitol (---), glucose (—), maltose (---), fructose (---), and sucrose (- · -). The anodic signal in the region ca. -600 to -200 mV (wave E) corresponds to the aldehyde group (glucose and maltose). The peak signal in the region -200 to +400 mV (peak F) corresponds to oxidation of aldehyde (glucose and maltose) and alcohol groups (all five compounds). Whereas all compounds tested exhibit the anodic response corresponding to peak F, responses for sucrose (a disaccharide) and oligosaccharides (not shown) exhibit a narrower peak maxima than is observed for glucose and maltose in Figure 4. Nevertheless, a maximum response is obtained at $E_{\text{det}} = +200$

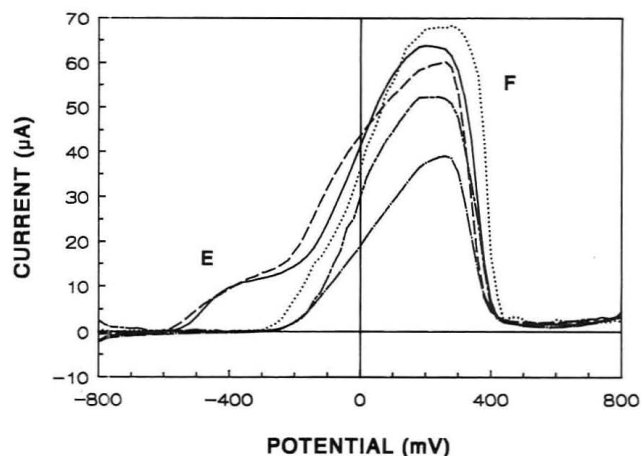


Figure 4. PV response for five carbohydrates at the Au RDE in 0.1 M NaOH. Conditions: 900 rpm rotation speed; others as in Figure 3; optimized waveform in Table I except for E_{det} . Solutions (0.1 mM): (---) sorbitol; (—) glucose; (---) fructose; (- · -) sucrose; (---) maltose.

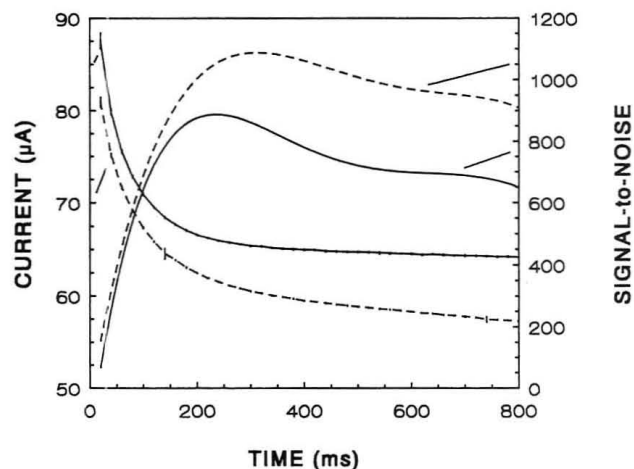


Figure 5. PV response and S/N as a function of t_{del} for 0.1 mM (—) glucose and (---) maltose at the Au RDE in 0.1 M NaOH. Conditions: 900 rpm rotation speed; optimized waveform in Table I except for t_{del} .

mV for all carbohydrates and application of this value in the PAD waveform enables the universal and highly sensitive detection of all carbohydrates. The anodic formation of surface oxide contributes only a small anodic signal at $E_{\text{det}} = +200$ mV, and virtually no cathodic response is obtained for reduction of dissolved O_2 .

Whereas the $i-E$ response obtained by CV can give a moderately good indication of a useful value of E_{det} for PAD waveforms, optimal timing parameters cannot possibly be deduced from the CV response. Hence, it is with regard to this aspect of waveform optimization that the PV technique yields maximum benefit. For this purpose, E_{det} is chosen to correspond to the maximum response observed in $i-E_{\text{det}}$ plots (Figure 4) and the response is recorded during independent incremental variations of several timing parameters. Figure 5 shows variations of the PAD response and S/N for glucose (—) and maltose (---) as a result of variation of t_{del} . For any value $t_{\text{del}} > \text{ca. } 20$ ms, a significant anodic response is obtained for both glucose and maltose. Of more importance is the observation that the S/N has a maximum value for $t_{\text{del}} = \text{ca. } 200$ and 300 ms for glucose and maltose, respectively. The value $t_{\text{del}} = \text{ca. } 240$ ms is recommended as optimal for general detection of glucose and maltose.

The shapes of the $i-t_{\text{del}}$ plots in Figure 5 are consistent with previous speculation.¹ Most significant is the observation that the signal for maltose diminishes more rapidly than that for glucose. This fact is attributable to the rapid fouling of the Au surface by the detection product of maltose, whereas

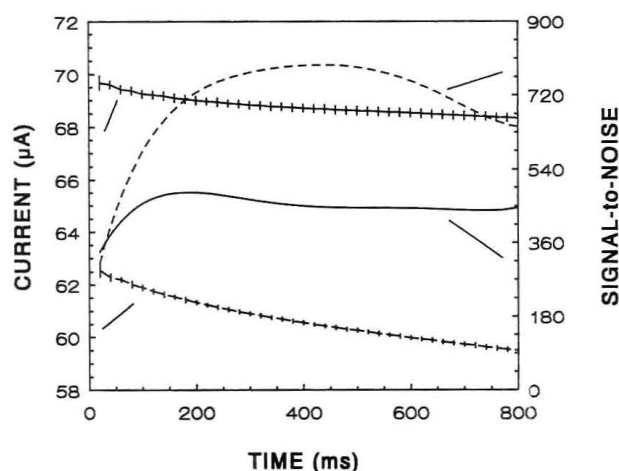


Figure 6. PV response and S/N as a function of t_{int} for (—) glucose and (---) maltose at the Au RDE in 0.1 M NaOH. Conditions/solutions are as in Figure 4.

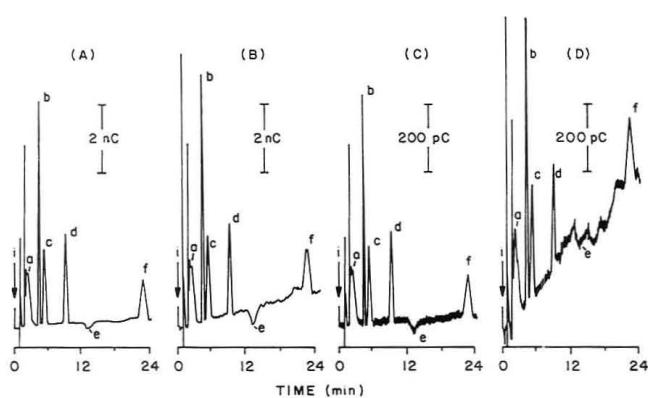


Figure 7. Comparison of LC-PAD results with variations of t_{del} and t_{int} in the PAD waveform. Conditions: CarboPac PA1 column; 0.1 M NaOH mobile phase; 1.0 mL min^{-1} flow rate; 25- μL injection volume; optimized waveform in Table I, except as noted. Parameters: (A) $t_{\text{del}} = 240$ ms, $t_{\text{int}} = 200$ ms; (B) $t_{\text{del}} = 20$ ms, $t_{\text{int}} = 200$ ms; (C) $t_{\text{del}} = 240$ ms, $t_{\text{int}} = 20$ ms; (D) $t_{\text{del}} = 20$ ms, $t_{\text{int}} = 20$ ms. Peaks (100 pmol): (a) sorbitol; (b) glucose; (c) fructose; (d) sucrose; (f) maltose. Comment: peak e represents injected dissolved O_2 .

the product of glucose detection exhibits minimal electrode fouling. Most of the monosaccharides and disaccharides tested exhibit $i-t_{\text{del}}$ responses which fall off at rates intermediate to those in Figure 5 for glucose and maltose.

Figure 6 shows the PV response for glucose (—) and maltose (---) as a result of the variation of t_{int} . Over the range of values tested, the signals change very little. The S/N for glucose reaches a nearly constant value for $T_{\text{int}} > \text{ca. } 200$ ms, and the S/N for maltose shows a broad maximum for $t_{\text{int}} = \text{ca. } 200\text{--}600$ ms. On the basis of these results, a value of $t_{\text{int}} = 200$ ms is chosen as the optimal value. Further testing reveals this value of t_{int} is appropriate for all carbohydrates. A further consideration supporting this choice of t_{int} is that 200 ms is a multiple of 16.667 ms (i.e., $1/60 \text{ Hz}^{-1}$). Hence, $t_{\text{int}} = 200$ ms minimizes the contribution of noise originating from both 60- and 50-Hz power sources.¹⁰

To illustrate the significance of the data in Figures 5 and 6, chromatograms are compared in Figure 7 obtained using $t_{\text{del}} = 240$ ms (A and C) and 20 ms (B and D) with $t_{\text{int}} = 200$ ms (A and B) and 20 ms (C and D). For each value of t_{int} , the background noise and baseline drift are dramatically worse for the shorter value of t_{del} . It is evident from Figure 7 that the S/N is superior for $t_{\text{int}} = 200$ ms.

As discussed for the optimization of t_{del} , the anodic signals for many carbohydrates do not reach steady-state values over the lifetime of the detection period (t_{det}). The attenuation of anodic signal is attributable to fouling of the electrode

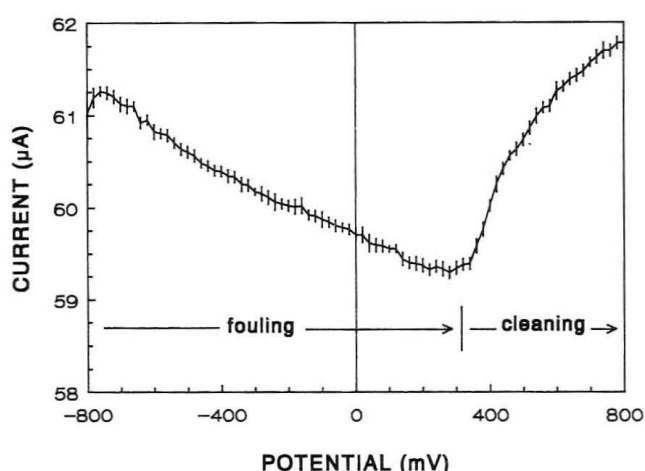


Figure 8. PV response as a function of E_{oxd} for glucose at the Au RDE in 0.1 M NaOH. Conditions/solutions are as in Figure 4.

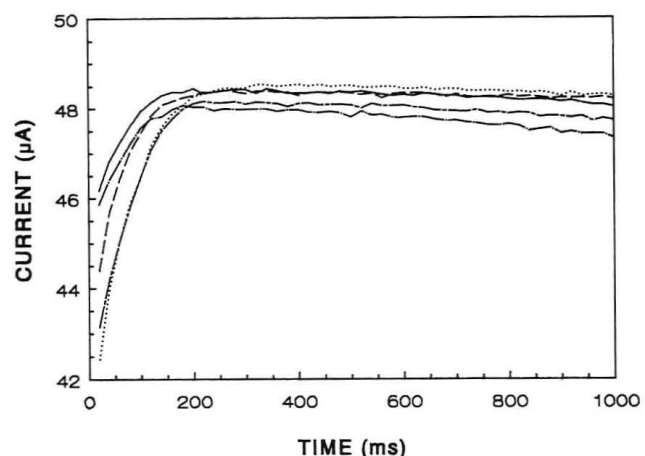


Figure 9. PV response as a function of t_{oxd} at five E_{oxd} values for glucose. E_{oxd} (mV): (···) 600; (---) 700; (—) 800; (- · -) 900; (—) 1000.

surface by the accumulation of adsorbed detection products and, to a lesser degree, the slow formation of surface oxide at E_{det} . It is for these reasons that detection of carbohydrates at Au (and Pt) electrodes with constant applied (dc) potentials is not successful. However, the activity of the electrode surface can be efficiently renewed within an optimized PAD waveform (Table I) by a positive potential step to achieve oxidative cleaning with formation of surface oxide ($E_{\text{oxd}} = \text{ca. } +200$ to $+800$ mV) followed by a negative step for reductive dissolution of the oxide ($E_{\text{red}} < -100$ mV; see Figure 2 and the associated discussion).

Optimization of E_{oxd} and t_{oxd} . Shown in Figure 8 is the PAD response for glucose with variation of E_{oxd} for $t_{\text{oxd}} = 180$ ms. As E_{oxd} is changed from -800 to $+300$ mV, the once-clean electrode becomes progressively fouled by the detection products because there is no surface oxide formed within the PAD waveform. However, as E_{oxd} is increased above $\text{ca. } +300$ mV, the amount of surface oxide formed at this potential is sufficient to evoke oxidative cleaning of the electrode surface and the anodic signal increases.

The optimal value of E_{oxd} is somewhat dependent upon the choice of t_{oxd} . Shown in Figure 9 is variation of the PAD response for glucose as a function of t_{oxd} for several values of E_{oxd} in the range $+600$ to $+1000$ mV. Clearly, for the values of E_{oxd} shown, $t_{\text{oxd}} = \text{ca. } 180$ ms is sufficient for the efficient oxidative cleaning of the electrode surface. The values $E_{\text{oxd}} = +800$ mV and $t_{\text{oxd}} = 180$ ms are recommended as optimal. Some evidence indicates that the rate of oxidative surface cleaning might be accelerated at large values of E_{oxd} at which

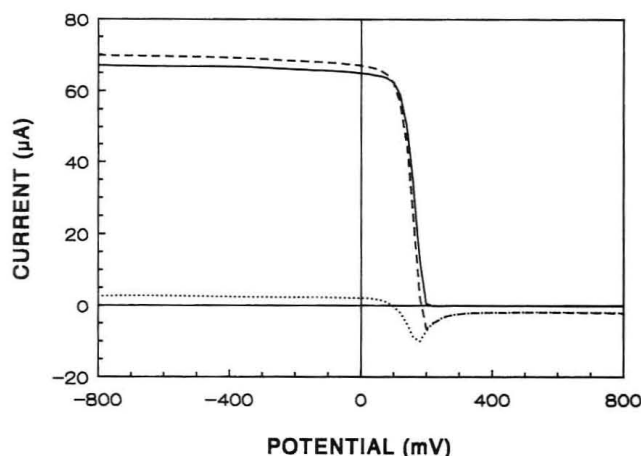


Figure 10. PV response as a function of E_{red} for glucose at the Au RDE in 0.1 M NaOH. Conditions are as in Figure 4. Solutions: (---) residual; (—) 0.1 mM glucose; (· · ·) difference.

the rigorous evolution of O_2 can occur.¹⁴ However, the choice of $E_{\text{oxd}} = +800$ mV avoids problems that can result from formation of O_2 bubbles which can adhere to the electrode surface and, thereby, interfere with the transport of analyte to the electrode.

Optimization of E_{red} and t_{red} . The surface oxide formed during application of E_{oxd} in the PAD waveform quickly results in loss of electrode response for carbohydrates. Hence, it is essential that the values of E_{red} and t_{red} are chosen to achieve complete reductive dissolution of the surface oxide. Figure 10 shows the variation of the PAD response for glucose as a function of E_{red} for $t_{\text{red}} = 300$ ms. The response is constant for $E_{\text{red}} = -800$ to $+100$ mV and, therefore, any value in this range is sufficient to dissolve the surface oxide formed at E_{oxd} . At $E_{\text{red}} > +200$ mV, reductive dissolution of surface oxide does not occur and carbohydrate response is terminated. Values of $E_{\text{red}} \leq -300$ mV are sufficient to minimize oxidation of carbohydrates prior to application of E_{det} , and -300 mV is chosen as the optimum value for E_{red} .

A secondary consequence of incomplete removal of surface oxide for the chosen values of E_{red} and t_{red} is that reduction of oxide can persist at E_{det} with a significant contribution to the residual response in LC-PAD. This residual response is very sensitive to fluctuations in temperature and pH. Hence, LC-PAD results obtained under conditions of incomplete oxide reduction have exhibited baseline signals which drift for more than 2 h after initiation of the PAD waveform. Conversely, when surface oxide is completely removed in the PAD waveform, baselines are stabilized within ca. 10 min.² Another consequence of inadequate oxide removal is a decreased analytical signal because the electrode surface is not fully utilized for the detection process. These factors have previously been noted with regard to the determination of amino alcohols by LC-PAD.¹⁵

Shown in Figure 11 is the PAD response for glucose (—) and maltose (---) as a function of t_{red} for $E_{\text{red}} = -300$ mV. The response for glucose reaches a plateau for $t_{\text{red}} > \text{ca. } 100$ ms, whereas $T_{\text{red}} > \text{ca. } 300$ ms is required to reach a maximum response for maltose. This difference is attributed to the difference in the extent of adsorption of the detection products for these two compounds. We recommend $t_{\text{red}} = 360$ ms as optimal in the general application of PAD for carbohydrates. Experience indicates this choice of t_{red} allows for latitude in the selection of E_{oxd} within the range $+600$ to $+800$ mV.

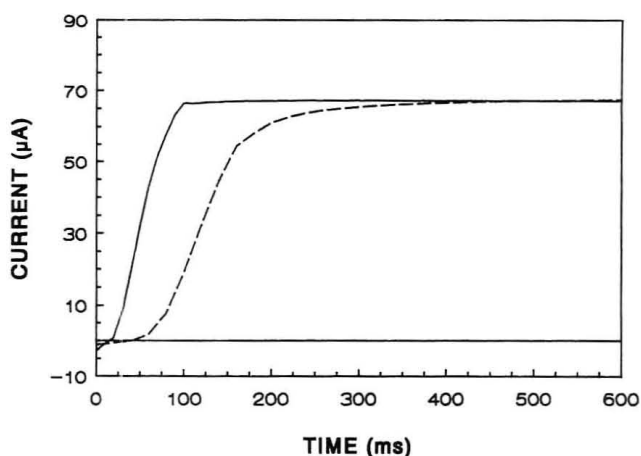


Figure 11. PV response as a function of t_{red} for (—) glucose and (---) maltose at the Au RDE in 0.1 M NaOH. Conditions/solutions are as in Figure 4.

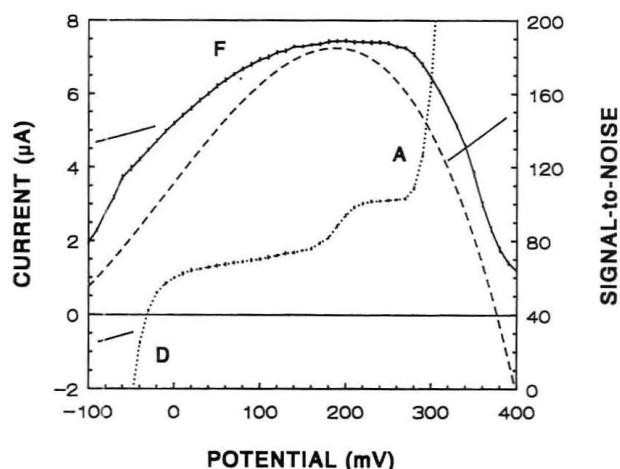


Figure 12. PV response and S/N as a function of E_{det} for glucose in 0.1 M NaOH. Conditions are as in Figure 4. Curves: (· · ·) aerated supporting electrolyte; (—) aerated 10 μM glucose; (---) signal-to-noise ratio.

PV and LC-PAD Response with Optimized Waveforms. Figure 12 shows the PV response for the Au RDE in 0.1 M NaOH with (—) and without (· · ·) the presence of 10 μM glucose during the positive scan of E_{det} . All other waveform parameters correspond to the optimal values given in Table I. The S/N is shown corresponding to the presence of glucose. In these experiments, solutions were not deaerated so to better simulate the inevitable presence of dissolved O_2 in LC-PAD. The labels correspond to those shown in Figure 2. For the high sensitivity used, the residual response (—) shows clearly that $E_{\text{det}} = \text{ca. } 0$ to $+300$ mV corresponds to very low signals for both oxide formation and O_2 reduction. The response for 10 μM glucose is in the form of a broad peak, which is consistent with Figure 2. The corresponding S/N (· · ·) easily identifies the optimal $E_{\text{det}} = \text{ca. } +200$ mV (S/N = 190). The PAD response for glucose at the Au RDE was determined for these conditions to be linear in the range 0–500 μM . The regression line is described by the equation $\mu\text{A} = 0.678 (\mu\text{M}) + 1.346$ with a correlation coefficient (r) of 0.999 995. The above procedure was repeated at the Au electrode of the flow-through thin-layer cell typically used in LC-PAD. The PV response for a positive E_{det} scan during continuous flow of sample was very similar to that in Figure 12 for the RDE with a maximum value of S/N for $E_{\text{det}} = \text{ca. } +200$ mV.

Figure 13 shows the LC-PAD response of a solution containing 10 pmol each of sorbitol, glucose, fructose, sucrose, and maltose in 0.1 M NaOH using the optimized PAD waveform described in Table I. The relative standard

(14) Johnson, D. C.; Polta, J. A.; Polta, T. Z.; Neuburger, G. G.; Johnson, J. L. *J. Chem. Soc., Faraday Trans. 1* 1986, 82, 1081–98.

(15) LaCourse, W. R.; Jackson, W. A.; Johnson, D. C. *Anal. Chem.* 1989, 61, 2466–71.

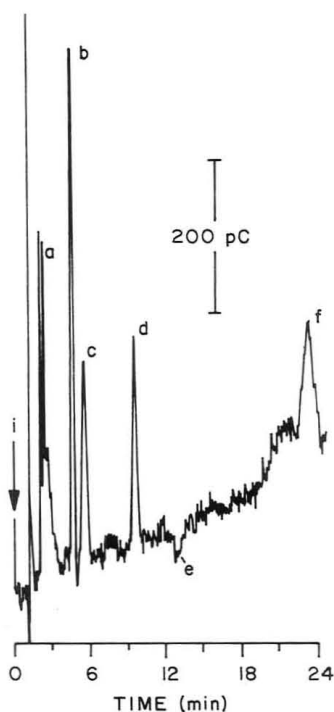


Figure 13. Chromatographic separation using optimized PAD waveform (Table I). Conditions are as in Figure 7. Peaks (10 pmol): (a) sorbitol; (b) glucose; (c) fructose; (d) sucrose; (f) maltose. Comment: peak e represents injected dissolved O_2 .

deviations (RSD) for six injections of each compound are 1.2, 1.7, 3.5, and 6.4 for glucose, fructose, sucrose, and maltose, respectively. Limits of detection ($S/N = 3$) are calculated to be 2, 4, 4, and 8 pmol injected for glucose, fructose, sucrose, and maltose, respectively. Because sorbitol is essentially not retained, the RSD and limit of detection for sorbitol were not determined.

Effects of pH and organic Modifiers. All carbohydrates that lack a formal charge are weakly acidic with pK_a values in the range ca. 12–14. As a result, carbohydrates are readily separated in highly efficient anion-exchange columns using alkaline mobile phases. The chromatographic k' values increase with decreasing pK_a and, i.e., increasing molecular weight.^{5,6} In addition, glycosylated compounds can be separated by a variety of chromatographic mechanisms including reversed-phase chromatography. Therefore, it is important to consider the optimization of PAD waveforms as a function of all variables normally considered when the various chromatographic separations are optimized, i.e., pH, ionic strength, organic modifiers, temperature, etc. Because these parameters can influence the rates for formation and dissolution of surface oxide and the sensitivity of electrocatalytic response mechanisms at Au electrodes, the availability of a definitive method for optimization of PAD waveforms is well warranted.

The effect of pH variation on the oxide formation process can be explained on the basis of the pH-dependent nature of the oxide formation reaction, i.e., $Au(H_2O)_{ads} \rightarrow Au-OH + H^+ + e^-$. The optimal E_{det} value corresponds approximately to the potential for the onset of oxide formation (see Figure 3). Furthermore, optimal values of E_{oxd} and E_{red} are approximately fixed with respect to the potential for the onset of oxide formation. Hence, for a given change in pH (ΔpH), the optimal values of E_{det} , E_{oxd} , and E_{red} must be adjusted by the amount $-60\Delta pH \text{ mV}^{-1}$,^{2,16} from the values recommended in Table I for 0.1 M NaOH. For a 0.2 M NaOH mobile phase,

E_{det} , E_{oxd} , and E_{red} are decreased by 20 mV to compensate for the increased alkalinity. For a 0.02 M NaOH mobile phase, commonly applied for assays of monosaccharide mixtures derived from glycoproteins, the PAD potentials should be increased by 40 mV to compensate for the decreased alkalinity.

Application of a positive pH gradient in HPIC-PAD can be beneficial for separations of mixtures of carbohydrates having a large range of molecular weights with the expected large range of k' values observed for isocratic elution. However, with an increase in pH comes a negative shift in the potential for the onset of oxide formation. Consequently, a large positive (anodic) shift in the baseline signal can result when E_{det} is held constant throughout development of the gradient.¹⁶ This problem can be alleviated by substitution of a pH-sensitive glass-membrane electrode for the Ag/AgCl reference electrode in the electrochemical cell. The potential response of a glass-membrane electrode is ca. -60 mV pH^{-1} , and hence, the value of E_{det} is automatically adjusted during execution of the pH gradient.¹⁶

Typical ionic strengths (I) in HPIC-PAD are in the range 50–100 mM, and variations within this range are of virtually no consequence to the optimization of PAD waveform parameters. However, under conditions of ion-gradient elution (e.g., increasing acetate concentration in HPIC-PAD), baseline drifts have been observed (data not shown).² In this case, we recommend postcolumn addition of a solution with high ionic strength to effectively "buffer" the ionic strength in the effluent stream passing through the electrochemical detector cell.

The presence of organic modifiers to the mobile phases in LC-PAD can have a much greater consequence on the optimized PAD waveform than is caused by changes in I and pH. This is true especially when the modifiers are adsorbed at the electrode surface and interfere with access by the carbohydrate molecules to specific reaction sites on the electrode with a corresponding attenuation of analytical response. Furthermore, adsorbed organic modifiers can suppress the oxide-formation process with the necessity of increasing E_{oxd} values.

Large temperature fluctuations (i.e., $\gg 1^\circ\text{C}$) can cause significant changes in the sensitivity of PAD response, especially for compounds whose detection is under mixed or surface control. Whereas the majority of present-day LC-PAD applications rely on the thermostatic control normally found in well-designed analytical laboratories, we can foresee applications that can benefit from better control of temperature (i.e., $< 1^\circ\text{C}$).

CONCLUSIONS

The application of PAD waveforms in pulsed voltammetry (PV) has been extended to the optimization of potential and timing parameters for PAD waveforms applied in LC-PAD for a variety of possible chromatographic conditions. Because the effects of variation of the waveform parameters are not mutually exclusive, it is important to reexamine the effects of variation of each parameter after approximate optimal values have been determined. Hence, we recognize the ultimate benefit of integrating the present PV strategy with automated simplex or other optimization protocols.

ACKNOWLEDGMENT

Financial support from Dionex Corp. is acknowledged with gratitude.

(16) LaCourse, W. R.; Mead, D. A., Jr.; Johnson, D. C. *Anal. Chem.* 1990, 62, 220–4.

Examination of Conditions under Which the Reduction of the Cobaltocenium Cation Can Be Used as a Standard Voltammetric Reference Process in Organic and Aqueous Solvents

R. S. Stojanovic and A. M. Bond*

Department of Chemical and Analytical Sciences, Deakin University, Waurn Ponds 3217, Victoria, Australia

The two one-electron processes for reduction of the cobaltocenium cation as the hexafluorophosphate salt have been studied extensively in both aprotic and protic solvents at a hanging mercury drop electrode and at conventionally and micro-sized platinum, gold, and glassy carbon disk electrodes of various radii. Under carefully chosen conditions, both the Cc^+/Cc^0 and Cc^0/Cc^- couples (Cc = cobaltocene) can be used as reversible voltammetric reference systems. However, the Cc^+/Cc^0 couple is the preferred reference process since the combination of a very negative potential and possible overlap problems with the solvent response sometimes prevents the Cc^0/Cc^- couple from being used as a practical voltammetric reference system. Furthermore, the half-wave potential for the Cc^+/Cc^0 system was calculated to be -1.35 ± 0.01 V vs the widely used Fc^+/Fc reference couple (Fc = ferrocene) and is essentially independent of electrode material, electrolyte, and solvent relative to the ferrocene reference potential. In contrast, the half-wave potential for the Cc^0/Cc^- couple relative to the ferrocene reference potential is significantly dependent on the nature of the solvent.

INTRODUCTION

There has been considerable interest in finding redox couples that can be used as reference redox systems in both organic and aqueous solvents.¹⁻⁵ The use of a standard redox couple not only acts as an internal standard with which potentials can be measured but also may minimize the contribution from the usually unknown aqueous–nonaqueous junction potential encountered when, for example, aqueous reference electrodes are used in nonaqueous solvent media. Ideally, the potential of the reference system also should be independent of solvent. However, it should be stressed that while it is useful to refer measured potentials to the potential of the reference system, this does not imply that the potentials of systems proposed so far are solvent independent.

The systems ferrocenium ion/ferrocene (Fc^+/Fc) and to a lesser extent cobaltocenium ion/cobaltocene (Cc^+/Cc) have been advocated as suitable reference systems, since both couples meet many of the criteria for a successful reference system.^{2,6-10} However, perhaps surprisingly, no detailed evaluation of the cobaltocene system for this purpose is

available under a wide range of conditions. The most stable cobaltocene derivative is the 18-electron $(\eta^5-C_5H_5)_2Co^+$ or bis- $(\eta^5-cyclopentadienyl)cobalt(III)$ cation which is isoelectronic with the 18-electron neutral ferrocene compound.^{11,12} Since only one form of a redox couple is required to be added to solution during a voltammetric experiment, the cobaltocenium cation is usually employed in preference to the less stable 19-electron cobaltocene (bis- $(\eta^5-cyclopentadienyl)cobalt(II)$) for use as a reference compound in electrochemical studies. The other form of the redox couple is generated via the voltammetric experiment.

Two reduction processes involving Cc^+/Cc^0 and Cc^0/Cc^- may be available for use as reference redox systems in both organic and aqueous media.¹³⁻²⁶ However, while the Cc^+/Cc^0 redox couple has on occasions been used as an alternative to the ferrocene system for reporting electrochemical data, the Cc^0/Cc^- process has yet to be examined for use as a reference process. In view of the need to find more suitable and reliable reference systems in both organic and aqueous solvents,^{7,8} further examination of the cobaltocene system for instrumental and reference potential calibration purposes is required. In particular, since the potentials for the cobaltocene redox processes are very different from those for ferrocene, this standard is likely to be available as an in situ reference

(6) Gagné, R. R.; Koval, C. A.; Lisensky, G. C. *Inorg. Chem.* 1980, 19, 2854.

(7) Gritzner, G.; Kúta, J. *Pure Appl. Chem.* 1982, 54, 1527.

(8) Gritzner, G.; Kúta, J. *Pure Appl. Chem.* 1984, 56, 461.

(9) Bond, A. M.; McLennan, E. A.; Stojanovic, R. S.; Thomas, F. G. *Anal. Chem.* 1987, 59, 2853 and references cited therein.

(10) Schneider H.; Strehlow H. *J. Electroanal. Chem.* 1966, 12, 530.

(11) Morris, M. D.; Kok, G. L. In *Encyclopedia of Electrochemistry of the Elements*; Bard, A. J., Ed.; Dekker: New York, 1979; Vol. XIII, p 1.

(12) Kotz, J. C. In *Topics in Organic Electrochemistry*; Fry, A. J., Britton, W. E., Eds.; Plenum Press: New York, 1986; p 81.

(13) Vlcek, A. *Collect. Czech. Chem. Commun.* 1965, 30, 952.

(14) Gubin, S. P.; Smirnova, S.; Denisovich, L. *J. Organomet. Chem.* 1971, 30, 257.

(15) El Murr, N.; Dabbard, R.; Laviron, E. *J. Organomet. Chem.* 1973, 47, C13.

(16) Geiger, W. E., Jr.; Smith, D. E. *J. Electroanal. Chem. Interfacial Electrochem.* 1974, 50, 31.

(17) Geiger, W. E., Jr. *J. Am. Chem. Soc.* 1974, 96, 2632.

(18) Geiger, W. E., Jr.; Bowden, W. L.; El Murr, N. *Inorg. Chem.* 1979, 18, 2358.

(19) Weaver, M. J. *J. Electroanal. Chem. Interfacial Electrochem.* 1985, 186, 179.

(20) Alpatova, N. M.; Krishtalik, L. I.; Ovsyannikova, E. V.; Leonova, E. V.; Shirokii, V. L. *Elektrokhimiya* 1989, 25, 1341.

(21) Geiger, W. E., Jr. In *Laboratory Techniques in Electroanalytical Chemistry*; Kissinger, P. T., Heineman, W. R., Eds.; Dekker: New York, 1984; p 490.

(22) Page, J. A.; Wilkinson, G. W. *J. Am. Chem. Soc.* 1952, 74, 6149.

(23) El Murr, N. *Transition Met. Chem.* 1981, 6, 321.

(24) Ovsyannikova, E. V.; Krishtalik, L. I.; Alpatova, N. M.; Shirokii, V. L.; Leonova, E. V. *Elektrokhimiya* 1989, 25, 1348.

(25) Bowyer, W. J.; Engelman, E. E.; Evans, D. H. *J. Electroanal. Chem. Interfacial Electrochem.* 1989, 262, 67.

(26) Bond, A. M.; Cooper, J. B. *J. Electroanal. Chem. Interfacial Electrochem.* 1990, 315, 143.

* To whom correspondence should be addressed at the Department of Chemistry, Latrobe University, Bundoora, 3083, Victoria, Australia.

(1) Pleskov, V. A. *Usp. Khim.* 1947, 16, 254.

(2) Koeppe, W. M.; Wendt, H.; Strehlow, H. *Z. Elektrochem.* 1960, 64, 483.

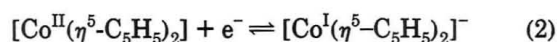
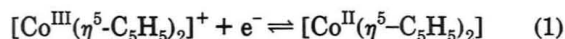
(3) Rusina, A.; Gritzner, G.; Vlcek, A. Proceedings of the IVth International Congress on Polarography, Prague, Czechoslovakia, 1966; p. 79.

(4) Gritzner, G.; Gutmann, V.; Schmid, R. *Electrochim. Acta* 1968, 13, 919.

(5) Bauer, D.; Beck, J. P. *Bull. Soc. Chim. Fr.* 1973, 1252.

process when the compound of interest is redox active at potentials similar to those of ferrocene.

In the present work, detailed voltammetric studies on the two reduction processes of cobaltocenium hexafluorophosphate have been undertaken in both aprotic and protic solvents at mercury electrodes and at conventional and microsized²⁷ platinum, gold, and glassy carbon disk electrodes of various radii. Both aprotic and protic solvents with varying dielectric constants such as dichloromethane (CH₂Cl₂), acetonitrile (CH₃CN), ethanol (CH₃CH₂OH), and water (H₂O) in the presence of different supporting electrolytes were examined to determine if conditions can be found under which the electrode processes



are simple reversible one-electron charge-transfer processes, suitable for use as voltammetric reference redox systems for instrumental and reference potential calibration. Finally, the purity of the solvent may also need to be considered and studies in both liquid chromatographic grade and more highly purified solvent were compared. These extensive studies form the basis of our final recommendation that under specified conditions both the Cc⁺/Cc and Cc/Cc⁻ couples can be used as voltammetric reference processes in both organic and aqueous solvents, although care must be taken with use of the latter process, as nonidealities exist under some circumstances.

EXPERIMENTAL SECTION

Reagents and Solvents. Cobaltocenium hexafluorophosphate (($\eta^5\text{-C}_5\text{H}_5$)₂CoPF₆) (Strem Chemicals, Newburyport, MA), lithium sulfate (BDH), lithium perchlorate (BDH), sodium fluoride (Hopkins and Williams), tetraethylammonium perchlorate (Et₄NClO₄) and tetrabutylammonium tetrafluoroborate (Bu₄NBF₄) (Southwestern Analytical Chemicals) were of analytical reagent or electrochemical grade and were dried under vacuum and subsequently stored in a desiccator prior to use. Triply distilled mercury (Engelhard Industries) was used in studies at the hanging mercury drop electrode.

Unless otherwise stated electrochemical measurements were made at 25.0 ± 0.1 °C in either water obtained from a Millipore 25TS (twin stage) reverse osmosis water purification system (Millipore, Bedford, MA) or liquid chromatographic grade solvent (Mallinckrodt) containing 0.1 M of a supporting electrolyte and deoxygenated with high-purity nitrogen. Organic solvents also were further purified by the recommended methods²⁸⁻³⁰ so that voltammetric data obtained in these more purified solvents could be compared to data obtained in liquid chromatographic grade solvent as obtained from the manufacturer (which is the order of purity commonly used in voltammetric studies in organic solvents).

Electrodes. Solid electrodes used were glassy carbon, GC, (area: 0.078 cm²), gold (area: 0.024 cm²), and platinum (area: 0.021 cm²) disks obtained from Bioanalytical Systems Inc. A PARC Model 303 static mercury drop electrode in the hanging mercury drop mode (HMDE) (area: 0.018 cm²) (Princeton Applied Research) or a Model E411 HMDE (area: 0.02 cm²) (Metrohm, Herisau, Switzerland) were used as mercury electrodes. The method for determining the area of each solid electrode has been described previously,⁹ while the surface areas of the mercury electrodes were determined from reduction of 1

× 10⁻³ M cadmium(II) solution in water (0.1 M KCl) by cyclic voltammetry and the equation

$$i_p = (2.69 \times 10^5) n^{3/2} A D^{1/2} C v^{1/2} \quad (3)$$

where i_p is the peak current (A), n (2 for cadmium(II)) is the number of electrons, A is the electrode area (cm²), D is the diffusion coefficient (D for cadmium(II) is 7.0 × 10⁻⁶ cm² s⁻¹ at 25 °C³¹), C is concentration (mol cm⁻³), and v is the scan rate (V s⁻¹).

The construction of Au and Pt microdisk electrodes have been described elsewhere,³² while a GC microdisk electrode was obtained from PAR (Princeton Applied Research). The radii of all microdisk electrodes were determined under steady-state conditions (scan rate 10 mV s⁻¹) via the oxidation of 1 × 10⁻³ M Fc in acetonitrile and the equation

$$i_L = 4nFDc r \quad (4)$$

where i_L is the diffusion-controlled limiting current, F is Faraday's constant, r is the radius of the microelectrode, D for ferrocene is 2.3 × 10⁻⁵ cm² s⁻¹ at 22 °C,²⁵ and other terms have previously been defined. All solid electrodes were polished consecutively with 0.5- and 0.05- μm alumina slurries and rinsed thoroughly with distilled water prior to each experiment.

Several reference electrode systems were used such as a Ag/Ag⁺ (0.1 M AgNO₃) double-fritted system in acetonitrile, a Ag/AgCl (saturated LiCl) double-fritted system in dichloromethane, and a Ag/AgCl (saturated KCl) reference electrode in water. However, the commonly recommended^{7,8} reversible Fc⁺/Fc redox couple was used as an internal standard and all cobaltocene data are quoted against this reference system. This enabled the standard reduction potentials for all processes to be compared in a variety of solvents, and thereby reducing the choice of reference electrode to one of experimental convenience.

Instrumentation. All voltammetric measurements (staircase waveform) with conventionally sized electrodes were performed with a BAS-100A electrochemical analyzer (Bioanalytical Systems) and a three-electrode system consisting of a working electrode (HMDE, GC, Au, Pt), a reference electrode, and a platinum wire auxiliary electrode.

All measurements with microelectrodes were performed with the BAS 100A instrument coupled to the BAS preamplifier (PA-1) and BAS Faraday cage. Typically, a two-electrode configuration was employed, consisting of a working electrode and a Ag wire pseudo reference electrode to avoid the errors introduced by a high-impedance conventional reference electrode³³ as well as minimizing the risk of contamination caused by the leakage of ions from conventional reference electrodes. Some microelectrode experiments were also performed using a three-electrode arrangement, as described previously for conventionally sized electrodes.

Experimental Procedure. All glassware was placed in an acid bath containing 2 M nitric acid for approximately 24 h and rinsed thoroughly with distilled water. All voltammetric measurements were performed in a thermostatically controlled jacketed cell at 25 ± 0.1 °C, except for measurements in dichloromethane at 2 ± 0.1 °C, which were performed in a Dewar flask. The solutions were deoxygenated with nitrogen for a minimum of 3 min. The nitrogen was passed through a trap containing the solvent of interest prior to being passed over the solutions during measurements. A 1 × 10⁻³ M stock solution of ($\eta^5\text{-C}_5\text{H}_5$)₂CoPF₆ in water was stirred for approximately 2 h, and standard solutions were prepared by serial dilution. Solutions containing ($\eta^5\text{-C}_5\text{H}_5$)₂CoPF₆ in organic solvents were prepared in a similar manner.

RESULTS AND DISCUSSION

Reduction of ($\eta^5\text{-C}_5\text{H}_5$)₂CoPF₆ in Acetonitrile. (a) Conventional Electrodes. Acetonitrile is a moderate dielectric constant ($\epsilon = 35.9$)³⁴ aprotic solvent, which is

(27) Bond, A. M.; Oldham, K. B.; Zoski, C. G. *Anal. Chim. Acta* 1989, 216, 177 and references therein.

(28) Mann, C. K. *Electroanal. Chem.* 1969, 3, 57.

(29) Marcus, Y. *Pure Appl. Chem.* 1985, 57, 860.

(30) Kadish, K. M.; Anderson, J. E. *Pure Appl. Chem.* 1987, 59, 707.

(31) Macero, D. J.; Rulfs, C. L. *J. Am. Chem. Soc.* 1959, 81, 2942.

(32) Bond, A. M.; Luscombe, D. L.; Oldham, K. B.; Zoski, C. G. *J. Electroanal. Chem. Interfacial Electrochem.* 1988, 249, 1.

(33) Hermann, C. C.; Ferrault, G. C.; Pilla, A. A. *Anal. Chem.* 1968, 40, 1173.

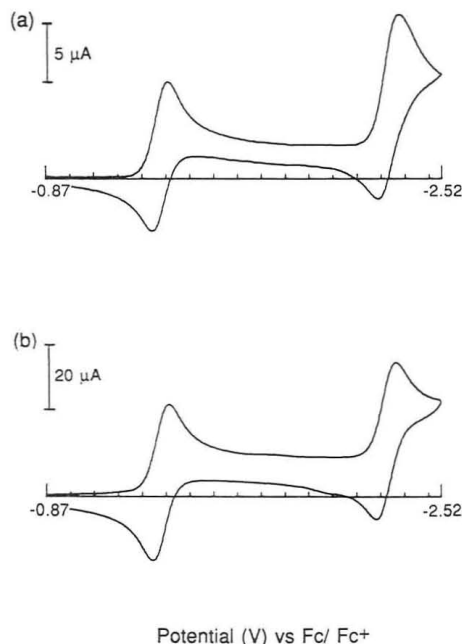


Figure 1. Cyclic voltammograms obtained at conventionally sized electrodes at 25 ± 0.1 °C for the two reduction processes with a 1×10^{-3} M solution of $(\eta^5\text{-C}_5\text{H}_5)_2\text{CoPF}_6$ in acetonitrile (0.1 M Bu_4NBF_4) at a scan rate of 100 mV s^{-1} at (a) a HMDE and (b) a glassy carbon electrode.

commonly used in electrochemistry. Figure 1 shows cyclic voltammograms obtained at the HMDE and GC electrode for the reduction of a 1×10^{-3} M solution of $(\eta^5\text{-C}_5\text{H}_5)_2\text{CoPF}_6$ in CH_3CN (0.1 M Bu_4NBF_4) at 25 ± 0.1 °C at a scan rate of 100 mV s^{-1} . Under these conditions, two well-defined reduction processes are observed at both the HMDE and GC electrode. The negative potential discharge region, which is a function of the solvent, solvent purity, electrolyte, and electrode material, prevents the very negative second reduction step from being as readily observed at conventionally sized Au and Pt electrodes unless the solvent is carefully purified, in which case both reduction processes also are well defined at these electrode surfaces in acetonitrile.

Extensive analysis of cyclic voltammetric data summarized in Table I at a scan rate of 100 mV s^{-1} at 25 ± 0.1 °C showed the first reduction process to be both chemically and electrochemically reversible at all electrodes. Although the peak to peak separation (ΔE_p) is slightly in excess of the expected 56 mV for a reversible one-electron process at 25 °C, this discrepancy in ΔE_p is attributable to uncompensated solution resistance since the known reversible one-electron oxidation of ferrocene under identical conditions also gives a similar peak to peak separation. The reversible half-wave potential ($E_{1/2}$) for this process was found to have an average value of $-1.350 \pm 0.003 \text{ V}$ vs Fc^+/Fc and is essentially independent of all working electrodes and supporting electrolytes. Process 1 is therefore confirmed^{2,21} to be suitable as an internal standard in acetonitrile.

The experimental data at the GC, Au, and Pt electrodes for the second reduction process in acetonitrile correspond to a simple reversible charge-transfer process, as was the case for the first reduction step, provided purified solvent is used. In liquid chromatographic grade solvent, overlap with the background reduction process occurs, particularly when gold or platinum electrodes are used. However, data at the HMDE do not correspond to completely ideal behavior. The wave height for the forward step is always greater than that for the

reverse step and the ratio of the oxidation and reduction peak currents ($i_p^{\text{ox}}/i_p^{\text{red}}$) is considerably less than unity. Additionally, the ΔE_p value is slightly greater than that observed at solid electrodes. However, the $E_{1/2}$ value for this process is also essentially independent of electrode material and supporting electrolyte with an average value of $-2.300 \pm 0.003 \text{ V}$ vs Fc^+/Fc , as is the difference between the half-wave potentials of the two processes ($\Delta E_{1/2}$) at a scan rate of 100 mV s^{-1} (average value of $951 \pm 4 \text{ mV}$).

The effect of the scan rate on the cyclic voltammograms obtained at the HMDE and GC electrode for a 1×10^{-3} M solution of $(\eta^5\text{-C}_5\text{H}_5)_2\text{CoPF}_6$ in CH_3CN in various supporting electrolytes at 25 ± 0.1 °C is summarized in Table II. Over the range of scan rates examined, the $E_{1/2}$ and $i_p^{\text{ox}}/i_p^{\text{red}}$ values were found to be virtually independent of scan rate for the first reduction process at both the HMDE and GC electrodes, while $E_{1/2}$ and $i_p^{\text{ox}}/i_p^{\text{red}}$ values were also found to be independent of scan rate for the second reduction process at the GC electrode, but not at the HMDE. For an uncomplicated reduction process, a plot of i_p^{red} vs $v^{1/2}$ at a conventionally sized electrode should be linear with intercepts at the origin. Such a plot yielded a linear fit for both processes at the GC electrode in acetonitrile, while linearity was only observed for the first reduction process at the HMDE in acetonitrile. Experimental differences between $\Delta E_{1/2}$ values lie within a 20-mV range at the HMDE and GC electrode over the range of scan rates examined. Thus, the second reduction process for cobaltocene can be used as a reference at the glassy carbon electrode (and gold and platinum electrodes, provided the solvent is sufficiently pure), whereas at a mercury electrode weak interaction of cobaltocene with the mercury surface makes this electrode material less suitable than the solid electrodes.

(b) Microelectrodes. Provided the electrode radius is sufficiently small and the scan rate is sufficiently slow,²⁷ sigmoidal-shaped steady-state voltammograms may be obtained at microdisk electrodes in many high-resistance solvents with negligible iR drop problems^{26,35} using the same potential waveform as for cyclic voltammetry at conventionally sized electrodes. Microelectrode measurements used under steady-state conditions may therefore be more useful in high-resistance organic solvents than conventionally sized electrodes for reference potential calibration purposes.

Figure 2 shows typical voltammograms obtained for the Cc^+/Cc process with a 1×10^{-3} M solution of $(\eta^5\text{-C}_5\text{H}_5)_2\text{CoPF}_6$ in acetonitrile (0.1 M Bu_4NBF_4) at 25 ± 0.1 °C at GC, Au, and Pt microdisk electrodes having radii around $5 \mu\text{m}$ using a scan rate of 10 mV s^{-1} . At slow scan rates essentially sigmoidal-shaped curves are observed for the first reduction process at all electrodes, as expected for steady state behavior, with the forward and reverse scans being superimposed. As the scan rate is progressively increased, the planar diffusion component becomes more significant (electrode sphericity is decreased) and the waves during the forward and reverse potential scans do not identically retrace each other. At sufficiently fast scan rates of potential, peaks are observed as for measurements with macro-sized electrodes. Voltammetric data at GC, Au, and Pt microdisk electrodes at 25 ± 0.1 °C as a function of scan rate are summarized in Table III. The $E_{1/2}$ values (average = $-1.350 \pm 0.003 \text{ V}$ vs Fc^+/Fc) for the first reduction process were found to be essentially constant and in agreement with values obtained under transient conditions at conventionally sized electrodes. These data confirm that the $E_{1/2}$ values measured from steady-state measurements may be used as a reference potential in acetonitrile.

(34) Lund, H. In *Organic Electrochemistry: An Introduction and a Guide*, 2nd ed.; Baizer, M. M., Lund, H., Eds.; Dekker: New York, 1983; p 192.

(35) Howell, J. O.; Wightman, R. M. *Anal. Chem.* 1984, 56, 524.

Table I. Cyclic Voltammetric Data at a Scan Rate of 100 mV s⁻¹ for Reduction of 1 × 10⁻³ M Cobaltocenium Hexafluorophosphate at Conventionally Sized Electrodes in Acetonitrile at 25 ± 0.1 °C

electrode	electrolyte (concn (M))	process 1 (C ^{c+} /C ^{c0})				process 2 (C ^{c0} /C ^{c-})				$\Delta E_{1/2}^c$ (mV)
		$E_p^{\text{red } a}$ (V)	$i_p^{\text{ox}}/i_p^{\text{red}}$	$E_{1/2}^a$ (V)	ΔE_p^b (mV)	$E_p^{\text{red } a}$ (V)	$i_p^{\text{ox}}/i_p^{\text{red}}$	$E_{1/2}^a$ (V)	ΔE_p^b (mV)	
HMDE	Et ₄ NClO ₄ (0.1)	-1.382	0.99	-1.350	64	-2.341	0.87	-2.301	79	951
	Bu ₄ NBF ₄ (0.1)	-1.378	0.99	-1.347	62	-2.336	0.88	-2.298	76	950
GC	Et ₄ NClO ₄ (0.1)	-1.384	0.99	-1.350	67	-2.338	0.99	-2.304	68	954
	Bu ₄ NBF ₄ (0.1)	-1.380	1.00	-1.348	64	-2.332	0.99	-2.297	70	949
Au ^d	Et ₄ NClO ₄ (0.1)	-1.387	0.99	-1.352	69	-2.336	1.00	-2.301	70	949
	Bu ₄ NBF ₄ (0.1)	-1.377	1.00	-1.345	68	-2.334	1.00	-2.300	68	955
Pt ^d	Et ₄ NClO ₄ (0.1)	-1.384	0.98	-1.348	72	-2.335	0.99	-2.300	70	952
	Bu ₄ NBF ₄ (0.1)	-1.386	0.99	-1.352	69	-2.332	0.99	-2.297	70	945

^a Reported as volts vs Fc⁺/Fc; actual reference electrode was Ag/Ag⁺ (0.1 M AgNO₃) in acetonitrile. $E_{1/2} = (E_p^{\text{ox}} + E_p^{\text{red}})/2$. ^b $\Delta E_p = E_p^{\text{red}} - E_p^{\text{ox}}$. ^c $\Delta E_{1/2} = E_{1/2}(\text{process 1}) - E_{1/2}(\text{process 2})$. ^d Data for process 2 could only be obtained in purified solvent at this electrode.

Table II. Effect of Scan Rate on Cyclic Voltammetric Data at Conventionally Sized HMDE and GC Electrodes for Reduction of 1 × 10⁻³ M Cobaltocenium Hexafluorophosphate in Acetonitrile at 25 ± 0.1 °C

electrode	electrolyte (concn (M))	scan rate (mV s ⁻¹)	process 1 (C ^{c+} /C ^{c0})				process 2 (C ^{c0} /C ^{c-})				$\Delta E_{1/2}^c$ (mV)
			i_p^{red} (μA)	$i_p^{\text{ox}}/i_p^{\text{red}}$	$E_{1/2}^a$ (V)	ΔE_p^b (mV)	i_p^{red} (μA)	$i_p^{\text{ox}}/i_p^{\text{red}}$	$E_{1/2}^a$ (V)	ΔE_p^b (mV)	
HMDE	Et ₄ NClO ₄ (0.1)	10	1.71	0.97	-1.344	66	2.39	0.77	-2.285	80	941
		50	4.55	0.99	-1.348	64	5.20	0.82	-2.294	79	946
		100	6.26	0.99	-1.350	64	9.21	0.87	-2.301	79	951
		500	14.1	1.00	-1.354	76	22.6	0.89	-2.303	93	949
		1000	19.5	1.00	-1.352	94	27.9	0.91	-2.305	112	953
	Bu ₄ NBF ₄ (0.1)	10	2.84	0.98	-1.346	69	3.64	0.79	-2.286	88	940
		50	4.89	0.98	-1.351	62	6.19	0.81	-2.297	80	946
		100	6.22	0.99	-1.347	62	11.1	0.88	-2.298	76	950
		500	15.4	1.00	-1.350	78	28.0	0.90	-2.302	100	952
		1000	21.2	1.00	-1.348	90	32.5	0.93	-2.302	116	954
GC	Et ₄ NClO ₄ (0.1)	10	10.7	0.98	-1.351	72	12.8	0.97	-2.292	74	941
		50	21.4	0.99	-1.349	75	22.9	0.99	-2.298	71	954
		100	29.2	0.99	-1.350	67	34.1	0.99	-2.304	68	954
		500	55.2	1.00	-1.351	89	70.8	1.01	-2.307	97	956
		1000	78.9	1.00	-1.353	104	91.9	1.00	-2.305	110	952
	Bu ₄ NBF ₄ (0.1)	10	8.95	0.99	-1.348	63	9.97	0.97	-2.286	72	938
		50	18.9	1.00	-1.345	68	21.6	0.99	-2.291	70	944
		100	26.1	1.00	-1.348	64	32.7	0.99	-2.299	70	951
		500	50.4	1.01	-1.352	91	63.6	1.00	-2.306	98	954
		1000	72.2	1.00	-1.353	104	84.1	1.00	-2.309	114	956

^a Reported as volts vs Fc⁺/Fc; actual reference electrode was Ag/Ag⁺ (0.1 M AgNO₃) in acetonitrile. $E_{1/2} = (E_p^{\text{ox}} + E_p^{\text{red}})/2$. ^b $\Delta E_p = E_p^{\text{red}} - E_p^{\text{ox}}$. ^c $\Delta E_{1/2} = E_{1/2}(\text{process 1}) - E_{1/2}(\text{process 2})$.

The Tomes potential difference ($E_{1/4} - E_{3/4}$)³⁶ was used to confirm electrochemical reversibility. The $E_{1/4} - E_{3/4}$ values for all electrodes over the range of scan rates examined were found to be Nernstian 58 ± 2 mV compared with the theoretical value of 56 mV for an electrochemically reversible one-electron process at 25 °C. In addition, plots of E vs $\log [(i_d - i)/i]$ where E = potential, i = current, and i_d = diffusion limiting current were linear with slopes close to the 59 mV theoretically expected for a one-electron reversible process at 25 °C. These data suggest that departures from ideality observed at conventional electrodes are attributable to a small amount of uncompensated resistance. The variation of limiting current with electrode radius for the first reduction process of Cc⁺ in acetonitrile obeys eq 4 at Au and Pt microelectrodes, and the first reduction process behaves as a simple reversible system for electrodes with radii in the range 5–50 μm and a scan rate of 10 mV s⁻¹.

Figure 2d shows a voltammogram obtained at the GC microdisk electrode over an extended potential range so as to include both reduction processes. At a scan rate of 10 mV s⁻¹ both processes are sigmoidal in shape and both limiting currents are controlled solely by radial diffusion. The $E_{1/4} - E_{3/4}$ values for the second reduction process at a scan rate of 10 mV s⁻¹ were found to have an average equal to 58 ± 2 mV compared with the theoretical value of 56 mV for an electrochemically reversible one-electron process at 25 ± 0.1

°C. A plot of E vs $\log [(i_d - i)/i]$ was linear with a slope close to the 59 mV expected for a reversible process. The $E_{1/2}$ (average = -2.302 ± 0.003 V vs Fc⁺/Fc) and $\Delta E_{1/2}$ (average = 953 ± 3 mV) were found to be essentially constant and in agreement with values obtained at conventional size electrodes, as expected for a reversible process. This result confirms that the second reduction step when measured at solid electrodes may also be an ideal process in acetonitrile for use as a reference redox process, provided solvent of sufficient purity is used.

Reduction of (η⁵-C₅H₅)₂CoPF₆ in Dichloromethane. (a) Conventional Electrodes. Dichloromethane is a widely used aprotic electrochemical solvent which has a low dielectric constant ($\epsilon = 8.9$).³⁴ Unfortunately, the highly resistive nature of CH₂Cl₂ often prevents highly accurate measurements from being made with conventionally sized electrodes because of problems with ohmic (iR) drop. As is the case in acetonitrile, data obtained (Table IV) for the first reduction step with a 1 × 10⁻³ M solution of (η⁵-C₅H₅)₂CoPF₆ in CH₂Cl₂ (0.1 M Bu₄NBF₄) at all electrodes at a scan rate of 100 mV s⁻¹ at 25 ± 0.1 °C suggest that the first reduction step may be described as a reversible diffusion-controlled process. While the ΔE_p values obtained at each electrode are significantly greater than the theoretical values for an electrochemically reversible process, this distortion is attributable to uncompensated solution resistance, as demonstrated by microelectrode data (see later). The $i_p^{\text{ox}}/i_p^{\text{red}}$ values are slightly less than unity,

(36) Tomes, J. *Collect. Czech. Chem. Commun.* 1937, 9, 50.

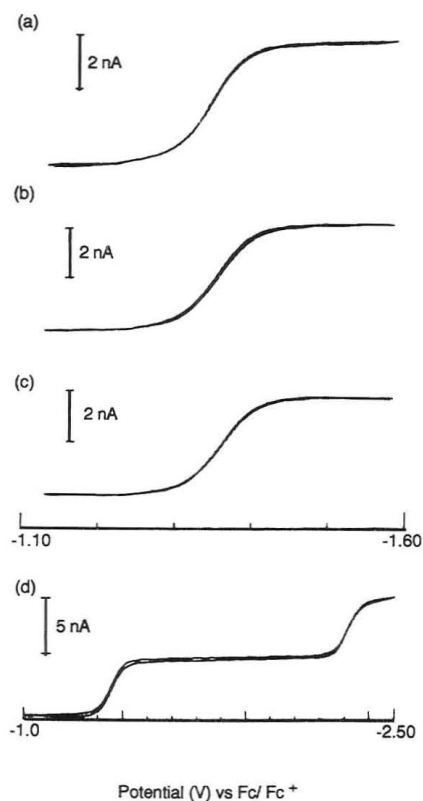


Figure 2. Voltammograms obtained at microelectrodes at 25 ± 0.1 °C for the first (a–c) and both (d) reduction processes with a 1×10^{-3} M solution of $(\eta^5\text{-C}_5\text{H}_5)_2\text{CoPF}_6$ in acetonitrile (0.1 M Bu_4NBF_4) at a scan rate of 10 mV s^{-1} at (a, d) a $5.8\text{-}\mu\text{m}$ -radius glassy carbon disk microelectrode, (b) a $5.2\text{-}\mu\text{m}$ -radius gold disk microelectrode, and (c) a $5.1\text{-}\mu\text{m}$ -radius platinum disk microelectrode.

again probably because of uncompensated solution resistance. Importantly, the calculated $E_{1/2}$ values were found to be essentially independent of electrode material and electrolyte with an average value of $-1.357 \pm 0.007 \text{ V vs Fc}^+/\text{Fc}$. A comparison with data obtained in acetonitrile under similar conditions shows that the average $E_{1/2}$ values for the first reduction process at all electrodes are in agreement in both solvents at the $\pm 10\text{-mV}$ level. This result suggests that in aprotic solvents the system Cc^+/Cc is a highly reversible couple whose redox potential relative to ferrocene does not change significantly as the dielectric constant changes from moderate to low values.

Parts a and b of Figure 3 show a comparison of cyclic voltammograms obtained for the second reduction process at a HMDE at 25 ± 0.1 and 2 ± 1 °C at a scan rate of 100 mV s^{-1} using liquid chromatographic grade solvent. At 25 °C, the second reduction step in this quality of solvent merges with the solvent background response. However at 2 °C a well-defined response is observed at the HMDE for the second reduction process even in liquid chromatographic grade solvent. The second response merges almost completely with the solvent process at the other electrode surfaces examined unless the solvent is carefully purified, in which case both processes are extremely well defined at all electrodes. The data for the second reduction process approach ideal behavior, provided conditions are chosen in which overlap with the solvent reduction process is avoided, even though the experimentally observed peak to peak separations are considerably greater than Nernstian due to uncompensated resistance. The ratio $i_p^{\text{ox}}/i_p^{\text{red}}$ approaches unity as the scan rate is increased. Plots of i_p^{red} vs $\nu^{1/2}$ are linear for both reduction processes at both 25 ± 0.1 and 2 ± 1 °C in purified dichloromethane.

The $E_{1/2}$ value for the second reduction process at the HMDE at 25 ± 1 °C was found to have an average value of

$-2.359 \pm 0.004 \text{ V}$ over the range of scan rates examined. The differences in $\Delta E_{1/2}$ values (average of $1004 \pm 6 \text{ mV}$) over the range of scan rates examined were found to be approximately 50 mV greater than those obtained in acetonitrile. The $E_{1/2}$ for the second reduction process and, therefore, the separation in potential between the two processes appears to be slightly solvent dependent in aprotic solvents relative to the ferrocene redox couple. The second reduction process may be used as a standard in carefully purified solvent. However, the proximity to the background reduction process may cause difficulties in less purified solvent media where lower temperatures and mercury electrodes are most likely to lead to the second process being easily measured.

(b) Microelectrodes. With a 1×10^{-3} M solution of $(\eta^5\text{-C}_5\text{H}_5)_2\text{CoPF}_6$ in dichloromethane (0.1 M Bu_4NBF_4) at 25 ± 0.1 °C and a scan rate of 10 mV s^{-1} , essentially sigmoidal-shaped steady-state curves are observed for the first reduction process at GC, Au, and Pt microdisk electrodes, as was the case in acetonitrile. The $E_{1/2}$ values (average = $-1.351 \pm 0.004 \text{ V vs Fc}^+/\text{Fc}$) are similar at GC, Au, and Pt microdisk electrodes and are also similar to those obtained at conventionally sized electrodes, while $E_{1/4} - E_{3/4}$ values (average = $59 \pm 3 \text{ mV}$) are close to the Nernstian value of 56 mV . The variation of limiting current with electrode radius for the reduction of Cc^+ is analogous to data obtained in acetonitrile at slow scan rates for electrodes with radii in the range $5\text{--}50 \mu\text{m}$, and a simple reversible process is observed in dichloromethane for the first reduction process, as was the case in acetonitrile at 25 ± 0.1 °C.

A useful feature associated with microelectrodes is that voltammetric measurements often can be made at potentials not accessible with conventionally sized electrodes.²⁷ An extended working range was observed in dichloromethane at microelectrodes which enabled the second reduction step of Cc^+ to be observed at a $5.8\text{-}\mu\text{m}$ GC microdisk electrode at 25 ± 0.1 °C in liquid chromatographic grade solvent. If the temperature of the liquid chromatographic grade solvent is lowered to 2 ± 1 °C, as was done for measurements with conventionally sized mercury electrodes, the second reduction process is almost completely resolved from the solvent process. However, if the solvent is purified by the IUPAC recommended method, both processes are very well defined at GC, Au, and Pt electrodes, with the second process being completely resolved from the solvent reduction process even at 25 °C (Figure 3c). Consequently, use of the second reduction step in dichloromethane is therefore not as easy as in acetonitrile under some of the conditions examined. If the second reduction process is to be used as a reference in dichloromethane, then the use of carefully purified solvent or a glassy carbon microelectrode or mercury electrodes at lower temperatures is recommended. Voltammetric data obtained at microelectrodes in dichloromethane are summarized in Table V.

Reduction of $(\eta^5\text{-C}_5\text{H}_5)_2\text{CoPF}_6$ in Ethanol. (a) Conventional Electrodes. Ethanol is a protic solvent which has a medium dielectric constant ($\epsilon = 24.5$).³⁴ Cyclic voltammograms for the two-step reduction of Cc^+ have been reported at mercury electrodes in basic ethanol solution.¹⁵ Cyclic voltammograms obtained for the first reduction process at a range of working electrodes for a 5×10^{-4} M solution of $(\eta^5\text{-C}_5\text{H}_5)_2\text{CoPF}_6$ in ethanol (0.1 M Bu_4NBF_4) at a scan rate of 100 mV s^{-1} and a temperature of 25 ± 0.1 °C exhibit close to ideal behavior. Voltammetric data for all conventionally sized electrodes at a scan rate of 100 mV s^{-1} and 25 ± 0.1 °C are summarized in Table VI. The $E_{1/2}$ value obtained for the first reduction process in this protic solvent has an average value of $-1.349 \pm 0.004 \text{ V vs Fc}^+/\text{Fc}$ at all electrodes and is similar to that obtained in acetonitrile and dichloromethane at the $\pm 10\text{-mV}$ level.

Table III. Voltammetric Data Obtained at Glassy Carbon, Gold, and Platinum Microelectrodes as a Function of Scan Rate for Reduction of 1×10^{-3} M Cobaltocenium Hexafluorophosphate in Acetonitrile (0.1 M Bu_4NBF_4) at 25 ± 0.1 °C

electrode (radius (μm))	scan rate (mV s^{-1})	process 1 (Cc^+/Cc^0)		process 2 (Cc^0/Cc^-)		$\Delta E_{1/2}^d$ (mV)	comment ^b
		$E_{1/4} - E_{3/4}$ (mV)	$E_{1/2}^a$ (V)	$E_{1/4} - E_{3/4}$ (mV)	$E_{1/2}^a$ (V)		
GC (5.8)	10	57	-1.347	57	-2.298	951	R
	20	56	-1.352	57	-2.305	953	R
	50	70	-1.350	66	-2.305	955	R, L
	100	68	-1.348	69	-2.300	952	R, L
Au (5.2) ^c	10	58	-1.349	56	-2.299	952	R
	20	57	-1.350	56	-2.298	952	R
	50	56	-1.352	57	-2.302	954	R
	100	60	-1.352	59	-2.300	952	R
	500	58	-1.350	60	-2.302	952	R, L
Pt (5.1) ^c	10	57	-1.348	58	-2.298	954	R
	20	57	-1.347	56	-2.300	953	R
	50	60	-1.351	58	-2.302	951	R
	100	56	-1.350	60	-2.302	952	R
	500	60	-1.348	60	-2.302	954	R, L

^a Volts vs Fc^+/Fc . ^b R: radial (edge diffusion), sigmoidal-shaped curve. R, L: radial (edge diffusion) dominant, but small peak present due to linear diffusion. L: linear diffusion dominant, peak-shaped curve. ^c Data for process 2 could only be obtained in purified solvent for this electrode. ^d $\Delta E_{1/2} = \Delta E_{1/2}(\text{process 1}) - \Delta E_{1/2}(\text{process 2})$.

Table IV. Cyclic Voltammetric Data Obtained at a Scan Rate of 100 mV s^{-1} for Reduction of 1×10^{-3} M Cobaltocenium Hexafluorophosphate at Conventionally Sized Electrodes in Dichloromethane at 25 ± 0.1 °C

electrode	electrolyte (concn (M))	process 1 (Cc^+/Cc^0)				process 2 ^c (Cc^0/Cc^-)				$\Delta E_{1/2}^d$ (mV)
		$E_p^{\text{red } a}$ (V)	$i_p^{\text{ox}}/i_p^{\text{red}}$	$E_{1/2}^a$ (V)	ΔE_p^b (mV)	$E_p^{\text{red } a}$ (V)	$i_p^{\text{ox}}/i_p^{\text{red}}$	$E_{1/2}^a$ (V)	ΔE_p^b (mV)	
HMDE	Et_4NClO_4 (0.1)	-1.398	0.96	-1.356	84	-2.414	0.97	-2.362	104	1006
	Bu_4NBF_4 (0.1)	-1.392	0.97	-1.351	82	-2.408	0.94	-2.359	98	1008
GC	Et_4NClO_4 (0.1)	-1.407	0.97	-1.359	95	-2.423	0.98	-2.368	110	1009
	Bu_4NBF_4 (0.1)	-1.402	0.99	-1.355	94	-2.415	0.97	-2.360	110	1005
Au	Et_4NClO_4 (0.1)	-1.393	0.98	-1.351	83	-2.410	0.98	-2.360	100	1009
	Bu_4NBF_4 (0.1)	-1.390	0.97	-1.348	84	-2.405	0.97	-2.356	98	1008
Pt	Et_4NClO_4 (0.1)	-1.417	0.96	-1.369	97	-2.424	0.97	-2.368	112	999
	Bu_4NBF_4 (0.1)	-1.411	0.96	-1.364	94	-2.415	0.97	-2.362	106	998

^a Reported as volts vs Fc^+/Fc ; actual reference electrode was Ag/AgCl (saturated LiCl) in dichloromethane. ^b $\Delta E_p = E_p^{\text{red}} - E_p^{\text{ox}}$. ^c Accurate data for process 2 could only be obtained in purified solvent. ^d $\Delta E_{1/2} = E_{1/2}(\text{process 1}) - E_{1/2}(\text{process 2})$.

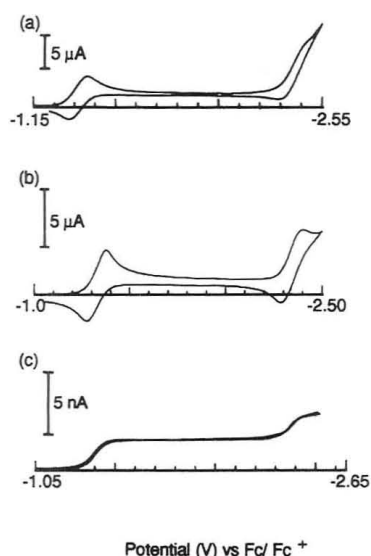


Figure 3. Voltammograms obtained for reduction of a 1×10^{-3} M solution of $(\eta^5\text{-C}_5\text{H}_5)_2\text{CoPF}_6$ in dichloromethane (0.1 M Bu_4NBF_4) at (a, b) a HMDE and (c) a 5.8- μm -radius glassy carbon microelectrode for the two reduction processes: (a) 25 ± 0.1 °C, scan rate 100 mV s^{-1} , liquid chromatographic grade solvent; (b) 2 ± 1 °C, scan rate 100 mV s^{-1} , liquid chromatographic grade solvent; (c) 25 ± 0.1 °C, scan rate 10 mV s^{-1} , purified solvent.

The second reduction process in ethanol is only readily observed at mercury electrodes using either liquid chromatographic grade or purified solvent. Overlap problems with the solvent response occur at the other electrodes examined. Cyclic voltammograms at the HMDE are shown in Figure 4

for a 5×10^{-4} M solution of cobaltocenium hexafluorophosphate in ethanol (0.1 M Bu_4NBF_4) as a function of scan rate at 25 ± 0.1 °C. Close to ideal behavior for a simple reversible system is observed for the first reduction process at all scan rates examined. However, the second reduction process at slow scan rates is not reversible, as evidenced by the ratio $i_p^{\text{ox}}/i_p^{\text{red}}$. As the scan rate is increased, well-defined peaks are observed on both the forward and reverse scans and the ratio $i_p^{\text{ox}}/i_p^{\text{red}}$ approaches unity. This behavior corresponds to a mechanism in which the electron transfer is reversible and a chemical reaction following the second charge-transfer process is irreversible. An average value of -2.376 ± 0.010 V vs Fc^+/Fc was obtained for $E_{1/2}$ of the second reduction process at scan rates in excess of 100 mV s^{-1} . The $\Delta E_{1/2}$ value (average = 1030 mV) is slightly larger than those obtained in acetonitrile and dichloromethane. The data imply that the second reduction process could be used as a standard at mercury electrodes with scan rates in excess of 100 mV s^{-1} , but not at lower scan rates or at the other electrode surfaces examined.

(b) Microelectrodes. Ideal steady-state voltammograms are observed for the Cc^+/Cc process with a 5×10^{-4} M solution of $(\eta^5\text{-C}_5\text{H}_5)_2\text{CoPF}_6$ in ethanol (0.1 M Bu_4NBF_4) at GC, Au, and Pt microelectrodes at slow sweep rates at 25 ± 0.1 °C. Voltammetric data as a function of scan rate are summarized in Table VII. $E_{1/2}$ values (average = -1.350 ± 0.004 V) are similar for all electrodes, while $E_{1/4} - E_{3/4}$ values (average = 62 ± 4 mV) are slightly larger than the Nernstian value of 56 mV. The variation of limiting current with electrode radius for the reduction of Cc^+ in ethanol (0.1 M Bu_4NBF_4) at Au and Pt microelectrodes is linear and analogous to data obtained in aprotic solvents at slow scan rates, and a simple

Table V. Voltammetric Data Obtained at Glassy Carbon, Gold, and Platinum Microelectrodes as a Function of Scan Rate for Reduction of 1×10^{-3} M Cobaltocenium Hexafluorophosphate in Dichloromethane (0.1 M Bu_4NBF_4) at 25 ± 0.1 °C

electrode (radius (μm))	scan rate (mV s^{-1})	process 1 (Cc^+/Cc^0)		process 2 ^c (Cc^0/Cc^-)		$\Delta E_{1/2}^d$ (mV)	comment ^b
		$E_{1/4} - E_{3/4}$ (mV)	$E_{1/2}^a$ (V)	$E_{1/4} - E_{3/4}$ (mV)	$E_{1/2}^a$ (V)		
GC (5.8)	10	60	-1.352	61	-2.361	1009	R
	20	59	-1.354	60	-2.363	1011	R, L
	50	62	-1.356	62	-2.364	1008	R, L
Au (5.2)	10	57	-1.348	58	-2.357	1009	R
	20	60	-1.346	60	-2.359	1013	R
	50	54	-1.346	60	-2.360	1014	R
	100	61	-1.350	62	-2.358	1008	R, L
	500	60	-1.353	63	-2.360	1007	R, L
Pt (5.1)	10	59	-1.349	59	-2.354	1005	R
	20	55	-1.347	59	-2.356	1009	R
	50	60	-1.351	62	-2.360	1009	R
	100	60	-1.353	62	-2.356	1003	R, L
	500	62	-1.354	62	-2.359	1005	R, L

^a Volts vs Fc^+/Fc . ^b R: radial (edge diffusion), sigmoidal-shaped curve. R, L: radial (edge diffusion) dominant, but small peak present due to linear diffusion. L: linear diffusion dominant, peak-shaped curve. ^c Process 2 is readily observed in purified dichloromethane. In liquid chromatographic grade solvent the process overlaps with the "solvent" discharge limit. ^d $\Delta E_{1/2} = E_{1/2}(\text{process 1}) - E_{1/2}(\text{process 2})$.

Table VI. Cyclic Voltammetric Data at a Scan Rate of 100 mV s^{-1} at Conventionally Sized Electrodes for Reduction of 5×10^{-4} M Cobaltocenium Hexafluorophosphate in Ethanol at 25 ± 0.1 °C

electrode	electrolyte (concn (M))	process 1 (Cc^+/Cc^0)				process 2 (Cc^0/Cc^-)				
		E_p^{red} (V)	$i_p^{\text{ox}}/i_p^{\text{red}}$	$E_{1/2}^a$ (V)	ΔE_p^b (mV)	E_p^{red} (V)	$i_p^{\text{ox}}/i_p^{\text{red}}$ (V)	$E_{1/2}^a$ (mV)	ΔE_p^b (mV)	$\Delta E_{1/2}^c$ (mV)
HMDE	Bu_4NBF_4 (0.1)	-1.376	0.97	-1.346	60	-2.398	0.74	-2.362	72	1016
	Et_4NClO_4 (0.1)	-1.375	0.96	-1.344	62	-2.400	0.72	-2.365	70	1021
GC	Bu_4NBF_4 (0.1)	-1.386	0.97	-1.356	69	<i>e</i>	<i>e</i>	<i>e</i>	<i>e</i>	<i>e</i>
	Et_4NClO_4 (0.1)	-1.385	0.95	-1.351	68	<i>e</i>	<i>e</i>	<i>e</i>	<i>e</i>	<i>e</i>
Au	Bu_4NBF_4 (0.1)	-1.390	0.94	-1.350	81	<i>e</i>	<i>e</i>	<i>e</i>	<i>e</i>	<i>e</i>
	Et_4NClO_4 (0.1)	-1.387	0.96	-1.347	80	<i>e</i>	<i>e</i>	<i>e</i>	<i>e</i>	<i>e</i>
Pt	Bu_4NBF_4 (0.1)	-1.393	<i>d</i>	-1.352	82	<i>e</i>	<i>e</i>	<i>e</i>	<i>e</i>	<i>e</i>
	Et_4NClO_4 (0.1)	-1.387	<i>d</i>	-1.345	84	<i>e</i>	<i>e</i>	<i>e</i>	<i>e</i>	<i>e</i>

^a Reported as volts vs Fc^+/Fc ; actual reference electrode was Ag/Ag^+ (0.1 M AgNO_3) in acetonitrile. $E_{1/2} = (E_p^{\text{ox}} + E_p^{\text{red}})/2$. ^b $\Delta E_p = E_p^{\text{red}} - E_p^{\text{ox}}$. ^c $\Delta E_{1/2} = E_{1/2}(\text{process 1}) - E_{1/2}(\text{process 2})$. ^d E_p^{ox} and related parameters for process 2 not measurable due to close proximity of solvent discharge. ^e Accurate measurements not possible due to proximity of solvent discharge process.

Table VII. Voltammetric Data Obtained at Glassy Carbon, Gold, and Platinum Microelectrodes as a Function of Scan Rate for Reduction Process 1 (Cc^+/Cc^0) for 5×10^{-4} M Cobaltocenium Hexafluorophosphate in Ethanol (0.1 M Bu_4NBF_4) at 25 ± 0.1 °C

electrode (radius (μm))	scan rate ^a (mV s^{-1})	$E_{1/4} - E_{3/4}$ (mV)	$E_{1/2}^b$ (V)	comment ^c
GC (5.8)	10	60	-1.344	R
	20	62	-1.348	R, L
	50	64	-1.342	R, L
	100	68	-1.350	L
Au (5.2)	10	62	-1.348	R
	20	63	1.352	R
	50	65	-1.354	R, L
	100	68	-1.347	L
Pt (5.1)	10	62	-1.350	R
	20	60	-1.351	R
	50	67	-1.355	R, L
	100	68	-1.354	L

^a Peak current rather than limiting current observed at a scan rate of 100 mV s^{-1} and $E_{1/2}$ calculated as $(E_p^{\text{ox}} + E_p^{\text{red}})/2$. ^b Volts vs Fc^+/Fc . ^c R: radial (edge diffusion), sigmoidal-shaped curve. R, L: radial (edge diffusion) dominant, but small peak present due to linear diffusion. L: linear diffusion dominant, peak-shaped curve.

reversible process is observed at 25 ± 0.1 °C. The use of GC microdisk electrodes extends the working potential range and allows the second reduction step to be observed in ethanol. However, the second reduction process is not completely resolved from the solvent response and mercury electrodes are to be preferred if this process is to be used as a reference in ethanol.

Reduction of $(\eta^5\text{-C}_5\text{H}_5)_2\text{CoPF}_6$ in Water. (a) Conventional Electrodes. Water is undoubtedly the most com-

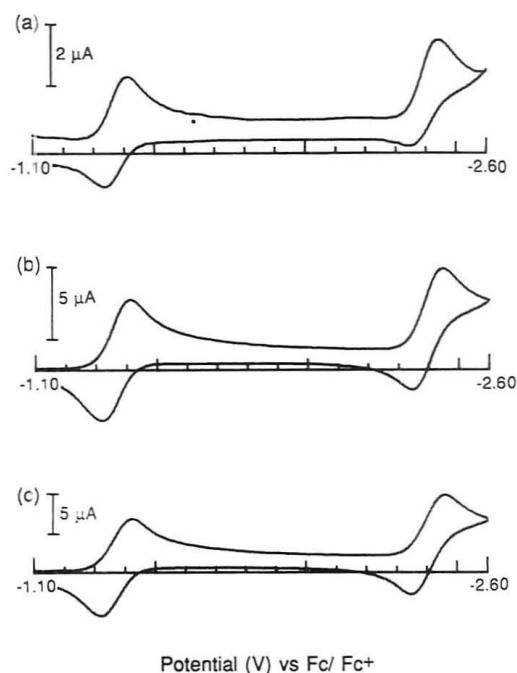


Figure 4. Cyclic voltammograms at a HMDE at 25 ± 0.1 °C for the two reduction processes with a 5×10^{-4} M solution of $(\eta^5\text{-C}_5\text{H}_5)_2\text{CoPF}_6$ in ethanol (0.1 M Bu_4NBF_4) at a scan rate of (a) 100 mV s^{-1} , (b) 500 mV s^{-1} , and (c) 1000 mV s^{-1} .

monly used electrochemical solvent and is a protic solvent which has a relatively high dielectric constant ($\epsilon = 80$).³⁴ Cyclic voltammetry was used to examine the reduction of the cobaltocenium cation in the presence of different supporting

Table VIII. Effect of Scan Rate on Cyclic Voltammetric Data at the HMDE and GC Electrodes for the Reduction of 1×10^{-4} M Cobaltocenium Hexafluorophosphate in Water with Various Supporting Electrolytes at 25 ± 0.1 °C

electrode	electrolyte (concn (M))	scan rate (mV s ⁻¹)	process 1 (Cc ⁺ /Cc ⁰)				process 2 (Cc ⁰ /Cc ⁻)				
			$E_p^{\text{red } a}$ (V)	$i_p^{\text{ox}}/i_p^{\text{red}}$	$E_{1/2}^a$ (V)	ΔE_p^b (mV)	$E_p^{\text{red } a}$ (V)	$i_p^{\text{ox}}/i_p^{\text{red}}$	$E_{1/2}^a$ (V)	ΔE_p^b (mV)	$\Delta E_{1/2}^c$ (mV)
HMDE	Li ₂ SO ₄ (0.1)	10	-1.389	0.97	-1.359	60	-1.961	<i>e</i>	-1.929	64	570
		50	-1.416	0.92	-1.380	72	-1.983	0.97	-1.945	60	565
		100	-1.434	0.89	-1.394	80	-1.995	0.99	-1.963	62	569
		500	-1.448	0.86	-1.400	97	-1.991	1.00	-1.956	70	548
		1000	<i>d</i>	<i>d</i>	<i>d</i>	<i>d</i>	-2.010	1.08	-1.972	76	<i>d</i>
GC		100	-1.433	0.64	-1.370	125	<i>e</i>	<i>e</i>	<i>e</i>	<i>e</i>	
HMDE	LiClO ₄ (0.1)	10	-1.394	0.98	-1.363	62	-1.971	<i>e</i>	-1.940	62	577
		50	-1.414	0.93	-1.381	65	-1.984	0.98	-1.955	59	574
		100	-1.428	0.87	-1.389	78	-1.992	0.99	-1.962	60	573
		500	-1.457	0.84	-1.410	93	-2.006	1.03	-1.971	69	561
		1000	<i>d</i>	<i>d</i>	<i>d</i>	<i>d</i>	-2.218	1.00	-1.979	79	<i>d</i>
GC		100	-1.426	0.67	-1.367	118	<i>e</i>	<i>e</i>	<i>e</i>	<i>e</i>	
HMDE	NaF (0.1)	10	-1.399	0.97	-1.362	63	-1.974	<i>e</i>	-1.942	64	<i>d</i>
		50	<i>d</i>	<i>d</i>	<i>d</i>	<i>d</i>	-1.984	<i>e</i>	-1.951	63	<i>d</i>
		100	<i>d</i>	<i>d</i>	<i>d</i>	<i>d</i>	-1.993	0.96	-1.958	71	<i>d</i>
		500	<i>d</i>	<i>d</i>	<i>d</i>	<i>d</i>	-2.016	0.99	-1.977	79	<i>d</i>
		1000	<i>d</i>	<i>d</i>	<i>d</i>	<i>d</i>	-2.023	1.00	-1.983	82	<i>d</i>
GC		100	-1.418	0.54	-1.362	112	<i>e</i>	<i>e</i>	<i>e</i>	<i>e</i>	

^a Reported as volts vs Fc⁺/Fc, actual reference electrode was Ag/AgCl (saturated KCl). $E_{1/2} = (E_p^{\text{ox}} + E_p^{\text{red}})/2$. ^b $\Delta E_p = E_p^{\text{red}} - E_p^{\text{ox}}$. ^c $\Delta E_{1/2} = E_{1/2}(\text{process 1}) - E_{1/2}(\text{process 2})$. ^d Presence of adsorption prevented accurate measurements from being made. ^e Not measurable due to close proximity of solvent discharge.

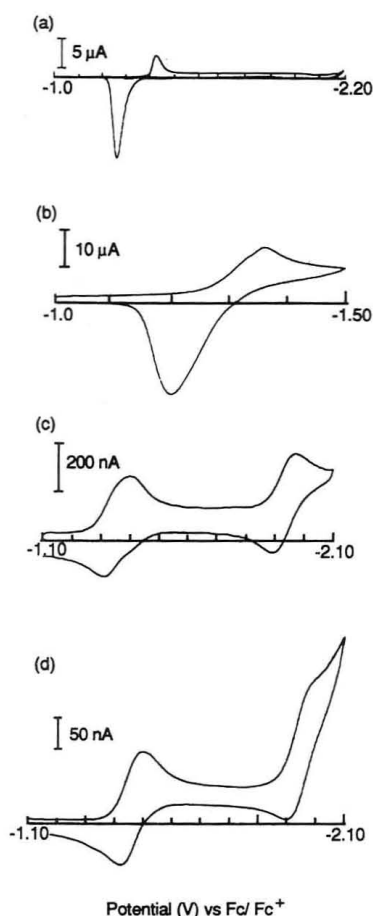


Figure 5. Cyclic voltammograms obtained under different conditions at conventionally sized electrodes at 25 ± 0.1 °C for reduction of $(\eta^5\text{-C}_5\text{H}_5)_2\text{CoPF}_6$ in water (0.1 M Li₂SO₄): (a) 1×10^{-3} M solution at a HMDE with a scan rate of 100 mV s^{-1} ; (b) 1×10^{-3} M solution at a glassy carbon electrode with a scan rate of 100 mV s^{-1} ; (c) 1×10^{-4} M solution at a HMDE with a scan rate of 100 mV s^{-1} ; (d) 5×10^{-5} M solution at a HMDE with a scan rate of 10 mV s^{-1} .

electrolytes (Li₂SO₄, LiClO₄, NaF) using HMDE, GC, Au, and Pt working electrodes. Parts a and b of figure 5 show cyclic voltammograms obtained at a HMDE and GC electrode for the reduction of a 1×10^{-3} M solution of $(\eta^5\text{-C}_5\text{H}_5)_2\text{CoPF}_6$ in 0.1 M Li₂SO₄ at 25 ± 0.1 °C at a scan rate of 100 mV s^{-1} .

At this concentration, a single reduction step is observed at both the HMDE and GC electrodes which is complicated by adsorption and/or precipitation phenomena, presumably related to the insolubility of the reduction product (cobaltocene) in aqueous media. Therefore, on reduction of high concentrations of Cc⁺, the surface of the electrode is effectively blocked, preventing the second reduction step from being observed in aqueous media. No response is observed at Pt and Au electrodes since the hydrogen evolution process limits the accessible working range.

In contrast to measurements in other solvents examined, much lower concentrations of Cc⁺ are required if the Cc⁺/Cc⁰ and Cc⁰/Cc⁻ couples are to be used as reference processes in water. Figure 5c shows the voltammogram obtained at a HMDE for the two-step reduction of a 1×10^{-4} M solution of $(\eta^5\text{-C}_5\text{H}_5)_2\text{CoPF}_6$ in 0.1 M Li₂SO₄ at a scan rate of 100 mV s^{-1} , while Figure 5d shows the voltammogram of a 5×10^{-5} M solution of $(\eta^5\text{-C}_5\text{H}_5)_2\text{CoPF}_6$ in 0.1 M Li₂SO₄ at a scan rate of 10 mV s^{-1} at 25 ± 0.1 °C. Under these more dilute conditions two well-defined processes are observed at the HMDE, whereas only the first reduction process is observed at the GC electrode because the available solvent limit range is inadequate. Voltammetric data for both processes at a HMDE in various supporting electrolytes are summarized in Table VIII.

It can be seen from the shape of the cyclic voltammogram in Figure 5d and voltammetric data in Table VIII, that if the concentration and sweep rate are sufficiently low, the influence of the adsorption decreases and close to a simple one-electron charge-transfer step is observed for the first reduction process. At slow scan rates (10 mV s^{-1}) with the HMDE the first reduction step is observed in all supporting electrolytes, and voltammetric data approach ideal behavior, with the peak to peak separation and the ratio $i_p^{\text{ox}}/i_p^{\text{red}}$ approaching the Nernstian value of 56 mV and unity, respectively. The average $E_{1/2}$ value at the HMDE for the first reduction process with a scan rate of 10 mV s^{-1} was $-1.361 \pm 0.002 \text{ V}$ vs Fc⁺/Fc, with the least complicated voltammograms being obtained with Li⁺ electrolyte. As the scan rate is increased ($500\text{--}1000 \text{ mV s}^{-1}$), the first reduction step becomes distorted relative to the ideal reversible shape, which illustrates the complex nature of this process in water. Slow scan rate conditions are therefore recommended for use of this process as a reference standard.

Voltammetric data for the second reduction process also approach the behavior expected for a simple one-electron diffusion-controlled process at low concentrations. Unfortunately, as the concentration of Cc^+ is decreased, the second reduction process becomes obscured by the hydrogen ion reduction wave and is difficult to characterize at slow scan rates (less than 100 mV s^{-1}), even at the HMDE, as shown in Figure 5d. The average $E_{1/2}$ value obtained at the HMDE for the second reduction process was found to be $-1.961 \pm 0.003 \text{ V}$ in all electrolytes at a scan rate of 100 mV s^{-1} and with a Cc^+ concentration of $1 \times 10^{-4} \text{ M}$. The ΔE_p and i_p^{ox}/i_p^{red} values for both processes therefore approach ideal behavior under the conditions noted above. In addition $\Delta E_{1/2}$ values (average = 568 mV) are essentially electrode, electrolyte, and scan rate independent at the $\pm 20\text{-mV}$ limit. However, $\Delta E_{1/2}$ values are significantly less than in other solvents examined. Since the potentials of Cc^+/Cc^0 are similar in all solvents relative to the Fc^+/Fc redox potential, this implies that the potential of the Cc^0/Cc^- couple is quite solvent dependent, relative to the ferrocene redox couple.

(b) Microelectrodes. The observation of peaked rather than sigmoidal-shaped responses for the first reduction process for $1 \times 10^{-3} \text{ M } Cc^+$ concentrations in water at a $5.8\text{-}\mu\text{m}$ -radius GC microdisk electrode is consistent with adsorption of Cc^+ and/or a complex nucleation and precipitation mechanism occurring for sparingly soluble and neutral cobaltocene produced at the electrode surface. Experiments in which the peak height on the reverse scan was examined as a function of switching potential or deposition time show that the peak height on the reverse scan increases with a more positive switching potential or with an increasing holding time at a fixed potential when more time is available for precipitation, which further supports this conclusion.

The effect of decreasing the concentration of Cc^+ , reduces the nonideality obtained at a microelectrode. However, the presence of the background current from the reduction of the hydrogen ion prevents a useful response from being observed at the $5.8\text{-}\mu\text{m}$ GC microdisk electrode at concentrations below 10^{-5} M and no completely ideal response suitable for a reference redox couple could be obtained with microelectrodes in water. Microelectrode measurements using the reduction of Cc^+ in water were therefore found to be less useful than those obtained with conventionally sized mercury electrodes for reference potential calibration purposes in aqueous media.

CONCLUSIONS

An investigation of the two-step reduction of $[(\eta^5\text{-C}_5\text{H}_5)_2\text{Co}]^+$ in a range of solvents at conventionally and micro-sized electrodes have revealed that under certain specified con-

ditions the Cc^+/Cc^0 couple and in some instances the Cc^0/Cc^- couple can be used as voltammetric reference systems. The reversible half-wave potential for the Cc^+/Cc^0 couple determined by voltammetric data in aprotic solvents was $-1.35 \pm 0.01 \text{ V}$ vs the Fc^+/Fc couple at $25 \pm 0.1 \text{ }^\circ\text{C}$ and is essentially independent of the electrode material and electrolyte in acetonitrile and dichloromethane. In protic solvents, the $E_{1/2}$ values occur at slightly more negative potentials relative to the ferrocene potential. The Cc^+/Cc^0 couple is therefore confirmed to be a useful voltammetric reference compound in a range of solvents since the $E_{1/2}$ value can be determined under many conditions. In contrast, the half-wave potential for the Cc^0/Cc^- couple was found to be considerably more solvent dependent and furthermore cannot always be determined accurately at $25 \pm 0.1 \text{ }^\circ\text{C}$ because of overlap and interaction with the "solvent" response and for a range of other reasons. The average reversible half-wave potential for the second reduction process at $25 \pm 0.1 \text{ }^\circ\text{C}$ was calculated to be $-2.300 \pm 0.003 \text{ V}$ in acetonitrile, $-2.359 \pm 0.004 \text{ V}$ in dichloromethane, $-2.376 \pm 0.010 \text{ V}$ in ethanol, and $-1.961 \pm 0.003 \text{ V}$ vs the Fc^+/Fc couple in water at a HMDE. The difference in the reversible half-wave potentials between the two reduction processes also was found to be solvent dependent relative to the ferrocene couple, with particularly significant differences being observed in water, relative to the value obtained in other solvents examined. While there has been considerable theoretical and practical interest⁹ in the solvent dependence of reversible potential data for different redox processes, since the Fc^+/Fc couple was chosen as an internal standard in this work, then except for differences on the potentials of these processes data presented are also related to how the ferrocene reference potential varies with solvent, and not solely to the absolute solvent dependence of the cobaltocene redox potentials. Consequently, no independent conclusions on the solvent dependence of the cobaltocene potentials can be made on the basis of data presented in this paper. On the basis of charge considerations, it is, in fact, probable that the solvent dependence of the Cc^0/Cc^- redox couple would directly correlate with that for the Fe^0/Fc^- process in the same way that the solvent dependence of the potentials of Fc^+/Fc^0 and Cc^+/Cc^0 redox couple appear to mimic each other.

ACKNOWLEDGMENT

The authors thank John Cooper for providing some of the data reported in purified solvent media.

RECEIVED for review March 5, 1992. Accepted September 21, 1992.

Long-Term, On-Line Monitoring of Microbial Biofilms Using a Quartz Crystal Microbalance

David E. Nivens,^{*,†,‡} James Q. Chambers,[†] Tina R. Anderson,[‡] and David C. White^{†,§}

Department of Chemistry and Center for Environmental Biotechnology, University of Tennessee, Knoxville, Tennessee 37932, and Environmental Science Division, Oak Ridge National Laboratory, Oak Ridge, Tennessee 37831

A quartz crystal microbalance was used to nondestructively monitor the formation of *Pseudomonas cepacia* biofilms. These experiments involved long-term monitoring over days. Long-term monitoring initially encountered problems associated with baseline drift which were not observed in short-term electrochemical experiments or studies performed in vacuum or air. The extent of baseline drift produced by fluctuations in hydrostatic pressure and temperature was ascertained. Results showed that 5-MHz AT-cut quartz crystals sealed into flow cells and exposed to aqueous environments were more sensitive to pressure and temperature changes than crystals exposed to air. A test system was designed to eliminate these interferences in order to monitor the frequency shift caused by the attachment and surface growth of *P. cepacia* cells. A calibration curve for the frequency shift corresponding to a given number of bacteria within a biofilm was generated, and the detection limit of the technique was determined to be 3×10^5 cells-cm⁻². The calibration curve was utilized to produce graphs of the number of attached cells versus time, and the first derivative curves were used to study rates of biofilm formation.

INTRODUCTION

Microorganisms are ubiquitous in most aqueous environments. Many of these microbes, which are present in aqueous systems such as lakes, oceans, municipal and industrial water systems, and even reagent bottles on laboratory benches, have a peculiar *modus operandi* in which they attach to surfaces and form gelatinous films termed biofilms. The literature on biofilms and biofilm processes has been extensively reviewed.¹⁻³ Biofilms are dynamic by nature and can influence interfacial, liquid phase, and surface chemistry. For instance, biofilms degrade waste in water treatment plants,⁴ reduce heat transfer in heat-exchange units,⁵ are a source of chemical as well as microbial contamination in water systems,⁶ and facilitate corrosion of metal structures.⁷ In medicine, biofouling has been implicated in the failure of implanted devices

such as catheters,⁸ voice prostheses,⁹ and endocardial pacemakers.¹⁰

Classical microbiological studies of biofilms involve methods that require the removal of the sample from its aqueous environment and subsequent microscopic, microbiological, or biochemical analyses. These off-line methodologies are plagued with problems resulting from sample removal and/or rinsing procedures that can alter or damage the biofilms. In addition, off-line methods are notoriously labor-intensive and do not provide instantaneous feedback. Therefore, microbiologists and microbial ecologists covet techniques that can provide *in situ* data on the formation of microbial biofilms.

On-line detection of developing biofilms has been accomplished with both microscopic and analytical techniques. Originally, microscopic techniques utilized time-lapsed videotape to record phase-contrast images of bacteria attaching to cellulose membranes.¹¹ Scanning confocal laser microscopy increased the resolution of the images and generated excellent three-dimensional views of biofilms.¹² Attenuated total reflection Fourier transform infrared spectroscopy provided molecular details about the inner portion of biofilms by generating infrared absorption spectra from bacteria located approximately 1 μ m from the surface of germanium crystals.¹³

The quartz crystal microbalance (QCM) is used to examine interfacial phenomena and study the formation of abiotic polymer films. This technique utilizes an AT-cut quartz crystal, a broad-band oscillator, and a frequency counter to monitor mass changes on the quartz resonator. Reviews of the QCM technique have been published.¹⁴⁻¹⁶ In biological systems, the QCM technique detected adenosine 5'-phosphosulfate reductase and human chorionic gonadotropin¹⁷ and indirectly detected microorganisms in the liquid phase by monitoring metabolite production.¹⁸ However, little attention has been given to use of the QCM for long-term monitoring in aqueous environments.

In the study described herein, the QCM was employed to monitor the attachment and surface growth of the bacterium

* Corresponding author: David E. Nivens, Center for Environmental Biotechnology, 10515 Research Drive, Building 1, Suite 300, Knoxville, TN 37932.

[†] Department of Chemistry, University of Tennessee.

[‡] Center for Environmental Biotechnology, University of Tennessee.

[§] Environmental Science Division, ORNL.

(1) *Adsorption of Microorganisms to Surfaces*; Marshall, K. C., Bitton, G., Eds.; John Wiley & Sons: New York, 1980.

(2) *Structure and Function of Biofilms*; Characklis, W. G., Wilderer, P. A., Eds.; John Wiley & Sons: New York, 1989.

(3) *Biofilms*; Characklis, W. G., Marshall, K. C., Eds.; John Wiley & Sons: New York, 1990.

(4) Bryers, J. D.; Characklis, W. G. In *Biofilms*; Characklis, W. G., Marshall, K. C., Eds.; John Wiley and Sons: New York, 1990; pp 671-696.

(5) Characklis, W. G. In *Biofilms*; Characklis, W. G., Marshall, K. C., Eds.; John Wiley & Sons: New York, 1990; pp 523-584.

(6) Patterson, M. K.; Husted, G. R.; Rutkowski, A.; Mayette, D. C. *Ultrapure Water* 1991, 8, 18.

(7) *Microbially Influenced Corrosion and Biodeterioration*; Dowling, N. J., Mittelman, M. W., Danko, J. C., Eds.; The University of Tennessee Press: Knoxville, 1990.

(8) Mahieu, H. F.; van Saene, H. K. F.; Rosingh, H. J.; Schutte, H. K. *Arch. Otolaryngol., Head Neck Surg.* 1986, 112, 321-228.

(9) Marrie, T. J.; Nelligan, J.; Costerton, J. W. *Circulation* 1982, 66, 1339-1346.

(10) Marrie, T. J.; Noble, M. N.; Costerton, J. W. *J. Clin. Microbiol.* 1983, 18, 1388-98.

(11) Kjelleberg, S.; Humphrey, B. A.; Marshall, K. C. *Appl. Environ. Microbiol.* 1982, 43, 1166.

(12) Lawrence, J. R.; Korber, D. R.; Hoyle, B. D.; Costerton, J. W.; Caldwell, D. E. *J. Bacteriol.* 1991, 173, 6558-6567.

(13) Nivens, D. E.; Chambers, J. Q.; Anderson, T. R.; Tunlid, A.; Smit, J.; White, D. C. *J. Microbiol. Methods*, in press.

(14) Deakin, M. R.; Buttry, D. A. *Anal. Chem.* 1989, 61, 1147A-1154A.

(15) Suhmacher, R. *Angew. Chem., Int. Ed. Engl.* 1990, 29, 329-343.

(16) Buttry, D. A. In *Electrochemical Interfaces*; Abruna, H. D., Ed.; VCH Publishers: New York, 1991, pp 531-566.

(17) Ebersole, R. C.; Ward, M. D. *J. Am. Chem. Soc.* 1988, 110, 8623-8628.

(18) Ebersole, R. C.; Foss, R. P.; Ward, M. D. *Bio/Technology* 1991, 9, 450-454.

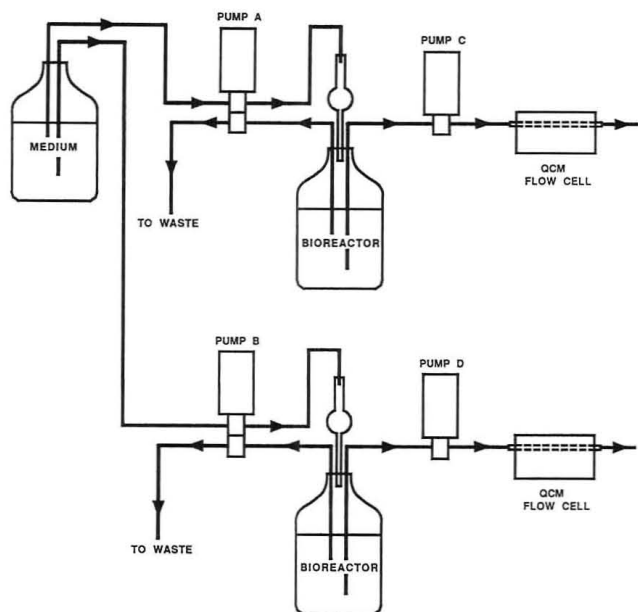


Figure 1. Diagram of flow system showing the direction of flow. Pumps A and B control the dilution rate in the bioreactors, and pumps C and D control the flow rate into the QCM flow cell.

Pseudomonas cepacia, which is a common contaminant in ultrapure water systems. This study was designed to simulate a microbial contamination event in a sterile water system. Microbial adhesion experiments involved long-term monitoring of frequency signals from quartz resonators and required strategies to eliminate signals due to random fluctuations in environmental parameters such as temperature and pressure.

EXPERIMENTAL SECTION

Bacterial Strain. *P. cepacia* (25416) was obtained from the American Typic Culture Collection (Rockville, MD). Stock cultures were maintained on nutrient agar slants and stored at -70°C in nutrient broth with 25% glycerol.

Growth Medium. The growth medium contained 5.7×10^{-6} M K_2PO_4 , 5.5×10^{-6} M glucose, 4.6×10^{-6} M NH_4Cl , 1.0×10^{-6} M MgSO_4 , 3.0×10^{-7} M CaCl_2 , 2.1×10^{-7} M NaCl , and a dilute Wolfe's mineral solution¹⁹ (9×10^{-8} M nitritotriacetic acid, 1.2×10^{-8} M MnSO_4 , 4×10^{-9} M FeSO_4 , 4×10^{-9} M CoSO_4 , 4×10^{-9} M ZnSO_4 , 2×10^{-9} M H_3BO_3 , 5×10^{-10} M CuSO_4 , 6×10^{-10} M NaSeO_4 , and 5×10^{-10} M NaMoO_4) in 18 M Ω -cm water. The final solution was titrated to pH 7.2. All chemicals were reagent-grade. The medium was sterilized with a 0.2- μm pore size filter.

Flow System. The flow system consisted of a medium reservoir, two constant-volume stirred bioreactors, two stainless steel heat exchange tubes (0.64-cm outer diameter), two flow cells, silicone tubing, four pumps, and two waste reservoirs (Figure 1). The 500-mL bioreactors were outfitted with an inlet drip tube, an exit line, an air stone, a stir bar, and a vent. The drip tube provided discontinuous flow which prevented microbial back-contamination of the medium reservoir. The exit line was positioned to maintain the volume of the flask at 350 mL. The flow rate into and out of the bioreactors was controlled with pumps A and B and was approximately 3.5 mL/min. The flow rates through the flow cells, which were controlled with pumps C and D, ranged from 2.4 to 3.2 mL/min. Because *P. cepacia* is a strict aerobe, the bioreactor fluid was stirred and sparged with air. Each flow cell was constructed from a block of Delrin (20 cm in length by 10 cm in width by 7.6 cm in thickness) cut into two sections. One section of the block was milled to form the flow channel and contained a resistance temperature detector (RTD), while a 2.54-cm-diameter AT-cut quartz crystal was sealed with silicone glue into the other section. The two sections were

sealed with a silicone gasket and bolted together. The volume of the flow cell was approximately 30 mL. The flow cells were sterilized by ethylene oxide, while the rest of the flow system was autoclaved (20 psi and 120°C for 25 min). The waste lines exited into a constant volume overflow tube that was housed within a sterile reservoir. The overflow tube was located approximately 1 m above the flow cell to maintain stable back-pressure on the flow cell.

QCM Analysis. Both sides of 5-MHz AT-cut quartz crystals (Valpey-Fischer, Hopkinton, MA) were coated with approximately 1000 Å of chromium followed by 2500 Å of gold in a keyhole pattern of different radii. A gold surface with a radius of 3 mm was exposed to air and a gold surface with a radius of 5 mm was exposed to the aqueous environment. Wires soldered onto the gold electrodes provided the electrical connection to the oscillator boards that were contained within Al boxes mounted onto the flow cells. Eight 9-V batteries connected in parallel provided power for up to 16 days. A voltage regulator chip provided a stable 5-V input signal. The oscillation frequency was measured at 5-min intervals by a dual-channel 775A frequency counter (Keithley Instruments, Cleveland, OH). Resistance measurements, also taken at 5-min intervals, were performed with a Keithley 196 digital voltmeter and 705 scanner to determine the temperature in the flow cell. The QCM flow cells and the heat-exchange tubing were placed in a Faraday cage/constant temperature box ($\pm 0.15^{\circ}\text{C}$), and the entire flow system was housed in a constant temperature room ($\pm 0.3^{\circ}\text{C}$).

An Asyst (Rochester, NY) program was written to control data acquisition through a general-purpose interface bus. In addition, Asyst was used to convert the frequency shift data into cell count data, differentiate the cell count data, and smooth the differentiated data using a low-pass Blackman filter with a cut-off frequency of 1 h^{-1} .

Experimental Procedures. Studies were performed to establish the magnitude of the frequency shifts associated with pressure and temperature changes. Temperature studies were performed in the flow cell under no-flow conditions. The frequency response was monitored as the bath temperature was increased at 0.2 and 0.3°C intervals from 22°C to 28°C and subsequently returned to 22°C . The temperature of the solution was monitored with the RTD. The exit line was vented to atmospheric pressure.

In the pressure-response experiments, pressure was controlled by a needle valve downstream of the flow cell and monitored with pressure gauges. An upstream pump recirculated water through the system at a flow rate of 3.2 mL/min using reinforced high-pressure silicone tubing. The pressure was increased, and the observed pressure and frequency shift was recorded. The observed frequencies were referenced to the frequency in the flow cell with the needle valve completely open. The temperature was maintained at $25.00 \pm 0.15^{\circ}\text{C}$.

In the microbial biofilm experiment, stability tests were performed prior to the start of the experiments. The first test examined the short-term stability of the frequency signal in air. If it remained stable within ± 0.5 Hz over a 5-min interval, the medium was pumped into the bioreactors and subsequently into the flow cells at flow rates ranging from 2.4 to 3.2 mL/min. The flow through the flow cell was calculated to be laminar with a worst case Reynolds's number of 30. Constant drift (1–3 Hz/h) was usually associated with new quartz resonators. This drift may be associated with chemical modifications of the gold surface, such as gold oxidation and chemical adsorption. Within 24 h, the temperature of the flow system equilibrated, and a 24-h culture containing actively growing bacteria was inoculated into the bioreactor. The number of bacteria in the inoculum was determined by acridine orange epi-fluorescent microscopy (described below). After inoculation, the biofouling event was monitored by the QCM. At the end of each experiment, the number of bacteria in the liquid phase and the number of cells attached to the surface were determined.

Bacterial Cell Counts. The number of bacteria in the inoculum, liquid phase, and biofilm were determined by an acridine orange (dibenzo[*b,e*]pyridine) staining procedure utilizing stained black Nuclepore filters (Costar, Cambridge, MA).

(19) Balch, W. E.; Fox, G. E.; Nagrum, L. J.; Woese, G. R.; Wolfe, R. S. *Microbiol. Rev.* 1979, 43, 260–296.

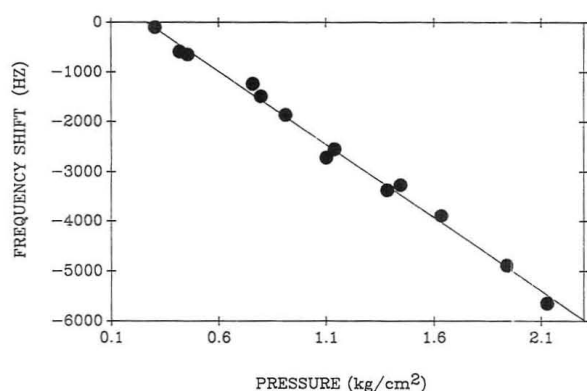


Figure 2. Plot of the frequency shift of a 5-MHz AT-cut quartz crystal with pressure change at a flow rate of 4 mL/min and 25.0 ± 0.15 °C. The data can be fit to a linear function with the equation, $y = 2940x + 781$ ($r^2 = 0.997$).

The AO counting method²⁰ is commonly used in microbiology to estimate biomass and was the method of choice in these experiments because no other methods that estimate biomass have low enough detection limits. The staining procedure involved transferring an aliquot of a bacterial cell suspension to the filter apparatus and subsequent addition of 2 mL of a 2.7×10^{-4} M acridine orange solution. After approximately 3 min, the filter was removed, dried, placed on a drop of immersion oil, and visualized with a microscope equipped with a 100-W mercury vapor source and epi-fluorescent collection optics (Nikon, Garden City, NJ). Twenty-five microscopic fields (100 by 100 μm) were counted, and the mean and standard deviation of the cell counts were determined.

Direct counting of bacteria on the gold surface was not possible because *P. cepacia* grows in colonies on surfaces. Biofilm bacteria were fixed by replacing the medium with 2.5% glutaraldehyde in 0.1 M phosphate buffer (pH 7.2). After fixation, a 2.8-cm-diameter plastic tube and a silicone gasket were placed around the quartz crystal, and 10 mL of sterile phosphate solution was added. The solution was sonicated for 10 s at 15 W to remove the bacteria from the surface. The quartz crystals were examined after sonication to ensure complete removal. The bacterial suspension was transferred to the filter apparatus, stained, and counted.

Scanning Electron Microscopy. Biofilm microorganisms attached to the quartz resonators were fixed in 2.5% glutaraldehyde in 0.1 M potassium phosphate buffer for 30 min. The crystals were removed from the flow cells, dried with a series of acetone/water solutions, and postfixed with osmium tetroxide. Following evaporation of 100 Å of gold/palladium alloy, the sample was examined using an ETEC Autoscan microscope.

RESULTS AND DISCUSSION

Pressure Effects. Elevated pressures were investigated because these conditions would be encountered in water systems. The frequency of the QCM in our experiments proved to be more sensitive to pressure changes than those reported for QCM's exposed to vacuum or air. Using a QCM to monitor the mass of particles suspended in the atmosphere, Olin and Sems reported that ambient fluctuations of ± 0.07 $\text{kg}\cdot\text{cm}^{-2}$ caused a frequency shift of less than 1 Hz.²¹ However, we found that the frequency shift data for a given increase in hydraulic pressure fit a linear function ($r^2 = 0.996$) with a slope of -2970 $\text{Hz}\cdot\text{cm}^{-2}\cdot\text{kg}^{-1}$ for pressure increased to $+2.1$ $\text{kg}\cdot\text{cm}^{-2}$ (Figure 2).

The increased sensitivity of the QCM to pressure changes can be traced to the manner in which the pressure was applied in our experiments. One side of the crystal was exposed to hydrostatic pressure, while the other side remained at

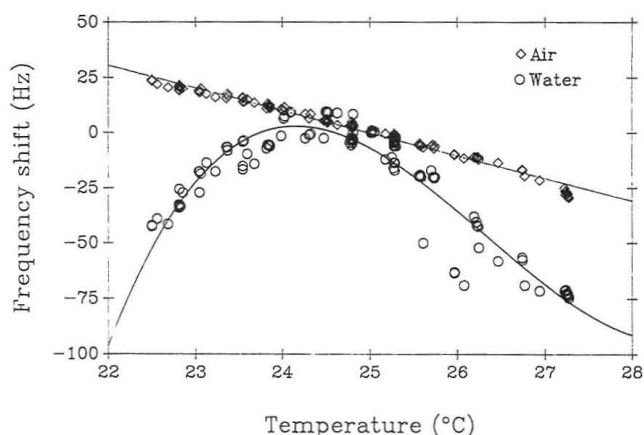


Figure 3. Comparison of the frequency shift versus temperature for a stressed AT-cut quartz crystal exposed to sterile water under no-flow conditions at ambient pressures (O) and an unstressed crystal in air (\diamond).

atmospheric pressure. For pressure increases on one side of the crystal, Heusler et al. found that the relationship between pressure and frequency shift was parabolic when pressure was varied from $+0.12$ to -0.12 $\text{kg}\cdot\text{cm}^{-2}$.²² A $+0.12$ $\text{kg}\cdot\text{cm}^{-2}$ pressure increase produced approximately a -175 -Hz shift. It was suggested that increasing the hydrostatic pressure on one side of the crystal results in a distortion in the crystal which in turn produces the frequency shift.

Temperature Effect. The effect of temperature on the oscillation frequency has been documented for AT-cut quartz crystals, where the temperature coefficient for an AT-cut quartz crystal at 25 °C is typically about 0.05 $\text{ppm}\cdot\text{°C}^{-1}$, and the temperature response can be fit to a third-order equation.²³ However, when the 5-MHz AT-cut quartz crystals are sealed into a flow cell and one side of the crystal is exposed to water, the temperature response is dramatically changed (Figure 3). For temperatures ranging between 22 and 28 °C, the frequency response of the crystals can be represented by a linear function in air and a parabolic function for a quartz crystal sealed into a flow cell and filled with water (no flow). Zero hertz was arbitrarily assigned to 25.000 °C. Increased temperature responses for crystals sealed in a flow cell and exposed to water have also been reported by Buttry¹⁶ who suggested that this effect could be attributed to viscosity and density changes associated with pure water at increased temperatures. However, increasing the temperature from 20 to 30 °C produces a monotonic decrease in water density from 0.998 to 0.996 $\text{g}\cdot\text{cm}^{-3}$ and monotonic increase in viscosity from 1.0020 to 0.7975 cP.²⁴ Thus, density and viscosity changes do not explain the parabolic nature of this curve. As with the pressure response, it can be hypothesized that the hydraulic pressure caused mechanical stress on the crystal sealed in a flow cell, which in turn altered the temperature response of the crystal. In order to avoid frequency shifts caused by temperature fluctuations, the temperature was maintained at 25.00 ± 0.15 °C.

Effects of Microbial Biofilms. Tests were performed to ascertain the stability of the QCM under sterile conditions with constant temperature and pressure. The measured frequency shift resulting from the introduction of sterile medium into the flow cell was -2028 ± 241 Hz. A value of -670 Hz is calculated using the relationship derived by Gordon and Kanazawa for viscous over layers.²⁵ The discrepancy in

(20) Hobbie, J. E.; Daley, R. J.; Jasper, S. *Appl. Environ. Microbiol.* 1977, 33, 1225-1228.

(21) Olin, J. G.; Sems, G. J. *Atmos. Environ.* 1971, 5, 653-668.

(22) Heusler, K. E.; Grzegorzewski, A.; Jackel, L.; Pietrucha, J. *Ber. Bunsen-Ges. Phys. Chem.* 1988, 92, 1218-1225.

(23) *Application of Piezoelectric Quartz Crystal Microbalance*; Lu, C., Czanderna, A., Eds.; Elsevier: New York, 1984.

(24) *Handbook of Chemistry and Physics*; Weast, R. C., Astle, M. J., Beyer, W. H., Eds.; CRC Press, Inc.: Boca Raton, FL, 1988.

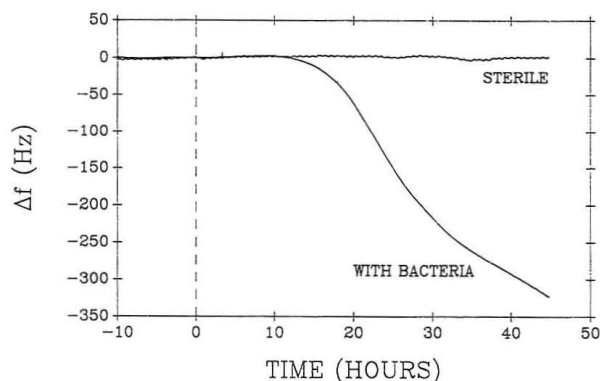


Figure 4. Graph comparing the frequency response of the QCM monitoring a sterile flowing medium versus biofilm formation. Inoculation time is at time zero, and the frequency at the inoculation time was arbitrarily set to 0.0 Hz.

these results is caused in part by the hydrostatic pressure in the flow cell. A stable frequency was monitored for a 54-h interval and the long-term drift noise was ± 4.0 Hz (Figure 4). In addition, the short-term noise was less than 0.5 Hz for a given 5-min interval.

Figure 4 compares the frequency shift data for a flow system inoculated with *P. cepacia* cells with the frequency data of the sterile control. In this graph, negative time represents the stabilization period following the introduction of water and prior to inoculation at time zero. In the experiment of Figure 4, 3 mL of a culture containing $(7 \pm 3) \times 10^7$ bacteria·mL⁻¹ was inoculated into a bioreactor. The dead volume of the tubing was approximately 70 mL, and the flow rate was 2.4 mL/min, thus unretained substances should arrive in the flow cell in approximately 30 min. However, the frequency did not decrease until approximately 10 h. The delay probably resulted from adsorption of the inoculum-bacteria to surfaces upstream of the flow cell and only a few inoculum-bacteria (less than the detection limit) attached to the quartz resonator. In an ancillary experiment performed in flasks, most *P. cepacia* cells in the liquid phase adsorbed to the side of the flasks within minutes (result not shown). The attachment event has been described as a two-step process: reversible adsorption followed by irreversible chemisorption possibly facilitated by extracellular polymers, organelles, or fimbriae.¹ Therefore, inoculum-bacteria must desorb or produce daughter cells to generate liquid-phase cells that can adsorb downstream onto the quartz resonator.

Attached bacteria utilize adsorbed nutrients²⁶ and/or nutrients from the bulk phase, replicate, and form colonies. The negative frequency shift after 10 h results mainly from surface growth of the attached bacteria. However, a portion of the signal also may result from viscosity and density changes in the solution at the QCM interface caused by actively growing bacteria or biomass from newly adsorbed liquid-phase bacteria. As the biomass increases, the frequency continues to decrease. After a -325-Hz frequency shift, the surface density of microorganisms was determined to be 3.3×10^7 cells·cm⁻² by the AO counting procedure. *P. cepacia* cells are rod shaped with an approximate length of 1 μ m and a width of 0.5 μ m. Thus, the surface coverage of the bacteria is calculated to be approximately 17%.

Similar experiments were stopped at different frequency shifts, and the number of bacteria on the surface were determined. The calibration curve of measured frequency shift versus the number of *P. cepacia* cells within the biofilm matrix is presented in Figure 5. The relationship between biofilm cell counts and frequency shift is monotonic for 2

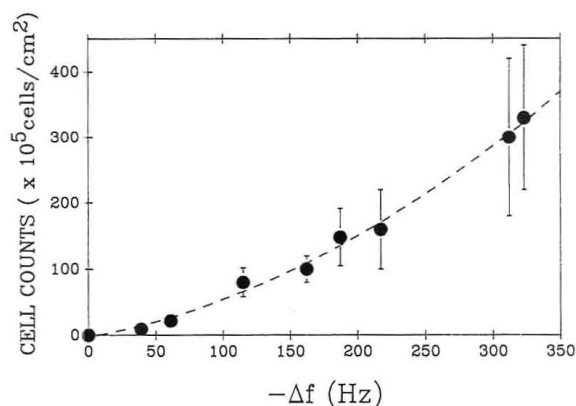


Figure 5. Plot of the number of attached bacteria within a biofilm versus frequency shift. Empirically, the plot can be fit to a second-order equation (eq 1, $r^2 = 0.995$).

orders of magnitude but not linear. Empirically, the plot can be represented by a parabolic function ($R^2 = 0.995$) with the equation

$$N_c = -2.84 + 0.37|\Delta f| + 0.002|\Delta f|^2 \quad (1)$$

where N_c is 10^5 cells·cm⁻² and Δf is the frequency shift. A conservative estimate of the limits of detection were calculated from the equation for the curve and the long-term drift noise. The detection limit was determined to be 3×10^5 *P. cepacia* bacteria·cm⁻².

A comparison of the precision of the cell counts and frequency measurements is of interest. The AO cell counting method typically has large relative errors resulting from nonuniform surface coverage of bacteria on the filters.²⁰ The QCM frequency shifts, on the other hand, are very precise: 5-MHz frequency signals were measured to 0.01-Hz accuracy and long-term drift noise was ± 4 Hz.

The nonlinearity of the calibration curve may be attributed to microbiological effects such as (1) colony formation, (2) cell shrinkage, and (3) extracellular polymer production. Scanning electron and AO epi-fluorescent microscopy showed that *P. cepacia* cells tend to remain closely packed in colonies that were evenly distributed on the surface of the resonator. Moreover, growth within the colonies is longitudinal along the solid/liquid interface, and larger colonies contained cells that do not contact the surface (Figure 6). This type of contiguous colonization behavior has been observed by computer-enhanced microscopy for *Pseudomonas fluorescens*.²⁷ It can be hypothesized that the shear wave, which in water penetrates approximately 2500 Å,²⁵ may not propagate far enough into nonrigid biofilms to detect bacteria not contacting the surface. The acoustic properties of a *P. cepacia* cell are unknown and may not remain constant. Secondly, bacteria within biofilms on densely populated portions of the surfaces (colonies) could decrease in size due to nutrient limitation, thus increasing the number of bacteria per unit biomass. Bacteria decrease in size under nutrient limited conditions.²⁸ Finally, bacteria produce extracellular polymers that may alter the viscoelastic properties of biofilms which in turn effects the frequency response. For example, *Pseudomonas atlantica* produces extracellular polymers in response to physiological stress.²⁹ These extracellular poly-

(27) Lawrence, J. R.; Delaquis, P. J.; Korber, D. R. *Microb. Ecol.* 1983, 14, 1.

(28) Humphrey, B.; Kjelleberg, S.; Marshall, K. C. *Appl. Environ. Microbiol.* 1983, 45, 43.

(29) Uhlinger, D. J.; White, D. C. *Appl. Environ. Microbiol.* 1983, 45, 64.

(30) Sauerbrey, G. *Z. Phys.* 1959, 155, 206.

(31) Miller, J. G.; Bolef, D. I. *J. Appl. Phys.* 1968, 39, 4589.

(32) Lu, C.; Lewis, O. J. *J. Appl. Phys.* 1972, 43, 4385.

(25) Gordon, J. G.; Kanazawa, K. K. *Anal. Chem.* 1985, 57, 1770.

(26) Power, K.; Marshall, K. C. *Biofouling* 1988, 1, 163.

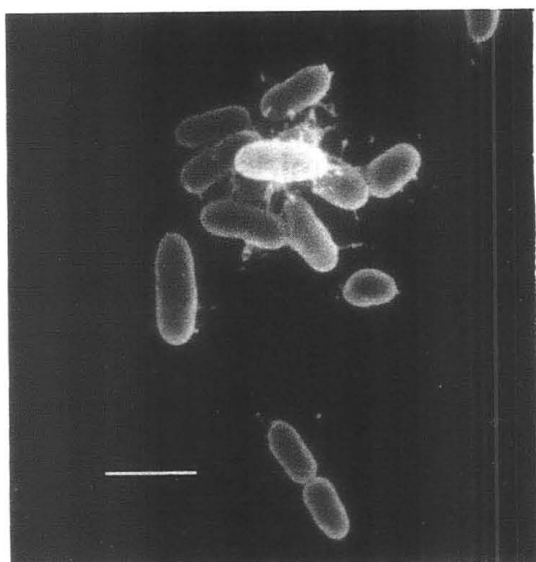


Figure 6. Electron micrograph showing colony formation on the oscillating gold surface of a QCM. *P. cepacia* tends to colonize the surface along the solid/liquid interface but eventually forms layers that do not contact the surface. The filamentous substance is assumed to be extracellular polymers. The bar equals 1 μm .

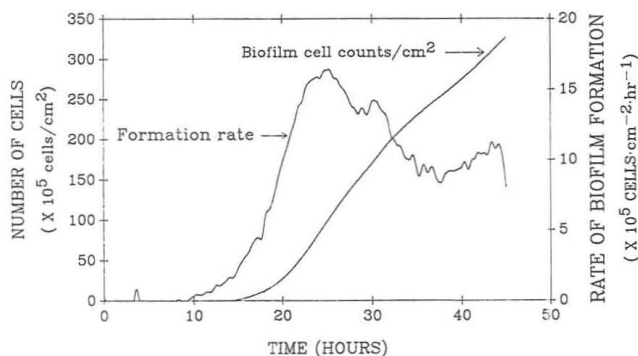


Figure 7. Graph presenting the cell count data versus time as predicted by eq 1 for the data shown in Figure 4 (left axis). The graph also shows the first derivative of the cell counts versus time data (right axis). This first derivative plots shows the instantaneous rate of biofilm formation versus time.

mers act as molecular bridges creating chemical bonds, dipole interactions, and/or hydrophobic interactions between the surface and the microbes present in the biofilm.³ Evidence for the existence of extracellular polymer in colonies and mature *P. cepacia* biofilms has been observed in electron micrographs where the polymers have collapsed in preparation and appear as filaments (Figure 6).

(33) Ingraham, J. L.; Maaloe, O.; Neidhardt, F. C. *Growth of the Bacterial Cell*; Sinauer Associates, Inc.: Sunderland, MS, 1983; p 3.

The calibration curve (Figure 5) was also used to predict the number of bacteria attached to the oscillating gold surface. Using the empirically derived equation for the calibration curve, the frequency shift curve from Figure 4 was converted into bacterial counts per unit area curve (Figure 7). From these data, the first derivative of the bacterial count data with respect to time was generated to determine the replication/attachment rate of bacteria within the biofilm. From Figure 7, the rate of biofilm formation increased dramatically at 10 h and achieved a maximum rate of 1.7×10^6 cells·cm⁻²·h at approximately 25 h.

Mathematical models for conversion of Δf into mass have been derived.³⁰⁻³² Sauerbrey developed an equation that directly relates the Δf to the mass load but assumes that the shear modulus of the attached layer is the same as quartz.³⁰ Relating Δf to biofilm-biomass is inappropriate because nonrigid living biofilms violate this assumption. Nonetheless, application of the Sauerbrey equation and eq 1 at the frequency shift corresponding to the detection limit gave an estimate of the wet mass of a single attached *P. cepacia* cell of 0.8 pg, which is comparable to the literature values of 1 pg obtained for an *Escherichia coli* cell grown on rich medium.³³ Frequency conversion models other than the Sauerbrey theory are more appropriate for viscoelastic layers but require prior knowledge of the acoustic properties of the adsorbed layers. Little is known about the viscoelastic properties of biofilms, but it would seem likely that these properties are dynamic and change with the physiological status of the bacteria within a biofilm.

In summary, the results presented here demonstrate that the QCM methodology can monitor sterile aqueous environments for days. Thus, it may be possible to use the QCM as an extremely sensitive remote sensing device for microbial contamination in ultrapure water systems. In addition, these results were consistent with the general knowledge of biofilm formation. The technique can also monitor the rate of biofilm formation. Future experiments will consider the effect of varying surface and liquid-phase chemistry on biofilm formation and will attempt to employ temperature and pressure compensation methods.

ACKNOWLEDGMENT

The research was supported by the National Aeronautics and Space Administration (NAS8-38493), the National Science Foundation (CHE-8718057), and the Office of Navy Research (N00014-88-k-0012). The oscillation board was a gift of Owen B. Melroy, IBM, San Jose, CA. The authors thank C. Dial, J. Sniatecki, and J. Stafford for their respective contributions.

RECEIVED for review July 17, 1992. Accepted October 16, 1992.

Vector Representation, Feature Selection, and Fingerprinting: An Application of Pattern Recognition to Pyrolysis-Gas Chromatography/Mass Spectrometry of Nucleosides

Rachhpal S. Sahota[†] and Stephen L. Morgan*

Department of Chemistry & Biochemistry, University of South Carolina, Columbia, South Carolina 29208

An approach for representing chromatograms as vectors using mass spectra to validate peak comparisons has been developed. Feature selection was employed to produce standard vectors that enhance discrimination between different classes of samples. Pyrolysis-gas chromatography/mass spectrometry fingerprints for five nucleosides were generated from replicate analyses. Unknowns were classified by Euclidean and Mahalanobis distance measures from these representative fingerprints. A combination of fingerprinting and feature selection is also shown to be effective in recognizing unique chemical markers for different classes of samples.

INTRODUCTION

The availability of lower cost bench-top mass spectrometric (MS) detectors has made qualitative identification of chemical components of complex mixtures common in gas chromatography (GC). Analytes of interest are often targeted with sample clean-up steps and selected ion data acquisition for maximum selectivity and sensitivity. However, GC/MS is also applied when the specific analytes of interest are not precisely known in advance. In such profiling applications, chromatographic and/or MS data interpretation has ranged from regression methods for calibration to multivariate statistical methods for fingerprinting and classification.¹ Analytical pyrolysis,^{2,3} in which samples are thermally degraded in the absence of oxygen, has been a particularly fertile area for chemometrics.²⁻¹⁰ The composition of the original sample is indirectly inferred from the pyrolyzate mixture, separated by capillary GC prior to MS or analyzed directly by MS. Capillary pyrograms can be complex and may consist of several hundred chromatographic peaks. Further, the absence of pure standards often hinders identification of pyrolysis products. Attempts at comparing, classifying, and understanding these patterns generally invite multivariate data handling methods.

How to represent chromatographic patterns in a data structure is a basic problem in the application of chemometrics to chromatography. The significance of this first step is evident from the fact that a raw pyrogram may represent over a megabyte of data, whereas the final representation is usually of the order of a few dozen bytes only. It is desirable to retain as much information as possible while reducing data. Samples or objects are initially represented as vectors, where each vector element represents a feature of the measurement space. Mapping a chromatogram to a vector involves using peak areas or peak heights as feature values in the sample/object vector. An ideal situation would be to have chromatograms with highly reproducible retention times and well separated and evenly spaced peaks. In this case, there is no ambiguity in assigning feature values to the corresponding vector. In real situations, peaks are unevenly distributed in retention time. Certain segments of the time axis may have many closely spaced peaks in contrast to other segments with fewer widely spaced peaks. Slight random shifts in retention times may lead to mapping of the same peak (chemical component) to different features in different chromatograms. Variations in sample introduction can also decrease reproducibility of GC, Py-GC, and Py-MS patterns.

A variety of different techniques have been employed to circumvent these problems. Visual comparison of chromatograms to select representative peaks is conceptually simple and commonly used. Criteria for peak selection include that the peaks were reproducible and of measurable heights,⁶ that the peaks were easy to distinguish and well resolved,¹¹ or that the peaks provided discriminating ability.¹² Selected peaks are then assigned peak ID's (or feature numbers) and the total number of such hand-picked peaks defines the dimensionality of the object vector. Manual peak selection is subjective, however, and two problems arise: only prominent peaks tend to be picked and only a small number of chromatograms can be handled without introducing significant errors.

Most of the difficulty in automating peak selection can be attributed to the complexity and variability of chromatograms. Figure 1 shows replicate Py-GC/MS total ion abundance chromatograms of the same sample obtained with the identical chromatographic and MS operating parameters. Peak "A" has identical retention times and mass spectra in the two chromatograms. When integrated with identical integration software settings, this peak is the sixteenth peak in the first chromatogram and the eighteenth peak in the second chromatogram. Similarly, peak "B" (number 32) in the first chromatogram has the same retention time and mass spectrum as peak number 37 in the second chromatogram.

To map a peak consistently to the same feature in the representation vector, the time axis is usually divided into

* Author to whom correspondence should be addressed.

[†] Current address: Research & Development, Procter & Gamble Pharmaceuticals, P.O. Box 191, Norwich, NY 13815-0191.

(1) Brown, S. D. *Anal. Chem.* 1990, 62, 84R-101R.

(2) Irwin, W. J. *Analytical Pyrolysis*; Marcel Dekker: New York, 1982.

(3) Meuzelaar, H. L. C.; Haverkamp, J.; Hileman, F. D. *Pyrolysis Mass Spectrometry of Recent and Fossil Biomaterial*; Elsevier Scientific Publishing: Amsterdam, 1982.

(4) Eshuis, W.; Kistemaker, P. G.; Meuzelaar, H. L. C. In *Analytical Pyrolysis*; Jones, C. E. R., Cramers, C. A., Eds.; Elsevier: Amsterdam, 1977; pp 151-166.

(5) MacFie, H. J. H.; Gutteridge, C. S. *J. Anal. Appl. Pyrol.* 1982, 4, 175.

(6) Morgan, S. L.; Jacques, C. A. *Anal. Chem.* 1982, 54, 741-747.

(7) Windig, W.; Haverkamp, J.; Kistemaker, P. G. *Anal. Chem.* 1983, 55, 81-89.

(8) Morgan, S. L.; Walla, M. D.; Rogers, J. C. *Chromatography* 1987, 2, 12.

(9) Dröge, J. B. M.; Rinsma, W. J.; Van't Klooster, H. A.; Tas, A. C.; Van der Greef, J. *J. Chemom.* 1987, 1, 231-241.

(10) Harrington, P. B.; Voorhees, K. J. *Anal. Chem.* 1990, 62, 729.

(11) Brazell, R. S.; Jenkins, R. A.; Bayne, C. K. *Anal. Chim. Acta* 1982, 139, 247-256.

(12) Milina, R.; Dimov, N.; Dimitrova, M. *Chromatographia* 1983, 17, 29-32.

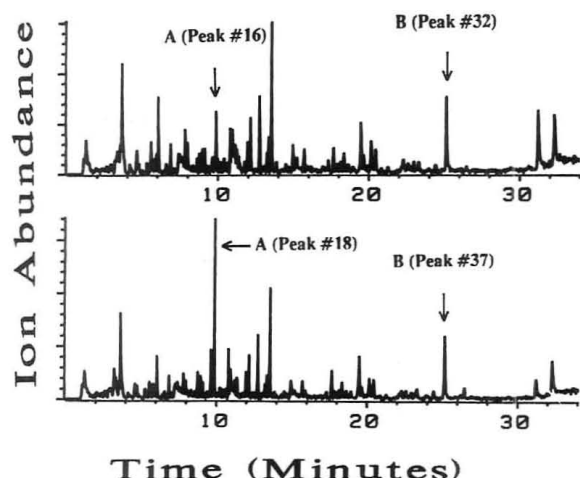


Figure 1. Replicate chromatograms illustrating variability in integration yielding different numbers of peaks.

small segments of time windows of equal¹³⁻¹⁵ or unequal¹⁶ width. The number of time windows defines the dimensionality of the representation vector. Feature values are assigned using the peak height or area of the most intense peak in the corresponding window^{13,16,17} or using the sum of all peak heights or areas in that window.^{15,18} Standardization of the time axis with reference peaks and stretching or compressing of the time axis by "rubber banding" can also aid in matching of retention times.¹⁸ With mass spectra, binary encoding with 1's and 0's has also been used to mark the presence or absence of a peak in a given window.¹⁹ The choice of window widths is problematic. Windows that are too wide may merge too many peaks together, with a resultant loss of information. Window widths that are too narrow increase the dimensionality of the vector space and may produce many features containing no peak information.

Engman et al.²⁰ have used a variable-size window approach to define chromatographic windows for pattern recognition. Varhegyi and Alexander²¹ discuss a chromatographic pre-processing approach in which the distribution of peak retention times is displayed in a histogram and used to generate a standard vector of chromatographic features. Brekke et al.²² used a "soft" maximum entropy criterion with NMR spectra to define variable-size windows in which the most intense peaks are left unchanged and the less intense peaks are summed together; this approach may also have utility with GC or GC/MS data.

In mapping peaks in windows to pattern features, regions of the chromatogram densely populated with peaks will be affected by slight shifts in retention times and peak overlaps. As seen in Figure 1, the same peak may be mapped to different features in different chromatograms. Another side effect is the increase in the number of patterns necessary for a given analysis. For most multivariate analysis techniques, the required number of patterns is proportional to the dimen-

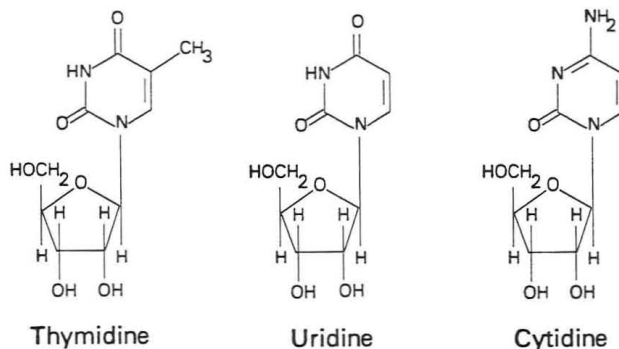
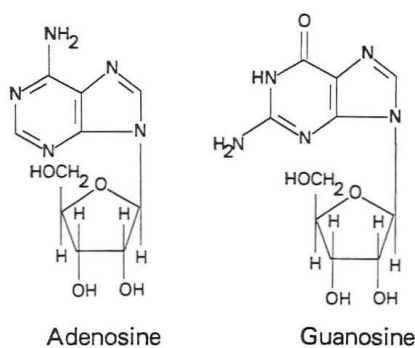


Figure 2. Chemical structures of five nucleosides.

sionality of the vector space.²³ If the dimensionality of the vector space is extremely large or if a large number of features have zero values, singular covariance matrices may result—a highly undesirable outcome for multivariate analysis. The optimum window width requires a compromise between including sufficient information for discrimination and not requiring too many samples. It is important to distinguish chemically significant classification from chance discrimination. The probability of chance linear separation between classes of samples increases with increased vector di-dimensionality.^{13,23-25}

In the present study, a vector-based representation method for chromatograms using mass spectra of peaks to map chromatogram peaks to features was employed to develop fingerprint pyrograms for five nucleosides (adenosine, guanosine, thymidine, cytidine, and uridine). These Py-GC/MS fingerprints were then employed for identification of nucleosides using either Euclidean or Mahalanobis distances. Investigating the ways in which feature selection can be employed to enhance classification and to recognize discriminating features (chemical markers) in the pyrograms were further objectives of this work.

MATERIALS AND METHODS

Chemicals. Five nucleosides (adenosine, guanosine, thymidine, cytidine, and uridine) were obtained from Sigma Chemical Co. (St. Louis, MO). The structure of these compounds is shown in Figure 2. Each nucleoside was dissolved in distilled water to a concentration of 2.5 mg/mL. Since the solubility of guanosine in water is less than 2.5 mg/mL at room temperature, this solution was warmed to 60 °C to dissolve the sample.

Pyrolysis-Gas Chromatography/Mass Spectrometry. A Model 120 Pyroprobe was equipped with a platinum coil pyrolyzer and quartz-lined interface (Autoclave Engineers, Chemical Data Systems, Oxford, PA). GC/MS was carried out on a Hewlett-Packard 5988 GC/MS system (Palo Alto, CA) equipped with a

(13) Kullik, E.; Kaljurand, M.; Koel, M. *J. Chromatogr.* 1976, 126, 249-256.

(14) McConnell, M. L.; Rhodes, G.; Watson, U.; Novotny, M. *J. Chromatogr.* 1979, 162, 495-506.

(15) Smith, C. S.; Morgan, S. L.; Parks, C. D.; Fox, A. *J. Anal. Appl. Pyrol.* 1990, 18, 97-115.

(16) Kullik, E.; Kaljurand, M.; Koel, M. *J. Chromatogr.* 1975, 112, 297-300.

(17) Clark, H. A.; Jurs, P. C. *Anal. Chem.* 1979, 51, 616-623.

(18) Parrish, M. E.; Good, B. W.; Hsu, F. S.; Hatch, F. W.; Ennis, D. M.; Douglas, D. R.; Shelton, J. H.; Watson, D. C. *Anal. Chem.* 1981, 53, 826-831.

(19) Scott, D. R. *Chemom. Intell. Lab. Syst.* 1988, 4, 47-63.

(20) Engman, H.; Mayfield, H. T.; Mar, T.; Bertsch, W. *J. Anal. Appl. Pyrol.* 1984, 6, 137.

(21) Varhegyi, G.; Alexander, G. *J. Chromatogr.* 1985, 318, 247-253.

(22) Brekke, T.; Barth, T.; Kvalheim, O. M.; Sletten, E. *Anal. Chem.* 1990, 62, 49-56.

(23) Lavine, B. K.; Jurs, P. C.; Henry, D. R. *J. Chemom.* 1988, 2, 1-10.

(24) Stouch, T. R.; Jurs, P. C. *J. Chem. Inf. Comput. Sci.* 1985, 25, 45-50.

(25) Stouch, T. R.; Jurs, P. C. *J. Chem. Inf. Comput. Sci.* 1985, 25, 92-98.

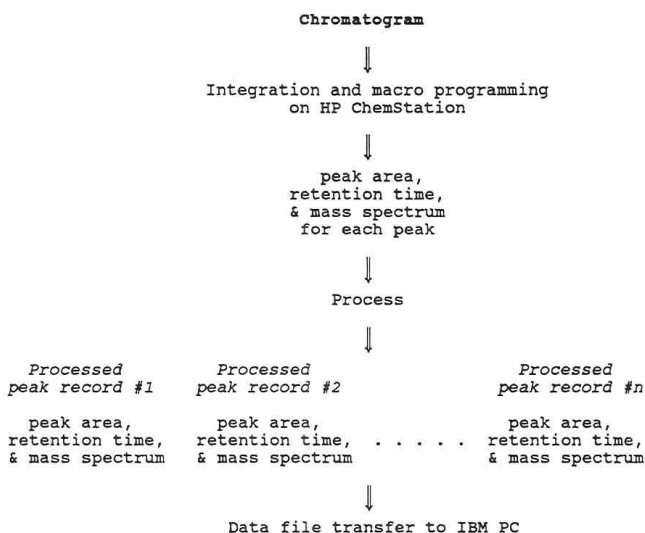


Figure 3. Chromatographic and mass spectral processing on Hewlett-Packard ChemStation prior to data file transfer to MS-DOS-compatible computer.

HP-5890 GC. All samples were analyzed in a random order over a period of 3–4 days.

Quartz sampling tubes were cleaned in hot nitric acid, rinsed in distilled water, and dried. A 10- μ L sample (25 μ g of nucleoside) was placed with a micropipet inside the quartz sampling tube and dried in an oven at 90 °C. The tube was then placed inside the platinum coil of the Pyroprobe and the probe inserted in the GC interface (230 °C). The system was then purged with helium carrier gas for 3 min before pyrolysis to eliminate air from the pyrolysis interface and GC column.

Samples were pyrolyzed at a final temperature setting of 750 °C, with the pyrolysis interval set to 5 s, and the Pyroprobe ramp setting in the "off" position (maximum rate). Actual pyrolysis temperatures and temperature rise times experienced by the sample, particularly in a quartz boat experiment, are less than the actual instrument settings. Probe calibration may be performed if considered necessary for interlaboratory comparisons or for accurate temperature specification.²⁶ Pyrolysis products were separated on a 25-m \times 0.25-mm free fatty acid phase (FFAP) fused silica capillary column (Quadrex, New Haven, CT) operated at a linear flow velocity of 35 cm/s. The GC oven temperature was programmed from 30 to 230 °C. The mass selective detector monitored 40–500 m/z in the total ion mode under "Autotune" conditions using 70-eV ionization.

Computing and Plotting. Preprocessing of GC/MS data was performed on the Hewlett-Packard GC/MS ChemStation using standard integration utilities combined with macroprogramming and processing programs written in HP Pascal. All other programs were written in Turbo Pascal version 5.5 (Borland International, Scotts Valley, CA) and QuickBASIC version 4.5 (Microsoft Corp., Seattle, WA), compiled, and executed on MS-DOS-compatible (Microsoft Corp., Seattle, WA) computers. Principal component analysis and graphics were performed using SYSTAT version 4.0 (SYSTAT Inc., Evanston, IL). Graphics were plotted on a LaserJet IIP printer (Hewlett-Packard Co., Palo Alto, CA).

REPRESENTATION OF CHROMATOGRAMS

Preprocessing of GC/MS data on the HP ChemStation prior to file transfer to the MS-DOS-compatible computer is summarized in Figure 3. Integration parameters were adjusted to produce between 20 and 25 peak areas for each chromatogram. Peak information was stored as a record with three fields—retention time, peak area, and mass spectrum at the peak maxima. Files containing arrays of peak records for a chromatogram (referred to as the *chromatogram array*) were transferred to an MS-DOS-compatible computer (Zenith

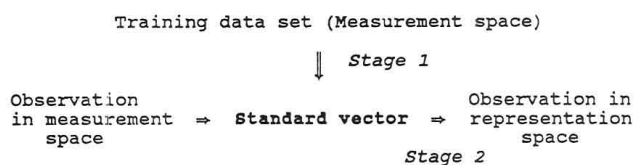


Figure 4. The two stages for representation of a chromatogram as a vector in representation space.

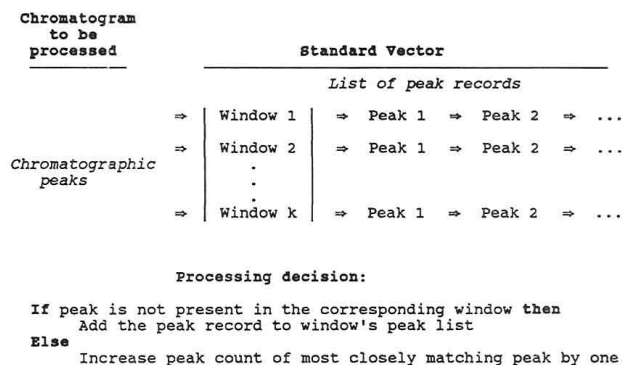


Figure 5. Steps in generating a standard vector from a set of chromatograms.

Z-248) as previously described.²⁷ Transferring the data allowed off-line processing on MS-DOS-based computers rather than on the dedicated-instrument ChemStation. The entire data processing could be accomplished either on a dedicated instrument computer or on an off-line system. The approach presented here is not limited or unique to the HP ChemStation.

With the data now on the MS-DOS-compatible computer, chromatograms were mapped into the representation space using the two-stage process shown in Figure 4.

Stage 1. A target array was defined with records similar to that of a chromatogram array, but with an extra peak count field to keep track of the number of times each different chromatographic peak appears in the data set. Initially the target array was empty. Peaks in each chromatogram array in the training set were merged into the target array, one by one as follows. An arbitrary time window width W , equal to the maximum possible variation in a peak retention time (0.25 min in the present work), was defined. The mass spectrum of the peak being merged was compared with those of all the peaks of the target array with retention times within $\pm W$ of its retention time. If a matching peak was found, this incoming peak was dropped and the peak count of the most closely matched peak in the target array was incremented by one. Otherwise, the peak was added to the growing target array, and its peak count was set equal to one. To efficiently search the growing target array, the retention time axis was initially divided into consecutive intervals of width W , and the peak records of the target array were maintained as lists associated with these intervals. All peaks in the list associated with a particular time interval thus had retention times within that interval. Peaks in each list were kept ordered by their retention times. To test the uniqueness of a peak, the list associated with the window corresponding to its retention time and those associated with the two adjacent windows were searched.

Figure 5 summarizes this procedure. The decision of whether two chromatographic peaks, A and B, match one another was made by comparing their mass spectra using the similarity index

$$S_{ij} = \sum m_i m_j / \sqrt{(\sum m_i^2 \sum m_j^2)} \quad (1)$$

where m_i and m_j represent the mass spectral intensity at each

(26) Wells, G.; Voorhees, K. J.; Futrell, J. H. *Anal. Chem.* 1980, 52, 1782–1784.

(27) Rogers, J. C.; Watt, B. E.; Sahota, R. S.; Morgan, S. L. *J. Chromatogr. Sci.* 1989, 27, 688.

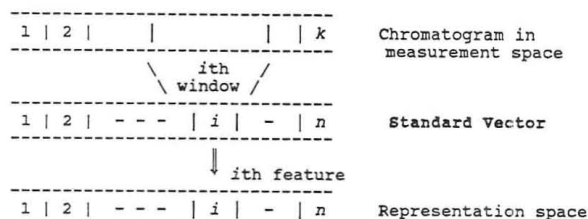


Figure 6. Mapping of a chromatogram in measurement space into the vector representation space.

mass for spectra i and j , respectively, and Σ represents the summation over the entire range of ion masses.²⁸ For the present data set, two peaks were assumed to match if their similarity exceeded 0.9. These choices of mass spectral similarity and threshold are arbitrary, and others could be used.²⁹

Mass spectra of the same chemical component may not be exactly similar in two replicate chromatograms. Since peaks are merged into the target array in the sequence they are processed, a peak with a more representative mass spectrum for a particular chromatographic peak may have a smaller peak count and ultimately be dropped in the next step (described below) simply because it is processed after a less representative peak of the same set. To avoid this problem, two iterations were performed. During the first iteration, all peaks were merged, but peak counts were kept at zero and not incremented. The first iteration identifies all unique peaks in the data set and saves a place for each unique peak in the target array. During the second iteration, all chromatogram arrays in the data set were again merged with this target array and the peak count changed as defined above. No new peaks will be added during the second iteration because the target array already contains at least one peak to match every peak in the data set. By separating the formation of the target array from the actual peak counting in two different iteration steps, any possible bias due to the order that the chromatograms are processed is avoided.

After all chromatogram arrays were merged, the target array contained all unique peaks present in the training set. The number of times each unique peak occurred in the training set was given by its peak count. With the objective of deleting less reproducible peaks from the target vector, a useful criterion would be to delete all peaks with peak counts less than the number of chromatograms in the smallest class of samples in the training set. If the training set contains only one class (e.g., as discussed below in fingerprinting the nucleosides), peaks having peak counts less than the total number of observations in the training set can be deleted. The array of retained peak records sorted by their retention times constitute the *standard vector*.

Stage 2. The second stage, summarized in Figure 6, was the reverse of stage one. A representation vector for a chromatogram was created by matching, within each defined window, peak by peak with the standard vector. The number of records, n , in the standard vector defined the dimensionality of the representation space. A representation vector V for chromatogram array A was created in the following manner. Let w_i be the interval for retention times of the peaks for which a match would be investigated with the i th record of the standard vector during stage 1. The i th record in the standard vector was matched with all the peaks with retention times in the interval w_i in A . If a matching peak was found then the area of the peak was assigned to the i th feature of V . If more than one peak was matched, then the peak area of the peak with the highest mass spectral similarity was

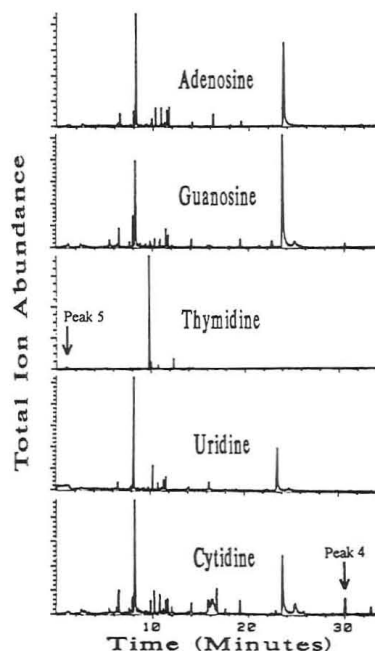


Figure 7. Representative total ion abundance pyrograms of the five nucleosides.

used. If no peak with a minimum acceptable match was found in A with a retention time in interval w_i , a value of zero was assigned to feature i in V .

RESULTS AND DISCUSSION

Feature Selection. The Py-GC/MS data set contained 48 pyrograms (8 for cytidine and 10 for each of the remaining four nucleosides). Representative pyrograms for the five nucleosides are shown in Figure 7. Except for thymidine, all nucleosides produced very similar pyrograms. Visual discrimination between the pyrograms of all five of these nucleosides was difficult. Even in the case of thymidine, no unique characteristic peak was easily distinguishable. So that each group would have 10 chromatograms during stage 1 of standard vector formation, two chromatograms for cytidine were repeated. These two cytidine chromatograms were deleted from the data set after stage 1 was completed. Only peaks with peak counts equal to or greater than 10 (the number of chromatograms in each class) were included in the standard vector.

The standard vector for the whole data set included 43 peaks, defining 43 dimensions of the representation space. Figure 8 shows a projection of all 48 data points (not-normalized or autoscaled) in the three-dimensional space of the first three principal components of these data. Except two points representing adenosine that were merged with points representing pyrograms of guanosine, all five nucleoside groups are well separated.

Peaks with peak counts higher than 10 (the number of pyrograms in each group of nucleosides) are common to more than one group. To select features for the purpose of discriminating between different classes, these peaks could be deleted from the standard vector. Because a peak having a peak count of 20 or more can be present in all samples from two groups, all peaks having a peak count higher than 19 were eliminated from the data set. Thirty peaks were retained on this reduced data set. Projections of the 48 points (not normalized or autoscaled) on the first three principal components of this new representation space are shown in Figure 9.

As a measure of the separability of the data after these different feature selection options, the ratio of the traces of the between-class (S_b) and within-class (S_w) covariance

(28) HP 59970 MS ChemStation, Operators Manual; Publication No. 59970-90016; Hewlett-Packard Company: Palo Alto, CA, March 1986.

(29) Heller, S. R.; Koniver, D. A.; Fales, H. M.; Milne, G. W. A. *Anal. Chem.* 1974, 46, 947-950.

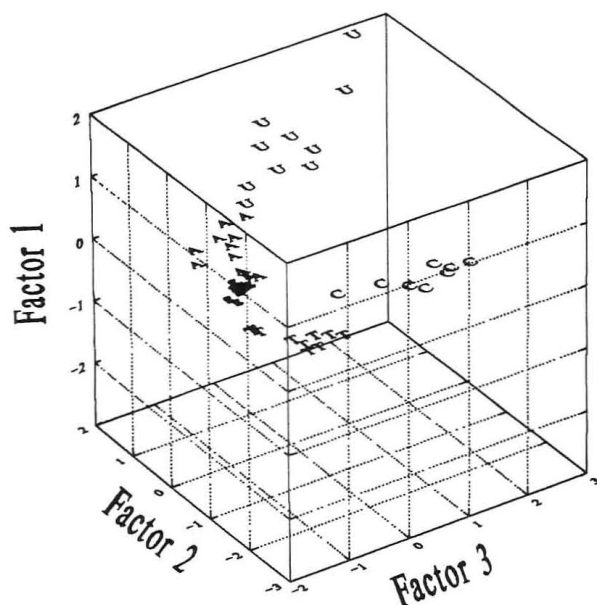


Figure 8. Projection of 48 data points in the three-dimensional space of the first three principal components for the Py-GC/MS data set on five nucleosides. Separability (eq 2) = 0.658. Symbols: A, adenosine; g, guanosine; C, cytidine; U, uridine; T, thymidine.

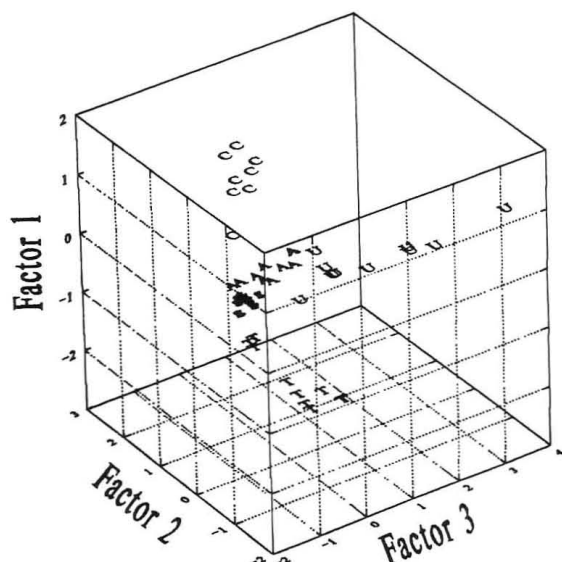


Figure 9. Projection of 48 data points in the three-dimensional space of the first three principal components computed after discarding features representative of more than 19 pyrograms. Separability (eq 2) = 0.731. Symbols: A, adenosine; g, guanosine; C, cytidine; U, uridine; T, thymidine.

matrices³⁰ was computed:

$$J = \text{tr}(S_b) / \text{tr}(S_w) \quad (2)$$

where "tr" indicates the sum of the diagonal elements of a matrix. As this measure is coordinate system-dependent, data sets were autoscaled before this calculation. For the 43-dimensional data set of Figure 8, the separability criterion was 0.658. For the 30-dimensional data set of Figure 9, the separability criterion improved to 0.731, representing better class separation.

Another feature selection method that can enhance class separability is to generate standard vectors for each nucleoside class separately. A new combined standard vector for the entire data set is then generated by merging the standard vectors for each individual class. Figure 10 shows the three-dimensional projection of the resulting 34-dimensional data

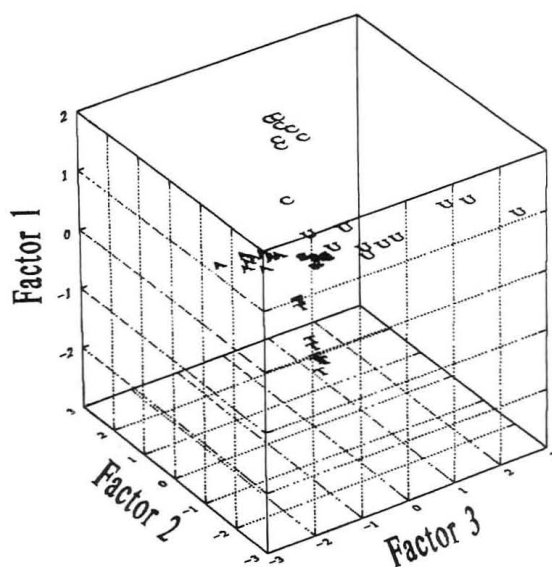


Figure 10. Projection of 48 data points in the three-dimensional space of the first three principal components. The standard vector was a composite of individual standard vectors obtained from the five nucleoside data subsets. Separability (eq 2) = 0.697. Symbols: A, adenosine; g, guanosine; C, cytidine; U, uridine; T, thymidine.

set (not normalized or autoscaled) on its first three principal components. The class separability given by eq 2 is now 0.697. The reason for the improvement in class separability over that shown in Figure 8 is that, during the generation of a standard vector for an individual nucleoside, peaks that are not characteristic of that nucleoside alone are dropped.

Chromatographic Fingerprinting. Observations from any one nucleoside data set were used in the training set to obtain a standard vector. As described above, using this standard vector, observations in the training set were then mapped into the representation space. The standard vector, together with the group centroid and the confidence intervals, was used as a fingerprint to represent that nucleoside. Distances can then be calculated for all pyrograms in the training set from the group centroid, and confidence intervals can be computed for a specified level of confidence.

Single-tailed confidence intervals were computed by the usual formula^{31,32}

$$\text{confidence interval} = \bar{x} \pm t_{\alpha, \phi} s_x \quad (3)$$

where \bar{x} is the mean distance of observations in the training set from their centroid, s_x is the standard deviation, α is the risk level associated with the $(100 - \alpha)\%$ confidence interval, and ϕ is the degrees of freedom.

To compare the pyrogram of an unknown sample to a nucleoside fingerprint, the standard vector for that nucleoside was used to map the unknown pyrogram into the representation space. The distance for the unknown sample from the test group centroid was then calculated. Confidence intervals computed from the training set were used to accept or reject this unknown sample as a member of the test nucleoside group.

Two different distance measures, Euclidean and Mahalanobis distances, were investigated. The squared Euclidean distance from a sample vector and the group centroid is defined by

$$D^2 = \|\mathbf{X} - \boldsymbol{\mu}\|^2 = (\mathbf{X} - \boldsymbol{\mu})^T (\mathbf{X} - \boldsymbol{\mu}) \quad (4)$$

where \mathbf{X} represents the sample vector, $\boldsymbol{\mu}$ represents the centroid vector for the test group, and the superscript "T"

(31) Hopkins, K. D.; Glass, G. V.; Hopkins, B. R. *Basic Statistics for the Behavioral Sciences*, 2nd ed.; Prentice-Hall, Inc.: Englewood Cliffs, NJ, 1987.

(32) Deming, S. N.; Morgan, S. L. *Experimental Design: A Chemometric Approach*; Elsevier: Amsterdam, 1987.

(30) Fukunaga, K. *Introduction to Statistical Pattern Recognition*, 2nd ed.; Academic Press, Inc.: Boston, 1990; pp 446-447.

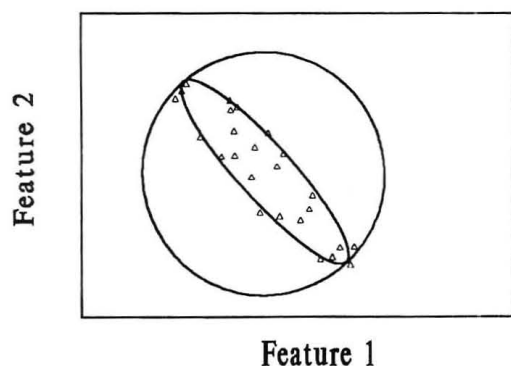


Figure 11. Confidence intervals on a simulated data set for Mahalanobis (ellipse) and Euclidean distances (outer circle).

indicates a matrix transpose.³³ Mahalanobis distances are described by an ellipsoid circumscribing the data.³⁴ The distance D between the position vector of a point \mathbf{X} to the group centroid vector μ is given by

$$D^2 = (\mathbf{X} - \mu)^T \Sigma^{-1} (\mathbf{X} - \mu) \quad (5)$$

where Σ is the variance-covariance matrix of the training data set, and the superscript “-1” indicates a matrix inverse. Since μ and Σ are generally unknown, estimates \bar{x} and \mathbf{S} are computed from a sample of size n , and eq 5 is replaced by

$$D^2 = (\mathbf{X} - \bar{x})^T \mathbf{S}^{-1} (\mathbf{X} - \bar{x}) \quad (6)$$

where

$$\mathbf{S} = [1/(n-1)] \sum_{i=1}^n (x_i - \bar{x})^T (x_i - \bar{x}) \quad (7)$$

Mahalanobis distances describe an ellipsoid, and the boundary defined by Euclidean distances is a sphere (Figure 11). Mahalanobis distances are smaller in the direction along the elongated principal components of the data set. Euclidean distance makes no compensation for differences in variability along different directions.

This fingerprinting strategy was validated by cross-validation.³⁵ Each pyrogram was omitted one at a time from the training set. A standard vector was generated from the remaining pyrograms, and group centroids and confidence intervals were computed. The omitted pyrogram was then classified using this set of standard vector, centroid, and confidence intervals. For each nucleoside data subset, 9 of the 10 observations (7 out of 8 in case of cytidine) were used for training. The remaining one observation from that nucleoside subset and the 38 (40 in case of the cytidine data subset) observations from the other four nucleoside data subsets were tested for acceptance. For perfect classification accuracy, in all 10 (or 8 for cytidine) iterations, 10 (or 8) left out observations from the same nucleoside data set should be accepted and the remaining 380 (320 in case of cytidine) should be rejected.

Table I shows the cross-validation results for the nucleoside data set using Euclidean and Mahalanobis distances. Although Mahalanobis distances might be expected to give better results, confidence intervals based on Euclidean distances perform better with this particular data set. The reason is the small size of the data set. Mahalanobis distances rely on the variance-covariance structure of the data set and a variance-covariance matrix will not be well-determined if

Table I. Acceptance and Rejection Accuracies of Unknown Samples Using Euclidean and Mahalanobis Distances

nucleoside	Euclidean distance		Mahalanobis distance	
	acceptance accuracy, %	rejection accuracy, %	acceptance accuracy, %	rejection accuracy, %
adenosine	90	95	90	93
guanosine	100	82	90	95
thymidine	100	100	90	100
uridine	90	83	70	95
cytidine	100	95	100	93

the number of observations in a data set is less than $2n$,^{33,36} where n is the number of features. Since during each cross-validation iteration, only nine (seven in case of cytidine) pyrograms represent a training set, a limit of four (three in the case of cytidine) was set on the maximum number of peaks that could be present in a fingerprint. Euclidean distances are not affected as much by this relationship between number of features and number of observations in the data set. For Euclidean distances, at least as many peaks as there were samples in the data set were retained in the standard vector during any given iteration. Since retaining a very low number of peaks may make a fingerprint less representative of a data set, Mahalanobis distances may be outperformed by Euclidean distances on a relatively smaller data set.

In this work, 99% confidence intervals were employed with Mahalanobis distances and 95% confidence intervals were used for Euclidean distances. Since confidence intervals for Euclidean distances define a sphere, they cover larger areas than necessary in the directions marking lower relative variance in the data set (Figure 11). When the different classes under consideration lie very close to one another, as was the case with the nucleoside data, rejection accuracy for the observations not belonging to the class under consideration decreases. Confidence intervals were set at a lower confidence for Euclidean distances in an attempt to maintain a high rejection accuracy. Euclidean distance rejection accuracies were still lower than the Mahalanobis rejection accuracies as shown in Table I. Euclidean distances may also be more susceptible to influence by outliers than the more parametric-based Mahalanobis distance approach. Quality control in the form of outlier detection schemes, both for individual chromatograms and individual peaks, might reduce such difficulties.

Recognition of Chemical Markers. The vector representation technique can be used to find chemical markers representative of the individual classes. Because the cytidine data subset had only eight samples, two pyrograms were repeated in that subset so that each nucleoside subset had ten observations. Five standard vectors were generated, each representing a different nucleoside data subset. Each standard vector contained peaks with peak counts of 10 or more. Higher than 10 peak counts are not uncommon, because a peak in the standard vector can match with more than one neighboring peaks in a chromatogram. These standard vectors were merged to obtain a common standard vector for the whole data set. This common standard vector was then matched with the whole data set to obtain peak counts for each peak in the vector. Since each peak will have a peak count of at least 10, peaks with peak counts equal to 10 cannot represent more than one nucleoside class and are representative of that nucleoside class. During this matching of the common standard vector with the entire data set, a trace can be set to find out which peaks match which nucleoside data sets. Peaks which match with peaks from only one nucleoside data set and are present in every chromatogram in that data set can be singled out. Eight such peaks were selected. Four

(33) Duda, R. O.; Hart, P. E. *Pattern Classification and Scene Analysis*; John Wiley: New York, 1973; Chapter 2.

(34) Mahalanobis, P. C. *Proc. Natl. Inst. Sci. India* 1936, 2, 49-55.

(35) Lachenbruch, P. A.; Mickey, M. R. *Technometrics* 1968, 10 (1), 1-11.

(36) Lambert, M. H.; Scheraga, H. A. *J. Comp. Chem.* 1989, 10, 770-797.

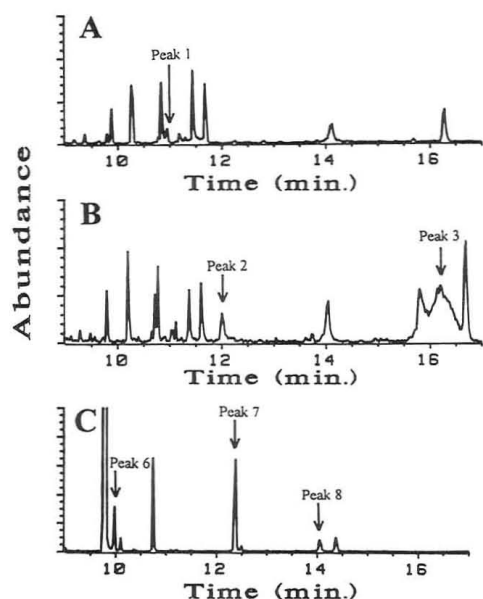


Figure 12. Total ion abundance pyrograms (expanded region from 8 to 18 min) identifying unique chemical marker peaks for (A) adenosine (peak 1), (B) cytidine (peaks 2 and 3, with peak 4 marked in Figure 7), and (C) thymidine (peaks 6–8, with peak 5 marked in Figure 7).

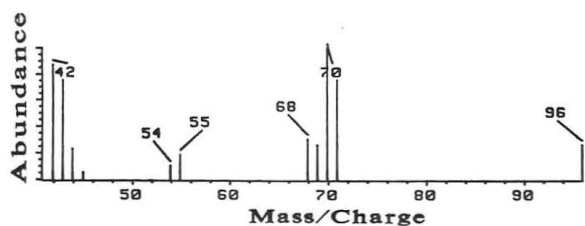


Figure 13. Mass spectrum of the unique chemical marker peak found in adenosine pyrograms (Figure 12A, peak 1).

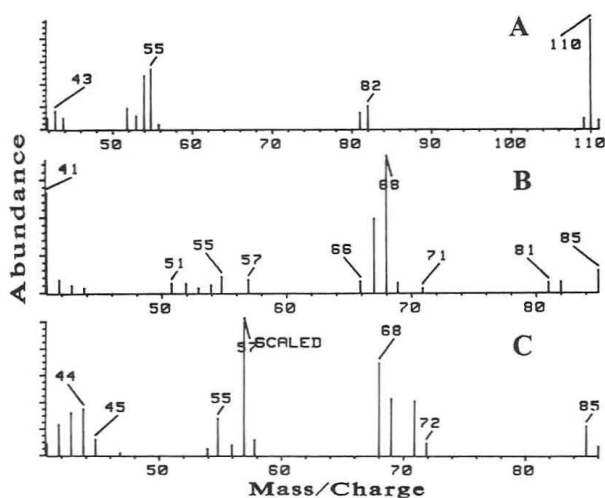


Figure 14. Mass spectra of three unique chemical marker peaks found in cytidine pyrograms (Figures 7 and 12B, peaks 2–4).

of these peaks were characteristic of thymidine, three were characteristic of cytidine, and one was characteristic of adenosine. No unique peaks were found to be characteristic of guanosine and uridine. This fact also explains the relatively lower rejection accuracy in Table I for these two nucleoside classes and the lower acceptance accuracy with uridine.

The characteristic chromatographic peaks for adenosine (peak 1), cytidine (peaks 2–4), and thymidine (peaks 5–8) are marked in Figures 7 and 12, and their mass spectra are shown in Figures 13–15. The NIH/EPA mass spectral library was searched for the best matches to these mass spectra. Table II lists the top five matches for each of the eight chemical markers. At this time, matching with pure standards to further identify these chemical markers has not been per-

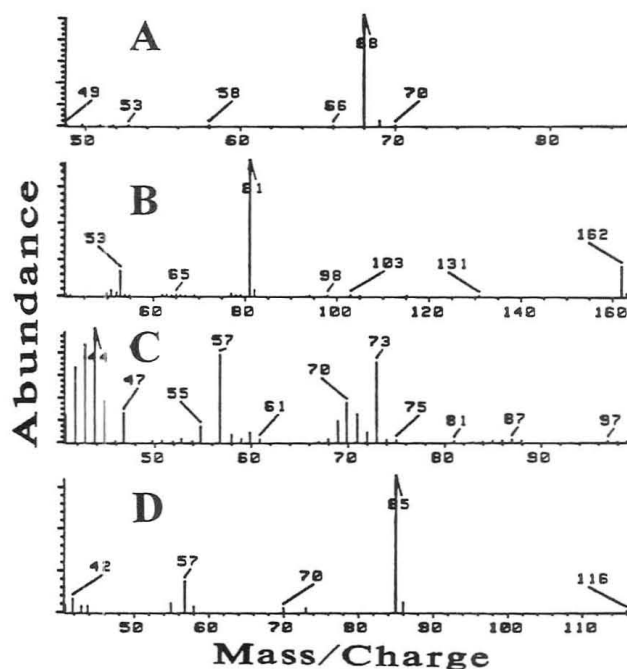


Figure 15. Mass spectra of four unique chemical marker peaks found in thymidine pyrograms (Figures 7 and 12C, peaks 5–8).

formed. However, the list of matches for each peak provides some information on the likely structures present in these markers.

CONCLUSIONS

The vector representation approach described here offers a viable method for preprocessing GC/MS data prior to multivariate statistical analysis. Qualitative mass spectral information is used to define features. The data representation process is integrated with feature selection to facilitate fingerprinting and recognition of chemical markers.

Feature selection methods are usually based on figures of merit such as the probability of correct classification, the ratio of within-class variance to between-class variance, or some other univariate criteria.^{37–39} The qualitative reasons for selecting or rejecting a given feature are not considered. The present technique marks a departure from this approach by selecting discriminating feature on a qualitative basis, even before a data structure is precisely defined.

The fingerprinting approach described here can be contrasted with more traditional classification methods based on distances from a class centroid or center of gravity.^{40–43} Cluster analysis algorithms also make use of distance measurements between an observation and a given group centroid or between different group centroids.⁴⁴ Both Mahalanobis^{42,43} and Euclidean^{40,41} distances have been used for classification. Our fingerprinting approach uses the standard vector for a given class of sample (nucleoside) to represent or define the unknown observation *before* measuring its distance to the class centroid. The standard vector maps peaks of the unknown chromatogram to vector features that have been defined on the basis of chromatograms from a specific class (nucleoside). An unknown chromatogram representing a

(37) Devijver, P. A.; Kittler, J. *Pattern Recognition: A Statistical Approach*; Prentice/Hall International: Englewood Cliffs, NJ, 1982.

(38) Forina, M.; Lanteri, S.; Armanino, C. *Top. Curr. Chem.* **1987**, *141*, 91–143.

(39) Sahota, R. S.; Morgan, S. L. *Anal. Chem.*, **1992**, *64*, 2383–2392.

(40) Varmuza, K. *Anal. Chem. Acta* **1980**, *122*, 227–240.

(41) Rotter, H.; Varmuza, K. *Anal. Chim. Acta* **1977**, *95*, 25–32.

(42) Shah, N. K.; Gemperline, P. J. *Anal. Chem.* **1990**, *62*, 465–470.

(43) Mark, H. L.; Tunnel, D. *Anal. Chem.* **1985**, *57*, 1449–1456.

(44) Everitt, B. *Cluster Analysis*, 2nd ed.; Halsted Press: New York, 1980.

Table II. Five Best Matches from the NIH/EPA Mass Spectral Library for the Eight Peaks Recognized as Unique Chemical Markers for Adenosine, Cytidine, and Thymidine^a

adenosine peak 1	1-butanol, 3-methyl-, carbonate (2:1) (2050-95-5) ^b hexanal, 3-methyl- (19269284) 1-propanamine, <i>N</i> -nitroso- <i>N</i> -propyl- (621-64-7) propanoic acid, 2-methyl-, 2-methylbutyl- (2445-69-4) carbonic acid, dipentyl ester (2050-94-4)
cytidine peak 2	1,4-benzenediol (123-31-9) 1 <i>H</i> -pyrrole-2,5-dione, 1,1'-(1,8-octanediyl)bis- (28537-73-7) 1 <i>H</i> -imidazole-2-carboxaldehyde, 1-methyl- (13750-81-7) <i>p</i> -benzoquinone, compd with resorcinol (26734-94-1)
cytidine peak 3	1,3-benzenediol (108-46-3) 1,6-heptadiene, 2,5-dimethyl- (68701-90-6) 2,3-nonadiene (22433347) cyclobutaneethanol, 1-methyl-2-(1-methylethenyl)- (26532-22-9) cyclobutaneethanol, 1-methyl-2-(1-methylethenyl)- (30346-21-5) 1 <i>H</i> -imidazole (288-32-4)
cytidine peak 4	cyclohexanol, 2-methyl- (583-59-5) heneicosane, 11-cyclopentyl- (6703-81-7) 1 <i>H</i> -imidazole, 1-(1-oxopentyl)- (69393-13-1) nonane, 2-bromo-5-ethyl- (55162-38-4) cycloheptanol (502410)
thymidine peak 5	cyclobutane, 1,2-dipropenyl- (22769-00-2) 1 <i>H</i> -imidazole (288-32-4) cyclobutane, 1,2-diethenyl-3-methyl- (22704-00-3) 2-propenamamide, <i>N</i> -(3,4-dichlorophenyl)- <i>N</i> - (56247-87-1) 1-naphthalenecarboxylic acid 1,4,4a,5,8 (58822-93-8)
thymidine peak 6	benzoic acid, 4-chloro-2-[2-furanylmethyl (74793-84-3) benzoic acid, 5-(aminosulfonyl)-4-chloro (54-31-9) benzoic acid, 4-chloro-2-[2-furanylmethyl (74793-12-7) 2-cyclopentene-1-carboxyl acid, 1-methyl- (68317-73-7) ethane, 2-bromo-2-chloro-1,1-difluoro-1- (679-89-0)
thymidine peak 7	1-octanamine, <i>N</i> -methyl- <i>N</i> -nitroso- (34423-54-6) 1-butanamine, <i>N</i> -methyl- <i>N</i> -nitroso- (7068-83-9) 1-octanamine, <i>N</i> -methyl- <i>N</i> -nitroso- (54789-28-5) 1,2,4,5-tetrazine, hexahydro-1,2,4,5-tet (20717-38-8) oxetane, 2-propyl- (4468-64-8)
thymidine peak 8	lup-20(29)-en-21-ol, 3,28-bis[tetrahydroxo (55401-92-8) 1,3-dioxolane-4-ethanol, 2,2,4-trimethyl- (64018-44-6) silane, tetrafluoro- (7783611) lup-20(29)-en-21-ol, 3,28-bis[tetrahydroxo (55401-93-9) indeno[3a,4-b]oxiren-2-ol, octahydro-4a (67920-65-4)

^a Peaks 1–8 are identified in Figures 7 and 12 and their mass spectra given Figures 13–15. Note that some names are truncated. ^b Numbers in parentheses are CAS registry numbers supplied by the author.

different nucleoside is likely to be poorly represented and hence rejected. Fuzzy logic has also been proposed for fingerprinting of Py-GC data.^{45,46} The approach described here is conceptually simple and provides information on chemical markers in addition to class membership.

Once a chemical marker for a class of samples is identified, the ultimate objective of many pattern recognition schemes has been reached. Using a validated chemical marker, traditional difficulties associated with dimensionality of the data set, required number of samples, or the way data is represented all disappear. Recognition of a chemical marker suggests the possibility of a qualitative chemical explanation from the discrimination obtained.

With the nucleoside data presented here, eight marker peaks were recognized. Although we have listed the first five NIH/EPA mass spectral library search matches for each peak, identifying these peaks is not the subject of this paper. These searches cannot be exhaustive because of the limited size of the library data base and the data reduction done to speed up library searching. Additionally, these peaks may not be pure chemical components. However, these peaks represent unique discriminating features and can be used as chemical markers for the qualitative identification of sample classes. The recognition of such marker peaks may direct subsequent studies to determine their chemical origin.

The MS dimension of GC/MS data has been used here to validate mapping peaks to features in the representation vector. This approach allows meaningful integration of data representation with subsequent analysis. A distinct advantage of this approach is the possibility of working with relatively smaller data sets. With the data set sizes used in this work, during fingerprinting the training set would contain nine (seven in case of cytidine) samples. For computation of Mahalanobis distances, at most three or four features could be retained to compute reasonably well-determined covariance matrices. During some fingerprinting iterations, these complex Py-GC/MS data were represented by only two features. That these complex data sets can be meaningfully represented by only two or three features exemplifies the strength of this vector representation approach.

ACKNOWLEDGMENT

This work was supported by Grant IN107 from the American Cancer Society, by Contract DAAL03-88-K-0075 from the U.S. Army Office of Research and by a grant from the Department of Defense Research Instrumentation program. The donation of the HP Pascal programming system from the Hewlett-Packard Company is also acknowledged.

(45) Otto, M.; Bandemer, H. *Anal. Chim. Acta* 1986, 184, 21–31.

(46) Torell, J. M.; Evans, J. O.; Valcarce, R. V.; Smith, G. G. *J. Anal. Appl. Pyrol.* 1988, 14, 223–236.

Quantitative Analysis by On-Line Supercritical Fluid Extraction/Fourier Transform Infrared Spectrometry

Cynthia Hume Kirschner and Larry T. Taylor*

Department of Chemistry, Virginia Polytechnic Institute and State University, Blacksburg, Virginia 24061

A system is described wherein the supercritical fluid extracts of compounds can be analyzed on-line by FT-IR without prior chromatographic separation. A 1-m- \times 0.010-in.-i.d. stainless steel transfer line was used between the extraction vessel/system cryotrap and the high-pressure IR flow cell. Extraction can be directly conducted as static, dynamic, static-dynamic, or dynamic-cryotrap with minor system alterations. Quantitation was performed by integrating the area of the extract plug, plotted in terms of detector signal versus time. The system was perfected for the extraction and quantification of *n*-tetracosane (C₂₄) from Cellite, but has subsequently been applied to more complex systems, such as fiber/fabric finishing oils, with comparable success. The detection limit for C₂₄ by on-line SFE/FT-IR was calculated to be 74 ng. The relative speed and reproducibility of the method make it a viable alternative to the liquid extraction/IR methods used in industrial process analysis that require increasingly EPA-regulated solvents.

INTRODUCTION

Supercritical fluids have garnered great attention as alternative solvents for extraction and chromatography. Ideally suited for thermally labile, nonpolar compounds, supercritical fluid extraction (SFE) and chromatography (SFC) have been applied independently and in tandem to a broad spectrum of sample types. Perhaps one of the key advantages of SFC is its capacity to interface readily with both GC- and LC-type detectors. Flame ionization detection (FID) is widely used as a universal detector for SFC and SFE/SFC, but applications requiring greater analyte information have been best served by more selective detection, such as Fourier transform infrared spectrometry (FT-IR).¹ Flow cell SFC/FT-IR has the benefit of being a nondestructive technique, permitting placement of a second detector (such as an FID) post flow cell for added data collection.² The addition of SFE to flow cell SFE/FT-IR only increases its method potential, as it eliminates unnecessary sample handling by combining sample preparation with sample analysis.

A principal advantage of SFE is the reduced use or elimination of organic solvents that are often required to remove the analyte from its matrix. This feature has made on-line SFE techniques particularly attractive to industries whose current sample preparation techniques require solvents that are undergoing increased EPA regulation (i.e. chlorinated solvents). For many of these type applications, however, chromatographic separation of the extract is not required. Instead, sample preparation and analysis are routinely conducted by mixing the matrix with an appropriate solvent, removing a portion of the solvent extract from the mixing

flask, and determining the analyte quantity in this extract by, for example, its infrared absorbance. This type of technique is fast and readily automatable and therefore difficult to surpass as a means of analysis. In order for an SFE method to compete, it must exhibit high reproducibility, low RSDs, and be equally fast.

Thus, for such analyses in which chromatography is not needed, direct SFE/FT-IR becomes a sought option. Off-line SFE/FT-IR is readily achieved by trapping the extracted analytes in an IR-suitable solvent (i.e. perchloroethylene) and observing the infrared absorbance of the analyte-containing extract through a liquid cell.³ On-line analyses, however, are inherently more intricate due to the difficulties of trapping analytes and quantitatively transferring them into the FT-IR. Despite such obstacles, on-line SFE/FT-IR has been developed, and our study demonstrates its viability as an alternative to liquid-solid extraction-IR analysis methods. Ikushima et al. recently cited their development of an on-line SFE/FT-IR system.⁴ They employed a JASCO Model 880-PU syringe pump in connection to a JASCO Model FT-IR 7300 spectrometer to obtain the extraction dynamics of stearic acid methyl ester, linoleic acid methyl ester, and DL- α -tocopherol. In contrast to their system, however, the system we show here can be readily plumbed to perform not only on-line dynamic SFE/FT-IR for extraction monitoring, but also on-line static, static-dynamic, and dynamic-cryotrap SFE/FT-IR. The system parameters, ruggedness, and reproducibility of our system have been studied with a simple hydrocarbon, *n*-tetracosane (C₂₄). In addition to the data given for C₂₄, however, the method has already been applied to more "real-world" applications, such as extraction and analysis of finishing oils from fiber and fabric matrices, with equally promising results.^{5,6}

EXPERIMENTAL SECTION

An MPS225 SFE/SFC system was employed (Suprex, Pittsburgh, PA), utilizing a slightly revamped flow schematic from the system as marketed to minimize pump contamination.⁷ The system flow paths are outlined in Figure 1. In lieu of a column, a 1-m- \times 0.010-in.-i.d. transfer line of high-quality stainless steel (Upchurch Scientific, Oak Harbor, WA) was installed. This line was joined by a zero dead volume union to the 50- μ m fused-silica transfer line leading to the high-pressure IR flow cell (Nicolet, Madison, WI). Adequate back-pressure was maintained by a 60- μ m-i.d. deactivated fused-silica tapered restrictor attached to the flow cell exit transfer line. The restrictor tip was housed within the FID heating block to reduce plugging of the exit orifice.

(3) Lopez-Avila, V.; Beckert, W. F. Presented at the 1992 Pittsburgh Conference and Exposition on Analytical Chemistry and Applied Spectroscopy, New Orleans, LA, March 9-12, 1992; paper 678.

(4) Ikushima, Y.; Saito, N.; Hatakeda, K.; Ito, S.; Arai, M.; Arai, K. *Ind. Eng. Chem. Res.* 1992, 31, 574-580.

(5) Kirschner, C. H.; Taylor, L. T.; Seemuth, P. D. Presented at the 1992 Pittsburgh Conference and Exposition on Analytical Chemistry and Applied Spectroscopy, New Orleans, LA, March 9-12, 1992; paper 1064.

(6) Kirschner, C. H.; Taylor, L. T.; Seemuth, P. D. Presented at the 4th International Symposium on Supercritical Fluid Chromatography and Extraction, Cincinnati, OH, May 19-22, 1992.

(7) Hedrick, J. L.; Taylor, L. T. Unpublished data.

(1) Griffiths, P. R.; de Haseth, J. A. *Fourier Transform Infrared Spectrometry*; Wiley & Sons: New York, 1986.

(2) Lee, M. L.; Markides, K. E. *Analytical Supercritical Fluid Chromatography and Extraction*; Chromatography Conferences, Inc.: Provo, UT, 1990.

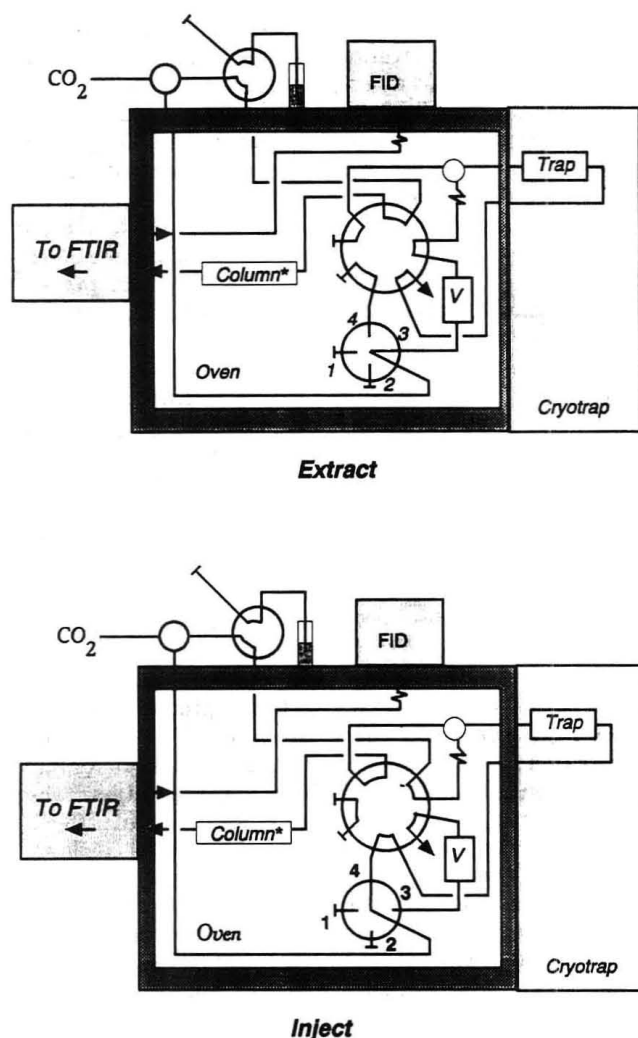


Figure 1. System flow schematic, as plumbed for SFE/SFC/FT-IR. For SFE/FT-IR, the column is replaced by a 1-m \times 0.010-in. stainless steel transfer line.

Stainless steel extraction vessels (0.167 mL) were purchased from Keystone Scientific (Bellefonte, PA). A Nicolet 710 SX FT-IR spectrometer and computer data system were used to collect and interpret the IR data. The system thermostatically maintained the flow cell at 35 °C and the flow cell transfer lines at the corresponding oven temperature (75–120 °C). FT-IR data were collected at 3 scans/s and 8-cm⁻¹ resolution. The FT-IR flow cell had a volume of 1.4 μ L and a 5-mm path length.

SFE-grade carbon dioxide was provided for this project by Air Products and Chemicals Inc. (Allentown, PA). Other necessary gases, such as syphon-grade carbon dioxide for use in cryotrapping, were purchased from Airco (Roanoke, VA). Analyte standards were obtained from Aldrich Chemical Co. (Milwaukee, WI), and any necessary solvents were purchased from Fisher Scientific (Pittsburgh, PA). The Celite extraction matrix was purchased from Supelco, Inc. (Bellefonte, PA).

RESULTS AND DISCUSSION

In removing the column from the system, a transfer line is necessary in order to permit ample IR background scans prior to analyte extract elution. Long sections of small-i.d. fused-silica (50–100 μ m) provided the element of time required, but they tended to separate mixed component extract plugs slightly, which made quantitation of the total extract plug more difficult. Larger i.d. fused silica (i.e. 250 μ m) would have served well as a transfer line, but it cannot typically withstand the high pressures associated with SFE/SFC. Thus, a 1-m- \times 0.010-in.-i.d. high-quality stainless steel transfer line proved most effective as well as rugged. Inter-

change of this line with a column when necessary is easily facilitated as similar fittings may be used, and the line can be configured to occupy roughly the same space as a standard 10-cm \times 1-mm packed column.

Quantitation of the IR signal was performed with the Nicolet 620 computer. The system was set up for a standard SFC/FT-IR analysis. The analyte was extracted, trapped, recovered, and passed through the IR flow cell as a single plug. Once the analyte had totally eluted and the baseline had been reestablished, data collection was stopped and a Grant-Schmidt plus reconstruction of the infrared data was plotted. Elution of the analyte was performed under constant supercritical fluid (CO₂) pressure and temperature, and analyte quantity was derived from the total area of the peak given on the Gram-Schmidt reconstruction. So long as the analyte absorbance is of relatively low intensity, quantitation by this method should be linear and valid.⁸ In the event of coextractants, an infrared window of 20–40 cm⁻¹ at which the analyte uniquely absorbs can be chosen, and a plot of the detector signal versus time for the run data can be made over this region. The integrated area of the peak produced by this plot can be interpreted as analyte quantity by correlating the value to a calibration curve. Alternatively, quantitation may be conducted from the infrared spectrum by determining the integrated absorbance or absorbance intensity for a given analyte. Quantitative data given in this study were generated from the Gram-Schmidt reconstruction by correlating the resulting peak area to concentration on a calibration curve. Quantitation performed from the infrared spectrum (i.e. integrated absorbance of a specific IR region) proved to be equally reproducible, although slightly more time consuming as an IR spectrum must first be generated from the collected data files.

The linearity and reproducibility of this IR quantitation method were tested as follows. Five standards of C₂₄ were prepared in carbon tetrachloride, ranging in concentration from 20.3 to 0.253 mg/mL. For each standard, 0.5 μ L was injected onto the transfer line via a Valco electronic valve assembly located on top of the SFE/SFC system. The injection flow path is shown in Figure 1 for the system in the "Extract" mode. Upon injection, the standard is solubilized by CO₂ and passed through the SFE/FT-IR transfer line into the IR flow cell. Oven temperature was held at 75 °C for all injections, as were the IR transfer lines. The IR flow cell was held at 35 °C. The CO₂ liquid flow rate was estimated at 0.3 mL/min for a pressure of 300 atm and density of 0.77 g/mL. For five replicate injections of each of the five standards, the integrated peak areas from the reconstruction yielded RSDs from 3.3% to 14.7%. Slope (m) was calculated to be 687, the y -intercept (i) was 51.7, and the correlation factor (r) was 0.999 12. From this plot, it was evident that minimal error is incurred by this means of quantitation and that IR response is in fact linear over the analyte concentration range tested. The higher RSD value was attained at the lowest concentration value (0.127 μ g). At lower quantities, the limitation is one of detector noise versus signal since smaller sample quantities mean lower intensity peaks. Variations in signal can also arise depending upon when the analyte enters and exits the flow cell. The signal-to-noise (S/N) ratio for injections made at the lowest standard concentration was calculated to be 23. Using the propagation of errors statistical method⁹ and the m , i , x , and y values from the calibration curve, the limit of detection (LOD) was determined to be 40 ng for analysis of C₂₄ in supercritical CO₂ by direct injection FT-IR. The required statistical equations are given in Table I.

(8) Sparks, Daniel T.; Lam, Richard B.; Isenhour, Thomas L. *Anal. Chem.* 1982, 54, 1922–1926.

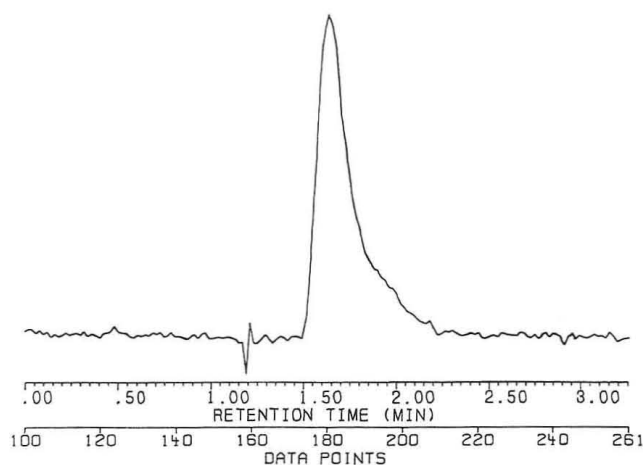


Figure 2. Gram-Schmidt reconstruction of C_{24} extractant plug. y-axis units of total detector signal are in volts/scan.

Table I. Statistical Equations for Calculation of LOD and LOQ⁹

$$S_{y/x} = \left\{ \sum_i (y_i - \hat{y}_i)^2 / n - 2 \right\}^{1/2}$$

$$S_m = S_{y/x} / \left\{ \sum_i (x_i - \bar{x})^2 \right\}^{1/2}$$

$$S_i = S_{y/x} \left\{ \sum_i x_i^2 / n - \sum_i (x_i - \bar{x})^2 \right\}^{1/2}$$

$$C_L = k[S_b^2 + S_i^2 + (i/m)^2 S_m^2]^{1/2} / m$$

y_i = observed integrated peak area for a given x value

\hat{y}_i = calculated peak area for a given x value

x_i = analyte concentration value (μg)

\bar{x} = analyte average concentration value

i = y intercept

m = slope

k = physical constant ($k = 3$ for LOD; $k = 10$ for LOQ)

$S_b = 0$ (zero peak area attained for any given blank)

S_i = error in intercept

S_m = error in slope

$S_{y/x}$ = y/x point error

C_L = limit of detection/limit of quantification (depending upon k value)

Likewise, a calibration curve was then established for C_{24} by on-line SFE/FT-IR. Extraction vessels (0.167 mL) were filled halfway with Celite (≈ 20 – 25 mg), and 20 μL of a C_{24} standard in dichloromethane was injected onto each standard bed. Once the solvent had evaporated, the vessel was sealed and inserted into the system, and its contents were analyzed by SFE/FT-IR. Conditions for extraction were 300 atm, 75 °C oven, and -20 °C trap, with a CO_2 density of 0.77 g/mL and a liquid flow rate of 1 mL/min for 10 min. Upon completion of extraction, the stainless steel trap was quickly heated to 180 °C as repressurized CO_2 flowed through it to achieve removal of the analyte from the trapping surface and entrance into the FT-IR. Conditions for the FT-IR portion of the experiment were 75 °C transfer lines, 35 °C flow cell, 0.30 mL/min CO_2 liquid flow rate at 300 atm, and 3 scans/s data collection at 8- cm^{-1} resolution. Four replicates were done for each of the five calibration points, ranging from 10.8 to 0.216 μg of C_{24} . A GSR for a 1.0- μg sample of C_{24} is given in Figure 2. The plotted calibration line had a slope of $m = 1200$, a y intercept of $i = 88.8$, and a correlation factor of $r = 0.99998$. The lower limits of the concentration range again posed the greatest problem for the method. For masses of 1–10 μg , the RSD was 3–5%, whereas the lowest quantity (0.216 μg) had a less acceptable RSD of 12%. Detection limits were based upon the intensity of the absorbance region chosen for quantitation; use of weaker absorbing windows for an analyte would naturally produce poorer detection limits. For C_{24} ,

the infrared signal was integrated over the 2951–2916- cm^{-1} region. Using the propagation of errors statistical technique and calibration curve data as before,⁹ the detection limit for C_{24} by on-line SFE/FT-IR was valued at 74 ng, and the limit of quantitation (LOQ) was determined to be 250 ng. Our lowest calibration curve point was below the calculated LOQ value, but since the average integrated area for this sample concentration was greater than 10 times the standard deviation of the four sample runs, the point is considered valid. Lower concentrations (i.e. <200 ng), however, proved to be less than 10σ and therefore nonquantifiable, although certainly detectable.

One factor which can hinder or enhance results is the choice of a y -threshold value. We used a fixed restrictor with this system which, with time and analyte buildup, produced gradually decreasing flow rates. A decline in the flow rate can naturally affect the analyte plug height and width adversely from run to run. Also, because cryotrapping was used in this study, differences can exist between small samples versus larger samples in the amount of time required to remove the analyte from the trapping surface. To minimize variation from one run to the next, a y -threshold value was appointed. Peak area was integrated only over those files which had a y signal at or above our designated threshold value (i.e. $y = 20$). It should also be mentioned that reproducibility and noise are quite dependent upon the chosen flow rate for the transfer of analyte into the IR flow cell. Faster flows (i.e. ≥ 0.5 mL/min CO_2 liquid flow) will promote the elution of the analyte as a sharp, single plug and reduce the tailing effects seen with slower flow rates (0.1 mL/min CO_2 liquid flow). Such rapid flows, however, produce inherently noisy IR backgrounds as the flow cell content is changing with every scan. Thus, a compromise should be sought in the choice of flow rate, and it may prove highly beneficial to employ a variable restrictor rather than a fixed restrictor to more readily maintain this optimal flow rate.

To demonstrate the ability of this technique to discern between different components in a mixture, a sample containing caffeine as well as C_{24} was run. A methylene chloride solution containing C_{24} and caffeine was injected onto a Celite-filled vessel to produce 3 μg of each analyte upon evaporation of the solvent. Extraction was performed at 300 atm for 10 min, with the oven at 75 °C and the trap at -10 °C. Fluid flow rate through the vessel was estimated to be 0.6 mL/min. Upon injection of analyte from the trap into the FT-IR flow cell, pressure was maintained at 300 atm with temperature and flow conditions as noted previously for the C_{24} standard runs. A second run of the same sample concentration was performed with injection at 425 atm, a slightly higher pressure which results in higher fluid density as well as increased flow rate. For both runs, a Gram-Schmidt reconstruction of the sample was produced. Figure 3 shows the elution of the mixture through the flow cell at the two different pressures/flow rates. At 300 atm, C_{24} elutes prior to caffeine, as seen in the figure by the shouldering peak. At 425 atm, however, the two analytes are removed almost simultaneously from the trapping surface and are thus pushed through the flow cell to form a more singular peak. Either by selection of the appropriate pressure or by simple replotting of the data over a carbonyl window region (i.e. 1685–1665 cm^{-1}), the passage of the caffeine through the flow cell can be separated from the passage of C_{24} without need of chromatography. Separation is not necessarily required, however, to produce an IR spectrum of a mixture component. If an IR spectrum is collected for pure C_{24} separately, it can be subtracted from the IR spectrum for the binary sample to produce the pure caffeine spectrum. Using this subtraction technique, the IR

(9) Long, G. L.; Winefordner, J. D. *Anal. Chem.* 1983, 55, 712A–724A.

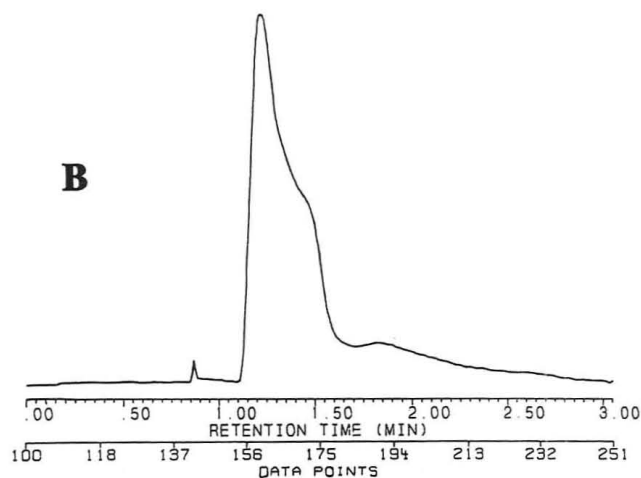
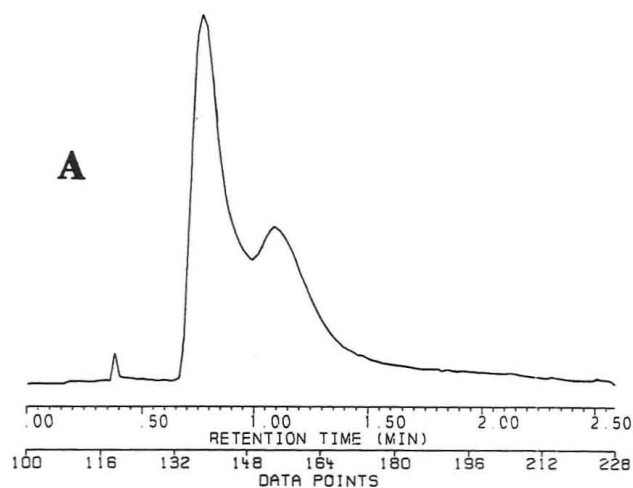


Figure 3. Gram-Schmidt reconstructions of C_{24} /caffeine extractant plugs. y -axis units of total detector signal are in volts/scan. Plug profile A is at 300-atm injection pressure; plug profile B is at 425-atm injection pressure.

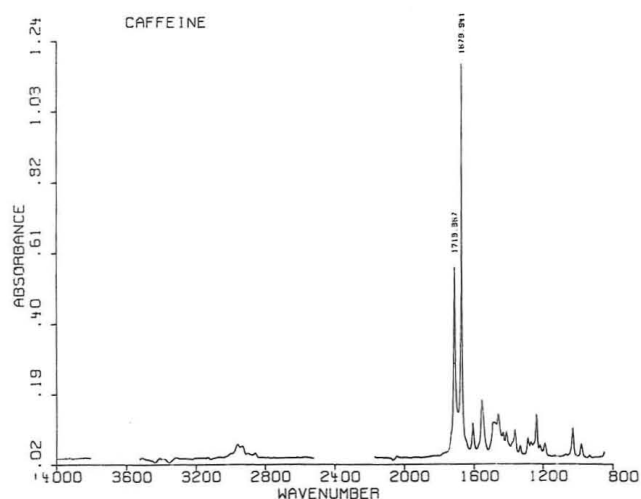


Figure 4. IR spectrum of caffeine via subtraction of C_{24} spectrum from a C_{24} /caffeine sample spectrum. Conditions are as for SFE/FT-IR of C_{24} standards.

spectrum for caffeine was produced from the C_{24} /caffeine sample run at 425 atm and is given in Figure 4. This spectrum is consistent with those obtained from previous SFC/FT-IR experiments using caffeine as an analyte.

The data given here have all been for the dynamic-cryotrapping mode of system operation. Cryotrapping enables analytes to be removed from a matrix and deposited onto a technically more inert surface. For analytes with complex

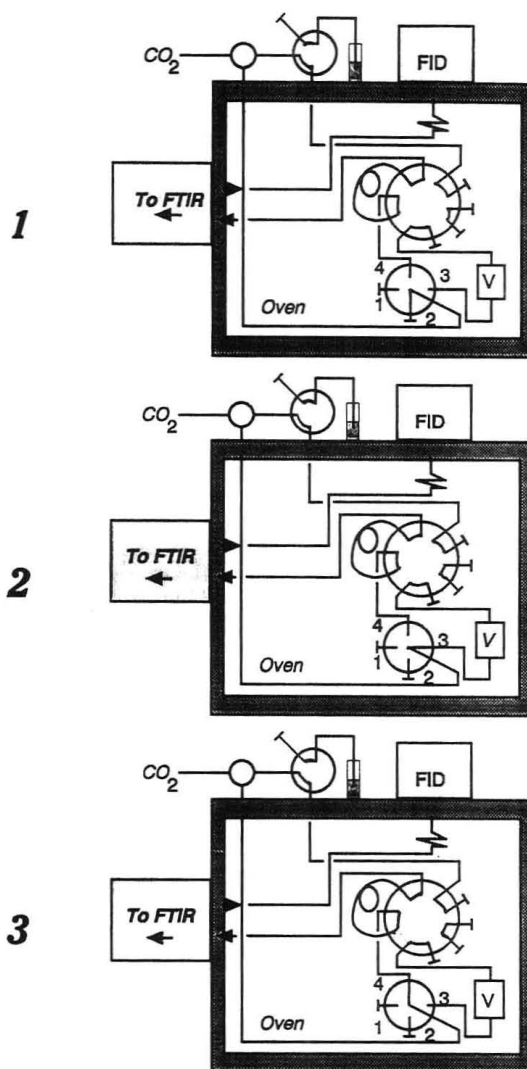


Figure 5. Direct static SFE/FT-IR flow schematic: A = extract; B = sample loop fill; C = sample loop purge/inject.

matrices, this method is highly advantageous. For pure analytes or for analytes with simple matrices, however, cryotrapping can be "overkill", as it effectively means two sample extractions for a given run. As stated previously, the system can be readily replumbed to perform either static, dynamic, or static-dynamic "trapless" SFE/FT-IR. Figures 5-7, show the minor changes required to perform these type extractions. For static extraction, the vessel is pressurized with CO_2 and given time to solubilize the analyte (Figure 5A). The 10-port valve is then switched to allow filling of the sample loop with the analyte-saturated fluid (Figure 5B). Lastly, the 4-way dead-end flow path valve is rotated to allow fluid to flush through the sample loop and into the FT-IR (Figure 5C). Afterward, both valves are returned to their original positions (Figure 5A) to either acquire another aliquot of sample or, upon change of vessels, begin a new extraction. The system can be modified for dynamic direct SFE/FT-IR by making the changes indicated in Figure 6. The system equilibrates to the desired pressure, temperature, and density on 4-way flow path valve position 2 (Figure 6A). Upon switching to position 3, CO_2 flushes through the vessel and into the FT-IR flow cell (Figure 6B). To conduct static-dynamic SFE/FT-IR, the same plumbing scheme is used with different valve configurations. The system is equilibrated with the 10-port valve at the "load" position and the 4-way flow path valve on position 2 (Figure 7A). The 4-way flow path valve is then switched to position 3, the vessel fills with CO_2 , and static extraction is conducted for the desired length

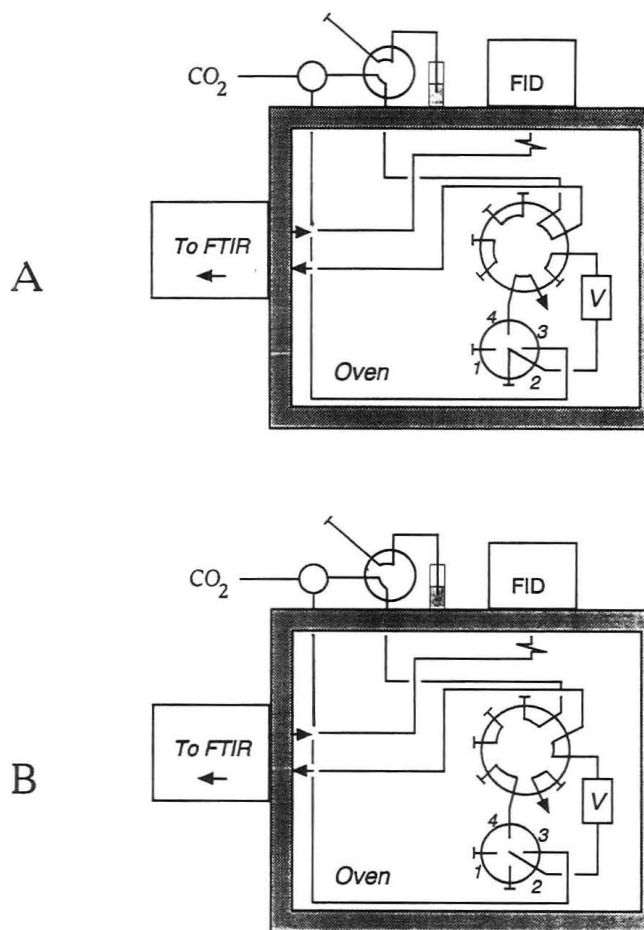


Figure 6. Direct dynamic SFE/FT-IR flow schematic: A = system equilibration; B = dynamic SFE.

of time (Figure 7B). The 10-port valve is then switched to "inject" to allow the effluent to flush the analyte-saturated CO₂ into the FT-IR as well as dynamically extract any remaining analyte from the matrix (Figure 7C). A study of five replicate extractions of 10- μ g sample of C₂₄ shows the reproducibility of static-dynamic SFE/FT-IR to be quite good (2% RSD). Use of alternative plumbing schemes can therefore provide fast results for appropriately soluble analytes, with no loss of analyte due to incomplete trapping and/or recovery.

For analytes which are readily solubilized in CO₂, the direct dynamic and direct static-dynamic SFE/FT-IR methods are quite successful. The elimination of the trapping process should reduce both analysis time as well as potential analyte loss due to incomplete trapping and/or recovery. Analytes which are not as readily solubilized by supercritical CO₂, however, pose more of a problem. Figure 8 shows the anticipated differences in extraction profile between a highly soluble analyte (A) and an analyte which is solubility limited (B) in supercritical CO₂. Note that for the solubility limited analyte, dynamic extraction will yield a lengthy, low-volume plug in the FT-IR that may prove difficult to quantify. It may, in fact, produce a flat plateau peak profile rather than a curve, evidence of an analyte having reached its maximum solubility within the fluid. Static-dynamic extraction may yield plug shape improvement for both solubility cases since it permits concentration of the analyte in a small volume of CO₂ prior to a dynamic flushing of the vessel. The third segment of Figure 8 represents potential plug shape for both solubility cases in which cryotrapping has been employed. For any analyte bound within a difficult matrix, cryotrapping can yield excellent results and be a definite improvement over trapless methods. Disregarding such matrix effects, the

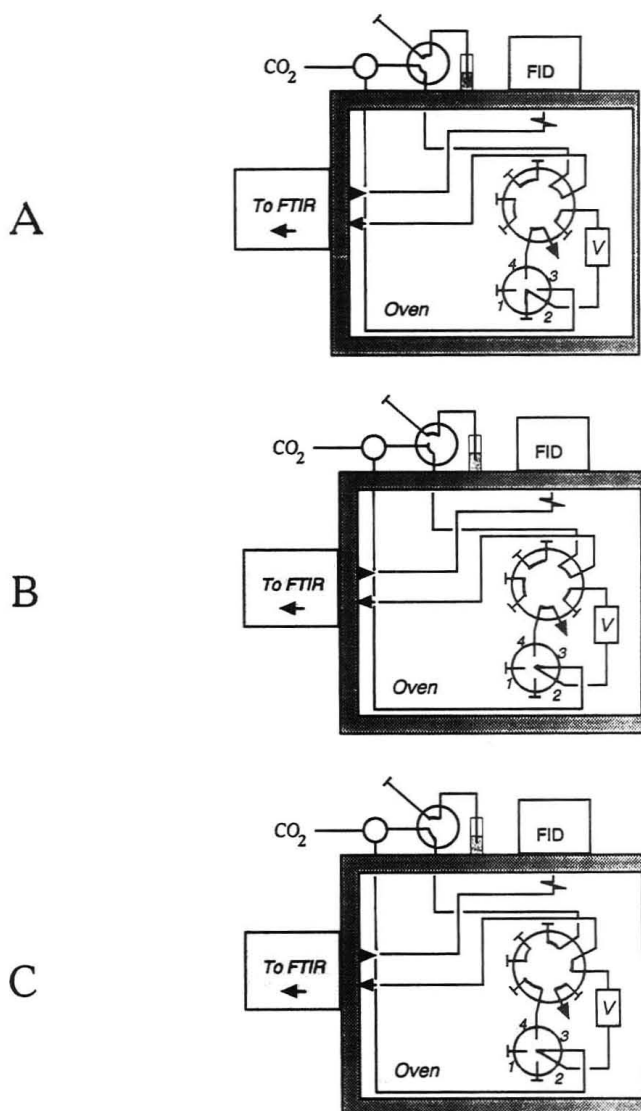


Figure 7. Direct static/dynamic SFE/FT-IR flow schematic: A = system equilibration; B = static SFE; C = dynamic SFE.

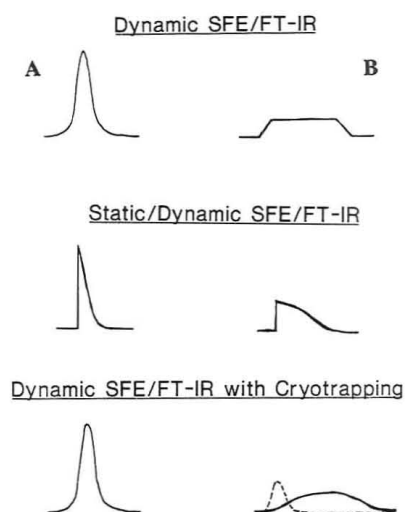


Figure 8. Extraction profiles for SF-soluble versus SF-solubility limited Analytes: A = not solubility limited; B = solubility limited; * = direct extraction/injection into FT-IR with no trapping.

results from cryotrapping SFE/FT-IR can vary depending upon the trap temperature and CO₂ density, as well as analyte solubility. Cryotrapping may result in peak broadening for even highly soluble analytes, depending upon how effectively the extract is removed from the trap and focused onto the

head of the column. For a solubility limited analyte, the result can also vary. The dashed line in the figure represents an analyte which has been effectively removed from the trapping surface, as opposed to the solid line which depicts a far more gradual elution of the analyte from the trap. It would be assumed, however, that if a solubility limited analyte with no matrix interactions extracts gradually for the direct SFE methods, it will likewise require a similar amount of time/fluid to be removed from the trap. In these cases, changes in conditions (i.e. increased fluid density or use of modified fluid) may prove more beneficial than changes in plumbing.

The hypothetical plug shapes represent the elution of single components with different solubilities. Multicomponent extractants make such problems even more complex, as the components may have vastly different degrees of solubility. The resulting profile may be broad and more indicative of total solubility limitation, when in fact several components may be highly to moderately soluble in CO₂. The gradual extraction of the less soluble components can sufficiently broaden the extraction plug to make quantitation difficult. For such cases as these where solubility limitations pose a problem, dynamic extraction with cryotrapping may be necessary so that the analyte(s) may be exhaustively extracted first and then transferred into the FT-IR as a whole. But, as was shown in Figure 8, this can prove to be an imperfect solution, since an analyte which is solubility limited in CO₂ can sometimes have as much difficulty removing itself from a trapping surface as it did from the original analyte matrix. Alternatively, direct static-dynamic extraction may help concentrate the more soluble elements of a mixture and hence create a more quantifiable extraction plug while the less soluble elements continue to gradually extract. The principal advantage of this is that by not trapping the analytes onto a surface, loss of analyte and subsequent contamination of the system due to incomplete recovery may be avoided. Thus, the ability of the SFE/FT-IR system to perform a variety of

extraction methods is a definite advantage, especially for the study of complex mixtures containing analytes of varying solubility.

CONCLUSIONS

The analysis of C₂₄ is perhaps neither novel nor exciting, but in this instance, it highlights a method which we believe to be both. The direct interface of SFE to FT-IR provides an alternative to liquid extraction/IR methods that require environmentally hazardous solvents, and exclusion of the column provides an additional small to substantial time savings. The method further proves itself in terms of reproducible quantitation, especially when one considers that the error values stated are for the inclusive method (sample preparation and analysis combined). The method can also be used to study extraction dynamics, as the solubility of analytes in CO₂ can be directly monitored by the FT-IR for varying extraction conditions. Presently, our studies of the extraction and quantification of several different fiber finishing oils from textile products are yielding excellent results, with RSDs of 5–9%.^{5,6} We have no doubt that there are other similar applications to be made with this system, and with equivalent degrees of success.

ACKNOWLEDGMENT

The authors extend appreciation to Dr. Paul Seemuth for his valued input toward this project and corresponding studies and to Nicolet Instruments for the use of the flow cell apparatus. We also acknowledge Air Products and Chemicals, Inc. for the generous donation of SFE-grade CO₂ to the project. Support for this project and related studies was graciously provided by the DuPont Co.

RECEIVED for review June 11, 1992. Accepted October 12, 1992.

TECHNICAL NOTES

Real-Time Measurement of Dimethyl Sulfoxide in Ambient Air

H. Berresheim,^{*†} D. J. Tanner,[‡] and F. L. Eisele[‡]

Georgia Institute of Technology, Atlanta, Georgia 30332

INTRODUCTION

Dimethyl sulfoxide (DMSO) is formed in the atmosphere as an intermediate product of the OH addition reaction with dimethyl sulfide (DMS).¹ In turn, OH also attacks DMSO to form dimethyl sulfone (DMSO₂), one of the stable end products of atmospheric DMS oxidation. Recently, it has been hypothesized² that the emission of dimethyl sulfide (DMS) from the world's oceans and its oxidation in the atmosphere may be responsible for controlling cloud formation over remote oceanic regions. Therefore, it has been further suggested that atmospheric DMS chemistry plays a significant role in global climate change. To verify this hypothesis instrumental techniques must be used or developed which are capable of measuring DMS, its major oxidants, and its individual oxidation products, including DMSO, in the real atmosphere, preferably with a high time resolution. Previously, we have already reported the successful development of different mass spectrometric techniques for real-time measurement of DMS, SO₂, CH₃S(O₂)OH, H₂SO₄, and OH in the atmosphere.³⁻⁵ In this paper we describe a new highly sensitive method for real-time measurement of DMSO in ambient air.

The first measurements of gaseous DMSO and DMSO₂ in the atmosphere were reported by Harvey and Lang.⁶ Typical levels for both compounds were in the low parts-per-trillion by volume (pptv) range. Further measurements over the North Atlantic showed a large range of concentrations observed for both compounds covering at least 3 orders of magnitude.⁷ The method used by these investigators has recently been described in more detail by Lang and Brown.⁸ It involves preconcentration sampling of both compounds from air by adsorption on Tenax GC contained in stainless steel tubes. The loaded tubes are extracted with methanol, and the extracts are further concentrated by solvent evaporation and then analyzed on a gas chromatograph equipped with a Hall electrolytic conductivity detector. Sample extraction and analysis are performed off-line in the laboratory usually within hours to weeks after the samples have been collected and stored in a refrigerator.

This method has two major disadvantages which limit its usefulness in studying the chemical mechanisms involved in atmospheric DMS oxidation and may even produce biased results. First, sampling integration times are typically on the order of 8 h or longer for determination of low pptv levels

of DMSO and DMSO₂. Therefore, only daily-based average concentrations of both compounds can be determined with this method. Since real-time measurements are not possible, the kinetics of DMS oxidation and production of DMSO and DMSO₂ cannot be studied under real atmospheric conditions. Second, the method may be biased by possible artifact formation of DMSO and DMSO₂ occurring in the Tenax traps during sampling due to air oxidation of DMS which is also trapped on Tenax GC. Lang and Brown⁸ reported tests in which no artifact formation of DMSO or DMSO₂ was observed using mixtures of DMS and ozone-enriched air. The use of an oxidant scrubber was considered to be unnecessary. However, other investigators have observed significant losses of DMS occurring in air-sampling traps and have emphasized the use of a scrubber to prevent this problem.⁹ To this date, neither the oxidant nor the product species involved in the observed loss of DMS during preconcentration sampling have been identified. Therefore, results obtained from measurements of DMSO and DMSO₂ using preconcentration sampling without an efficient scrubber in the sampling line may be ambiguous and must be interpreted with caution.

In this paper we describe a new technique for measuring DMSO in ambient air at sub-pptv levels which does not require sample preconcentration. This technique is based on atmospheric pressure chemical ionization mass spectrometry (APCI/MS) and involves the use of a flow reactor which has been described in detail in an earlier paper.³ The high sensitivity of APCI/MS for measuring DMSO in air was first recognized by Karasek and co-workers.^{10,11} They used DMSO as a prototype gas to demonstrate the sensitivity of APCI in combination with ion mobility spectrometry, a technique which they termed plasma chromatography (PC). This system could be further coupled with a quadrupole mass spectrometer. For a combined PC/MS system a detection limit of 1 pptv DMSO in dry air was estimated based on 10-min signal integration.¹² Similar to this previous application the present APCI/MS technique makes use of the relatively high proton affinity of DMSO (211 kcal/mol) compared to H₂O (166 kcal/mol) and most other atmospheric trace gases.¹³ The present system can detect DMSO mixing ratios in ambient air down to approximately 0.5 pptv at 60-s signal integration.

EXPERIMENTAL SECTION

Apparatus and Method. The apparatus used in the present work has been described in detail in an earlier paper.³ Therefore,

[†] School of Earth and Atmospheric Sciences.
[‡] Georgia Tech Research Institute, Physical Sciences Laboratory.
(1) Yin, F.; Grosjean, D.; Seinfeld, J. H. *J. Atmos. Chem.* **1990**, *11*, 390.
(2) Charlson, R. J.; Lovelock, J. E.; Andreae, M. O.; Warren, S. G. *Nature* **1987**, *326*, 655.
(3) Eisele, F. L.; Berresheim, H. *Anal. Chem.* **1992**, *64*, 283.
(4) Eisele, F. L.; Tanner, D. J. *J. Geophys. Res.* **1991**, *96*, 9295.
(5) Tanner, D. J.; Eisele, F. L. *J. Geophys. Res.* **1991**, *96*, 1023.
(6) Harvey, G. R.; Lang, R. F. *Geophys. Res. Lett.* **1986**, *13*, 49.
(7) Pszenny, A. P.; Harvey, G. R.; Brown, C. J.; Lang, R. F.; Keene, W. C.; Galloway, J. N.; Merrill, J. T. *Global Biogeochem. Cycles* **1990**, *4*, 367.

(8) Lang, R. F.; Brown, C. J. *Anal. Chem.* **1991**, *63*, 186.
(9) Saltzman, E. S.; Cooper, D. J. *Biogenic Sulfur in the Environment*; ACS Symposium Series; American Chemical Society: Washington, DC, 1989, Vol. 393, p 330.
(10) Karasek, F. W. *Res./Dev.* **1970**, *21*, 25.
(11) Cohen, M. J.; Karasek, F. W. *J. Chromatogr. Sci.* **1970**, *8*, 330.
(12) Franklin GNO Corp. *Alpha/II plasma chromatograph-mass spectrometer* PCP, Inc.: West Palm Beach, FL, 1970.
(13) Lias, S. G.; Liebman, J. F.; Levin, R. D. *J. Phys. Chem. Ref. Data* **1984**, *13*, 695.

only a brief summary of the experimental setup is given here. One major section of the apparatus consists of a selected-ion, chemical ionization flow reactor. A tailor-made carrier gas mixture is continuously passing through the reactor in a laminar flow. After entering the reactor, the carrier gas is ionized by α bombardment from a radioactive ^{241}Am source, forming specific reactant ions. On the other hand, the sample molecules enter the reactor through a central axis tube downstream from the ^{241}Am source and are subsequently ionized by proton-transfer reactions with the carrier gas reactant ions. The spatial separation between the production of reactant ions and subsequent chemical ionization of the sample is crucial to the high sensitivity and specificity achievable with the present apparatus. This spatial separation significantly reduces the number of radical or metastable species interfering in the production of sample ions, making the ion chemistry in the reactor straightforward, and results in the formation of well-known product ions. Wall losses are virtually eliminated due to the laminar flow conditions in the reactor.

In the present application the targeted sample species is DMSO. As mentioned earlier, DMSO has a relatively high proton affinity compared to most other atmospheric gases. This allows for an efficient production of $(\text{DMSO})\text{H}^+$ product ions by proton exchange with initial NH_4^+ ions in the flow reactor. Subsequently, DMSO concentrations are determined from the $(\text{DMSO})\text{H}^+/\text{NH}_4^+$ ion ratio. Because of the high proton affinity of DMSO, the sample air can be introduced directly into the flow reactor without requiring prior gas chromatographic (GC) separation of DMSO from other atmospheric compounds. This major advantage makes it possible for the first time to measure DMSO in air on a continuous basis with a high time resolution (typically 60-s sample integration in ambient air). The carrier gas mixture used in the present application consists of N_2 containing a few parts per billion by volume (ppbv) of NH_3 and H_2O . The N_2 gas is supplied from a liquid nitrogen dewar and cleaned from impurities in a high-pressure (20 psi) liquid nitrogen trap. Downstream from the trap and prior to entering the reactor the carrier gas is mixed with a continuous flow of NH_3 (12 ng/min at 30 °C) originating from an in-line NH_3 permeation device (VICI Metronics). Using a typical N_2 flow rate of 1 L/min, this produces a NH_3 mixing ratio of approximately 15 ppbv in the carrier gas. Radioactive bombardment of the carrier gas mixture prior to sample ionization in the reactor produces $(\text{H}_2\text{O})_n\text{H}^+$ ions which undergo charge-transfer reactions with NH_3 to form $(\text{H}_2\text{O})_m\text{NH}_4^+$ due to the higher proton affinity of NH_3 (204 kcal/mol) compared to H_2O . Both n and m depend on the H_2O and NH_3 content of the carrier gas used and on temperature and pressure. When encountering the sample air, the ammonium ions react with DMSO molecules to produce $(\text{DMSO})\text{H}^+$ ions which are then guided by electrical fields into the N_2 buffer gas and through small sample apertures into a low-pressure collisional dissociation chamber and from there into a modified Extrel quadrupole mass spectrometer. In the present application sample air was continuously flowing into the reactor at a rate of 0.1 L/min through a $1/32$ -in.-o.d. Teflon line guided inside the stainless steel central axis tube. The sample flow into the reactor was maintained by keeping the reactor slightly (1 Torr) below ambient pressure.

Calibration. Gaseous DMSO standards in the low pptv range were produced using a DMSO permeation device (VICI Metronics) in combination with a multistage flow dilution system.³ The permeation rate of the DMSO source (7.4 ± 0.4 ng/min at 35 °C) was determined by repeatedly measuring the weight loss of the permeation cell over a period of 3 months using a Mettler microbalance. Except for the gravimetric measurements, the DMSO cell was permanently stored in a permeation oven at 35 °C under a constant flow of ultraclean N_2 gas. In the laboratory DMSO standards were produced using N_2 as the dilution gas. Measurements in the field were calibrated by standard addition using dynamic mixtures of the DMSO/N_2 effluent from the permeation system with ambient air.

RESULTS AND DISCUSSION

The choice of carrier gas in the present selected-ion APCI/MS technique is crucial for obtaining optimal results with respect to a specific sample species. For many applications

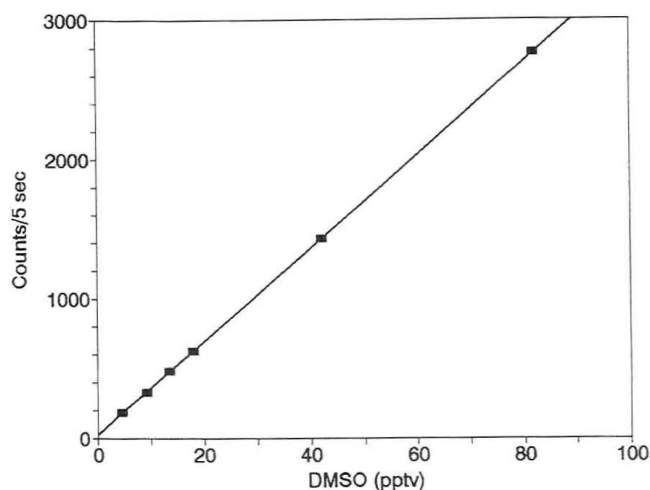


Figure 1. Typical calibration curve for DMSO at 5-s signal integration. Individual points represent means from 10 repetitive measurements. Standard error bars are smaller than symbols shown.

the use of N_2 carrier gas with $(\text{H}_2\text{O})_n\text{H}^+$ as the primary reactant ion species is probably sufficient. However, during a preliminary attempt to measure DMSO in the field on Sapelo Island, GA, in April 1990 very ambiguous results were obtained. Direct chemical ionization of the sample air was used; i.e., initial reactant ions and sample product ions were formed in the same reaction region. A large number of varying and unknown reactant ion species were formed in the flow reactor which either did not react with DMSO or in some cases may have reacted but led to dissociative products. The results were thus ambiguous, and calibration was not possible. In addition to the large number and diversity of initial reactant ion species occurring in the flow reactor the problems encountered in these earlier field experiments were likely related to large differences between the proton affinities of DMSO and species such as H_2O involving relatively high-energy transfer reactions. Therefore, a more specific gentler method of ionizing DMSO was chosen, using NH_3 in the carrier gas to make NH_4^+ the dominant reactant ion species. Since the proton affinity of NH_3 (204 kcal/mol) is also relatively high but lower than that of DMSO, the production of $(\text{DMSO})\text{H}^+$ ions in this mode is not affected by species other than NH_4^+ and no dissociation of the product ions is observed because the energy transfer during the reaction is relatively small (0.3 eV).

Figure 1 shows a typical DMSO calibration curve (blank subtracted) based on a signal integration time of 5 s ($r^2 = 0.9994$, slope = 33.4, intercept = 26.1 counts). Stable concentrations lower than approximately 4 pptv were difficult to produce due to limitations of the gas flow dilution system. During ambient air measurements standard addition calibrations were performed using a 60-s integration cycle for better precision. The estimated 2σ detection limit of the described method in ambient air is 0.5 pptv DMSO at 60-s integration. Figure 2 shows results obtained from field measurements of DMSO with the present system. To our knowledge these data represent the first real-time measurements of DMSO in ambient air. The measurements were conducted on April 24, 1991, at a Pacific coastal site (Cheeka Peak) in northwestern Washington. The site is located on the Olympic peninsula near Cape Flattery at an elevation of approximately 500 m above sea level. The measurements were made with a time resolution of 60 s. The results clearly show a correlation between daylight intensity and production of DMSO due to photochemical oxidation of DMS. Peak DMSO levels up to 3.2 pptv were observed in phase with solar radiation peaks in the late morning hours and at noontime. DMSO levels were below the detection limit at night. As

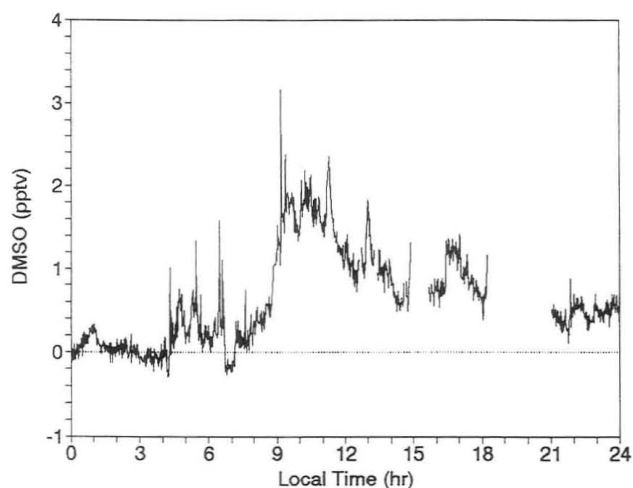


Figure 2. DMSO concentrations measured in marine air at a Pacific coastal site in northwestern Washington on April 24, 1991. Signal integration was 60 s. A discussion of the negative values is given in the text.

shown in Figure 2 the data scattering around the detection limit also include some negative values which resulted from a background signal variation equivalent to ± 0.2 pptv DMSO at 60-s integration. Standard addition calibrations in ambient air were typically made once or twice a day (here between 18 and 21 h) and were also subject to the observed background signal variation. The overall accuracy of the method including

calibration is estimated to be approximately 20%. In the future isotopically labeled DM^{34}SO will be used in standard addition calibrations to eliminate the present calibration problem and further improve the accuracy of the method.

As mentioned earlier, a systematic study of atmospheric DMS oxidation requires measurements of both DMSO and DMSO_2 in air. Dimethyl sulfone is a relatively stable compound with a much weaker basicity compared to DMSO. Therefore, direct measurements of atmospheric DMSO_2 in the low pptv range are not possible with the present technique. Certain modifications are required to convert DMSO_2 into a more reactive product. We are currently developing a selected-ion APCI/MS technique specifically for real-time atmospheric DMSO_2 measurements. The sample analysis involves on-line GC separation of DMSO_2 from other sulfur compounds followed by postcolumn pyrolysis to SO_2^{14} in the presence of a gold catalyst. The SO_2 produced by decomposition of DMSO_2 is then analyzed as described earlier.³ Preliminary experiments using DMSO_2 standards in the pptv range have shown very promising results.

ACKNOWLEDGMENT

We thank T. S. Bates of NOAA/PMEL and R. J. Charlson of the University of Washington for the opportunity to conduct field measurements at Cheeka Peak research station. This work was supported by the National Science Foundation, Grants ATM-8813594 and ATM-9021522, and by the Georgia Tech Research Institute, Grant E8904-046.

RECEIVED for review April 10, 1992. Accepted October 5, 1992.

(14) Busfield, W. K.; Ivin, K. J. *Trans. Faraday Soc.* 1961, 57, 1044.

Method for Batch Processing Small Wood Samples to Holocellulose for Stable-Carbon Isotope Analysis

Steven W. Leavitt* and Shelley R. Danzer

Laboratory of Tree-Ring Research, University of Arizona, Tucson, Arizona 85721

INTRODUCTION

Cellulose and holocellulose have become the preferred material for isotopic analysis of tree rings because of the singular composition of cellulose relative to whole tissue which has many compounds of different isotopic composition¹ and because cellulosic compounds are relatively immobile and remain confined to the growth rings in which they were actually formed, whereas whole tissue contains some mobile compounds which may move across ring boundaries.² Holocellulose is a combination of cellulose (a glucan polymer) and hemicellulose (mixtures of polysaccharides).³ Standard methods for extraction of holocellulose from wood with chlorine dioxide or acid sodium chlorite have the effect of removing most of the lignin, but prolonged treatment to remove the final few percent of lignin results in some loss of hemicelluloses.⁴ For the purpose of streamlining the processing of wood samples to holocellulose, and especially to increase ease of handling and to limit loss of small samples with which we commonly work, we have devised a modified method of processing built around the basic "Jayme-Wise" technique of acid sodium chlorite delignification summarized by Green.⁴ Traditionally, samples are processed in large thimbles through various extractions, at times requiring removal and transfer to other separate vessels. In our method, a batch of 25–30 samples is collectively processed using one large beaker and one flask after initial solvent extraction of the batch in a single soxhlet. We describe here a test of the method in which both yield and stable-carbon isotope composition were measured on samples progressively taken through processing to various degrees of acid chlorite reaction.

EXPERIMENTAL SECTION

Apparatus. Small samples of air-dried, ground (30–40-mesh) plant matter (usually 0.1–0.2 g if abundant and much smaller in the case of samples of limited supply) are placed into individual pouches made of glass-fiber filter paper. We have found the Schleicher & Schuell (Keene, NH 03431) no. 30 glass fiber paper as 5.5-cm circles or as 6-cm squares cut from large 8-in. × 10-in. sheets performs quite well, whereas other types such as Whatman GF/A 5.5-cm glass micropore filter circles disaggregate too much during processing. The filter paper is shaped into a pouch by forming it around the round end of a 14-mm-diameter test tube and placing it into the round 18-mm top opening of a plastic test tube holder. With a 10-hole test tube holder, 10 pouches can be lined up at a time to receive ground plant samples. For routine preparation of holocellulose where mass measurements are not needed during processing, a small plastic or glass tab (ca. 5-mm diameter) with a number inscribed is placed into the pouch along with the sample, and the sample name and corresponding tag number are recorded. The plastic tags degrade with time so they must be inspected prior to each use and replaced if necessary. The pouches are cinched up with waxed lacing string or waxed ribbon flossing tape (dental). Because of the corrosive nature of

the treatment, we tie the pouch with two separate lengths of string in case one fails. An alternate method of securing the pouch is with 4-in. nylon cable ties (typically available from electronic supply stores). When weight determinations are to be made at various stages during processing, it is important to be able to identify the pouches from the outside, so a number or letter is inscribed directly onto the cable-tie "buckle" of each sample. Excess flossing tape or cable tie, and excess pouch flap material above the tie is then trimmed away. Inscription and reading of these small numbers is aided with a binocular microscope. The results described herein employ the latter method of labeling samples.

Procedure. In the first processing step, extractives such as waxes, oils, and resins are removed. A set of 25–30 samples can usually fit into a soxhlet extractor (50-mm i.d., 200-mL capacity to siphon top). The reservoir flask is filled with a 2:1 toluene/ethanol mixture and run overnight (ca. 16–18 h). After shutdown and cooling, samples are poured from the soxhlet and allowed to dry for 1–2 h before returning them to a soxhlet in which the reservoir flask is filled with 100% ethanol and then extracting them for another 16–18 h. Samples are poured from the soxhlet to dry for 1–2 h before boiling in a 1000-mL beaker filled with deionized water for 6 h. Some inorganic salts and low molecular weight polysaccharides including gums and starches are soluble in hot water.³ The pouches (still wet) are then transferred to a 1500-mL Erlenmeyer flask containing ca. 700 mL of deionized water with an addition of sodium chlorite (NaClO₂, technical grade) in the amount of 6–8 g along with 1 mL of glacial acetic acid. The flask is placed on a hot plate at 70 °C with a 50-mL Erlenmeyer flask inverted over the top of the large flask and allowed to react overnight. The following day, three more additions of sodium chlorite and acetic acid are made at 2-h intervals, and the reaction is continued over the second night. The following morning, the samples are rinsed by decanting the solution and adding deionized water. After allowing to sit for 0.5–1 h, the process is repeated until the conductivity of the supernatant is less than 0.5 μmhos cm⁻¹ (SI, 0.5 μS cm⁻¹). We find this usually takes 5–7 such rinsings. Samples are then oven-dried overnight, and the pouches are opened by cutting the string or cable tie to recover the cellulose. Care must be taken in removing the cellulose because it is usually white like the glass-fiber paper. Because the holocellulose tends to clump together, it is fairly easy to remove but sometimes a binocular microscope or hand lens may be used to facilitate the process.

For our test of the method, we first started out with 25 pouches filled with wood (sample no. UA-ALTP-4), a modern spruce (*Picea glauca*) sample from Alaska. Samples were progressively taken out at various steps of the bleaching process on a schedule outlined in Table I. Two additional groups of four modern spruce samples were each treated together with separate batches of 24–25 other samples that were being routinely processed for other projects in order to compare our uniform processing with the test results. A third additional group of four spruce samples was treated with a batch of 16 other samples. Finally, a group of four large splits of spruce wood (ca. 0.4–0.5 g each) were extracted in large, separate glass thimbles, poured from their thimbles, and boiled and bleached in separate beakers and flasks.

The holocellulose yield was calculated as the percent of oven-dried (70 °C) holocellulose mass scraped from the pouches relative to the original mass of air-dried, ground wood. Samples were combusted in a recirculation microcombustion line at 800 °C in the presence of excess oxygen. The CO₂ product was cryogenically purified and analyzed mass spectrometrically. The ¹³C/¹²C ratios are expressed as δ¹³C values with respect to the PDB standard⁵

(1) Deines, Peter *Handbook of Environmental Isotope Geochemistry*; Elsevier: Amsterdam, 1980; Vol. 1, Chapter 9.

(2) Long, Austin; Arnold, Larry D.; Damon, Paul E.; Lerman, Juan C.; Wilson, Alex T. *Radiocarbon Dating*; University of California Press: Berkeley, 1979; pp 532–537.

(3) Petterson, Roger C. *The Chemistry of Solid Wood*; American Chemical Society: Washington, DC, 1984; pp 57–126.

(4) Green, John W. *Methods of Carbohydrate Chemistry*; Academic: New York, 1963; pp 9–21.

(5) Craig, Harmon *Geochim. Cosmochim. Acta* 1957, 12, 133–149.

Table I. Bleaching Schedule after Initial Solvent and Hot-Water Extraction of 25 Splits of Test Sample

date	time, h	action
6 March	1630	hot plate on at 70 °C, 8.03 g of NaClO ₃ and 1 mL of glacial acetic acid added
7 March	0815	four samples removed from solution (batch 1)
	0820	7.99 g of NaClO ₃ and 1 mL of glacial acetic acid added
	1025	four samples removed (batch 2)
	1030	7.90 g of NaClO ₃ and 1 mL of glacial acetic acid added
	1225	four samples removed (batch 3)
	1230	8.05 g of NaClO ₃ and 1 mL of glacial acetic acid added
8 March	1435	four samples removed (batch 4)
	1440	6.10 g of NaClO ₃ and 1 mL of glacial acetic acid added
	0815	four samples removed (batch 5)
9 March	0820	6.35 g of NaClO ₃ and 1 mL of glacial acetic acid added
	0805	last five samples removed (batch 6)

through the use of secondary standards. To judge the accuracy, one split of NBS-21 graphite standard combusted to CO₂ following the experiment gave $\delta^{13}\text{C} = -28.46\text{‰}$ compared to the reported value of -28.13‰ .⁶ Additionally, NBS-19 marble and NBS-20 limestone standards analyzed after reaction with 100% phosphoric acid to produce CO₂ gave $\delta^{13}\text{C}$ values of $+1.91\text{‰}$ and -0.48‰ , respectively, whereas their reported true values are $+1.93\text{‰}$ and -1.06‰ , respectively. A "softwood standard" ground wood material obtained from the Laboratory of Isotope Geochemistry, University of Arizona, was processed to holocellulose using our method. The $\delta^{13}\text{C}$ result was -23.65‰ ($s = 0.32$, $n = 2$) which may be compared to results previously obtained using standard sodium chlorite methods which yielded $\delta^{13}\text{C}$ of -23.55‰ ($s = 0.07$, $n = 2$).⁷ Repeated combustion and analysis ($n = 8$) of a holocellulose lab standard to monitor precision during the course of the experiment produced a standard deviation of 0.23‰ .

RESULTS AND DISCUSSION

The results of this study are contained in Table II, including the characteristics of the resulting "holocellulose", the condition of the cable tie with which the pouch was secured, the percent holocellulose yield, and the stable-carbon isotopic composition ($\delta^{13}\text{C}$). There is a progressive decrease in yield with length of processing, with batches 5 and 6 representing a particularly dramatic, highly statistically significant decrease in yields associated with their extended treatment. For comparison, Hägglund⁸ reported the residue after acid sodium chlorite (or chlorine dioxide) treatment to be in the range of 60–63% for spruce and pine samples, and 62–74% for a variety of hardwood samples. Pettersen³ found the "Cross and Bevan cellulose" content of 8 white spruce and 19 black spruce as 61% and 60%, respectively. Cross and Bevan cellulose is the product after chlorine dioxide bleaching followed by extraction with hot aqueous sodium sulfite solution; this "cellulose" retains a large quantity of the original hemicelluloses.⁴ At the extended level of delignification represented in batches 5 and 6, even the plastic cable ties were beginning to decompose.

The $\delta^{13}\text{C}$ of the original whole wood is -25.92‰ ($n = 4$, $s = 0.12$). The isotopic composition of the holocellulose shows a shift toward increased enrichment in ¹³C (less negative $\delta^{13}\text{C}$) with continued treatment. This is consistent with loss of lignins which tend to be isotopically more ¹³C-depleted than cellulose and especially hemicellulose.¹ The increasingly ¹³C-enriched composition of batches 5 and 6 is puzzling because hemicelluloses are more ¹³C-enriched than cellulose, so that as hemicellulose is decomposed one would expect the re-

maining residue to become more ¹³C-depleted. This result may represent degradation of specific, more ¹³C-enriched than average, hemicelluloses under extreme chlorite delignification conditions. Alternatively, under these harsh conditions perhaps even some of the cellulose is degrading. The $\delta^{13}\text{C}$ averages of batches 1, 2, 3, and 4 were not statistically different from one another, but batches 5 and 6 were significantly heavier than the first four.

The three groups of four splits of the modern spruce wood which were processed along with separate batches of 24, 25, and 16 other unrelated wood samples, respectively, using our standard acid chlorite procedure provide an interesting comparison. The average yield for the first group of four was $62.1 \pm 1.3\%$ and the $\delta^{13}\text{C}$ was -24.67‰ ($s = 0.22\text{‰}$). The second group of four had an average yield of $59.7 \pm 1.3\%$ and a $\delta^{13}\text{C}$ of -24.66‰ ($s = 0.33\text{‰}$); all samples were fully white except one. The third group of four had a yield of $50.8 \pm 1.6\%$ and a $\delta^{13}\text{C}$ of -24.94‰ ($s = 0.17\text{‰}$). These yields suggest the treatment of 25–30 samples produces a holocellulose product approximately consistent with that reported in the literature and intermediate in extent between that received by samples in batch 4 and that received from the extended bleaching in batches 5 and 6 of the test run. Complete treatment of 20 samples resulted in lower yields, but the apparently lower $\delta^{13}\text{C}$ of the third group was not significantly different from the first two groups. The $\delta^{13}\text{C}$ values from runs with 25–30 samples are not statistically different from those of batches 5 and 6 of the test run. It thus appears that our routine with 25–30 samples effectively represents the holocellulose content, but at the same time produces an isotopic composition suggesting a greater degree of lignin removal. Yields were not calculated for the final group of four samples which were treated in thimbles and separate glassware, but their average $\delta^{13}\text{C}$ was -24.66‰ ($s = 0.21\text{‰}$). This is consistent with our results using the pouch method.

The seemingly high standard deviations of the $\delta^{13}\text{C}$ means, even for the whole wood tissue splits, is comparable to the standard deviation for combustions of the lab standard over the period of the experiment. However, sample heterogeneity may also contribute to the scatter in $\delta^{13}\text{C}$ beyond that simply attributable to the actual delignification treatment effects. Sample no. UA-ALTP-4 was from a full disk of wood from the trunk of a tree that was ground and mixed. There is actually much inhomogeneity among and within tree rings of an individual tree,⁹ and the ultimate combustion to CO₂ of only ca. 3 mg of holocellulose from a sample originally in excess of 150 g in size may also contribute to some of the variability.

CONCLUSIONS

With appropriate caution, the processing of small samples of plant matter in glass-fiber pouches provides a reliable method of treatment that eliminates much of the extra glassware needed in traditional methods, and it eliminates material losses which might otherwise occur from transferring samples from one vessel to the next and in filtering. Our standard processing (25–30 samples bleached from late afternoon one day to morning of the day after, with a total of four additions of NaClO₃ and acetic acid) appears to produce a good holocellulose product, similar in yield to that reported in the literature using the standard techniques for large samples, and approximating a treatment intermediate between that of batch 4 and batch 5 in the bleaching test conducted herein. Further treatment and treatment of fewer samples runs the risk of major loss of mass which includes

(6) Coplen, Tyler B.; Kendall, Carol; Hopple, Jessica *Nature* 1983, 302, 236–238.

(7) Siegel, Randall D. *Paleoclimatic Significance of D/H and ¹³C/¹²C Ratios in Pleistocene and Holocene Wood*; M.S. Thesis, University of Arizona: Tucson, 1983.

(8) Hägglund, Erik *Chemistry of Wood*; Academic: New York, 1951.

(9) Leavitt, Steven W.; Long, Austin *Ecology* 1986, 1002–1010.

Table II. Characteristics and Yields of Cellulose Batches

batch	character of cellulose	cable tie	mean yield, % (1s)	mean $\delta^{13}\text{C}$, ‰ (1s)
1	yellow; powdery	good condition	73.1 (0.3)	-25.27 (0.15)
2	yellow, but less so on outside; less powdery	good condition	72.3 (0.6)	-25.32 (0.17)
3	light yellow	good condition	70.5 (1.8)	-25.13 (0.20)
4	mostly white, slight yellow inside	good condition	68.8 (0.8)	-25.09 (0.11)
5	white, hard packed	broke on 2 of 4	53.1 (1.9)	-24.64 (0.15)
6	white, very hard packed	broke on 5 of 5	48.9 (2.2)	-24.61 (0.18)

hemicellulose and perhaps even cellulose in the extreme. Small significant differences in yield also occur during insufficient treatment.

The stable-carbon isotopic composition of the residue generally shows a pattern of increasing $\delta^{13}\text{C}$ with treatment, at least initially consistent with the loss of isotopically "light" lignin. The continued ^{13}C enrichment of samples under prolonged delignification conditions suggests that selective loss of certain hemicelluloses and/or attack on cellulose is enriching the residue further in ^{13}C .

Because of the variation of both yield and $\delta^{13}\text{C}$ associated with the extent of delignification processing, a protocol for constant and uniform processing of samples is essential. However, if precise yield determination is not needed, it

appears that overbleaching is not as critical to accurate measurement of holocellulose $\delta^{13}\text{C}$.

ACKNOWLEDGMENT

This work was supported by NSF Grant No. ATM-9096319. Kyle DeWitte carefully prepared and weighed samples and Teresa Newberry analyzed CO_2 from the samples at the Laboratory of Isotope Geochemistry, Department of Geosciences, University of Arizona.

RECEIVED for review June 8, 1992. Accepted October 20, 1992.

AC FEATURES

A-page Feature Article Guidelines

ANALYTICAL CHEMISTRY regularly publishes INSTRUMENTATION, REPORT, ANALYTICAL APPROACH, and A/C INTERFACE feature articles in the A-page section. In contrast to research articles, which are written for the specialist, A-page articles are written for the nonspecialist. Because they are intended to interest a large number of readers, we encourage authors to provide a popularized and educational perspective. These articles should not be definitive, comprehensive reviews; extensive citation of the research literature should be avoided. The total number of references should not exceed 30–40, and a suggested reading list may be substituted for a formal literature-cited section. In addition, commercial overtones should be minimized, and a discussion of the work of one or two groups only is generally not desirable. Although A-page articles are frequently invited, unsolicited articles are considered if the topics are appropriate. Articles submitted for publication are subject to editorial and peer review. Suggestions for appropriate reviewers are encouraged.

Instrumentation

INSTRUMENTATION feature articles focus on some aspect of a measurement system relevant to analytical science. Areas of interest include both instrument design and applications in fields such as chromatography and separations science, MS, lasers, surface analysis, materials chemistry, spectroscopy, electroanalytical chemistry, bioanalytical chemistry, and biotechnology. Advances in sensitivity, selectivity, and speed should be emphasized. Presentations should provide sufficient information to allow readers to assess both the advantages and the disadvantages of new versus currently available instruments, and to determine how the information provided compares with and/or complements that obtained from other techniques and instruments.

Report

REPORT articles are intended to broaden readers' professional interests and keep them aware of the role of analytical chemistry in the scientific arena and in society in general. Suitable subject matter includes but is not limited to state-of-the-art coverage of important, broad techniques; historical views of certain facets of the field; tutorial presentations of newly developing technical areas; applications of techniques to areas of topical interest,

such as environmental chemistry and biomedicine; and philosophical presentations dealing with any facet of analytical practice.

Analytical Approach

ANALYTICAL APPROACH articles focus on the kind of analytical problem solving that is of concern to laboratories involved with the analysis of real-world samples. Additional popular topics arise from samples of great interest to the general public, including archaeological materials, art objects, or forensic specimens. Articles should include a description of the problem and related background material that gives some perspective on its economic or societal significance. Following this, the author should describe the reasoning behind the particular analytical approach taken to solve the problem.

A/C Interface

A/C INTERFACE articles focus on the influence of computers and automation on the practice of analytical chemistry. Suitable subject matter includes but is not limited to hardware and software for analytical chemistry, laboratory automation and robotics, data acquisition and analysis, chemometrics, and chemical information systems and databases.

Manuscript Format

Manuscript length varies with the type of presentation but should not exceed 25 double-spaced pages. A maximum of six figures can be included to complement or enhance the text. Camera-ready versions of the figures are usually needed for complex diagrams and spectra; otherwise, drafts of the figures are acceptable if they clearly indicate the information to be conveyed. If any figures have appeared previously or are adapted from other publications, please indicate this in the manuscript and your submission letter. Please follow the literature citation style in the JOURNAL's research section.

A brief biographical sketch and informal photograph of the author(s) should also be included for publication at the end of the article. The JOURNAL's editors and artists will assist you in effective and attractive presentation of the material. A copy of the final manuscript on diskette would also be appreciated.

Send four copies of the manuscript to ANALYTICAL CHEMISTRY, 1155 Sixteenth St., N.W., Washington, DC 20036. Please indicate in your cover letter that the paper you are submitting is for consideration as an A-page feature article.

AC RESEARCH

Manuscript Requirements

Scope

The journal is devoted to the dissemination of new and original knowledge concerning all branches of analytical chemistry. Fundamental articles may address the general principles of chemical measurement science and need not directly address existing or potential analytical methodology. Articles may be entirely theoretical with regard to analysis or may report experimental results that bear on theory. Articles may contribute to any of the phases of analytical operations, including sampling, chemical reactions, separations, instrumentation, measurements, and data processing. Articles dealing with known analytical methods should offer either a unique and original application or a significant improvement of the method.

In addition to regular research papers, *Correspondence* and *Technical Notes* are published. *Correspondence* may be brief disclosures of new analytical concepts of unusual significance. They may also represent important comments on the work of others, in which case the authors of the work being discussed will, ordinarily, be allowed to reply. *Technical Notes* should be brief descriptions of novel apparatus or techniques, requiring real ingenuity on the author's part, that offer definite advantages over those already available.

Papers involving extensive use of computers will be judged by the usual criteria of originality, technical content, and value to the field. They should include a statement of the objectives, the procedural steps to the objectives, and the results. However, *details* of procedural steps, including programs, should be omitted. Availability of the latter through commercial collections or by writing to the author should be clearly indicated in the text. Computational techniques for calculations of well-known analytical methods cannot be considered.

Submission of manuscripts

Papers submitted to ANALYTICAL CHEMISTRY are considered with the understanding that they have not been published and are not under consideration elsewhere.

Four complete double-spaced copies of the manuscript are required, with text, tables, and illustrations of a size that can be mailed to reviewers under one cover.

In addition, include with your manuscript: (i) any paper of yours that is in press or under consideration elsewhere and includes information that would be helpful in evaluating the work submitted to ANALYTICAL CHEMISTRY; (ii) written permission from any author whose work is cited as a personal communication, unpublished work, or work in press but who is not an author of your manuscript.

Authors are encouraged to suggest reviewers for their work; such reviewers may be used at the discretion of the editors.

Send all copies of the manuscript with cover letter to Royce W. Murray, Editor, ANALYTICAL CHEMISTRY, Department of Chemistry, Venable and Kenan Laboratories, University of North Carolina, Chapel Hill, NC 27599-3290 (919-962-2541; fax 919-962-2542).

Title

Use specific and informative titles with a high keyword content. Avoid trade names. Use one complete title rather than a title and subtitle.

Authorship

Give authors' names in as complete a form as possible: first names, initials, and surnames. Give the complete mailing address of the place where the work was done and include the current address of each author, if different, on the title page of the manuscript, using a footnote to indicate the difference. The corresponding author is indicated by an asterisk.

Abstract

Abstracts are required for all manuscripts but will not be published with *Correspondence* and *Technical Notes*. The abstract (80–200 words) should describe briefly and clearly the purpose of the research, the principal results, and the major conclusions. Remember that the abstract will be the most widely read portion of the paper and will be used by abstracting services.

Upcoming research

On a separate page, state in 30 words or less the significant results obtained, emphasizing precision and accuracy data when possible. Do not repeat the title. These statements are published in an issue that precedes the full article and are not necessary for *Correspondence* or *Technical Notes*.

Text

Consult the publication for general style. Write for the specialist. It is not necessary to include information and details or techniques that should be common knowledge to the specialist.

General organization. Indicate the breakdown among and within sections with center heads and side heads. Results and Discussion follow the Experimental Section. Keep all information pertinent to a particular section, and avoid repetition.

Introduction. The introduction should state the purpose of the investigation and its relation to other work in the same field but should not include an extensive review of the literature. If the manuscript describes a new method, reasons should be given to indicate why it is preferable to older methods.

Experimental section. Use complete sentences (i.e., do not use outline form). Be consistent in voice and tense.

Apparatus: List only devices of a specialized nature. Do not include equipment that is standard in an analytical

laboratory and used in the normal way.

Reagents: List and describe preparation of special reagents only. Do not list reagents normally found in the laboratory and preparations described in standard handbooks and texts.

Procedure: Because procedures are intended as instructions for other workers, give adequate details of critical steps to permit the work to be repeated. Published procedures should be cited but not described, except where the presentation involves substantial modifications. Omit details of procedures that are common knowledge to those working in the field.

Safety considerations: Describe all safety considerations, including any procedures that are hazardous, any reagents that are toxic, and any procedures requiring special precautions, in enough detail so that workers repeating the experiments can take appropriate safety measures. Appropriate procedures and references for the neutralization or deactivation, as well as ultimate disposal, of unusual byproducts should be included.

Results and discussion. The results may be presented in tables or figures; however, many simple findings can be presented directly in the text with no need for tables or figures. The discussion should be concise and deal with the interpretation of the results. In most cases, combining results and discussion in a single section will give a clearer, more compact presentation.

Conclusions. Use conclusions only when necessary for interpretation and not to summarize information already given in the text or abstract.

References. References that are considered part of the permanent literature should be numbered in one consecutive series by order of mention in the text. The complete list of literature citations should be placed on a separate page, double-spaced, at the end of the manuscript. Reference numbers in the text should be superscripted. Please note that the accuracy of the references is the responsibility of the author.

Use *Chemical Abstracts Service Source Index* abbreviations for journal names and include publication year, volume, and page number (inclusive pagination is recommended). Include *Chemical Abstracts* reference for foreign publications that are not readily available. List submitted articles as "in press" only if formally accepted for publication, and give the volume number and year if known. Otherwise use "submitted to" or "unpublished work" with place where work was done and date. Include name, affiliation, and date for "personal communications."

Please use the format given in the following examples.

- (1) Koile, R. C.; Johnson, D. C. *Anal. Chem.* **1979**, *51*, 741-44.
- (2) Willard, H. H.; Merritt, L. L., Jr.; Dean, J. A.; Settle, F. A., Jr. *Instrumental Methods of Analysis*, 6th ed.; Van Nostrand: New York, 1981; Chapter 2.

Acknowledgment. Authors may acknowledge technical assistance, gifts, and the source of special materials. Credit for financial support, meeting presentation information, and auspices under which work was done, including permission to publish, are also appropriate.

Figures and tables. Do not use figures or tables that duplicate each other or material already in the text. Straight line graphs will not normally be published; give the information in a table, or in a sentence or two in the text. Do not include tables or figures that have already been published.

Tables: Prepare tables in a consistent form, furnish each with an appropriate title, and number consecutively with Roman numerals in the order of reference in the text. Type each table on a separate page, and collate at the end of the manuscript.

Figures: Submit original drawings (or sharp glossy prints) of graphs and diagrams prepared on tracing cloth or plain white paper. If structures are given in the text, original drawings should be provided. All lines, lettering, and numbering should be sharp and unbroken. If coordinate paper is used, use nonphotographic blue cross-hatch lines. Do not use a typewriter to letter illustrations.

Design illustrations to fit the width of one journal column (8.3 cm). The width of original drawings should be twice the publication size. Letters and symbols should be about 4 mm high on the original (2 mm in reduced journal version). Lettering on copy should be in proportion. Label ordinates and abscissas of graphs along the axes and outside the graph proper.

Supply good prints of photographs. Sharp contrasts are essential. Label each figure on the back with the name of the corresponding author and the figure number. Number all figures consecutively with Arabic numerals in the order of reference in the text.

If drawings are mailed under separate cover, identify them by name of author and title of manuscript.

Color reproduction is possible provided that the Editor deems it necessary and that the author bears a portion of the incremental charges. An estimate of these charges will be given upon request. A letter acknowledging the author's willingness to defray the additional cost of color reproduction of figures should accompany the revised manuscript.

Figure captions: Include, on one page, a list of all captions and legends for illustrations. Make the legend a part of the caption rather than inserting it within the figure.

Nomenclature

Nomenclature should conform with current American usage. Insofar as possible, authors should use systematic names similar to those used by the International Union of Pure and Applied Chemistry and the Chemical Abstracts Service. For CA nomenclature advice, consult the Manager of Nomenclature Services, Chemical Abstracts Service, P.O. Box 3012, Columbus, OH 43210. A name generation service is available through the Registry Services Department, Chemical Abstracts Service, P.O. Box 3343, Columbus, OH 43210.

Avoid trivial names. Well-known symbols and formulas may be used if no ambiguity is likely. Define trade names and abbreviations at point of first use.

Use SI units of measurement (with acceptable exceptions) and give dimensions for all terms. If nomenclature is specialized, as in mathematical and engineering reports, include a Nomenclature section at the end of the paper, giving definitions and dimensions for all terms. Type all equations and formulas clearly and number all equations in consecutive order.

General information about American Chemical Society publications, including preparation of manuscripts, is given in *The ACS Style Guide* (1986), available from Distribution Office, American Chemical Society, 1155 Sixteenth St., N.W., Washington, DC 20036 (800-227-5558 in the continental U.S.; in Washington, DC, or outside the U.S., call 202-872-4363).

Ethical Guidelines to Publication of Chemical Research

The guidelines embodied in this document were adopted by the editors of the Books and Journals Division (now the Publications Division) of the American Chemical Society in January 1985, endorsed by the Society Committee on Publications, and reaffirmed at the 1989 conference of Editors.

PREFACE

The American Chemical Society serves the chemistry profession and society at large in many ways, among them by publishing journals which present the results of scientific and engineering research. Every editor of a Society journal has the responsibility to establish and maintain guidelines for selecting and accepting papers submitted to that journal. In the main, these guidelines derive from the Society's definition of the scope of the journal and from the editor's perception of standards of quality for scientific work and its presentation.

An essential feature of a profession is the acceptance by its members of a code that outlines desirable behavior and specifies obligations of members to each other and to the public. Such a code derives from a desire to maximize perceived benefits to society and to the profession as a whole and to limit actions that might serve the narrow self-interests of individuals. The advancement of science requires the sharing of knowledge between individuals, even though doing so may sometimes entail foregoing some immediate personal advantage.

With these thoughts in mind, the editors of journals published by the American Chemical Society now present a set of ethical guidelines for persons engaged in the publication of chemical research, specifically, for editors, authors, and manuscript reviewers. These guidelines are offered not in the sense that there is any immediate crisis in ethical behavior, but rather from a conviction that the observance of high ethical standards is so vital to the whole scientific enterprise that a definition of those standards should be brought to the attention of all concerned.

We believe that most of the guidelines now offered are already understood and subscribed to by the majority of experienced research chemists. They may, however, be of substantial help to those who are relatively new to research. Even well-established scientists may appreciate an opportunity to review matters so significant to the practice of science.

Formulation of these guidelines has made us think deeply about these matters. We intend to abide by these guidelines, strictly, in our own work as editors, authors, and manuscript reviewers.

GUIDELINES

A. ETHICAL OBLIGATIONS OF EDITORS OF SCIENTIFIC JOURNALS

1. An editor should give unbiased consideration to all manuscripts offered for publication, judging each on its merits without regard to race, religion, nationality, sex, seniority, or institutional affiliation of the author(s). An editor may, however, take into account relationships of a manuscript immediately under consideration to others previously or concurrently offered by the same author(s).

2. An editor should consider manuscripts submitted for publication with all reasonable speed.

3. The sole responsibility for acceptance or rejection of a manuscript rests with the editor. Responsible and prudent exercise of this duty normally requires that the editor seek advice from reviewers, chosen for their expertise and good judgment, as to the quality and reliability of manuscripts submitted for publication. In reaching a final decision, the editor should also consider additional factors of editorial policy.

4. The editor and members of the editor's staff should not disclose any information about a manuscript under consideration to anyone other than those from whom professional advice is sought. (However, an editor who solicits, or otherwise arranges beforehand, the submission of manuscripts may need to disclose to a prospective author the fact that a relevant manuscript by another author has been received or is in preparation.) After manuscripts have been accepted for publication, the editor and members of the editor's staff may disclose or publish manuscript titles and authors' names, but no more than that unless the author's permission has been obtained.

5. An editor should respect the intellectual independence of authors.

6. Editorial responsibility and authority for any manuscript authored by an editor and submitted to the editor's journal should be delegated to some other qualified person, such as another editor of that journal or a member of its Editorial Advisory Board. Editorial consideration of the manuscript in any way or form by the author-editor would constitute a conflict of interest, and is therefore improper.

7. Unpublished information, arguments, or interpretations disclosed in a submitted manuscript should not be used in an editor's own research except with the consent of the author. However, if such information indicates that some of the editor's own research is unlikely to be profitable, the editor could ethically discontinue the work. When a manuscript is so closely related to the current or past research of an editor as to create a conflict of interest, the editor should arrange for some other qualified person to take editorial responsibility for that manuscript. In some cases, it may be appropriate to tell an author about the editor's research and plans in that area.

8. If an editor is presented with convincing evidence that the main substance or conclusions of a report published in an editor's journal are erroneous, the editor should facilitate publication of an appropriate report pointing out the error and, if possible, correcting it. The report may be written by the person who discovered the error or by an original author.

B. ETHICAL OBLIGATIONS OF AUTHORS

1. An author's central obligation is to present an accurate account of the research performed as well as an objective discussion of its significance.

2. An author should recognize that journal space is a precious resource created at considerable cost. An author therefore has an obligation to use it wisely and economically.

3. A primary research report should contain sufficient detail and reference to public sources of information to permit the author's peers to repeat the work.

4. An author should cite those publications that have been influential in determining the nature of the reported work and that will guide the reader quickly to the earlier work that is essential for understanding the present investigation. Except in a review, citation of work that will not be referred to in the reported research should be minimized.

5. Any unusual hazards inherent in the chemicals, equipment, or procedures used in an investigation should be clearly identified in a manuscript reporting the work.

6. Fragmentation of research reports should be avoided. A scientist who has done extensive work on a system or group of related systems should organize publication so that each report gives a well-rounded account of a particular aspect of the general

study. Fragmentation consumes journal space excessively and unduly complicates literature searches. The convenience of readers is served if reports on related studies are published in the same journal, or in a small number of journals.

7. In submitting a manuscript for publication, an author should inform the editor of related manuscripts that the author has under editorial consideration or in press. The relationships of such manuscripts to the one submitted should be indicated.

8. It is in general inappropriate for an author to submit manuscripts describing essentially the same research to more than one journal of primary publication. However, there are exceptions as follows: (a) resubmission of a manuscript rejected by or withdrawn from publication in one journal; (b) submission of overlapping work to a second journal in another field, if workers in the other field are unlikely to see the article published in the first journal, providing that both editors are informed; and (c) submission of a manuscript for a full paper expanding on a previously published brief preliminary account (a "communication" or "letter") of the same work.

9. An author should identify the source of all information quoted or offered, except that which is common knowledge. Information obtained privately, as in conversation, correspondence, or discussion with third parties, should not be used or reported in the author's work without explicit permission from the investigator with whom the information originated. Information obtained in the course of confidential services, such as refereeing manuscripts or grant applications, should be treated similarly.

10. An experimental or theoretical study may sometimes justify criticism, even severe criticism, of the work of another scientist. When appropriate, such criticism may be offered in published papers. However, in no case is personal criticism considered to be appropriate.

11. The co-authors of a paper should be all those persons who have made significant scientific contributions to the work reported and who share responsibility and accountability for the results. Other contributions should be indicated in a footnote or an "Acknowledgments" section. An administrative relationship to the investigation does not of itself qualify a person for co-authorship (but occasionally it may be appropriate to acknowledge major administrative assistance). Deceased persons who meet the criterion for inclusion as co-authors should be so included, with a footnote reporting date of death. No fictitious name should be listed as an author or co-author. The author who submits a manuscript for publication accepts the responsibility of having included as co-authors all persons appropriate and none inappropriate. The submitting author should have sent each living co-author a draft copy of the manuscript and have obtained the co-author's assent to co-authorship of it.

C. ETHICAL OBLIGATIONS OF REVIEWERS OF MANUSCRIPTS

1. Inasmuch as the reviewing of manuscripts is an essential step in the publication process, and therefore in the operation of the scientific method, every scientist has an obligation to do a fair share of reviewing.

2. A chosen reviewer who feels inadequately qualified to judge the research reported in a manuscript should return it promptly to the editor.

3. A reviewer (or referee) of a manuscript should judge objectively the quality of the manuscript, of its experimental and theoretical work, of its interpretations and its exposition, with due regard to the maintenance of high scientific and literary standards. A reviewer should respect the intellectual independence of the authors.

4. A reviewer should be sensitive to the appearance of a conflict of interest when the manuscript under review is closely related

to the reviewer's work in progress or published. If in doubt, the reviewer should return the manuscript promptly without review, advising the editor of the conflict of interest or bias. Alternatively, the reviewer may wish to furnish a signed review stating the reviewer's interest in the work, with the understanding that it may, at the editor's discretion, be transmitted to the author.

5. A reviewer should not evaluate a manuscript authored or co-authored by a person with whom the reviewer has a personal or professional connection if the relationship would bias judgment of the manuscript.

6. A reviewer should treat a manuscript sent for review as a confidential document. It should neither be shown to nor discussed with others except, in special cases, to persons from whom specific advice may be sought; in that event, the identities of those consulted should be disclosed to the editor.

7. Reviewers should explain and support their judgments adequately so that editors and authors may understand the basis of their comments. Any statement that an observation, derivation, or argument had been previously reported should be accompanied by the relevant citation. Unsupported assertions by reviewers (or by authors in rebuttal) are of little value and should be avoided.

8. A reviewer should be alert to failure of authors to cite relevant work by other scientists, bearing in mind that complaints that the reviewer's own research was insufficiently cited may seem self-serving. A reviewer should call to the editor's attention any substantial similarity between the manuscript under consideration and any published paper or any manuscript submitted concurrently to another journal.

9. A reviewer should act promptly, submitting a report in a timely manner. Should a reviewer receive a manuscript at a time when circumstances preclude prompt attention to it, the unreviewed manuscript should be returned immediately to the editor. Alternatively, the reviewer might notify the editor of probable delays and propose a revised review date.

10. Reviewers should not use or disclose unpublished information, arguments, or interpretations contained in a manuscript under consideration, except with the consent of the author. If this information indicates that some of the reviewer's work is unlikely to be profitable, the reviewer, however, could ethically discontinue the work. In some cases, it may be appropriate for the reviewer to write the author, with copy to the editor, about the reviewer's research and plans in that area.

D. ETHICAL OBLIGATIONS OF SCIENTISTS PUBLISHING OUTSIDE THE SCIENTIFIC LITERATURE

1. A scientist publishing in the popular literature has the same basic obligation to be accurate in reporting observations and unbiased in interpreting them as when publishing in a scientific journal.

2. Inasmuch as laymen may not understand scientific terminology, the scientist may find it necessary to use common words of lesser precision to increase public comprehension. In view of the importance of scientists' communicating with the general public, some loss of accuracy in that sense can be condoned. The scientist should, however, strive to keep public writing, remarks, and interviews as accurate as possible consistent with effective communication.

3. A scientist should not proclaim a discovery to the public unless the experimental, statistical, or theoretical support for it is of strength sufficient to warrant publication in the scientific literature. An account of the experimental work and results that support a public pronouncement should be submitted as quickly as possible for publication in a scientific journal. Scientists should, however, be aware that extensive disclosure of research in the public press might be considered by a journal editor as equivalent to a preliminary communication in the scientific literature.



COPYRIGHT STATUS FORM

Name of American Chemical Society Publication

Author(s)

Ms No.

Ms Title

Received

This manuscript will be considered with the understanding you have submitted it on an exclusive basis. You will be notified of a decision as soon as possible.

[THIS FORM MAY
BE REPRODUCED]

Print or
Type
Author's
Name and
Address

COPYRIGHT TRANSFER

The undersigned, with the consent of all authors, hereby transfers, to the extent that there is copyright to be transferred, the exclusive copyright interest in the above cited manuscript, including the printed version in any format (subsequently referred to as the "work"), to the **American Chemical Society** subject to the following (Note: if the manuscript is not accepted by ACS or if it is withdrawn prior to acceptance by ACS, this transfer will be null and void and the form will be returned.):

- A. The undersigned author and all coauthors retain the right to revise, adapt, prepare derivative works, present orally, or distribute the work provided that all such use is for the personal noncommercial benefit of the author(s) and is consistent with any prior contractual agreement between the undersigned and/or coauthors and their employer(s).
- B. In all instances where the work is prepared as a "work made for hire" for an employer, the employer(s) of the author(s) retain(s) the right to revise, adapt, prepare derivative works, publish, reprint, reproduce, and distribute the work provided that all such use is for the promotion of its business enterprise and does not imply the endorsement of the American Chemical Society.
- C. Whenever the American Chemical Society is approached by third parties for individual permission to use, reprint, or republish specified articles (except for classroom use, library reserve, or to reprint in a collective work) the undersigned author's or employer's permission will also be required.
- D. No proprietary right other than copyright is claimed by the American Chemical Society.
- E. For works prepared under U.S. Government contract or by employees of a foreign government or its instrumentalities, the American Chemical Society recognizes that government's prior nonexclusive, royalty-free license to publish, translate, reproduce, use, or dispose of the published form of the work, or allow others to do so for noncommercial government purposes. State contract number: _____

SIGN HERE FOR COPYRIGHT TRANSFER: I hereby certify that I am authorized to sign this document either in my own right or as an agent for my employer.

Print Authorized Name(s) and Title(s)

Original Signature(s) (in Ink)

Date

CERTIFICATION AS A WORK OF THE U.S. GOVERNMENT

This is to certify that **ALL** authors are or were bona fide officers or employees of the U.S. Government at the time the paper was prepared, and that the work is a "work of the U.S. Government" (prepared by an officer or employee of the U.S. Government as part of official duties), and, therefore, it is not subject to U.S. copyright. (This section should NOT be signed if the work was prepared under a government contract or coauthored by a non-U.S. Government employee.)

INDIVIDUAL AUTHOR OR AGENCY REPRESENTATIVE

Print Author's Name

Print Agency Representative's Name and Title

Original Signature of Author (in Ink)

Date

Original Signature of Agency Representative (in Ink)

FOREIGN COPYRIGHT RESERVED (NOTE: if your government permits copyright to be transferred, refer to section E and sign this form in the top section.)

- If **ALL** authors are employees of a foreign government that reserves its own copyright as mandated by national law, **DO NOT SIGN THIS FORM**. Please check this box as your request for the FOREIGN GOVERNMENT COPYRIGHT FORM (Blue Form) which you will be required to sign. If you check this box, mail this form to: Copyright Administrator, Publications Division, American Chemical Society, 1155 Sixteenth Street, N.W., Washington, D.C. 20036, U.S.A. Otherwise, mail this form to the editor.

AUTHOR INDEX

- Adams, J., 7
Anderson, T. R., 65
Ann, Q., 7
Avdeef, A., 42
- Berresheim, H., 84
Bond, A. M., 56
- Cai, Z., 21
Chait, B. T., 1
Chambers, D. M., 14
Chambers, J. Q., 65
Chan, A. D. C., 32
Cohen, S. L., 1
Comer, J. E. A., 42
- Danzer, S. R., 87
- Eisele, F. L., 84
- Ewing, A. G., 27
- Giblin, D. E., 21
Glish, G. L., 14
Goeringer, D. E., 14
Gross, M. L., 21
- Harrison, D. J., 32
Hayes, M. A., 27
- Johnson, D. C., 50
- Kheterpal, I., 27
Kirschner, C. H., 78
- LaCourse, W. R., 50
Leavitt, S. W., 87
- Malem, F., 37
Mandler, D., 37
McLuckey, S. A., 14
Mirza, U. A., 1
Morgan, S. L., 70
- Nivens, D. E., 65
- Ramanujam, V. M. S.,
21
- Sahota, R. S., 70
Spalding, R. F., 21
Stojanovic, R. S., 56
- Tanner, D. J., 84
Taylor, L. T., 78
Thomson, S. J., 42
- White, D. C., 65

5 Sure-fire Ways to Save Time On Your Scientific Shopping Year-round

The American Chemical Society's * ANNUAL BUYERS' GUIDES *

Your complete sources of where to buy everything from labware to plasticizers, monoclonal antibodies to molecular modeling software. Convenient, multiple-access indexing lets you find what you need at a glance. Reader Service Reply Cards and telephone listings help you make the right decisions fast!

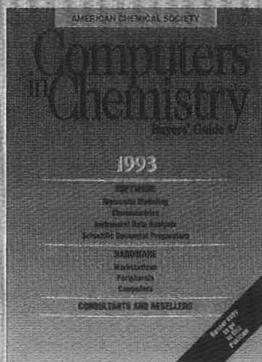
FREE to Qualified Buyers and Specifiers*

1 Analytical Chemistry LabGuide Edition



The first place to turn to build, and maintain, the best-equipped operation around! Gain ready access to state-of-the-art instruments, equipment, and supplies...research and analytical services...and laboratory chemicals and standards. A "must" for any lab!

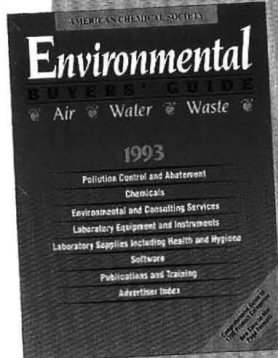
3 Computers in Chemistry Buyers' Guide



Edited specifically for chemists, engineers, and chemical plant and chem lab managers, this essential directory alerts and guides users to the latest

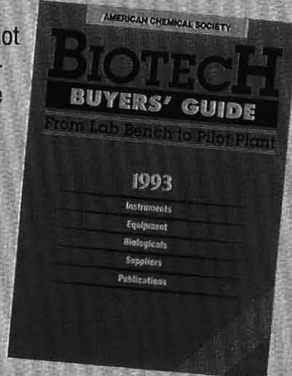
options in computers, peripherals, software, and more.

2 Environmental Buyers' Guide



Air monitors and samplers, water treatment chemicals, waste disposal equipment. Design, engineering and construction services. Lab reagents, gases and solvents. There's no better or more thorough purchasing resource than this full-range, one-stop guide for environmental managers, scientists, and engineers.

4 Biotech Buyers' Guide



From lab bench to pilot plant, an indispensable compendium of cutting-edge biotech products and services for any scientist or engineer (specialists in biochemistry to neuroscience...analytical chemistry to

pharmacology) involved in this cutting-edge field.

5 Chemyclopedia

The authoritative manual for purchasers and users of custom and commercial chemicals. User-friendly and complete, chemical listings include trade names (if any); available forms and grades; packaging and containers; special handling requirements; applications and end uses — even CAS Registry Numbers!

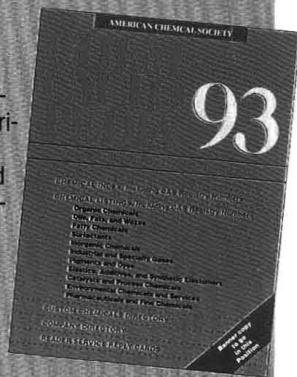
What's more, information is indexed by chemical names and by company/supplier, including addresses, telephone and fax numbers, and telex codes. Valuable briefings in each category review factors affecting availability and price.

* Libraries and other institutions, \$50 (Chemyclopedia, \$60)

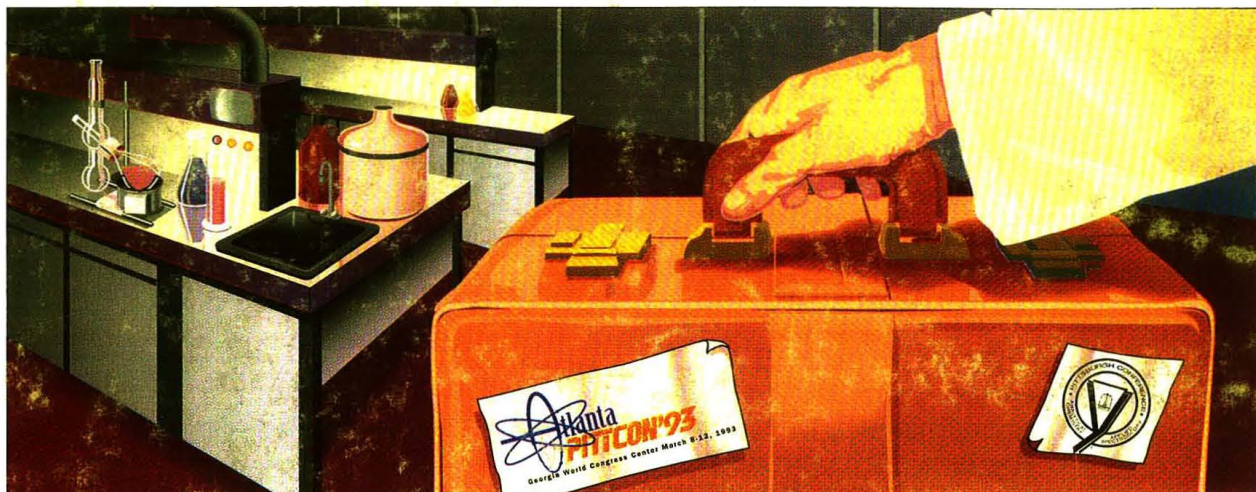
Please address your request or order to:

American Chemical Society
Buyers' Guides, Room 210
1155 Sixteenth Street, N.W.
Washington, D.C. 20036

Your job title and/or letterhead preferred



HAVE SUITCASE, WILL TRAVEL



Have your suitcase packed and ready to go to the 44th Annual Pittsburgh Conference and Exposition.

PITTCON®'93 is home to the world's largest exposition of laboratory equipment and analytical instrumentation. Each year a majority of the exhibitors target **PITTCON®** to unveil their new products. Join the more than 30,000 scientists from industry, government and academia who will attend **PITTCON®'93**

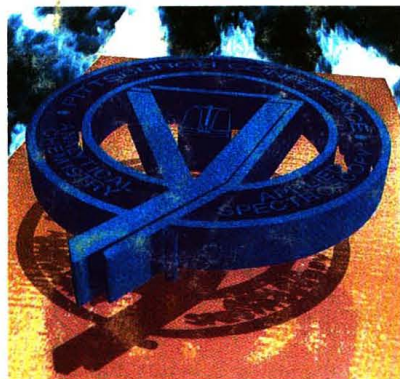
Of course, the exposition alone is reason enough to attend, but **PITTCON®'93** offers much more:

- **WORLD CLASS TECHNICAL PROGRAM**— featuring invited symposia, contributed sessions and short courses on all phases of analytical chemistry and applied spectroscopy, and many related fields
- **EMPLOYMENT BUREAU**— assisting contacts between job candidates and prospective employers
- **LOW REGISTRATION FEES**— a minimal fee for a maximum event
- **HOUSING AND TRANSPORTATION**— insuring the best rates, services and facilities for conferees
- **SOCIAL PROGRAM**— offering a variety of activities for registered conferees and their spouses

So pack that suitcase and be ready to experience **PITTCON®'93** in Atlanta!

For more information, call the Pittsburgh Conference office at

1-800-825-3221



March 8-12, 1993
Georgia World
Congress Center,
Atlanta, Georgia

PITTCON®'93

Dept 7F, Suite 332, Penn Center Blvd. Pittsburgh, PA 15235-5503
(412) 825-3220 • Fax: (412) 825-3224